CONTRIBUTION TO THE ADVANCED ANALYSIS AND PREVENTION OF THE MECHANISMS OF NATURAL FIRE INDUCED STRUCTURAL COLLAPSE IN HIGH-RISE BUILDINGS

APORTACIÓN AL ANÁLISIS AVANZADO Y PREVENCIÓN DE LOS MECANISMOS DE COLAPSO ESTRUCTURAL DE EDIFICIOS DE GRAN ALTURA ANTE UNA SOLICITACIÓN DE INCENDIO REAL

Doctoral Thesis presented by / *Tesis Doctoral presentada por*

Angel Guerrero Castells *Ingeniero Industrial con Suficiencia Investigadora*

in February 2009 to obtain the degree of Doctor in Industrial Engineering

en Febrero de 2009 para obtener el grado de Doctor Ingeniero Industrial.

Thesis Directors / *Directores de la Tesis:*

Dr Frederic Marimon Carvajal from the / *de la Universidad Politécnica de Cataluña*

Dr Francesco Pesavento from the / *de la Università degli Studi di Padova*

PROGRAMA DE DOCTORADO DE ANÁLISIS ESTRUCTURAL

Departamento de Resistencia de Materiales y Estructuras en la Ingeniería

Escuela Técnica Superior de Ingenieros Industriales de Barcelona

Chapter 6

ANALYSIS OF COOLING PROCESSES IN HIGH STRENGTH CONCRETES

THIS PAGE IS INTENTIONALLY
LEFT BLANK

Chapter 6

ANALYSIS OF COOLING PROCESSES IN HIGH STRENGTH CONCRETES

The first aim of this chapter is to analyze both phenomenologically and from a mechanistic point of view the effect of a spectrum of cooling processes on the hygro-thermo-chemo-mechanical state of a structural element, manufactured with High-Strength concrete, during the development of a natural fire in a High-Rise Building. In order to ensure a practical usefulness of the results, the spectrum of cooling processes whose effect is to be analyzed must be wide enough to ensure that they are representative of all of the most expectable actions to be developed by the Fire Fighting Services during the progress of a fire. However, the precise featuring of the Fire Fighting Services cooling actions is not a purpose of this Thesis and in any case will need independent research works.

A second aim taking profit of the results arising from the first part of this Chapter is to develop a comparative analysis to compare the final hygro-thermo-chemo-mechanical state of a structural element after the development of different types – and subtypes – of cooling processes, including comparisons about the Environment vs. Structural element's Surface cooling attacks, among different start instants and for several velocities of the cooling processes.

A third aim of this chapter is to provide enough information to analyze the influence on the hygro-thermo-chemo-mechanical behaviour of the structural element during the cooling processes of several parameters non-related to the own cooling processes. The analysis of the influence of these parameters – such as the initial moisture content of concrete, its intrinsic permeability, the rate of temperature increase (fire intensity), the porosity, compressive strength, type of aggregate and, in general, the whole set of hygro-thermo-chemical properties of concrete – would generate an extension of the Spalling Nomograms initially obtained just for heating processes and described previously on Chapter 4, task not included in this Thesis but proposed as an extended task for future research works.

It must be remarked that it is not an objective of this chapter to discern a complete and definitive conclusion about the favourable or unfavourable effect of the cooling actions developed by the Fire Fighting Services during the progress of a fire, since this aim would need much more analyses than those that might be reasonable for the contents and amount of work expectable for a single Thesis. Nevertheless, some partial conclusions in this sense are included herein.

6.1 IDENTIFICATION OF THE ORIGINAL CONTRIBUTION

As just stated, the main original contributions of the works presented in this chapter are the following. Some parallel minor contributions are also identified within the text of this Chapter.

a. The phenomenological and mechanistic analysis of the effect of a spectrum of cooling processes – representative of the most expectable actions to be developed by the Fire Fighting Services during the progress of a natural fire in a High-Rise Building – on the hygro-thermo-chemo-mechanical state of a structural element manufactured with High-Strength concrete.

b. The development of a comparative analysis to compare the final hygro-thermo-chemo-mechanical state of a structural element after the development of different types – and subtypes – of cooling processes, including comparisons about the Environment vs. Structural element's Surface cooling attacks, among different start instants and for several velocities of the cooling processes.

c. The supply of the information needed for the analysis of the influence on the hygro-thermo-chemo-mechanical behaviour of the structural element during the cooling processes of several parameters non-related to the own cooling processes – such as the initial moisture content of concrete, its intrinsic permeability, the rate of temperature increase (fire intensity), the porosity, compressive strength, type of aggregate and, in general, the whole set of hygro-thermo-chemical properties of concrete –, and for the generation of an extension of the Spalling Nomograms initially obtained just for heating processes and described previously on Chapter 4. Although the generation of the stated Spalling Nomograms for the cooling stage is not an aim of this Thesis and it is proposed as an extended task for future research works, in Appendix 6A is analyzed if the variation of any of these parameters leads to an increase of the maximum value of the adopted Spalling Index I_{s4} (i.e. the risk of Thermal Spalling) during the cooling stage of the cases dealt in this Chapter.

6.2 DEFINITION AND METHODOLOGY TO DEVELOP THE PHENOMENOLOGICAL AND MECHANISTIC ANALYSIS OF THE COOLING PROCESSES

In order to achieve the contributions presented on the previous paragraph, the methodologies described on the following subparagraphs will be applied at each stage of this work to the analysis case defined on next paragraphs.

6.2.1 Definition and Methodology for the evaluation of the Spalling Criteria

As explained in detail both in Chapter 4 and in the chapter concerning the historical evolution of spalling evaluation methodologies, the selected spalling index [1] is obtained choosing the following factors favouring thermal spalling: high local values of gas overpressure, p^g- p_{atm}, and mechanical damage parameter, d, high values of averaged transversal traction stresses, $\overline{\sigma}_{th}$, and constrained elastic energy $\overline{U}$. The considered factors impeding thermal spalling are high average values of traction strength, $\overline{f}_t$, and specific fracture energy, $\overline{G}f$, for the material layer between a current position and the heated surface. Additionally, to obtain a non-dimensional quantity, [1] introduced a reference pressure (assume as equal to atmospheric pressure, p_{atm}) and a characteristic element dimension L (e.g. thickness for a wall, radius for a cylindrical specimen). Finally, internal geometrical parameters involved are unknown and are jointly described by a scaling factor, C_s, which is a non-dimensional parameter. Therefore, the fourth spalling index selected herein, I_{s4}, is given by the following relation:

$$I_{s4} = \frac{\overline{\sigma}_{th} \cdot \overline{U} \cdot d}{\overline{f}_t \cdot \overline{G}_f} \cdot \frac{p^g - p_{atm}}{p_{atm}} \cdot L \cdot C_s \tag{6.1}$$

Herein,

- The values of $\overline{\sigma}_{th}$, d, $\overline{U}$, p^g and the temperatures at each position are obtained from Hitecosp software [2] and then averaged for the material layer between a current position and the heated surface.
- The values of the specific fracture energy are obtained from experimental tests [3]
- The value of $\overline{f}_t$ is obtained from the material tensile strength equation for the temperature at each temperature and then averaged as described.

6.2.2 Definition of other Parameters and Criteria required to complete the accomplishment of the Analysis

The definition and evaluation of a spalling index such as that described on previous paragraph is not enough by itself to accomplish the phenomenological and mechanistic analysis

of the effect of a spectrum of cooling processes on the hygro-thermo-chemo-mechanical state of a structural element manufactured with High-Strength concrete. Hence, a set of parallel variables and parameters is needed. Their description and justification of their selection are included in next subparagraphs.

6.2.2.1 STATE VARIABLES AND RELATED PARAMETERS

A proper choice of state variables for description of concrete at high temperature is of particular importance [4]. From a practical point of view, the physical quantities used, should be possibly easy to measure during experiments, and from a theoretical point of view, they should uniquely describe the thermodynamic state of the medium [5]. They should also assure a good numerical performance of the computer code based on the resulting mathematical model. The necessary number of the state variables may be significantly reduced if existence of local thermodynamic equilibrium at each point of the medium is assumed. In such a case physical state of different phases of water can be described by use of the same variable. When fast hygro-thermal phenomena in concrete at high temperature are analysed, the assumption is debatable, but it is almost always used in modelling.

Having in mind all the aforementioned remarks, now are briefly presented the state variables chosen for the numerical model used in the calculations, some of which are selected to accomplish the phenomenological and mechanistic analysis of cooling processes. Use of temperature (the same for all constituents of the medium because of the assumption about the local thermodynamic equilibrium state) and solid skeleton displacement vector is rather obvious, thus it needs no further explanation. As a hygrometric state variable various physical quantities, which are thermodynamically equivalent, may be used, e.g. volumetric- or mass moisture content, vapour pressure, relative humidity, or capillary pressure. Analysing concrete at high temperature, one must remember that at temperatures higher than the critical point of water (i.e. 647.3 K) there is no capillary (or free) water present in the pores of concrete, and there exists only the gas phase of water, i.e. vapour. Then, very different moisture contents may be encountered at the same moment in a heated concrete, ranging from full saturation with liquid water (e.g. in some nuclear vessels or in so called “moisture clog” zone in a heated concrete [6]) up to almost completely dry material. For these reasons it is not possible to use, in a direct way, one single variable for the whole range of moisture contents. Instead, an appropriate Stefan’s problem could be formulated, with different state variables in zones separated by moving interfaces. However, such an approach is numerically very costly, e.g. [7,8], and usually avoided in practical applications, as already mentioned in [9].

For description of concrete moisture state, Bazant et al. used in their model [10,11] the relative humidity, but in zones fully saturated with liquid water, where pressures higher than the atmospheric one can occur, a different meaning must be given to this variable, permitting its value to be higher than one, what is physically inadmissible. Then, application of a shrinkage coefficient, relating strain changes with changes of the relative humidity, is consistent with the phenomenological approach, used in [10,11], but not with the mechanistic one. Apparently, the most natural choice for the state variable seems to be mass- or volumetric moisture content, which are well defined for the whole range of temperatures and pressures in concrete. However, these quantities are not continuous at interfaces between different materials, and are not well adapted for numerical simulations, both in fully saturated conditions and in a range of very low moisture contents. Moreover, there is not any direct, physically sound (from the mechanistic point of view) relation between moisture content and stresses. Another possible choice for the moisture state variable is vapour pressure, which however has no physical meaning in a medium fully saturated with water and then, it creates serious numerical problems for moisture contents close to these conditions, as shown by our extensive tests.

The moisture state variable proposed in [9] was capillary pressure, which was shown to be a thermodynamic potential of the physically adsorbed water and, with an appropriate interpretation, can be also used for description of water at pressures higher than the atmospheric one, [12]. The capillary pressure has been shown to assure good numerical performance of the computer code, [9,13-15], and is very convenient for analysis of stress state in concrete, because there is a clear relation between pressures and stresses, [16,17]. Hence, the chosen primary variables of the model used in the calculations of this chapter are the volume averaged values of: gas pressure, p^g, capillary pressure, p^c, temperature, T, and displacement vector of the solid matrix, **u**. On the other hand, the state variables and related parameters chosen for the analyses developed in this Chapter are (by apart from those explained in more detail on paragraphs 6.2.2.2 to 6.2.2.4 because of their especial relevance) the following ones:

p^g,	Gas Pressure,	p^v,	Vapour Pressure,
p^a,	Dry Air Pressure,	T,	Temperature,
S,	Saturation degree,	RH,	Relative Humidity,

6.2.2.2 TOTAL, MECHANICAL AND THERMO-CHEMICAL DAMAGE OF CONCRETE

Beyond the variables and parameters exposed on last paragraph, two parameters more are needed in order to describe sufficiently both the concrete dehydration and the crack development. During heating, concrete at high temperature is exposed to complicated physical and chemical transformations [18] causing changes of its inner structure, what has also a sensible influence on the material properties. From a practical point of view, among the most important macroscopic consequences of these processes are concrete dehydration and crack development, resulting in a significant decrease of mechanical properties of concrete at high temperatures. The material stress – strain behaviour in such conditions is highly non-linear and depends not only on the temperature and dehydration degree, but also on the history of mechanical loading during heating [18].

All these phenomena should be accounted for during analysis of the performance of concrete structures at high temperatures. Some time ago [9,13-15] the changes of concrete strength properties were expressed as functions of the mechanical damage and temperature (only heating processes were analysed), hence any information about the thermally induced material deterioration was not available directly. However, the latter one may be of importance for proper assessment of the state of concrete structure previously exposed to high temperature, e.g. after fire or nuclear accident, because thermo-chemical deterioration is irreversible. For these reasons [4] introduced a parameter describing the degree of the latter process advancement, called thermo-chemical damage, V, because it accounts for changes of material stiffness, both due to thermally induced micro-cracks, caused mainly by stresses at micro- and meso-level, (e.g. resulting from different thermal expansion coefficients of cement paste and aggregate, and from local increase of dehydration products' volume), and due to decrease of concrete strength properties caused by the dehydration process (thus related to the Γ_{dehydr} value). Analysis of the experimental results for several HPC concretes showed, that the chemical effects (dehydration) cannot be distinguished with sufficient accuracy from the micro-thermo-mechanical ones, [19].

The thermo-chemical damage parameter, V, is defined in terms of the experimentally determined evolution of Young's modulus of mechanically undamaged material (i.e. heated to a given temperature, without any additional mechanical load), E_o, expressed as a function of temperature,

$$V = 1 - \frac{E_o(T)}{E_o(T_a)} \tag{6.2}$$

where T_a= 20°C is room temperature.

Mechanical damage of concrete is considered following the scalar isotropic model by Mazars [20,21]. In this model, the damaged material at given temperature, *T*, is supposed to behave elastically and to remain isotropic. Its Young's modulus at this temperature, $E(T)$, can be obtained from the value of mechanically undamaged material at the same temperature, $E_o(T)$, and mechanical damage parameter, *d*, being a measure of cracks' volume density in the material,

$$E(T) = (1-d)\,E_o(T) \tag{6.3}$$

A total effect of the mechanical and thermo-chemical damages, to which the material is exposed at the same time, is multiplicative, i.e. the total damage parameter, *D*, is defined by the following formula,

$$D = 1 - \frac{E(T)}{E_o(T_a)} = 1 - \frac{E(T)}{E_o(T)}\frac{E_o(T)}{E_o(T_a)} = 1 - (1-d)\cdot(1-V) \tag{6.4}$$

and not just by the sum of the two components of damage.

Therefore, the classical effective stress concept [22] is modified to take into account both the mechanical and thermo-chemical damage, so a further reduction of resistant section area due to thermo-chemical degradation is added to that caused by the mechanical damage, i.e. the section reduction by cracking:

$$\tilde{\boldsymbol{\sigma}} = \boldsymbol{\sigma}\frac{S}{\tilde{S}} = \frac{\boldsymbol{\sigma}}{(1-d)(1-V)} \tag{6.5}$$

where *S* and $\tilde{S}$ mean total and resistant area of the damaged material, $\boldsymbol{\sigma}$ is the tensor of nominal stress and $\tilde{\boldsymbol{\sigma}}$ the tensor of "modified" effective stress (in Mazars' sense [20,21]).

This definition of modified effective stress leads to the following form of elastic energy:

$$\rho\psi_e = \frac{1}{2}(1-d)(1-V)\boldsymbol{\Lambda}_0 : \boldsymbol{\varepsilon}^e : \boldsymbol{\varepsilon}^e \tag{6.6}$$

where the term ($\rho\psi_e$) is the scalar thermodynamic potential, Λ_0 the initial material stiffness matrix and $\boldsymbol{\varepsilon}^e$ elastic strain tensor.

In conclusion, for practical reasons only two of the three damage parameters previously explained are selected for the analysis of the phenomena involved in cooling processes (the third parameter, Thermo-Chemical Damage, can always be easily obtained from Total and Mechanical Damage):

D, Total Damage — *d*, Mechanical Damage

while the following variables affected by the abovementioned measures of the concrete dehydration and the crack development complete the set of mechanic parameters selected:

σ_{xx}, Longitudinal stress — σ_{yy}, Transversal stress
U, Elastic Energy

6.2.2.3 VELOCITY (AVAILABLE ENERGY) OF SPALLED-OFF PIECES

6.2.2.3.1 General Velocity of Spalled-Off Pieces

Once determined the time and position of appearance of the main fractures, by means of the damage parameters explained in last subparagraph, it must be analysed, at least through a simplified methodology, if concrete spalling is energetically possible through the comparison of the fracture energy and the stored energy similarly as it was already done in [1] and in Chapter 4

of this Thesis, discerning also if expectable type of spalling is either violent and explosive or slow in nature through the calculation of the velocity of the spalled pieces.

The steps to develop for each set of conditions to work out the parameters just described were explained on Chapter 4 and briefly described again on next table, for the concrete pieces spalled from one square metre, to ease the understanding of this Chapter:

Parameter	**Source / equation**
Possible thickness of the ruptured layer of concrete, Δx [m]	From numerical calculations and evaluation of the Spalling Index, fixed by the position and instant corresponding to the maximum valued of the Spalling Index I_{s4}.
Released elastic energy, ΔU [J]	Integrating the curve of the elastic energy density at the instant showing the highest value of the spalling index and in the range of the coordinates corresponding to the ruptured layer (and for a total surface of 1 m^2).
Total mass of spalled concrete, Δm [Kg]	ρ_0 [Kg/m^3] · Δx [m] · 1 m^2, where ρ is the density at ambient temperature for each kind of material
Total Area of rupture, ΔA_{fr} [m^2]	Assuming certain average dimensions of the spalled pieces of concrete: calculated for 1 m^2 of total surface considering that the average piece of concrete has dimensions $\Delta x \cdot \Delta x \cdot \Delta x$ (for a smaller value of the total surface of all cracks created during concrete fracturing, i.e. for larger dimensions of the spalled material pieces, their kinetic energy would be higher).
Energy consumed for fracturing, ΔE_{fr} [J]	$\Delta E_{fr} = \Delta A_{fr} \cdot G_f$ Where G_f is the specific fracture energy obtained from experimental tests [11], 200 J/m^2
Kinetic energy E_{k0} [J] taking into account only the released elastic energy ΔU [J]	$E_{k0} = \Delta U - \Delta E_{fr}$
Contribution to the concrete fracturing done by the compressed gas, W [J]	Initial assumptions and data: - Initial pressure: p_1 corresponding to the position of the main fracture at the instant showing the maximum value of the spalling index, - It is assumed that during spalling the gas expands adiabatically (good approximation for very quick processes) to the atmospheric pressure $p_2 \approx 0{,}1$ MPa, - Initial width of the crack: 0,5 mm (the higher the initial crack width, the higher would be the value of the work performed by gas), Then, the work performed by compressed gas can be estimated from: $W = \frac{p_1 \cdot V_1 - p_2 \cdot V_2}{k-1}$ $p_2 \cdot (V_2)^k = p_1 \cdot (V_1)^k$, $where\, k = c_p / c_v$ k is the specific heat ratio characteristic for a given gas, c_p and c_v are the isobaric and isochoric specific heats of a gas, and V_1 and V_2 are the initial and final gas volumes.
Estimation for the total kinetic energy ΔE_k [J], taking into account both the released elastic energy and the work performed by compressed gas during its expansion to the atmospheric pressure	$\Delta E_k = \Delta E_{k0} + W$
Average velocity of the concrete spalled pieces, v [m/s]	$v = \sqrt{\frac{2 \cdot \Delta E_k}{\rho_0 \cdot \Delta x \cdot 1m^2}}$

Table 6-1. *Scheme for the energetic analysis*

Whenever the total kinetic energy value is positive (i.e. the sum of the stored elastic energy and the work performed by compress gas during its expansion to the atmospheric pressure is greater than the energy needed for the rupture) and, consequently, the average velocity of the concrete spalled pieces is greater than zero, the concrete spalling will be energetically possible (either explosive or progressive spalling depending on ΔE_k value, the mass of spalled concrete and the gas pressure).

6.2.2.3.2 Velocity affected by Mechanical Damage

Although the comparison of the fracture energy and the stored energy, leading to a calculation of the velocity of spalled-off pieces, is a quite intuitive result, those instants and depths where total kinetic energy is positive (i.e. thermal spalling is energetically viable) do not necessarily present a cracking level sufficiently high to ensure that thermal spalling will be mechanically viable (one must remember that one of the assumptions of the energetic analysis described on last paragraph is that the width of the crack existing at the instant and position of the energetic calculation is of 0,5 millimetres). Therefore, instead of considering a general velocity of spalled-off pieces by itself, only those instants and depths of the structural element at which mechanical damage is higher than 0,1 (10 per cent of the material is cracked) will be understood as mechanically suitable for thermal spalling to occur (this criteria will be referred to from now on as '$v \cdot d$ criterion', where v and d are the velocity and mechanical damage calculated respectively).

The reason for the introduction of this criterion besides the spalling index I_{s4} presented on paragraph 6.2.1, by apart from discerning the expectable type of thermal spalling, is that – as it was previously explained on table 4-43 partially reproduced here in table 6-2 – the instant and depth at which the spalling index I_{s4} reaches its maximum value will not necessarily indicate the first instant when thermal spalling will be both energetically and mechanically viable. Hence, on table 6-2 are represented in green letters the instants and depths where spalling is not possible either because the total kinetic energy is not positive and/or because the level of cracking is not enough. In orange letters are represented the cases where spalling is energetically possible but the level of cracking may still be insufficient. Finally, in red letters are represented the cases where thermal spalling is energetically possible and the level of cracking is high enough to ensure its viability.

#45–TH12K019RH60PAR1C90	$\frac{\Delta E_k\,[J]}{d\,[-]}$					
t [s] / x [m]	120	240	360	480	600	720
0,001	-170	1.457	116	73	-190	-281
	0,000	0,000	0,425	0,480	0,513	0,550
0,002	-275	1.299	392	342	20	-85
	0,000	0,000	0,429	0,503	0,530	0,562
0,003	-372	1.158	684	518	269	66
	0,000	0,000	0,312	0,525	0,548	0,573
0,004	-456	1.021	697	638	457	186
	0,000	0,000	0,235	0,551	0,565	0,582
0,005	-514	883	578	725	593	373
	0,000	0,000	0,205	0,542	0,582	0,594
0,010	-569	157	562	589	1.023	873
	0,000	0,000	0,124	0,199	0,317	0,660

Table 6-2. *Time and spatial evolution of the total kinetic energy ΔE_k and the mechanical damage d, for C90 material (refer to Table 4-43 for deeper information)*

Meanwhile, highlighted in yellow colour are the instants and depths corresponding to the time and position where the maximum value of the I_{s4} spalling index has been obtained, observing clearly that these instants and depths do not match those where thermal spalling is energetically and mechanically possible In the paragraphs concerning the results obtained, these differences will be observed much more in detail.

6.2.2.4 MAXIMUM TEMPERATURE IN CONCRETE AND REINFORCING BARS

The maximum value of the temperature reached at each position of the structural element during the whole set of heating and cooling processes is also of extreme importance for some of the mechanical properties of both the concrete matrix and for the steel reinforcing bars built inside it. Hence, next are introduced a set of mechanical properties that are clearly affected by the maximum temperature reached at a certain position during each of the analyzed cases, and whose evaluation will consequently need the provision of temperature maps and registering of maximum temperature values. Although there are many properties affected by the maximum temperature achieved (both mechanical and thermal) in this paragraph are especially focused the reduction in concrete strength at elevated temperature, the reduction in steel reinforcing bars strength and, as an interface of both materials, the reduction in the adherence breakage stress between reinforcing bars and the concrete matrix.

Regarding the reduction in strength of High Strength concretes at elevated temperature, for instance European regulations such as *Eurocode 2: Design of concrete structures - Part 1.2* [23] establish, in its Section 6, the rule exposed on Table 6-3 is used to consider this reduction (f_{ck} is the characteristic strength). Herein temperature is needed to discern strength reduction that will have to be taken into account within the calculation of the load-carrying capacity of any structural element in a fire situation. Three classes of materials are given in Table 6.3; however, the values given for each of these classes rely on a limited amount of test results. Taking this into account, the recommended class for concrete C 55/67 and C 60/75 is Class 1; for concrete C 70/85 and C80/95 is Class 2, and for concrete C90/105 is Class 3. In this chapter we are dealing with Classes 1 and 2 concretes.

Concrete temperature θ °C	$f_{c,\theta}/f_{ck}$		
	Class 1	Class 2	Class 3
20	1,00	1,0	1,0
50	1,00	1,0	1,0
100	0,90	0,75	0,75
200			0,70
250	0,90		
300	0,85		0,65
400	0,75	0,75	0,45
500			0,30
600			0,25
700			
800	0,15	0,15	0,15
900	0,08		0,08
1000	0,04		0,04
1100	0,01		0,01
1200	0,00	0,00	0,00

Table 6-3. *Reduction of strength at elevated temperature (High Strength concretes) established in [23]*

In this sense, either applying the rules provided by regulations or deriving the strength reduction from experimental tests such as those exposed on figure 6-1, the maximum temperature reached at each point of a structural element constitutes a basic data needed. For instance, figure 6-1 shows the strength-temperature relationships both for the unstressed residual property test and for the comparison of the strength-temperature relationships obtained under the stressed test method for four HSC mixtures in a test program [24] against the design rules for

calculating concrete compressive strength at elevated temperatures prescribed by the Eurocodes [23] for calcareous aggregate concrete and siliceous aggregate concretes:

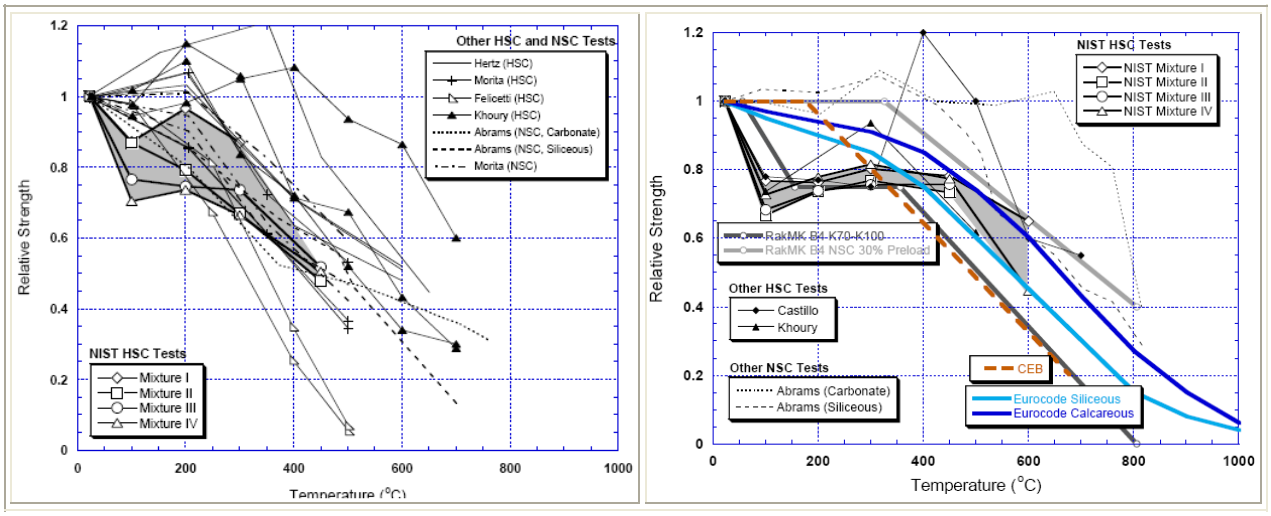

Figure 6-1. *Strength-Temperature relationships corresponding to: Left Figure) Unstressed residual property test [24]; Right Figure) Stressed test method [24] and comparison against the design rules prescribed by the Eurocodes [23].*

On the other hand, related to reinforcing steel bars if, for instance, European regulations such as the already stated *Eurocode 2: Design of concrete structures - Part 1.2* [23] are to be used to assess the fire resistance of a concrete structural element, the strength and deformation properties of reinforcing steel at elevated temperatures shall be obtained from the stress-strain relationships specified in figure 6-2 and tables 6-4 and 6-5. As it is observed, herein the maximum temperature achieved at the reinforcing position again constitutes a basic starting data.

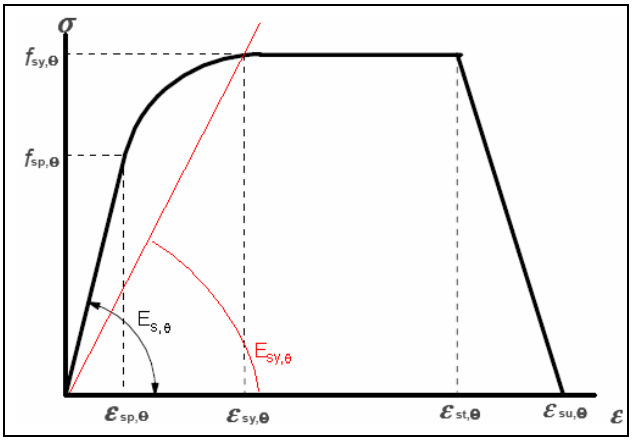

Range	Stress $\sigma(\theta)$	Tangent modulus
$\varepsilon_{sp,\theta}$	$\varepsilon E_{s,\theta}$	$E_{s,\theta}$
$\varepsilon_{sp,\theta} \le \varepsilon \le \varepsilon_{sy,\beta}$	$f_{sp,\theta} - c + (b/a)[a^2 - (\varepsilon_{sy,\theta} - \varepsilon)^2]^{0,5}$	$\frac{b(\varepsilon_{sy,\theta} - \varepsilon)}{a\left[a^2 - (\varepsilon - \varepsilon_{sy,\theta})^2\right]^{0,5}}$
$\varepsilon_{sy,\beta} \le \varepsilon \le \varepsilon_{st,\beta}$	$f_{sy,\theta}$	0
$\varepsilon_{st,\beta} \le \varepsilon \le \varepsilon_{su,\beta}$	$f_{sy,\theta}[1-(\varepsilon - \varepsilon_{st,\theta})/(\varepsilon_{su,\theta} - \varepsilon_{st,\theta})]$	-
$\varepsilon = \varepsilon_{su,\beta}$	0,00	-
Parameter *)	$\varepsilon_{sp,\theta} = f_{sp,\theta} / E_{s,\theta}$ $\varepsilon_{sy,\theta} = 0,02$ $\varepsilon_{st,\theta} = 0,15$ $\varepsilon_{su,\theta} = 0,20$ Class A reinforcement: $\varepsilon_{st,\theta} = 0,05$ $\varepsilon_{su,\theta} = 0,10$	
Functions	$a^2 = (\varepsilon_{sy,\theta} - \varepsilon_{sp,\theta})(\varepsilon_{sy,\theta} - \varepsilon_{sp,\theta} + c/E_{s,\theta})$ $b^2 = c\,(\varepsilon_{sy,\theta} - \varepsilon_{sp,\theta})\,E_{s,\theta} + c^2$ $c = \frac{(f_{sy,\theta} - f_{sp,\theta})^2}{(\varepsilon_{sy,\theta} - \varepsilon_{sp,\theta})E_{s,\theta} - 2(f_{sy,\theta} - f_{sp,\theta})}$	

Figure 6-2. *Mathematical model for stress-strain relationships of reinforcing and prestressing steel at high temperatures [23].*

Steel Temperature θ[°C]	$f_{sy,\theta}/f_{yk}$ hot rolled	$f_{sy,\theta}/f_{yk}$ cold worked	$f_{sp,\theta}/f_{yk}$ hot rolled	$f_{sp,\theta}/f_{yk}$ cold worked	$E_{s,\theta}/E_s$ hot rolled	$E_{s,\theta}/E_s$ cold worked
1	2	3	4	5	6	7
20	1,00	1,00	1,00	1,00	1,00	1,00
100	1,00	1,00	1,00	0,96	1,00	1,00
200	1,00	1,00	0,81	0,92	0,90	0,87
300	1,00	1,00	0,61	0,81	0,80	0,72
400	1,00	0,94	0,42	0,63	0,70	0,56
500	0,78	0,67	0,36	0,44	0,60	0,40
600	0,47	0,40	0,18	0,26	0,31	0,24
700	0,23	0,12	0,07	0,08	0,13	0,08
800	0,11	0,11	0,05	0,06	0,09	0,06
900	0,06	0,08	0,04	0,05	0,07	0,05
1000	0,04	0,05	0,02	0,03	0,04	0,03
1100	0,02	0,03	0,01	0,02	0,02	0,02
1200	0,00	0,00	0,00	0,00	0,00	0,00

Table 6-4. *Class A values for the parameters of the stress-strain relationship of hot rolled and cold worked reinforcing steel at elevated temperatures [23]*

Steel temp. θ[°C]	$f_{py,\theta}/(0,9\,f_{pk})$ cw	$f_{py,\theta}/(0,9\,f_{pk})$ q & t	$f_{pp,\theta}/(0,9\,f_{pk})$ cw	$f_{pp,\theta}/(0,9\,f_{pk})$ q & t	$E_{p,\theta}/E_p$ cw	$E_{p,\theta}/E_p$ q & t	$\varepsilon_{pt,\theta}$ [-] cw, q&t	$\varepsilon_{pu,\theta}$ [-] cw, q&t
1	2	3	4	5	6	7	8	9
20	1,00	1,00	1,00	1,00	1,00	1,00	0,050	0,100
100	0,99	0,98	0,68	0,77	0,98	0,76	0,050	0,100
200	0,87	0,92	0,51	0,62	0,95	0,61	0,050	0,100
300	0,72	0,86	0,32	0,58	0,88	0,52	0,055	0,105
400	0,46	0,69	0,13	0,52	0,81	0,41	0,060	0,110
500	0,22	0,26	0,07	0,14	0,54	0,20	0,065	0,115
600	0,10	0,21	0,05	0,11	0,41	0,15	0,070	0,120
700	0,08	0,15	0,03	0,09	0,10	0,10	0,075	0,125
800	0,05	0,09	0,02	0,06	0,07	0,06	0,080	0,130
900	0,03	0,04	0,01	0,03	0,03	0,03	0,085	0,135
1000	0,00	0,00	0,00	0,00	0,00	0,00	0,090	0,140
1100	0,00	0,00	0,00	0,00	0,00	0,00	0,095	0,145
1200	0,00	0,00	0,00	0,00	0,00	0,00	0,100	0,150

Table 6-5. *Values for the parameters of the stress-strain relationship of cold worked (cw) (wires and strands) and quenched and tempered (q & t) (bars) prestressing steel at elevated temperatures [23]*

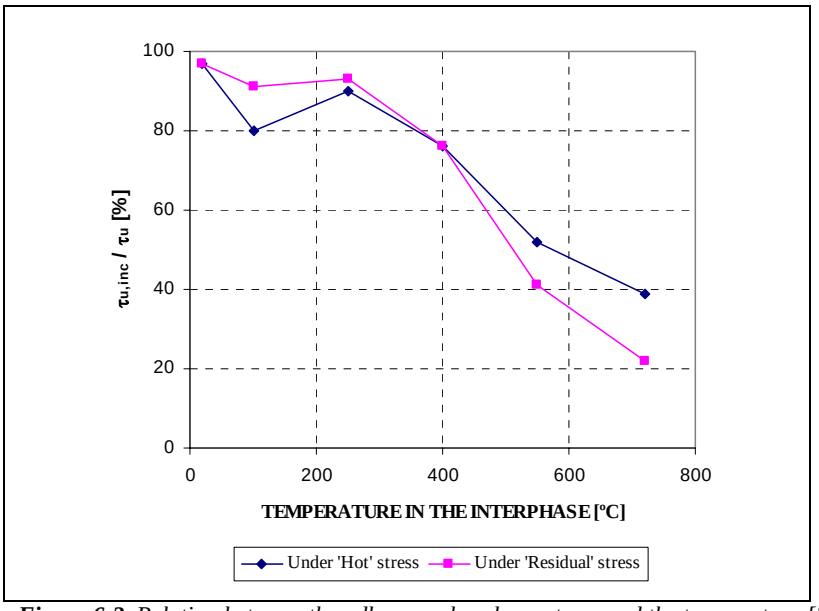

Figure 6-3. *Relation between the adherence breakage stress and the temperature [25].*

A critical aspect in the case of structural elements under fire is the variation of the adherence between reinforcing bars and concrete. The perturbation of this feature is higher after the fire than when the maximum temperature is reached (and higher for higher temperatures reached). Figure 6-3 shows the relation between the adherence breakage stress ($\tau_{u,inc}$) after the fire and that previous to it (τ_u). As it can be observed, the deterioration is very fast for temperatures higher than 300 ºC.

As a conclusion of this paragraph, it has been justified the necessity of exploiting the maximum temperature reached at each position during the complete set of heating and cooling processes composing each case, in order to enable the evaluation the final value of several basic mechanical (and thermal) properties needed to calculate the load-carrying capacity of any structural element in a fire situation.

6.2.3 Graphical representation forms selected for the results

All of the state variables, parameters and criteria selected and exposed on previous paragraphs to complete the accomplishment of the analysis of the phenomena occurred during cooling processes constitute, when a large number of calculations are to be done and described as it will be done later in this chapter, a huge amount of information that needs a clear and intuitive form of representation that enables an easier understanding from the reader.

As many of the results that are exposed herein are collected for each depth and for each instant during the complete calculation, the typical representation form of – for instance – the evolution of the Relative Humidity would be the Cartesian representation of dispersed data with smoothed lines, for all of the depths of the structural element and at a chosen number of instants during the heating and cooling processes duration, such as that shown on Figure 6-4. However, this type of representation tends to be much more complicated to analyze as more sample instants are represented. Furthermore, the necessity to choose a sample of representation instants is dangerous since some really fast but relevant occurring processes might be ignored.

Therefore, an alternative form of representation has been established. Since the amount of dealt information is huge (as it has been previously stated) Matlab software [26] has been used for this task. In figure 6-5 is shown the type of representation finally selected: instead of a Cartesian discrete graphic where *Depth* and *Relative Humidity* constitute the axes, a Cartesian continuum graphic is chosen where *Time [s]* and the *Distance to the heated/cooled surface [cm]* are the axes (the distance is represented only up to a distance to heated/cooled surface of 10,63 centimetres because the overall set of results exceeded the maximum amount of information capable to represent)while the represented parameter values are shown on a colour scaled base. In this way, no information is neglected whereas a continuum representation is developed by means of high-order interpolation techniques that do not introduce any distortion into the finite elements solution. In this way, the interpretation of the large amount of results is much easier, though the needed postprocessing effort is much higher.

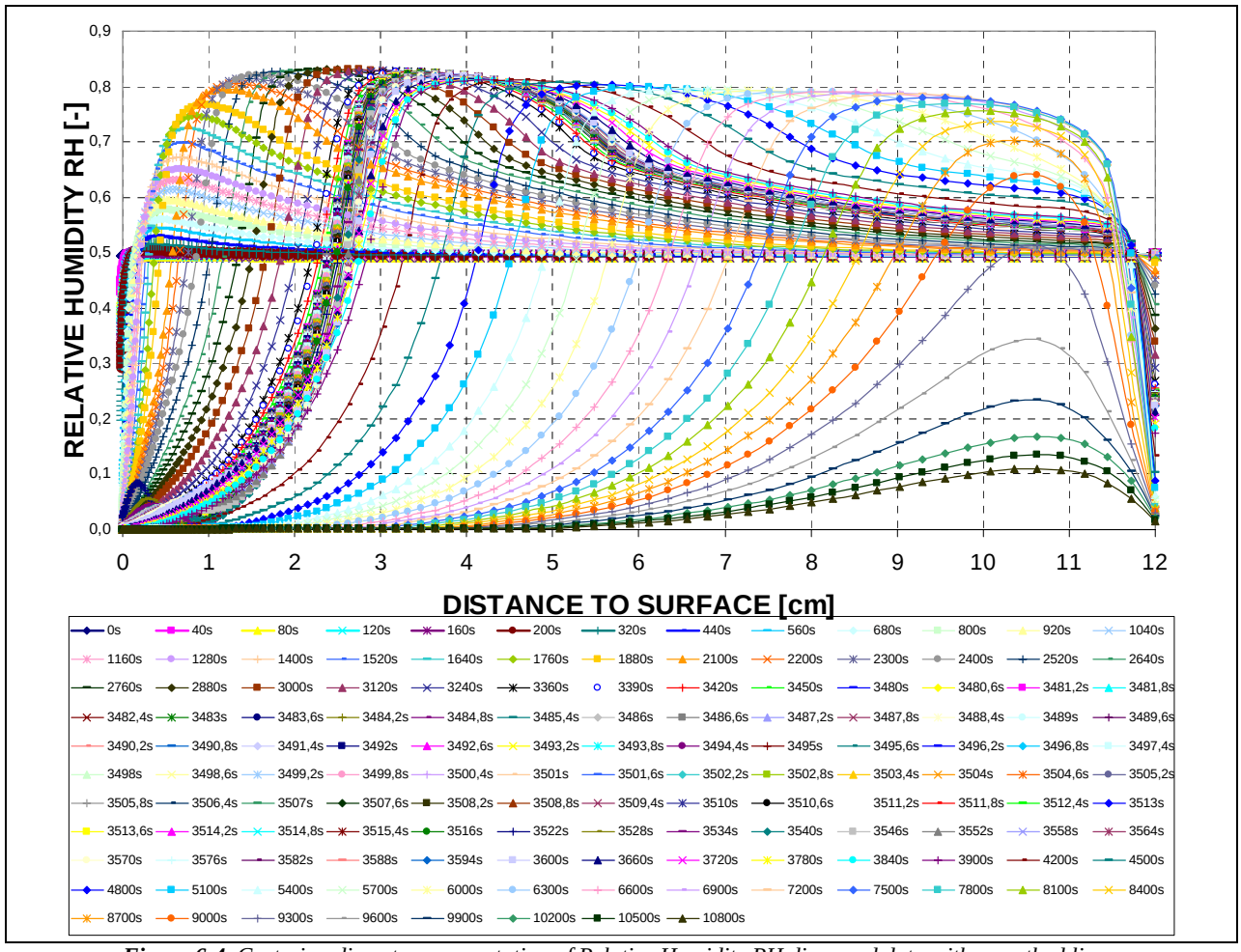

Figure 6-4. *Cartesian discrete representation of Relative Humidity RH dispersed data with smoothed lines.*

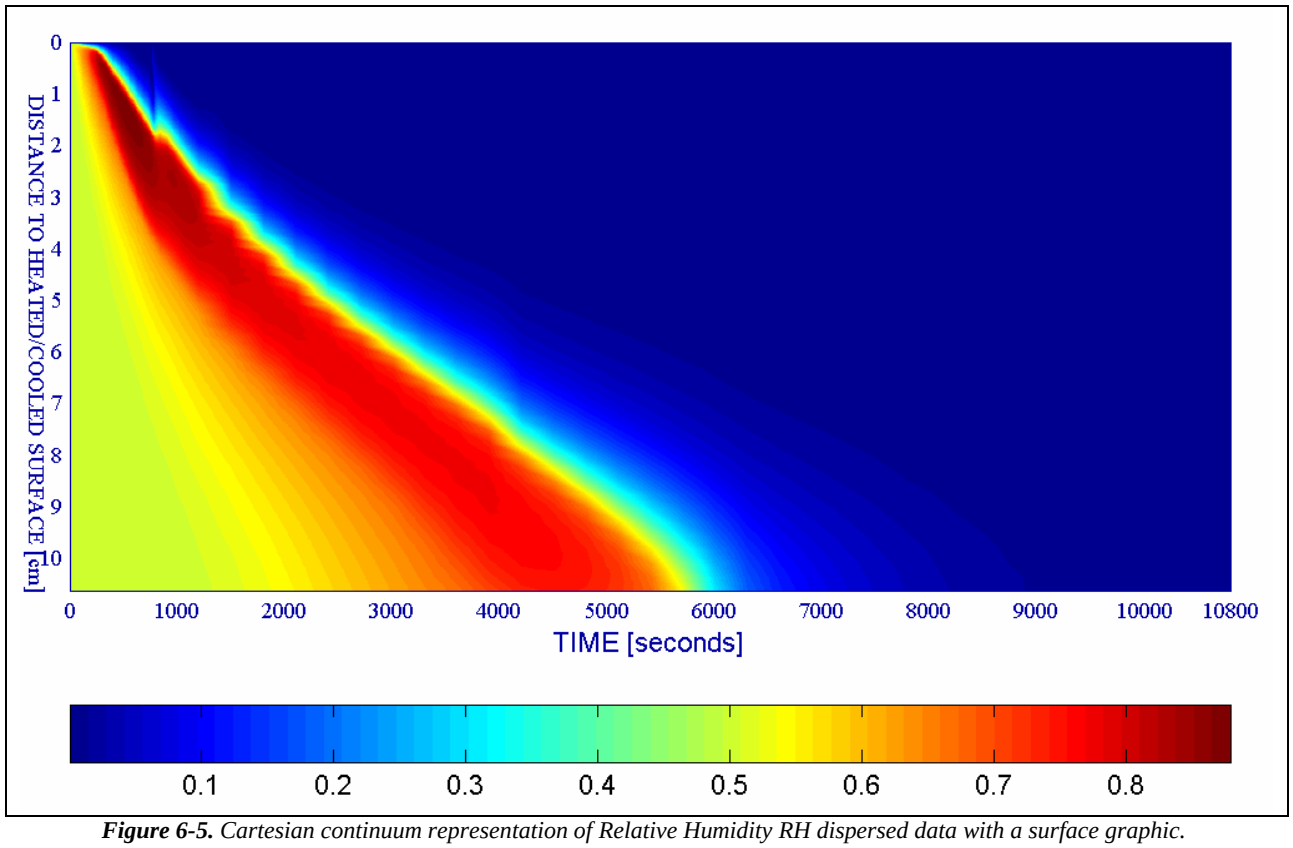

Figure 6-5. *Cartesian continuum representation of Relative Humidity RH dispersed data with a surface graphic.*

6.3 DEFINITION AND METHODOLOGY TO DEVELOP THE SUPPLY OF INFORMATION NEEDED FOR THE ANALYSIS OF THE INFLUENCE ON COOLING OF PARAMETERS NOT RELATED TO COOLING PROCESSES

In this paragraph it is explained the methodology to develop the supply of information needed for the analysis of the influence on the hygro-thermo-chemo-mechanical behaviour of the structural element during the cooling processes of several parameters non-related to the own cooling processes – such as the initial moisture content of concrete, its intrinsic permeability, the rate of temperature increase (fire intensity), the porosity, compressive strength, type of aggregate and, in general, the whole set of hygro-thermo-chemical properties of concrete –. The intention is to provide an atlas of information that enables the generation of an extension of the Spalling Nomograms initially obtained just for heating processes and previously described on Chapter 4.

The values adopted for each of the ranging parameters considered in this atlas, must be combined with all of the others. The whole set of the forty five resulting combinations of the parameters' values initially considered is described in Table 6-6. For a better and faster understanding and identification of the values characterizing each combination, the type of notation used to describe each of these forty five combinations is the following one:

TH**K***RH**PAR*C**, where,

TH** indicates the value of the thickness of the model (in cm) used in the computation – Parameter 3 –

K*** indicates the value of the intrinsic permeability (in m^2) – Parameter 2 –,

RH** indicates the value of the initial saturation degree (in %) – Parameter 1 –,

PAR* indicates the parametric heating curve taken into account in the computation, – Parameter 4 – explained in next paragraphs in detail.

C** indicates the material considered in the computation – Parameter 5 –.

Hence, for example, the combination TH12K018RH50PAR1C60 stands for a case characterised by a *thickness*=12 cm, $k=10^{-18}$ m^2, S_{init}*=50%, Parametric curve*=ISO Curve (Par1) and C60 material.

In some of the reference cases, several cooling start instants have been chosen in order to develop, in paragraph 6.5.3, an analysis of the influence of the cooling start instant on the phenomena occurred during cooling. The explanation of the selection of the cooling start instants and rates of cooling is included on paragraph 6.4.3.2. The set of represented results for each case is constituted by four Cartesian continuum representations of the following parameters, chosen as those more representative of the thermal spalling risk (what represents a total amount of 180 graphics introduced in paragraph 6.5.4 and included in Appendix 6A):

Spalling Index I_{s4}

Mechanical Damage *d*

General Velocity of Spalled-Off pieces *v*

Velocity affected by Mechanical Damage '$v \cdot d$ *criterion*'

It is remarkable that in all of these 180 graphics only the time interval corresponding to the First Surface Cooling simulated is represented, in order to achieve a higher level of detail in the representation. Conclusions arisen from this set of results are included in Appendix 6A and will enable discerning, as an extended task out of the scope of this Thesis and proposed for future research works, whether the initial values of the considered parameters have a significant influence on the hygro-thermo-chemo-mechanical phenomena occurred during cooling processes.

COOLING START TIME [s]	COOLING TYPE	COOLING SUBTYPE	CODE	Combination	PC1 (RH) [%]			PC2 (K) [m^2]			PC3 (TH) [cm]	PC4 (Heating curve)			PC5 (Mat)	
					40	50	60	10^{-19}	10^{-18}	10^{-17}	12	PAR1	PAR2	PAR4	C60	C90
600	SURF	FIRST COOL	1SFC	TH12K017RH40PAR1C60	X					X	X	X			X	
600	SURF	FIRST COOL	2SFC	TH12K018RH40PAR1C60	X				X		X	X			X	
600	SURF	FIRST COOL*	3SFC	TH12K019RH40PAR1C60	X			X			X	X			X	
600	SURF	FIRST COOL	4SFC	TH12K017RH50PAR1C60		X				X	X	X			X	
600	SURF	FIRST COOL	5SFC	TH12K018RH50PAR1C60		X			X		X	X			X	
600	SURF	FIRST COOL	6SFC	TH12K019RH50PAR1C60		X		X			X	X			X	
600	SURF	FIRST COOL	7SFC	TH12K017RH60PAR1C60			X			X	X	X			X	
600	SURF	FIRST COOL	8SFC	TH12K018RH60PAR1C60			X		X		X	X			X	
600	SURF	FIRST COOL*	9SFC	TH12K019RH60PAR1C60			X	X			X	X			X	
3360	SURF	FIRST COOL	10SFC	TH12K017RH40PAR2C60	X					X	X		X		X	
3360	SURF	FIRST COOL	11SFC	TH12K018RH40PAR2C60	X				X		X		X		X	
3360	SURF	FIRST COOL	12SFC	TH12K019RH40PAR2C60	X			X			X		X		X	
3360	SURF	FIRST COOL	13SFC	TH12K017RH50PAR2C60		X			X		X		X		X	
1800	SURF	FIRST COOL	14SFC	TH12K018RH50PAR2C60		X			X		X		X		X	
2400	SURF	FIRST COOL (10K/s)	14SFC	TH12K018RH50PAR2C60		X			X		X		X		X	
2400	SURF	FIRST COOL (15K/s)	14SFC	TH12K018RH50PAR2C60		X			X		X		X		X	
3000	SURF	FIRST COOL	14SFC	TH12K018RH50PAR2C60		X			X		X		X		X	
3360	SURF	FIRST COOL	14SFC	TH12K018RH50PAR2C60		X			X		X		X		X	
1260	SURF	FIRST COOL	15SFC	TH12K019RH50PAR2C60		X		X			X		X		X	
3360	SURF	FIRST COOL	15SFC	TH12K019RH50PAR2C60		X		X			X		X		X	
3360	SURF	FIRST COOL	16SFC	TH12K017RH60PAR2C60			X			X	X		X		X	
3360	SURF	FIRST COOL	17SFC	TH12K018RH60PAR2C60			X		X		X		X		X	
3360	SURF	FIRST COOL	18SFC	TH12K019RH60PAR2C60			X	X			X		X		X	
600	SURF	FIRST COOL	37SFC	TH12K017RH40PAR1C90	X					X	X	X				X
600	SURF	FIRST COOL	38SFC	TH12K018RH40PAR1C90	X				X		X	X				X
600	SURF	FIRST COOL	39SFC	TH12K019RH40PAR1C90	X			X			X	X				X
600	SURF	FIRST COOL	40SFC	TH12K017RH50PAR1C90		X				X	X	X				X
600	SURF	FIRST COOL	41SFC	TH12K018RH50PAR1C90		X			X		X	X				X
600	SURF	FIRST COOL*	42SFC	TH12K019RH50PAR1C90		X		X			X	X				X
600	SURF	FIRST COOL	43SFC	TH12K017RH60PAR1C90			X			X	X	X				X
600	SURF	FIRST COOL	44SFC	TH12K018RH60PAR1C90			X		X		X	X				X
600	SURF	FIRST COOL	45SFC	TH12K019RH60PAR1C90			X	X			X	X				X
3360	SURF	FIRST COOL	46SFC	TH12K017RH40PAR2C90	X					X	X		X			X
3360	SURF	FIRST COOL	47SFC	TH12K018RH40PAR2C90	X				X		X		X			X
3360	SURF	FIRST COOL	48SFC	TH12K019RH40PAR2C90	X			X			X		X			X
3360	SURF	FIRST COOL	49SFC	TH12K017RH50PAR2C90		X				X	X		X			X
1800	SURF	FIRST COOL	50SFC	TH12K018RH50PAR2C90		X			X		X		X			X

Remark 1: See the details about cooling process definition in the paragraph corresponding to each case.

Table 6-6. *Forty five resulting combinations of the parameters' values initially considered.*

(continued)

COOLING START TIME [s]	COOLING TYPE	COOLING SUBTYPE	CODE	Combination	PC1 (RH) [%]			PC2 (K) [m²]			PC3 (TH) [cm]	PC4 (Heating curve)			PC5 (Mat)	
					40	50	60	10^{-19}	10^{-18}	10^{-17}	12	PAR1	PAR2	PAR4	C60	C90
3360	SURF	FIRST COOL	50SFC	TH12K018RH50PAR2C90		X			X		X		X			X
1260	SURF	FIRST COOL	51SFC	TH12K019RH50PAR2C90		X		X			X		X			X
1560	SURF	FIRST COOL	51SFC	TH12K019RH50PAR2C90		X		X			X		X			X
3360	SURF	FIRST COOL	51SFC	TH12K019RH50PAR2C90		X		X			X		X			X
3360	SURF	FIRST COOL	52SFC	TH12K017RH60PAR2C90			X			X	X		X			X
3360	SURF	FIRST COOL	53SFC	TH12K018RH60PAR2C90			X		X		X		X			X
3360	SURF	FIRST COOL	54SFC	TH12K019RH60PAR2C90			X	X			X		X			X
4800	SURF	FIRST COOL	100SFC	TH12K019RH50PAR3C90		X		X			X			X		X

Remark 1: See the details about cooling process definition in the paragraph corresponding to each case.

Table 6-6 (continued). *Forty five resulting combinations of the parameters' values initially considered.*

6.4 DEFINITION OF THE ANALYSIS CASE

6.4.1 Description of the general features of the analysis case and causes for its selection

The structural element selected for the analyses developed in this chapter is analogous to that considered in *Chapter 4 – Spalling Nomograms*, since it was as more versatile as possible in order to achieve results applicable to most of the High Strength Concrete structural elements usually found in High-Rise Buildings. Its complete typological description is included in paragraph 4.3 and not repeated herein except for the slight differences introduced because of the especial features of the phenomena occurred during cooling processes.

Hence the selected numerical model, representing a slice of any High Strength Concrete structural element which may work in plain strain conditions and under one-dimensional fluxes of both heat and mass, is featured by the general layout shown on next figures, corresponding to a situation where the structural element is exposed to fire at only one face:

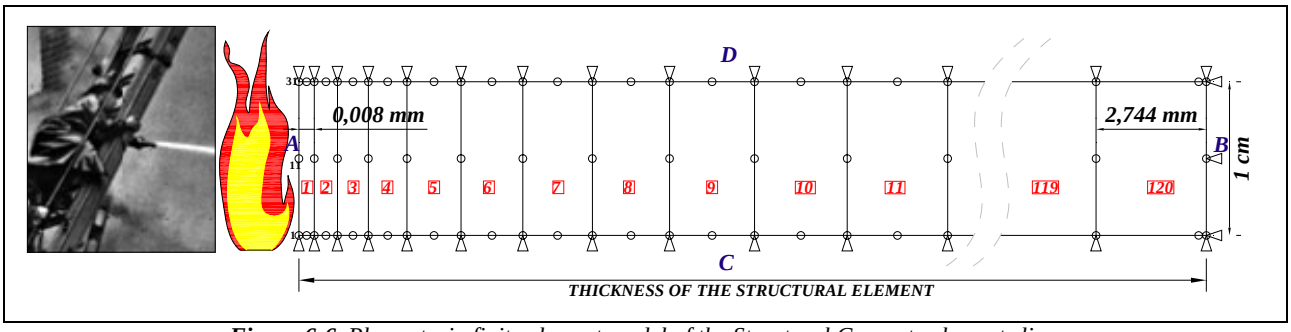

Figure 6-6. *Plane strain finite element model of the Structural Concrete element slice.*

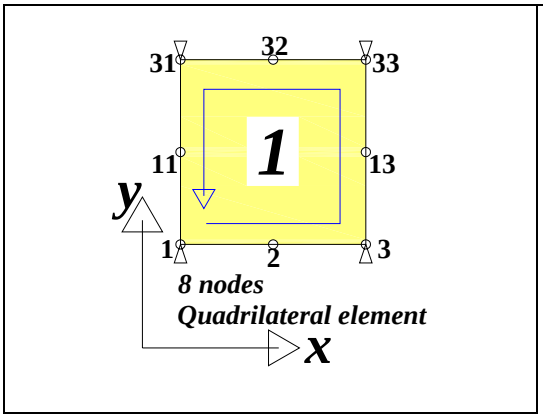

Figure 6-7. *Finite Element detail.*

Side	Variables	Values and coefficients
A	p^g	p^g = 101.325 Pa
	p^c	p^v = 1.300 Pa, β_c = 0,02 m/s
	T: convective	T = See Parameter 4 in paragraph 4.2.3.4
	T: radiative	$e\sigma_0 = 5{,}1 \times 10^{-8}$ W m^{-2} K^{-1}
B	u_x	$u_x = 0$
	p^g	p^g = 101.325 Pa
	p^c	Environm. Relative Humidity=50%, β_c=0,005m/s
	T : convective	Constant environment temperature: 298,15K
C,D	u_y	$u_y = 0$

Table 6-7. *Boundary conditions used in the numerical simulation.*

The general features and the mesh needed for the numerical simulation of the analysis case described herein have been modified because of the extremely sharp gradients of the state variables in the zone close to the heated and cooled surface, especially during the cooling processes. Hence, mesh is concentrated in the layers close to the heated/cooled surface while it is widened in the opposite face. It is remarkable that, although the aspect ratio of the finite elements close to the heated/cooled surface is quite large, the trials developed have ensured that this potential distortion does not introduce an impoverishment of solutions' quality because the problem solved is essentially unidirectional. Consequently, a model with a total number of 120 eight-nodes quadrilateral elements, with 40 degrees of freedom ($p_{g,i}$, $p_{c,i}$, T_i, $u_{x,i}$ and $u_{y,i}$ for each of the eight nodes) and a 3x3 order of integration, a total number of 603 nodes, and the boundary conditions exposed next has been implemented and calculated for each of the analyzed cases.

Related to the boundary conditions imposed, as it was explained in Chapter 4 the Cauchy's type boundary conditions (mixed radiative-convective) described on table 4-2 represent, in the case of the heated/cooled face, a constant in time value of the environment water vapour pressure – equal to 1.300 Pa –. This means that initially, at ambient temperature, the air relative humidity is around the 50 %, decreasing this value with time as the environment temperature increases (and vice versa if the environment temperature decreased). This type of condition is much more real, during the development of a natural fire, than keeping constant the relative humidity of the environment because during the fire evolution water vapour will be produced and eliminated. On the contrary on the opposite face, face B, the relative humidity value is fixed constant at a 50% during all the simulation because it is not expectable that it might vary significantly. In both cases, a constant gas pressure value equal to the atmospheric pressure has been considered.

The heating and cooling profiles applied to face A are one of the ranging parameters (Parameter 4) taken into account for the calculations developed in this chapter. Their definition is extensively described on paragraphs 4.3.2.4 (for heating profiles) and 6.4.3.2 (for cooling profiles) and they are always related to the evolution of the environment temperature (during heating) and both to the environment and the surface temperature (during cooling, depending on each type of cooling). The heat exchange coefficients are derived from prestigious bibliography [27] taking into account the physics and phenomena occurring at each of the environments.

Since the structural element dealt in these analyses may appear in different positions (vertical / horizontal) and distances to the flames, the following average values of the heat exchange coefficients have been selected:

- For the Heated/Cooled Environment – Surface A exchange:

  α_c = 20 W/m^2·K, since forced convection is expected,
  During heating, emissivity coefficient is equal to 0,85,
  During cooling, only convection (no radiation) is considered since it is expectable that the environment water vapour from nozzles water jet prevents radiation from the remaining fire to the surface.

- For the Constant Ambient Temperature Environment – Surface A exchange:

  α_c = 5 W/m^2·K, since natural (not forced) convection is expected,
  Only convection (no radiation) is considered since fire is already extinguished,

- For the non-Heated/Cooled Environment – Surface B exchange:

  α_c = 5 W/m^2·K, since natural convection is expected.

Finally, the mass exchange coefficients β_c between the environment and each surface are convective-type exchanges and have been taken as a thousandth of each heat exchange coefficients α_c, appearing their values on Table 4-2 of *Chapter 4 – Spalling Nomograms*.

According to the different stages of each heating/cooling curve defined by Parameter 4, curves that are shown on paragraph 6.4.3., simulations have been divided into several stages described by different time steps and frequency of results recording. The most common are the following ones, although in some cases time step has been reduced to reduce the computational time needed to achieve numerical convergence:

Type of process	**Time step (s)**	**Frequency of results record** (in seconds)
Environment Heating	From 1 to 3	120
Environment Cooling	From 1 to 12	From 30 to 600
Surface Cooling	From 0,01 to 0,1	From 6 to 10

Table 6-8. *Time step main features of each simulation stages.*

6.4.2 Description of the material selected

6.4.2.1 MATERIAL DESCRIPTION AND CAUSES FOR ITS SELECTION

For the analysis developed in this chapter, the materials selected (namely C60 and C90) are analogous to those extendedly described in paragraph 4.3.2.5 of *Chapter 4 – Spalling Nomograms*. As it was explained in that paragraph, the consideration of all of the physical-chemical processes that take place in High-Strength Concretes during heating and cooling processes within a numerical model needs the previous definition of a sophisticated set of thermal, chemical and mechanical properties of concrete (beyond those needed for the suitable characterization of water in both liquid and gas phases), extremely complicated to find in literature from existing experimental tests, properties that are enounced next:

- Cubic thermal expansion coefficient of solid β_s,
- Skeleton density ρ_s,
- Young's modulus E_c for compression,
- Young's modulus E_t for tension,
- Compressive strength f_c,
- Tensile strength f_t,
- Poisson's ratio ν,
- Characteristic length l,
- Degree of saturation S (isotherms of desorption),
- Stechiometric factor,
- Porosity ϕ,
- Intrinsic permeability,
- Thermal conductivity of dry concrete λ_{dry}, and
- Specific apparent heat C_{ps}

Furthermore these are not constant values but varying with temperature, so their temperature evolution is also needed. On paragraphs 4.3.2.5.2 and 4.3.2.5.3 of *Chapter 4 – Spalling Nomograms* are shown the values adopted in the available literature for two of the materials more widely used in High-Rise Buildings (see table 4-7) being, respectively, a High-Strength Concrete named C60 with a compressive strength of about 60 MPa at 20 ºC and a Very-High-Strength Concrete named C90 with a compressive strength above 80 MPa at ambient temperature. Although the values adopted for each of the material properties are analogous to those used in *Chapter 4 – Spalling Nomograms*, on next paragraph is introduced a correction necessary to simulate correctly the evolution of these properties during cooling processes, correction that we will call *Irreversible Definition of Material Properties during Cooling Processes*, and that constitutes one of the parallel minor contributions of this Chapter.

6.4.2.2 IRREVERSIBLE DEFINITION OF MATERIAL PROPERTIES FOR COOLING PROCESSES

Some of the material properties whose definition is necessary to accomplish the hygro-thermo-chemo mechanical calculations developed herein do not show a 'reversible' trend when temperature cycles are applied to structural elements. These properties, that will be enounced next, increase with temperature but do not decrease at all when temperature diminishes again.

Concrete Property	**Property Behaviour with Temperature**
Cubic thermal expansion coefficient of solid β_s	*A constant value equal to mean slope is assumed in this Thesis for all temperatures [2].*
Skeleton density ρ_s	*Heat treatment induces a mass loss (which results in a decrease in density) as well as a slight shrinkage during dehydration (which results in a slight increase in density). In fact the density of dry material is almost constant between 105ºC and 600 ºC so it is considered Irreversible with temperature.*
Young's modulus E_c for compression	*All of these mechanical properties are considered Reversible with temperature within the hygro-thermo-chemo-mechanical calculations developed herein. However, at any postprocessing calculation their residual value is taken into account according to what was exposed on paragraph 6.2.2.4. For example, in the Spalling Index I_{s4} calculation it is considered according to [3] a reduction in the tensile strength of about a 5 to 15 per cent after a cycle of temperature above 250 ºC, what it is caused probably by the reabsorption of environment humidity during cooling (see paragraph 6.5.2.6.2).*
Young's modulus E_t for tension	
Compressive strength f_c	
Tensile strength f_t	
Poisson's ratio ν	*A constant value equal to mean slope is assumed in this Thesis for all temperatures, due to the lack of further available experimental data during cooling [2].*
Characteristic length l	*A constant value equal is assumed for all temperatures [2].*
Degree of saturation S (isotherms of desorption)	*Sorption isotherms might be different from desorption isotherms due to hysteretic effects. However, the experimental definition of Sorption isotherms for cooling processes necessarily fall out of the scope of this Thesis, so hysteretic effects will be neglected herein. The study of sorption isotherms will be proposed as a task to accomplish in future research tasks.*
Stechiometric factor	*A constant value equal is assumed for all temperatures [2].*
Porosity ϕ	*Irreversible with temperature. Once the maximum temperature is reached it does not decrease again.*
Intrinsic permeability	*Reversible with temperature. However, it is affected by damage values so it will not show the same value at the same temperature during the heating and cooling processes.*
Thermal conductivity of dry concrete λ_{dry}	*Irreversible with temperature. Once the maximum temperature is reached it does not increase again*
Specific apparent heat C_{ps}	*Irreversible with temperature. Once the maximum temperature is reached it does not increase again*

Table 6-9. *Behaviour of Material Properties with Temperature cycles.*

6.4.3 Definition of Temperature Profiles

6.4.3.1 HEATING PROFILES

As it was explained on *Chapter 4 – Spalling Nomograms*, paragraph 4.3.2.4, as the temperature evolution in a High Strength Concrete element has an essential influence on the thermal spalling risk [24] the heating profiles selected for the calculations development need to be chosen covering the complete range of possible realistic fires that may arise in High-Rise Buildings rooms and/or offices.

Therefore, the adopted heating profiles are obtained, analogously to what is done in *Chapter 4*, from the time-temperature parametric curves defined in the Eurocode 1, Part 1-2 [28], since this is an European regulation widely spread and prestigious document where parametric curves have been defined on an experimental bases, definition that is described on paragraph 4.3.2.4.1 and applied next:

6.4.3.1.1 Value 1 (PAR1): ISO834

The first value to adopt results from applying to the equation used in Eurocode 1, Part 1-2 [28] to define parametric curves in heating stage,

$$\Theta_g = 20 + 1.325 \cdot (1 - 0{,}324 \cdot e^{-0{,}2 \cdot t^*} - 0{,}204 \cdot e^{-1{,}7 \cdot t^*} - 0{,}472 \cdot e^{-19 \cdot t^*}) \quad (6.7)$$

a value of $\Gamma = [O/b]^2 / (0{,}04 / 1.160)^2 = 1$ (where $t^* = t \cdot \Gamma$) which in this case represents an opening coefficient of about $O = 0{,}07\ m^{1/2}$ (see paragraph 4.3.2.4.2.1 for more details).

In such a way, the curve obtained matches the normalized time-temperature curve (ISO 834) defined in the regulation project prEN 13501-2 to represent a fire model completely developed in a fire sector. This selection has many advantages since this curve is widely spread and adopted to classify or to verify the fire resistance, both from the experimental and from the analytical points of view, so it enables an easier comparison of the results obtained with any source of comparable experimental results.

This curve represents a set of heating conditions more severe than most of the conditions that may appear during a natural fire in a High-Rise building. Its final form is the following:

PARAMETER 4 ***Heating profile PAR1***	***VALUE 1*** (Θ_g [ºC] ,t [min])
	$\Theta_g = 20 + 345 \cdot \log_{10}(8 \cdot t + 1)$

Table 6-10. *First Value selected for the Heating profile.*

6.4.3.1.2 Value 2 (PAR2): Slow Heating Curve with the lowest Opening Coefficient

The second value to adopt results from applying to the equation used in Eurocode 1, Part 1-2 [28] to define parametric curves in heating stage,

$$\Theta_g = 20 + 1.325 \cdot (1 - 0{,}324 \cdot e^{-0{,}2 \cdot t^*} - 0{,}204 \cdot e^{-1{,}7 \cdot t^*} - 0{,}472 \cdot e^{-19 \cdot t^*}) \quad (6.8)$$

the lowest value of the opening coefficient allowed in the Eurocode $O = 0{,}02\ m^{1/2}$ (and the rest of common values described on paragraph 4.3.2.4.1).

In such a way, the curve obtained is one of the slowest and less severe curves that may be obtained from the family of heating curves defined by parametric curves. It clearly represents a slow development fire that reaches its maximum temperature at a total time of three hours, time that is being considered as a maximum within the heating stage of simulations.

This curve represents a set of heating conditions less severe than most of the conditions that may appear during a natural fire in a High-Rise building. Its final form is the following:

PARAMETER 4 ***Heating profile PAR2***	***VALUE 2*** (Θ_g [ºC] ,t [h])
	$\Theta_g = 20+1.325\cdot(1-0{,}324\cdot e^{-0{,}0152\cdot t}-0{,}204\cdot e^{-0{,}1292\cdot t}-0{,}472\cdot e^{-1{,}444\cdot t})$

Table 6-11. *Second Value selected for the Heating profile.*

6.4.3.1.3 Value 3 (PAR4): Extremely Slow Heating Curve with an Opening Coefficient under the lowest admitted by Eurocode 1, Part 1-2

This heating profile is selected for a single trial (combination with Code #100) to analyze if conclusions obtained for Values 1 and 2 of the Heating profiles are also applicable to fires with a extremely low development. To achieve quite a slow heating profile, an opening coefficient below the minimum permitted in Eurocode 1, Part 1-2 [28] is used (O = 0,013 $m^{1/2}$), matching this heating profile with the one used in *Chapter 5 – Preliminary and Simplified Analysis of Cooling Effect on HSCs Spalling Behaviour* (paragraph 5.2.1 for more details)

PARAMETER 4 ***Heating profile PAR4***	***VALUE 3*** (Θ_g [ºC] ,t [h])
	$\Theta_g = 20+1.325\cdot(1-0{,}324\cdot e^{-0{,}0077\cdot t}-0{,}204\cdot e^{-0{,}06545\cdot t}-0{,}472\cdot e^{-0{,}7315\cdot t})$

Table 6-12. *Third Value selected for the Heating profile.*

while the heat exchange coefficient is selected, within the reasonable range of values for natural convection on air [5-20] W/m^{2}K, matching that corresponding to the average value considered in the simulations reported in *Chapter 5*, this is 7,6 W/m^{2}K (lower than the value of 20 W/m^{2}K selected for the rest of the cases in order to obtain an even slower heating profile).

6.4.3.1.4 Collection of the Heating Profiles selected

Finally, in figure 6-8 if we compare the three heating profiles selected against the whole range of possible parametric curves obtainable from Eurocode 1, Part 1-2 [28], it is observed that the only heating profiles outside the range of analysis are extremely fast heating ones. This is due, as it was explained on Chapter 4 – Spalling Nomograms, to the numerical difficulties arisen when considering very fast heating profiles such as Hydrocarbon Fire Curve:

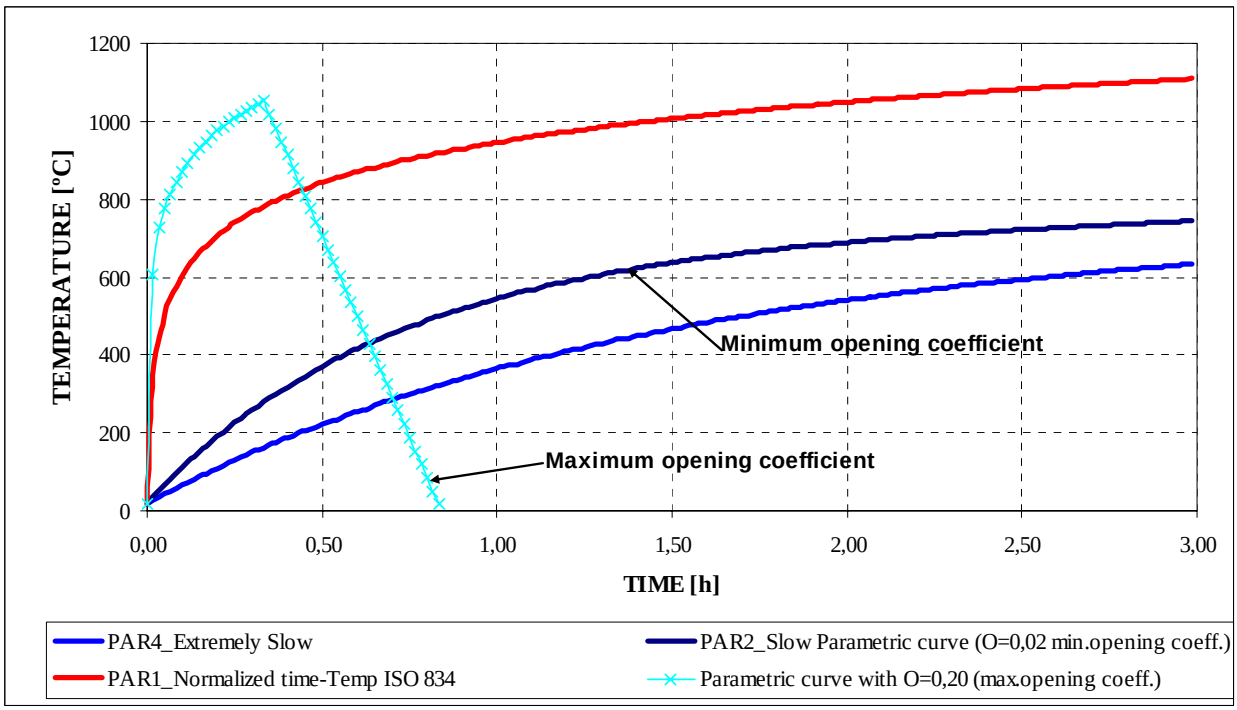

Figure 6-8. *Comparison of the possible heating profiles and the range defined by the selected curves PAR1, PAR2 and PAR4.*

6.4.3.2 COOLING PROFILES

6.4.3.2.1 Compartmental Fire Attack Techniques

6.4.3.2.1.1 Mechanisms of Fire Extinction

There are three methods of fire extinction depending on the nature of the attacked medium [29]:

Fuel Cooling: Consists on the cooling of the combustible solid fuel surface, which reduces the rate of pyrolysis and thus the supply rate of fuel to the flame zone. This reduces the rate of heat release by the fire; consequently the thermal feedback from the flame is also reduced and this increases the primary cooling effect of the suppression agent. The application of a water spray to the fuel bed is typical of this method although a straight-stream, or smoothbore attack, may be equally effective, if not more so.

Flame Cooling: Consists on the cooling of the flame zone directly; this reduces the concentration of free radicals (in particular the chain-branching initiators of the combustion reaction). Some proportion of the heat of reaction is taken up by heating an inert substance (such as water) and therefore less thermal energy is available to continue the chemical break-up of compounds in the vicinity of the reaction zone. One function of the latest water mist technology is to act in this manner; the fine droplets providing a very large surface area per unit mass of spray in order to increase the rate of heat transfer;

Flame Inerting: Consists on inerting the air feeding the flame by reducing the oxygen partial pressure by the addition of an inert gas (e.g. N_2, CO_2, vapour). This is equivalent to the removal of the oxidizer supply to the flame by the production of water vapour and is the dominant mechanism by which the Layman/Royer/Nelson concepts of indirect water fog attack achieve suppression. In a discussion of fixed system water-mist fire extinction mechanisms [30] added to the above three mechanisms some further effects associated with decreasing thermal radiation, dilution of the flammable vapour/air mixture, and chemical inhibition as playing a part in fire suppression.

6.4.3.2.1.2 Two Types of Structural Enclosure Fires

A compartment or enclosure fire involves a room or space within the confines of a structure. A fire involving two, or several, rooms/spaces is said to be a multi-compartment/enclosure fire. A fire that has developed beyond the definitions of compartmental, where elements of the structure have been breached and have become involved in fire, is said to be ‘structural’. Based upon the above mechanisms of fire extinction, there are two basic types of combustion that the fire-fighter may face in almost every compartment/structure fire, namely:

Fuel-Phase Fire: Two-dimensional fuel bed or surface fire (m^2)

Gaseous-Phase Fire: Three-dimensional gaseous-phase fire (m^3)

Gaseous-phase combustion may exist in several forms. It may begin with sporadic tongues of flame that detach themselves from the main fire plume as fire reaches the ceiling. These tongues of flame will snake eerily across the ceiling as pockets of accumulating fire gases surpass the lower flammable limit (*LFL*) burning in a lean state. These tongues of fire precede *rollover*, which occurs as the concentration of fire gases builds to create extensive flaming in the overhead. The effect of rollover is to radiate heat downward to other fuel surfaces in the compartment, causing them to pyrolize and add more fire gases into the space. These may ignite briefly in small but spectacular fire-balls about 2-3 feet from the floor or progress to a full compartmental flashover where the air appears to be burning throughout all spaces in the room. In other instances, the fire may be ventilation-restricted and smoulder in a state of extremely slow development. This incomplete combustion may cause high concentrations of fuel-rich gases

to accumulate within a compartment. There may be some ghosting flames that appear briefly in the lower portions of the room but fail to progress due to insufficient oxygen (oscillatory combustion). The creation of an opening to the room may allow air to join with the gases and ignition may occur in the region where they mix, along the level where the neutral plane or smoke interface exists. Such an ignition may rapidly lead to a full compartmental backdraft.

There is another situation (Fire Gas Ignition) where fire gases may ignite while in their ideal state of mix, accumulating in levels above the *LFL* but below the UFL. This generally causes what is termed *premixed gaseous combustion* – a very severe form of extreme fire behaviour that should be countered or dealt with as a primary action.

6.4.3.2.1.3 Methods of Fire Suppression Using Water

There are three methods of fire suppression using water that may be applied to deal with the above two types of fire:

Direct Attack: The traditional approach that deals with the majority of fires. This method relies on a stream of water to cool the fuel-surfaces involved in fire when applied directly onto them where accessible.

Indirect Attack: A method of applying water fog onto super-heated surfaces in the fire compartment to create a mass of steam that displaces the oxygen to smother the fire. This approach, based upon the principles of Lloyd Layman and commonly known as the *Iowa* or *Royer/Nelson* method, is normally applied from an exterior position. When applied under strict protocols this method is extremely effective in certain situations and may deal with combustion in both the fuel and gaseous-phases.

3D (three-dimensional) 'Offensive' Water Fog: A method introduced by Swedish fire-fighters during the early 1980s [31] using controlled nozzle pulsing actions or brief bursts of water fog to counter combustion in the gaseous-phase (offensively). This approach may also be used (defensively) to prevent/mitigate the effects of flashovers, backdrafts, or other ignitions of the fire gases. The term 3D refers to the volumetric mechanisms of combustion in the gaseous-phase and associated water applications are normally calculated in cubic dimensions (lpm/m^3).

No single method of suppression is able to deal with combustion existing both in the fuel and gaseous-phases of fire development with optimum effects. An ideal attack on a compartment fire may alternate [29] between a 3D offensive application of water fog to tackle the gaseous combustion and a direct straight stream attack to deal with the fuel-phase fire.

Mechanism of Extinction	Method of Suppression	Estimated Percentage of Use
Fuel Cooling	Direct Attack	95 Percent Structure Fires
Flame Cooling	3D Offensive Attack	40 Percent Structure Fires
Flame Inerting *	3D Offensive Action	85 Percent Structure Fires
Flame Inerting *	Indirect Attack	5 Percent Structure Fires

Table 6-13. *Mechanisms of fire extinction, methods of fire suppression and estimated percentages of use for each suppression tactic at UK structure fires [29]*

6.4.3.2.1.4 Water Spray, Fog or Mist

The use of fine water droplets for gaseous phase fire suppression has been studied for at least fifty years. There is a need for consistent terminology when discussing firefighting sprays, especially when considering the characteristic 'size' of the droplets. Average sizes of droplets that appear of most interest in firefighting terms (hand-held attack hose-lines) fall within the range of 100-1000 microns (0.1-1.0 mm). A spectrum of drop sizes classes them into five categories:

Colloidal	Below 1 micron – appears as smoke
Dust	Between 1-10 microns – appears as oil or sea fog
Fine	Between 10-100 microns – appears as clouds or mist
Average	Between 100-1000 microns – appears as drizzle or rain
Coarse	Between 1000-10000 microns – appears as coarse heavy droplets

Table 6-14. *A spectrum of water droplet sizes*

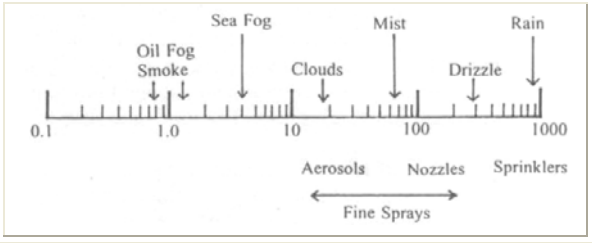

Figure 6-9. *Spectrum of drop diameters [32]*

In firefighting terms the size of an individual droplet, or some mean drop size within a spray is of great importance when discussing other attributes of the spray. The resistance offered by the surrounding air to the forward motion of the droplets is proportional to the droplet diameter. Therefore, the carrying power, or penetration, of the spray is strongly dependant upon the drop size distribution. The efficiency of heat transfer to water droplets, which is fundamental to their use in firefighting applications, is also dependant on droplet geometry and in particular the ratio of the total surface area of the spray to its volume. Maximizing this ratio is beneficial in promoting rapid absorption of heat from the environment and subsequent evaporation of the droplet. The practical penetration achieved by a particular spray is governed by the relative magnitudes of the kinetic energy of the initial liquid and the degree of aerodynamic resistance offered by the surrounding gas. All other things being equal, the penetration of a spray is much greater than for an individual drop, since the leading droplets impart forward momentum to the surrounding gas, reducing the air drag on the following drops and thus creating a 'pathway' for them, resulting in better overall penetration. There is a growing body of contemporary research concerned with the interaction between water droplets and buoyant fire plumes. This literature suggests there may exist a critical heat release rate above which a given drop size would not contribute to fire extinction due to its failure in reaching the relevant cooling zone.

The Annual Building Fire Research Laboratory (BFRL) Conference on Fire Research in 1998 produced an interesting (NIST) paper [33] that investigated the Mitigation of Compartment Jet Fires Using Water Sprays. The main objective of the study was to investigate the interaction of water-sprays with a burning gas layer at the ceiling in a ventilation controlled state, and close attention was paid to the effectiveness of different spray angles, droplet diameters, stream velocities and water flow-rates. Although the directions of sprays were downward, from the ceiling in this study, the mechanisms associated with flame cooling were of direct relevance to 3D applications by fire-fighters. It was generally observed that water applications into the gas layers using different spray angles of 30, 60, 75, 90, 120, 135 and 150 degrees produced varying reductions in compartmental temperatures but spray cones within the 60-75 degree range were found to be most effective in reducing the overall temperature. For these angles the limiting behaviour due to the effectiveness in penetrating the flame indicated that spray velocities in excess of 18 m/s (40 mph) should be used. The mean droplet diameters of 100 to 600 microns were analysed and it was further noted that droplets within the 300-micron (0,3 mm) range maximized any cooling effects within the compartment. In terms of flow-rate it was reported that, for these compartmental dimensions of 115 m^2 the 'most efficient' flow-rate (for gaseous-phase suppression) was around 113 lpm where 0.3 mm droplets formed the main bulk of the spray pattern. This equates close to 1 l/m^2 and correlates closely with the critical flow-rate (CFR) recorded in [34] (see figure 6-10).

Other authors [35] further attempted to estimate the heat transfer between flames and water sprays and produced a plot of convective heat transfer rate against drop velocity for drop sizes ranging from 50 microns to 2mm whilst assuming a flame temperature of 1.000 ºC. In general, higher velocities and smaller droplet diameters were found to increase the heat transfer rates. For

example, a 2mm droplet at 0,07m/s (terminal velocity in still air) produced a heat transfer rate of 167 kW/m^2 while the same droplet travelling at 2 m/s achieved a value of 293 kW/m^2. For a 50-micron drop at velocities of 0,01 m/s and 0,5 m/s the corresponding heat transfer rates were 1,7 MW/m^2 and 2,5 MW/m^2 respectively. It is this high-velocity application of fine water droplets that make HP hose-reel systems of 25 mm diameter so effective in the gaseous-phase. An estimation of droplet penetration was also studied in the research and it was noted that drops of larger initial size were able to penetrate further into the flame before complete evaporation occurred.

6.4.3.2.1.5 Dealing with Combustion in the Gaseous-phase

When a water spray pattern passes through the hot gases, heat transfers to the droplets, which then start to evaporate. As explained above, evaporation depends to a great extent on droplet diameter, temperature, and transport properties such as velocity.

- Sprays made up of smaller droplets present a larger surface area in relation to their volume and so heat up and evaporate faster, consequently absorbing more heat. Small droplets will evaporate quickly and will concentrate their suppressive effect on combustion occurring in the gas-phase.
- Large droplets will not entirely evaporate when passing through flames and hot gases, unless the flames are very deep, which usually is not the case in apartment fires. Instead, these droplets will mostly pass through the flames and collide with the burning material, or other superheated surfaces, causing a decrease in pyrolysis.

When water droplets travel through the gaseous-phase of a fire there is much heat and mass transfer between droplet and hot gas. There is also an element of 'drag' upon the droplets that will affect their velocity and trajectory. All these factors affect a droplet's ability to absorb heat from the gases. The fire's plume and convection currents within an enclosure also have a major effect upon the movement of droplets that are too small (below 0,1mm), where they may be simply carried away before they are able to have any great cooling effect.

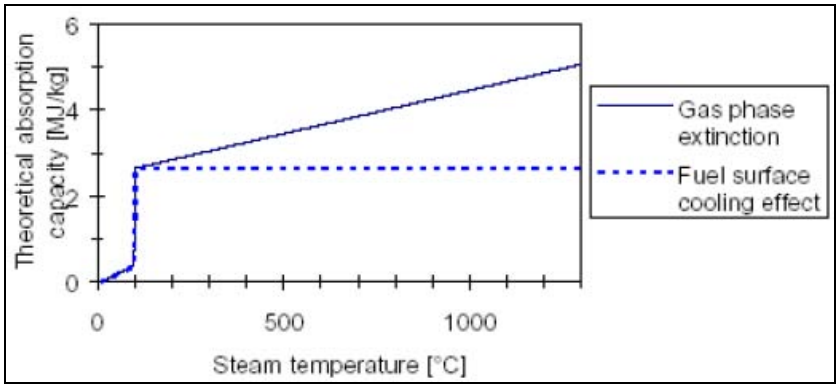

***Figure 6-10**. Theoretical heat absorption capacity of water in the gaseous-phase and on surface cooling..*

A wealth of scientific and empirical research attempts to define the ideal droplet size for use in manually applied firefighting streams. The general consensus is agreed that droplets falling within the mean range of 0,2mm – 0,4mm diameter provide the greatest effect in terms of 3D gaseous-phase cooling, dilution and suppression. The mean droplet diameters found in spray patterns provided by many of the world's combination fog/straight stream firefighting nozzles, when operated at 7 bars NP, generally fall within the 0,4mm – 1,0mm range. As nozzle pressures (NP) and stream velocities are increased the median droplet diameter decreases closer towards the 0,3mm ideal level. Although smaller droplets are undoubtedly more effective in the gaseous-phase, the slightly larger droplets are able to reach and cool boundary and fuel surfaces more effectively, preventing rapid reheating and ignition of fire gas accumulations. One observation

during a range of tests [36]) showed that, when discharged into the gaseous-phase, larger droplets cooled the enclosure walls more effectively:

- 0,3mm droplets cooled boundary wall by 57ºC within two minutes,
- 0,7mm droplets cooled boundary wall by 124ºC within two minutes, and
- 0,8mm droplets cooled boundary wall by 195ºC within two minutes.

This observation demonstrated and confirmed some interesting points:

- More cooling power reached the enclosure boundary when larger droplets were in use,
- More cooling power was utilized in the gaseous-phase when smaller droplets were applied,
- The application of larger droplets causes more evaporation (steam expansion) on the enclosure boundary but less evaporation (and contraction) in the gases. This imbalance is generally undesirable and serves as the root cause of much opposition to water-fog tactics by fire-fighters who have sometimes experienced steam burns from over zealous applications.

The National Research Council (NRC) Canada presented some interesting research data [37] as follows. The performance of the 3D water-fog attack strategy is generally determined by the nozzle characteristics (e.g., droplet size and velocity, spray angle, and flow rate), and application techniques (e.g., discharge angle, and duration of discharge). When using the 3D water fog technique (into the gaseous-phase), the nozzle and application techniques are different from those used in the direct and indirect attack methods. In theory, small droplets are more efficient in cooling and diluting the gases than large droplets, because of the larger total surface area available for evaporation and heat extraction. When the droplet diameter is reduced from 1,0mm (1000μm) to 0,1mm (100μm), the total surface area increases 10 times from 6 m^2 to 60 m^2 for 1 litre of water. However, on occasions, droplets may be so small that they are blown away on the convection currents before they are able to effectively take part in any cooling process.

ΔT [ºC]	100 μm	200 μm	300 μm	500 μm	1.000 μm
200	0,8 s	1,6 s	2,4 s	4,0 s	8,0 s
300	0,533 s	1,06 s	1,6 s	2,66 s	5,33 s
400	0,4 s	0,8 s	1,2 s	2,0 s	4,0 s
600	0,26 s	0,52 s	0,78 s	1,3 s	2,6 s
800	0,2 s	0,4 s	0,6 s	1,0 s	2,0 s
1.000	0,16 s	0,32 s	0,48 s	0,8 s	1,6 s

Table 6-15. *Lifetime (seconds) of water droplets with temperature [37]*

The cooling effectiveness of water spray for hot gases is also determined by the residence times of droplets that are available for absorbing heat from the gas – the longer the residence time, the better the cooling effectiveness of the spray. The residence time of various droplet patterns can be roughly assessed in still air by pulsing a brief burst of water-fog into the air. It can be seen that an effective fog pattern suited to a 3D application will discharge a range of droplets that demonstrate a visible residence time in air of around 4-6 seconds before striking the ground. This will represent the 'typical' fog pattern consisting of a droplet range within the 0,2-0,4mm range (for manually applied firefighting streams). Under fire conditions this actual residence time of droplets is relative to the temperature of the gases and the size of the droplet (Table 6-15). For example, 1,0mm (1000μm) droplets passing through an upper gas layer heated to 600ºC will exist for 2,6 seconds (Table 6-15) before evaporating entirely. In small compartments the larger droplets will reach boundary walls, ceiling and linings, causing excess steam. In larger compartments the smaller droplets evaporate within a few feet of the nozzle and

the effect is lost for the outer reaches of the compartment. Therefore, it is essential to understand the variables of droplet sizing and flow-rate in compartments varying in size up to and beyond $70m^2$.

The amount of water that is in a 'pulse' or 'burst' from a nozzle, applied in 3D fashion, depends upon the flow-rate, how long the flow-control is 'cracked' open and also by how much the flow-valve (ball/slide) is opened. Nozzle pulses, or bursts, may vary between short, medium and long in duration. The briefest pulse of water from a partially opened nozzle may be just half a second long and discharge around 0,2 litres of water into the overhead – that's a cupful of water! A three-second burst from a fully opened nozzle discharging 570lpm flow-rate might place around 28 litres of droplets into the overhead. The variance can clearly be seen. The nozzle operator must be trained to read fire conditions correctly and adjust their applications of 3D water-fog to suit each specific situation, avoiding excessive use of water-fog where necessary.

6.4.3.2.1.6 Fire-Fighting Services: their tactical flow-rates, baseline flows and extinguishing equipment.

Research works into actual flows used at 307 selected fires in non-residential buildings in London [38] suggested that most working fires were extinguished with a 605 lpm flow-rate or less and that 75% of fires did not increase in size following fire department arrival. These studies also revealed that only a very small percentage of structural fires exceeded about 93 m^2, requiring less than 30 fire-fighters to deal with the majority of incidents.

Parameter	Mean	St. dev.	Cases
Time Preheating – Ignition [min]	44,9	118,3	50
Time Ignition – Discover [min]	9,1	15,0	116
Time Discover – Arrival [min]	8,4	13,0	271
Time Arrival – Intervention [min]	2,0	2,8	153
Time Intervention – Spread stopped [min]	7,4	25,1	152
Time Spread stopped – Flames out [min]	13,3	87,8	238
Time Flames out – Fire dead [min]	40,3	203,5	236
Area when first discovered [m^2]	3,2	7,3	269
Area when first f/f arrived [m^2]	10,0	47,3	299
Final area of fire spread [m^2]	24,0	113,4	300

Table 6-16. *The mean and standard deviation of parameters and the number of fires on which they are based from the 307 fire study in London [38]*

A similar study in New Zealand [39] suggested that 87% of 290 working structural fires were extinguished using a flow of 605 lpm or less. Only 3% of structural fires required larger flows in the same study. Some authors [34] suggested that fire departments may use up to 100 times more water than is theoretically required. As large fires are of particular concern in High-Rise Buildings, the correlations x-x and y-y from research data displayed in Figure 6-11 are relevant, where it can be seen that real fire fighting flow-rates at large structure fires in the 1950s and 1960s were in excess of 1.703 lpm in compartments of spaces of 93 m^2.

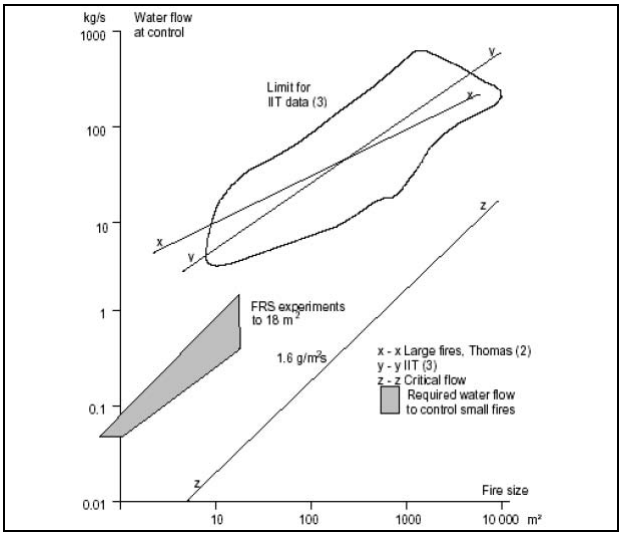

Figure 6-11. *The actual used water flow in relation to the area of the fire is shown. The data are derived from real fires, and taken from reports published in the late 1950's and 1960's. These may not be wholly reliable after forty years [34]*

The mentioned research [34] demonstrated that flow-rates of 113 lpm were unable to control developing compartment fires within a six-minute control criteria and that any such control achieved after this time would have been during the decay-phase of the fires progression. The same research demonstrated a flow-rate of 226 lpm was able to achieve extinction during the growth phase of the fire's development. Many empirical data from different sources suggest that the vast majority of working structural fires are smaller than $100m^2$ and are suppressed with a flow-rate below 600 lpm. Others [29] suggested flow-rates between 200-400lpm were generally successful in suppressing developing compartment fires up to $100m^2$. Therefore, these authors proposed a minimum tactical flow-rate (TFR) of 400lpm per $100m^2$ of compartmental fire involvement for attacks on both the fuel and gaseous phases of combustion and this includes a small margin for error. If the fire has spread to a stage where it involves actual structural members, the baseline flow-rate should be increased by at least 50 percent (600lpm per 100 m^2). In terms of tackling compartment fires in the gaseous phase, it should be mentioned that, in some author's experience [29], the strategy of 3D water-fog attack is limited to a maximum compartment size of 70 m^2.

There have been several international research studies [40] into the ideal base-line flow for a primary low-pressure attack hose-line and these have been fairly consistent in their approval for the 51mm hose-line flowing 450-560lpm. This research takes into account such relevant issues as (a) optimal flow-rate; (b) manoeuvrability and manual handling; (c) nozzle reaction; and (d) stowage and tactical deployment issues. Such hose-lines are fast becoming established as the ideal attack tools, for a primary offensive advancement by two fire-fighters into most compartment/structural fires where the fire area is contained within $100m^2$. In situations where a defensive mode of attack is necessary, or where any particular fire front is rapidly escalating through an established heavy fire loading, extensive structural fire involvement, or wind gusts (for example), then higher flows will be necessary. However, flows up to 950lpm from a 51mm hose-line are generally perfectly manageable by a team of two fire-fighters in a defensive or offensive 'holding position' (i.e.; the nozzle reaction would be too powerful to advance such a line whilst flowing).

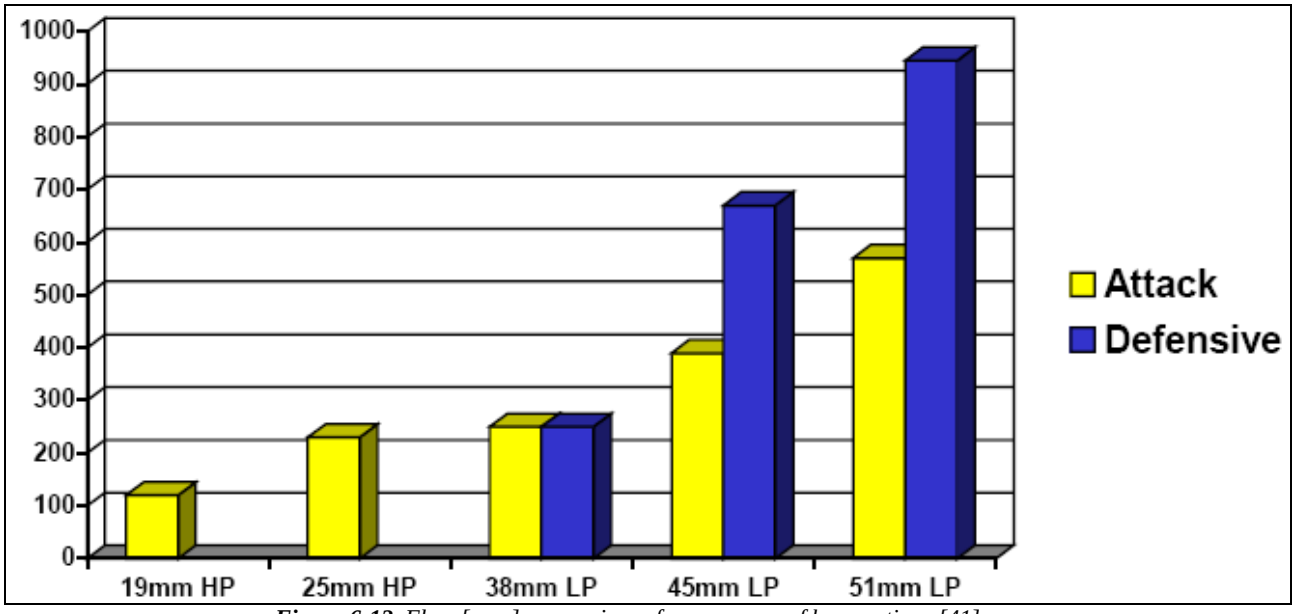

Figure 6-12. *Flow [gpm] comparisons from a range of hose options [41]*

Finally, related to the wide variety of the nozzles to be used by fire-fighting services and their capabilities, figures 6-13 to 6-16 are worthy to show some examples of their spray patterns and ranges for different water supplying systems conditions.

Figure 6-13. *A wide variety of models of nozzles [42]*

Tillverkare	Modell	Pris (SEK)	K - faktor	Tryck (bar)	Flöde (l/min)
Akron Brass Co	Turbojet	4500	18,4	3,4	340

Figure 6-14. *Akron Turbojet nozzle spray pattern and main features [42]*

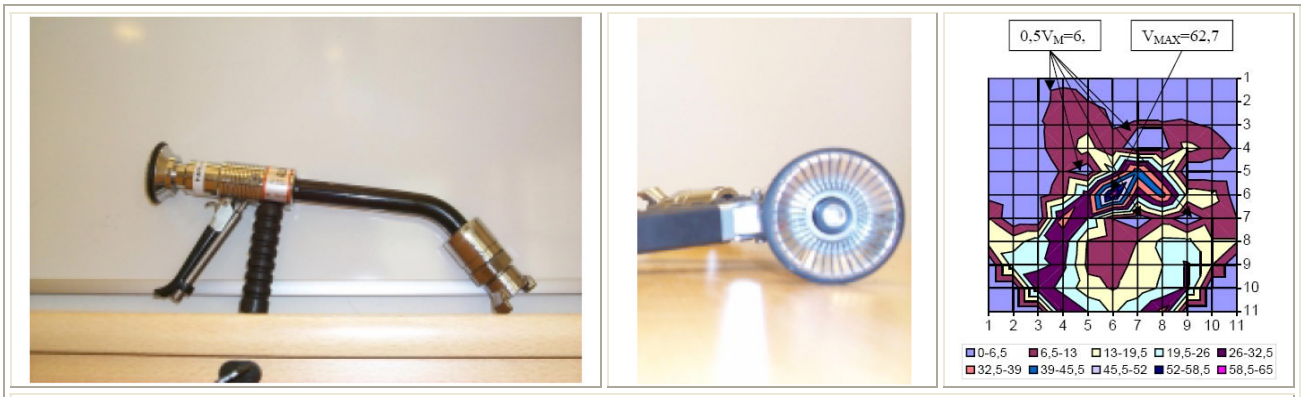

Tillverkare	Modell	Pris (SEK)	K - faktor	Tryck (bar)	Flöde (l/min)
Unifire AB	APG	2700	2,9	9,5	88

Figure 6-15. *Unifire APG nozzle spray pattern and main features [42]*

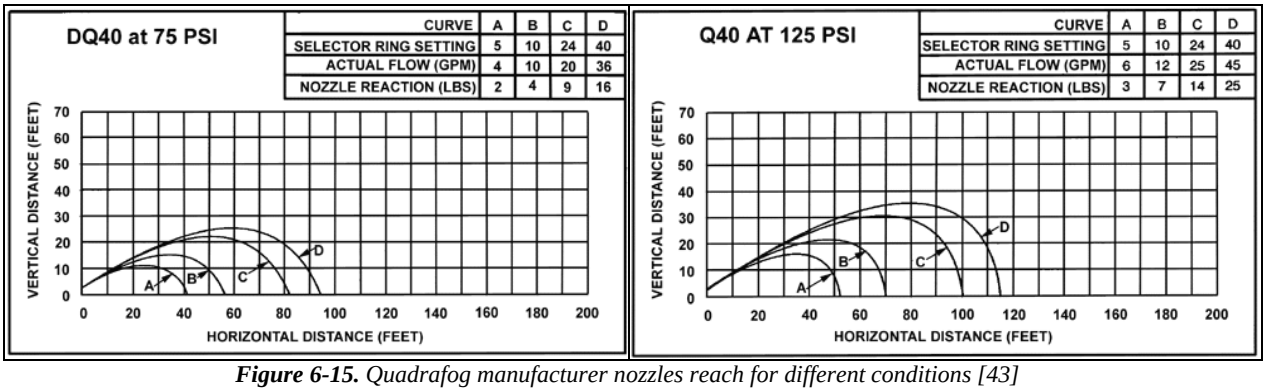

Figure 6-15. *Quadrafog manufacturer nozzles reach for different conditions [43]*

6.4.3.2.2 The Physics behind extinguishing with water

Next, physical and theoretical descriptions of water droplet dynamics in a fire environment are gathered to form a basis for more accurate definition of the cooling profiles to be applied to analyze the effect of cooling processes on the hygro-thermo-chemo-mechanical behaviour of structural elements manufactured with High Strength Concrete.

6.4.3.2.2.1 Formation of droplet from different types of nozzles

There are three different mechanisms for forming a spray:

- By creating a rotation in the spray (swirl),
- By colliding water jets,
- By direct droplet creation from a turbulent water jet, on leaving the nozzle.

The most common type in water systems is by direct droplet formation from a turbulent water jet. How the break-up of the jet takes place depends on the jet speed and diameter. There are, mainly, four different ways droplets can be formed from a water jet [44]:

A.- *'Rayleigh break-up' regime*. The droplet is formed far away from the nozzle. The diameter of the droplets is bigger than in the hole in the nozzle.

B.- *'First wind-induced break-up'*. Droplet formation occurs several nozzle diameters downstream of the nozzle outlet. The diameter of the droplets is about the same size as the hole in the nozzle.

C.- *'Second wind-induced break up'*. Droplet formation takes place a short distance downstream of the nozzle. The diameter of the droplets is smaller than the diameter of the hole in the nozzle.

D.- 'Atomization'. Droplet formation takes place at the exit from the nozzle. The diameter of the droplets is much smaller than the diameter of the hole in the nozzle.

Next figure shows a scheme of each of the four different ways droplets can be formed.

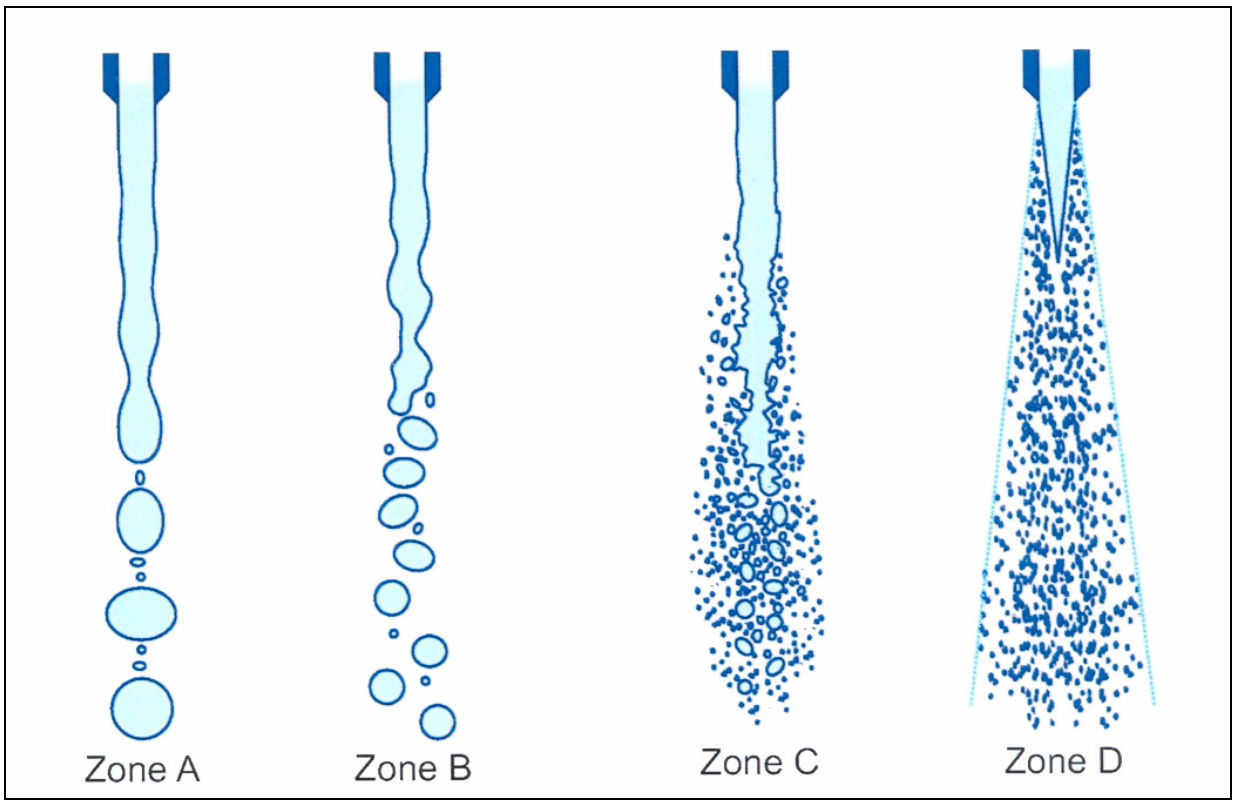

Figure 6-16. *Different kinds of droplet formation [44]*

The dominating factors that control the droplet formation mechanism are the Reynolds number and the Ohnesorge number. The Ohnesorge number, Oh, is the ratio between the viscous forces and the surface tension:

$$Oh = \frac{\mu}{\sqrt{\rho \cdot \sigma \cdot d}} \tag{6.9}$$

Where μ is the dynamic viscosity of the fluid [N·s/m^2], σ is the surface tension [N/m], ρ is the density and d is the diameter of the nozzle. For a typical high pressure nozzle with a internal diameter of 0,8 millimetres the Ohnesorge number is 0,004.

Next figure shows some digital images of jet/spray patterns corresponding to different cone angles:

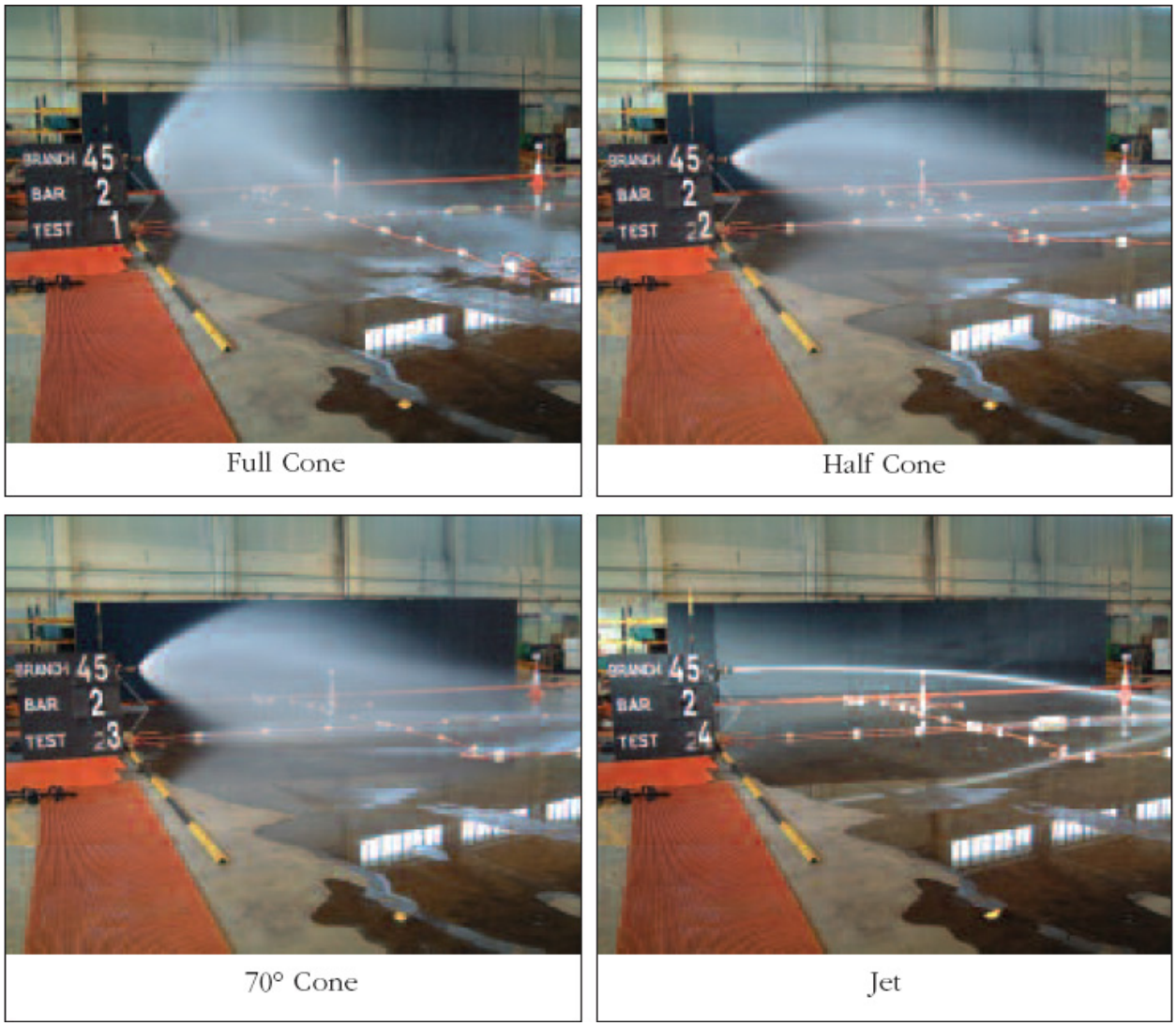

Figure 6-17. *Digital images of jet/spray patterns [45]*

6.4.3.2.2.2 Droplet size distribution

The creation of a spray results in droplets of different sizes. 'Small' droplets (< 2 mm) are more or less spherical and can be accurately described by a diameter. To describe the droplet distribution of the entire spray, statistical methods are normally used. One way to characterize a spray by a single parameter is to use the *Sauter* mean diameter, often written d_{32}. *Sauter* mean diameter is a number used to express the average droplet size in terms of the average ratio of volume to surface area of the droplets. *Sauter* mean diameter therefore is the diameter of a hypothetical droplet whose ratio of volume to surface area is equal to that of the entire spray.

The droplet size also depends on the pressure in the nozzle. The droplet size is reduced considerably up to a pressure of 7 bar. At higher pressures, the situation becomes more complex and droplet size is reduced at a much lower rate. Next figure shows the measured droplet size distribution at different pressures.

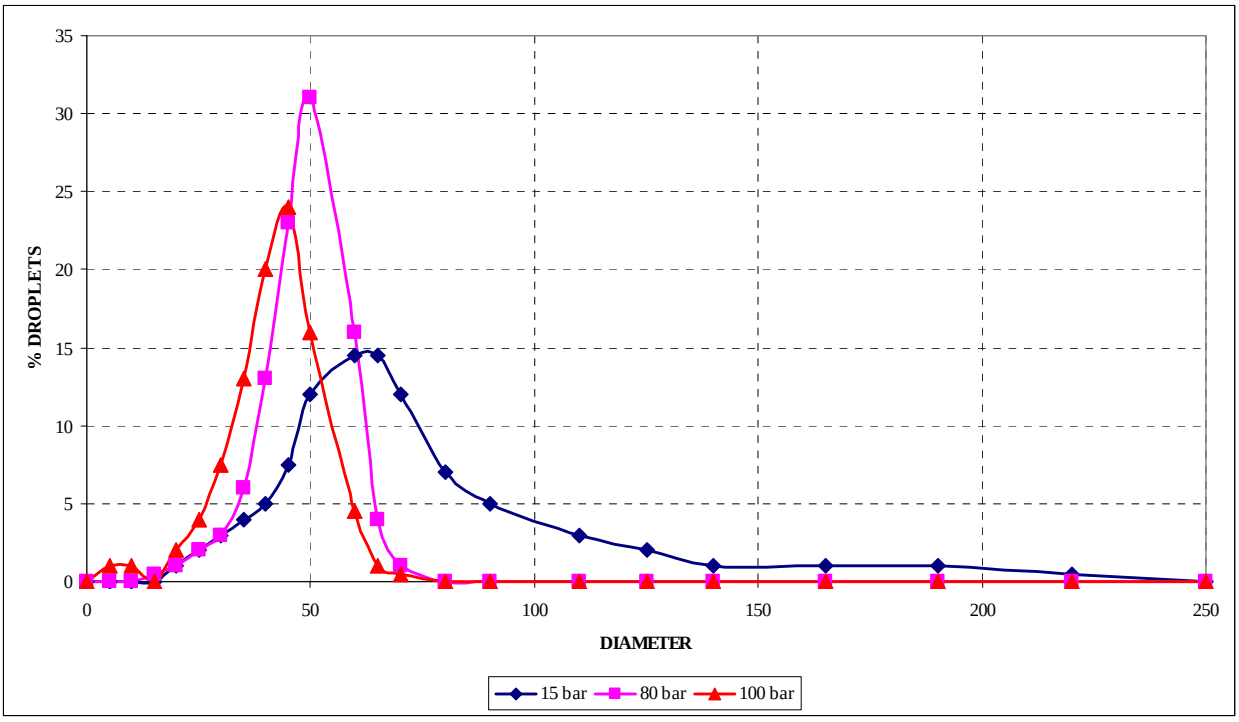

Figure 6-18. *Droplet size distribution [μm] at three different pressures [44] in water sprays at pressures higher than 7 bar.*

Table 6-17 shows the *Sauter* mean diameter variation at the three different pressures in figure 6-17. It can be observed that the diameter is only reduced by 50% when increasing the pressure from 15 to 100 bar.

PRESSURE	15 bar	80 bar	100 bar
***SAUTER* MEAN DIAMETER**	41,30 μm	33,07 μm	23,70 μm

Table 6-17. *d_{32} variation with pressure [135] in water sprays at pressures higher than 7 bar.*

6.4.3.2.2.3 Deceleration of droplets: aerodynamic properties of the spray

- FORCES ON A SINGLE DROPLET

A number of forces act on a droplet that is moving in air, e.g. the *Magnus, Saffman and Faxen* forces. However, many of them can be neglected compared to gravity and frictional forces [44].

The remaining forces that act on the droplet can be derived from Newton's second law:

$$\overline{F} = \frac{d}{dt}(m \cdot \overline{v}) = m \cdot \overline{g} - C_D \cdot \frac{\pi \cdot d^2 \cdot \rho_1}{8} \cdot (\overline{v} - \overline{v}_1) \cdot \left|\overline{v} - \overline{v}_1\right| \qquad (6.10)$$

where,

$\overline{F}$ is the total force which acts on the droplet,

m is the mass of the droplet = $\rho_w \cdot \frac{\pi \cdot d^3}{6}$

ρ_w is the density of water, d is the droplet diameter, $\overline{v}$ is the droplet velocity,

g is gravity, $\overline{v}_1$ is the velocity vector of the surrounding air,

C_D is the drag coefficient related to the Reynolds number of the droplet ($\frac{v \cdot d \cdot \rho_1}{\mu}$)

Due to the frictional force, the droplet will slow down. Setting the force $\overline{F}$ = 0 in the above equation, gives the terminal velocity of the droplet. For droplet Reynolds number less than 1, the drag coefficient can be calculated on the basis of Stokes law, C_D=25/Re. This means that the above equation can be solved analytically for droplets up to 80 μm. For droplets bigger than 80 μm (Re>1), the equation must be solved by numerical methods.

- DECELERATION OF SINGLE WATER DROPLETS WITH HIGH INITIAL SPEED

Water droplets that leave a spray nozzle at higher speed than the terminal velocity are quickly slowed down. Deceleration and throw length can be calculated by the previous equation, but in this high-speed case the calculation of the drag coefficient is more complex and the equation must be solved numerically.

As it has been observed in previous research works [44] small droplets decelerate very fast. A droplet size of 100 μm, typical for instance of water mist systems, decelerates in 0,01 seconds from 100 down to 10 m/s in a distance of 0,3 meters. During deceleration, the droplet may evaporate depending on the moisture content and temperature of the air. This influences the drag force and the droplet size, but it has only a minor influence on the drag force in previous equation [44]. On the other hand, the throw length for single water droplets with diameters under 100-200 μm is very short, even if they have an initial speed created by a water pressure of 100-200 bar in the nozzle. The only way to increase throw length is to reduce the relative velocity between the droplet and the surrounding air.

- RETARDATION OF WATER DROPLETS IN A SPRAY

The momentum lost by the droplet during deceleration is transferred to the surrounding air, which will therefore move in the same direction as the droplet. In a spray with many droplets, this implies that air will be sucked into the spray. The acceleration of air means that the relative velocity between the droplets and the surrounding air is reduced, increasing the throw length of the droplets.

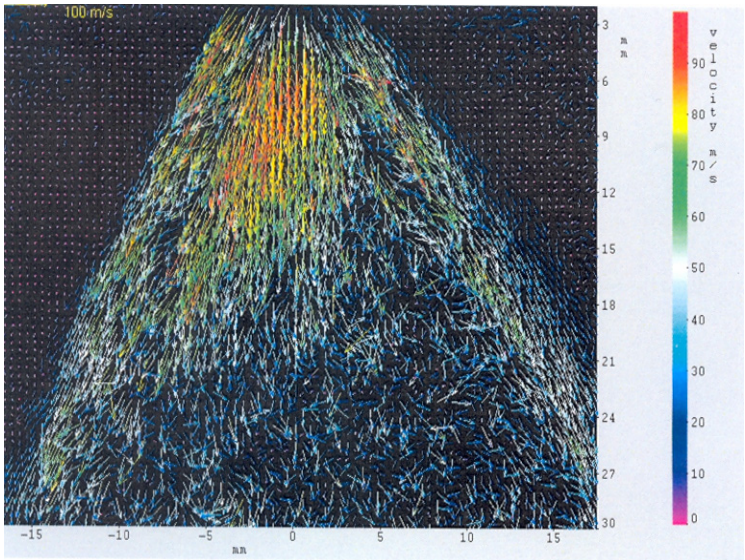

How this will occur depends on how the nozzle distributes the droplets. The most common spray patterns are full cone and hollow cone. In a full cone spray, the droplets are distributed evenly across the entire spray angle, whereas in a hollow cone, the droplets are mostly in the perimeter of the cone. Analyzing two pictures of droplets illuminated with a laser sheet and taken with a short time interval, the velocity field can be defined experimentally (this type of measuring equipment is called '*Particle Induced Velocimetry*', shown in figure 6-19).

Figure 6-19. *Velocity field in a spray (Hollow cone, 80 bar, nozzle diameter 0,8 mm) [44]*

From last figure it can be observed that the droplets in the spray are decelerated from 90-100 m/s down to 10-30 m/s in a distance of 0,3 metres and that the velocity field inside the hollow cone is very complex.

For nozzles that form a full cone spray the air velocity, v_1, in the spray can be calculated from [44]:

$$v_1 \approx \frac{\sqrt{m_w^* \cdot p^{0,5}}}{r}$$

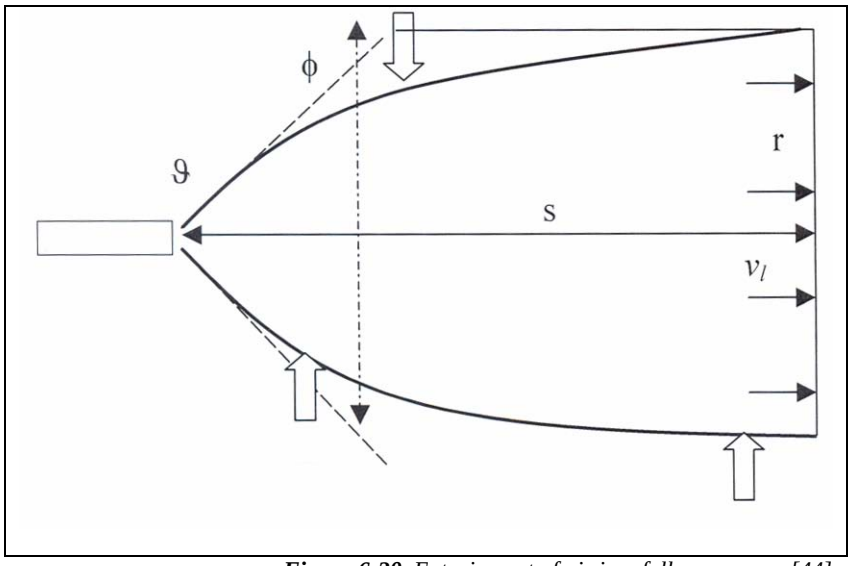

Figure 6-20. *Entrainment of air in a full cone spray [44]*

where m_w^* is the mass flow rate of water, p is the nozzle pressure and r is the spray radius calculated from:

$$r \approx s \cdot \tan\left(\left(\vartheta/2+\phi\right)\cdot\frac{1}{2}\right), \; for \vartheta \le 45^o$$
$$r = s \cdot \tan\left(\vartheta/4\right), \; for \; \vartheta > 45^o \qquad (6.11)$$

where ϑ is the cone angle, s is the distance from the nozzle and ϕ is defined in the entrainment picture above.

6.4.3.2.2.4 Evaporation of water droplets

Evaporation of water droplets depends on the temperature and moisture content in the surrounding air. In the following descriptions, only temperatures above 100ºC are considered. The heating of a droplet from the start to 100ºC is ignored, as the energy required is much smaller than the energy required to evaporate the droplet (see figure 6-21).

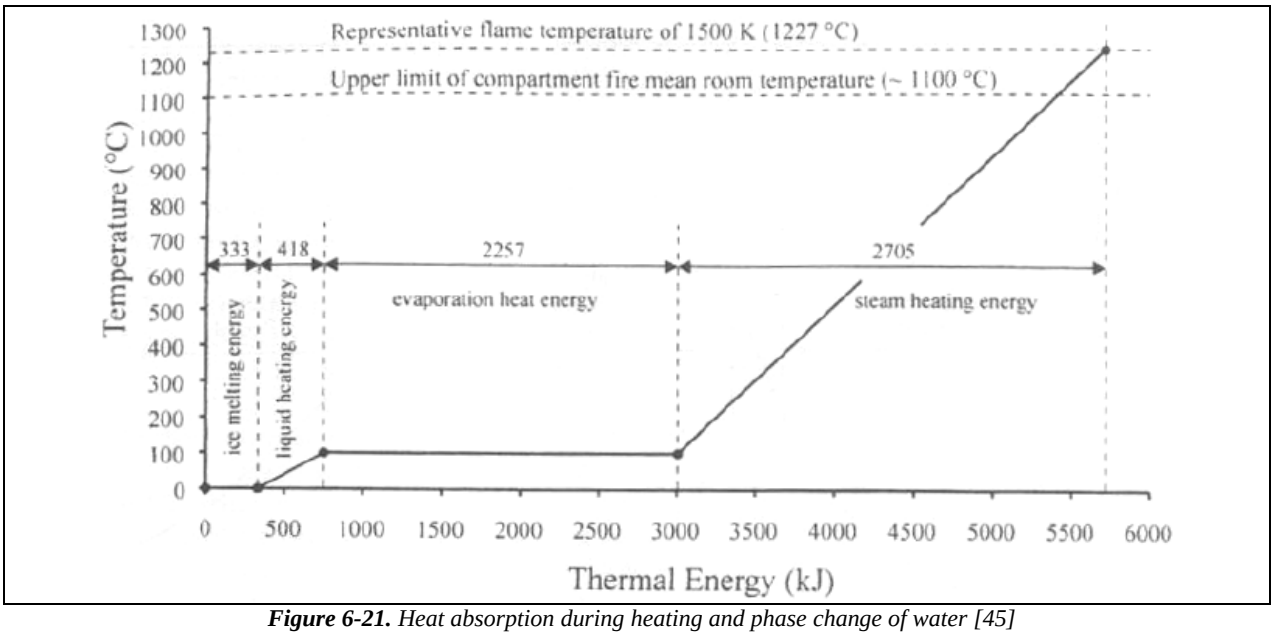

Figure 6-21. *Heat absorption during heating and phase change of water [45]*

The dynamic change of droplet volume is given by

$$\frac{dV}{dt} = \frac{1}{6}\Pi\frac{dd^3}{dt} = \frac{1}{6}\Pi\cdot 3d^2\frac{dd}{dt} = \frac{\Pi}{2}d^2\frac{dd}{dt} \tag{6.12}$$

The convective heat transfer to a droplet in hot air is proportional to the temperature difference ΔT between the air and the droplet, heat transfer coefficient h and the square of the droplet diameter, which gives

$$\frac{dQ}{dt} = h\cdot A\cdot\Delta T = h\cdot 4\cdot\pi\cdot\left(\frac{d}{2}\right)^2\cdot\Delta T \tag{6.13}$$

where Q is the energy.

If the heating of the droplet to 100ºC is ignored, the received energy leads only to evaporation of the droplet, which can be described as:

$$\frac{dQ}{dt} = -H_v\cdot\rho_w\cdot\frac{dV}{dt} = -H_v\cdot\rho_w\cdot\frac{\pi}{2}\cdot d^2\cdot\frac{dd}{dt} \tag{6.14}$$

where H_v is the heat of evaporation for water. The change in droplet diameter over time can then be written as:

$$\frac{dd}{dt} = -\frac{2\cdot h}{H_v\cdot\rho}\cdot\Delta T \tag{6.15}$$

- FOR WATER DROPLETS UNDER 0,1 MILLIMETRES

For small water droplets the heat transfer coefficient *h* is given by the dimensionless Nusselt number, *Nu*:

$$Nu = \frac{h\cdot d}{k} = 2 + 0{,}6\cdot \mathrm{Pr}^{0{,}33}\cdot \mathrm{Re}^{0{,}5} \tag{6.16}$$

This equation can be solved analytically for some simple cases.

For droplets smaller than 0,1 millimetres, the droplet is decelerated very rapidly and reaches terminal velocity quickly. At that velocity, natural convection will dominate and the Nusselt number will be equal to 2. Combining the above equations:

$$\frac{dd}{dt} = -\frac{4\cdot k\cdot\Delta T}{H_v\cdot\rho\cdot d} \tag{6.17}$$

If the temperature difference between the droplet and the air is constant over time, an integration of last equation leads to:

$$d^2 = d_0^2 - \beta\cdot t\ ,\ where\ \beta = \frac{8\cdot k\cdot\Delta T}{H_v\cdot\rho} \tag{6.18}$$

Table 6-18 shows the lifetime for droplets with different diameters and different gas temperatures:

Temperature Diameter [µm]	**150 ºC**	**200 ºC**	**300 ºC**	**400 ºC**	**600 ºC**
5	3,9	1,8	0,8	0,5	0,2
10	15,6	7,2	3,1	1,8	0,9
50	391,2	178,9	76,9	45,4	22,2
100	1.564,8	715,8	307,5	181,4	88,9

Table 6-18. *Lifetime for droplets in hot air, free falling [10^{-3} s] [44]*

However, during deceleration the convective heat transfer dominates, which will reduce the droplet lifetime even further.

Using the above equations, a system of partial differential equations are obtained that can be solved numerically:

DROPLET DIAMETER [μm]	DISTANCE [mm]	LIFE TIME, INITIAL SPEED 100 m/s
5	0,239	3,9 ms
10	7,87	15,5 ms
50	111	372,0 ms
100	387	1.400,0 ms

Table 6-19. *Initial speed 100 m/s, temperature in fire room 150 ºC [44]*

Table 6-19 shows how far a droplet is transported and the estimated droplet lifetime. In Table 6-20 the lifetime for droplets with and without initial speed is shown. It can be observed from this table that the lifetime of the droplet is not greatly influenced by the initial droplet speed.

DROPLET DIAMETER [μm]	LIFE TIME, FREE FALLING	LIFE TIME, INITIAL SPEED 100 m/s
5	3,9 ms	3,9 ms
10	15,6 ms	15,5 ms
50	391,2 ms	372,0 ms
100	1.564,8 ms	1.400,0 ms

Table 6-20. *Comparison of lifetime for free falling droplets with droplets with an initial speed of 100 m/s, at a gas temperature of 150 ºC [44]*

The reason for the slight difference in lifetimes is the fast deceleration of the droplet. It is remarkable that the droplet has a high speed only for a short period. The conclusion is that a high initial speed (high nozzle pressure) does not substantially increase the evaporation rate.

6.4.3.2.2.5 Extinguishing performance of water

Water can enhance extinguishment of fire in different ways:

- *Flame Extinguishing.* Droplets enter the flames. The flames are cooled to such low temperatures that they can no longer exist. Flames are extinguished. Hot surfaces will for a time continue to produce pyrolysis products that can be reignited.
- *Surface cooling*. The droplets hit the burning/hot surfaces, which are cooled down to a temperature that no longer can produce enough pyrolysis products to sustain a fire.
- The droplets blocks or reduces re-radiation from flames and thereby lowers the heating and pyrolysis rates from surfaces.

- FLAME EXTINGUISHING

Flame extinguishment can in principle be explained by the chemical reaction that takes place in the flames. An extinguishing media can either participate actively in the flame reactions or it can work as a collision partner and heat absorber (temperature is lowered). Water and water droplets mostly work as heat absorbers and to a lesser degree by depletion of oxygen and fuel. The basic idea behind this kind of extinguishment, '*fire point theory*', is to make an energy balance for the flames.

The thermal quenching concept is based on energy balance as stochiometry in the flame [44]:

$$X_w \cdot (L + \int_{T_0}^{373} C_{lw} dT + \int_{373}^{1550} C_{gw} dT) = X_f \cdot \Delta H_c - \sum X_p \cdot \int_{T_0}^{1550} C_{gp} dT - X_{N_2} \cdot \int_{T_0}^{1550} C_{gN_2} dT - \sum X_{di} \cdot \Delta H_{di} \quad (6.19)$$

where X_w represents the mole fraction of water, X_f is the mole fraction of fuel, X_p is the mole fraction of combustion products, X_{N2} is the mole traction of nitrogen, X_{di} is the mole fraction of dissociated molecules, C represents the molar heat capacity of *lw* (liquid water), *gw* (water vapour), *gp* (combustion products) and gN_2 (nitrogen), L is the latent heat of vaporization of water, ΔH_c is the heat of combustion and ΔH_{di} is the heat of dissociation.

Experimentally it has been found that a hydrocarbon flame will extinguish at an adiabatic flame of about 1550 K. It can be shown – using last equation – that for a premixed stoichiometric propane-air flame a concentration of 280 g of water per cubic metre can extinguish the flame (assuming that all water will be evaporated).

For a diffusion flame, an extinguishing concentration of 140-190 g of water per cubic metre would be required, as a diffusion flame has higher heat loss than a premixed flame. Experimental measurements on diffusion flames give values [44] which vary from 150 to 200 g of water per cubic metre air. This is very close to the theoretical calculation. If water vapour is used instead of water droplets, about double the amount of water is required.

- SURFACE COOLING

Water that reaches a burning surface is heated up and evaporates, thereby cooling the surface. The pyrolysis rate from the surface decreases and when it gets sufficiently small, about a heat release of 50-75 kW/m^2, flames on the surface can no longer exist. This case can also be described by the thermal extinguishing theory. Theory and experiments [44] show that the amount of water required to extinguish a wood based fire (pyrolysis rate under about 5 g/(s·m^2)) is ≈ 2 g/(s·m^2). If the surface is also subjected to radiation, the demand for water to extinguish the flame is increased dramatically. For example, at a radiation level on the surface of 25 kW/m^2, the demand of water increases to 10 g/(s·m^2).

When water is sprayed at a hot wall, it will absorb heat. Water has a high latent heat of vaporization, 2.260 kJ/Kg. By using water the right way, high cooling effects can be obtained. After the water has hit the wall, it will be warmed up while running down the wall. Some of the water will be evaporated. But the heat transfer from a hot wall to a water droplet is a very complex process, which depends on the collision speed of the droplet at the wall, the diameter of the droplet and the temperature of the wall. Here the dimensionless parameter, Weber number (*We*), is used to describe what happens at the collision.

6.4.3.2.2.6 Absorption of radiation in water droplets

Attenuation of radiation in a volume S of an absorbing gas is described by the *Lambert-Beers* law, written in differential form as:

$$\frac{di(\lambda, S)}{ds} = -K_a(\lambda, S) \cdot i(\lambda) \quad (6.20)$$

where i is the radiation intensity, λ the radiation wave length and K_a the absorption coefficient. The solution to this equation is the well-known expression:

$$i(\lambda, S) = i(\lambda, 0) \cdot e^{[K_a(\lambda) S]} \quad (6.21)$$

If the gas is also emitting radiation due to high temperatures, the following differential expression is used:

$$\frac{di(\lambda,S)}{ds} = -K_a(\lambda,S)\cdot i(\lambda) + K_a(\lambda,S)\cdot i_b(\lambda) \tag{6.22}$$

where i_b is the black-body radiation from the particle based on its temperature. The emission and absorption coefficients are assumed equal, based on Kirchoff's law that states that the emissivity and the absorbtivity of a gas are equal.

If the volume S contains particulate material (e.g. water droplets) that scatter radiation, the intensity attenuation obtained in S can be described by similar simple expressions as long as the physics of in-scattering (i.e. the radiation intensity increase due to scattering in surrounding particles) can be neglected. This simplification leads to a Lambert-Beer type of attenuation description:

$$\frac{di(\lambda,S)}{ds} = -K_s(\lambda,S)\cdot i(\lambda) \tag{6.23}$$

where λ is the radiation wave length and K_s is the scatter coefficient.

For a monodisperse particle cloud, K_s can be calculated from:

$$K_s = C_s \cdot N_0 \tag{6.24}$$

where C_s is the scattering area of a particle an dN_0 is the number of particles. Since the particle area is proportional to the square of the diameter, and the number of particles for a given mass fraction *f* depends on the particle diameter as $N_0 \propto f/d^3$ it can be stated that $K_s \propto f/d$, i.e. that the scattering coefficient increases with diminishing diameter for a given mass fraction.

The differential equation describing radiation attenuation based on absorption, emission and scattering is then obtained as:

$$\frac{di(\lambda,S)}{ds} = -\left(K_a(\lambda,S) + K_a(\lambda,S)\right)\cdot i(\lambda) + k_a(\lambda,S)\cdot i_b(\lambda) \tag{6.25}$$

If the coefficients are assumed constant, the following solution is obtained:

$$i(\lambda,S) = i(\lambda,0)\cdot e^{[-K(\lambda)S]} + i_b\cdot\left(1 - e^{[-K_a(\lambda)S]}\right), where\, K = K_a + K_s \tag{6.26}$$

If in-scattering is included in the model and spherical coordinates (θ,ϕ) are used, an integro-differential equation, the Radiation Transfer Equation is obtained:

$$\frac{di_\lambda(S,\theta,\phi)}{dS} = -(K_a + K_s)\cdot i_\lambda(S,\theta,\phi) + K_a\cdot i_{b\lambda}(S) + \frac{K_s}{4\cdot\pi}\cdot\int_0^{2\cdot\pi}\int_0^{\pi} i_\lambda(S,\theta',\phi')\cdot P(S'\to S)\cdot\sin\theta'\,d\theta'\,d\phi' \tag{6.27}$$

where index λ is used to indicate wave-length dependence and P is the phase function defined by

$$P(S'\to S) = \lim_{ds\to 0}\left(\frac{Energy\ scattered\ \ from\ the\ S'\ to\ the\ S-direction}{Energy\ scattered\ to\ S\ in\ isotropic\ scattering}\right) \tag{6.28}$$

i.e. P=1 when the scattering is isotropic (direction independent). The phase function can be derived from Maxwell's fundamental equations on electricity and magnetism.

When particle size is much less than the electromagnetic wave length (λ), a more simple, Rayleigh scattering model can be used, giving as phase function:

$$P(\Theta) = \frac{3}{4}\cdot\left(1+\cos^2(\Theta)\right) \tag{6.29}$$

where θ is the angle between the plane of the incident ray and the reflected ray.

For a 'large' opaque particle having a diffuse reflecting surface, the phase function

$$P(\Theta) = \frac{8}{3\cdot\pi}\cdot\left(\sin(\Theta) - \Theta\cdot\cos(\Theta)\right) \tag{6.30}$$

is obtained. Hence, Rayleigh scattering has a minimum in a plane orthogonal to the incident plane but diffusive scattering is dominated by backward scattering.

In conclusion, it is observed both that small droplets are better than larger droplets in reducing radiation and that they will evaporate very fast, taking place the main radiation absorption in the gas phase of water rather than the liquid phase.

6.4.3.2.3 Definition of the Cooling Profiles in sight of their Physical Background and Fire Fighting Experiences.

6.4.3.2.3.1 Start Time of Extinguishing Actions

There are significant differences on the start instant of the fire extinguishing actions in High-Rise Buildings depending, among other parameters, on the type and availability of active extinguishing measures.

Some regulations [28] are currently in evolution in order to take into account these differences, when calculating the fire load to be considered within further analyses of the structural state under fire conditions, establishing – within its Annex E – the following rule for its calculation:

$$q_{f,d}\,[MJ/m^2] = q_{f,k}\cdot m\cdot\delta_{q1}\cdot\delta_{q2}\cdot\delta_n \tag{6.31}$$

where, $q_{f,k}$ is the characteristic fire load density per floor surface unit [MJ/m^2],

m is the combustion coefficient,

δ_{q1} is a coefficient which takes into account the fire start risk due to the sector size,

δ_{q2} is a coefficient which takes into account the fire start risk due to the kind of activity developed in the building, and

$\delta_n = \prod_{i=1}^{10}\delta_{ni}$ is a coefficient which takes into account the different active measures of fire fighting (sprinklers, detection, automatic alarm transmission, fire-fighting services, …), which are defined as follows (see Table 6-21) and whose effect is clearly illustrated on figure 6-22:

$\delta_{n,I}$ Function of the active measures for fire fighting										
Automatic Extinction				Automatic Detection			Manual Extinction				
Automatic system for water extinguishing	Independent water supply sources			Automatic detection and alarm		Automatic alarm transmission to fire fighting headquarter	Self fire fighting service	External fire fighting service	Sure access paths	Fire fighting equip-ment	Soot control system
	0	1	2	of heat	of soot						
$\delta_{n,1}$	$\delta_{n,2}$			$\delta_{n,3}$	$\delta_{n,4}$	$\delta_{n,5}$	$\delta_{n,6}$	$\delta_{n,7}$	$\delta_{n,8}$	$\delta_{n,9}$	$\delta_{n,10}$
0,61	1,0	0,87	0,7	0,87 or 0,73		0,87	0,61 or 0,78		0,9 or 1 or 1,5 1,0 or 1,5	1,0 or 1,5	1,0 or 1,5

Table 6-21. *Coefficient $\delta_{n,i}$ to take into account different active fire fighting measures [28]*

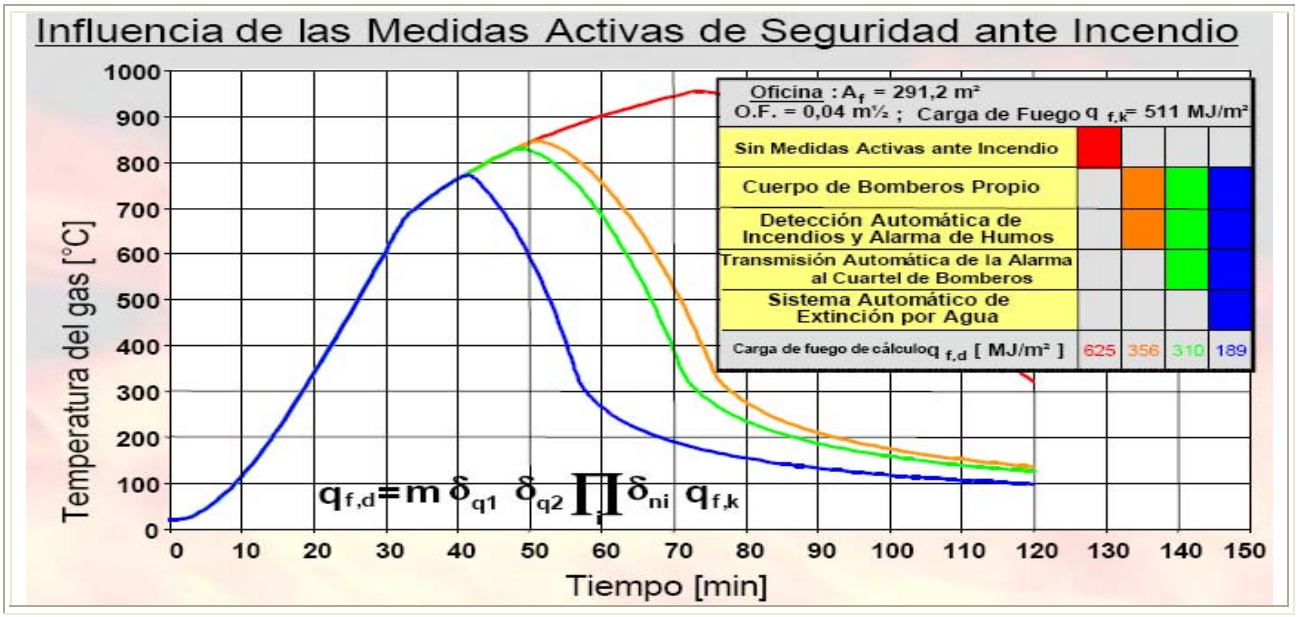

Figure 6-22. *Influence of active measures for fire fighting [46]*

Figure 6-22 shows that depending on the available active measures of fire fighting (sprinklers, detection, automatic alarm transmission, fire-fighting services, …) the start instant of cooling may vary considerably, from the shortest 40 minutes up to 75 minutes where no active fire fighting measures are available.

On the other hand, from some recent actual catastrophic events such as the fire and collapse of the World Trade Centre Towers 1 and 2 arise realistic and accurate information about the fire fighting services response times and about the use of active fire fighting measures [47]. The following chronology (Table 6-22) demonstrates that the emergency response to the World Trade Centre (WTC) was immediate. Within the first three minutes after the aircraft impact into WTC 1, (1) the Port Authority Police Department (PAPD) responded by providing information on the attack to the police desk; (2) The Fire Department of the City of New York (FDNY) dispatched 26 units to the WTC; and (3) The New York City Police Department (NYPD) called a department mobilization that included dispatching aviation units to the WTC for visual assessment. In less than 10 minutes, PAPD called a chemical mobilization; NYPD dispatched five Emergency Service Unit (ESU) teams and had two aviations units at the scene providing observations. In less than 30 minutes, 121 FDNY units had been dispatched to the scene and 30 units had signaled their arrival at the scene.

Event Time	Event Description
8:46 a.m.	*FDNY Battalion Chief reports that an airplane has struck the upper floors of a WTC building and transmits a first and second alarm (FDNY, McKinsey & Company, 2002)* *PAPD officer reports to the police desk an explosion at the WTC. (PAPD Radio Channel Y/Channel 2)*
8:48 a.m.	*26 FDNY units dispatched. (FDNY Dispatch log)* *NYPD calls for a department mobilization. (NYPD Special Operations Division (SOD) Radio Channel)*
8:49 a.m.	*NYPD requests that aviation units get into the air and make a visual assessment of the WTC (NYPD SOD Radio Channel)*
8:50 a.m.	*PAPD officer calls for a chemical mobilization. (PAPD Radio Channel W)*
8:52 a.m.	*A total of five NYPD Emergency Service Units dispatched. (NYPD, McKinsey & Company, 2002)* *NYPD aviation requests landing zone in the vicinity of the WTC. (NYPD SOD Radio Channel)* *NYPD aviation unit arrives at the WTC and examines possibilities of roof rescue. (NYPD, McKinsey & Company, 2002)*

8:54 a.m.	*NYPD aviation advises they have two units in the air to do aerial survey. (NYPD SOD Radio Channel)*
8:59 a.m.	*FDNY Chief calls for all but one Rescue Squad to the WTC. (FDNY Manhattan Dispatch Radio Channel)*
9:00 a.m.	*A total of 66 FDNY units have been dispatched at this time. (FDNY Dispatch log)*
9:03 a.m.	*FDNY Marine unit reports that a second plane struck WTC 2. (FDNY Manhattan Dispatch Radio Channel and FDNY, World Trade Center Incident Summary, 2001)*
9:15 a.m.	*A total of 121 FDNY units dispatched, and 30 FDNY units signal their arrival. (FDNY Dispatch log)*
9:29 a.m.	*FDNY dispatcher relays that a department-wide recall has been instituted. (FDNY, World Trade Center Incident Summary, 2001)*
9:59 a.m.	*A total of 171 FDNY units dispatched, and 74 FDNY units signal their arrival. (FDNY Dispatch log)*
10:29 a.m.	*A total of 214 FDNY units dispatched, and 103 FDNY units signal their arrival. (FDNY Dispatch log)*

Table 6-22. *Chronology of the Emergency Response to the World Trade Centre [47]*

After that 30 minutes necessary to arrive at the scene, an additional time interval is required to reach the fire floor and unfold active fire fighting measures, matching hence the intervention start interval from 40 to 75 minutes describe previously (see figure 6-22) and with that of 64,4 minutes (mean value) shown on Table 6-16, which is partially reproduced next:

Parameter	**Mean**	**St. dev.**	**Cases**
Time Preheating – Ignition [min]	44,9	118,3	50
Time Ignition – Discover [min]	9,1	15,0	116
Time Discover – Arrival [min]	8,4	13,0	271
Time Arrival – Intervention [min]	2,0	2,8	153
Total Mean Time Preheating – Intervention [min] = 64,4 minutes			

Table 6-16 (partially reproduced). *The mean and standard deviation of parameters and the number of fires on which they are based from the 307 fire study in London [38]*

6.4.3.2.3.2 Cooling Rate and duration of Extinguishing Actions

Since the temperature evolution in a HSC concrete element has an essential influence on the thermal spalling risk, the cooling curves selected for the analyses aim of this Chapter need to be chosen within the most realistic ones corresponding to High-Rise Buildings rooms and/or offices.

Therefore, the cooling curves adopted must be clearly representative of the temperature distributions during real fires. Some regulations, such as Eurocode 1 Part 1-2 [28], adopt with this aim time-temperature parametric curves in the cooling stage defined as follows:

$$\Theta_g = \Theta_{max} - 625 \cdot (t^* - t^*_{max} \cdot x) \qquad for \quad t^*_{max} \le 0{,}5$$

$$\Theta_g = \Theta_{max} - 250 \cdot (3 - t^*_{max}) \cdot (t^* - t^*_{max} \cdot x) \qquad for \quad 0{,}5 \le t^*_{max} \le 2$$

$$\Theta_g = \Theta_{max} - 250 \cdot (t^* - t^*_{max} \cdot x) \qquad for \quad t^*_{max} \ge 2, \tag{6.32}$$

$$where \quad t^* = t \cdot \Gamma$$

$$t^*_{max} = (0{,}2 \cdot 10^{-3} \cdot q_{t,d} / O) \cdot \Gamma$$

$$x = 1{,}0 \; if \; t_{max} > t_{lim}, or \; x = t_{lim} \cdot \Gamma / t^*_{max} \; if \; t_{max} = t_{lim}$$

$$(where \; t_{lim} \; is \; 25 \min \; for \; slow \; fires, 20 \min \; for \; medium \; fires \; and \; 15 \min \; for \; fast \; fires)$$

where,

Θ_g is the air temperature within the fire sector [ºC]

Θ_{max} is the maximum air temperature within the fire sector during the heating stage, corresponding to $t^* = t^*_{max}$ [ºC]

Γ $= [O/b]^2 / (0{,}04 / 1.160)^2$ [-]

b $= \sqrt{\rho \cdot c \cdot \lambda}$ with the following limits: 100<= b <=2.200 [$J/m^3s^{1/2}K$]

ρ is the density of the element closing the fire sector (At ambient temperature) [Kg/m^3]

c is the specific heat of the element closing the fire sector (At ambient temperature) [J/KgK]

λ is the thermal conductivity of the element closing the fire sector (At ambient temperature) [W/mK]

O is the opening coefficient: $A_v \cdot \sqrt{h_{eq}} / A_t$ [$m^{1/2}$]
with the following limits: 0,02 <= O <= 0,20

A_v is the total surface of the vertical openings at all of the walls [m^2]

h_{eq} is the averaged height of the windows at all of the walls [m]

A_t is the total surface closing the fire sector, including openings [m^2]

$q_{t,d}$ is the calculation value of the fire load density referred to the total area A_t of the envolvent $q_{t,d} = q_{f,d} \cdot A_f / A_t$ [MJ/m^2] with the following limits: $50 \leq q_{t,d} \leq 1.000$ [MJ/m^2].

$q_{f,d}$ is the calculation value of the fire load density referred to the floor built area A_f [MJ/m^2] described in Annex E of Eurocode 1 Part 1-2 [28].

If, for instance, it is analyzed the parametric cooling curve corresponding to different situations arising from the situation after the heating process described in paragraph 6.4.3.1.1. (opening coefficient O = 0,07 $m^{1/2}$) – corresponding to the normalized time-temperature curve (ISO 834) defined in the regulation project prEN 13501-2 – the cooling features obtained for a characteristic fire load density per floor surface unit, $q_{f,k}$, of 400 MJ/m^2, a combustion coefficient *m* equal to 1,0 (Annex E, paragraph E.3 of the Eurocode 1 Part 1-2 [28]), a δ_{q1} coefficient with a 1,50 value and a δ_{q2} coefficient with a value of 1,00 (both according to Table E.1 of the stated Annex E) are analyzed next:

Combination of Active Fire Fighting Measures	$\delta_n = \prod_{i=1}^{10} \delta_{ni}$ **(see 6.4.3.2.3.1)**	**$q_{f,d}$ [MJ/m^2]**
Without Active Fire Fighting Measures	1,00	600
The above + With a Self Fire Fighting Service	0,61	366
The above + With Automatic Fire Detection and Soot Alarm	0,53	319
The above + Automatic Alarm Transmission to Fire Fighting Headquarter	0,46	277
The above + Automatic System for Water Extinguishing	0,28	169

Table 6-23. *Fire Load Density corresponding to different combinations of Active Fire Fighting Measures*

The cooling (and heating) profiles corresponding to each of the combinations of the Active Fire Fighting Measures detailed on Table 6-23 are shown next:

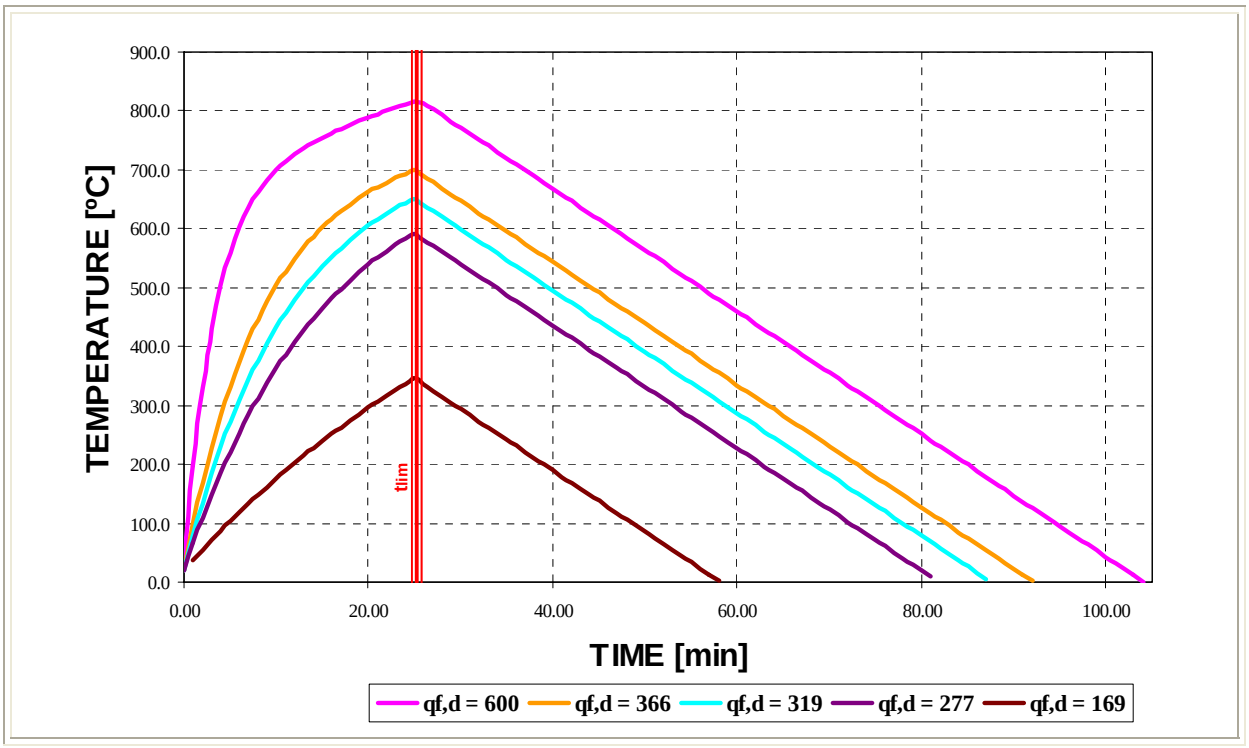

Figure 6-23. *Cooling (&heating) profiles corresponding to different combinations of Active Fire Fighting Measures (ISO curve)*

From this figure it is observed that the environmental cooling rate prescribed by the parametric curves of the Eurocode 1 Part 1-2 [28] is analogous for all of the combinations and with a value of – 0,172 ºC/second, with environmental cooling durations from 33 minutes (1.980 seconds) up to 79 minutes (4.740 seconds) depending on the case considered.

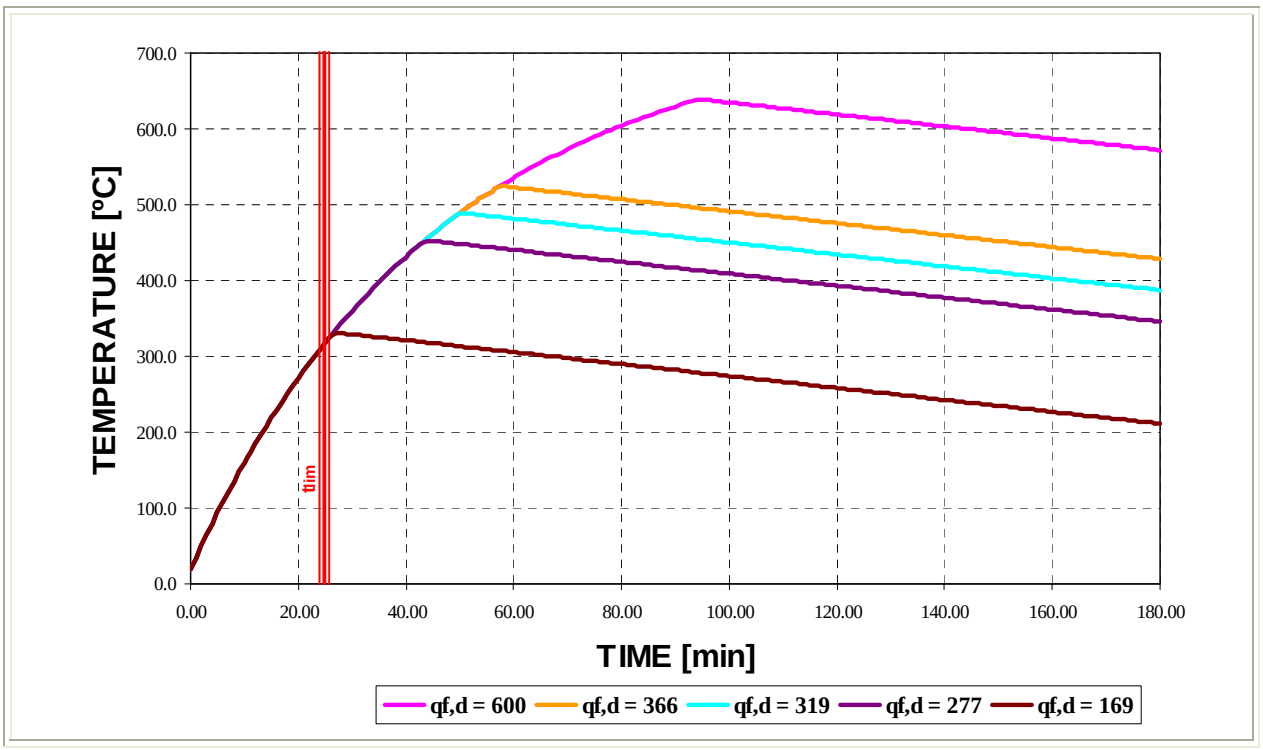

Figure 6-24. *Cooling (&heating) profiles corresponding to different combinations of Active Fire Fighting Measures (Slow curve)*

Analogously, if we analyze the parametric cooling curve corresponding to the slow heating process described in paragraph 6.4.3.1.2. – corresponding to the Eurocode 1, Part 1-2 [28] with the lowest value of the opening coefficient allowed in the Eurocode O = 0,02 $m^{1/2}$ – the cooling

features obtained for a characteristic fire load density per floor surface unit, $q_{f,k}$, of 400 MJ/m^2, a combustion coefficient *m* equal to 1,0 (Annex E, paragraph E.3 of the Eurocode 1 Part 1-2 [28]), a δ_{q1} coefficient with a 1,50 value and a δ_{q2} coefficient with a value of 1,00 (both according to Table E.1 of the stated Annex E) are those exposed on figure 6-24 (referred also to the combinations described on Table 6-23 of this Chapter). From this figure it is observed that the environmental cooling rate prescribed by the parametric curves of the Eurocode 1 Part 1-2 [28] is analogous for all of the combinations and with a value of – 0,013 ºC/second, with environmental cooling durations much longer.

Finally, if the maximum allowed value of the opening coefficient is considered (O = 0,20 m$^{1/2}$) instead of the minimum one, the cooling rate increases considerably up to – 1.438 ºC/second.

Hence, a wide range of the environment cooling rate value is possible depending on the ventilation conditions of the enclosure, so this range is taken into account in the cooling rates finally selected for these analyses and exposed on paragraph 6.4.3.2.4. This dispersion of cooling rate values is also confirmed from experimental tests described on [29], where extinguishing actions were experimentally developed by means of water mist devices of different water pressures and nominal flows, as it is observed on next table:

	Water Spray Characteristics			Water used overall during attack					Mean air cooling rate [ºC/s]
Test	Pump pressure [bar]	Nozzle pressure [bar]	Nominal flow [Kg/s]	Total mass [Kg]	Mean flow [Kg/s]	Number of sweeps [-]	Mass per sweep [Kg]	Capacity used [-]	
2	39	25±5	3,83	694	1,46	62	11,2	0,38	- 4,6
3	7,0	6,0±0,5	3,83	692	1,26	42	16,5	0,33	- 3,0
4	5,2	4,5±0,5	1,92	298	0,843	26	11,5	0,44	- 1,7
5	35	23±5	1,92	284	0,708	28	10,2	0,37	- 3,3
6	8,0	7,0±0,5	5,75	755	1,50	35	21,6	0,26	- 2,0

Table 6-24. *Experimental results from extinguishing actions by means of a water mist system for different water spray characteristics [29] and estimation, from experimental time-temperature curves, of the mean air-cooling rate.*

In last table it is observed that the mean gas temperature for all tests clearly demonstrates the greatest cooling effects were achieved during tests 2 and 5 (high-pressure booster line) although the flow-rate (30 gpm) used in Test 5 was unable to attain final control of the fuel-based fire within the test criteria of six minutes.

Besides this, although these parametric curves, generally prescribed for "natural" cooling processes, may introduce the extinguishing effect of active fire fighting measures and, especially, of Fire Fighting Services extinguishing actions, by means of the set of $\delta_{n,i}$ coefficients – described on paragraph 6.4.3.2.3.1, Table 6-21 and Figure 6-22, affecting the value of $q_{f,d}$ – they are always referring only to the air temperature but never to the structural elements surface temperature. Therefore, they are not able to describe their cooling effect when applied directly on structural elements surface, which is a part of the aim of this chapter.

As a consequence of this fact, the characterization of surface cooling processes (especially the determination of the surface cooling rate and its duration) must start either / both from experimental available data or / and from results of simulations developed through techniques of Computational Fluid Dynamics, both also of particular usefulness to complete environmental cooling characterization. Since – as it was explained in the Chapter concerning the state-of-the-art – no available experimental results have been found regarding the temperature evolution of the surface of structural elements were water is directly applied, the development of Computational Fluid Dynamics simulations has been adopted in order to discern this question, analyses that are described in detail on next paragraphs.

6.4.3.2.4 Definition of the Cooling Profiles in sight of the results of Computational Fluid Dynamics Simulations.

Within this paragraph, the development of a Computational Fluid Dynamics simulation of a natural fire in an office is addressed. The basic aim of this simulation is to arrange more information about the temperature evolution of the surface of structural elements where a water jet/spray is directly applied, since this is a basic information needed to discern the cooling effect on the hygro-thermo-chemo-mechanical state of a structural element manufactured with High-Strength concrete. However, it must be remarked – as it was already done in the introduction to this Chapter – that the precise featuring of the Fire Fighting Services cooling actions is not a purpose of this Thesis and in any case will need independent research works.

6.4.3.2.4.1 Introduction to the Computational Fluid Dynamics (CFD) and Fire Dynamics Simulator (FDS) Software.

The idea that the dynamics of a fire might be studied numerically dates back to the beginning of the computer age. Indeed, the fundamental conservation equations governing fluid dynamics, heat transfer, and combustion were first written down over a century ago. Despite this, practical mathematical models of fire (as distinct from controlled combustion) are relatively recent due to the inherent complexity of the problem. Indeed, in his brief history of the early days of fire research, Hoyt Hottel noted '*A case can be made for fire being, next to the life processes, the most complex of phenomena to understand*' [48].

The difficulties revolve about three issues: First, there are an enormous number of possible fire scenarios to consider due to their accidental nature. Second, the physical insight and computing power required to perform all the necessary calculations for most fire scenarios are limited. Any fundamentally based study of fires must consider at least some aspects of bluff body aerodynamics, multi-phase flow, turbulent mixing and combustion, radiative transport, and conjugate heat transfer; all of which are active research areas in their own right. Finally, the "fuel" in most fires was never intended as such. Thus, the mathematical models and the data needed to characterize the degradation of the condensed phase materials that supply the fuel may not be available. Indeed, the mathematical modelling of the physical and chemical transformations of real materials as they burn is still in its infancy [48].

In order to make progress, the questions that are asked have to be greatly simplified. To begin with, instead of seeking a methodology that can be applied to all fire problems, we begin by looking at a few scenarios that seem to be most amenable to analysis. Hopefully, the methods developed to study these "simple" problems can be generalized over time so that more complex scenarios can be analyzed. Second, we must learn to live with idealized descriptions of fires and approximate solutions to our idealized equations. Finally, the methods should be capable of systematic improvement. As our physical insight and computing power grow more powerful, the methods of analysis can grow with them.

To date, three distinct approaches to the simulation of fires have emerged [48]. Each of these treats the fire as an inherently three dimensional process evolving in time. The first to reach maturity, the "zone" models, describe compartment fires. Each compartment is divided into two spatially homogeneous volumes, a hot upper layer and a cooler lower layer. Mass and energy balances are enforced for each layer, with additional models describing other physical processes appended as differential or algebraic equations as appropriate. Examples of such phenomena include fire plumes, flows through doors, windows and other vents, radiative and convective heat transfer, and solid fuel pyrolysis. Descriptions of the physical and mathematical assumptions behind the zone modelling concept are given in separate papers by several authors, who chronicle developments through 1983. Model development since then has progressed to the point where documented and supported software implementing these models are widely available.

The relative physical and computational simplicity of the zone models has led to their widespread use in the analysis of fire scenarios [48]. So long as detailed spatial distributions of physical properties are not required, and the two layer description reasonably approximates reality, these models are quite reliable. However, by their very nature, there is no way to systematically improve them. The rapid growth of computing power and the corresponding maturing of computational fluid dynamics (CFD, from now on), has led to the development of CFD based "field" models applied to fire research problems. Virtually all this work is based on the conceptual framework provided by the Reynolds-averaged form of the Navier-Stokes equations (RANS), in particular the k-ε turbulence model pioneered by Patankar and Spalding. The use of CFD models has allowed the description of fires in complex geometries, and the incorporation of a wide variety of physical phenomena. However, these models have a fundamental limitation for fire applications – the averaging procedure at the root of the model equations.

RANS models were developed as a time-averaged approximation to the conservation equations of fluid dynamics. While the precise nature of the averaging time is not specified, it is clearly long enough to require the introduction of large eddy transport coefficients to describe the unresolved fluxes of mass, momentum and energy. This is the root cause of the smoothed appearance of the results of even the most highly resolved fire simulations. The smallest resolvable length scales are determined by the product of the local velocity and the averaging time rather than the spatial resolution of the underlying computational grid. This property of RANS models is typically exploited in numerical computations by using implicit numerical techniques to take large time steps.

Unfortunately, the evolution of large eddy structures characteristic of most fire plumes is lost with such an approach, as is the prediction of local transient events. It is sometimes argued that the averaging process used to define the equations is an '*ensemble average*' over many replicates of the same experiment or postulated scenario. However, this is a moot point in fire research since neither experiments nor real scenarios are replicated in the sense required by that interpretation of the equations. The application of '*Large Eddy Simulation*' (LES) techniques to fire is aimed at extracting greater temporal and spatial fidelity from simulations of fire performed on the more finely meshed grids allowed by ever faster computers.

The phrase LES refers to the description of turbulent mixing of the gaseous fuel and combustion products with the local atmosphere surrounding the fire. This process, which determines the burning rate in most fires and controls the spread of smoke and hot gases, is extremely difficult to predict accurately. This is true not only in fire research but in almost all phenomena involving turbulent fluid motion. The basic idea behind the LES technique is that the eddies that account for most of the mixing are large enough to be calculated with reasonable accuracy from the equations of fluid dynamics. The hope (which must ultimately be justified by comparison to experiments) is that small-scale eddy motion can either be crudely accounted for or ignored.

The equations describing the transport of mass, momentum, and energy by the fire-induced flows must be simplified so that they can be efficiently solved for the fire scenarios of interest. The general equations of fluid dynamics describe a rich variety of physical processes, many of which have nothing to do with fires. Retaining this generality would lead to an enormously complex computational task that would shed very little additional insight on fire dynamics. The simplified equations, developed by Rehm and Baum, have been widely adopted by the larger combustion research community, where they are referred to as the '*low Mach number*' combustion equations. They describe the low speed motion of a gas driven by chemical heat release and buoyancy forces. Oran and Boris provide a useful discussion of the technique as

applied to various reactive flow regimes, commenting that '*There is generally a heavy price for being able to use a single algorithm for both fast and slow flows, a price that translates into many computer operations per time step often spent in solving multiple and complicated matrix operations.*'.

The low Mach number equations are solved numerically by dividing the physical space where the fire is to be simulated into a large number of rectangular cells. Within each cell the gas velocity, temperature, etc., are assumed to be uniform; changing only with time. The accuracy with which the fire dynamics can be simulated depends on the number of cells that can be incorporated into the simulation. This number is ultimately limited by the computing power available. Present day, single processor desktop computers limit the number of such cells to at most a few million. This means that the ratio of largest to smallest eddy length scales that can be resolved by the computation (the '*dynamic range*' of the simulation) is on the order of 100. Parallel processing can be used to extend this range to some extent, but the range of length scales that need to be accounted for if all relevant fire processes are to be simulated is roughly 104 to 105 because combustion processes take place at length scales of 1 mm or less, while the length scales associated with building fires are of the order of tens of meters.

The software selected for the Computational Fluid Dynamics simulations to develop in this Chapter, the *Fire Dynamics Simulator* (FDS from now on) [48,49], is a Computational Fluid Dynamics (CFD) model of fire-driven fluid flow. The model solves numerically a form of the Navier-Stokes equations appropriate for low-speed, thermally-driven flow with an emphasis on smoke and heat transport from fires. The partial derivatives of the conservation equations of mass, momentum and energy are approximated as finite differences, and the solution is updated in time on a three-dimensional, rectilinear grid. Thermal radiation is computed using a finite volume technique on the same grid as the flow solver. Lagrangian particles are used to simulate smoke movement, sprinkler or water spray discharges, and fuel sprays.

Version 1 of FDS was publicly released in February 2000, version 2 in December 2001, version 3 in November 2002, and version 4 in July 2004. The version of FDS used in this Chapter is version 5, first released in October 2007 and, more precisely, the version FDS 5.2.

Smokeview [48,49] is a companion program to FDS that produces images and animations of the results. In recent years, its developer, Glenn Forney, has added to Smokeview the ability to visualize fire and smoke in a fairly realistic way. In a sense, Smokeview 5.2.2 now is, via its three-dimensional renderings, an integral part of the physical model, as it allows one to assess the visibility within a fire compartment in ways that ordinary scientific visualization software cannot.

6.4.3.2.4.2 The case analyzed with the Fire Dynamics Simulator (FDS) Software.

The selected case, through which more information about the temperature evolution of the surface of structural elements where a water jet/spray is directly applied is to be arranged – since this is a basic information needed to discern the cooling effect on the hygro-thermo-chemo-mechanical state of a structural element manufactured with High-Strength concrete – consists of an actual typical-plan office of $A_f = 43{,}12\ m^2$, a total walls surface of $A_t = 152{,}70\ m^2$ and 2,50 m in height:

the selected office is the office where this Thesis is being written, owned by the PhD Student and writer, as it constitutes a typical-plan office common to many High-Rise Buildings

in a building exclusively containing offices. The building is composed by seven offices per floor – each of similar plan – with a common corridor where a hose system with lay-flat hose is placed (the lecture of its manometer gives a 3,5 bar pressure).

The model ortho-plan of the office is shown on next figure:

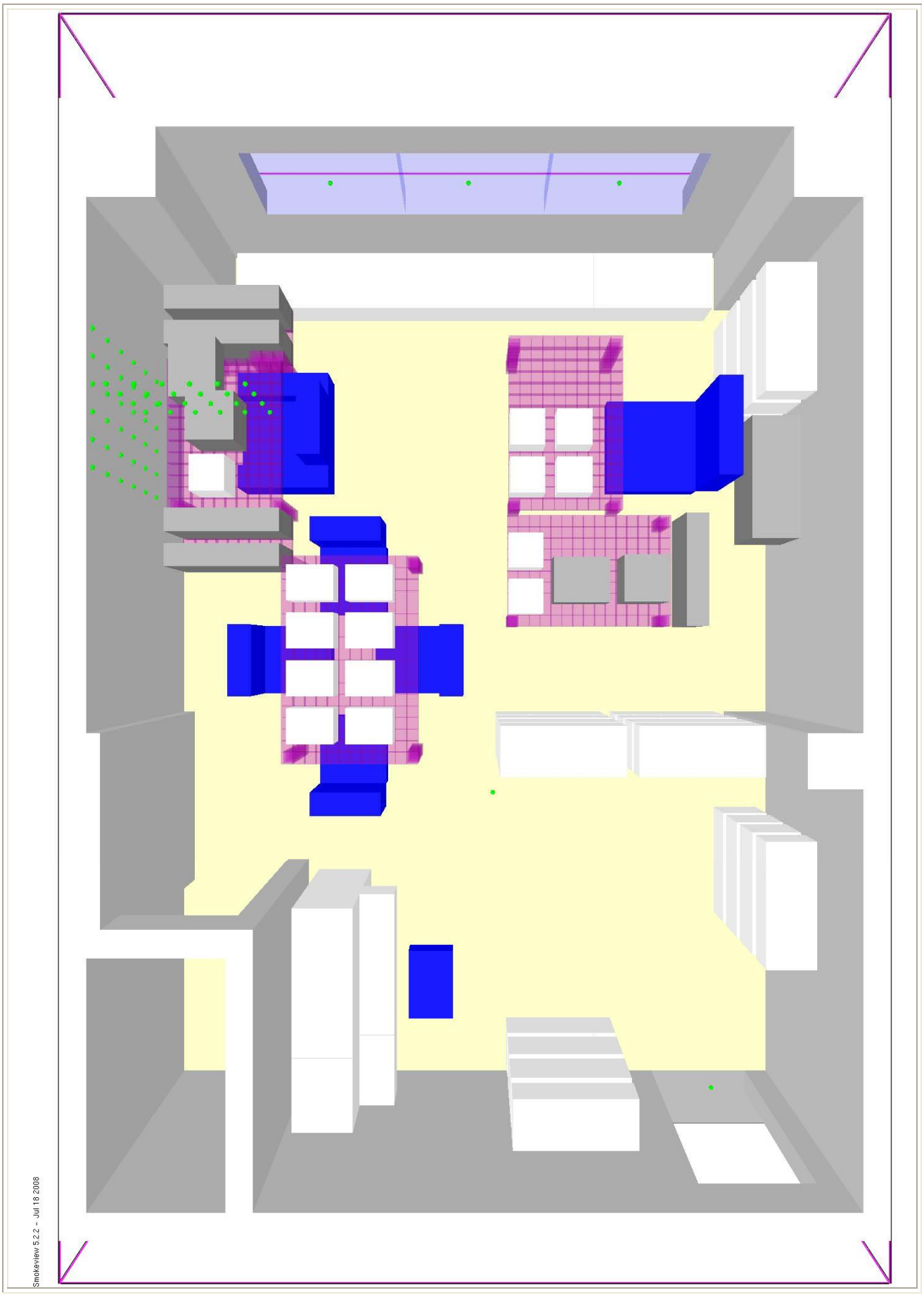

Figure 6-25. *Ortho-Plan of Guerrero's Office, selected for the Computational Fluid Dynamics Simulations developed herein.*

The selected office presents an opening coefficient of 0,061 $m^{1/2}$ due to three 1,60m·1,30m glass windows in its northern (outer) façade and a 0,70m·2,10m wooden door in its southern façade (corridor common to the seven offices in the floor), with a total opening area of A_o = 7,71 m^2 and an averaged opening height of 1,53 m. Initially, both the window farther from the fire starting focus and the door are considered to be open; the other two windows are initially closed and with a breakage temperature set on 300 ºC (temperatures progressively reached in the calculation) deducted from [50].

Its main furnace content is composed by glass and metal tables and shelves, upholstery chairs and armchairs and a wooden-made piano. Upholstered furniture makes up a significant fraction of the combustible load. A single couch can generate several megawatts of energy and sometimes lead to compartment flashover, as it is observed in the simulation of this case. Modelling a couch fire requires a simplification of its structure and materials. At the very least, we want the upholstery to be described as fabric covering foam:

```
&MATL   ID =                        'FABRIC'
        FYI =                       'Properties completely fabricated'
        SPECIFIC_HEAT =             1.0
        CONDUCTIVITY =              0.1
        DENSITY =                   100.0
        N_REACTIONS =               1
        NU_FUEL =                   1.
        REFERENCE_TEMPERATURE =     350.
        HEAT_OF_REACTION =          3000.
        HEAT_OF_COMBUSTION =        15000. /

&MATL   ID =                        'FOAM'
        FYI =                       'Properties completely fabricated'
        SPECIFIC_HEAT =             1.0
        CONDUCTIVITY =              0.05
        DENSITY =                   40.0
        N_REACTIONS =               1
        NU_FUEL =                   1.
        REFERENCE_TEMPERATURE =     350.
        HEAT_OF_REACTION =          1500.
        HEAT_OF_COMBUSTION =        30000. /

&SURF   ID =                        'UPHOLSTERY'
        FYI =                       'Properties completely fabricated'
        COLOR =                     'PURPLE'
        BURN_AWAY =                 .TRUE.
        MATL_ID(1:2,1) =            'FABRIC','FOAM'
        THICKNESS(1:2) =            0.002,0.1 /
```

Both the fabric and the foam decompose into fuel gases via single-step reactions. The fuel gases from each have different composition and heats of combustion. FDS automatically adjusts the mass loss rate of each. The attribute BURN_AWAY forces FDS to break up the couch into individual cell-sized blocks that will disappear from the calculation as soon as the fuel is exhausted (what is observed on the following figures in this Chapter). The surface is specified as consisting of two layers, with a thickness of 2 mm for the FABRIC and 10 cm for the FOAM. The 10 cm is chosen to be the same as the mesh cell size.

The existing fire load is also constituted by a considerable amount of books and paper articles used for this Thesis writing and almost uniformly distributed both in the shelves and in the several tables. Although the floor of the actual office is marble made, the floor considered in the simulation includes a carpet in order to accelerate the instant when high surface temperatures are reached and extinguishing is started (remember that this simulation is not addressed to the heating but to the forced cooling stage, and that the computational time of this model already exceeds six days). Some more details on the case geometry and model are included on the actual photographs and Smokeview [48,49] detailed drawings included next:

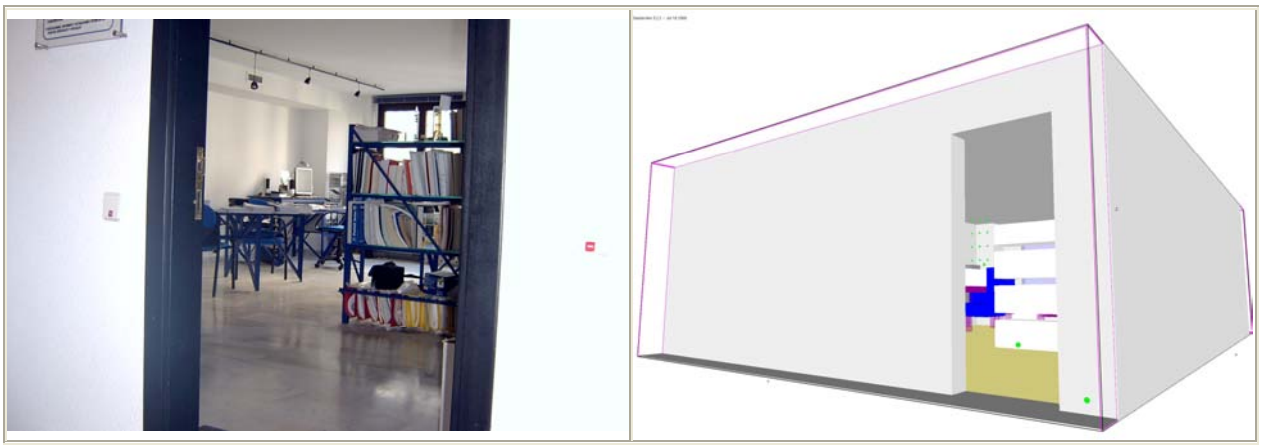

Figure 6-26. *Detail of the door entrance, from the corridor.*

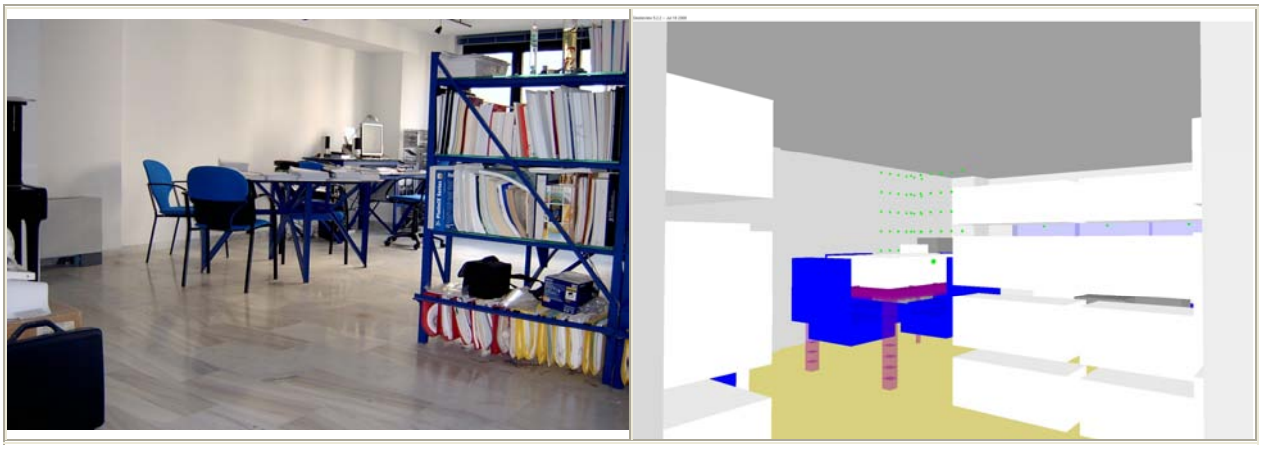

Figure 6-27. *Detail of the inner view, from the door entrance. This is the first location of the fire-fighter, at 1.260 seconds.*

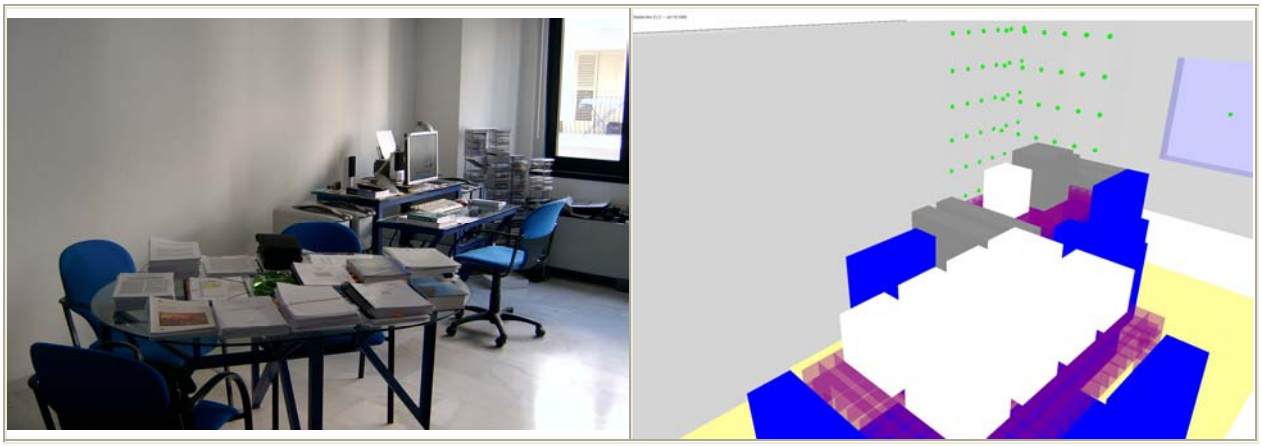

Figure 6-28. *Detail of the computers table, where fire begins, from the middle of the office. This is the position from which the fire-fighter applies the water jet on the wall behind the computers table, at 1.380 seconds (observe sensors rosette in the model).*

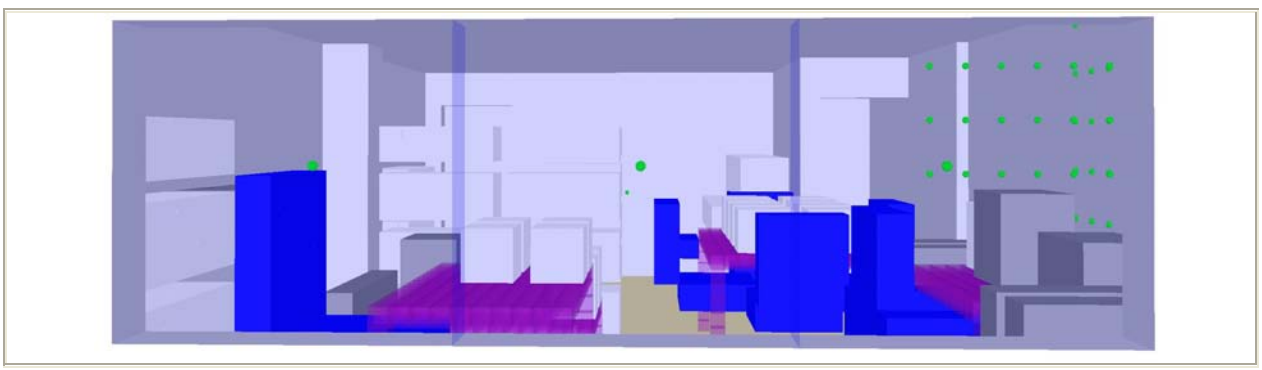

Figure 6-29. *Detail of the office's view from outside the northern façade windows (observe temperature sensor at each window).*

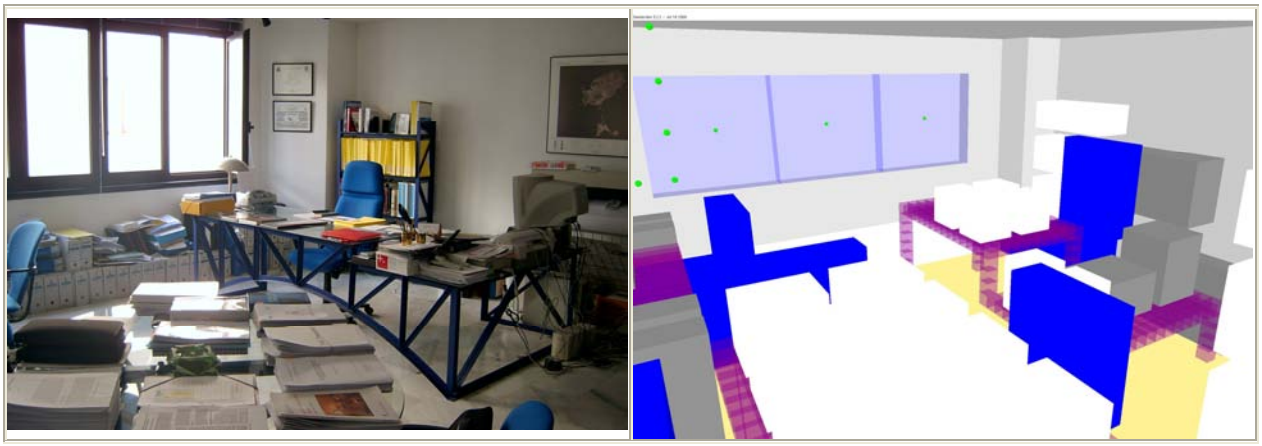

Figure 6-30. *Detail of the windows and the east part of the office, from the middle of the office. The window on the right side (east) is open from the beginning of the calculation. The other windows, centre and left or middle and west, are closed until their breakage temperature is reached (300 ºC).*

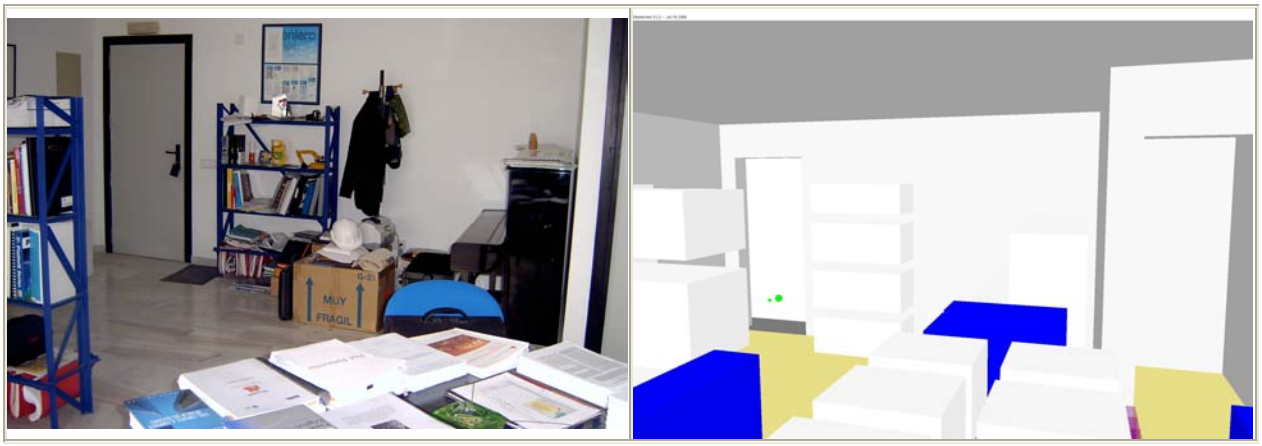

Figure 6-31. *Detail of the entrance zone, from the middle of the office.*

The structural elements surrounding the office are mainly composed by a 18,8 centimetres layer of concrete and a 12 millimetres lining of gypsum plaster. Taking into account the purpose of this simulation, at least we need to define the following material properties:

```
&MATL   ID =                    'GYPSUM PLASTER'
        FYI =                   'Quintiere, Fire Behavior'
        CONDUCTIVITY =          0.48
        SPECIFIC_HEAT =         0.84
        DENSITY =               1440. /

&MATL   ID =                    'CONCRETE'
        FYI =                   'Quintiere, Fire Behavior'
        CONDUCTIVITY =          1.8079
        SPECIFIC_HEAT =         0.855
        DENSITY =               2627.4 /

&SURF   ID =                    'WALL'
        RGB =                   200,200,200
        MATL_ID(1:2,1) =        'GYPSUM PLASTER','CONCRETE'
        THICKNESS(1:2) =        0.012,0.188 /
```

The mesh used consists of 135.000 cells uniformly distributed and sizing $0{,}10 \cdot 0{,}10 \cdot 0{,}10$ metres. The model includes a part of both the corridor and the outer environment in order to appreciate better the smoke evacuation. The complete input files of the FDS model are included on the Annexes of this Chapter.

An initially specified fire is modelled as the ejection of gaseous fuel from a solid surface or vent. This is essentially a burner, with a specified Heat Release Rate Per Unit Area, HRRPUA, in units of kW/m^2. In this case, the burner is defined as:

&SURF ID='BURNER', HRRPUA=1000., COLOR='RASPBERRY' /

applying 1.000 kW/m^2 to any surface with the attribute SURF_ID=’FIRE’:

&VENT XB= 5.80, 5.90, 4.20, 4.30, 0.60, 0.60, SURF_ID='BURNER' / Ignition source on computers table

which is a 0,10 · 0,10 metres burning surface placed on the cushion of the chair next to the computers table, so the total Heat Release Rate applied in the simulation is 10 kW.

Concerning the definition of the extinguishing action, a fire-fighter is supposed to act handling the hose system with lay-flat hose existing in the corridor (5 metres away from the door entrance) in the following stages:

Figure 6-32. *Photographs of the hose-nozzle employed by the fire-fighter.*

a) Fire fighter arrives to the office corridor at 20 minutes (1.200 seconds) from the start of the fire (the office is only at a second floor, but nine kilometres away from the fire fighting service headquarters and inside a town with narrow streets).

b) 60 seconds later, at 1.260 seconds, fire fighter is placed on the door handling the hose-nozzle (figure 6-27). Since the smoke layer is almost at the floor level at this instant, his first extinguishing actions are applying the water jet (the more atomized the merrier) towards the upper smoke layer. Three sweeps are simulated at 1.260 seconds, 1.300 seconds and 1.340 seconds with a duration of 10 seconds each. The intention of this series of real-purpose sweeps is to reproduce the 120 seconds period included in the simulation where environment temperature is supposed to remain constant before the surface cooling process starts.

c) After the third ‘smoke-spraying sweep’ is finished, at 1.350 seconds, the fire fighter squats and moves inwards until the middle of the office (figure 6-28). There, at 1.380 seconds he addresses the water jet to the wall behind the computers table (where fire was initiated) in order to cool it during a period of 10 seconds. In this case, the water jet has been concentrated (the nozzle has been partially closed) in order to reach better the overheated wall.

The main features of the water jet are those described next:

```
&PART    ID =                      ‘water’,
         WATER =                   .TRUE.,
         QUANTITIES =              'DROPLET_DIAMETER',
         AGE =                     30.,
         DIAMETER =                1000.,
         GAMMA_D =                 2.4,
         DROPLETS_PER_SECOND =     3000,
         DT_INSERT =               0.01      /
```

```
&PROP   ID =                  'nozzle_1',
        PART_ID =             'water',
        FLOW_RATE =           96 and 220,
        SPRAY_ANGLE =         3.,20.,
        DROPLET_VELOCITY =    8. /
&PROP   ID =                  'nozzle_2',
        PART_ID =             'water',
        FLOW_RATE =           96 and 220,
        SPRAY_ANGLE =         3.,6.,
        DROPLET_VELOCITY =    10. /
```

where '*nozzle_1*' is the configuration used from the door site and '*nozzle_2*' is that corresponding to the water jet applied to the wall, and whose meanings are detailed next:

Parameter	**Nozzle 1**	**Nozzle 2**
Median volumetric diameter of droplets, with the distribution assumed to be a combination of Rosin-Rammler and log-normal [μm]	1.000	
Width of the droplets distribution	2,4	
Maximum lifetime of droplets [seconds]	30	
Flow rate [liters/minute]	96 and 200 (see explanation below)	
Spray Angle [º]: A pair of angles (in degrees) through which the droplets are sprayed. The angles outline a conical spray pattern relative to the south pole of the sphere centered at the sprinkler with radius OFFSET (assumed 0 in this case). For example, SPRAY_ANGLE=30.,80. directs the water droplets to leave the nozzle through a band between 60º and 10º south latitude, assuming the orientation of the sprinkler is (0,0,-1). The droplets are uniformly distributed within this belt.	3 / 20	3 / 6
Droplet Initial Velocity [m/s]	8	10
Orientation (triplet)	1.0,0.95,3.00	1.0,0.95,0.80

Table 6-25. *Main features of the water spray / jet used in the simulations.*

Within the extinguishing parameters to define for the simulation, the water flow rate is a determinant factor since it governs the amount of heat exchange between the heated surface where the water jet is applied and the droplets.

Currently, in Spanish regulations there is not a minimum prescribed flow-rate for the hose systems with lay-flat hoses whereas a minimum dynamic pressure at the nozzle hole with a value of 2 bar is prescribed on paragraph 7.3 of the Appendix 1 of the Royal Decree 1942/1993, of 5 of November, by which it is approved the Regulation about the Installations for Protection from Fire [51]:

"../..

La red de tuberías deberá proporcionar, durante una hora, como mínimo, en la hipótesis de funcionamiento simultáneo de las dos BIE hidráulicamente más desfavorables, una presión dinámica mínima de 2 bar en el orificio de salida de cualquier BIE.

../.."

Nevertheless, prior major regulations effectively prescribed a minimum flow-rate at each hose which is nowadays still applied for the water supply systems dimensioning [52]. Hence, on the paragraph 4.2.2.1.d of the Royal Decree 2059/1991 by which it is approved the Basic Edification Rule for the Protection from Fires NBE-CPI/82, a minimum flow-rate of 1,6 l/sec was prescribed for lay-flat hoses of 25 millimetres (which is the most common and that actually installed in the selected case – see photographs in figure 6-32 –):

"../..

d)

La red de tuberías será de acero, de uso exclusivo para instalaciones de protección contra incendios y deberá diseñarse de manera que queden garantizadas, en cualquiera de las bocas de incendio equipadas, las siguientes condiciones de funcionamiento:

- La presión dinámica en punta de lanza será como mínimo de 3,5 kg/cm² (344 kPa) y como máximo de 5 kg/cm² (490 kPa).
- Los caudales mínimos serán de 1,6 l/s para bocas de 25 mm y 3,3 l/s para bocas de 45 mm.

Estas condiciones de presión y caudal se deberán mantener durante una hora, bajo la hipótesis de funcionamiento simultáneo de las dos bocas hidráulicamente más desfavorables.

../.."

Therefore, a general simulation with a flow-rate of 96 l/min (1,6 l/sec) will be developed for most of the cases since it is the most common installation in Spain. However, since lay-flat hoses of 45 millimetres can also be (more rarely) found in some Spanish High-Rise Buildings, for which a minimum flow-rate of 3,3 l/s is prescribe – 198 l/sec –, a second flow-rate value of 220 l/sec will also be accounted for in some particular cases (a bit oversized in order to include possible situations with peak values of pressure).

Finally, a rosette of thermocouples is introduced in the model to evaluate both the environment and the wall surface temperature evolution at several locations. Their locations have been strategically chosen in the zone where the water jet is applied at 1.380 seconds, including 36 thermocouples in the wall behind the computers table – to analyze the dispersion in the time-temperature curves at different points – and 24 thermocouples in the environment close to the wall. Next figures show the thermocouples distribution. The thermocouples are equidistantly placed to measure temperature each 20 centimetres in the horizontal direction and each 30 centimetres in the vertical one.

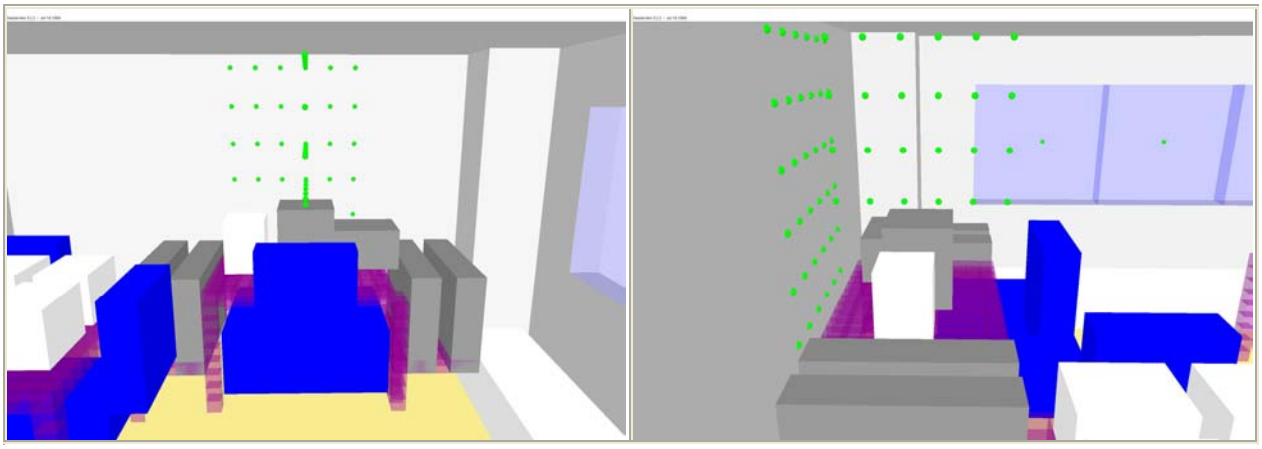

Figure 6-33. *Detail on the thermocouples distribution: left: wall surface; right: environment.*

X [m] / Z [m]	5,30	5,50	5,70	5,90	6,10	6,30
2,40	WALL11	WALL12	WALL13	WALL14	WALL15	WALL16
2,10	WALL21	WALL22	WALL23	WALL24	WALL25	WALL26
1,80	WALL31	WALL32	WALL33	WALL34	WALL35	WALL36
1,50	WALL41	WALL42	WALL43	WALL44	WALL45	WALL46
1,20	WALL51	WALL52	WALL53	WALL54	WALL55	WALL56
0,90	WALL61	WALL62	WALL63	WALL64	WALL65	WALL66

5,40	5,20	5,00	4,80	4,60	4,40	Y [m] / Z [m]
ENV11	ENV12	ENV13	ENV14	ENV15	ENV16	**2,40**
ENV21	ENV22	ENV23	ENV24	ENV25	ENV26	**2,10**
ENV31	ENV32	ENV33	ENV34	ENV35	ENV36	**1,80**
ENV41	ENV42	ENV43	ENV44	ENV45	ENV46	**1,50**

Table 6-26. *Thermocouples distribution, coordinates and nomenclature: lets: wall surface; right: environment.*

6.4.3.2.4.3 The main Results of the Computational Fluid Dynamics Simulations.

First of all, the main events happening during the fire evolution are shown on next figures:

119,5 s: Fire at chair cushion after 2 minutes of ignition.

360,0 s: The west window breaks due to its temperature (300 ºC).

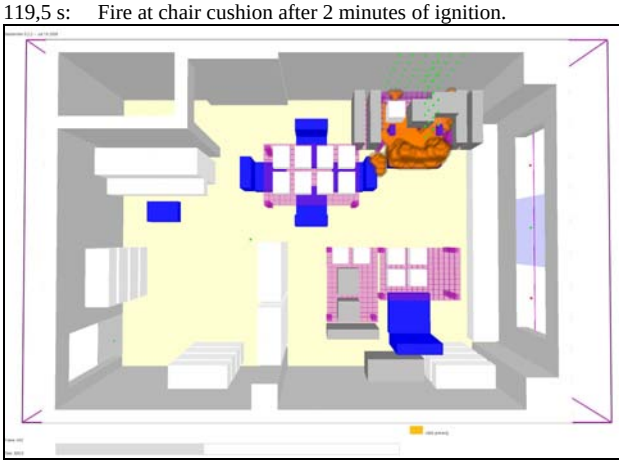

600,5 s: Fire begins to spread to neighbouring furniture after 10 min.

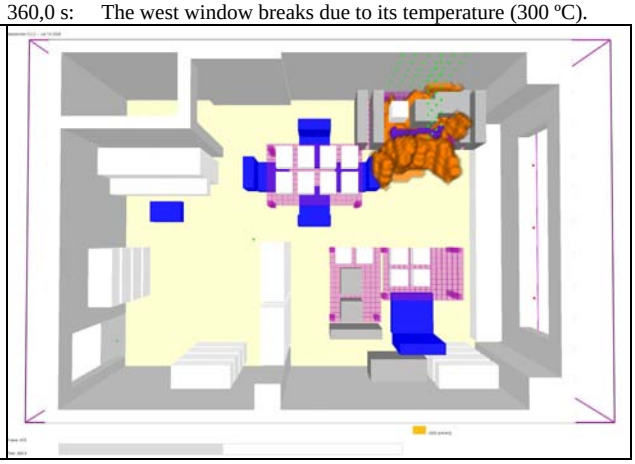

664,4 s: The middle window breaks due to its temperature.

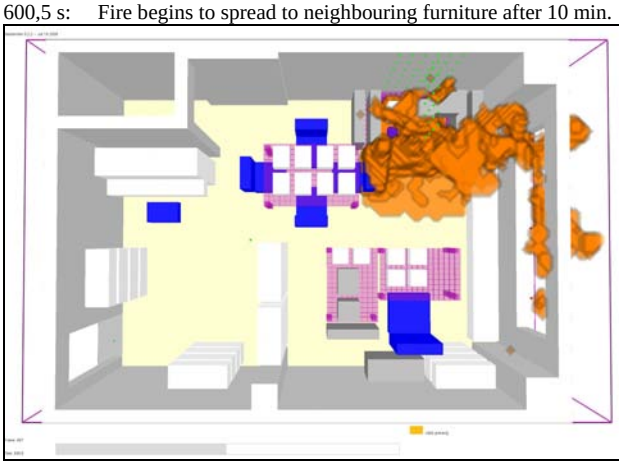

690,8 s: Big contribution of oxygen due to the middle window break.

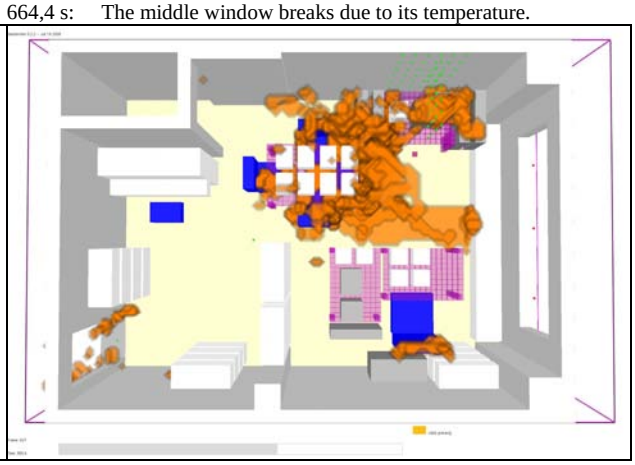

885,4 s:Flames reach the entrance door. Flashover has already happened.

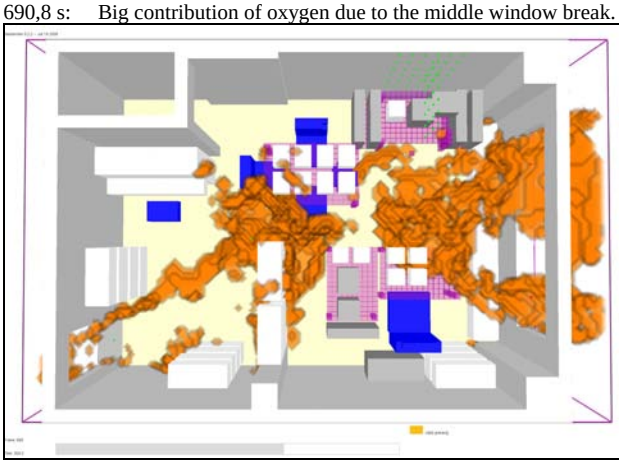

924,3 s: Flames are spread all around. Outer fire plume is considerable.

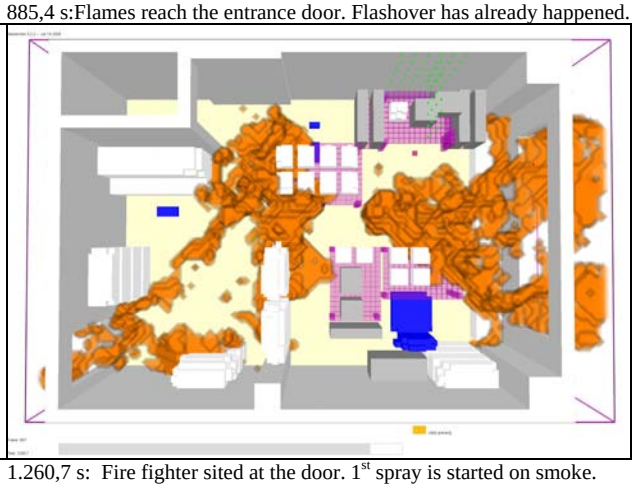

1.260,7 s: Fire fighter sited at the door. 1st spray is started on smoke.

1.271,8 s: Just after the end of the 1st spray application on smoke.

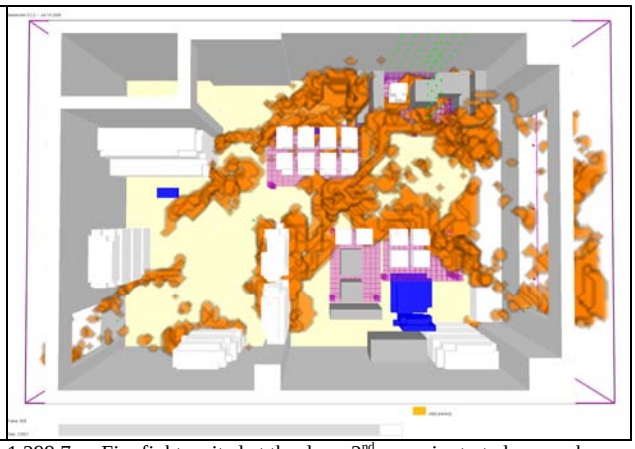

1.299,7 s: Fire fighter sited at the door. 2nd spray is started on smoke.

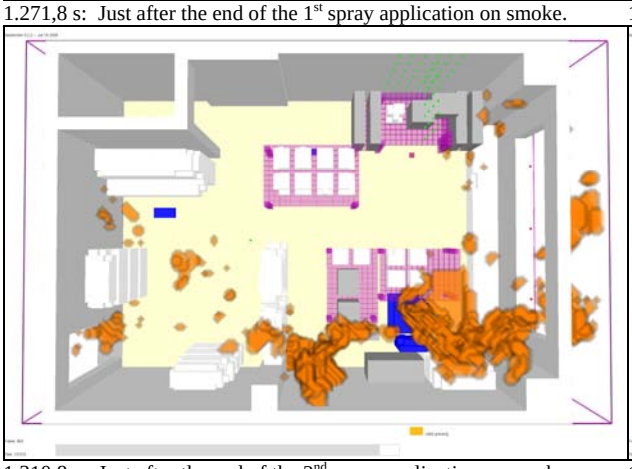

1.310,8 s: Just after the end of the 2nd spray application on smoke.

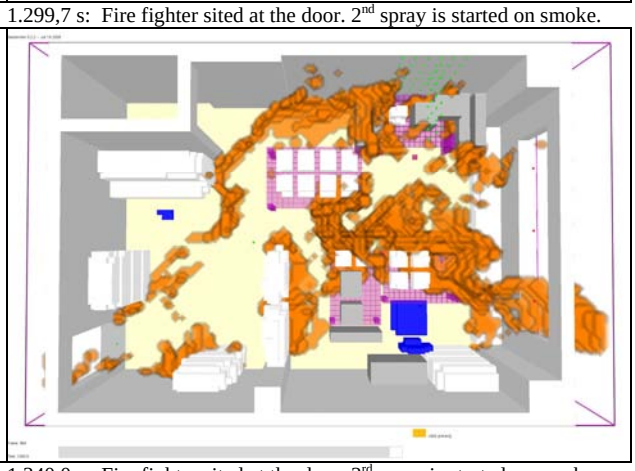

1.340,0 s: Fire fighter sited at the door. 3rd spray is started on smoke.

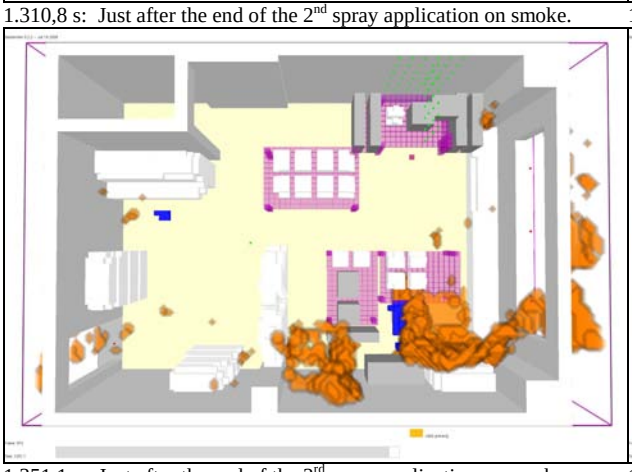

1.351,1 s: Just after the end of the 3rd spray application on smoke.

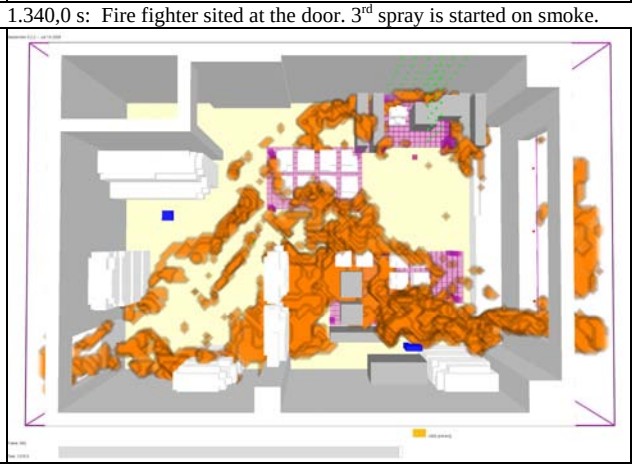

1.378,9 s: Fire fighter is sited at the middle of the office. Water jet is applied to the wall behind the computers table.

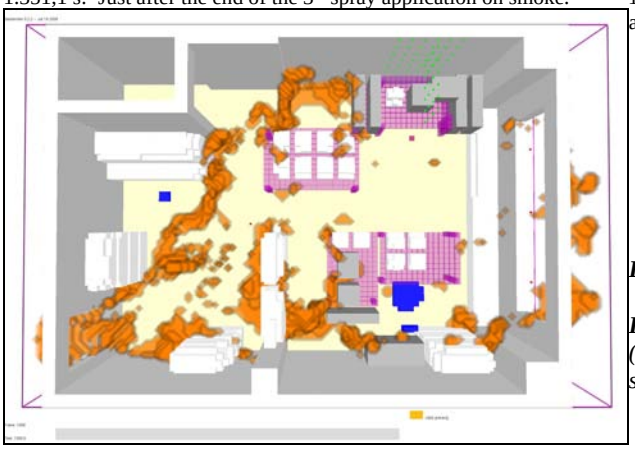

1.390,0 s: End of the application of the water jet on the wall surface.

Figure 6-34. *Fire evolution at several stages of the simulation.*

Remark: *note that upholstery furniture and other burning items (books) have been progressively disappearing from the simulation model due to its complete burning.*

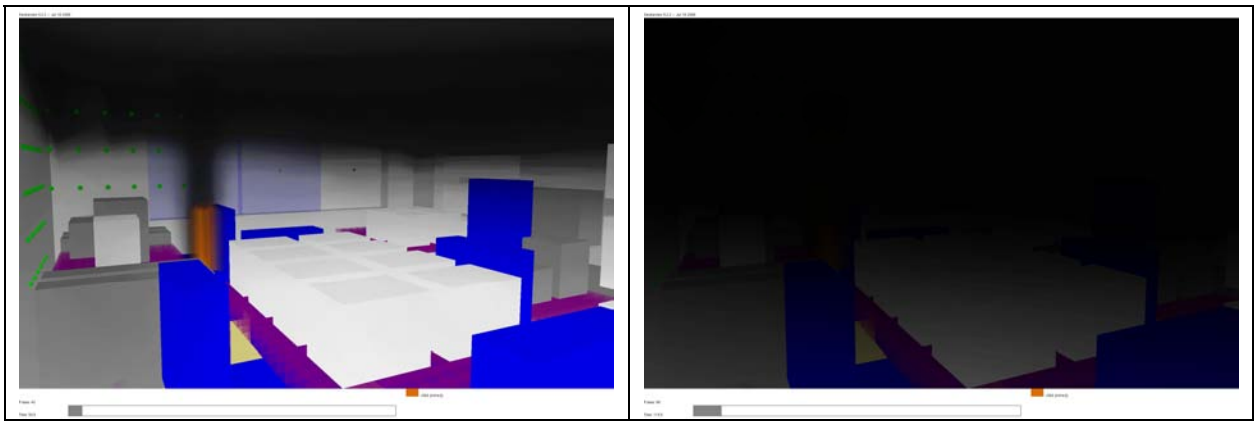

59,8 s: Smoke after 1 minute from fire ignition. 119,5 s: Smoke after 2 minutes from fire ignition.

Figure 6-35. *Detail on the loss of visibility, from the eyes height of a standing 1,70 m person, during the first two minutes.*

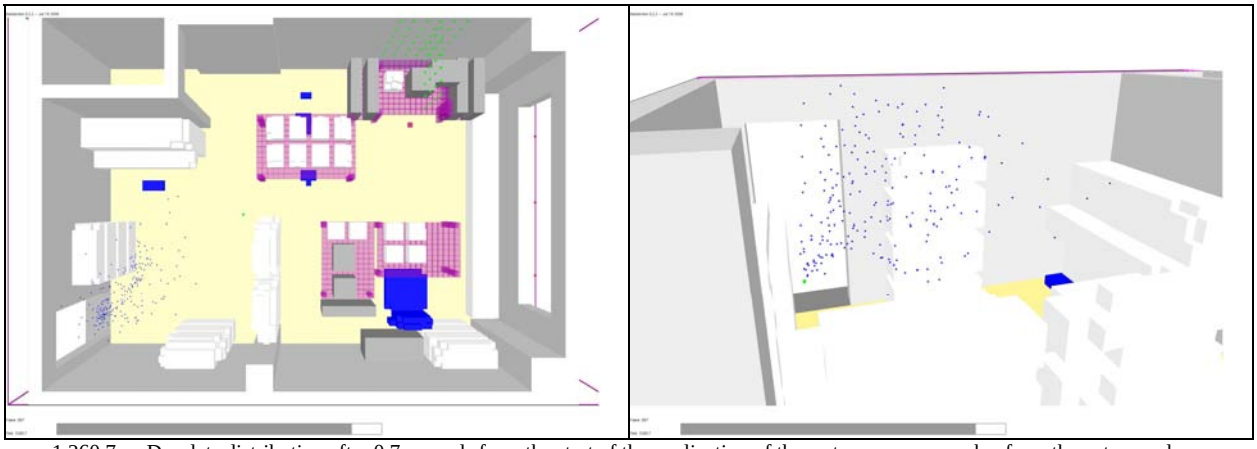

1.260,7 s: Droplets distribution after 0,7 seconds from the start of the application of the water spray on smoke, from the entrance door.

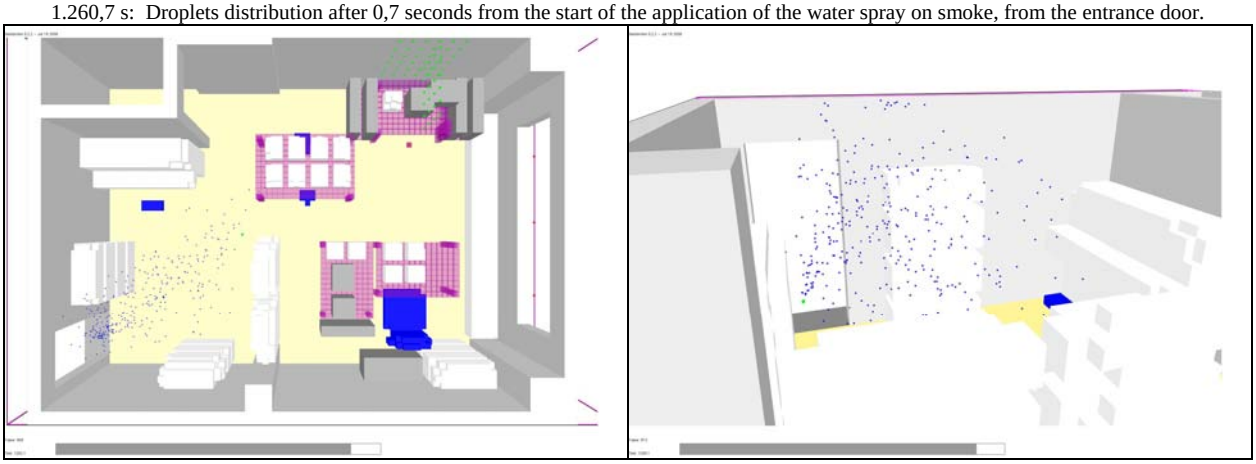

1.262,1 s: Water droplets 2,1 seconds after the first spray start. 1.269,1 s: Water droplets 9,1 seconds after the first spray start.

Figure 6-35. *Detail on the water droplets from the first spray applied to smoke.*

Figure 6-36 shows the complete sequence of the application of the water jet on the wall behind the computers table.

As it will be also observed in the graphics corresponding to the evolution of the temperature of the wall, the wall surface cooling is not only due to the cooling effect of the droplets that impact directly against it but also to those descending on the wall surface from the ceiling and upper zones of the wall.

It is remarkable that, within the calculations developed, the floor has been assumed to be porous in order to avoid extending unnecessarily the computational time needed to track the water particles by the floor once they reach it.

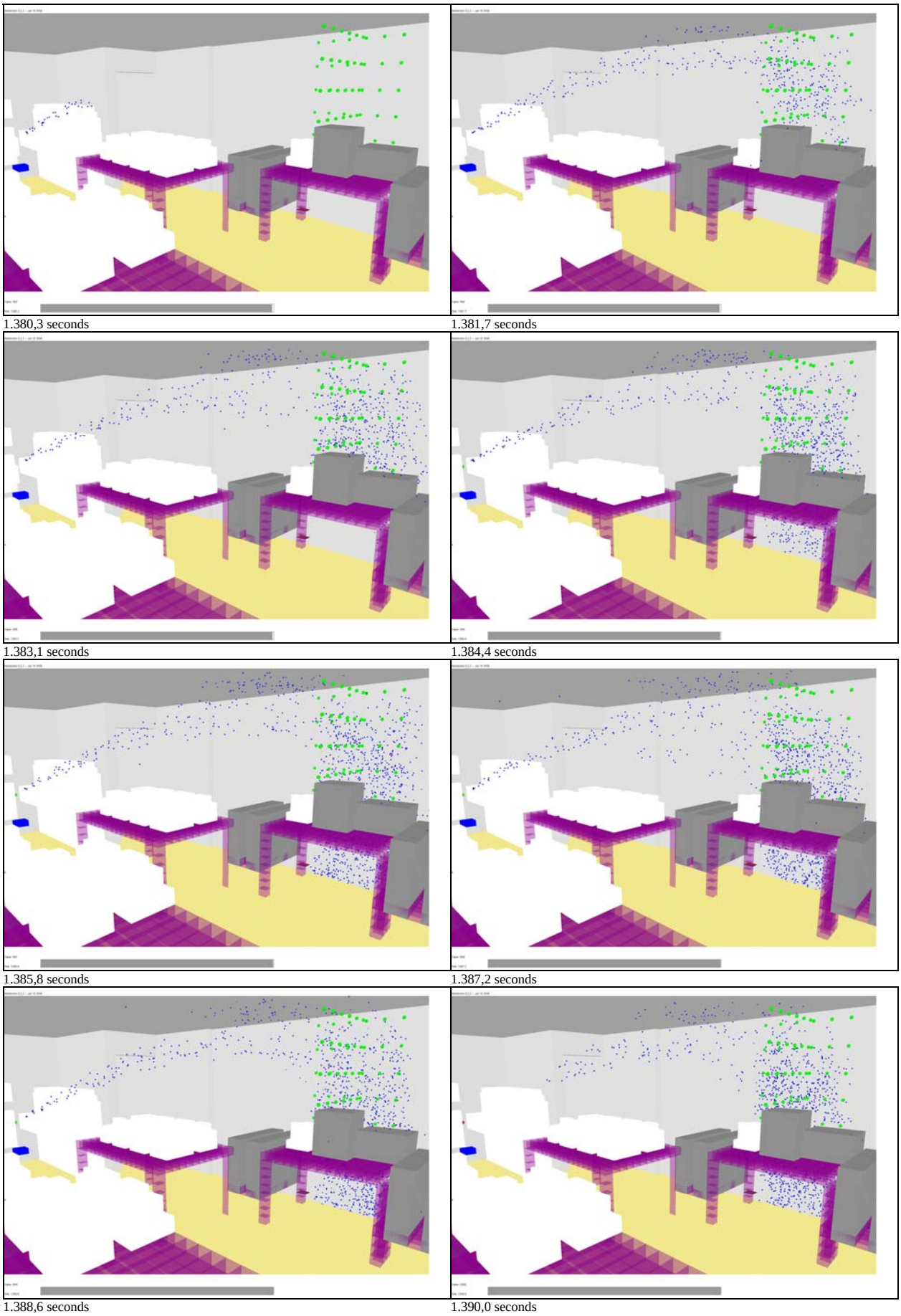

Figure 6-36. *Complete sequence of the application of the water jet on the wall surface (flow-rate 220 l/min) – represented: 3.000 droplets/sec –.*

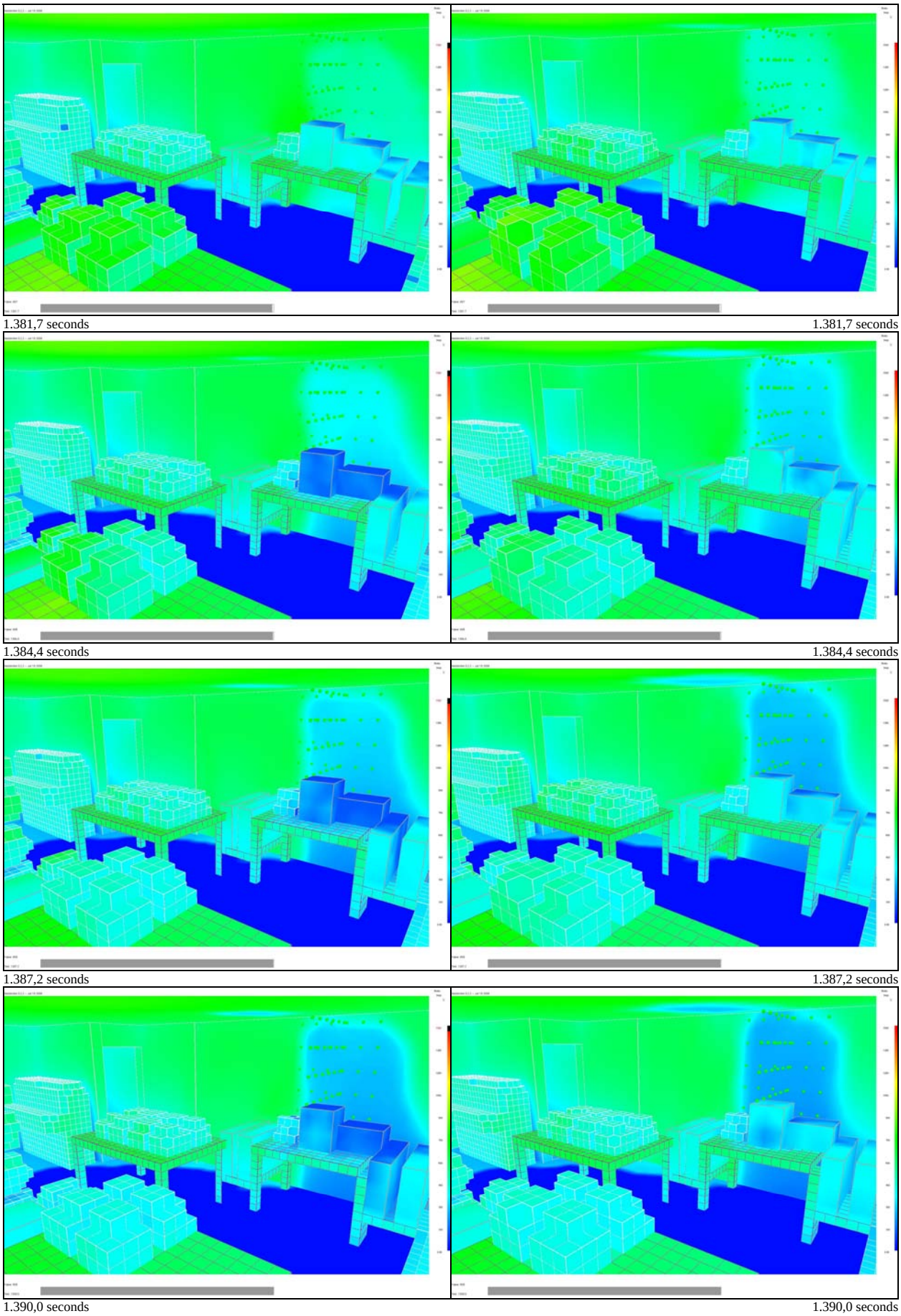

Flow rate: 96 l/min ***Figure 6-37.*** *Temperature evolution of the wall during the application of the water jet on its surface.* ***Flow rate: 220 l/min***

Concerning the main features of the water jet applied on the wall, the following variables and combinations have been considered in order to dispose of information as wide as possible about its effect:

Case name	*Droplets mean diameter [μm]*	*Flow-Rate [l/min]*	*Cone Angle [º]*	*Initial velocity [m/s]*	*Related Figures*	*Related Tables*
Office – 20	250	96	3º - 6º	10	6-40.a to 6-40.c	6-28.a
Office – 22			3º - 13º		6-40.d to 6-40.f	6-28.b
Office – 23			3º - 20º		6-40.g to 6-40.i	6-28.c
Office – 24			3º - 30º		6-40.j to 6-40.l	6-28.d
Office – 25			3º - 40º		6-40.m to 6-40.o	6-28.e
Office – 26			3º - 60º		6-40.p to 6-40.r	6-28.f
Office – 19	500		3º - 6º		6-41.a to 6-41.c	6-28.g
Office – 10	1.000		3º - 6º		6-42.a to 6-42.c	6-28.h
Office – 12			3º - 13º		6-42.d to 6-42.f	6-28.i
Office – 11			3º - 20º		6-42.g to 6-42.i	6-28.j
Office – 15			3º - 30º		6-42.j to 6-42.l	6-28.k
Office – 16			3º - 40º		6-42.m to 6-42.o	6-28.l
Office – 17			3º - 60º		6-42.p to 6-42.r	6-28.m
Office – 14			3º - 20º	15	6-43.a to 6-43.c	6-28.n
Office – 13			3º - 40º		6-44.a to 6-44.c	6-28.o
Office – 7		220	3º - 6º	10	6-45.a to 6-45.c	6-28.p

Table 6-27. *Atlas of cases analyzed to discern the wall surface cooling rate to adopt in the calculations.*

Figures 6-40 to 6-45 show the results corresponding to each of the cases detailed on Table 6-27. However figure 6-38 collects all of these results, showing the mean value of the cooling rate and the standard deviation found for each case:

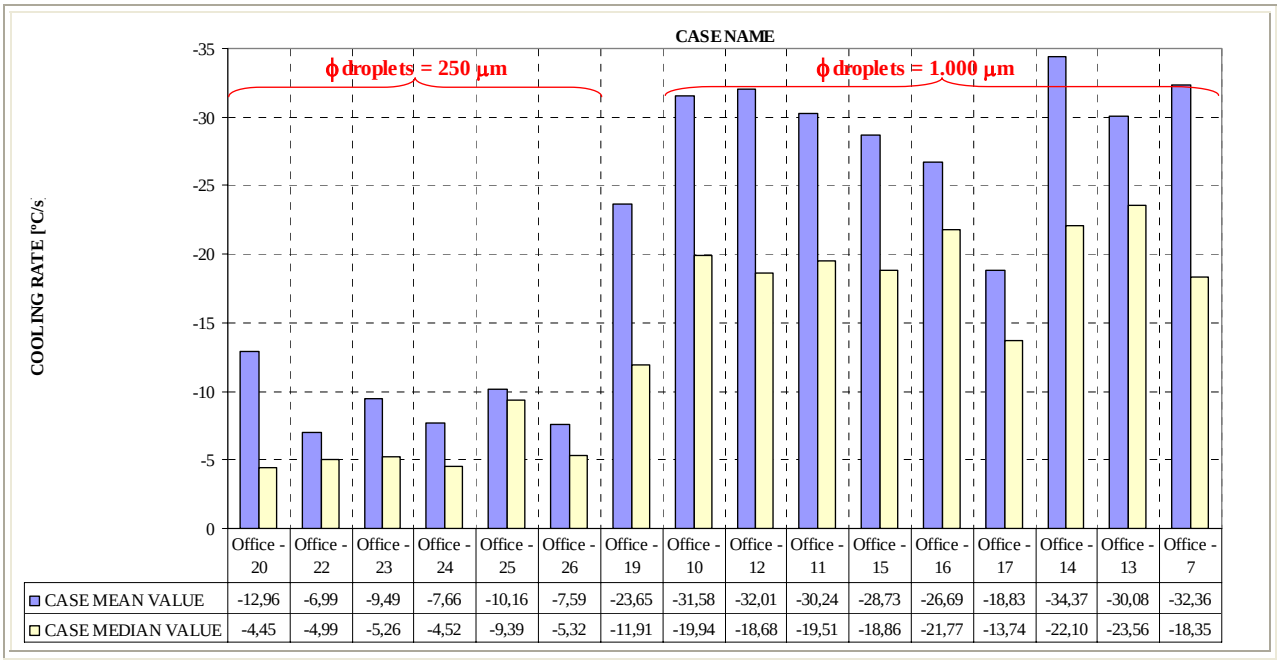

Figure 6-38. *Mean and median values of the cooling rate found for each of the analyzed cases.*

From figures 6-40 to 6-45 and Tables 6-28.a to 6-28.p it is observed that, for a flow-rate of 96 l/min, the overall mean value of the surface cooling rate (taking into account all the temperature lecture points) is extremely dependent on the initial value of the mean diameter of the droplets and less dependent (comparatively talking) on the cone angle of the water jet and on the initial velocity of the droplets.

This fact can be easily observed on figure 6-39:

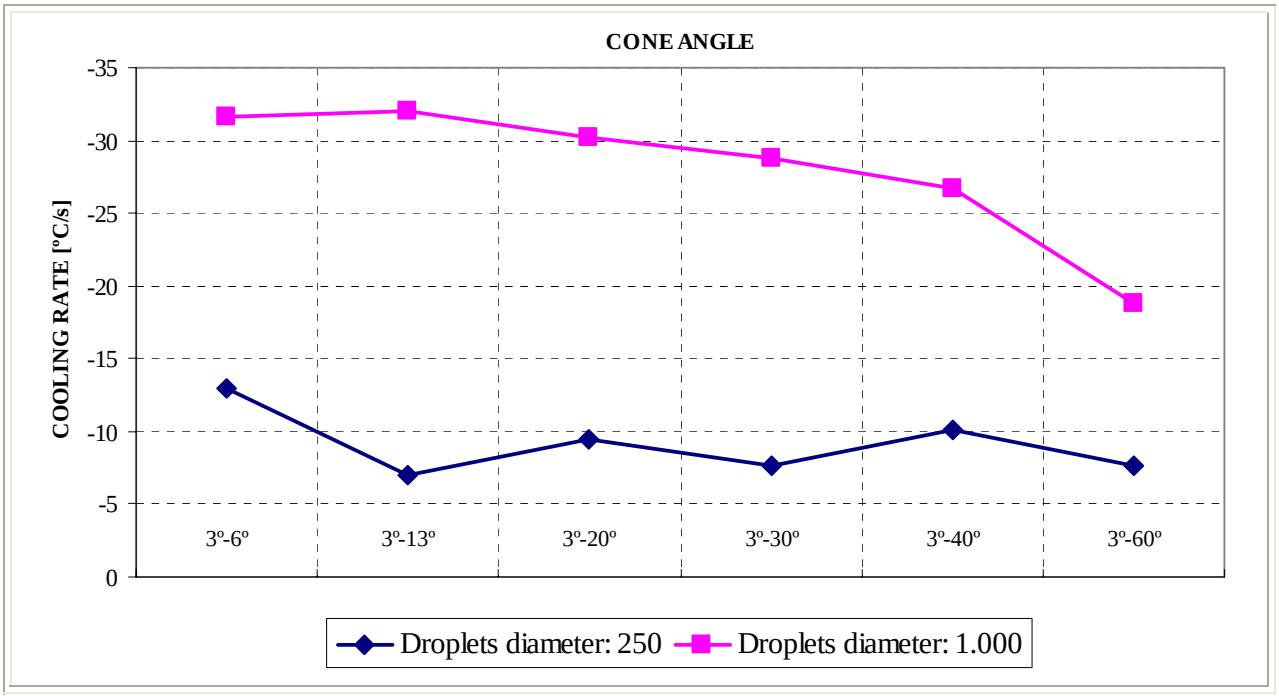

Figure 6-39. *Mean values of the cooling rate found for several cone angles (and for two values of the initial diameter of the droplets [μm]).*

In sight of the dispersion of the results obtained from the Computational Fluid Dynamics simulations depending on the main features of the water jet, the cooling rate values adopted for this Chapter must cover, as much as possible, the wide variety of the conditions that Fire-Fighters may find when attacking a natural fire in a High-Rise Building.

Therefore, taking into account the orders of magnitude discerned from the simulations detailed on this paragraph, a general cooling rate of -10 ºC/s will be adopted (since it constitutes a mean value of those results corresponding to a water jet with a droplets distribution featured by an initial mean diameter of 250 μm) whereas the cases with higher cooling rate values will be studied through particular analyses developed in paragraphs 6.5.2.6.1 and 6.5.2.6.2, which correspond to extremely high cooling rates of -136,6 ºC/s and -32,36 ºC/s respectively (deducted from the case with the higher flow-rate, namely, case *Office-7*, corresponding to the maximum and mean value of the cooling rate considering a flow-rate of 220 l/min, an initial velocity of the droplets of 10 m/s, a cone angle of 3º-6º and an initial mean diameter of the droplets of 1.000 μm).

By means of this methodology, the conclusions arisen from this Chapter will cover most of the expectable combinations of the parameters stated herein.

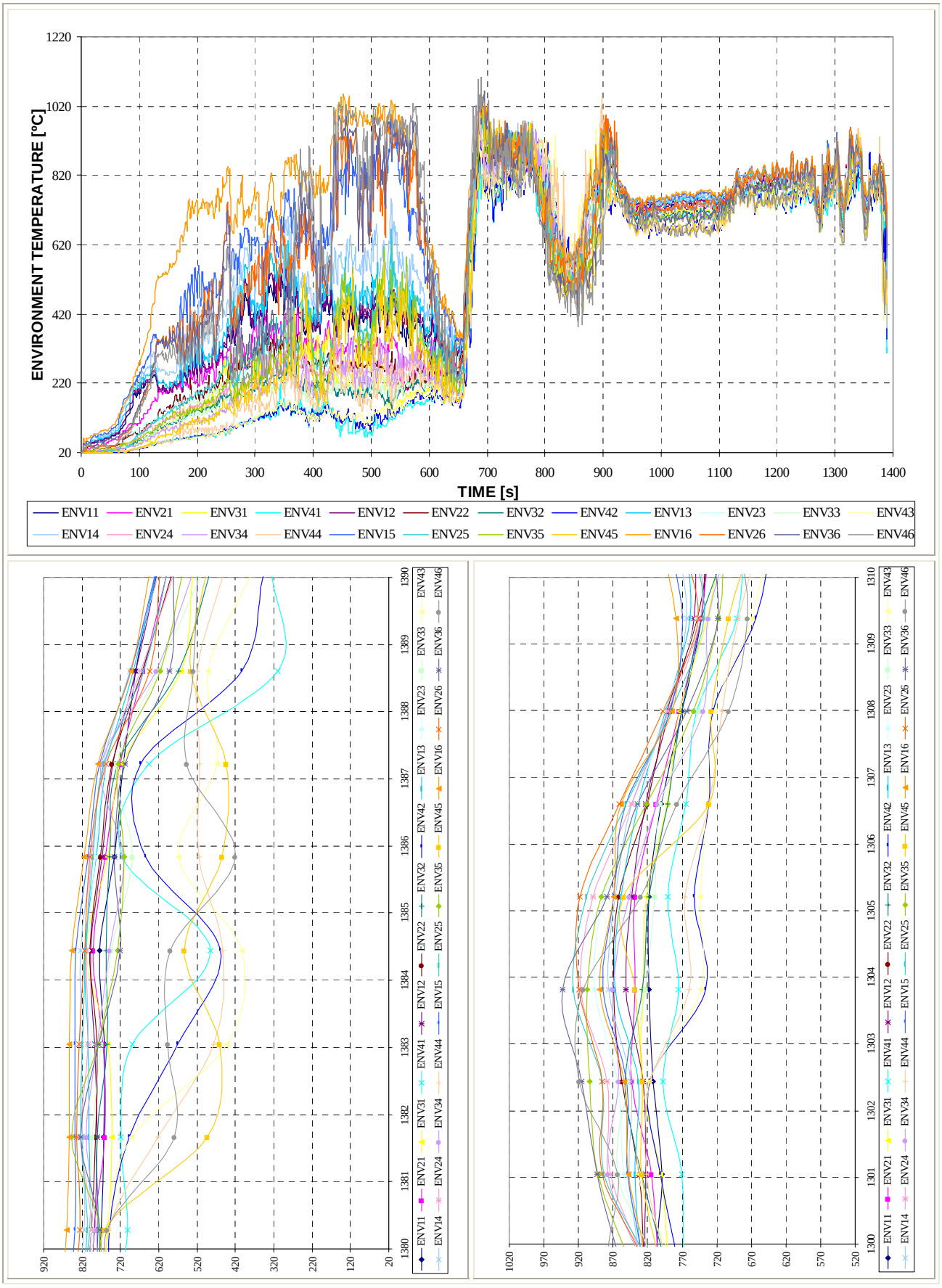

Figure 6-40.a. OFFICE-20.

Environment Temperature Evolution at the Control Points. Lower figures correspond to the detail on the 2nd environment cooling – from 1.300 to 1.310 seconds – and on the surface cooling – from 1.380 to 1.390 seconds –).

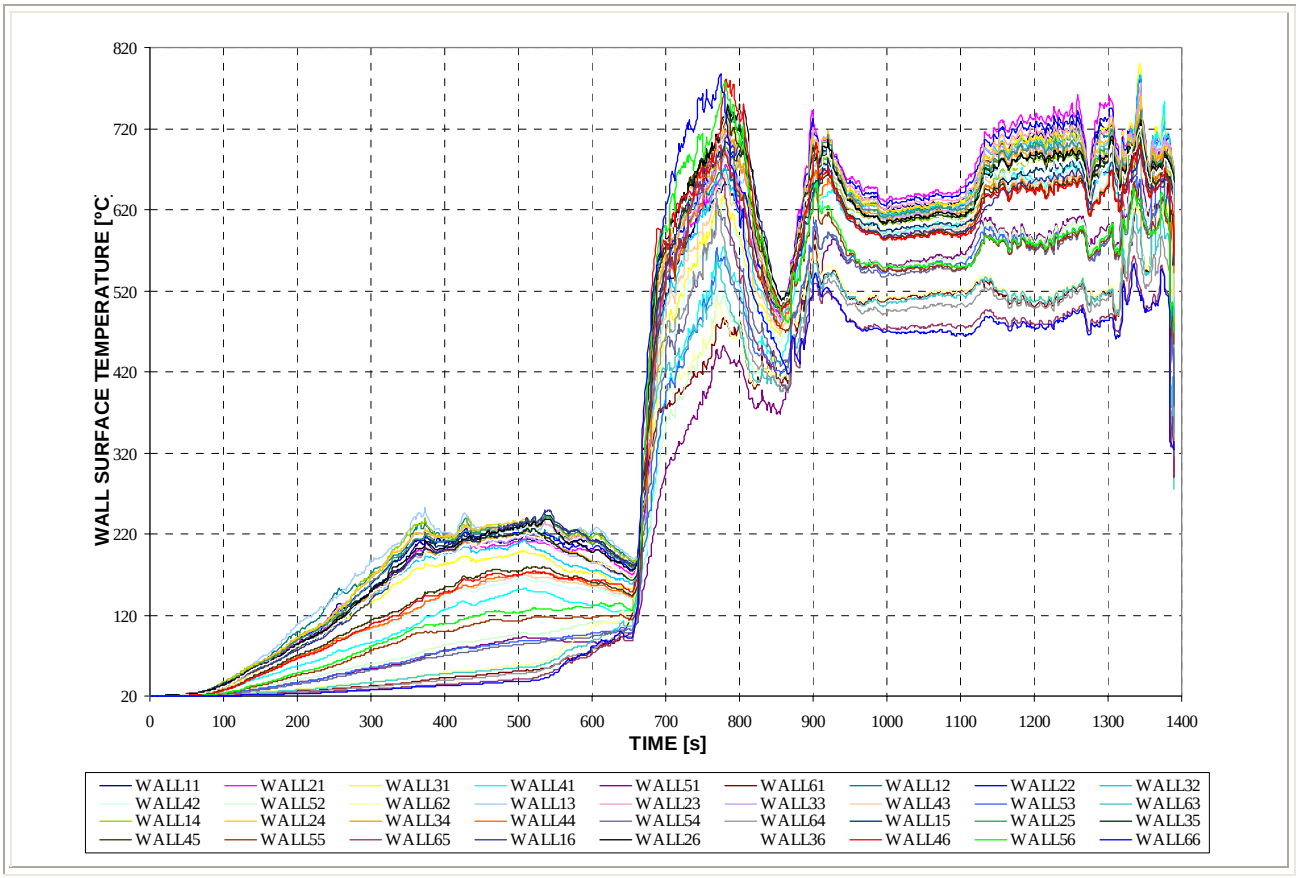

Surface Temperature Evolution at the Control Points.

Figure 6-40.b. OFFICE-20.

Surface Temperature Evolution at Control Points: detail on the surface cooling period –1.380 to 1.390s–

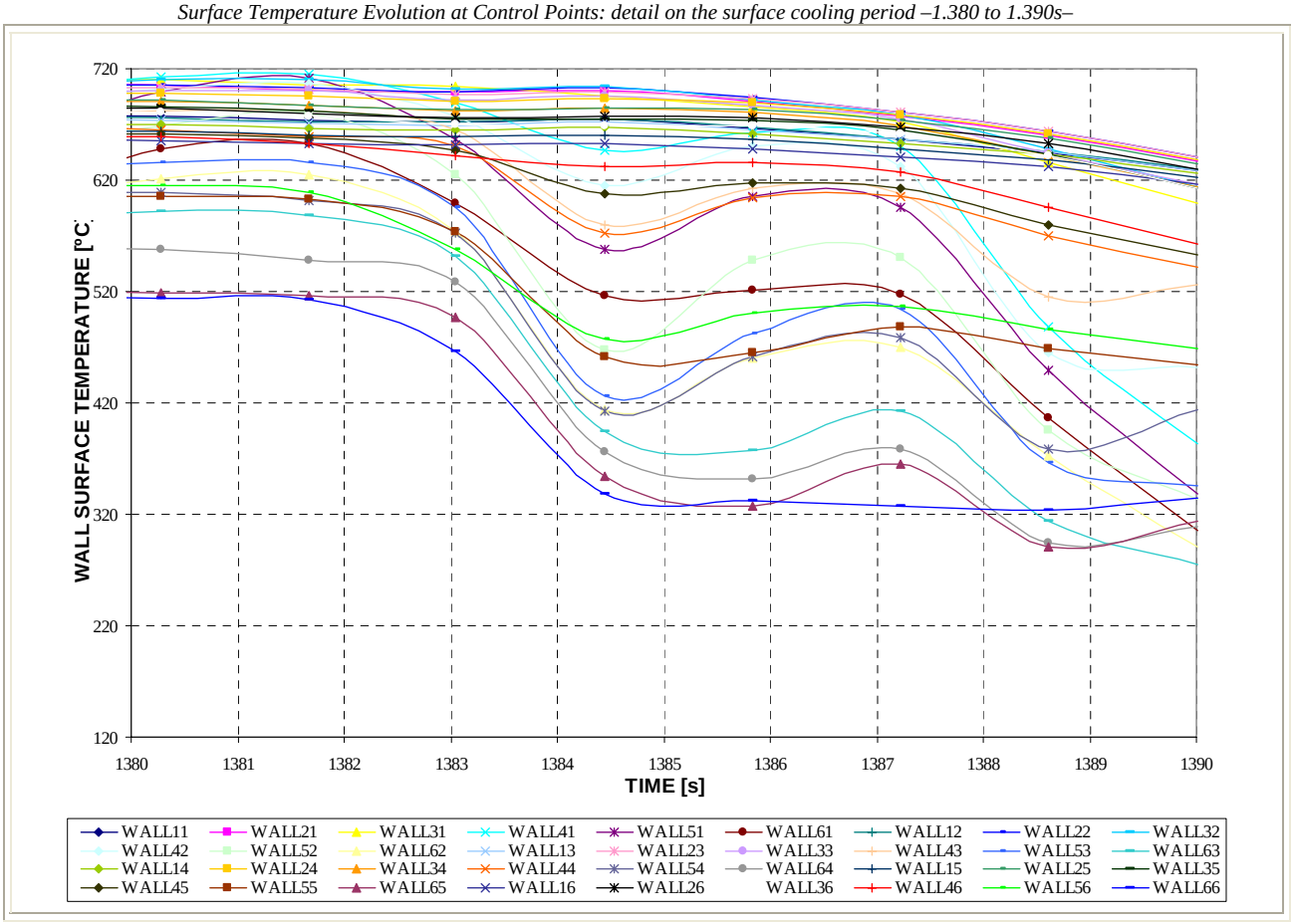

Figure 6-40.c. OFFICE-20.
Mean Cooling Rate and Standard Deviation at each of Surface Control Points.

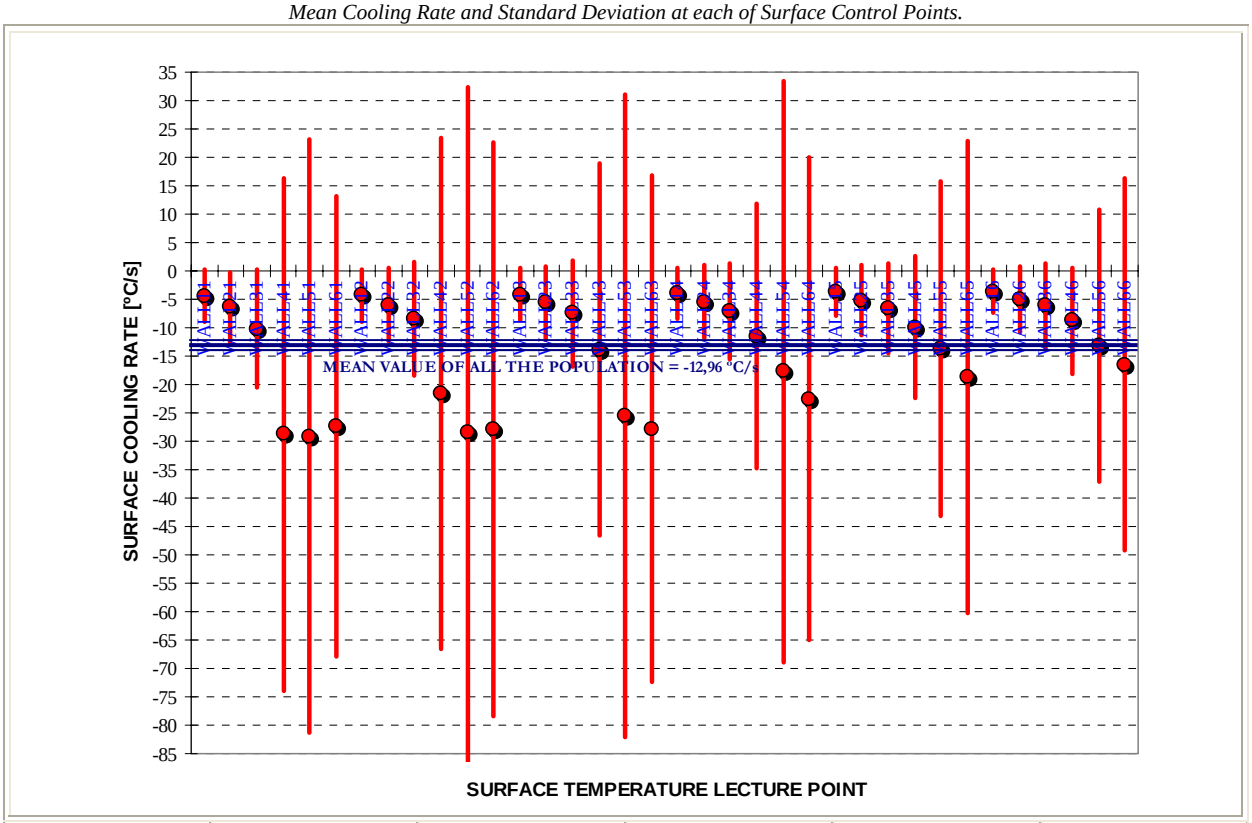

SURF. T LECTURE POINT	ARITHMETIC MEAN [°C/s]	STANDARD DEVIATION [°C/s]	MAXIMUM [°C/s]	MINIMUM [°C/s]	MEDIAN [°C/s]
WALL11	-4,5	4,6	-11,3	2,2	-4,8
WALL21	-6,4	6,2	-17,1	0,9	-5,5
WALL31	-10,2	10,3	-26,7	-1,5	-6,4
WALL41	-28,8	45,2	-117,4	11,5	-13,3
WALL51	-29,2	52,3	-105,6	33,5	-23,3
WALL61	-27,4	40,5	-79,7	26,7	-20,9
WALL12	-4,3	4,7	-11,8	2,3	-4,2
WALL22	-6,0	6,5	-17,0	2,5	-4,2
WALL32	-8,4	10,0	-23,9	1,5	-7,3
WALL42	-21,6	44,9	-120,5	24,6	-11,1
WALL52	-28,4	60,8	-113,0	57,2	-18,5
WALL62	-28,0	50,5	-114,8	32,6	-17,0
WALL13	-4,2	4,6	-12,1	2,3	-3,5
WALL23	-5,6	6,5	-17,0	2,1	-4,1
WALL33	-7,5	9,3	-21,6	2,8	-6,1
WALL43	-13,8	32,9	-67,1	23,5	-1,3
WALL53	-25,4	56,6	-121,7	40,3	-7,0
WALL63	-27,8	44,6	-112,9	25,6	-19,8
WALL14	-4,0	4,5	-12,1	1,8	-3,0
WALL24	-5,4	6,4	-17,1	1,9	-3,0
WALL34	-7,1	8,5	-20,7	1,9	-3,4
WALL44	-11,5	23,2	-56,3	23,2	-5,5
WALL54	-17,7	51,2	-115,2	35,0	-3,3
WALL64	-22,6	42,4	-109,9	19,0	-10,7
WALL15	-3,8	4,2	-11,8	1,3	-2,7
WALL25	-5,2	6,2	-16,8	1,5	-3,1
WALL35	-6,6	7,9	-21,4	-0,2	-3,9
WALL45	-9,9	12,5	-27,9	7,3	-5,7
WALL55	-13,7	29,4	-80,9	16,2	-6,2
WALL65	-18,7	41,5	-101,9	27,4	-8,1
WALL16	-3,6	3,9	-11,2	0,3	-2,4
WALL26	-4,9	5,8	-16,1	0,6	-3,1
WALL36	-6,2	7,5	-20,6	-0,1	-3,7
WALL46	-8,7	9,3	-23,3	2,4	-6,9
WALL56	-13,1	23,8	-57,9	16,7	-8,3
WALL66	-16,4	32,8	-92,0	8,0	-3,1

Table 6-28.a. OFFICE-20.
Statistic Parameters calculated on the Surface Cooling Rate at each Control Points.

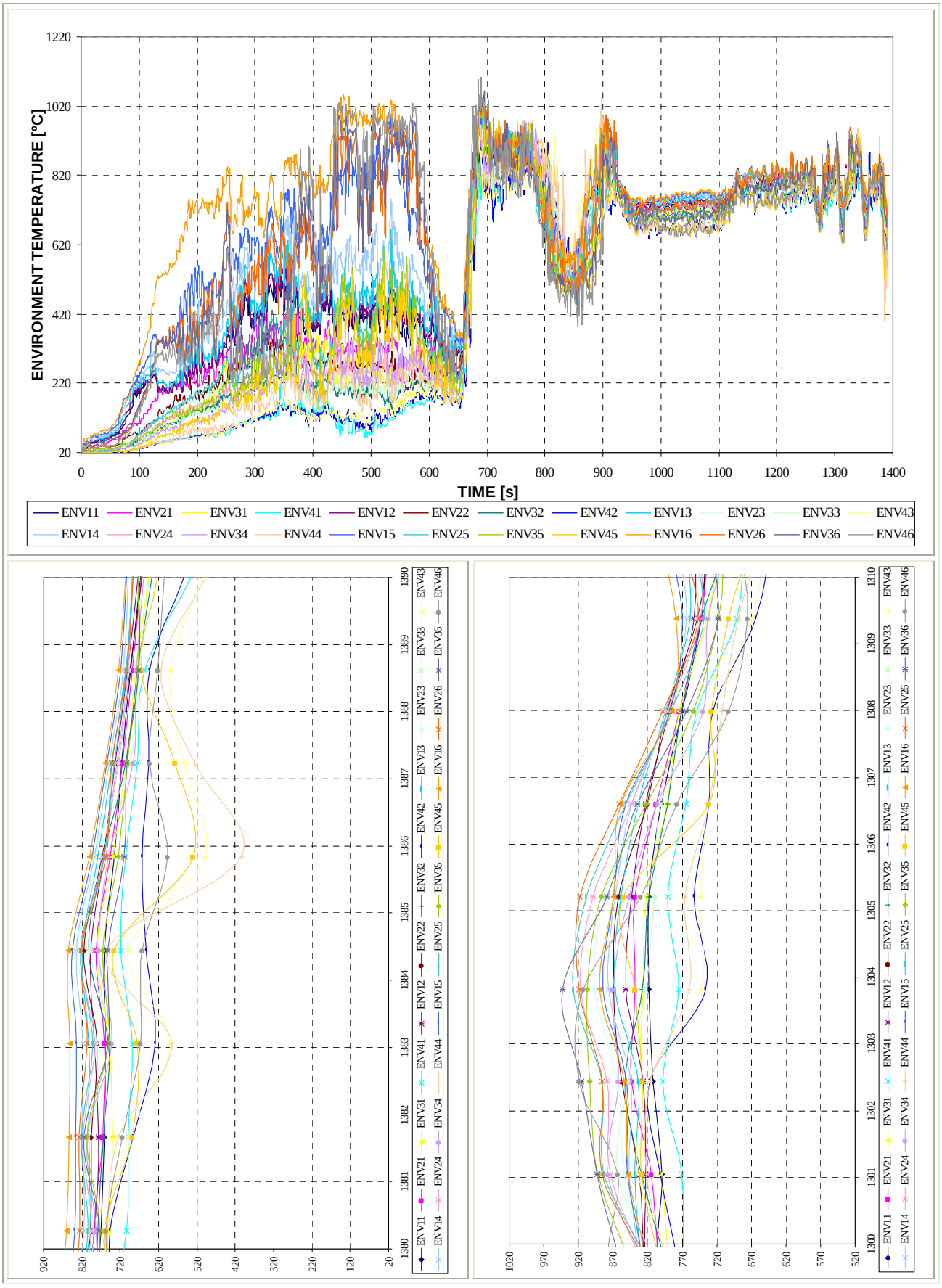

Figure 6-40.d. OFFICE-22.
Environment Temperature Evolution at the Control Points. Lower figures correspond to the detail on the 2nd environment cooling – from 1.300 to 1.310 seconds – and on the surface cooling – from 1.380 to 1.390 seconds –).

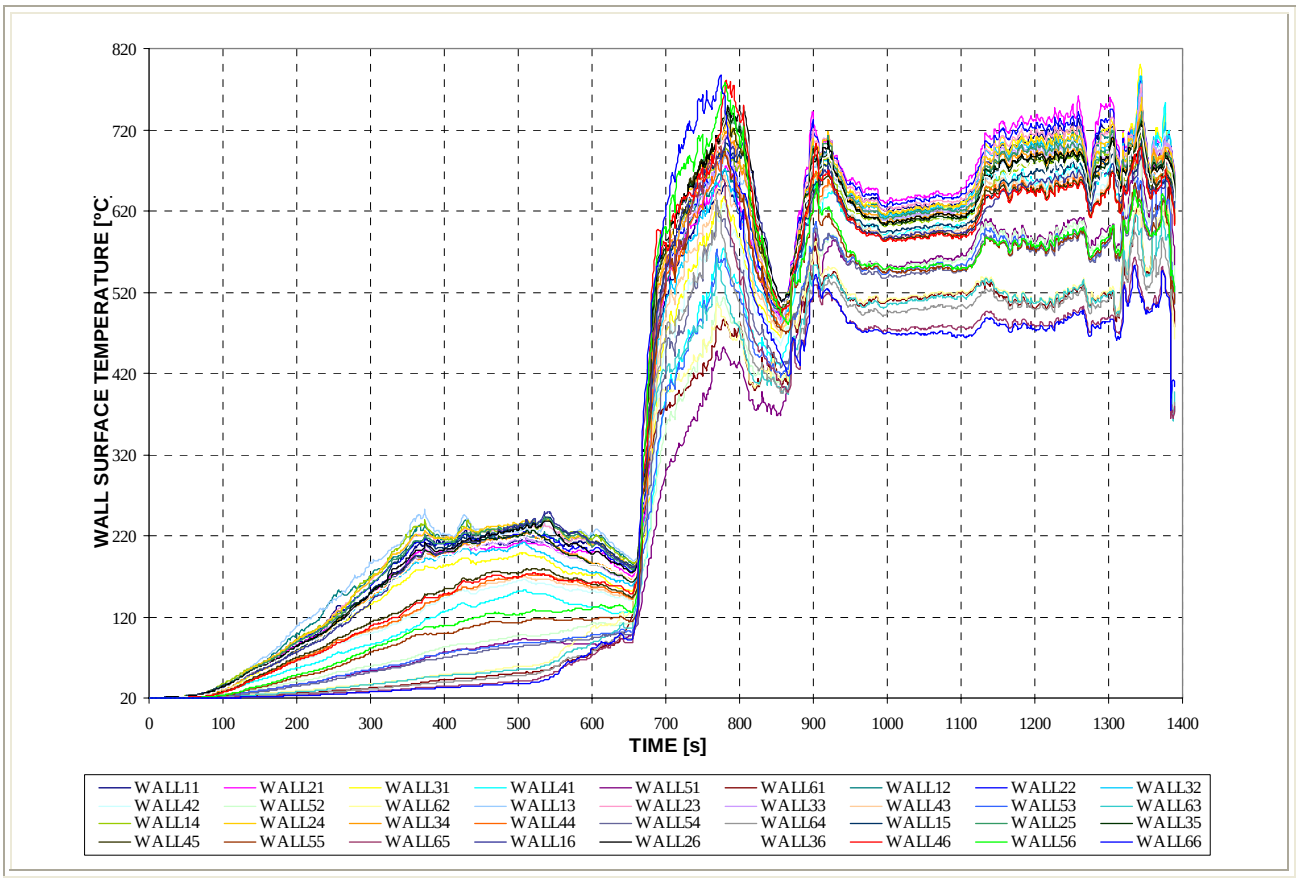

Surface Temperature Evolution at the Control Points.

Figure 6-40.e. OFFICE-22.

Surface Temperature Evolution at Control Points: detail on the surface cooling period –1.380 to 1.390s–

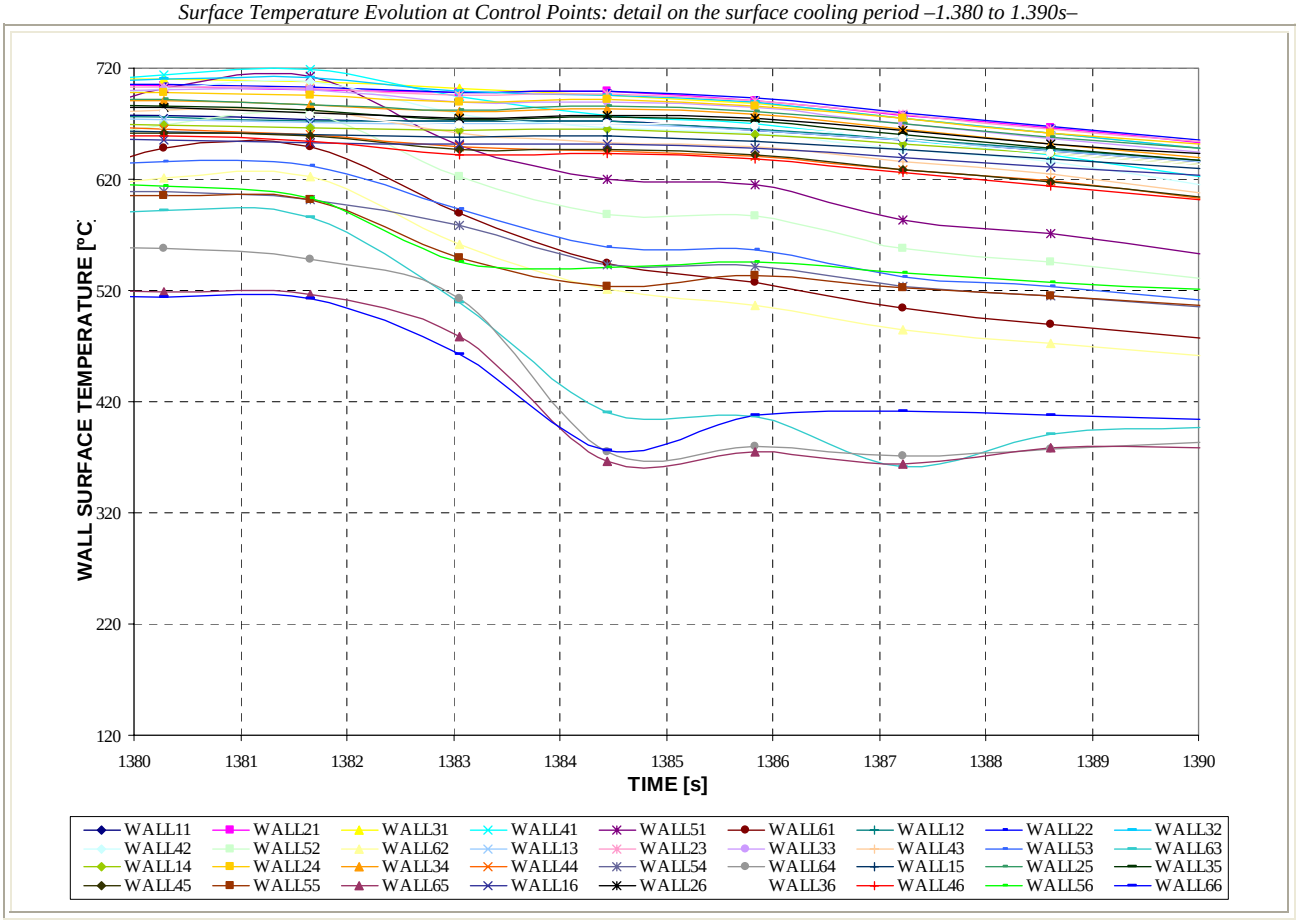

Figure 6-40.f. OFFICE-22.
Mean Cooling Rate and Standard Deviation at each of Surface Control Points.

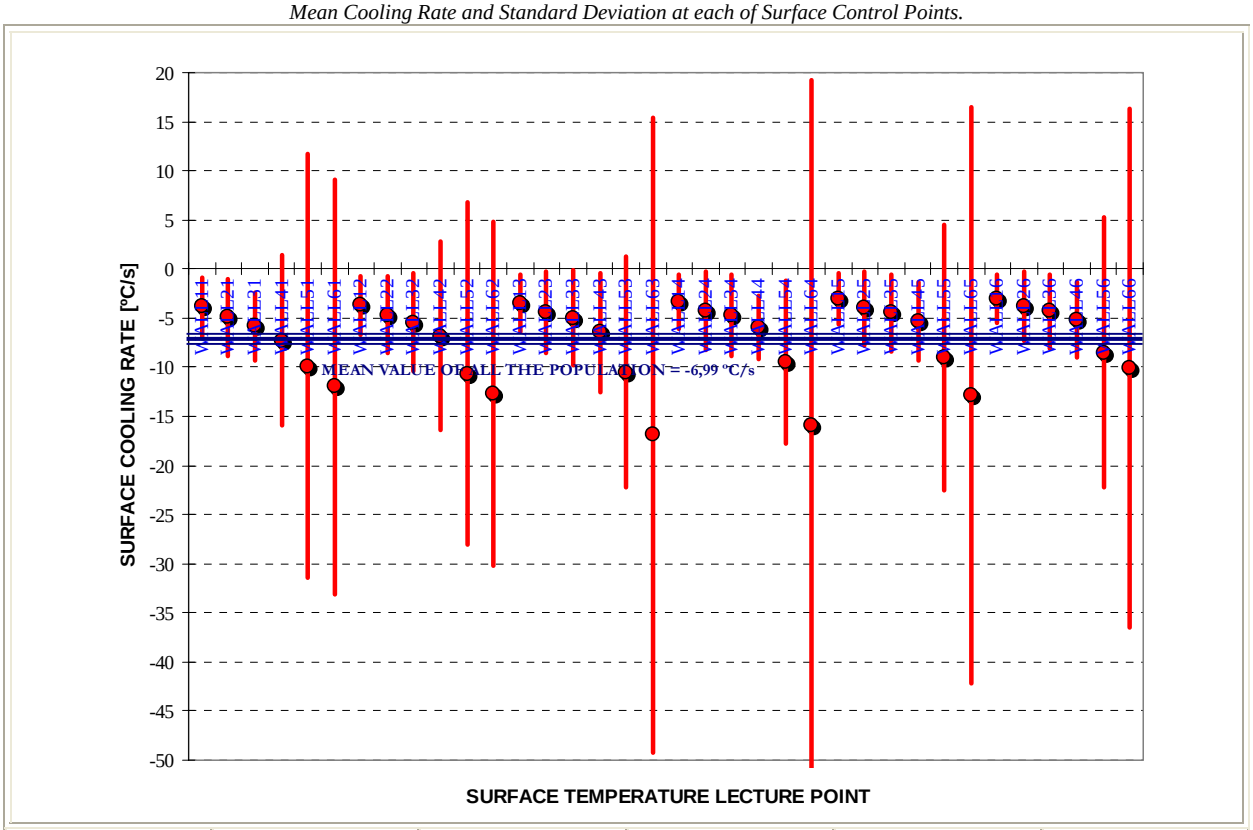

SURF. T LECTURE POINT	ARITHMETIC MEAN [ºC/s]	STANDARD DEVIATION [ºC/s]	MAXIMUM [ºC/s]	MINIMUM [ºC/s]	MEDIAN [ºC/s]
WALL11	-3,9	3,0	-7,5	-0,2	-4,3
WALL21	-4,9	3,9	-9,9	0,4	-4,5
WALL31	-5,8	3,5	-10,0	-1,7	-4,9
WALL41	-7,3	8,6	-17,9	6,9	-10,0
WALL51	-9,9	21,5	-44,1	27,4	-10,8
WALL61	-12,0	21,1	-43,3	27,3	-11,7
WALL12	-3,6	3,0	-7,1	-0,2	-3,8
WALL22	-4,7	3,9	-9,5	0,7	-3,9
WALL32	-5,4	5,0	-10,1	1,6	-7,0
WALL42	-6,8	9,6	-21,4	7,8	-8,6
WALL52	-10,7	17,5	-39,9	14,1	-9,6
WALL62	-12,7	17,5	-44,0	13,6	-10,1
WALL13	-3,5	2,9	-6,8	0,3	-3,2
WALL23	-4,4	4,1	-9,1	1,1	-4,6
WALL33	-5,0	4,9	-10,0	0,7	-5,9
WALL43	-6,5	6,1	-15,5	1,7	-6,9
WALL53	-10,5	11,8	-28,7	5,0	-7,6
WALL63	-16,9	32,3	-70,5	21,5	-3,8
WALL14	-3,3	2,8	-6,7	0,5	-2,8
WALL24	-4,2	4,0	-9,2	1,8	-4,2
WALL34	-4,7	4,1	-9,4	1,7	-4,2
WALL44	-6,0	3,2	-10,8	-2,4	-5,7
WALL54	-9,5	8,3	-25,2	-1,0	-6,8
WALL64	-15,8	35,1	-99,3	4,6	-4,0
WALL15	-3,1	2,6	-6,4	0,3	-2,5
WALL25	-4,0	3,8	-9,0	2,1	-3,3
WALL35	-4,5	4,0	-9,2	1,7	-4,3
WALL45	-5,3	4,0	-9,6	-0,3	-6,0
WALL55	-9,0	13,5	-37,2	7,2	-5,5
WALL65	-12,8	29,3	-79,8	10,1	-1,9
WALL16	-3,0	2,4	-6,2	0,1	-2,3
WALL26	-3,8	3,6	-8,8	1,7	-3,2
WALL36	-4,3	3,7	-9,3	1,2	-4,1
WALL46	-5,2	3,8	-8,8	0,6	-5,9
WALL56	-8,5	13,7	-41,0	3,8	-5,6
WALL66	-10,1	26,4	-61,9	23,1	-2,6

Table 6-28.b. OFFICE-22.
Statistic Parameters calculated on the Surface Cooling Rate at each Control Points.

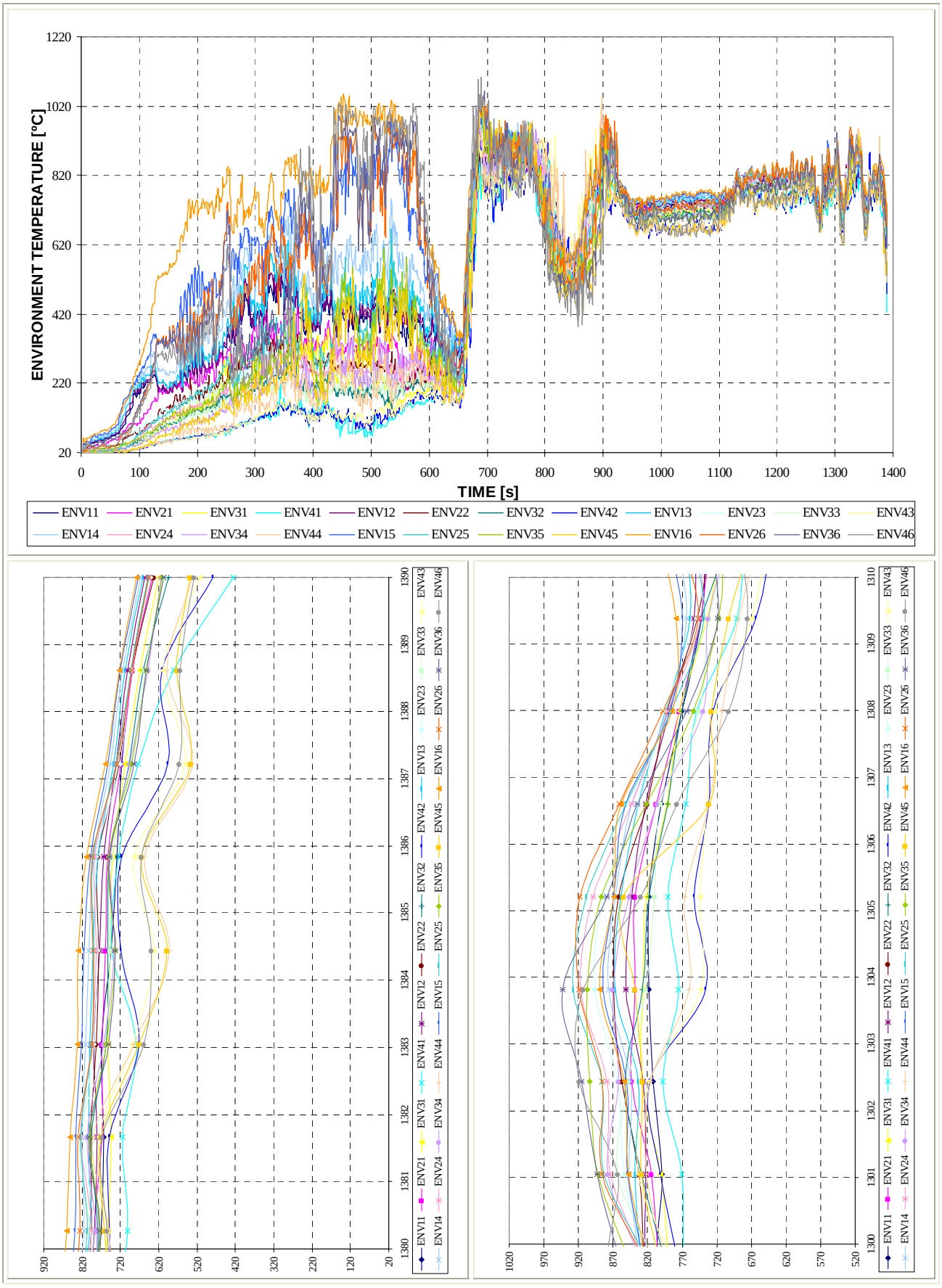

Figure 6-40.g. OFFICE-23.
Environment Temperature Evolution at the Control Points. Lower figures correspond to the detail on the 2nd environment cooling – from 1.300 to 1.310 seconds – and on the surface cooling – from 1.380 to 1.390 seconds –).

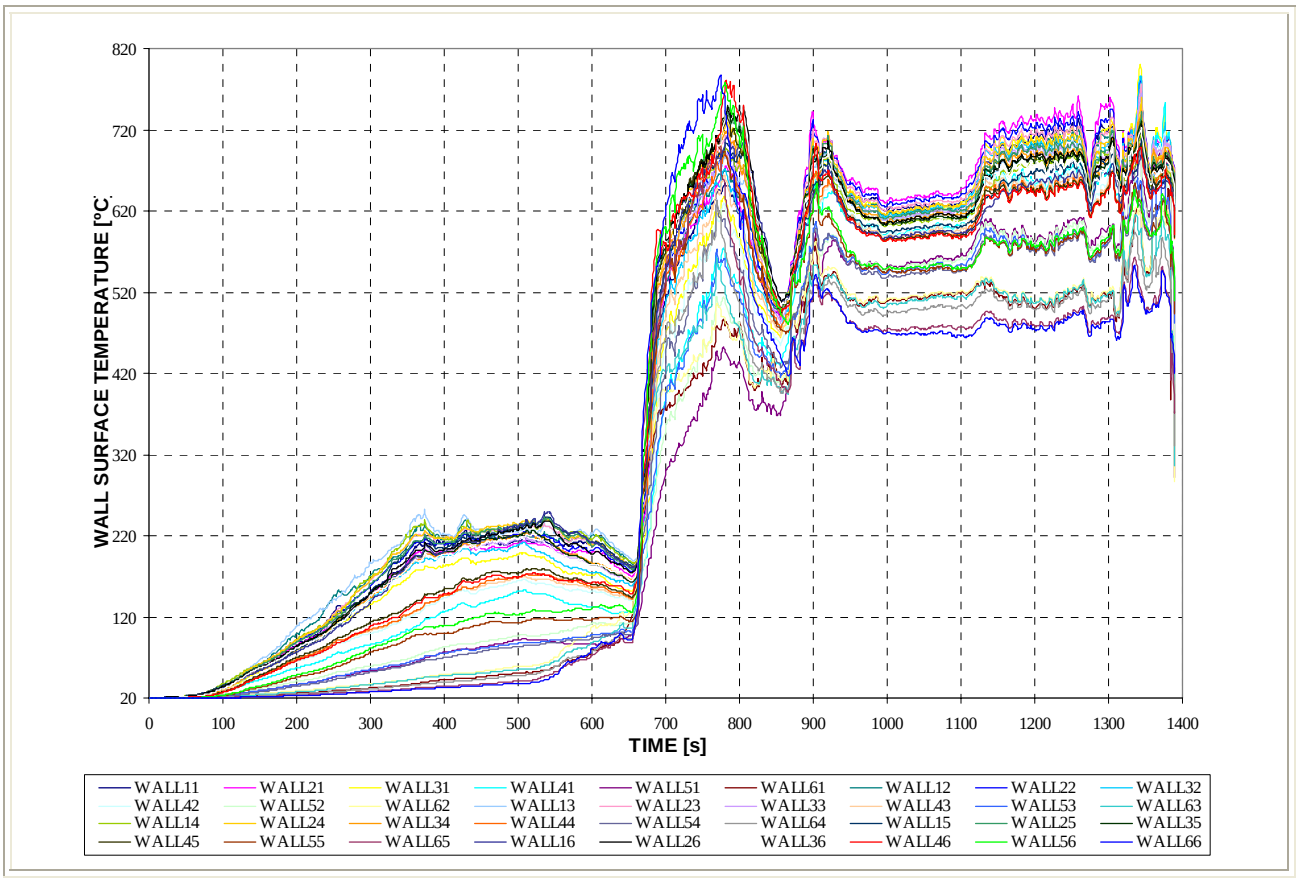

Surface Temperature Evolution at the Control Points.

Figure 6-40.h. OFFICE-23.

Surface Temperature Evolution at Control Points: detail on the surface cooling period –1.380 to 1.390s–

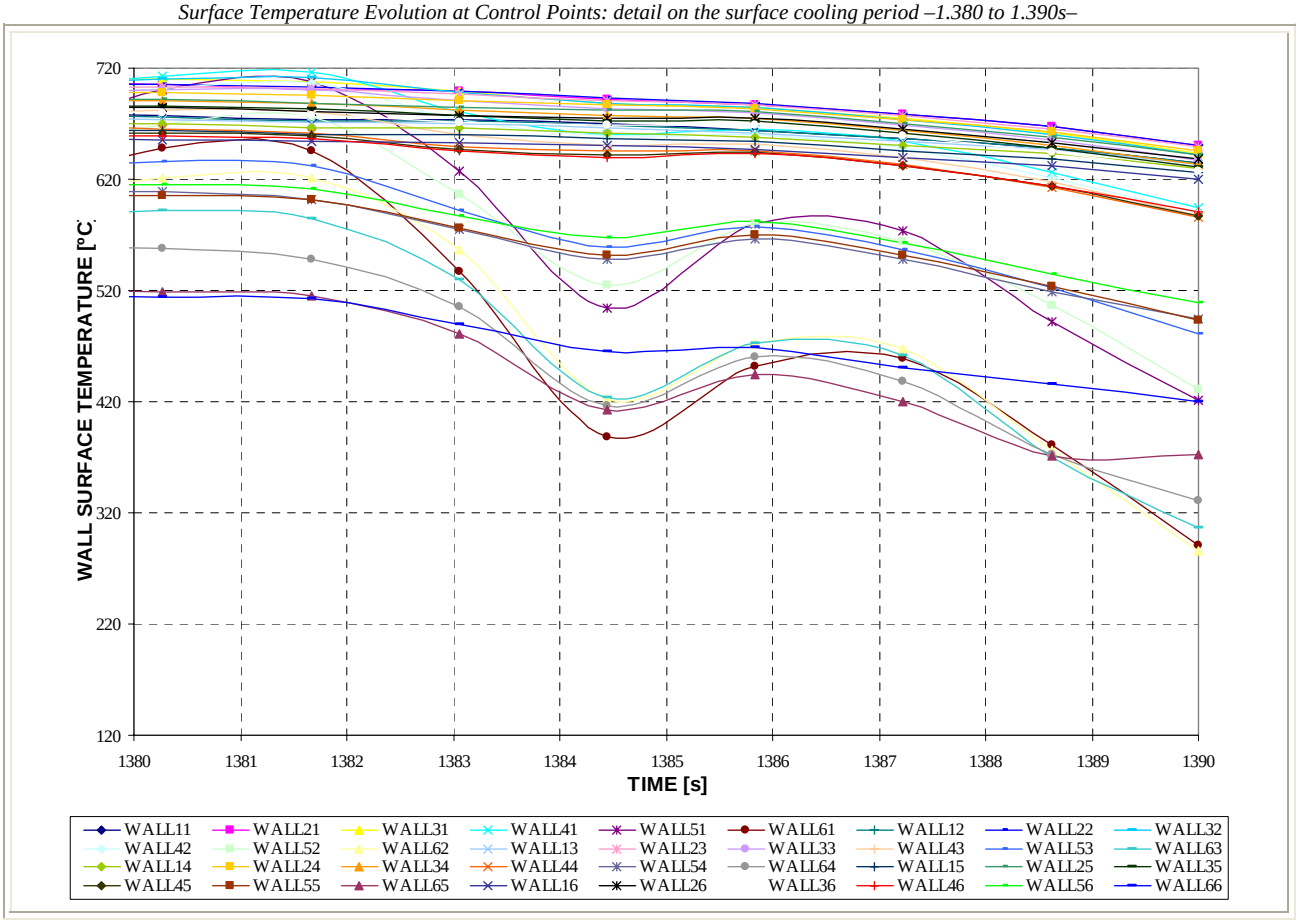

Figure 6-40.i. OFFICE-23.
Mean Cooling Rate and Standard Deviation at each of Surface Control Points.

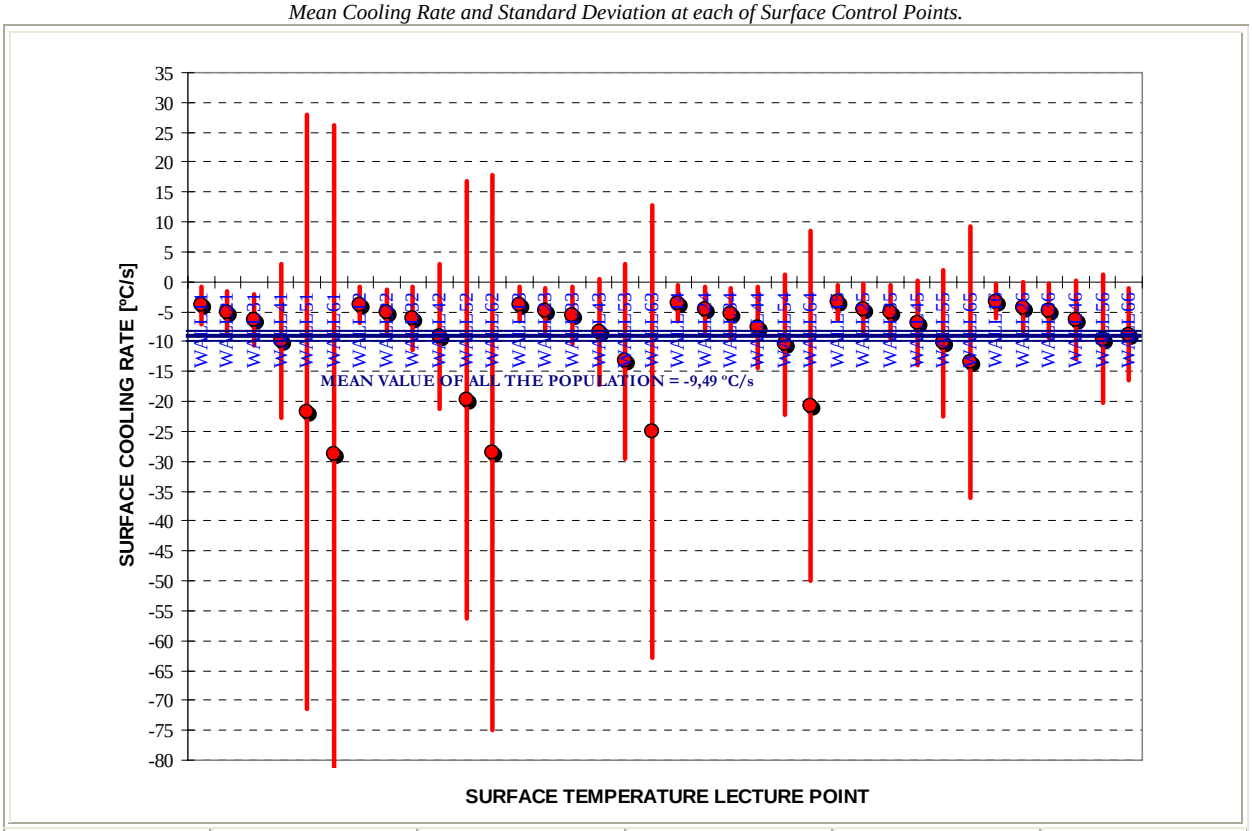

SURF. T LECTURE POINT	ARITHMETIC MEAN [ºC/s]	STANDARD DEVIATION [ºC/s]	MAXIMUM [ºC/s]	MINIMUM [ºC/s]	MEDIAN [ºC/s]
WALL11	-3,9	3,1	-9,4	0,4	-3,4
WALL21	-5,2	3,6	-12,3	-1,1	-4,1
WALL31	-6,3	4,2	-13,9	-1,5	-6,6
WALL41	-9,9	12,9	-25,9	6,4	-11,5
WALL51	-21,8	49,6	-89,1	54,3	-27,2
WALL61	-28,8	55,0	-106,8	45,1	-28,6
WALL12	-3,8	3,0	-9,3	-0,5	-3,0
WALL22	-5,1	3,7	-12,3	-1,5	-3,8
WALL32	-6,0	5,3	-13,7	1,3	-7,6
WALL42	-9,1	12,2	-23,4	7,3	-9,9
WALL52	-19,7	36,6	-58,5	39,5	-26,1
WALL62	-28,5	46,4	-96,9	36,4	-24,8
WALL13	-3,8	2,9	-9,3	-0,8	-3,0
WALL23	-4,9	3,9	-12,2	-0,6	-3,8
WALL33	-5,5	4,8	-13,0	0,6	-6,4
WALL43	-8,3	8,8	-21,8	1,6	-8,1
WALL53	-13,3	16,3	-29,8	12,6	-19,0
WALL63	-25,0	37,9	-76,1	34,5	-23,8
WALL14	-3,6	3,0	-9,1	-0,4	-2,8
WALL24	-4,7	4,0	-12,0	-0,3	-3,0
WALL34	-5,3	4,3	-13,0	-0,8	-4,1
WALL44	-7,6	6,8	-19,9	0,1	-5,8
WALL54	-10,5	11,7	-21,2	12,7	-15,1
WALL64	-20,7	29,3	-64,0	30,9	-22,8
WALL15	-3,4	3,0	-8,7	-0,1	-2,6
WALL25	-4,5	4,1	-11,5	-0,3	-2,6
WALL35	-5,1	4,5	-12,8	-0,4	-3,8
WALL45	-6,9	7,0	-19,3	1,3	-5,8
WALL55	-10,2	12,3	-22,0	13,1	-15,6
WALL65	-13,4	22,7	-49,0	22,9	-10,4
WALL16	-3,3	2,9	-8,3	-0,3	-2,2
WALL26	-4,2	4,1	-10,8	-0,1	-2,7
WALL36	-4,8	4,6	-12,3	0,3	-3,5
WALL46	-6,3	6,6	-17,0	2,6	-6,0
WALL56	-9,6	10,7	-20,1	10,2	-13,7
WALL66	-8,8	7,7	-18,0	2,9	-11,2

Table 6-28.c. OFFICE-23.
Statistic Parameters calculated on the Surface Cooling Rate at each Control Points.

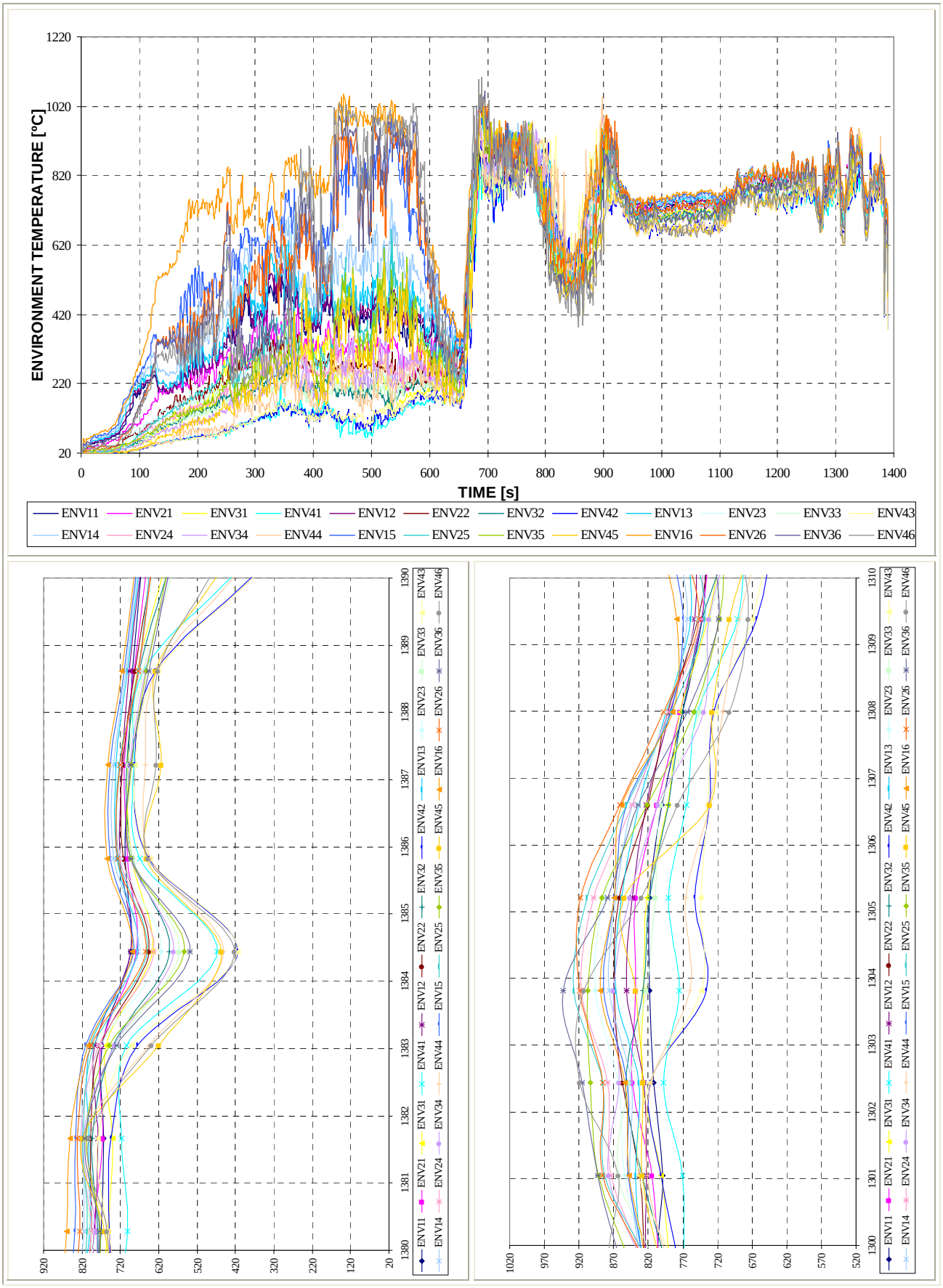

Figure 6-40.j. OFFICE-24.

Environment Temperature Evolution at the Control Points. Lower figures correspond to the detail on the 2nd environment cooling – from 1.300 to 1.310 seconds – and on the surface cooling – from 1.380 to 1.390 seconds –).

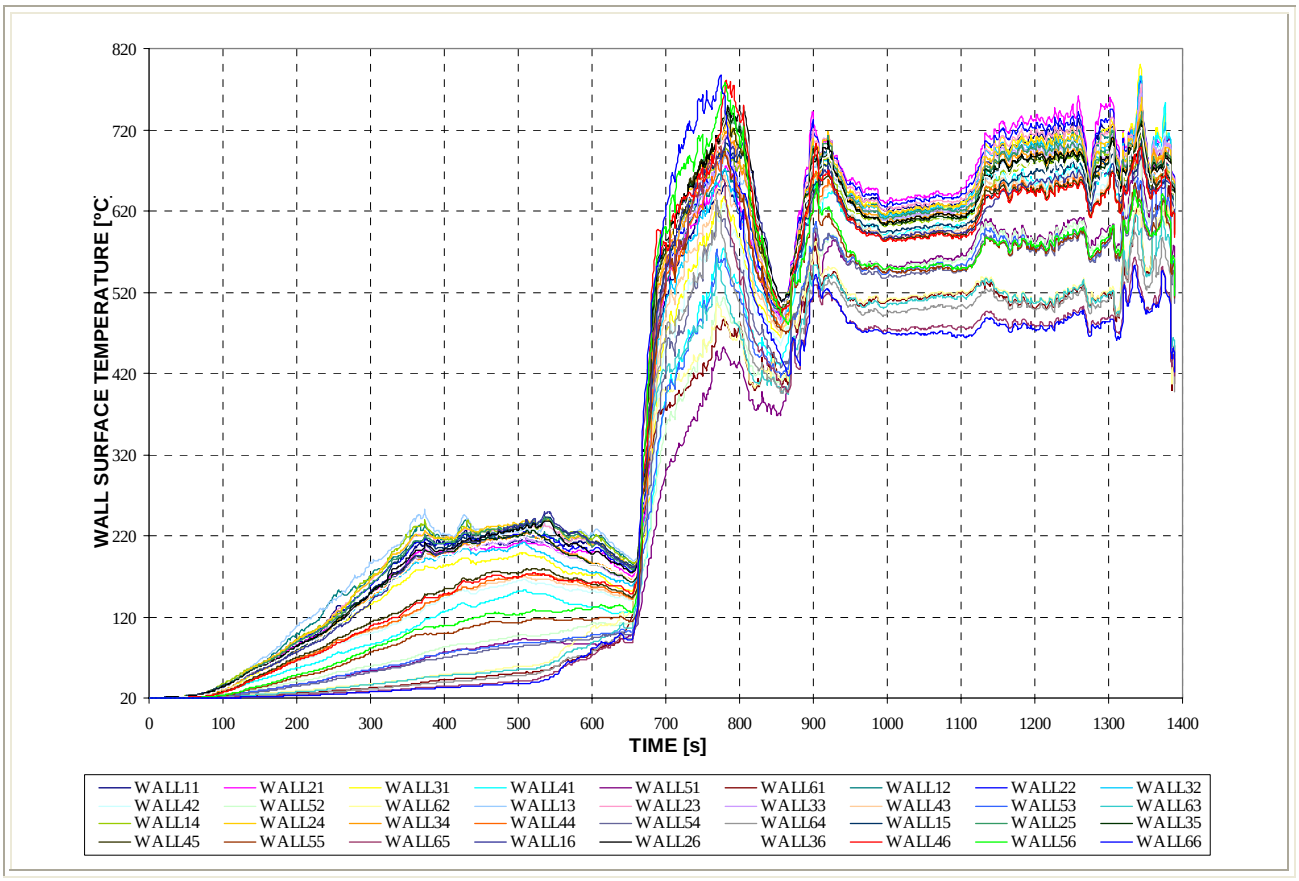

Surface Temperature Evolution at the Control Points.

Figure 6-40.k. OFFICE-24.

Surface Temperature Evolution at Control Points: detail on the surface cooling period –1.380 to 1.390s–

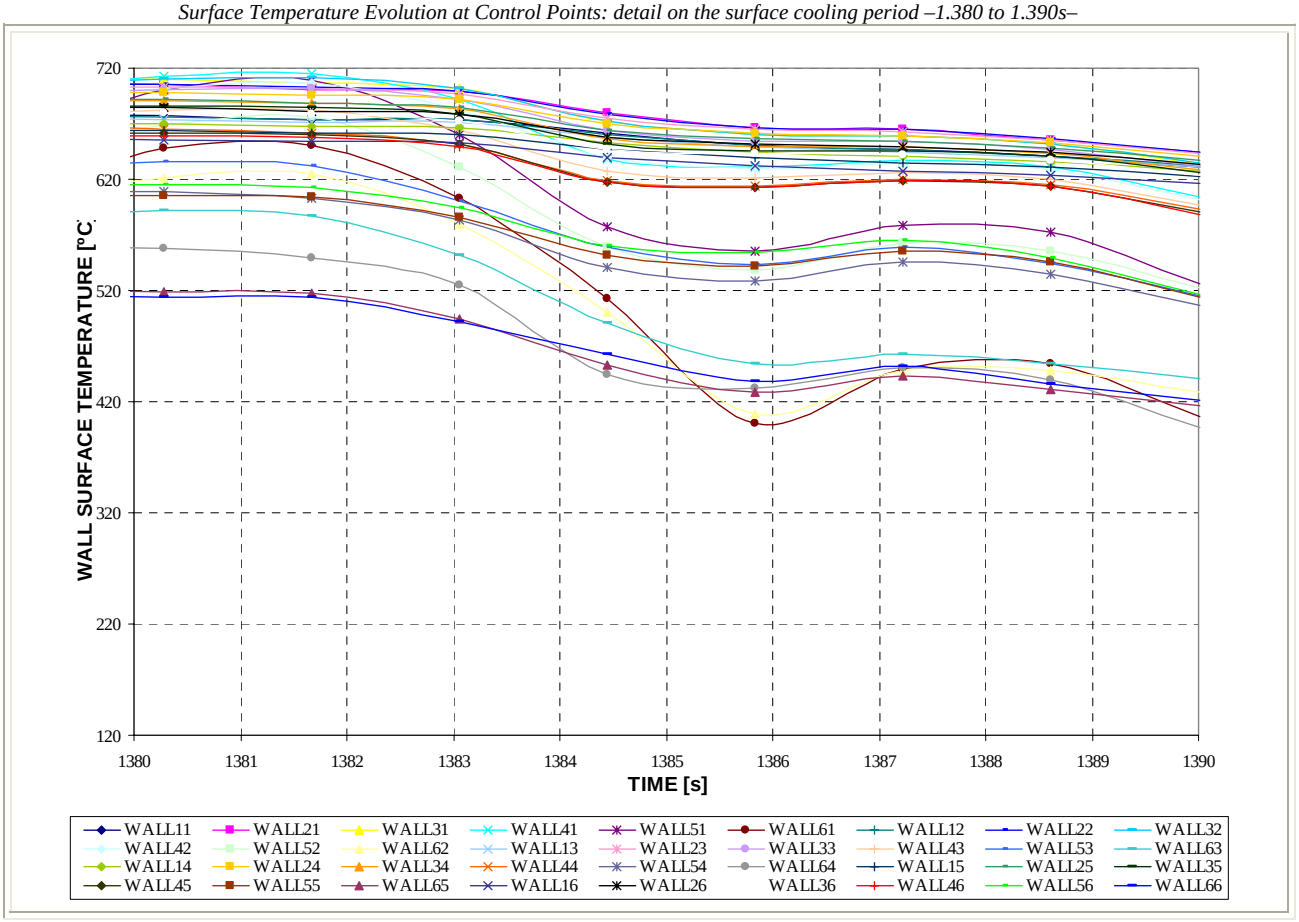

Figure 6-40.l. OFFICE-24.
Mean Cooling Rate and Standard Deviation at each of Surface Control Points.

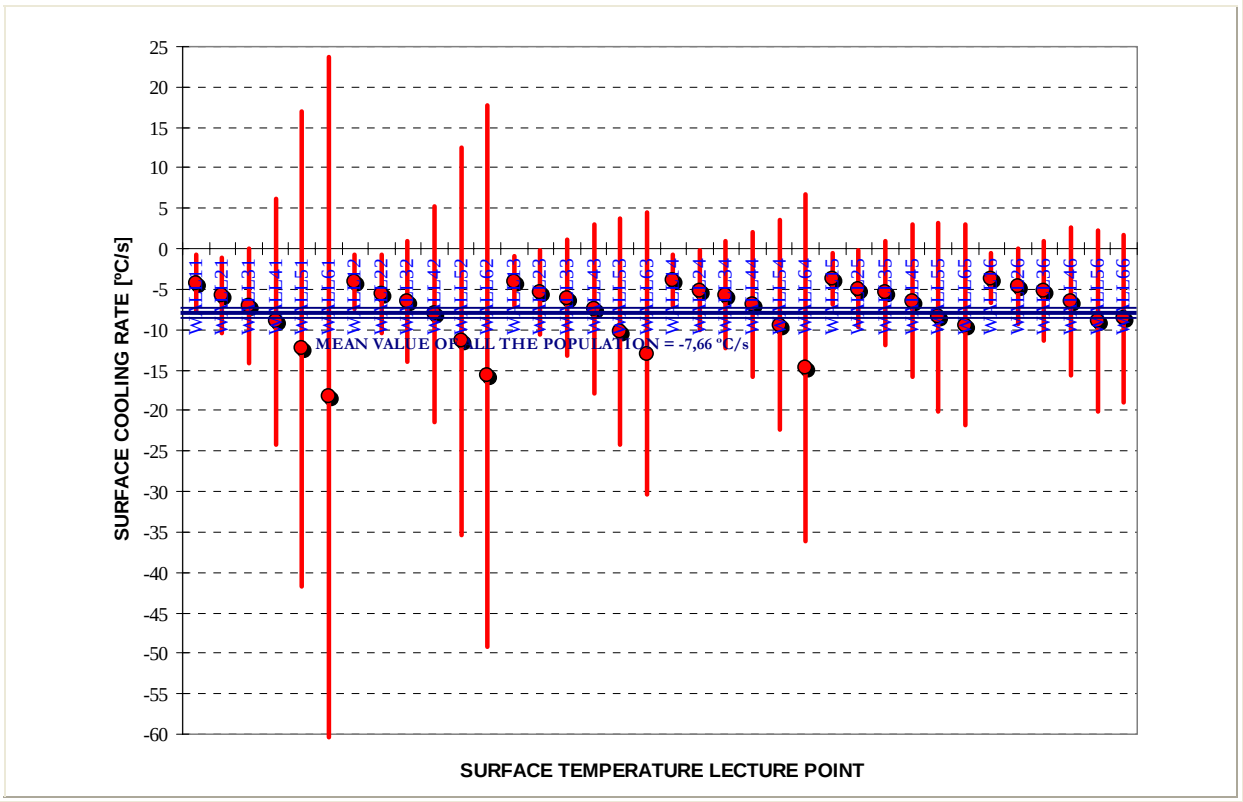

SURF. T LECTURE POINT	ARITHMETIC MEAN [ºC/s]	STANDARD DEVIATION [ºC/s]	MAXIMUM [ºC/s]	MINIMUM [ºC/s]	MEDIAN [ºC/s]
WALL11	-4,2	3,5	-9,4	0,4	-3,6
WALL21	-5,8	4,7	-14,2	-0,9	-4,8
WALL31	-7,1	7,0	-21,3	-0,6	-4,6
WALL41	-9,0	15,2	-38,5	6,4	-4,9
WALL51	-12,3	29,4	-60,0	26,4	-9,6
WALL61	-18,3	42,0	-81,2	35,2	-16,0
WALL12	-4,1	3,3	-9,5	0,0	-3,4
WALL22	-5,6	4,8	-14,8	-1,3	-4,1
WALL32	-6,6	7,5	-20,7	1,3	-6,6
WALL42	-8,0	13,3	-30,8	7,3	-5,4
WALL52	-11,4	23,9	-52,1	17,5	-10,1
WALL62	-15,7	33,5	-66,1	28,0	-7,1
WALL13	-4,0	3,0	-9,5	-0,7	-3,6
WALL23	-5,4	5,2	-15,7	-0,2	-4,5
WALL33	-6,1	7,2	-20,4	1,0	-5,8
WALL43	-7,4	10,4	-26,2	3,9	-4,6
WALL53	-10,2	14,1	-29,7	10,9	-10,8
WALL63	-13,0	17,5	-43,7	6,3	-8,2
WALL14	-3,9	3,2	-9,8	-0,5	-3,3
WALL24	-5,1	5,0	-15,4	-0,3	-4,0
WALL34	-5,7	6,6	-19,8	0,2	-4,0
WALL44	-6,9	8,9	-24,1	4,7	-3,8
WALL54	-9,4	12,9	-30,4	12,7	-8,5
WALL64	-14,6	21,5	-57,6	13,4	-8,5
WALL15	-3,7	3,1	-9,7	-0,4	-3,2
WALL25	-4,9	4,8	-15,1	-0,3	-3,3
WALL35	-5,4	6,4	-19,2	0,2	-4,0
WALL45	-6,5	9,4	-24,1	4,3	-3,3
WALL55	-8,4	11,7	-24,6	9,8	-7,0
WALL65	-9,4	12,4	-29,6	10,8	-9,5
WALL16	-3,6	3,0	-9,5	-0,6	-3,0
WALL26	-4,7	4,6	-14,7	-0,4	-3,1
WALL36	-5,2	6,1	-18,3	-0,1	-3,3
WALL46	-6,5	9,1	-22,4	3,6	-3,2
WALL56	-8,9	11,2	-23,7	7,8	-7,9
WALL66	-8,6	10,3	-21,2	9,3	-10,7

Table 6-28.d. OFFICE-24.
Statistic Parameters calculated on the Surface Cooling Rate at each Control Points.

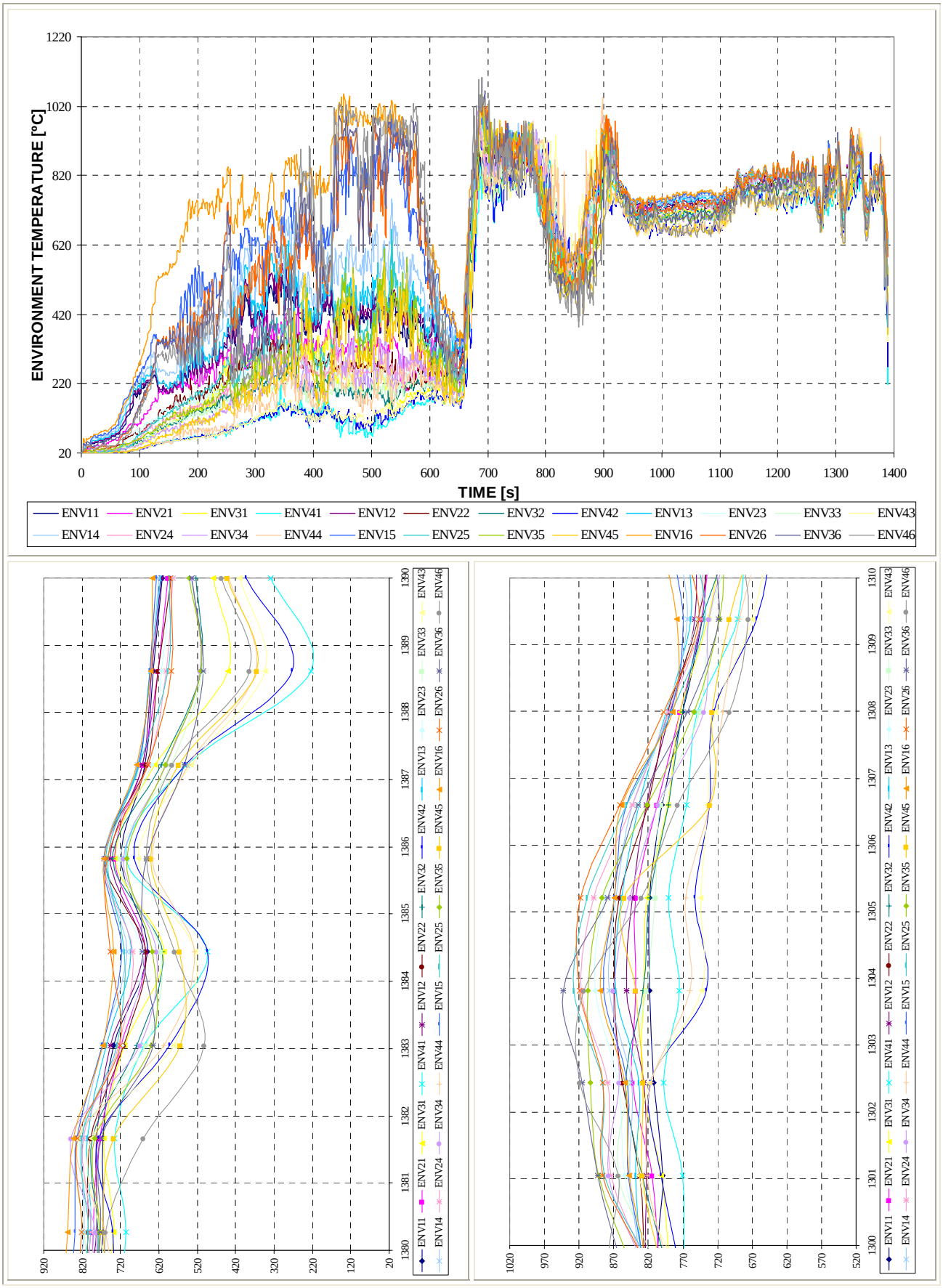

Figure 6-40.m. OFFICE-25.
Environment Temperature Evolution at the Control Points. Lower figures correspond to the detail on the 2nd environment cooling – from 1.300 to 1.310 seconds – and on the surface cooling – from 1.380 to 1.390 seconds –).

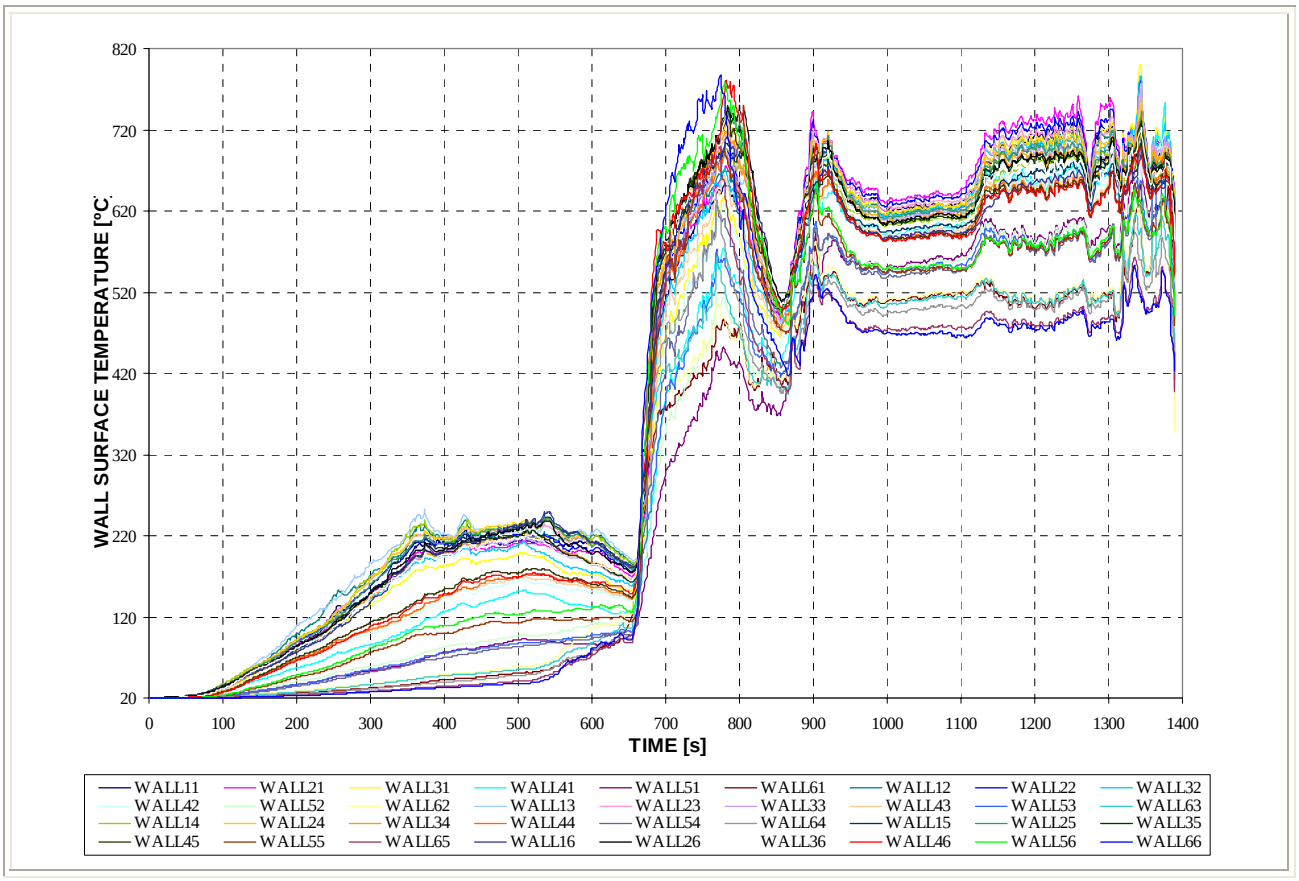

Surface Temperature Evolution at the Control Points.

Figure 6-40.n. OFFICE-25.

Surface Temperature Evolution at Control Points: detail on the surface cooling period –1.380 to 1.390s–

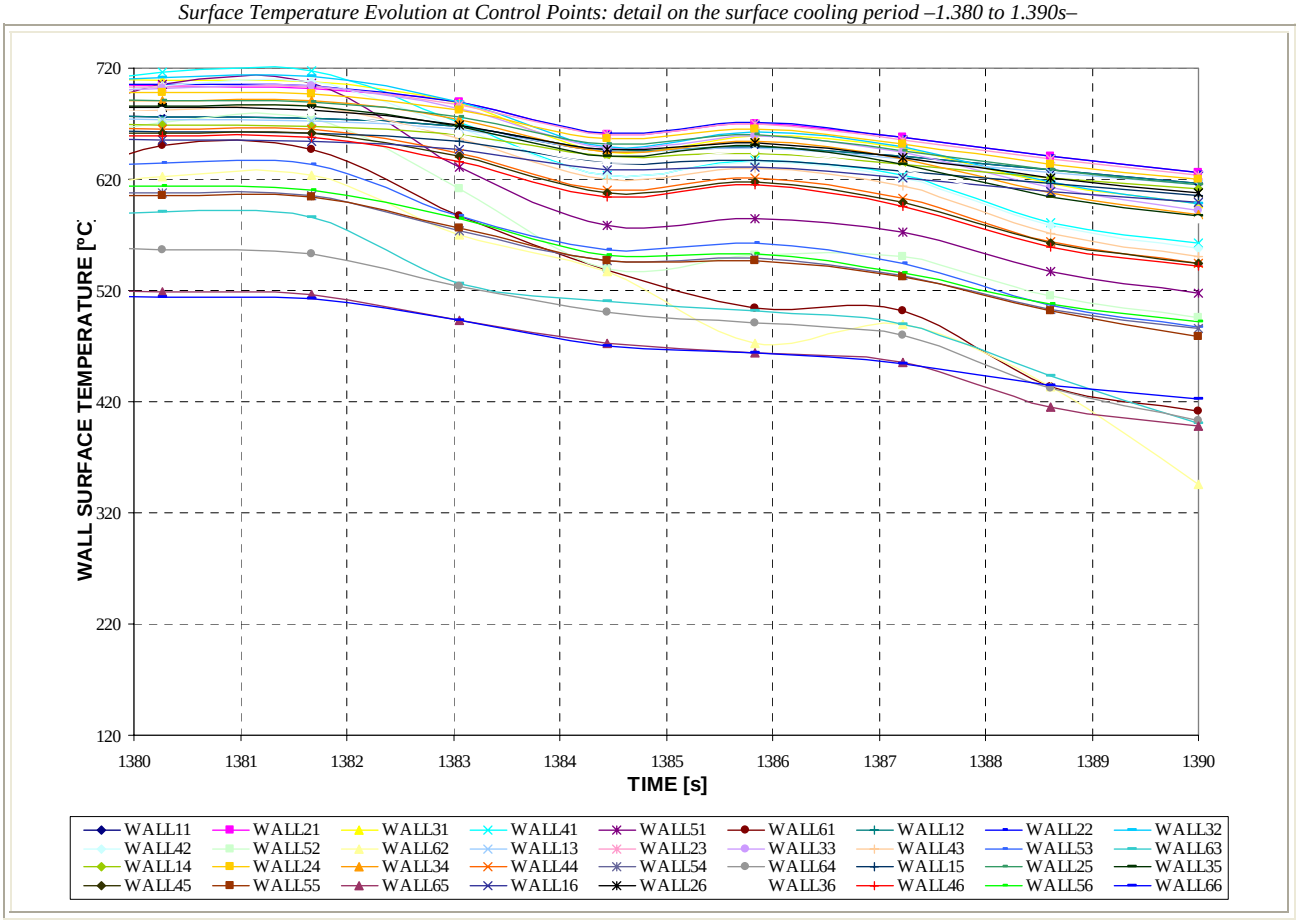

Figure 6-40.o. OFFICE-25.
Mean Cooling Rate and Standard Deviation at each of Surface Control Points.

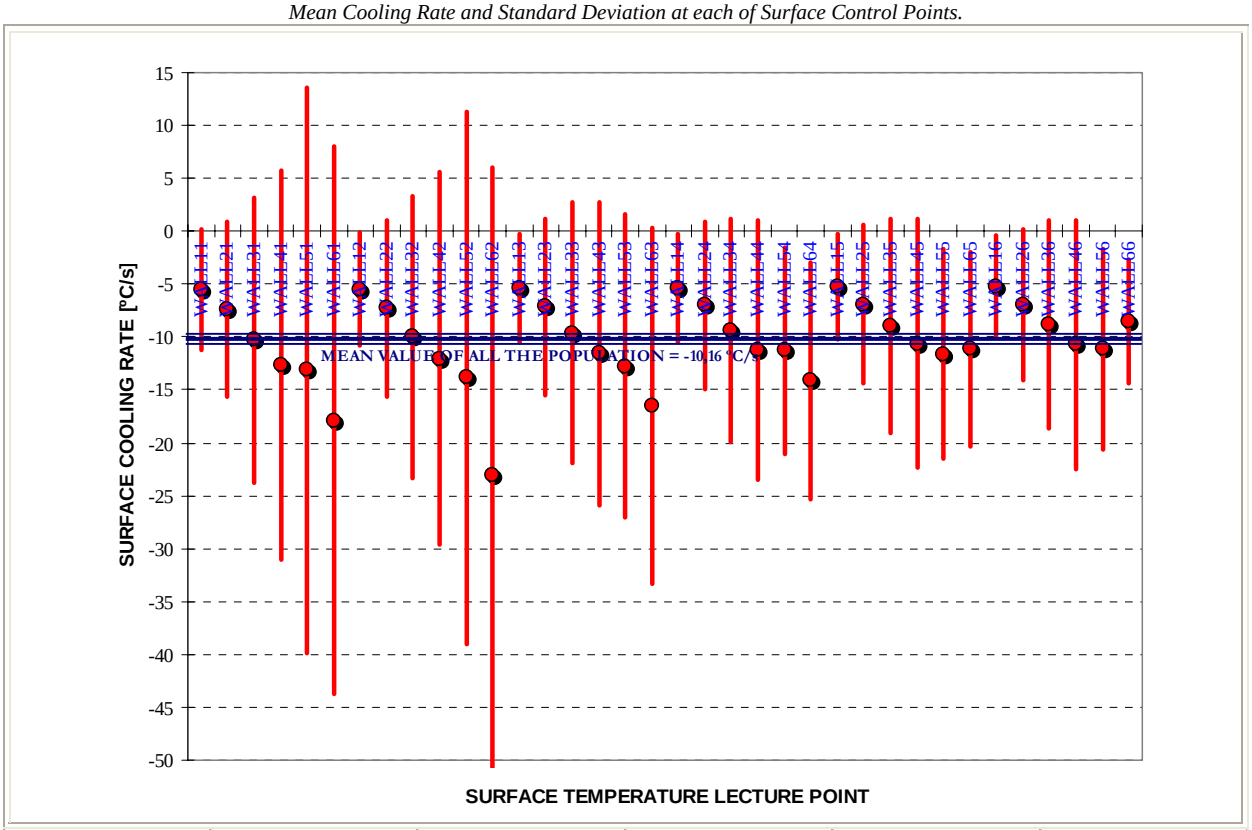

SURF. T LECTURE POINT	ARITHMETIC MEAN [ºC/s]	STANDARD DEVIATION [ºC/s]	MAXIMUM [ºC/s]	MINIMUM [ºC/s]	MEDIAN [ºC/s]
WALL11	-5,6	5,7	-15,8	2,5	-5,7
WALL21	-7,4	8,3	-21,0	6,9	-8,6
WALL31	-10,3	13,4	-31,8	10,7	-10,3
WALL41	-12,7	18,4	-34,0	9,7	-11,3
WALL51	-13,1	26,7	-54,4	30,9	-11,3
WALL61	-17,9	25,8	-49,1	29,0	-20,1
WALL12	-5,5	5,3	-14,6	1,8	-6,1
WALL22	-7,3	8,4	-20,2	6,9	-9,7
WALL32	-10,0	13,3	-29,1	9,7	-12,3
WALL42	-12,0	17,6	-30,9	9,4	-12,7
WALL52	-13,8	25,1	-51,8	15,3	-7,2
WALL62	-23,1	29,1	-62,5	14,6	-30,9
WALL13	-5,4	5,1	-14,0	1,7	-6,3
WALL23	-7,2	8,3	-19,4	6,5	-10,3
WALL33	-9,6	12,3	-25,6	8,4	-12,8
WALL43	-11,6	14,4	-30,8	7,8	-13,2
WALL53	-12,7	14,3	-33,8	4,6	-13,4
WALL63	-16,5	16,8	-43,3	4,7	-9,8
WALL14	-5,3	5,1	-13,9	1,9	-6,3
WALL24	-7,0	7,9	-17,9	5,9	-10,0
WALL34	-9,3	10,5	-21,6	7,6	-12,2
WALL44	-11,2	12,3	-28,5	8,3	-13,3
WALL54	-11,3	9,7	-22,9	1,9	-12,3
WALL64	-14,1	11,2	-34,5	-2,4	-12,2
WALL15	-5,2	5,0	-13,6	1,7	-6,1
WALL25	-6,9	7,5	-17,2	5,8	-9,6
WALL35	-9,0	10,1	-21,3	7,3	-12,4
WALL45	-10,7	11,8	-26,4	7,4	-13,2
WALL55	-11,6	9,9	-22,3	0,3	-13,6
WALL65	-11,1	9,2	-28,9	-1,4	-9,4
WALL16	-5,2	4,8	-13,1	1,2	-6,0
WALL26	-6,9	7,2	-16,4	5,0	-9,3
WALL36	-8,8	9,8	-21,6	7,0	-11,2
WALL46	-10,7	11,8	-26,7	7,8	-13,1
WALL56	-11,1	9,5	-23,5	0,8	-11,8
WALL66	-8,5	5,8	-16,6	-0,7	-8,0

Table 6-28.e. OFFICE-25.
Statistic Parameters calculated on the Surface Cooling Rate at each Control Points.

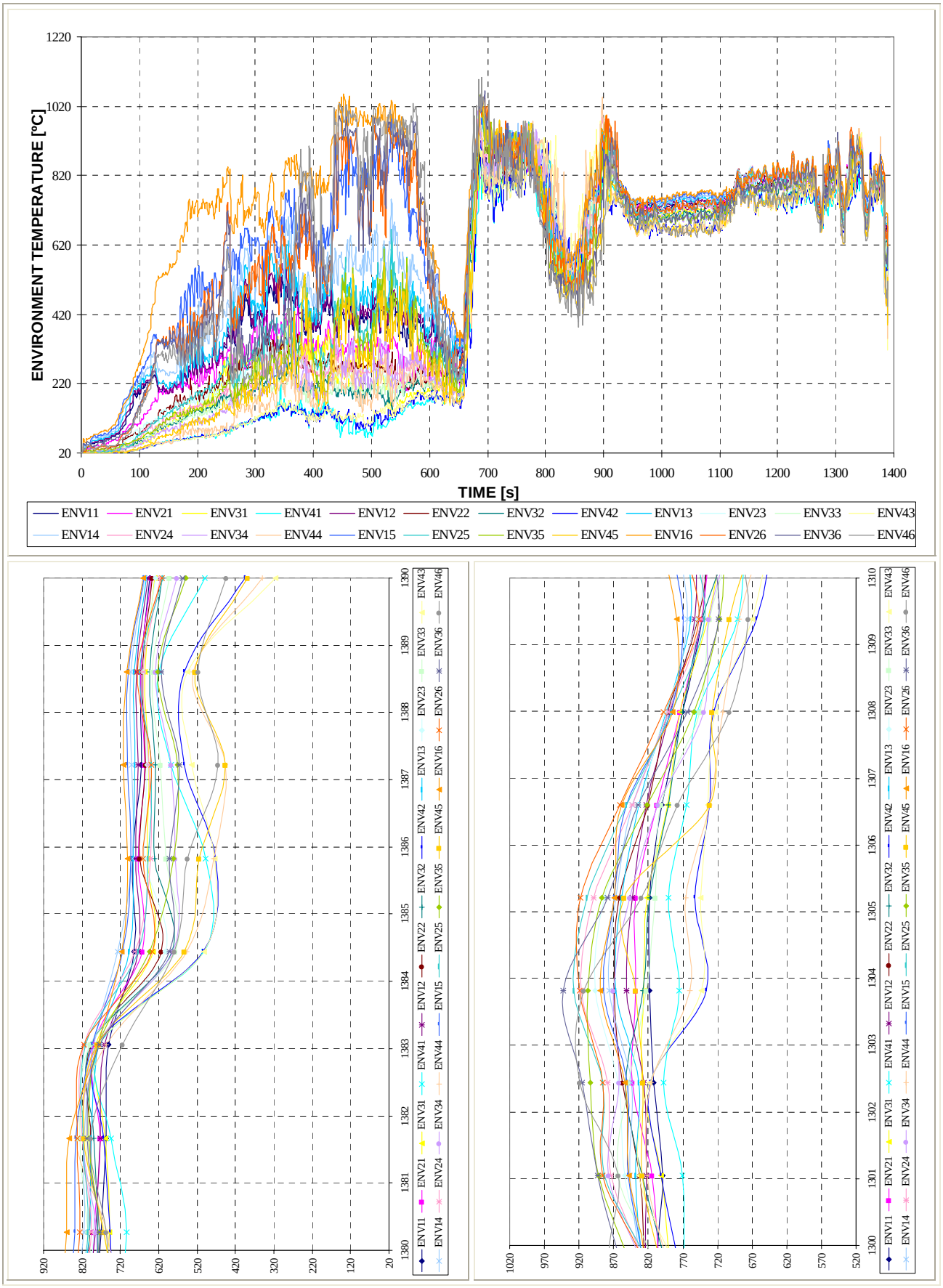

Figure 6-40.p. OFFICE-26.

Environment Temperature Evolution at the Control Points. Lower figures correspond to the detail on the 2nd environment cooling – from 1.300 to 1.310 seconds – and on the surface cooling – from 1.380 to 1.390 seconds –).

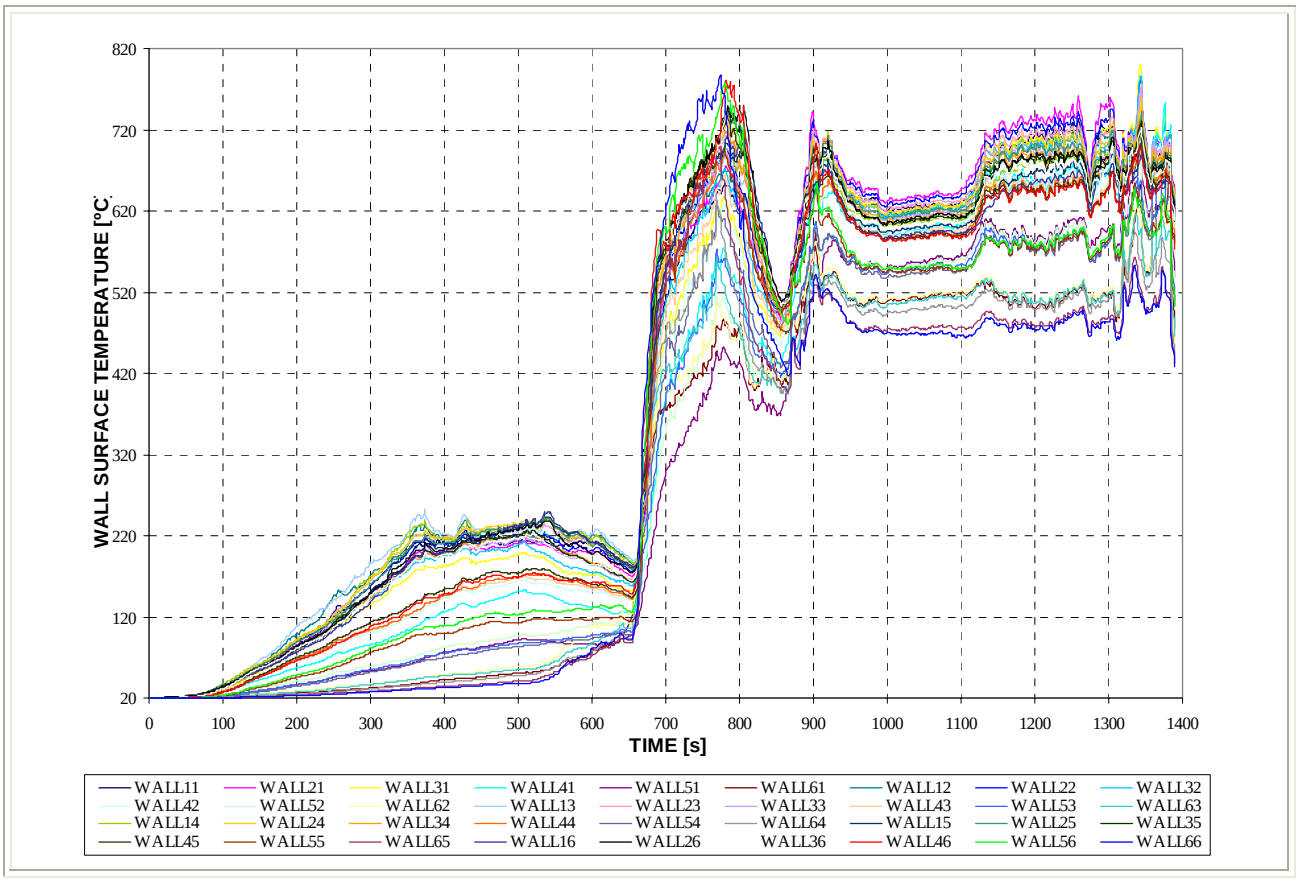

Surface Temperature Evolution at the Control Points.

Figure 6-40.q. OFFICE-26.

Surface Temperature Evolution at Control Points: detail on the surface cooling period –1.380 to 1.390s–

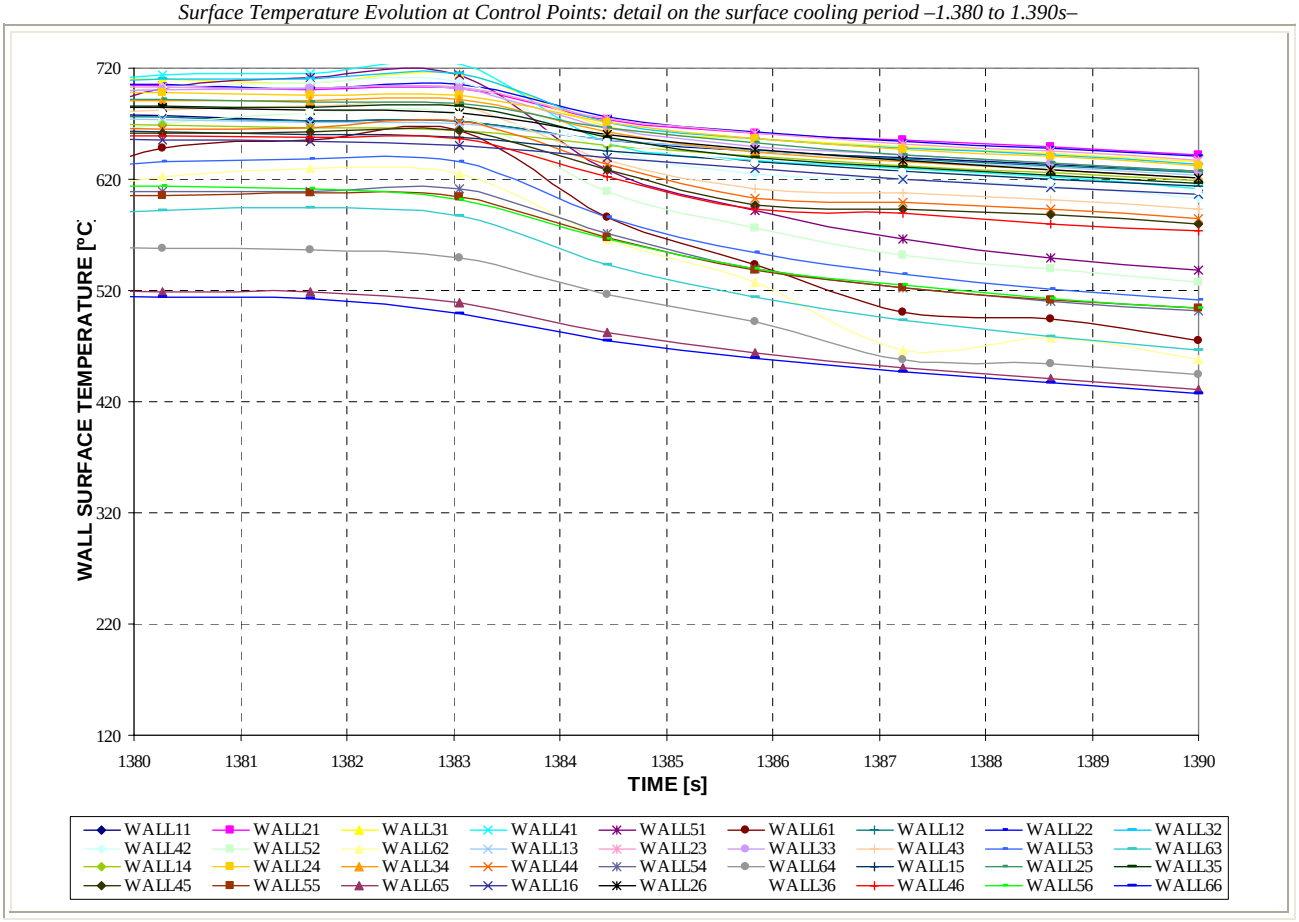

Figure 6-40.r. OFFICE-26.
Mean Cooling Rate and Standard Deviation at each of Surface Control Points.

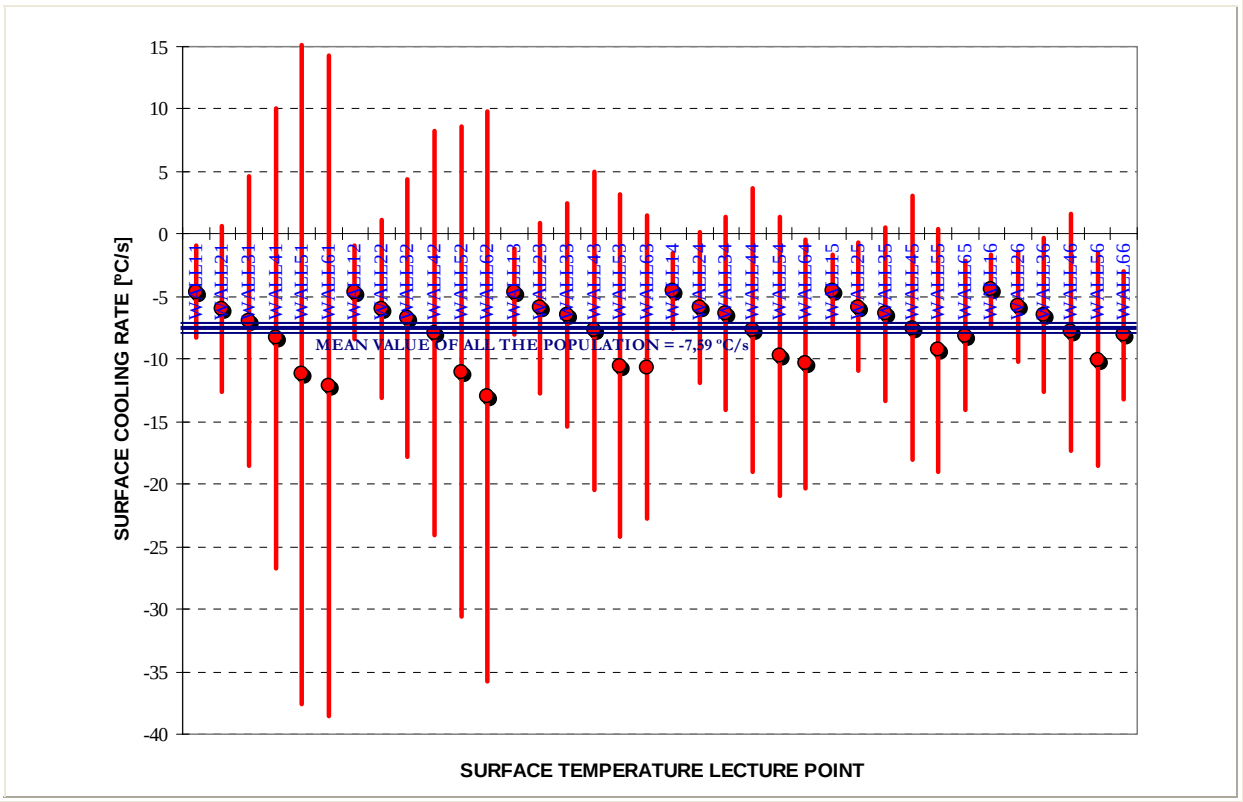

SURF. T LECTURE POINT	ARITHMETIC MEAN [ºC/s]	STANDARD DEVIATION [ºC/s]	MAXIMUM [ºC/s]	MINIMUM [ºC/s]	MEDIAN [ºC/s]
WALL11	-4,6	3,7	-12,3	-0,7	-4,3
WALL21	-6,0	6,6	-20,8	1,5	-4,5
WALL31	-6,9	11,6	-33,6	6,2	-4,7
WALL41	-8,3	18,4	-50,9	7,4	-5,3
WALL51	-11,2	26,4	-61,7	28,0	-10,0
WALL61	-12,2	26,4	-56,3	27,6	-9,1
WALL12	-4,6	3,7	-11,9	-0,4	-4,3
WALL22	-6,0	7,1	-21,3	2,4	-4,9
WALL32	-6,7	11,1	-31,8	3,4	-5,1
WALL42	-7,9	16,1	-43,8	8,1	-4,2
WALL52	-11,0	19,6	-48,7	14,3	-9,0
WALL62	-13,0	22,8	-44,3	13,8	-8,7
WALL13	-4,6	3,5	-11,0	-0,8	-4,5
WALL23	-5,9	6,8	-20,1	1,0	-5,1
WALL33	-6,4	8,9	-25,6	0,8	-5,0
WALL43	-7,7	12,7	-34,7	2,7	-3,5
WALL53	-10,5	13,7	-36,1	4,9	-8,2
WALL63	-10,7	12,1	-32,1	4,9	-9,7
WALL14	-4,6	3,0	-9,7	-0,6	-4,7
WALL24	-5,9	6,0	-17,9	-0,1	-5,3
WALL34	-6,3	7,7	-21,7	1,2	-5,2
WALL44	-7,7	11,3	-28,1	4,5	-3,7
WALL54	-9,8	11,1	-29,2	1,5	-7,3
WALL64	-10,4	10,0	-24,5	-0,8	-5,9
WALL15	-4,5	2,9	-8,9	-0,6	-4,8
WALL25	-5,9	5,1	-15,4	-0,4	-5,6
WALL35	-6,4	7,0	-19,7	0,4	-5,6
WALL45	-7,5	10,5	-25,8	1,4	-3,4
WALL55	-9,3	9,7	-26,2	1,1	-6,9
WALL65	-8,1	6,0	-18,9	0,0	-7,3
WALL16	-4,5	2,8	-8,6	-0,7	-4,8
WALL26	-5,8	4,5	-13,5	-0,6	-5,8
WALL36	-6,5	6,2	-17,6	-0,5	-5,7
WALL46	-7,9	9,4	-24,7	-0,5	-4,0
WALL56	-10,1	8,5	-25,4	-0,8	-7,9
WALL66	-8,1	5,1	-17,2	-0,6	-8,1

Table 6-28.f. OFFICE-26.
Statistic Parameters calculated on the Surface Cooling Rate at each Control Points.

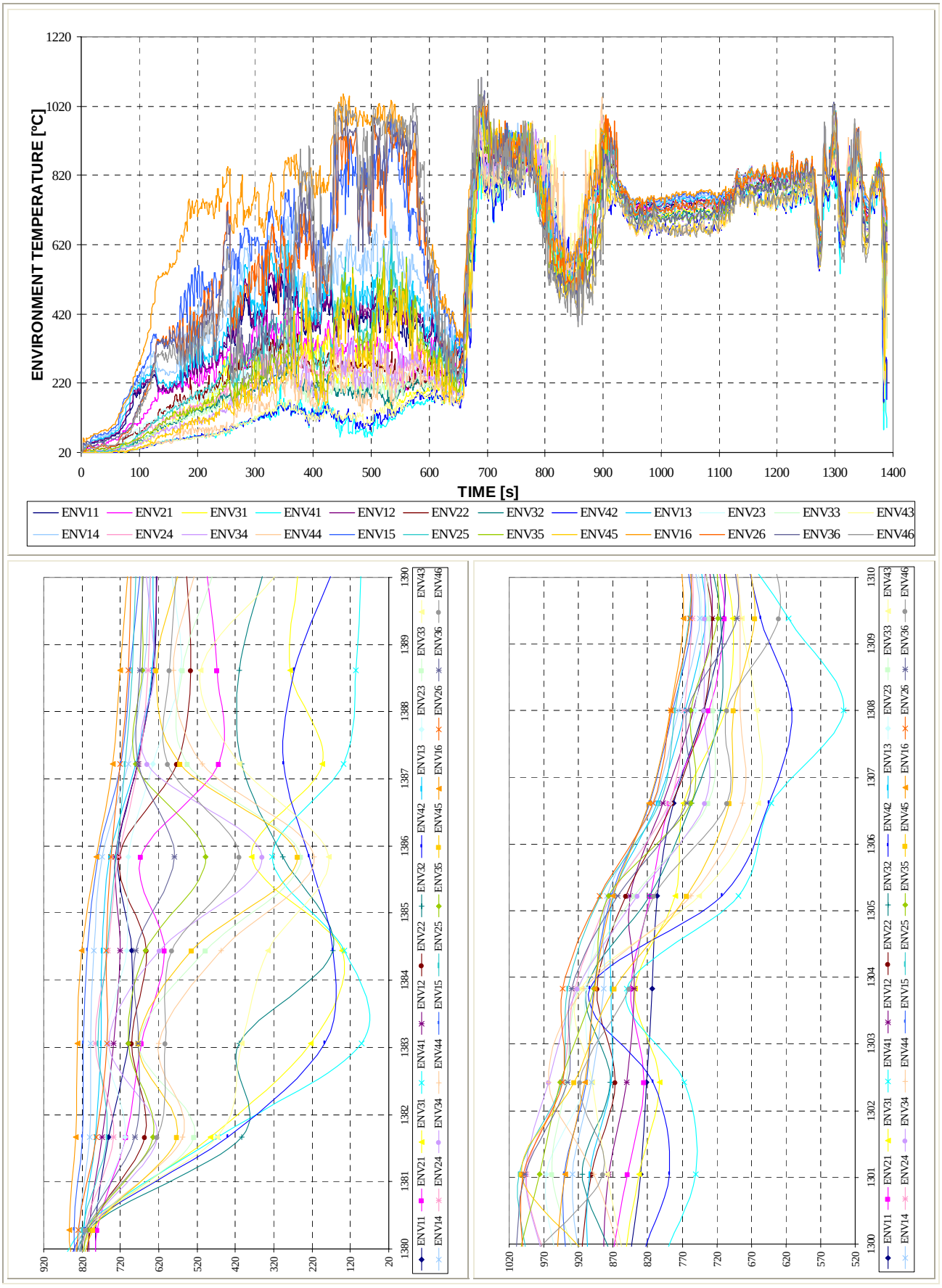

Figure 6-41.a. OFFICE-19.
Environment Temperature Evolution at the Control Points. Lower figures correspond to the detail on the 2nd environment cooling – from 1.300 to 1.310 seconds – and on the surface cooling – from 1.380 to 1.390 seconds –).

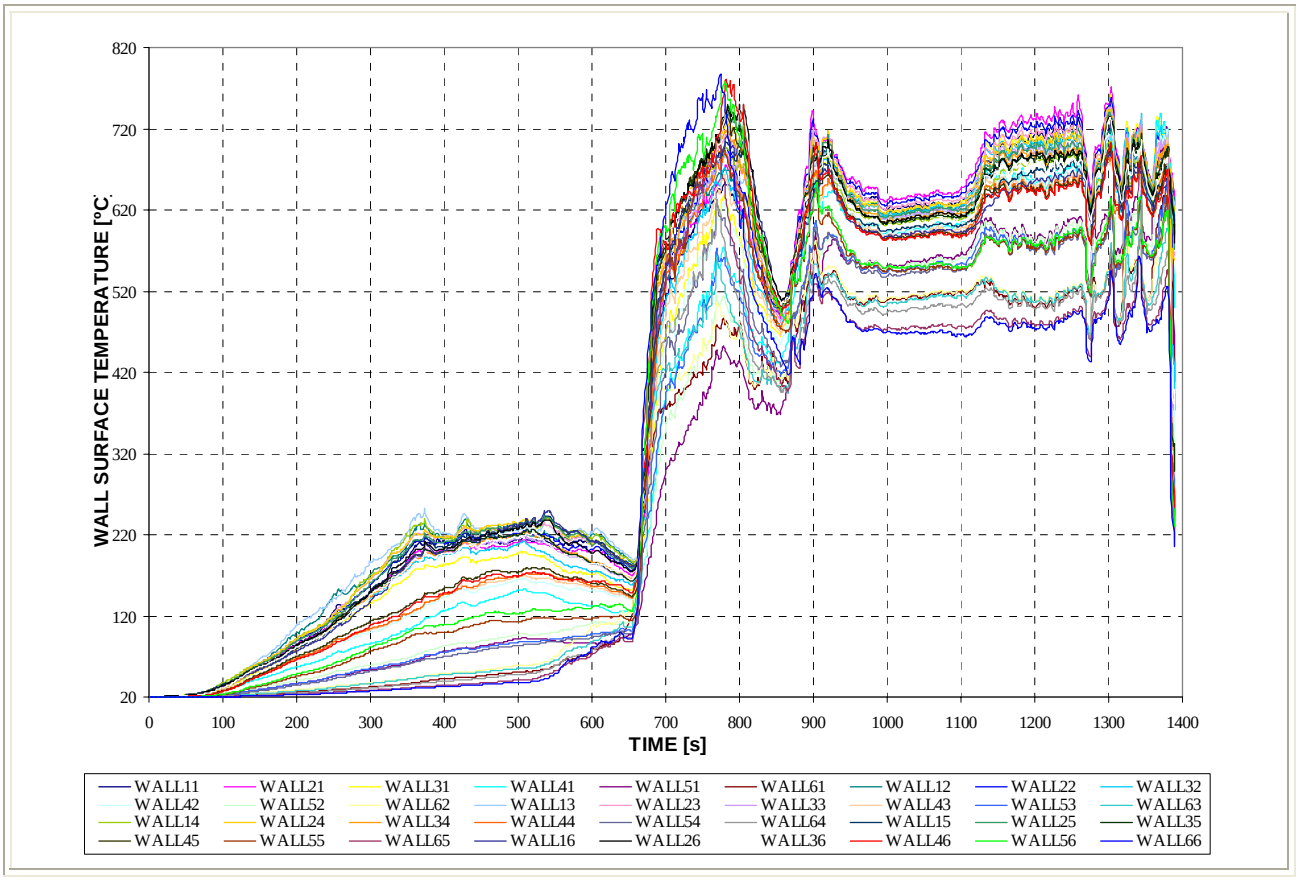

Surface Temperature Evolution at the Control Points.

Figure 6-41.b. OFFICE-19.

Surface Temperature Evolution at Control Points: detail on the surface cooling period –1.380 to 1.390s–

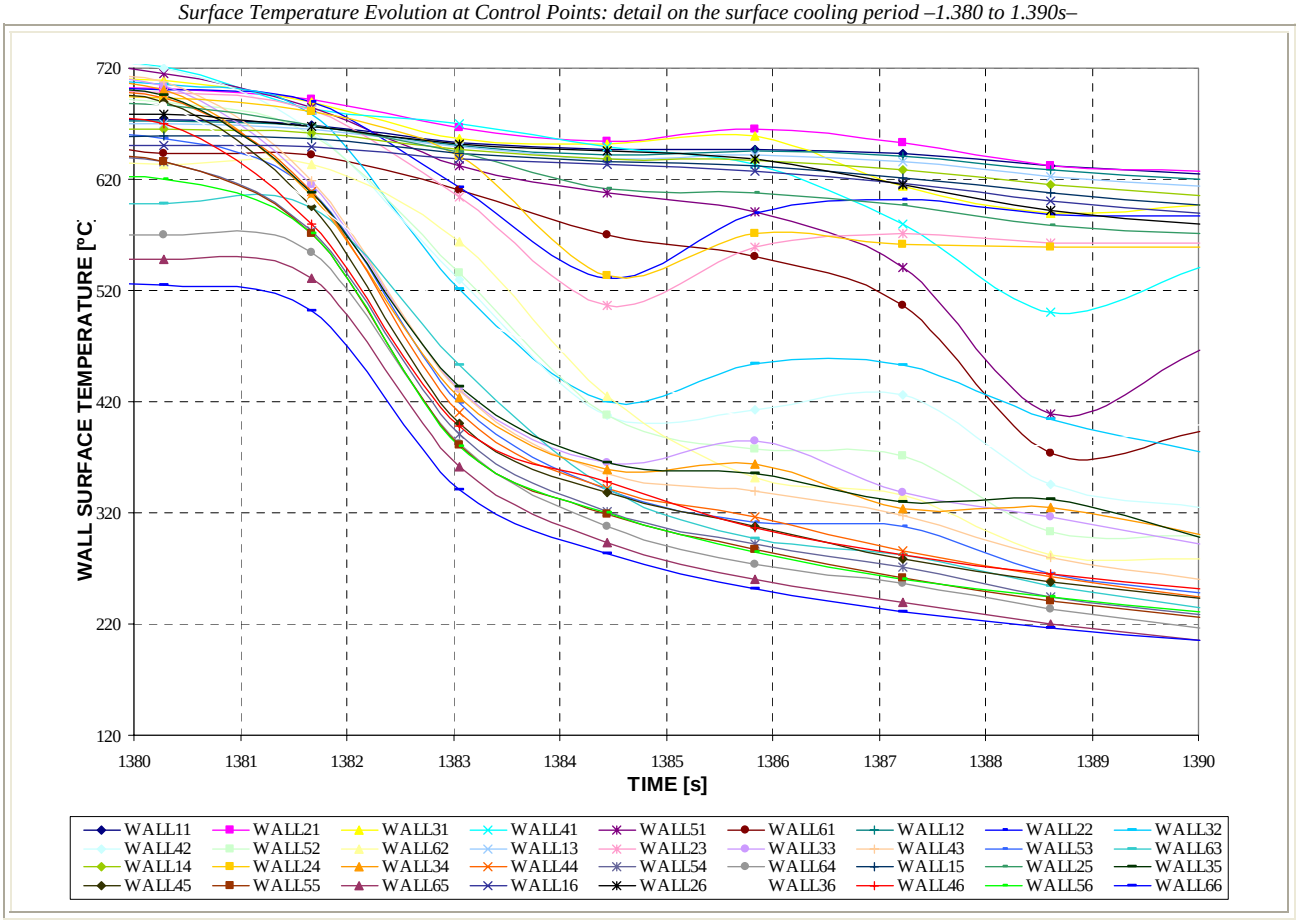

Figure 6-41.c. OFFICE-19.
Mean Cooling Rate and Standard Deviation at each of Surface Control Points.

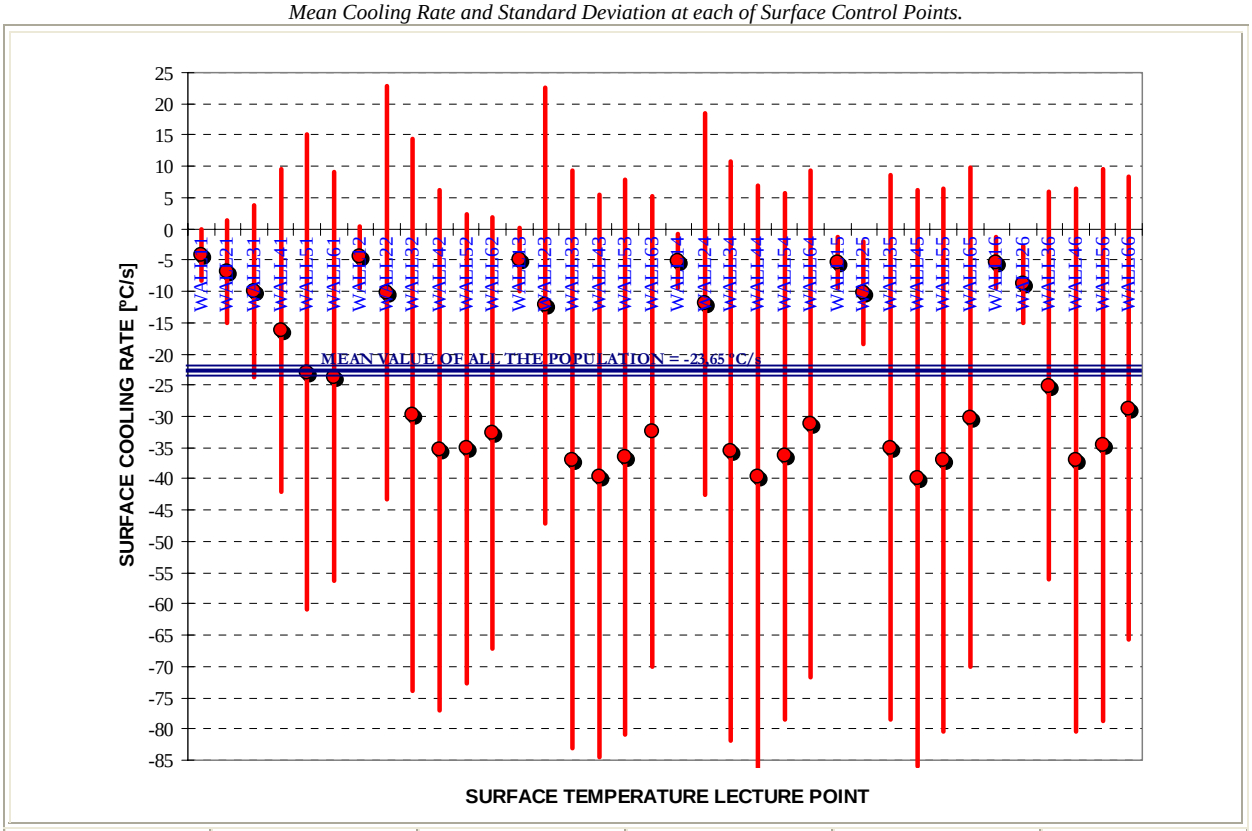

SURF. T LECTURE POINT	ARITHMETIC MEAN [ºC/s]	STANDARD DEVIATION [ºC/s]	MAXIMUM [ºC/s]	MINIMUM [ºC/s]	MEDIAN [ºC/s]
WALL11	-4,2	4,1	-11,4	1,3	-3,9
WALL21	-6,8	8,3	-18,6	8,3	-7,7
WALL31	-10,0	13,8	-31,9	5,0	-8,9
WALL41	-16,3	25,8	-56,9	29,0	-13,1
WALL51	-23,0	38,0	-94,8	41,0	-20,0
WALL61	-23,7	32,7	-95,7	14,0	-18,3
WALL12	-4,5	4,9	-12,3	2,2	-4,4
WALL22	-10,3	33,0	-58,3	42,2	-4,4
WALL32	-29,8	44,1	-113,1	24,6	-20,2
WALL42	-35,4	41,7	-96,0	9,4	-28,0
WALL52	-35,2	37,6	-92,1	-0,4	-21,7
WALL62	-32,6	34,5	-99,2	0,0	-25,1
WALL13	-4,9	5,0	-12,0	2,2	-5,0
WALL23	-12,2	34,9	-69,7	37,8	-3,1
WALL33	-36,9	46,2	-132,8	14,1	-24,9
WALL43	-39,5	45,0	-135,2	5,4	-21,4
WALL53	-36,4	44,4	-135,9	2,8	-26,1
WALL63	-32,4	37,7	-101,4	1,5	-16,8
WALL14	-5,2	4,4	-10,8	1,3	-6,2
WALL24	-12,0	30,4	-77,1	27,1	-4,3
WALL34	-35,5	46,4	-130,7	4,0	-23,4
WALL44	-39,7	46,5	-142,7	5,2	-20,2
WALL54	-36,3	42,1	-131,3	2,9	-20,3
WALL64	-31,3	40,6	-123,1	4,2	-14,5
WALL15	-5,4	4,0	-10,4	1,4	-6,3
WALL25	-10,3	8,2	-24,1	0,5	-10,5
WALL35	-35,0	43,5	-124,6	5,4	-21,6
WALL45	-39,8	46,1	-140,1	2,8	-21,6
WALL55	-37,0	43,3	-136,7	-0,7	-20,6
WALL65	-30,2	39,9	-121,5	4,2	-14,7
WALL16	-5,3	4,0	-10,7	1,4	-6,0
WALL26	-8,9	6,1	-17,0	0,8	-8,6
WALL36	-25,1	31,0	-70,5	13,3	-25,0
WALL46	-37,0	43,3	-130,9	4,8	-23,6
WALL56	-34,6	44,1	-137,5	3,3	-21,5
WALL66	-28,7	37,0	-115,0	0,1	-16,0

Table 6-28.g. OFFICE-19.
Statistic Parameters calculated on the Surface Cooling Rate at each Control Points.

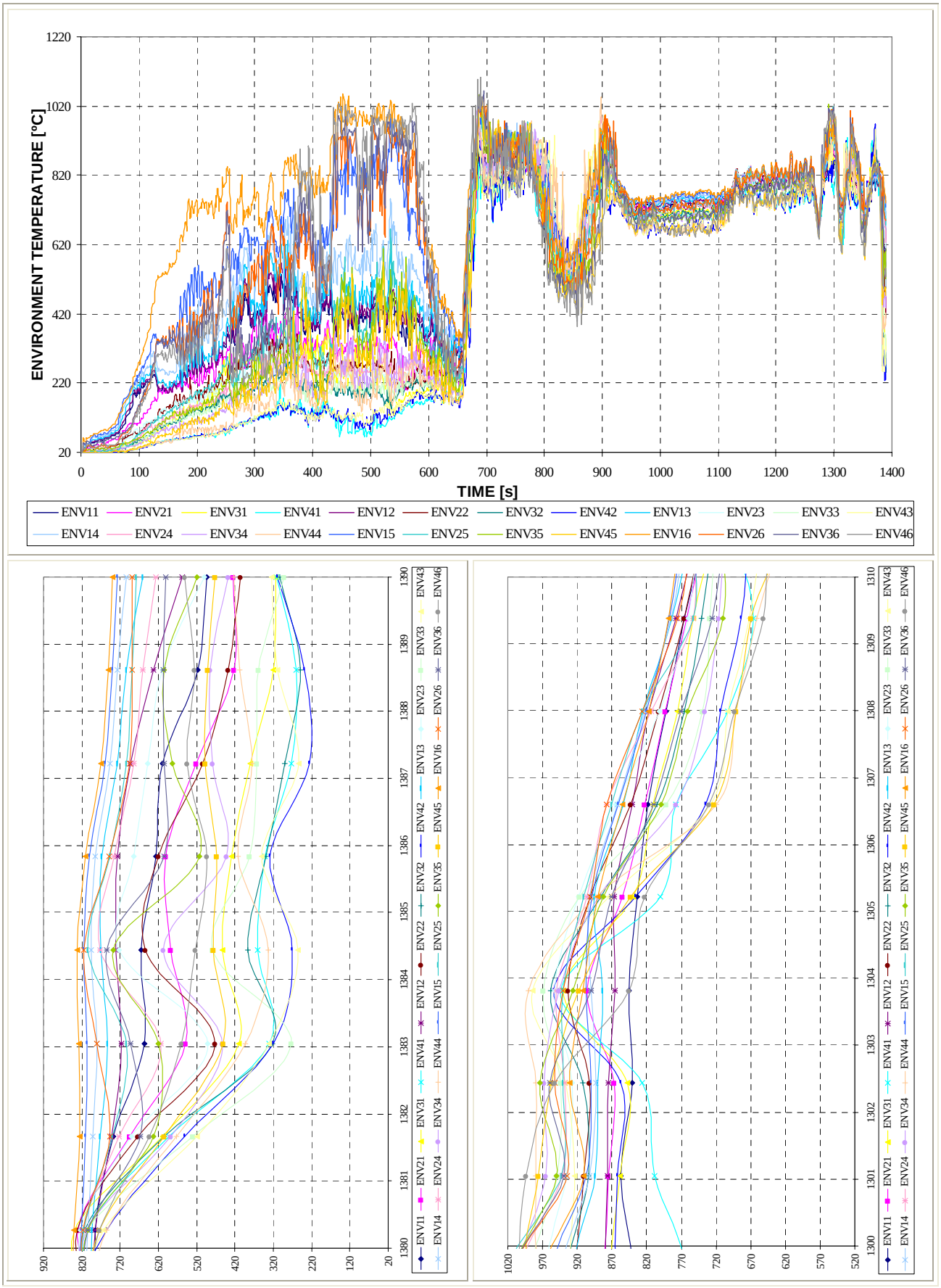

Figure 6-42.a. OFFICE-10.

Environment Temperature Evolution at the Control Points. Lower figures correspond to the detail on the 2nd environment cooling – from 1.300 to 1.310 seconds – and on the surface cooling – from 1.380 to 1.390 seconds –).

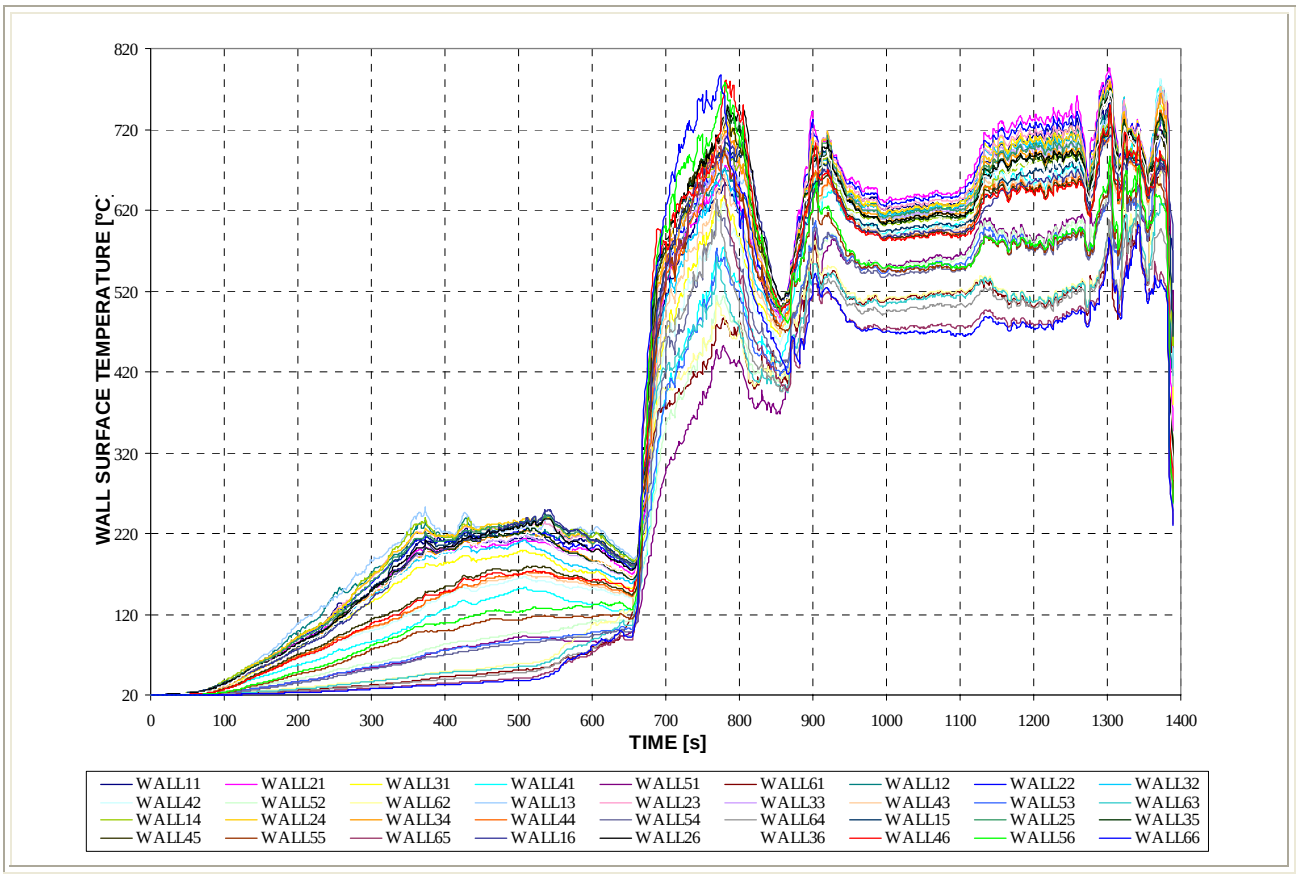

Surface Temperature Evolution at the Control Points.

Figure 6-42.b. OFFICE-10.

Surface Temperature Evolution at Control Points: detail on the surface cooling period –1.380 to 1.390s–

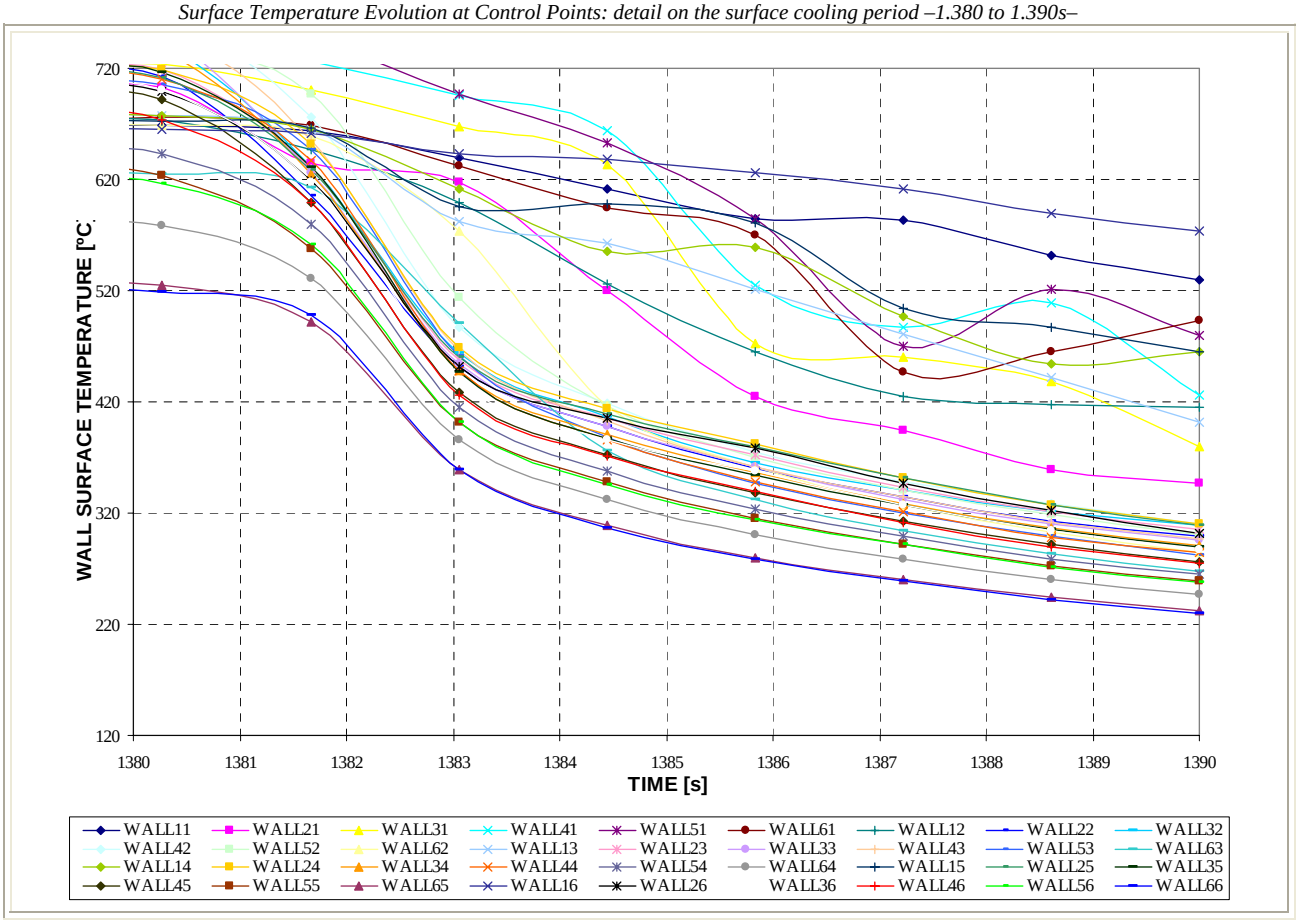

Figure 6-42.c. OFFICE-10.
Mean Cooling Rate and Standard Deviation at each of Surface Control Points.

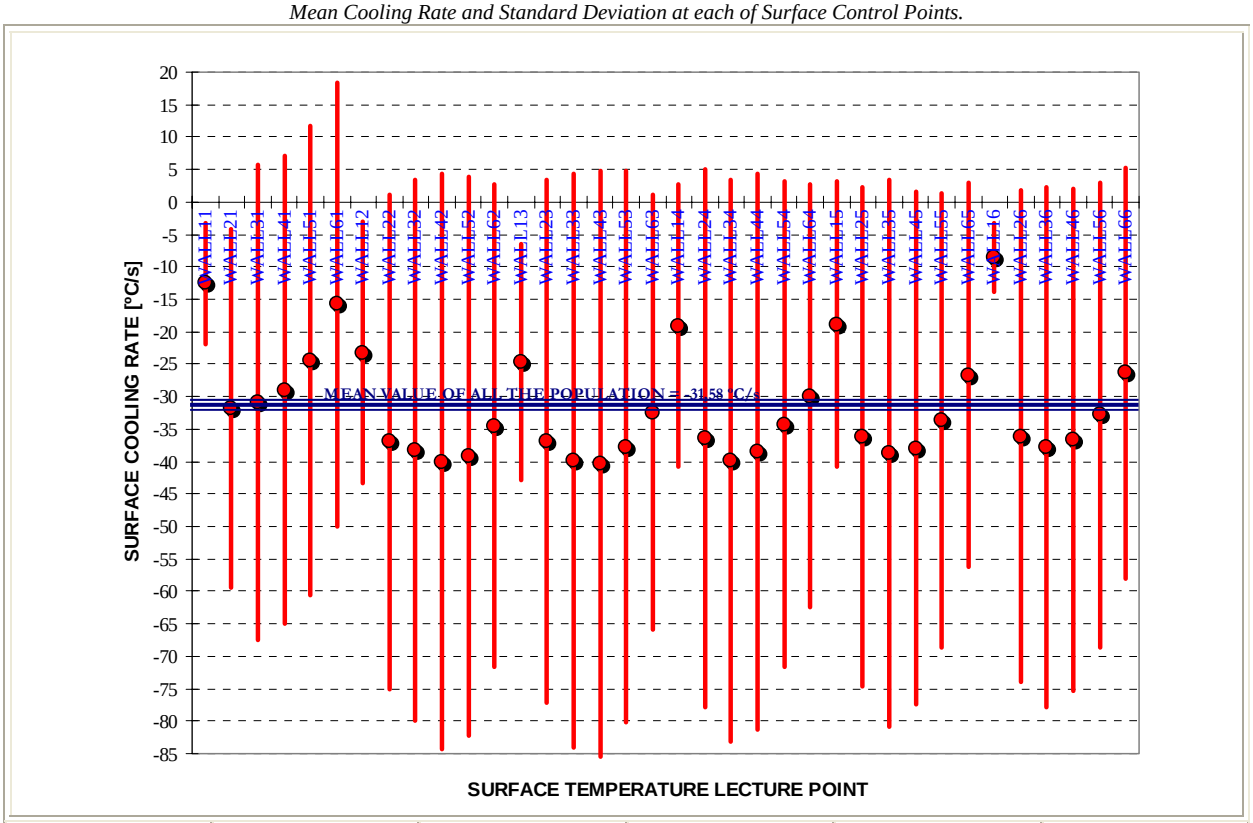

SURF. T LECTURE POINT	ARITHMETIC MEAN [°C/s]	STANDARD DEVIATION [°C/s]	MAXIMUM [°C/s]	MINIMUM [°C/s]	MEDIAN [°C/s]
WALL11	-12,5	9,4	-23,5	0,0	-16,2
WALL21	-31,7	27,6	-69,8	1,6	-23,6
WALL31	-30,9	36,6	-116,0	0,7	-20,0
WALL41	-29,0	36,0	-99,6	15,7	-22,4
WALL51	-24,5	36,2	-82,8	37,3	-31,0
WALL61	-15,7	34,1	-88,2	20,0	-11,9
WALL12	-23,2	20,1	-53,0	0,2	-24,5
WALL22	-37,0	38,2	-110,6	2,2	-22,8
WALL32	-38,3	41,7	-120,5	4,1	-23,9
WALL42	-40,0	44,4	-136,2	5,5	-25,3
WALL52	-39,2	43,1	-132,2	2,2	-25,6
WALL62	-34,5	37,2	-112,4	0,0	-20,8
WALL13	-24,7	18,2	-60,1	0,1	-28,4
WALL23	-36,9	40,2	-123,8	2,4	-22,2
WALL33	-39,8	44,2	-124,4	7,1	-23,4
WALL43	-40,4	45,1	-136,1	5,9	-24,3
WALL53	-37,8	42,5	-133,5	2,6	-24,3
WALL63	-32,4	33,5	-87,3	-2,3	-17,8
WALL14	-19,1	21,8	-44,7	8,4	-20,0
WALL24	-36,5	41,4	-131,4	2,2	-22,1
WALL34	-39,8	43,3	-127,6	2,0	-22,4
WALL44	-38,5	42,8	-135,8	-2,3	-23,4
WALL54	-34,2	37,4	-119,2	-1,8	-21,2
WALL64	-29,9	32,6	-104,4	-1,5	-19,3
WALL15	-18,8	21,9	-54,8	2,0	-12,6
WALL25	-36,2	38,5	-120,8	-0,1	-20,4
WALL35	-38,7	42,2	-132,3	-2,3	-21,6
WALL45	-37,9	39,5	-122,5	-4,6	-21,2
WALL55	-33,7	34,9	-113,0	-7,2	-19,9
WALL65	-26,7	29,6	-95,4	-2,3	-17,6
WALL16	-8,5	5,2	-15,2	-1,7	-10,0
WALL26	-36,1	38,0	-121,1	-2,2	-21,1
WALL36	-37,9	40,1	-127,7	-5,8	-21,1
WALL46	-36,6	38,8	-124,3	-5,9	-21,2
WALL56	-32,8	35,8	-115,8	-4,5	-19,5
WALL66	-26,4	31,6	-100,4	-2,2	-14,5

Table 6-28.h. OFFICE-10.
Statistic Parameters calculated on the Surface Cooling Rate at each Control Points.

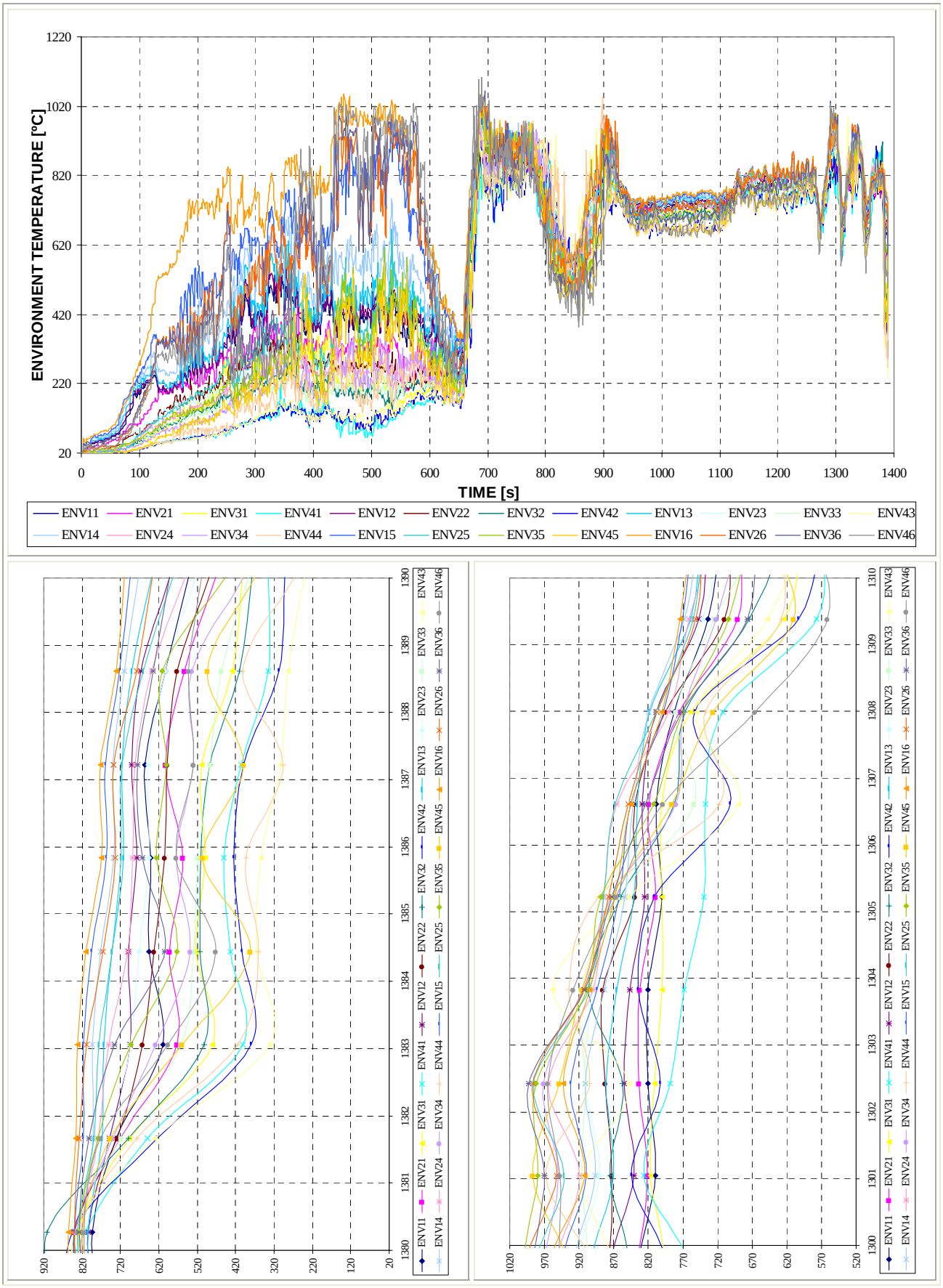

Figure 6-42.d. OFFICE-12.

Environment Temperature Evolution at the Control Points. Lower figures correspond to the detail on the 2nd environment cooling – from 1.300 to 1.310 seconds – and on the surface cooling – from 1.380 to 1.390 seconds –).

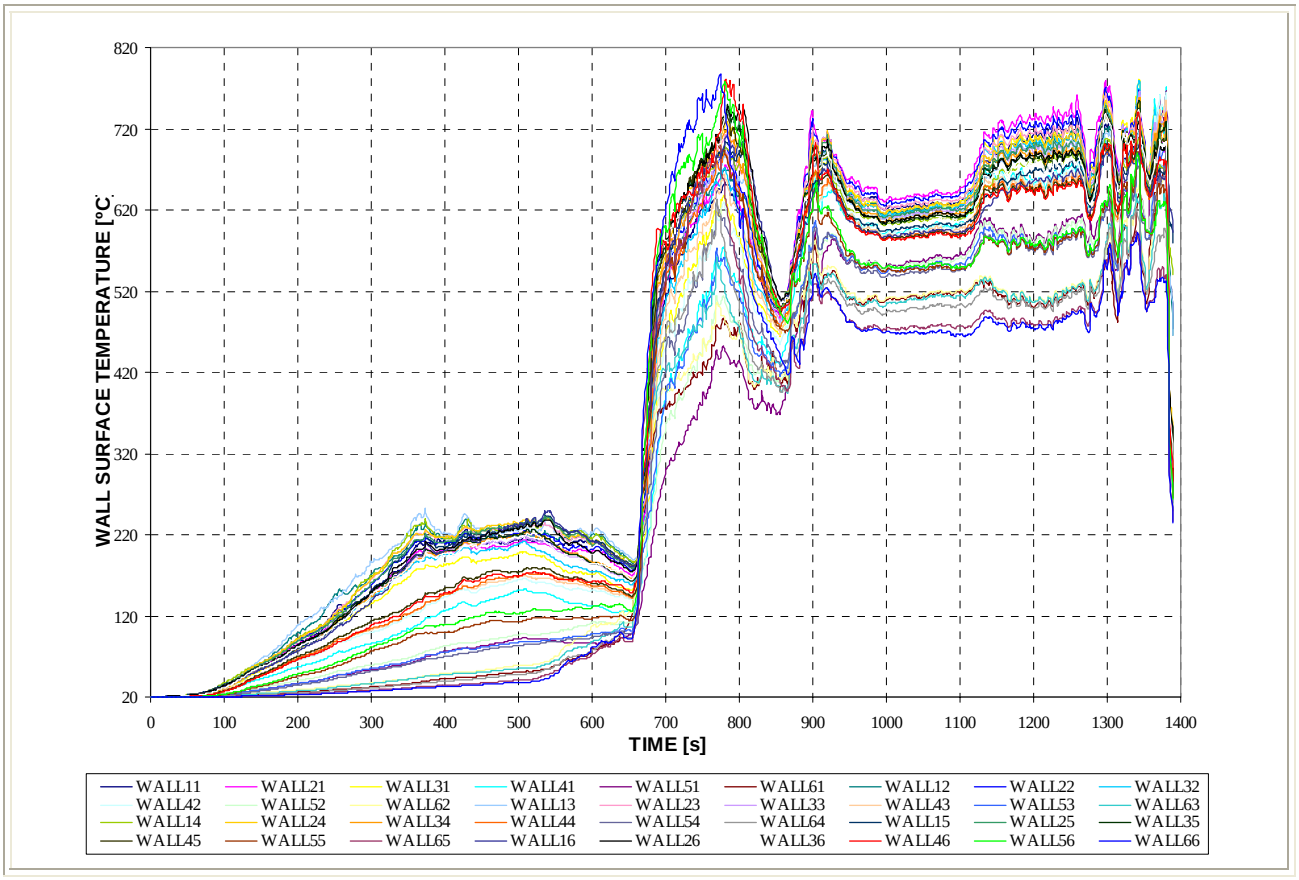

Surface Temperature Evolution at the Control Points.

Figure 6-42.e. OFFICE-12.

Surface Temperature Evolution at Control Points: detail on the surface cooling period –1.380 to 1.390s–

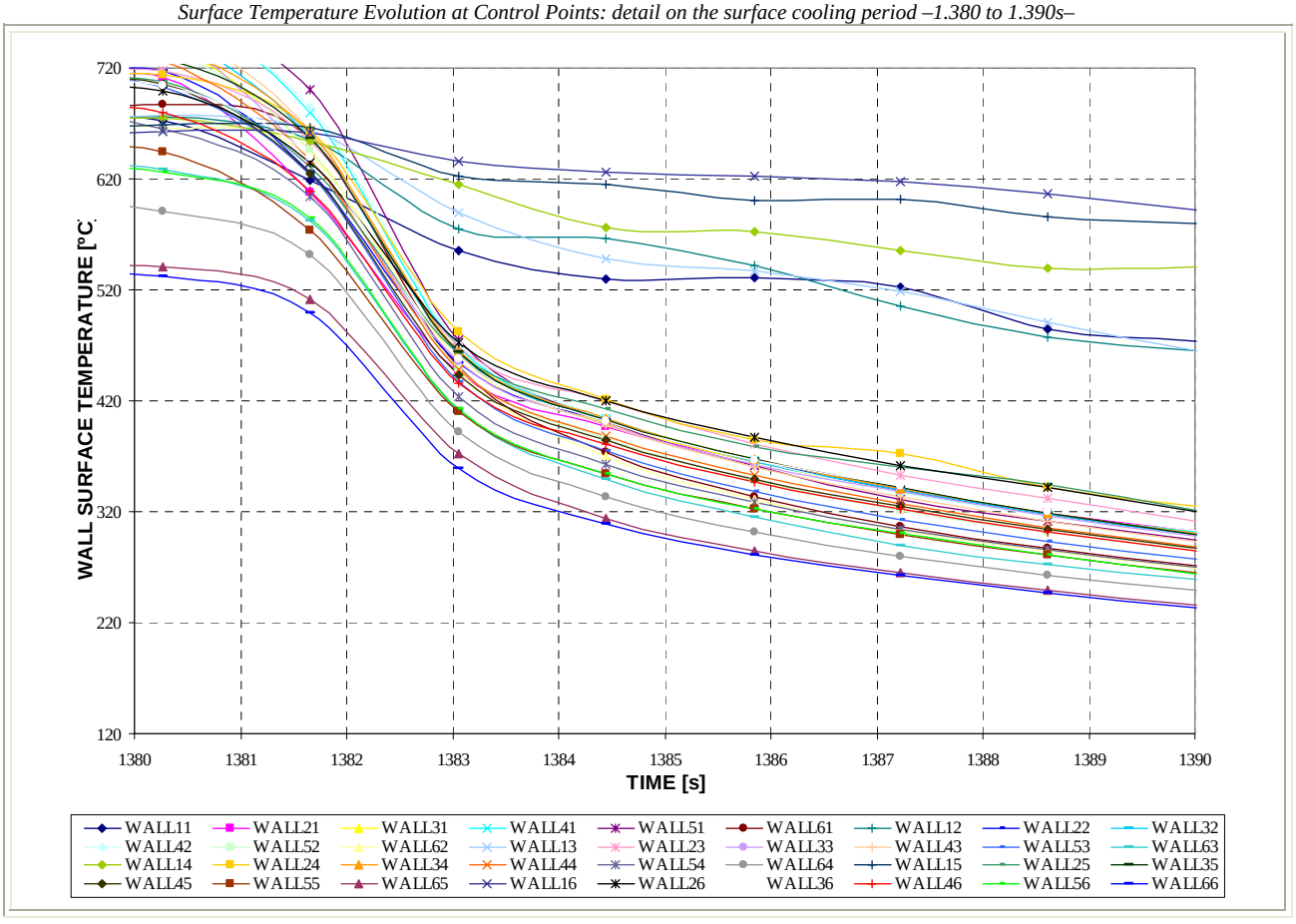

Figure 6-42.f. OFFICE-12.
Mean Cooling Rate and Standard Deviation at each of Surface Control Points.

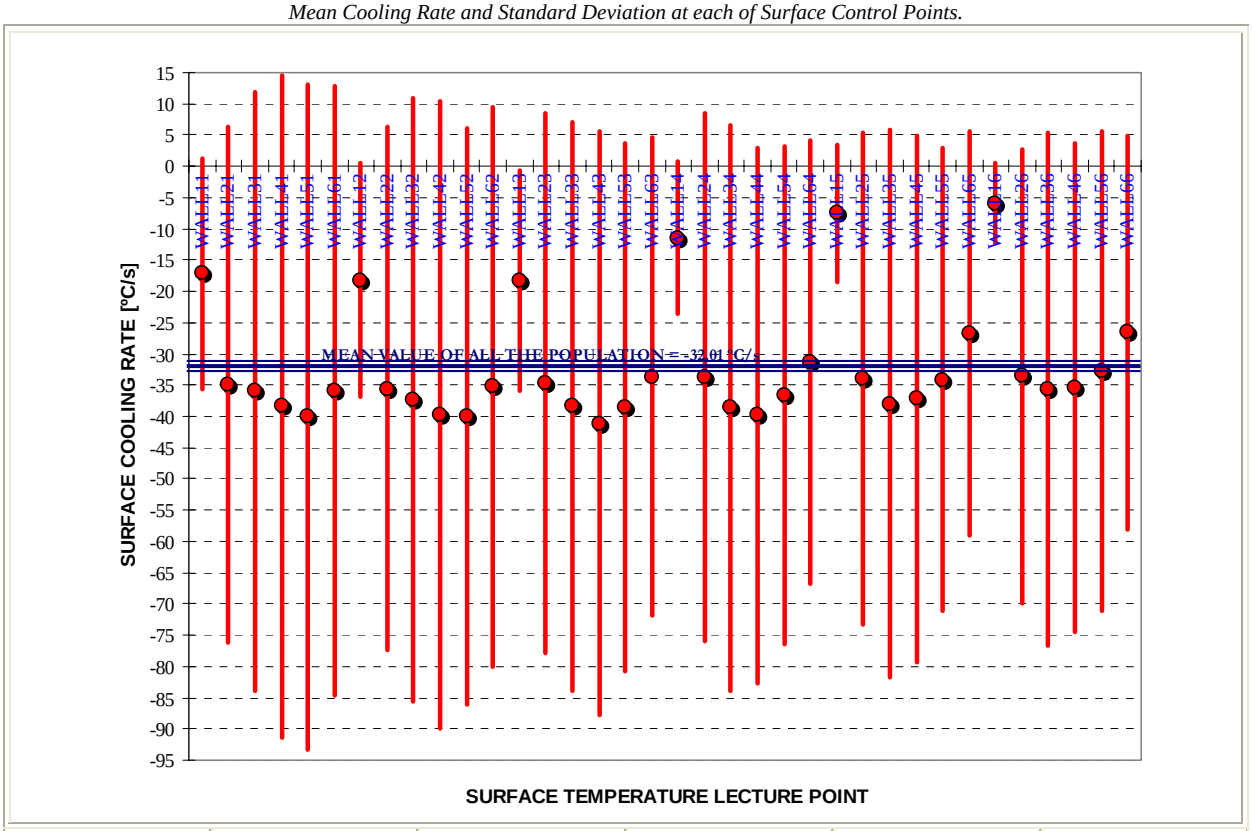

SURF. T LECTURE POINT	ARITHMETIC MEAN [ºC/s]	STANDARD DEVIATION [ºC/s]	MAXIMUM [ºC/s]	MINIMUM [ºC/s]	MEDIAN [ºC/s]
WALL11	-17,19	18,43	-45,65	4,75	-12,93
WALL21	-34,86	41,27	-116,06	14,29	-20,64
WALL31	-35,99	47,96	-134,50	26,43	-22,22
WALL41	-38,42	52,90	-150,45	28,68	-23,77
WALL51	-40,12	53,25	-160,91	16,01	-25,35
WALL61	-35,90	48,77	-147,70	10,64	-20,73
WALL12	-18,19	18,74	-57,54	6,01	-16,33
WALL22	-35,60	41,90	-122,66	14,66	-22,15
WALL32	-37,37	48,20	-139,69	22,10	-22,59
WALL42	-39,80	50,25	-151,74	14,42	-24,03
WALL52	-39,96	46,06	-140,34	4,61	-23,18
WALL62	-35,27	44,71	-137,78	2,57	-19,23
WALL13	-18,25	17,57	-53,22	5,80	-15,67
WALL23	-34,73	43,23	-132,69	13,25	-24,15
WALL33	-38,42	45,40	-129,15	14,83	-21,94
WALL43	-41,19	46,68	-144,26	1,94	-23,41
WALL53	-38,59	42,27	-133,14	-3,02	-22,33
WALL63	-33,63	38,15	-122,11	-3,70	-21,20
WALL14	-11,43	12,29	-28,61	4,88	-11,67
WALL24	-33,71	42,24	-129,78	9,55	-24,28
WALL34	-38,65	45,19	-140,38	5,37	-22,69
WALL44	-39,86	42,84	-134,92	-5,27	-21,74
WALL54	-36,59	39,83	-128,88	-8,32	-20,98
WALL64	-31,23	35,42	-113,90	-4,94	-19,45
WALL15	-7,55	11,02	-31,57	3,86	-4,77
WALL25	-33,97	39,33	-120,10	5,98	-20,59
WALL35	-37,95	43,80	-137,25	3,96	-21,94
WALL45	-37,19	42,10	-130,41	3,31	-21,27
WALL55	-34,12	36,98	-116,26	-0,96	-19,51
WALL65	-26,81	32,29	-99,96	4,19	-17,75
WALL16	-5,88	6,50	-18,14	2,98	-5,43
WALL26	-33,59	36,38	-115,11	3,67	-20,89
WALL36	-35,66	41,05	-129,54	2,74	-20,88
WALL46	-35,42	39,01	-123,02	0,30	-20,70
WALL56	-32,74	38,27	-122,54	-2,42	-19,67
WALL66	-26,60	31,51	-99,52	1,31	-16,76

Table 6-28.i. OFFICE-12.
Statistic Parameters calculated on the Surface Cooling Rate at each Control Points.

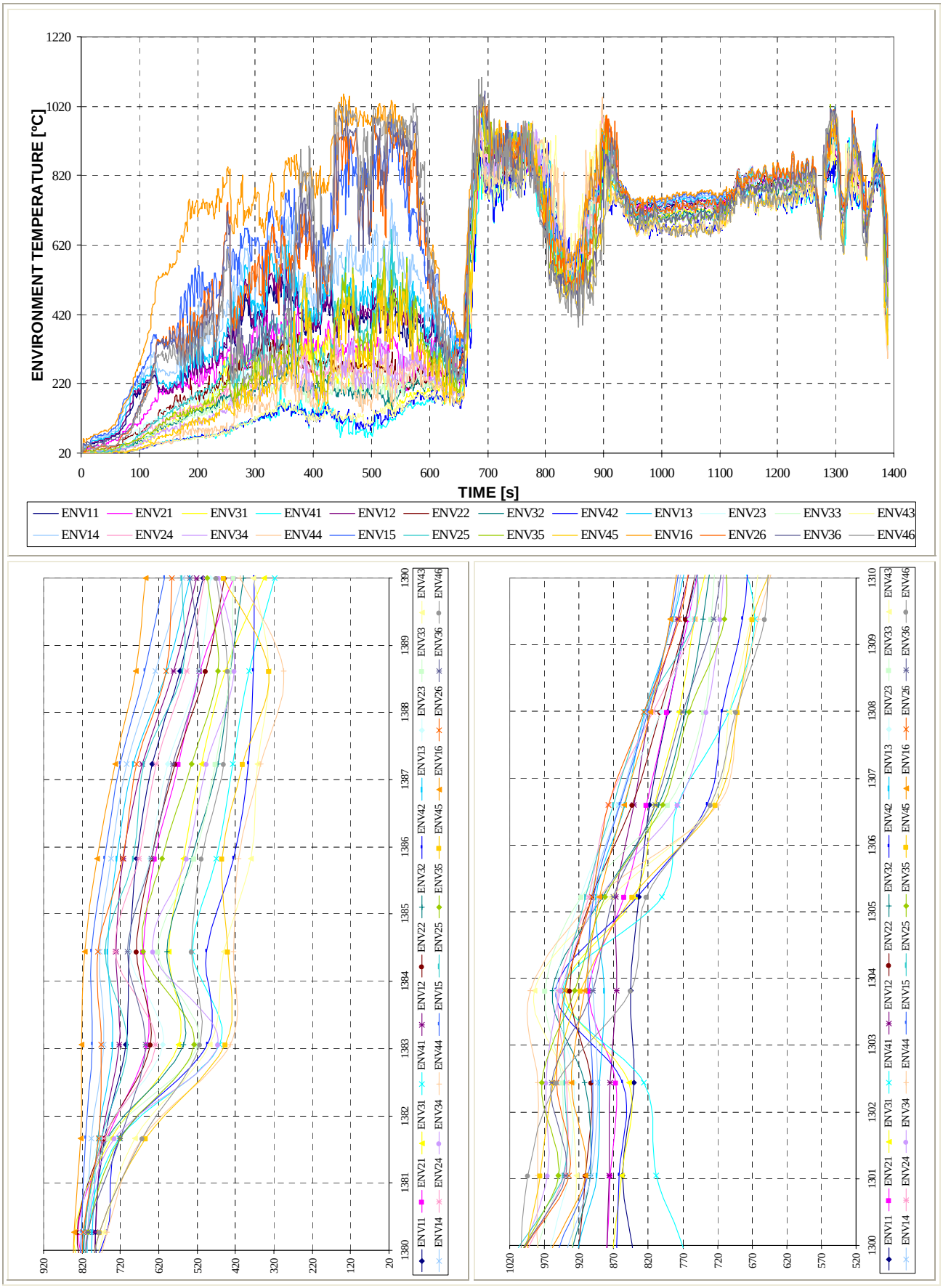

Figure 6-42.g. OFFICE-11.

Environment Temperature Evolution at the Control Points. Lower figures correspond to the detail on the 2nd environment cooling – from 1.300 to 1.310 seconds – and on the surface cooling – from 1.380 to 1.390 seconds –).

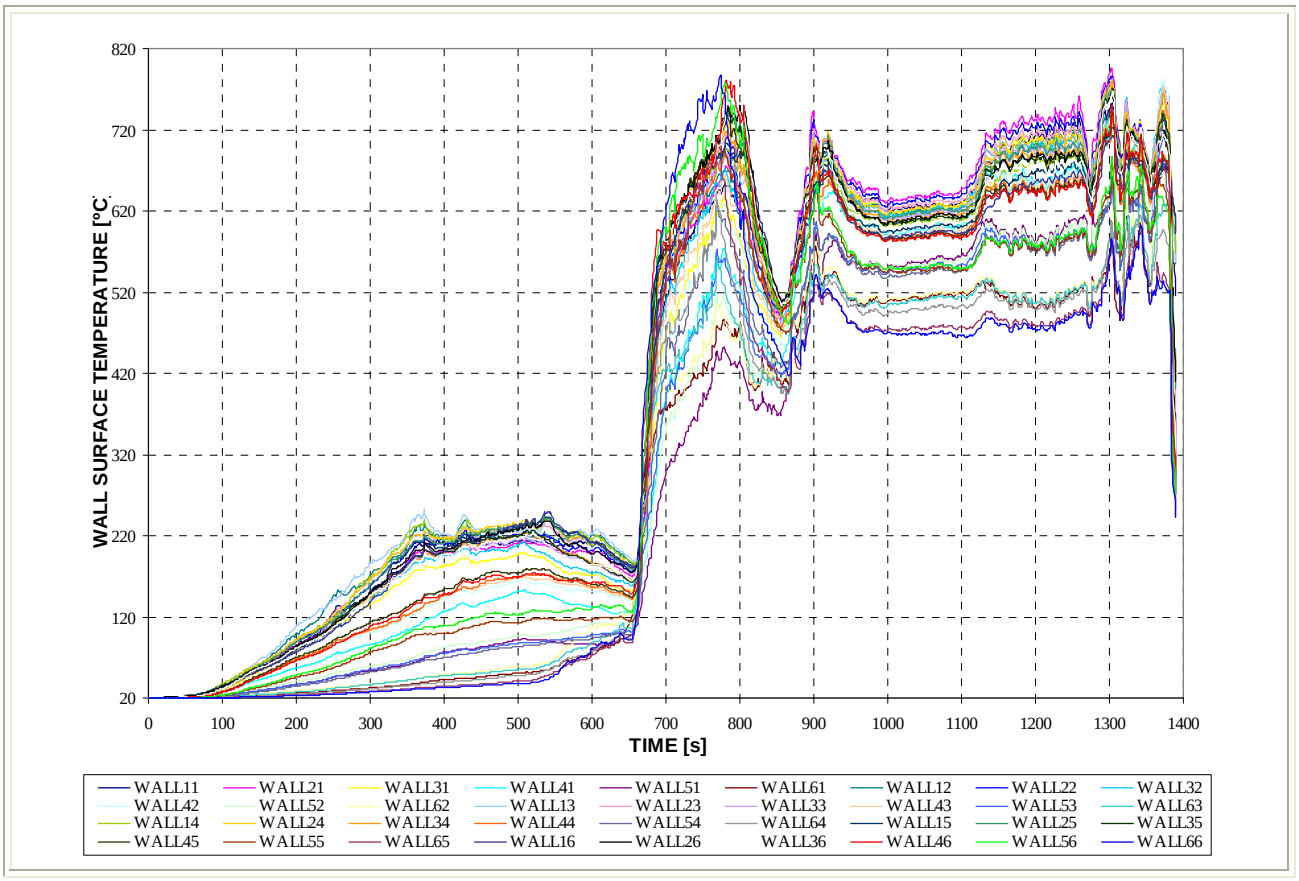

Surface Temperature Evolution at the Control Points.

Figure 6-42.h. OFFICE-11.

Surface Temperature Evolution at Control Points: detail on the surface cooling period –1.380 to 1.390s–

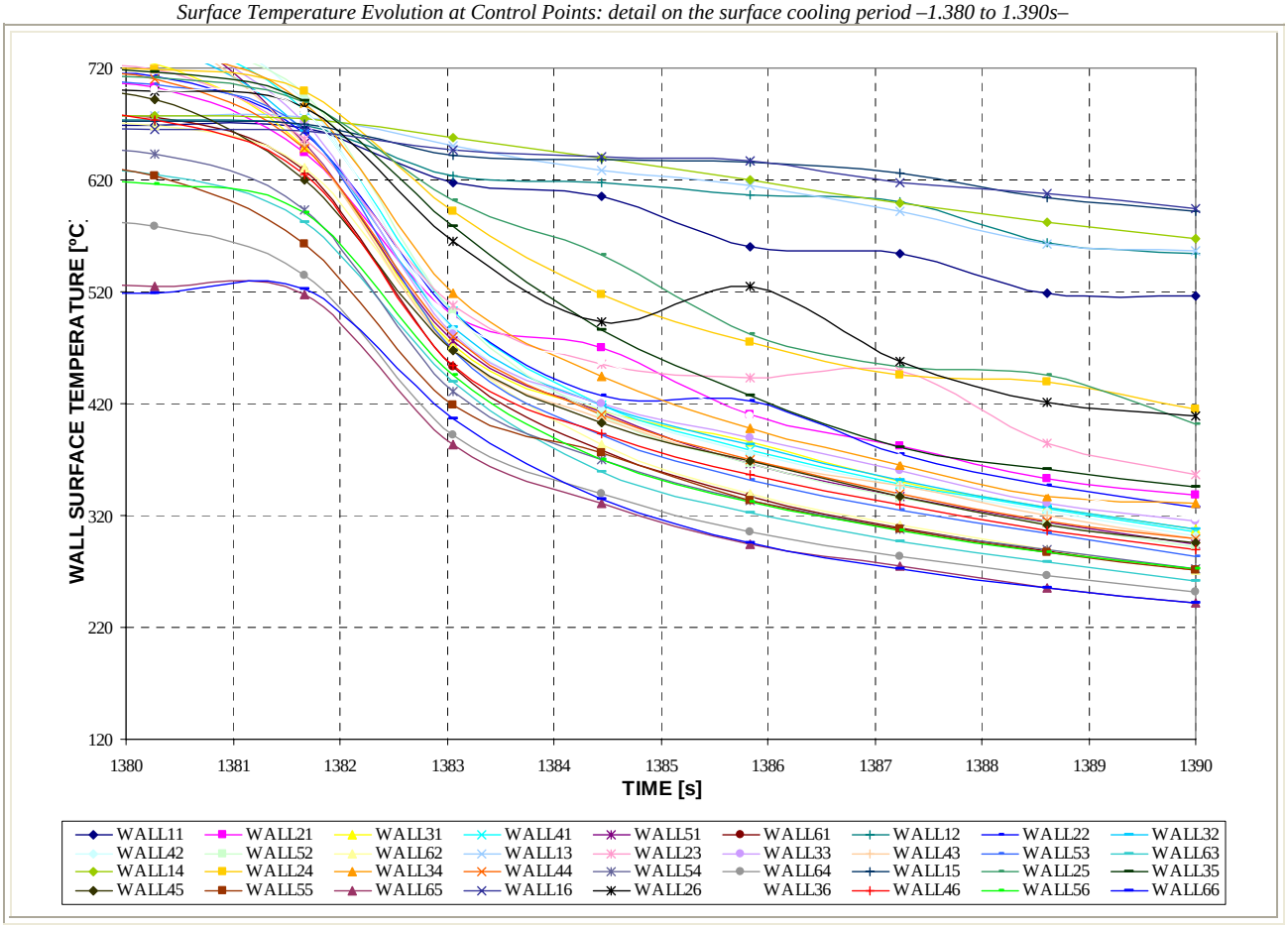

Figure 6-42.i. OFFICE-11.
Mean Cooling Rate and Standard Deviation at each of Surface Control Points.

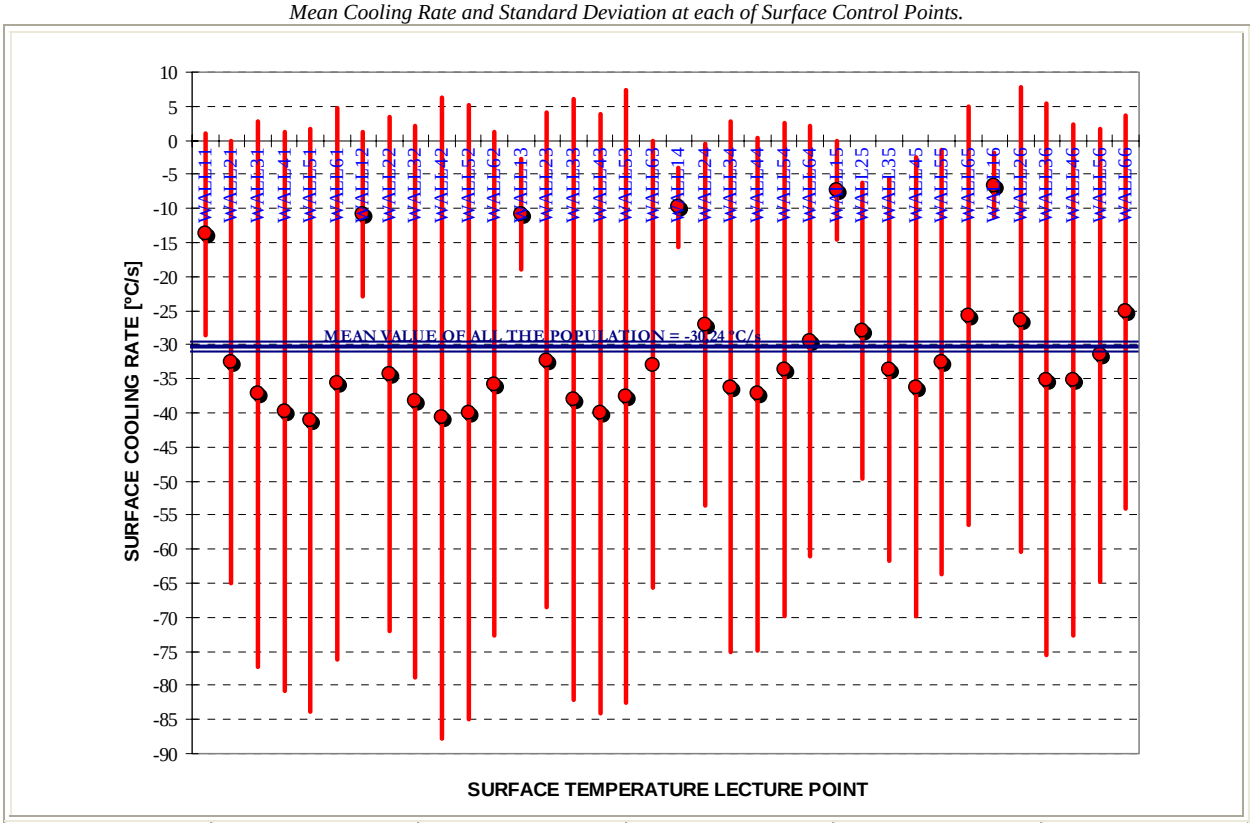

SURF. T LECTURE POINT	ARITHMETIC MEAN [°C/s]	STANDARD DEVIATION [°C/s]	MAXIMUM [°C/s]	MINIMUM [°C/s]	MEDIAN [°C/s]
WALL11	-13,74	14,83	-35,13	0,01	-6,29
WALL21	-32,59	32,51	-104,13	1,62	-21,44
WALL31	-37,25	40,09	-127,61	0,73	-22,92
WALL41	-39,79	40,92	-129,19	0,84	-25,43
WALL51	-41,16	42,80	-126,69	6,88	-27,31
WALL61	-35,68	40,41	-126,01	5,64	-24,93
WALL12	-10,74	12,07	-32,66	0,18	-5,52
WALL22	-34,39	37,73	-116,39	2,15	-27,13
WALL32	-38,35	40,43	-126,59	4,11	-23,88
WALL42	-40,76	47,00	-147,39	5,50	-24,64
WALL52	-39,93	45,01	-140,30	2,21	-26,18
WALL62	-35,75	37,04	-115,54	-0,03	-24,08
WALL13	-10,85	8,03	-20,70	0,10	-12,63
WALL23	-32,24	36,26	-106,93	4,73	-28,75
WALL33	-38,02	44,08	-136,27	7,11	-21,45
WALL43	-40,07	44,02	-132,27	5,86	-23,22
WALL53	-37,60	44,87	-140,94	2,64	-24,09
WALL63	-32,92	32,82	-103,11	-2,27	-22,32
WALL14	-9,84	5,75	-14,94	-0,44	-12,63
WALL24	-27,08	26,52	-77,33	2,17	-19,80
WALL34	-36,17	38,83	-121,70	1,96	-28,27
WALL44	-37,26	37,52	-121,52	-2,32	-25,56
WALL54	-33,60	36,14	-116,41	-1,77	-21,91
WALL64	-29,54	31,61	-102,16	-1,49	-20,51
WALL15	-7,42	7,25	-20,49	-1,21	-4,85
WALL25	-27,93	21,63	-62,74	-0,14	-26,41
WALL35	-33,65	28,03	-81,01	-2,30	-25,72
WALL45	-36,20	33,59	-109,07	-4,61	-23,48
WALL55	-32,53	31,17	-103,78	-7,21	-24,48
WALL65	-25,77	30,75	-96,33	-2,34	-14,07
WALL16	-6,60	4,70	-13,20	-1,08	-5,90
WALL26	-26,33	34,12	-85,59	22,62	-18,96
WALL36	-35,07	40,44	-132,55	-5,80	-24,13
WALL46	-35,23	37,50	-122,89	-5,94	-22,75
WALL56	-31,50	33,25	-104,85	-4,46	-18,07
WALL66	-25,18	28,87	-83,10	2,37	-14,45

Table 6-28.j. OFFICE-11.
Statistic Parameters calculated on the Surface Cooling Rate at each Control Points.

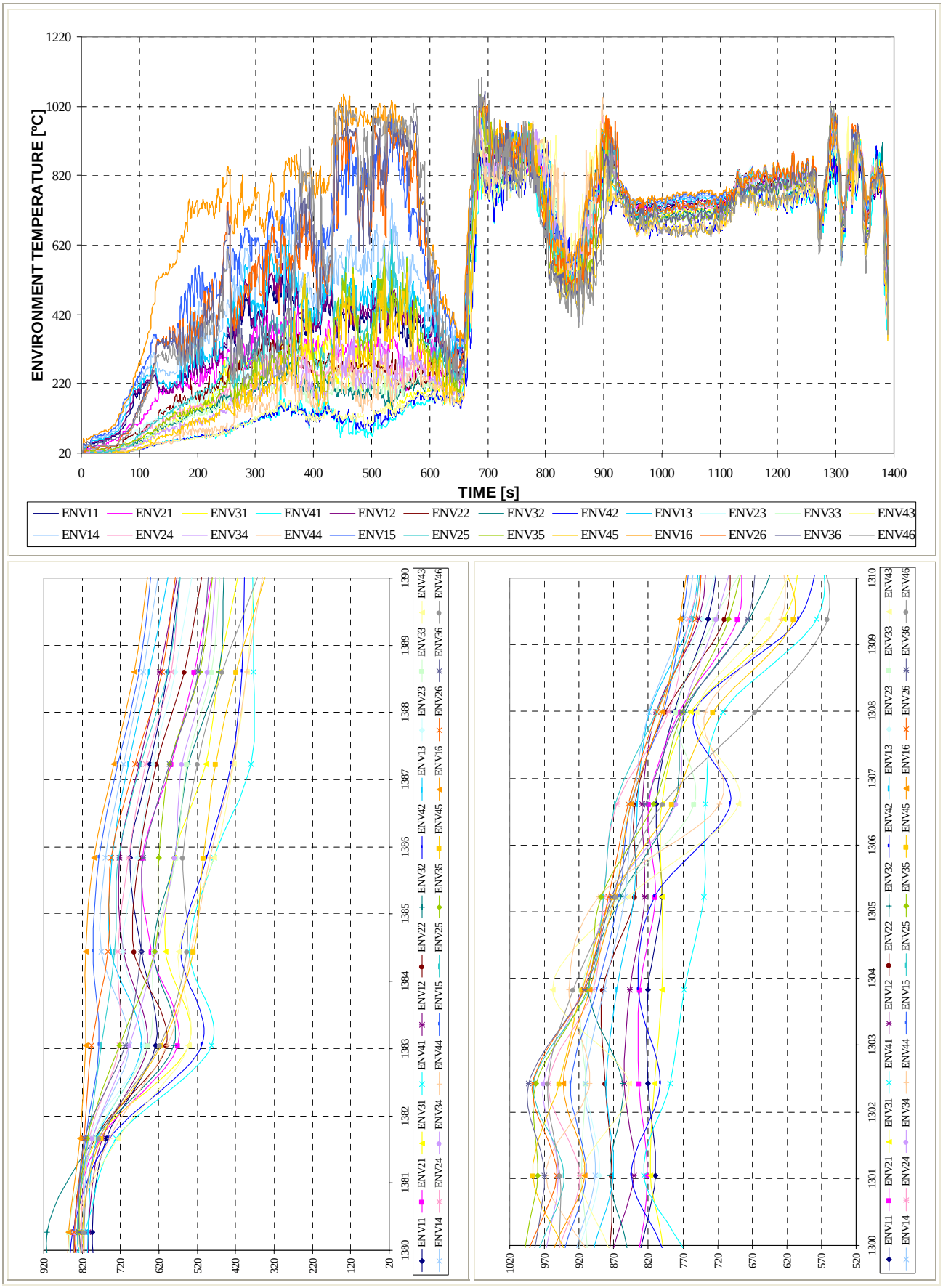

Figure 6-42.j. OFFICE-15.
Environment Temperature Evolution at the Control Points. Lower figures correspond to the detail on the 2nd environment cooling – from 1.300 to 1.310 seconds – and on the surface cooling – from 1.380 to 1.390 seconds –).

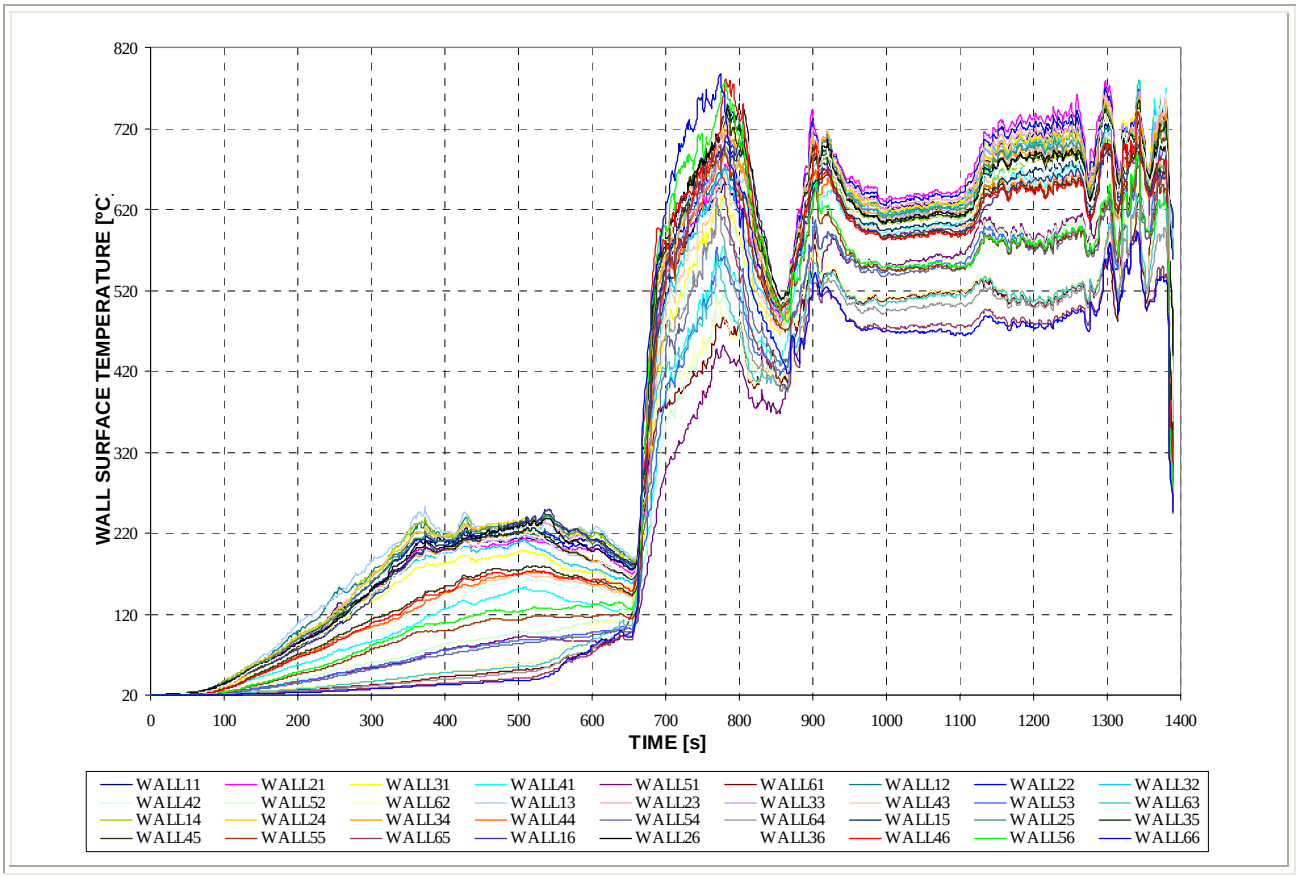

Surface Temperature Evolution at the Control Points.

Figure 6-42.k. OFFICE-15.

Surface Temperature Evolution at Control Points: detail on the surface cooling period –1.380 to 1.390s–

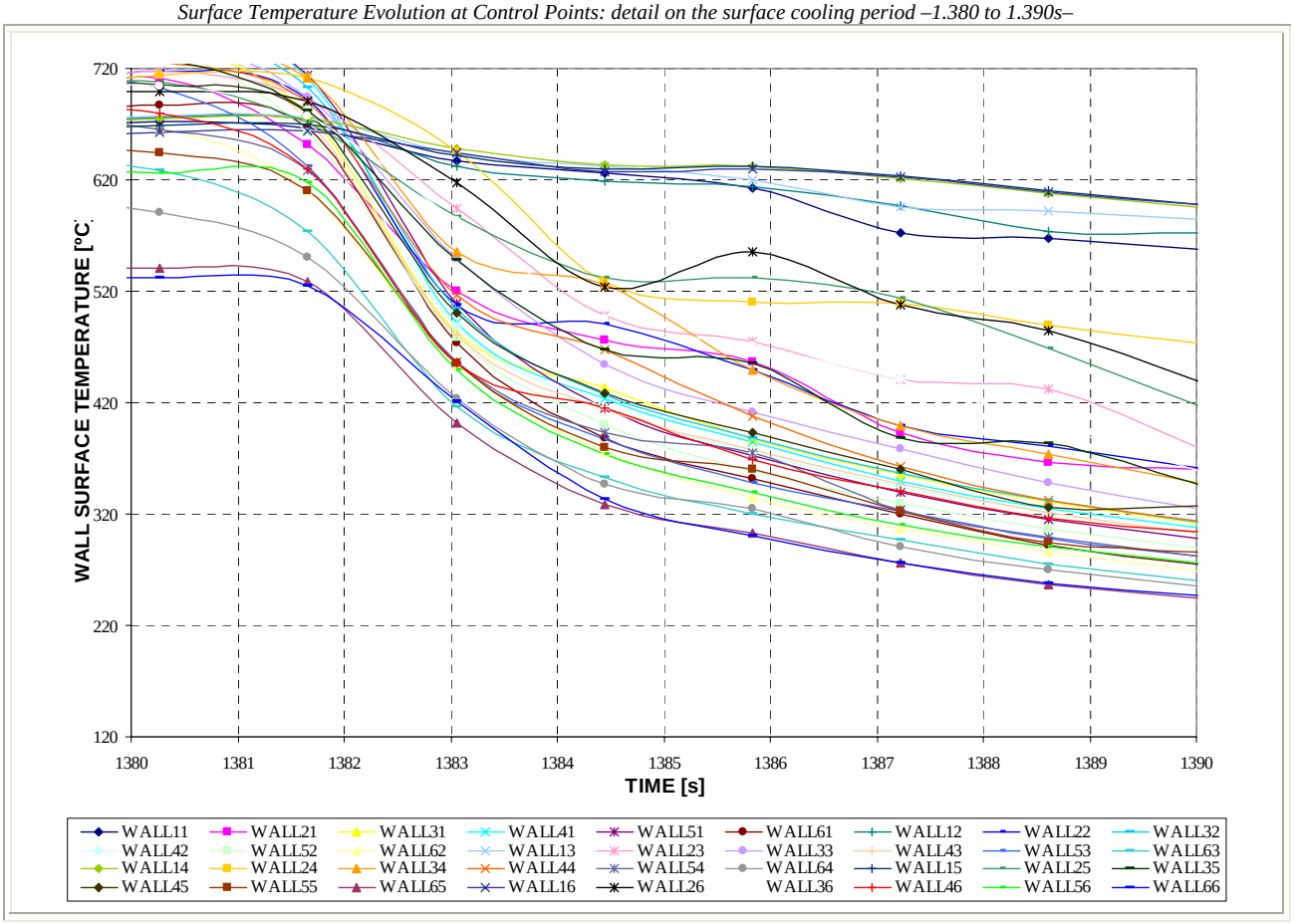

Figure 6-42.l. OFFICE-15.
Mean Cooling Rate and Standard Deviation at each of Surface Control Points.

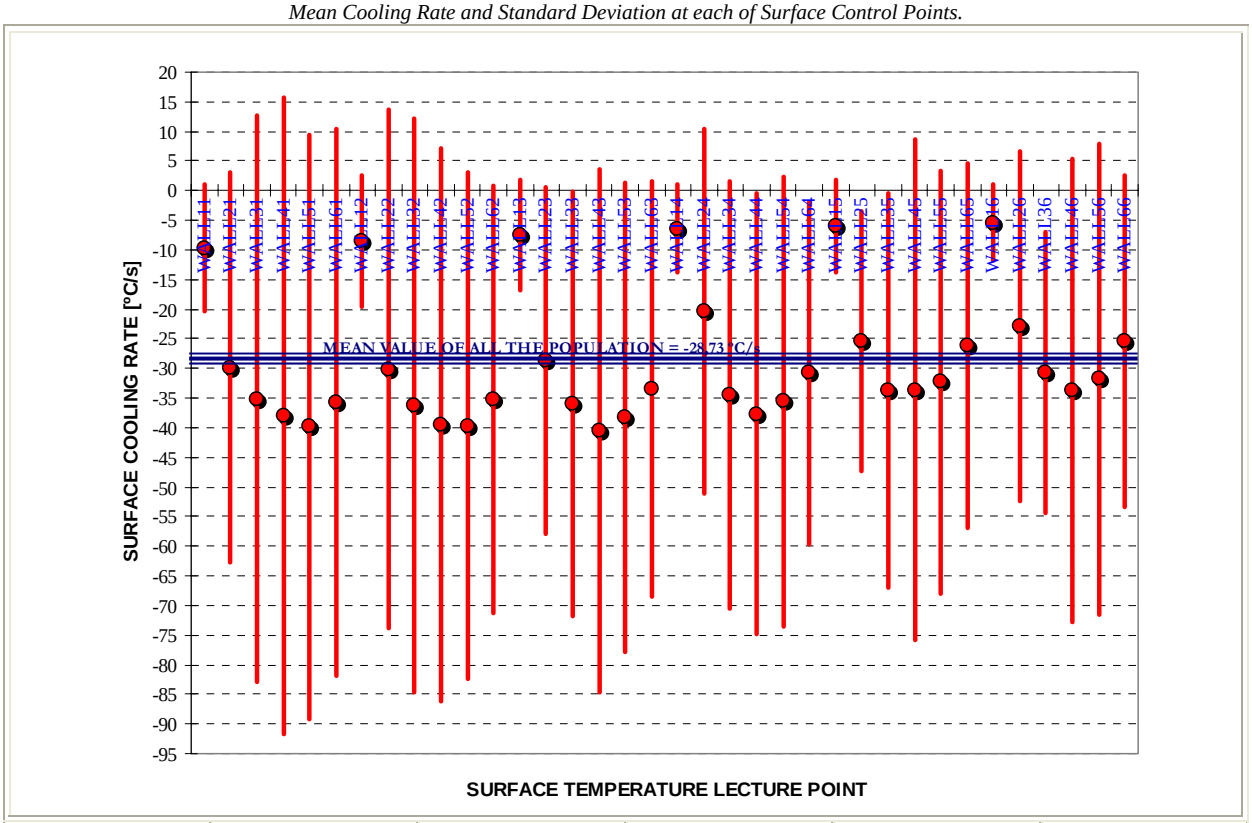

SURF. T LECTURE POINT	ARITHMETIC MEAN [°C/s]	STANDARD DEVIATION [°C/s]	MAXIMUM [°C/s]	MINIMUM [°C/s]	MEDIAN [°C/s]
WALL11	-9,68	10,74	-28,99	4,75	-7,62
WALL21	-29,83	32,99	-95,19	14,29	-24,84
WALL31	-35,19	47,78	-140,93	26,43	-28,05
WALL41	-37,94	53,69	-157,35	28,68	-26,94
WALL51	-39,88	49,39	-147,54	16,01	-27,46
WALL61	-35,66	46,13	-138,48	10,64	-21,48
WALL12	-8,61	11,09	-29,71	6,01	-6,80
WALL22	-30,13	43,77	-132,10	14,66	-16,20
WALL32	-36,24	48,31	-143,25	22,10	-25,39
WALL42	-39,46	46,59	-140,58	14,42	-25,79
WALL52	-39,68	42,79	-132,74	4,61	-25,67
WALL62	-35,31	36,08	-112,71	2,57	-24,61
WALL13	-7,55	9,27	-23,18	5,80	-6,72
WALL23	-28,70	29,18	-69,63	13,25	-21,89
WALL33	-35,98	35,84	-104,10	14,83	-27,33
WALL43	-40,46	44,09	-138,77	1,94	-24,25
WALL53	-38,20	39,65	-126,81	-3,02	-23,31
WALL63	-33,50	35,14	-113,19	-3,70	-20,41
WALL14	-6,43	7,41	-18,88	4,88	-8,09
WALL24	-20,37	30,81	-84,71	9,55	-12,36
WALL34	-34,41	36,10	-112,87	5,37	-19,78
WALL44	-37,67	37,18	-124,79	-5,27	-29,09
WALL54	-35,53	37,94	-123,73	-8,32	-22,08
WALL64	-30,81	28,87	-90,87	-4,94	-19,97
WALL15	-5,93	7,74	-20,01	3,86	-7,45
WALL25	-25,41	21,95	-60,04	5,98	-29,58
WALL35	-33,76	33,33	-96,45	3,96	-29,51
WALL45	-33,61	42,25	-129,37	3,31	-24,24
WALL55	-32,31	35,72	-111,04	-0,96	-22,25
WALL65	-26,15	30,83	-90,92	4,19	-16,33
WALL16	-5,43	6,41	-13,88	2,98	-6,82
WALL26	-22,82	29,54	-67,78	22,26	-24,44
WALL36	-30,66	23,72	-67,92	2,74	-25,83
WALL46	-33,77	39,07	-125,51	0,30	-24,45
WALL56	-31,74	39,70	-121,58	-2,42	-17,54
WALL66	-25,48	27,96	-74,57	1,31	-15,51

Table 6-28.k. OFFICE-15.
Statistic Parameters calculated on the Surface Cooling Rate at each Control Points.

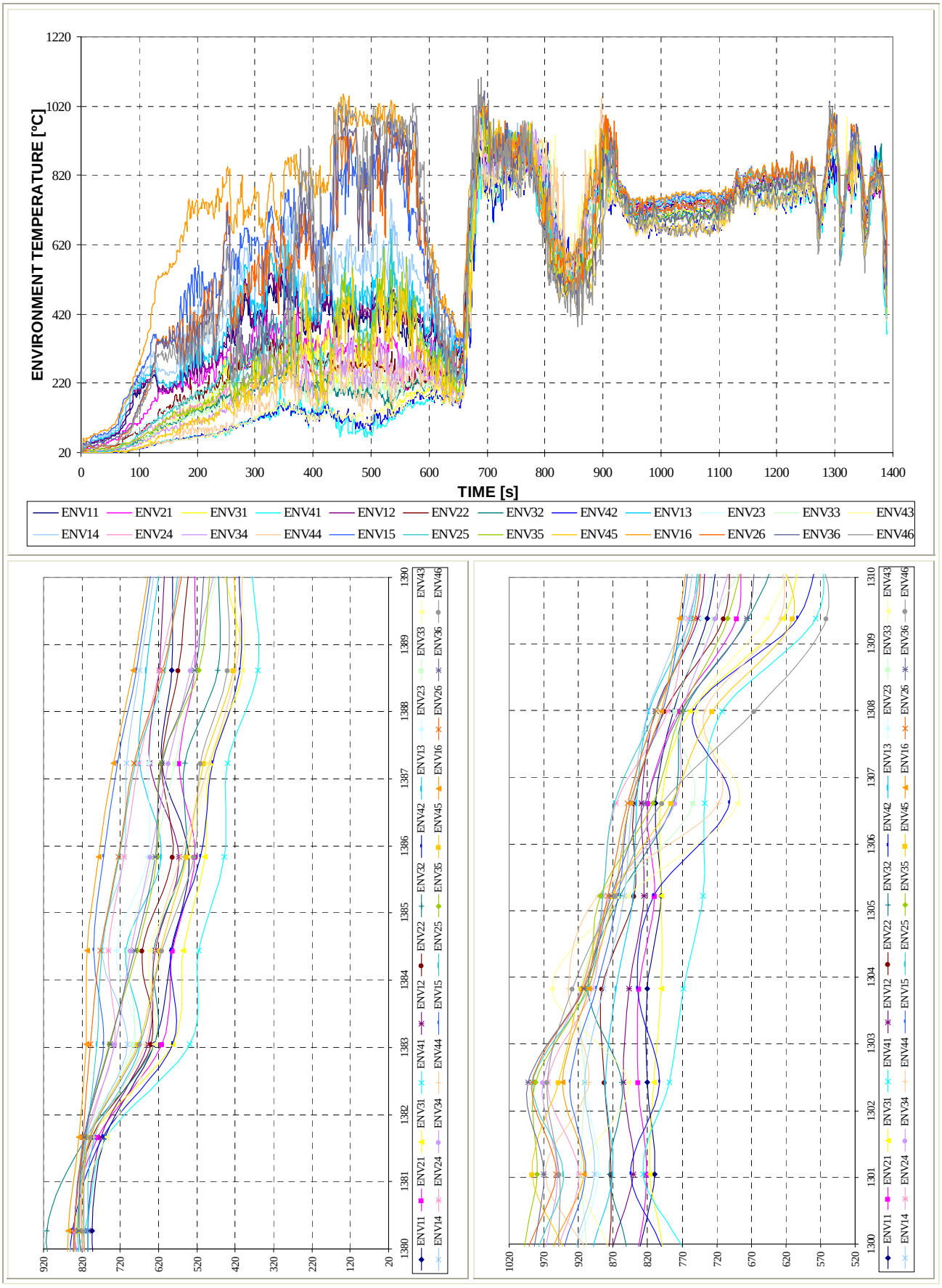

Figure 6-42.m. OFFICE-16.

Environment Temperature Evolution at the Control Points. Lower figures correspond to the detail on the 2nd environment cooling – from 1.300 to 1.310 seconds – and on the surface cooling – from 1.380 to 1.390 seconds –).

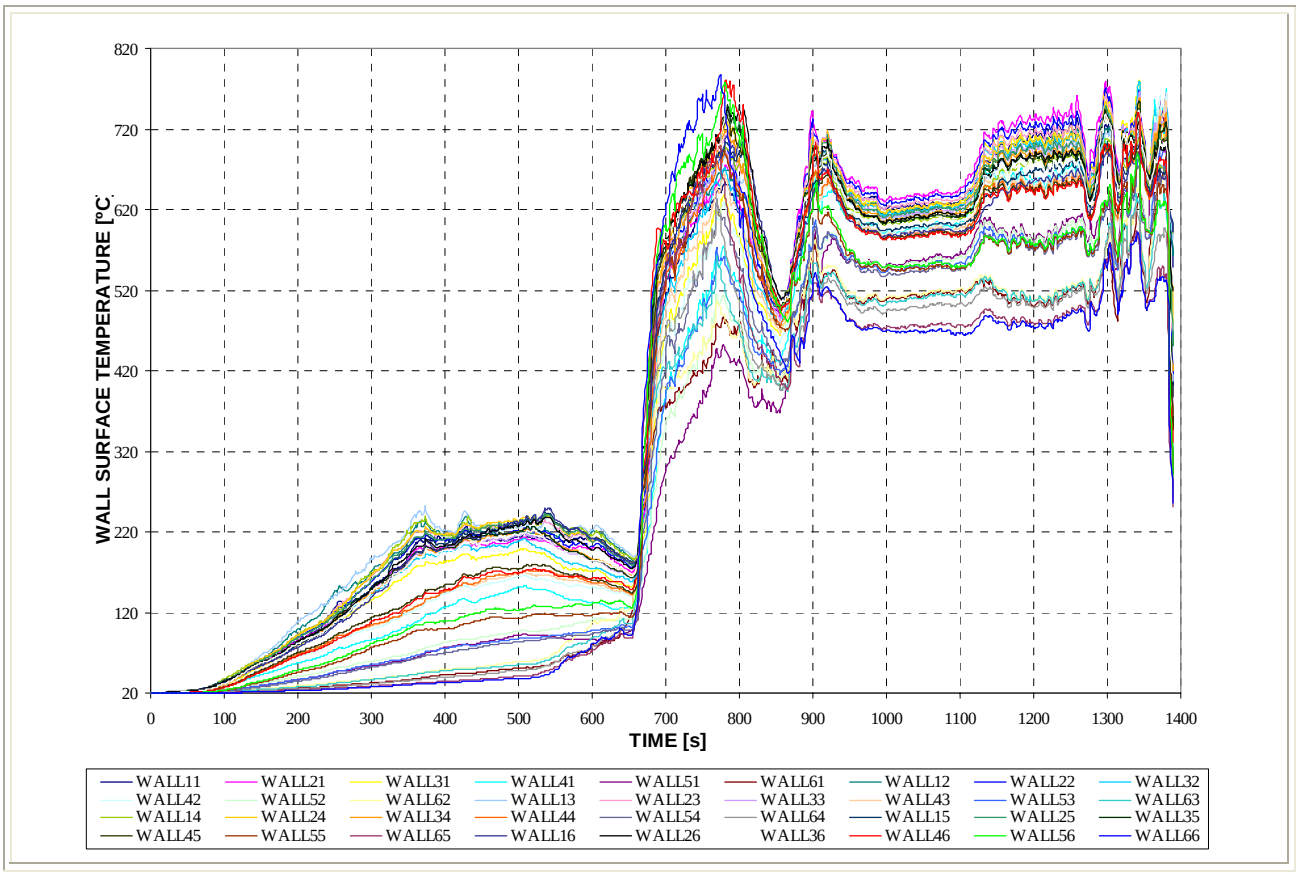

Surface Temperature Evolution at the Control Points.

Figure 6-42.n. OFFICE-16.

Surface Temperature Evolution at Control Points: detail on the surface cooling period –1.380 to 1.390s–

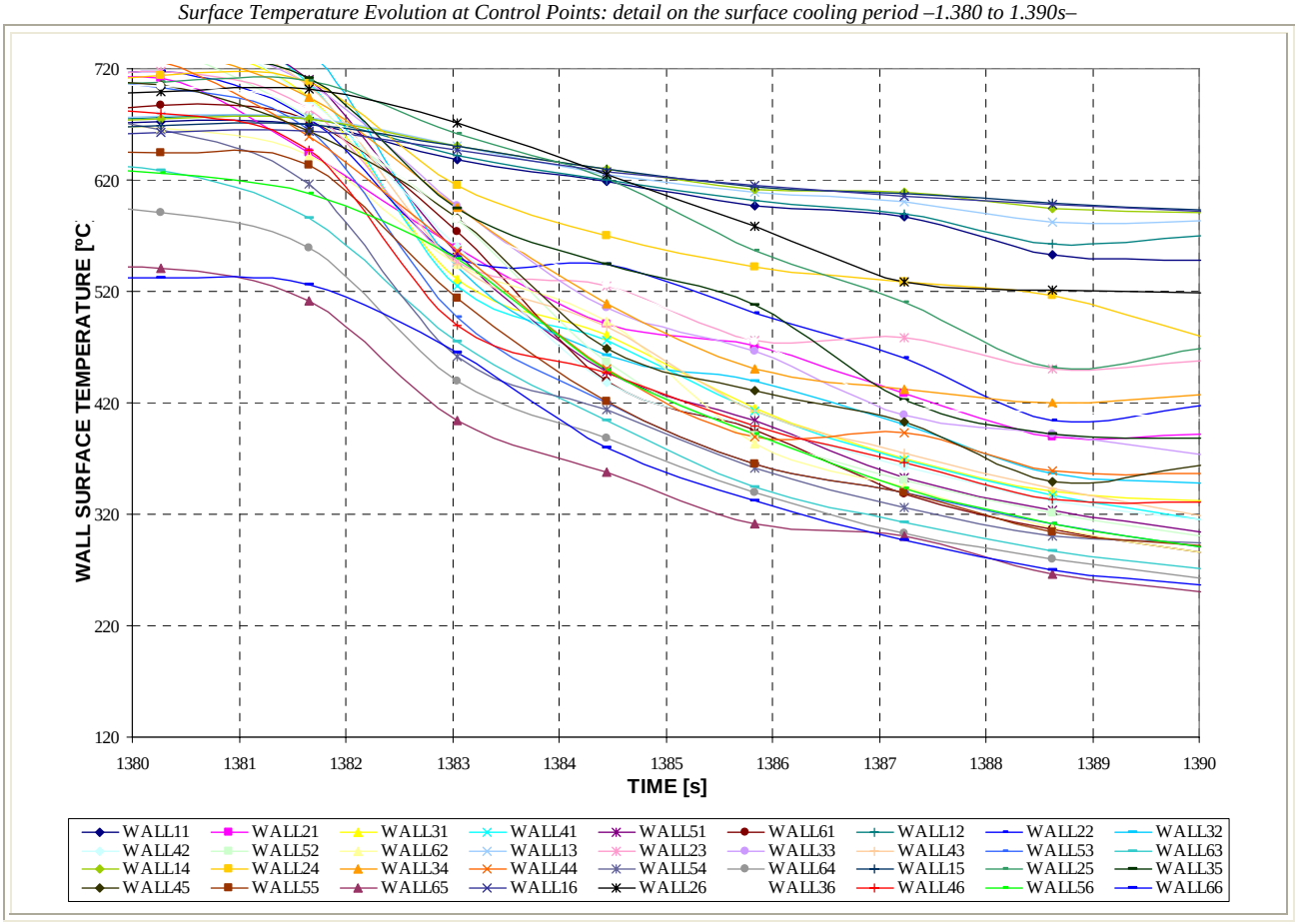

Figure 6-42.o. OFFICE-16.
Mean Cooling Rate and Standard Deviation at each of Surface Control Points.

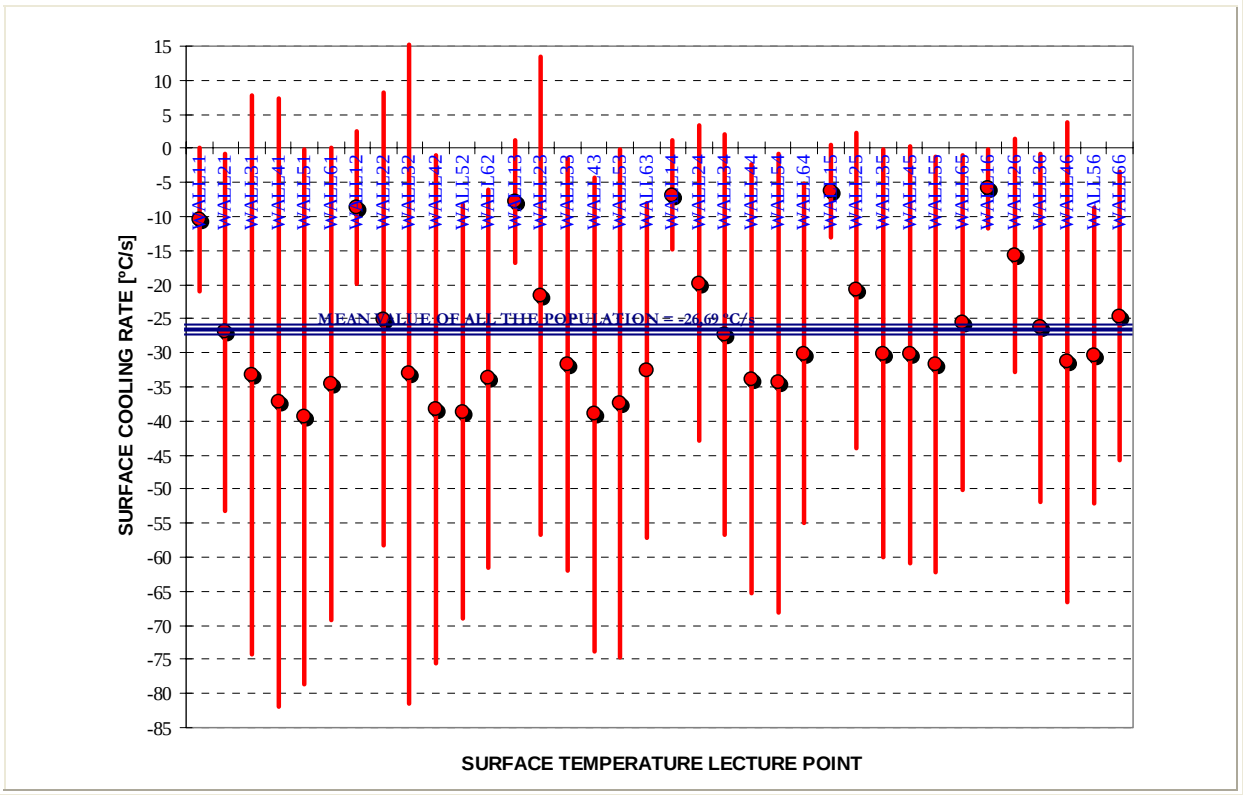

SURF. T LECTURE POINT	ARITHMETIC MEAN [ºC/s]	STANDARD DEVIATION [ºC/s]	MAXIMUM [ºC/s]	MINIMUM [ºC/s]	MEDIAN [ºC/s]
WALL11	-10,50	10,54	-24,26	4,75	-10,30
WALL21	-26,93	26,19	-61,67	14,29	-29,12
WALL31	-33,30	41,00	-117,54	26,43	-32,69
WALL41	-37,30	44,59	-130,54	28,68	-32,80
WALL51	-39,35	39,26	-112,53	16,01	-33,98
WALL61	-34,61	34,65	-95,65	10,64	-27,63
WALL12	-8,76	11,17	-23,30	6,01	-10,80
WALL22	-25,04	33,30	-89,49	14,66	-29,81
WALL32	-33,08	48,36	-138,74	22,10	-22,22
WALL42	-38,32	37,22	-94,91	14,42	-27,55
WALL52	-38,64	30,44	-91,03	4,61	-36,70
WALL62	-33,76	27,82	-79,14	2,57	-26,98
WALL13	-7,72	8,99	-18,84	5,80	-9,00
WALL23	-21,69	35,08	-98,15	13,25	-17,85
WALL33	-31,63	30,26	-79,15	14,83	-28,28
WALL43	-39,02	34,78	-114,29	1,94	-31,94
WALL53	-37,40	37,31	-120,84	-3,02	-23,75
WALL63	-32,57	24,62	-79,73	-3,70	-26,51
WALL14	-6,89	8,04	-17,39	4,88	-6,35
WALL24	-19,80	23,13	-66,91	9,55	-14,71
WALL34	-27,27	29,38	-71,40	5,78	-22,44
WALL44	-33,80	31,50	-76,03	3,19	-34,42
WALL54	-34,40	33,72	-111,92	-3,96	-29,55
WALL64	-30,07	24,84	-85,40	-4,94	-24,93
WALL15	-6,35	6,81	-14,96	3,86	-5,37
WALL25	-20,77	23,15	-46,01	11,82	-30,98
WALL35	-30,07	29,86	-84,58	3,96	-24,32
WALL45	-30,27	30,50	-83,44	10,56	-28,63
WALL55	-31,74	30,44	-85,82	-0,96	-22,05
WALL65	-25,57	24,62	-77,70	4,19	-22,59
WALL16	-5,94	5,84	-13,73	2,98	-6,10
WALL26	-15,75	17,15	-35,90	3,67	-13,07
WALL36	-26,32	25,57	-71,42	2,74	-25,53
WALL46	-31,35	35,24	-112,89	0,30	-24,04
WALL56	-30,43	21,73	-71,11	-2,42	-29,09
WALL66	-24,63	21,11	-61,39	1,31	-22,11

Table 6-28.l. OFFICE-16.
Statistic Parameters calculated on the Surface Cooling Rate at each Control Points.

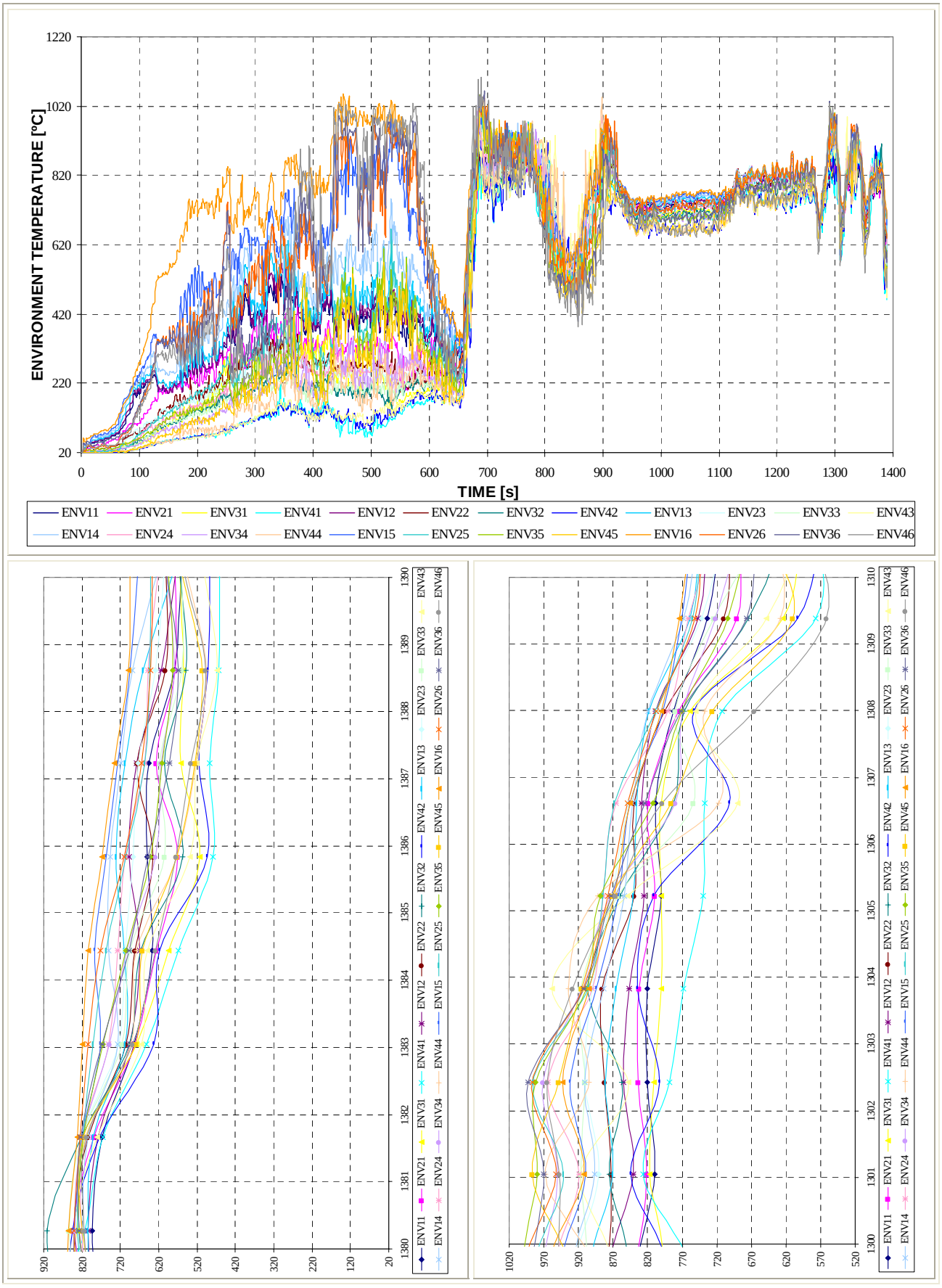

Figure 6-42.p. OFFICE-17.

Environment Temperature Evolution at the Control Points. Lower figures correspond to the detail on the 2nd environment cooling – from 1.300 to 1.310 seconds – and on the surface cooling – from 1.380 to 1.390 seconds –).

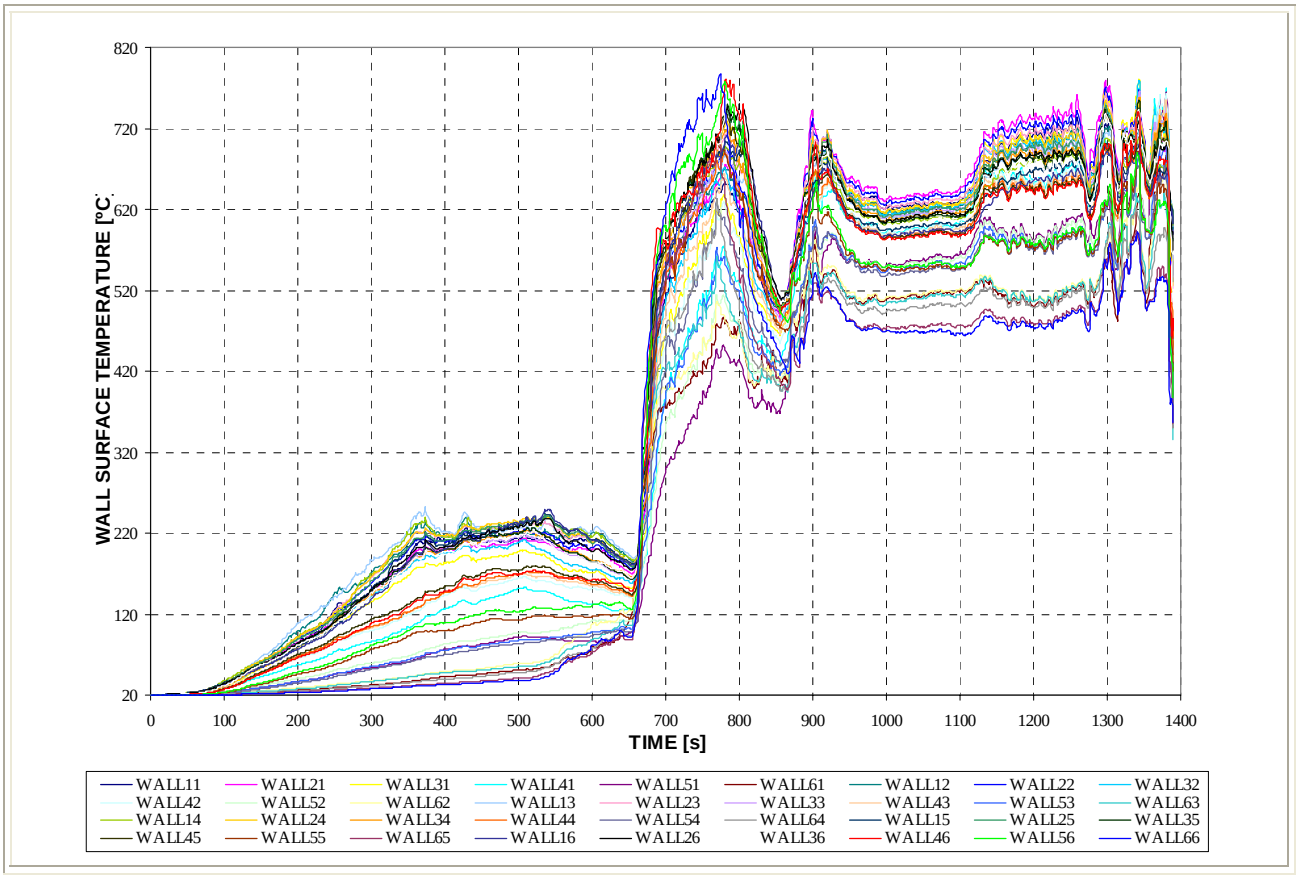

Surface Temperature Evolution at the Control Points.

Figure 6-42.q. OFFICE-17.

Surface Temperature Evolution at Control Points: detail on the surface cooling period –1.380 to 1.390s–

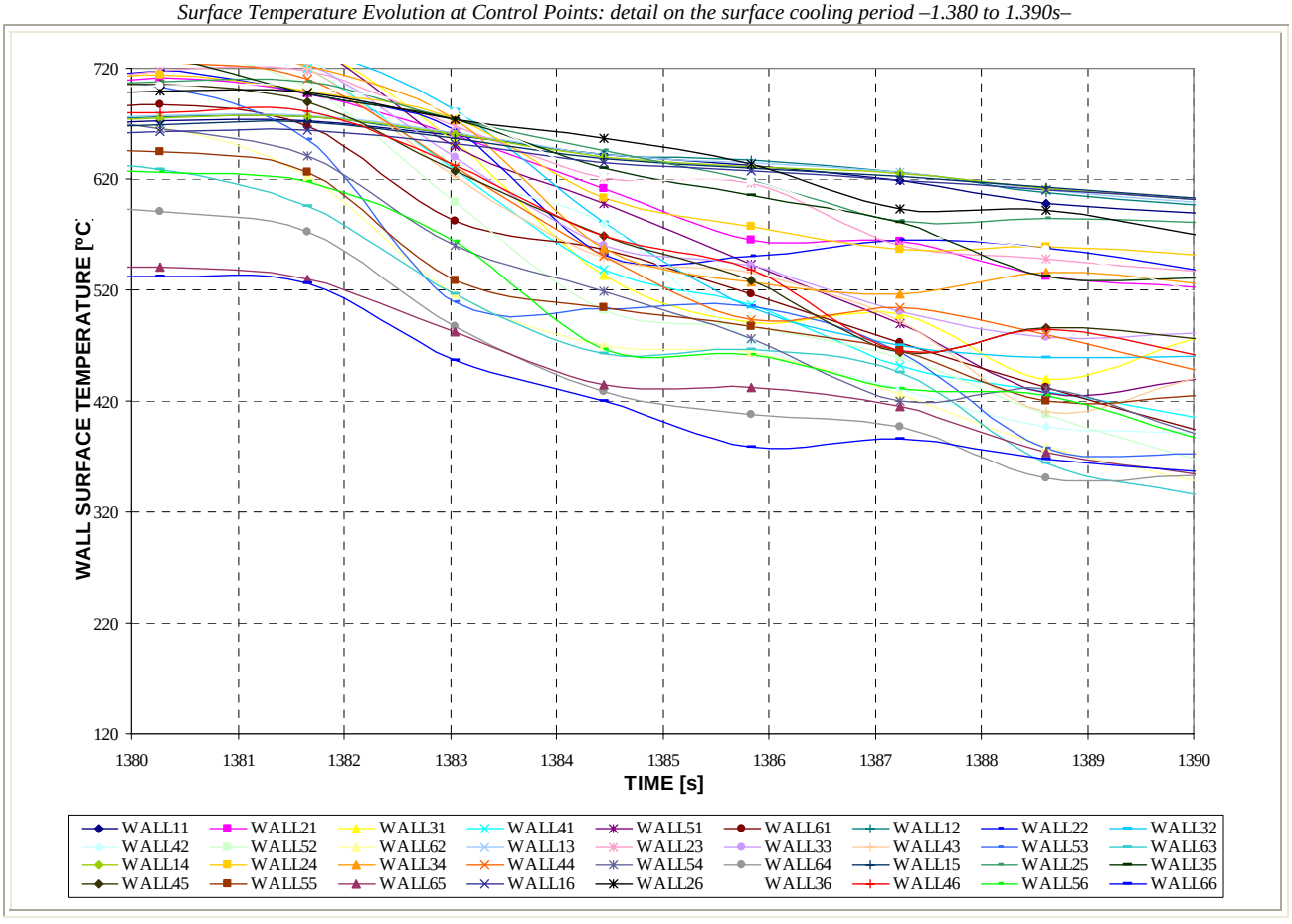

Figure 6-42.r. OFFICE-17.
Mean Cooling Rate and Standard Deviation at each of Surface Control Points.

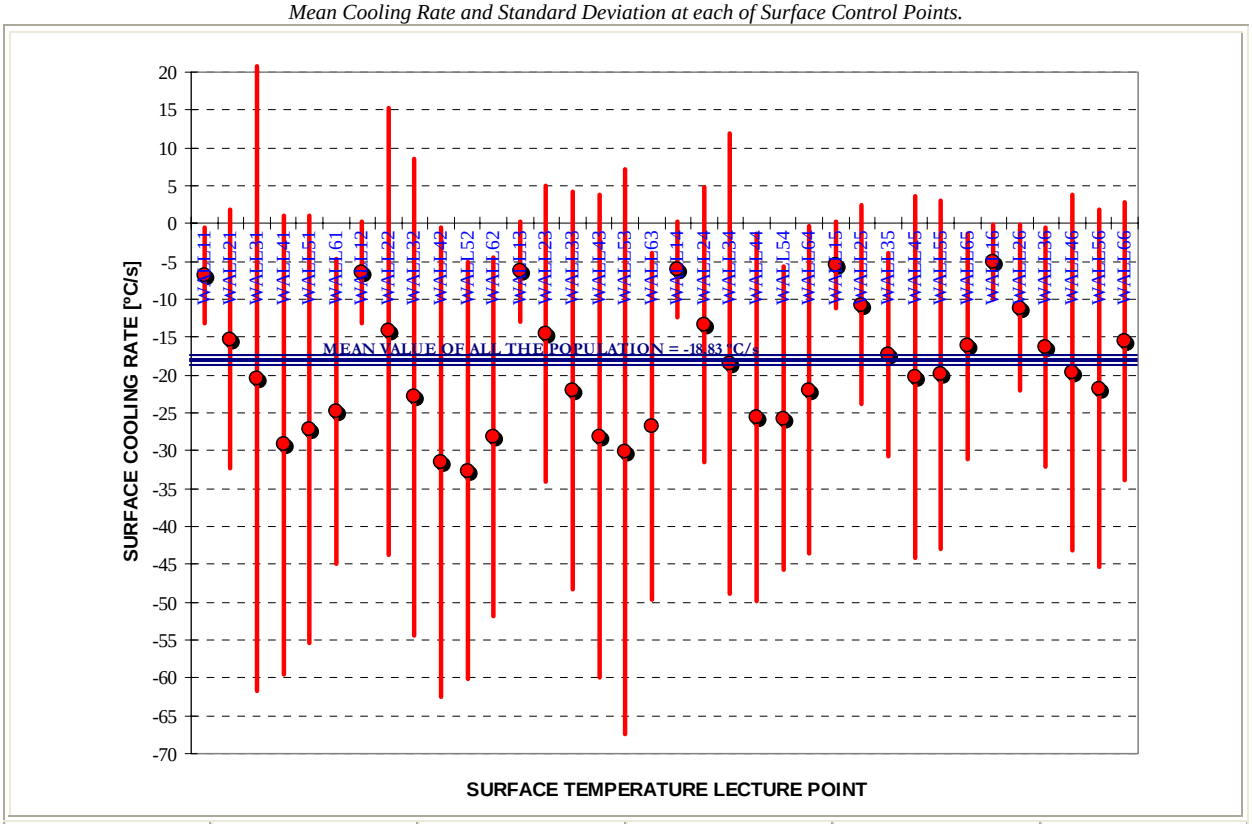

SURF. T LECTURE POINT	ARITHMETIC MEAN [ºC/s]	STANDARD DEVIATION [ºC/s]	MAXIMUM [ºC/s]	MINIMUM [ºC/s]	MEDIAN [ºC/s]
WALL11	-6,81	6,36	-14,46	4,75	-8,22
WALL21	-15,24	17,14	-34,49	14,29	-16,41
WALL31	-20,38	41,25	-85,61	26,43	-16,04
WALL41	-29,23	30,36	-65,26	28,68	-29,54
WALL51	-27,22	28,24	-67,13	16,01	-37,13
WALL61	-24,86	20,16	-61,48	10,64	-27,93
WALL12	-6,41	6,66	-13,14	6,01	-8,20
WALL22	-14,23	29,51	-79,86	14,66	-9,82
WALL32	-22,91	31,55	-72,45	22,10	-16,09
WALL42	-31,47	30,94	-76,45	14,42	-27,67
WALL52	-32,64	27,53	-74,66	4,61	-26,47
WALL62	-28,24	23,68	-76,14	2,57	-29,22
WALL13	-6,27	6,62	-13,75	5,80	-7,15
WALL23	-14,56	19,46	-39,97	13,25	-8,52
WALL33	-22,02	26,28	-60,76	14,83	-16,52
WALL43	-28,11	31,89	-70,47	21,78	-28,39
WALL53	-30,15	37,28	-105,11	1,57	-17,19
WALL63	-26,79	22,84	-58,85	2,07	-21,90
WALL14	-5,97	6,31	-14,17	4,88	-6,97
WALL24	-13,39	18,14	-51,25	9,55	-12,84
WALL34	-18,43	30,38	-83,73	13,73	-9,26
WALL44	-25,60	24,28	-57,63	8,43	-20,31
WALL54	-25,73	20,05	-58,08	8,00	-29,21
WALL64	-21,96	21,64	-61,64	2,09	-14,22
WALL15	-5,52	5,73	-13,72	3,86	-6,59
WALL25	-10,69	13,17	-26,20	5,98	-11,14
WALL35	-17,28	13,48	-35,60	3,96	-17,67
WALL45	-20,22	23,83	-46,74	15,91	-20,00
WALL55	-19,90	22,97	-70,03	3,20	-14,52
WALL65	-16,21	14,89	-34,43	4,19	-12,99
WALL16	-5,06	4,99	-12,56	2,98	-5,79
WALL26	-11,12	10,91	-28,68	3,67	-13,79
WALL36	-16,27	15,76	-41,14	2,74	-14,41
WALL46	-19,61	23,45	-51,88	13,94	-19,76
WALL56	-21,76	23,61	-70,02	-2,42	-13,56
WALL66	-15,58	18,35	-49,47	4,96	-10,29

Table 6-28.m. OFFICE-17.
Statistic Parameters calculated on the Surface Cooling Rate at each Control Points.

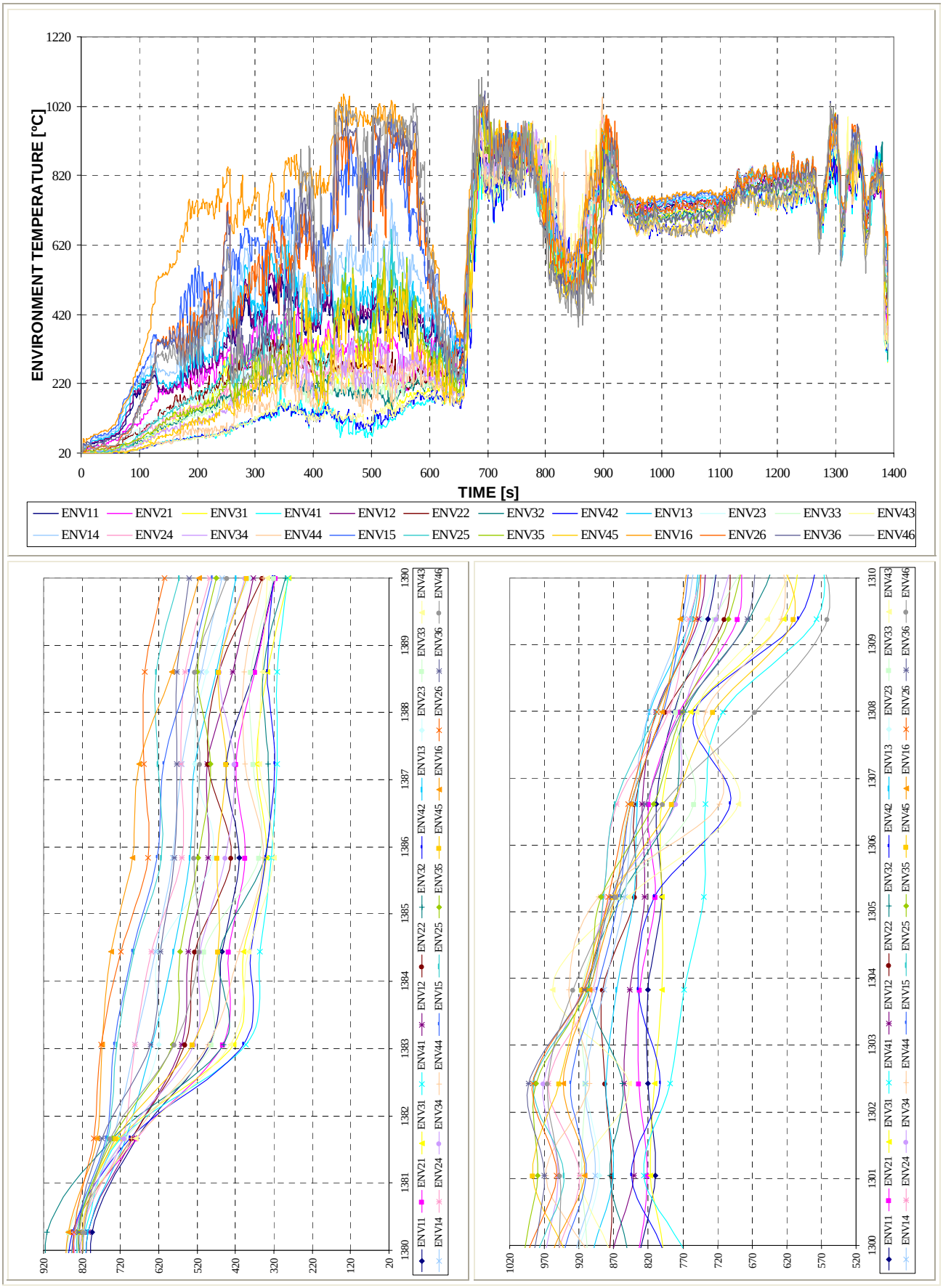

Figure 6-43a. OFFICE-14.
Environment Temperature Evolution at the Control Points. Lower figures correspond to the detail on the 2nd environment cooling – from 1.300 to 1.310 seconds – and on the surface cooling – from 1.380 to 1.390 seconds –).

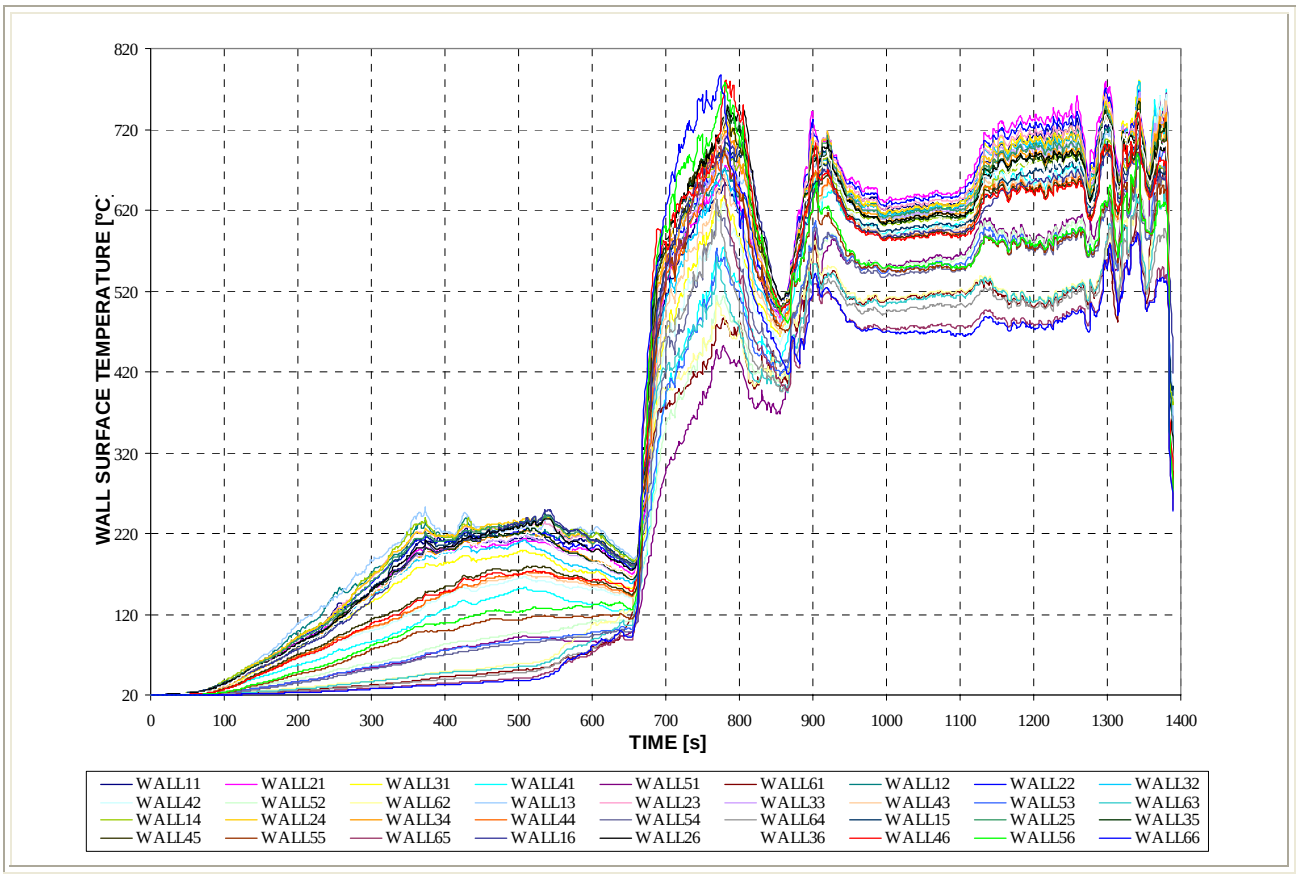

Surface Temperature Evolution at the Control Points.

Figure 6-43b. OFFICE-14.

Surface Temperature Evolution at Control Points: detail on the surface cooling period –1.380 to 1.390s–

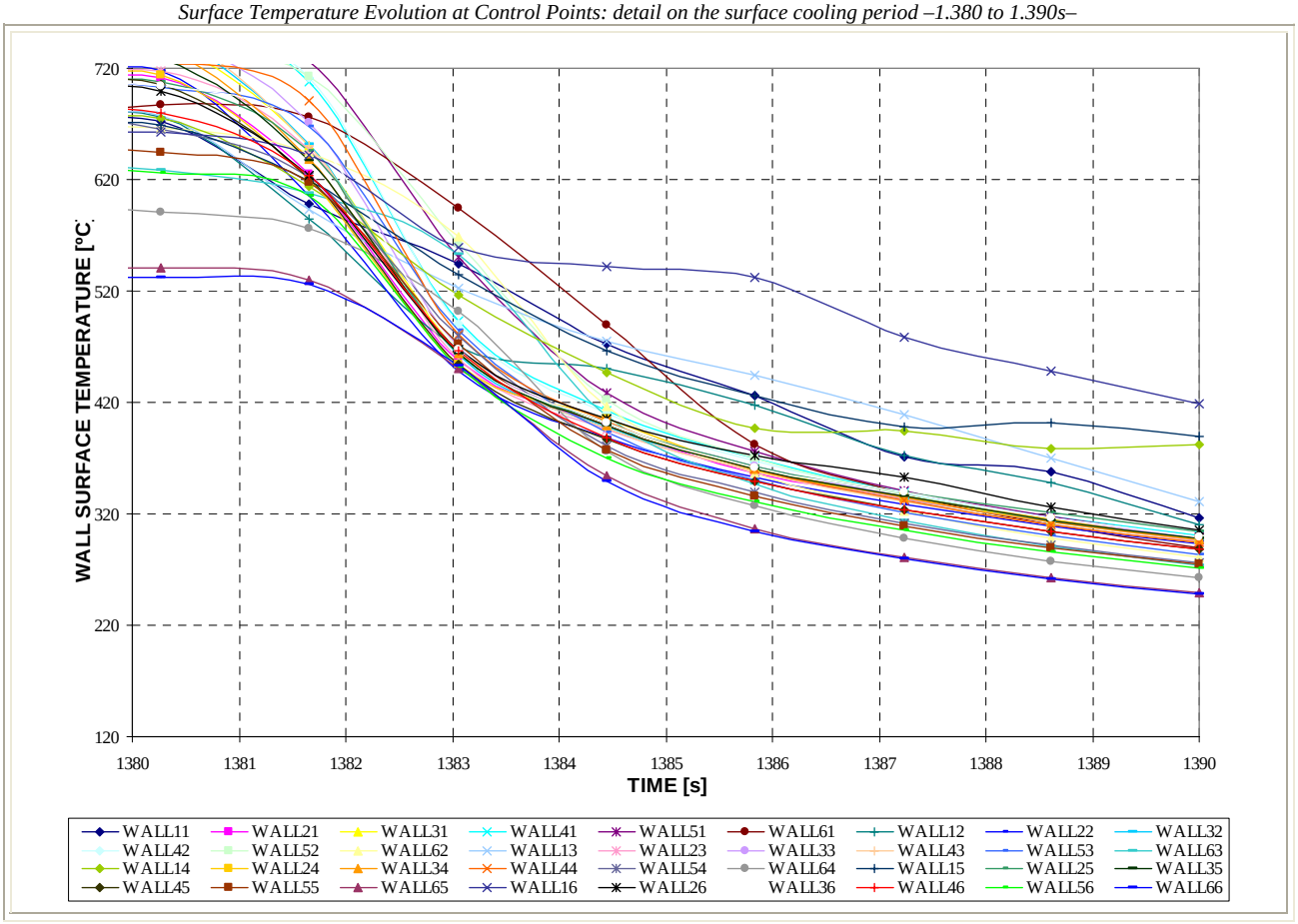

Figure 6-43c. OFFICE-14.
Mean Cooling Rate and Standard Deviation at each of Surface Control Points.

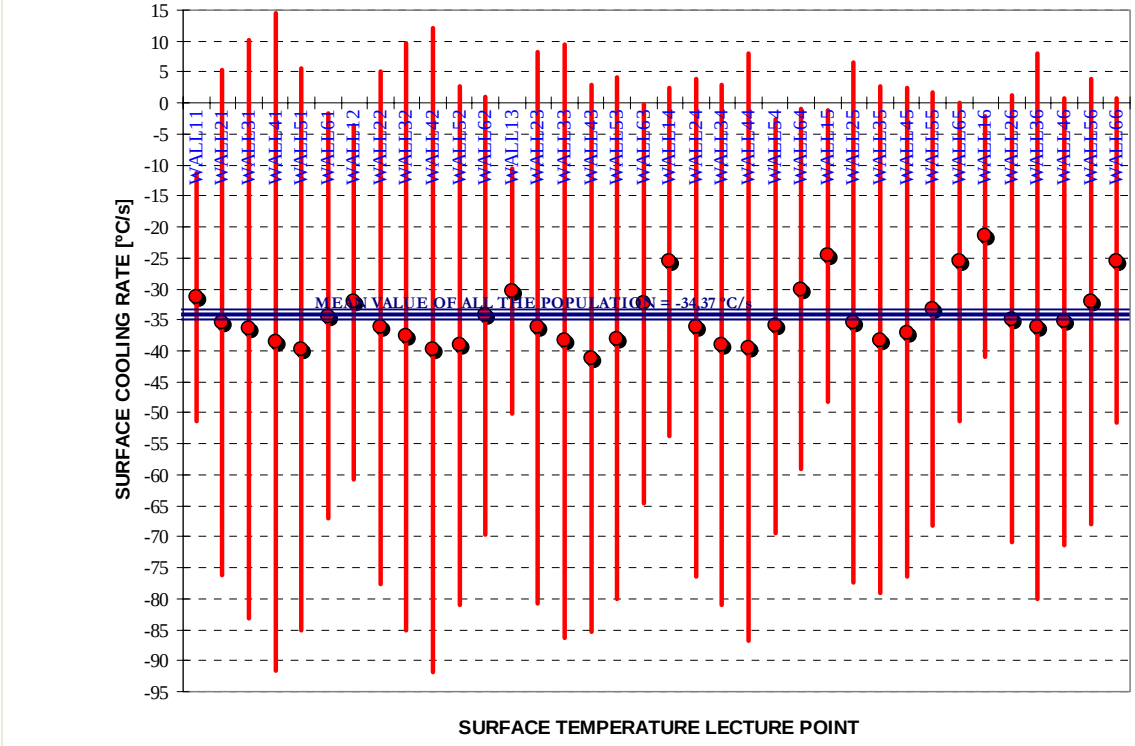

SURF. T LECTURE POINT	ARITHMETIC MEAN [°C/s]	STANDARD DEVIATION [°C/s]	MAXIMUM [°C/s]	MINIMUM [°C/s]	MEDIAN [°C/s]
WALL11	-31,36	20,05	-53,10	4,75	-35,80
WALL21	-35,46	40,79	-119,42	14,29	-23,16
WALL31	-36,41	46,66	-131,11	26,43	-24,19
WALL41	-38,57	53,02	-153,25	28,68	-26,08
WALL51	-39,81	45,33	-125,60	16,01	-26,34
WALL61	-34,35	32,60	-76,64	10,64	-26,02
WALL12	-32,11	28,57	-82,17	6,01	-25,42
WALL22	-36,25	41,44	-113,17	14,66	-21,79
WALL32	-37,64	47,44	-135,20	22,10	-23,20
WALL42	-39,78	51,99	-157,65	14,42	-25,83
WALL52	-39,14	41,76	-107,09	4,61	-21,08
WALL62	-34,31	35,35	-109,96	2,57	-20,77
WALL13	-30,36	19,75	-60,03	5,80	-27,85
WALL23	-36,19	44,53	-134,58	13,25	-22,36
WALL33	-38,41	47,82	-143,83	14,83	-23,82
WALL43	-41,17	44,16	-132,51	1,94	-23,76
WALL53	-38,03	42,07	-131,11	-3,02	-23,08
WALL63	-32,30	32,22	-104,57	-3,70	-20,27
WALL14	-25,60	28,07	-70,05	4,88	-23,36
WALL24	-36,22	40,11	-118,79	9,55	-24,78
WALL34	-39,03	41,98	-124,67	5,37	-23,29
WALL44	-39,42	47,50	-150,49	-5,27	-22,60
WALL54	-36,01	33,51	-102,73	-8,32	-24,76
WALL64	-30,07	29,08	-90,60	-4,94	-17,82
WALL15	-24,60	23,55	-60,36	3,86	-24,41
WALL25	-35,50	41,93	-130,10	5,98	-22,17
WALL35	-38,19	40,99	-124,44	3,96	-22,86
WALL45	-37,05	39,43	-120,45	3,31	-22,63
WALL55	-33,28	34,95	-103,64	-0,96	-19,25
WALL65	-25,63	25,67	-69,39	4,19	-15,84
WALL16	-21,50	19,42	-59,44	2,98	-17,94
WALL26	-34,90	36,07	-111,86	3,67	-21,69
WALL36	-36,04	43,97	-138,40	2,74	-22,46
WALL46	-35,21	36,06	-112,90	0,30	-23,09
WALL56	-32,13	35,92	-110,38	-2,42	-16,48
WALL66	-25,41	26,16	-74,36	1,31	-15,72

Table 6-28.n. OFFICE-14.
Statistic Parameters calculated on the Surface Cooling Rate at each Control Points.

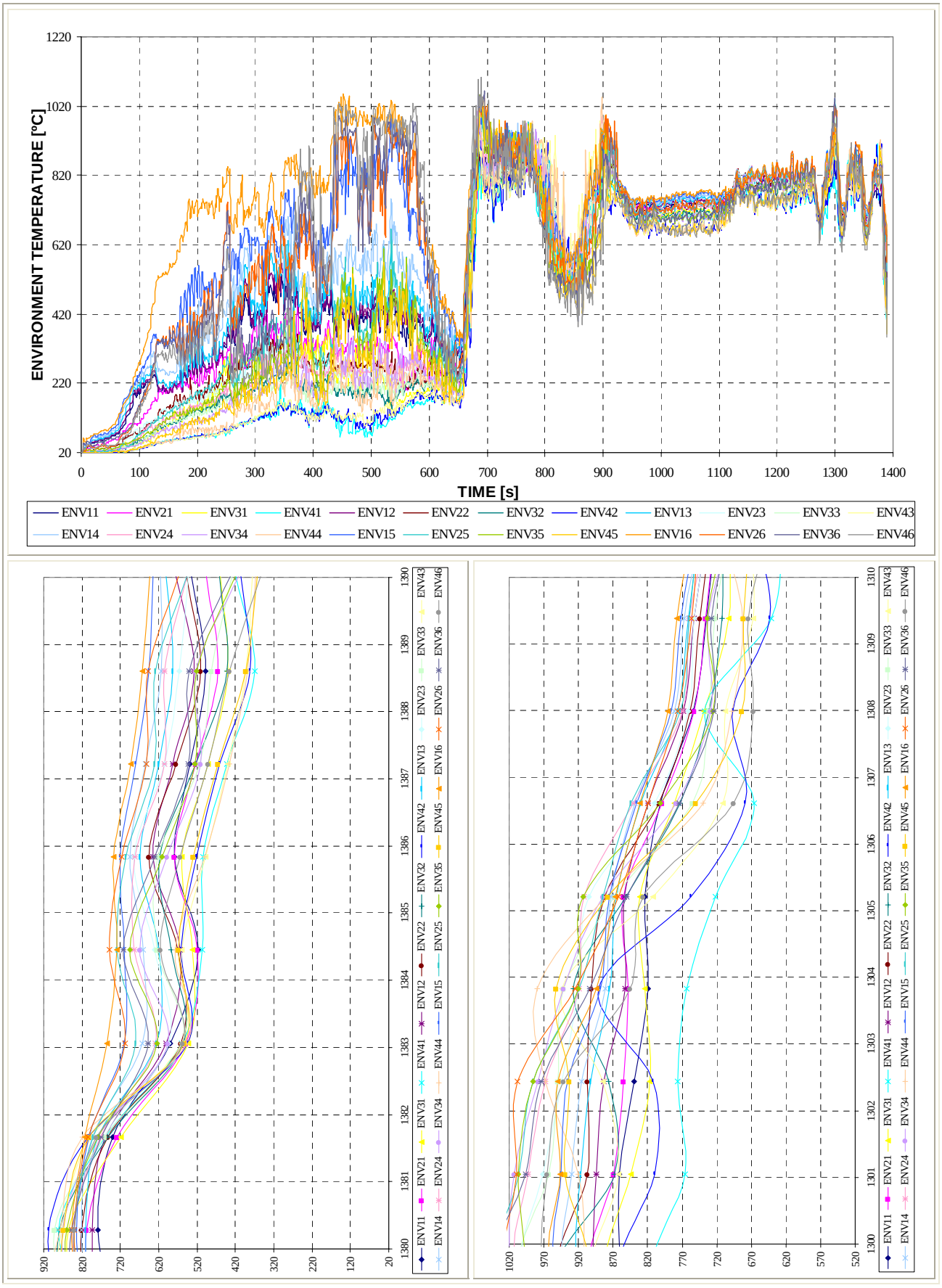

Figure 6-44.a. OFFICE-13.

Environment Temperature Evolution at the Control Points. Lower figures correspond to the detail on the 2nd environment cooling – from 1.300 to 1.310 seconds – and on the surface cooling – from 1.380 to 1.390 seconds –).

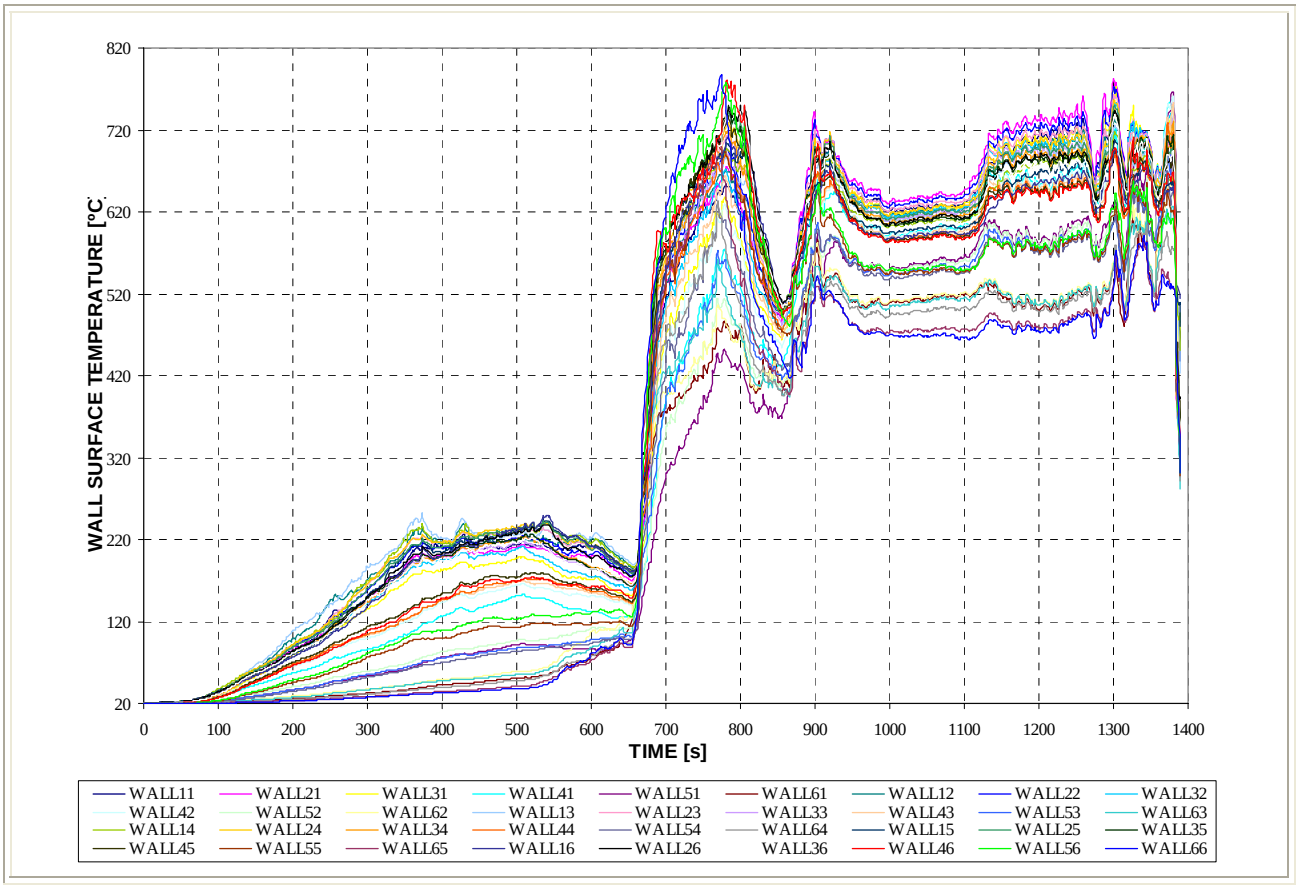

Surface Temperature Evolution at the Control Points.

Figure 6-44.b. OFFICE-13.

Surface Temperature Evolution at Control Points: detail on the surface cooling period –1.380 to 1.390s–

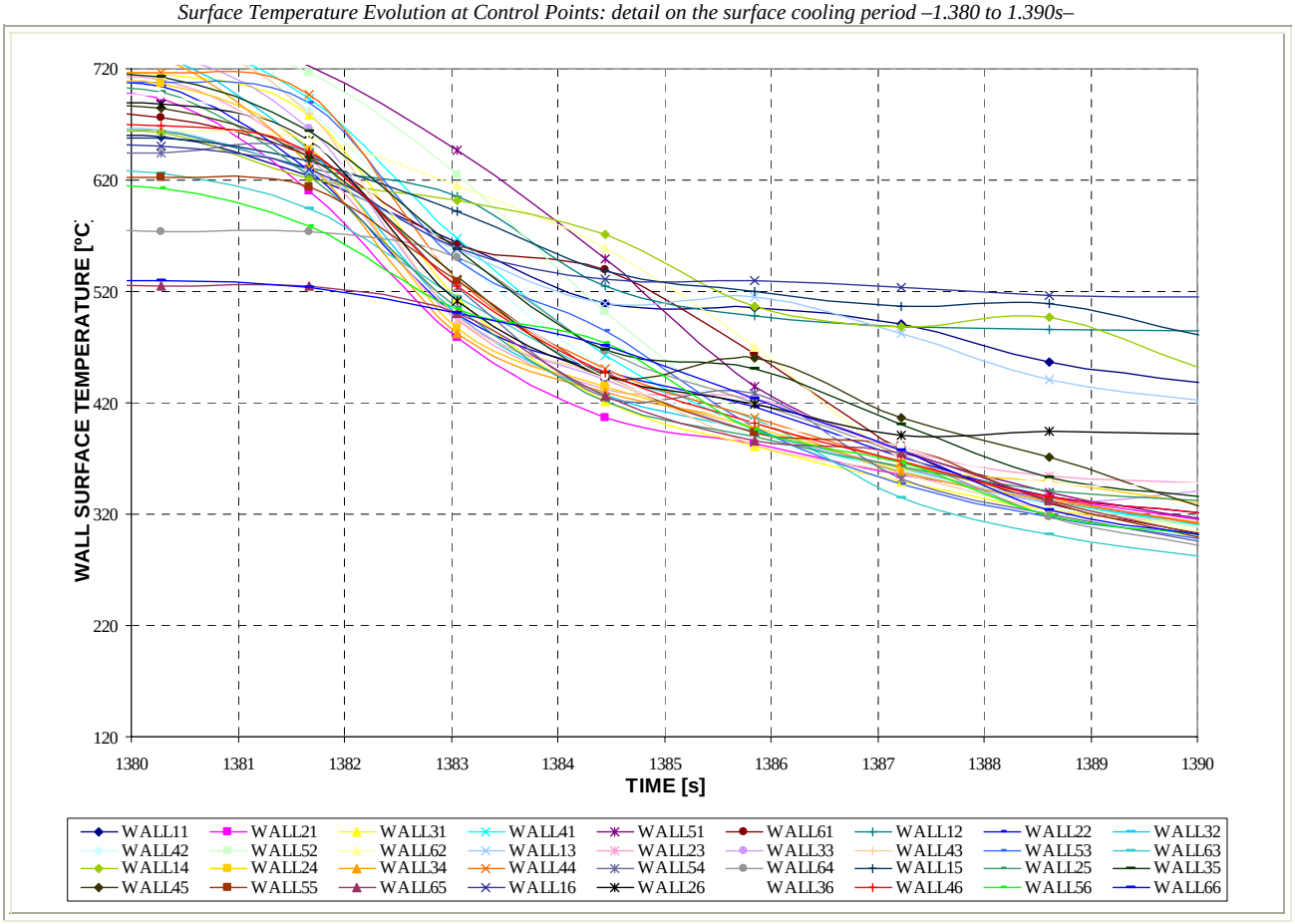

Figure 6-44.c. OFFICE-13.
Mean Cooling Rate and Standard Deviation at each of Surface Control Points.

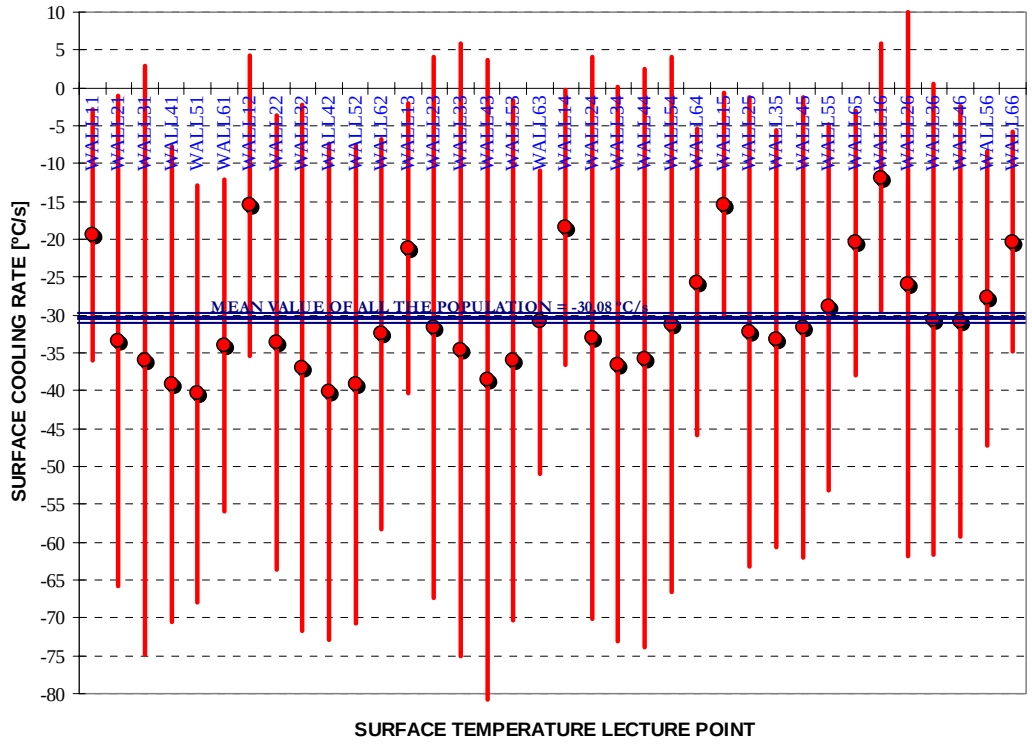

SURF. T LECTURE POINT	ARITHMETIC MEAN [°C/s]	STANDARD DEVIATION [°C/s]	MAXIMUM [°C/s]	MINIMUM [°C/s]	MEDIAN [°C/s]
WALL11	-19,44	16,59	-42,18	3,04	-18,87
WALL21	-33,45	32,42	-94,86	4,03	-18,71
WALL31	-36,01	38,82	-118,24	2,89	-24,23
WALL41	-39,16	31,46	-91,00	2,60	-34,23
WALL51	-40,41	27,56	-82,05	0,58	-37,00
WALL61	-33,93	21,89	-61,59	-2,54	-30,06
WALL12	-15,50	19,87	-57,70	4,87	-12,79
WALL22	-33,63	30,03	-92,82	7,11	-28,95
WALL32	-37,03	34,72	-105,81	5,89	-23,70
WALL42	-40,16	32,79	-93,57	3,93	-33,10
WALL52	-39,11	31,55	-88,39	1,58	-26,85
WALL62	-32,49	25,76	-72,32	-0,83	-29,54
WALL13	-21,18	19,21	-50,66	4,87	-25,64
WALL23	-31,67	35,72	-104,60	7,15	-24,93
WALL33	-34,60	40,50	-121,21	7,21	-28,12
WALL43	-38,55	42,24	-131,25	7,64	-31,26
WALL53	-35,99	34,26	-101,91	7,38	-29,02
WALL63	-30,92	19,98	-56,85	0,18	-26,23
WALL14	-18,40	18,13	-45,93	6,19	-18,18
WALL24	-33,08	37,14	-116,34	6,78	-26,51
WALL34	-36,50	36,57	-109,67	6,96	-25,70
WALL44	-35,72	38,17	-118,90	6,06	-26,18
WALL54	-31,24	35,25	-87,20	2,42	-20,04
WALL64	-25,63	20,29	-60,48	0,63	-25,96
WALL15	-15,43	14,83	-38,38	3,91	-14,41
WALL25	-32,21	31,02	-85,18	6,19	-21,18
WALL35	-33,18	27,50	-76,67	5,57	-34,60
WALL45	-31,62	30,42	-77,66	12,31	-31,38
WALL55	-28,92	24,16	-61,85	1,12	-29,75
WALL65	-20,47	17,50	-53,10	0,24	-20,10
WALL16	-11,81	17,66	-51,29	3,29	-4,81
WALL26	-25,99	35,92	-103,85	5,46	-19,64
WALL36	-30,63	31,09	-85,46	4,92	-26,54
WALL46	-30,86	28,50	-87,14	3,34	-23,71
WALL56	-27,75	19,46	-56,00	1,39	-23,15
WALL66	-20,31	14,59	-38,90	1,37	-19,05

Table 6-28.o. OFFICE-13.
Statistic Parameters calculated on the Surface Cooling Rate at each Control Points.

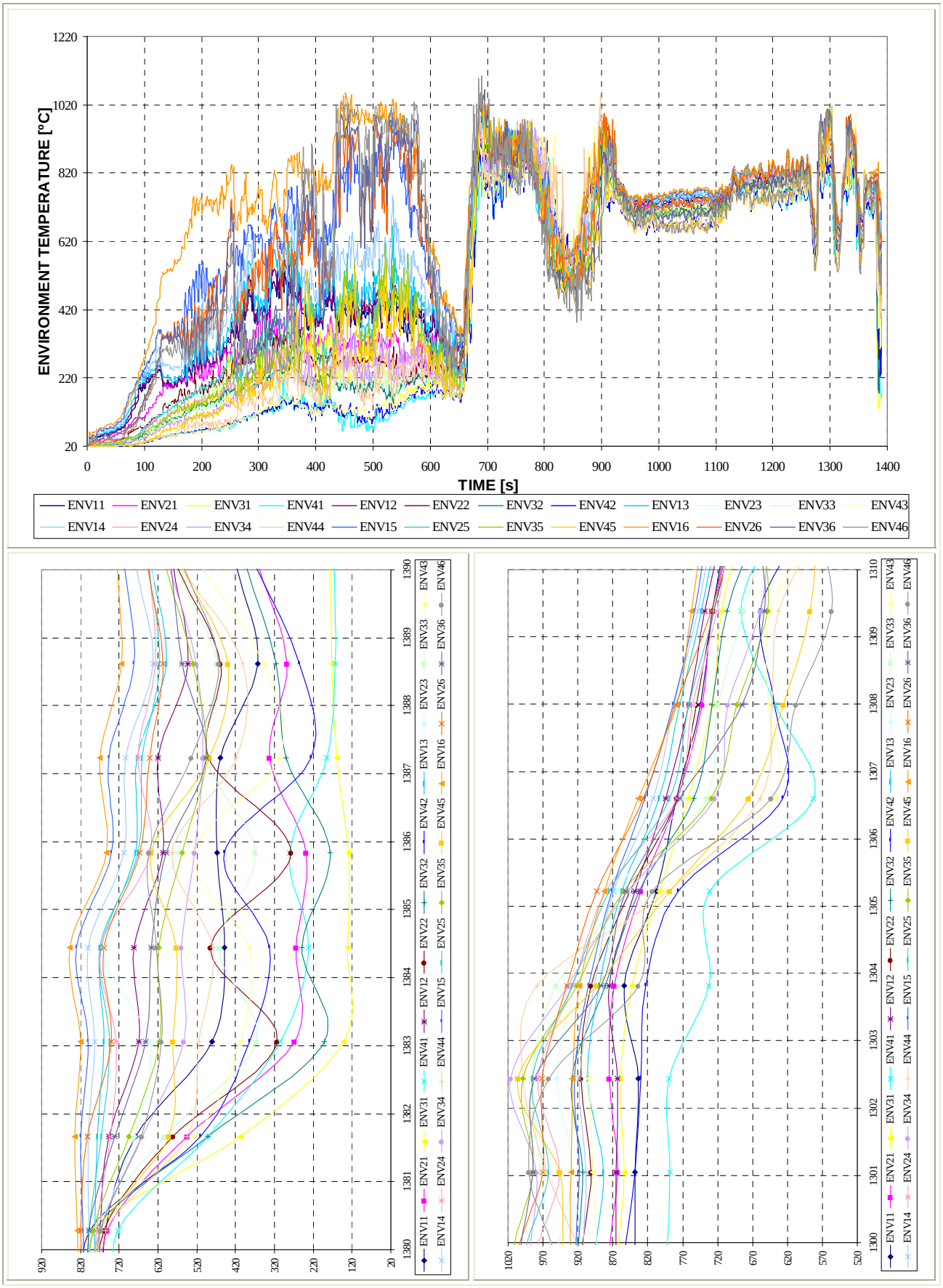

Figure 6-45.a OFFICE-7.

Environment Temperature Evolution at the Control Points. Lower figures correspond to the detail on the 2nd environment cooling – from 1.300 to 1.310 seconds – and on the surface cooling – from 1.380 to 1.390 seconds –).

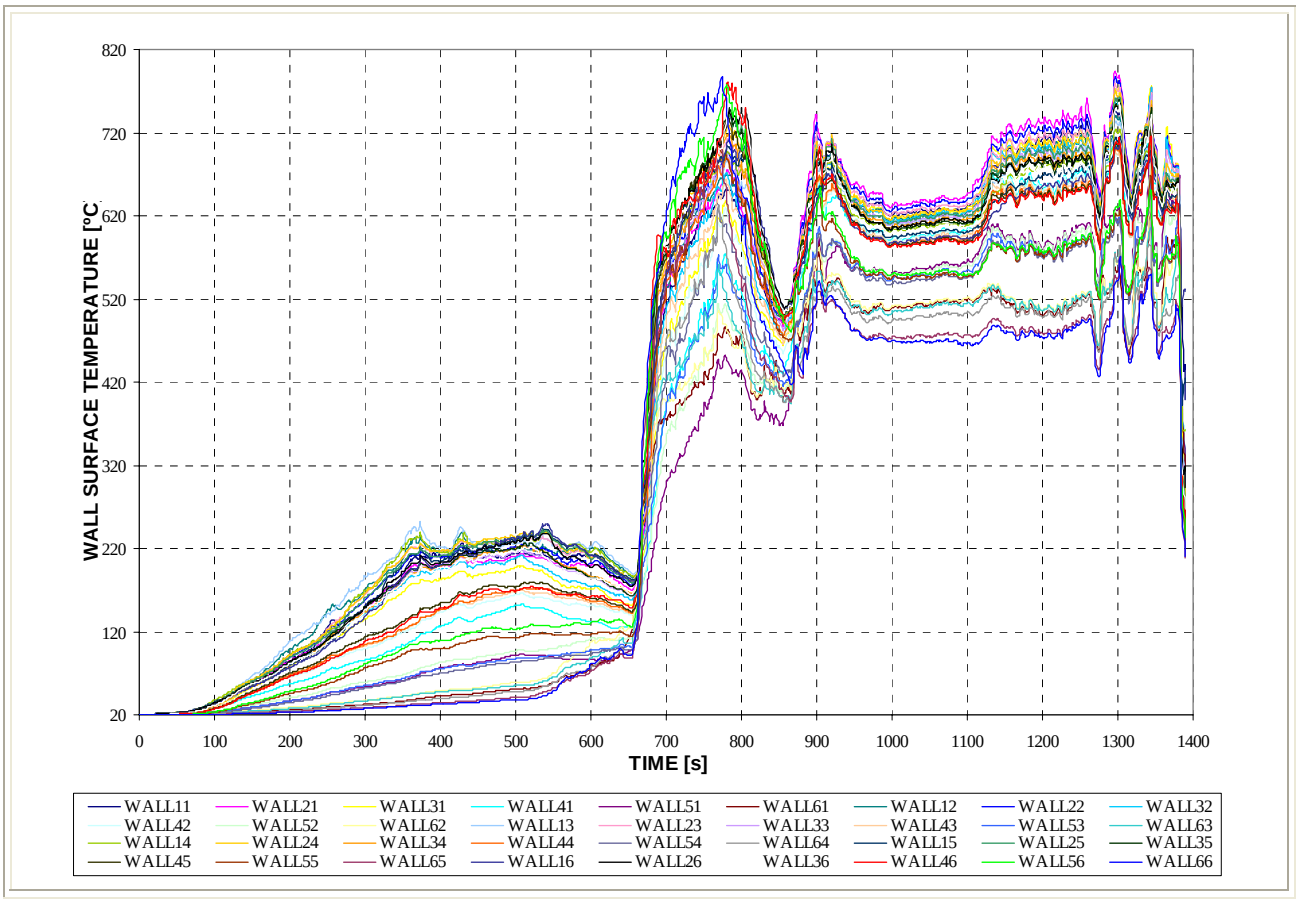

Surface Temperature Evolution at the Control Points.

Figure 6-45.b. OFFICE-7.

Surface Temperature Evolution at Control Points: detail on the surface cooling period –1.380 to 1.390s–

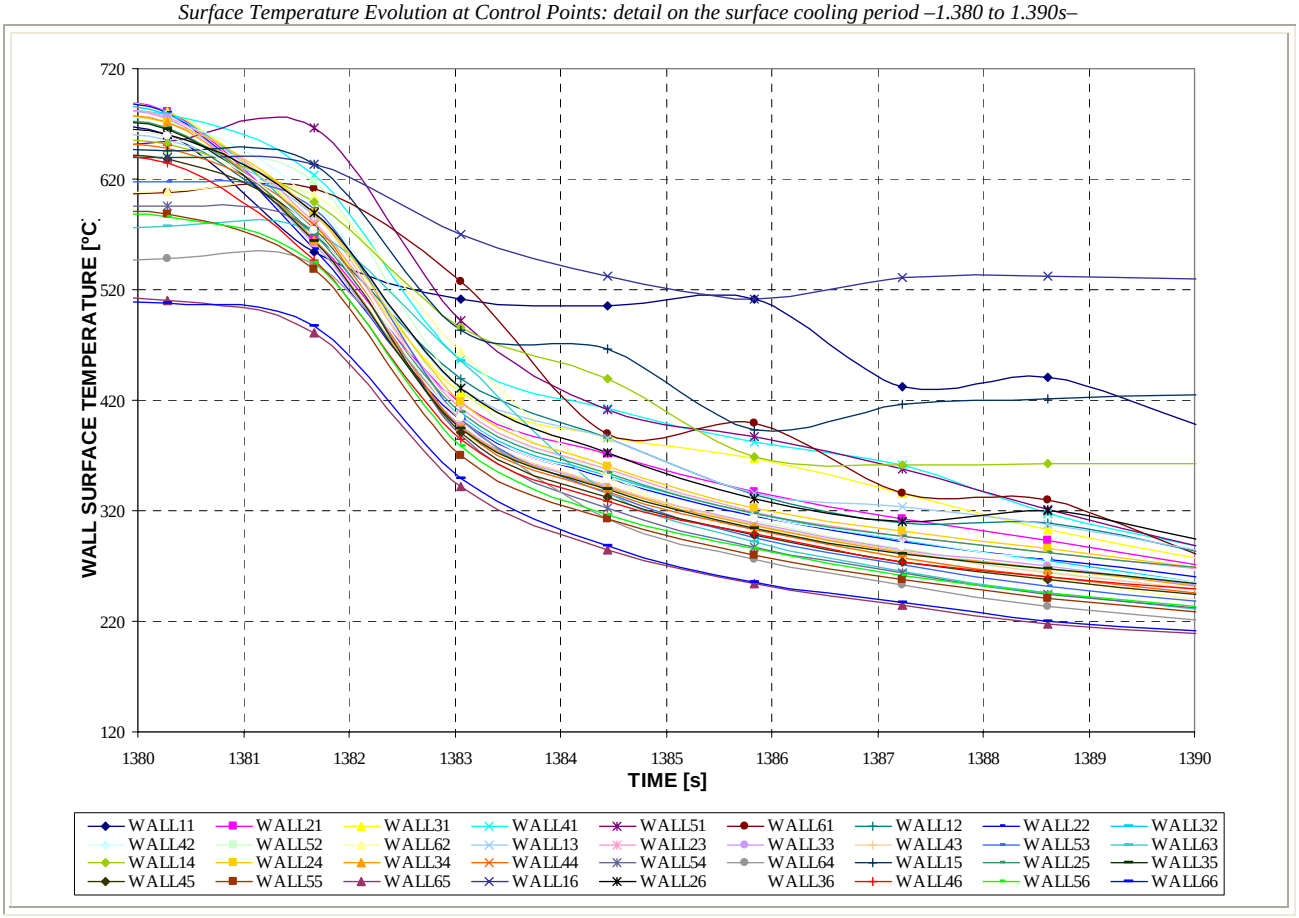

Figure 6-45.c. OFFICE-7.
Mean Cooling Rate and Standard Deviation at each of Surface Control Points.

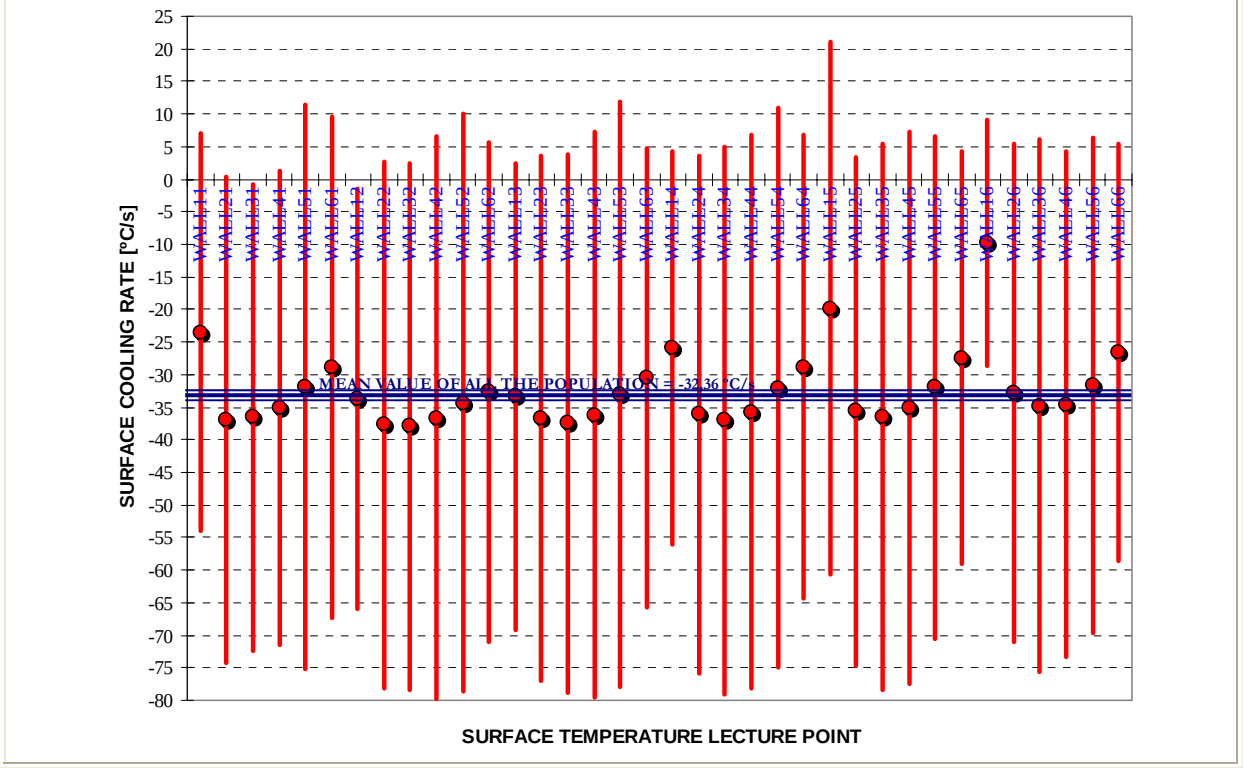

SURF. T LECTURE POINT	ARITHMETIC MEAN [°C/s]	STANDARD DEVIATION [°C/s]	MAXIMUM [°C/s]	MINIMUM [°C/s]	MEDIAN [°C/s]
WALL11	-23,5	30,6	-75,8	6,2	-17,6
WALL21	-36,9	37,3	-105,2	-0,4	-20,9
WALL31	-36,6	35,8	-107,7	-2,0	-23,4
WALL41	-35,0	36,4	-119,8	0,4	-26,8
WALL51	-31,8	43,3	-125,1	8,9	-22,3
WALL61	-28,9	38,5	-99,6	7,2	-19,4
WALL12	-33,8	32,3	-93,9	0,0	-27,8
WALL22	-37,7	40,5	-111,6	-0,4	-20,5
WALL32	-38,0	40,5	-120,5	0,2	-20,8
WALL42	-36,7	43,1	-133,2	6,8	-22,3
WALL52	-34,4	44,3	-134,2	7,9	-17,6
WALL62	-32,6	38,4	-101,5	4,9	-17,4
WALL13	-33,3	35,8	-112,0	0,0	-24,2
WALL23	-36,7	40,2	-120,8	-0,2	-21,6
WALL33	-37,5	41,4	-117,7	3,1	-20,4
WALL43	-36,1	43,5	-133,5	7,0	-21,5
WALL53	-33,0	44,9	-136,6	8,4	-17,2
WALL63	-30,4	35,2	-85,6	5,9	-16,7
WALL14	-25,9	30,2	-81,2	0,9	-19,4
WALL24	-36,1	39,7	-122,4	0,2	-21,2
WALL34	-37,0	42,0	-121,3	5,2	-20,9
WALL44	-35,8	42,5	-132,2	3,2	-21,2
WALL54	-32,0	43,0	-131,9	5,0	-16,6
WALL64	-28,8	35,6	-99,5	4,0	-15,3
WALL15	-19,8	40,9	-107,6	16,4	-4,5
WALL25	-35,6	39,1	-115,6	0,4	-20,3
WALL35	-36,4	41,9	-122,0	4,4	-20,6
WALL45	-35,1	42,3	-131,4	2,8	-21,1
WALL55	-32,0	38,6	-120,6	2,4	-19,7
WALL65	-27,4	31,6	-99,9	-2,5	-17,6
WALL16	-9,8	18,9	-45,8	14,0	-3,3
WALL26	-32,9	38,2	-114,0	7,3	-24,3
WALL36	-34,8	40,8	-122,2	3,3	-21,8
WALL46	-34,5	38,9	-116,4	0,5	-19,5
WALL56	-31,6	38,1	-119,5	0,5	-19,7
WALL66	-26,5	32,0	-98,2	1,6	-14,1

Table 6-28.p. OFFICE-7. (Highlighted in red is the most extreme value adopted in the calculations)
Statistic Parameters calculated on the Surface Cooling Rate at each Control Points.

6.4.3.2.5 Final Selection of the Cooling Profiles

Definitely, two types of cooling profiles are chosen in sight of what has been exposed on previous paragraphs:

- Environmental Cooling Profiles, where cooling effect is applied to the air in contact with the surface of the structural element,
- Surface Cooling Profiles, where cooling effect is applied directly to the surface of the structural element.

All of these processes are preceded by a 120 seconds interval where environment temperature is kept constant in order to ease the achievement of numerical convergence. Among them, several subtypes of cooling profiles are defined starting from different instants and depending on the actions following the cooling processes:

- Environmental Cooling Profiles: In all of them, the environmental temperature is progressively decreased according to the cooling rates detailed next and until it reaches ambient temperature, which is considered 25 ºC, following the calculations with a constant ambient temperature until the whole structural element show a temperature within the range *Ambient Temperature* ± 10ºC. This leads to very long calculations, since in general the subsequent cooling rates of the structural element are progressively slower once the environment is at ambient temperature.
  - ❖ '*Slow cooling*': It is characterized by a cooling rate of the air of only – 0,2 ºC/s.
  - ❖ '*Medium cooling*': It is characterized by a cooling rate of the air of – 2,0 ºC/s.
  - ❖ '*Fast cooling*': It is characterized by a cooling rate of the air of – 20,0 ºC/s.
- Surface Cooling Profiles: As explained in previous chapter, all of them are, in general, characterized by a cooling rate of the surface of the structural element of – 10,0 ºC/s (by apart of the particular cases analyzed with higher cooling rates, which will be described in detail later on specific paragraphs of this Chapter). The duration of the cooling process depends on the temperature of the surface at the instant when cooling starts, since it will continue until the ambient temperature is reached at the surface.
  - ❖ '*Followed by Heating*': After the surface cooling stage, the environment heating profile keeps governing the evolution of the temperature in the structural element. The heating profile is imposed until a total calculation time of 10.800 seconds (3 hours) has been reached from the beginning of the fire.
  - ❖ '*Followed by an imposed constant Surface Temperature*': Herein, the surface temperature is also decreased at the cooling rate previously described until the ambient temperature is reached on the surface. The difference with the case '*Followed by Heating*' is that at this instant the surface temperature is kept constant in order to simulate keeping the water jet applied on the surface for some time more. This 'extra' time of application of the water jet depends on the time when the superficial layers of the structural element become 'completely' damaged, since beyond this instant continuing the calculations is senseless.
  - ❖ '*Divided into Two/Three Periods*': The intention of this subtype of surface cooling is to simulate the action of the water jet applied on the surface of the structural element in several sweeps, which might be a realistic situation when fire fighters move the nozzle around in cyclic sweeps. Two or three sweeps of different durations are simulated depending on the initial temperature of the surface, but always the same cooling rate is applied. Among the several cooling subprocesses, the temperature of the surface is assumed to evolution governed by the environment heating profile.

In order to provide a better understanding of each cooling profile, in the following subparagraphs are shown some figures describing all of them. The complete set of analyzed cases is deeply described on paragraph 6.5.1., within the *Atlas of analyzed cases*.

6.4.3.2.5.1 Graphical Description of the Environment Cooling Profiles

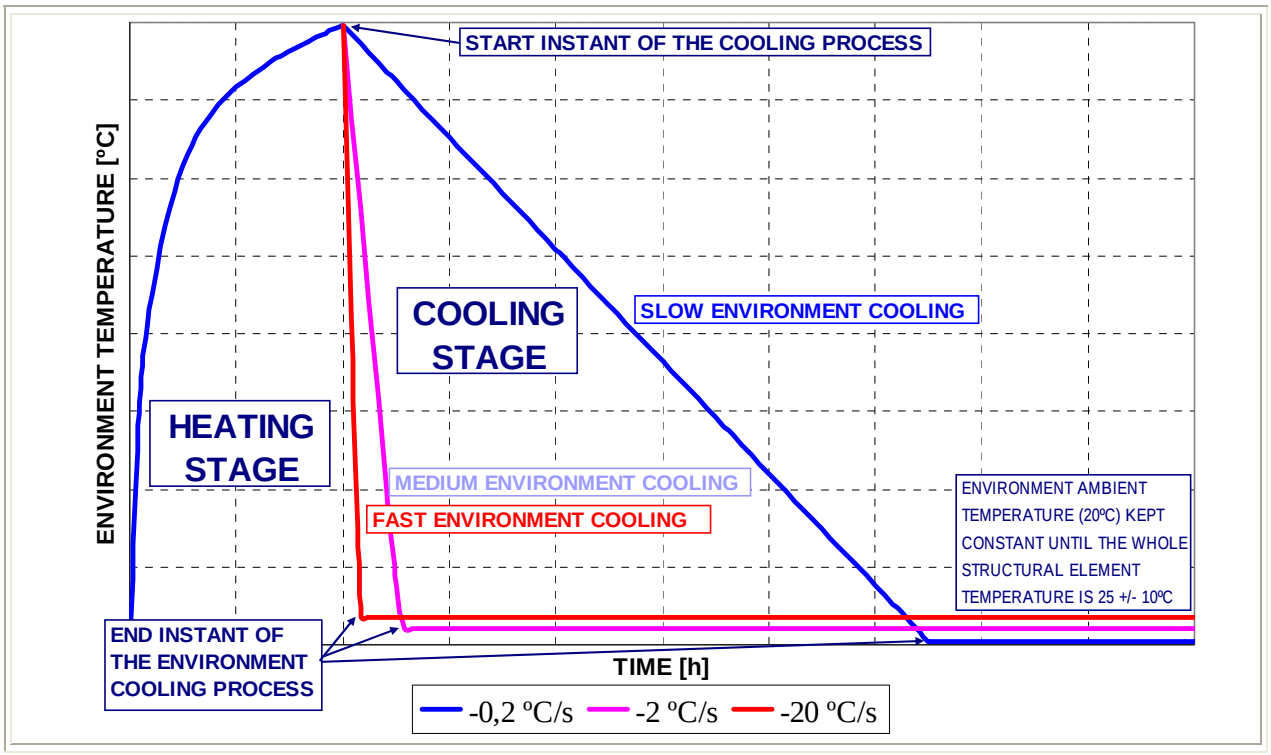

Figure 6-46. *Graphical Description of the Environment Cooling Profiles.*

6.4.3.2.5.2 Graphical Description of the Surface Cooling Profiles

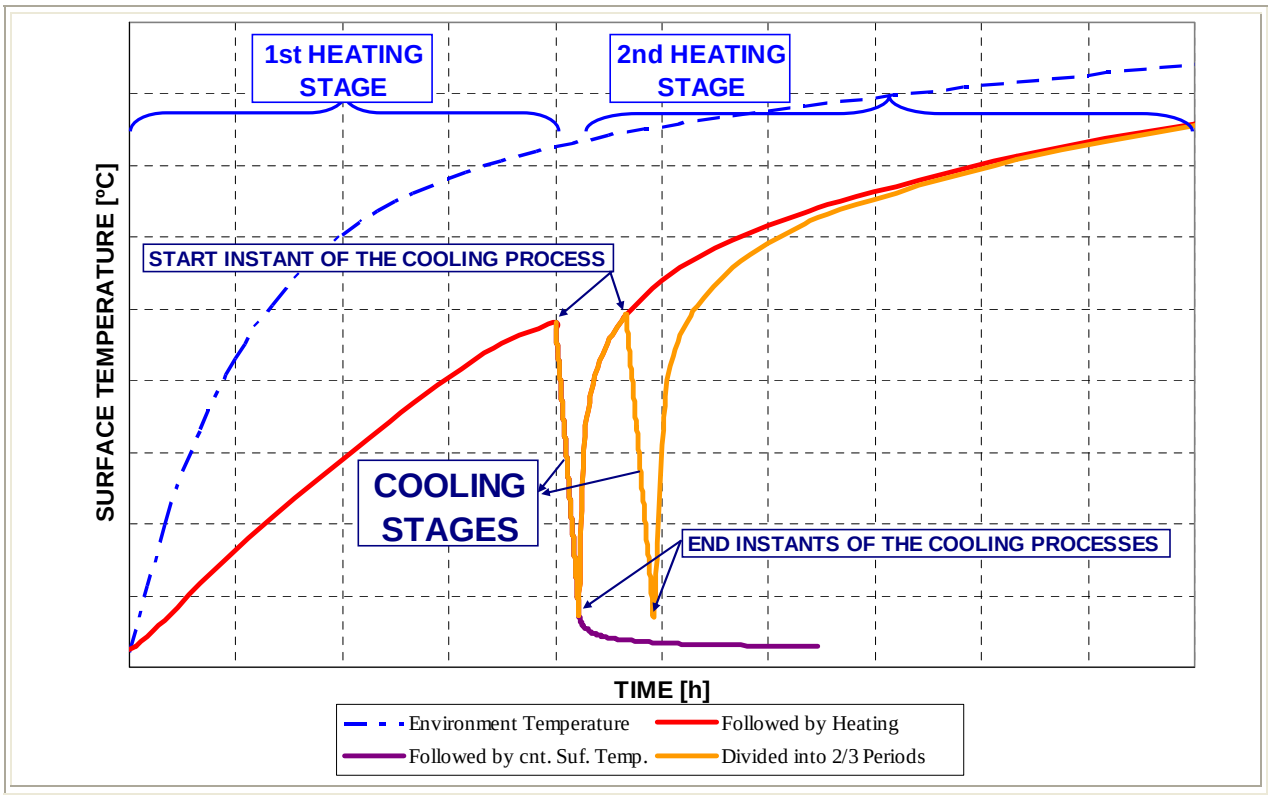

Figure 6-47. *Graphical Description of the Surface Cooling Profiles.*

6.4.3.2.5.3 Start Instants selected for the Cooling Processes

Some reference cases, where analyses are developed with a greater depth, are analyzed with the extinguishing action (cooling process) starting at several instants in order to discern the influence of the start instant on the overall hygro-thermo-chemo-mechanical processes occurring in the High Strength Concrete structural element (this comparison is developed on paragraph 196). The following selection of the start instant values is made from the basis that was explained on paragraph 6.4.3.2.3.1 for each of the previous heating curves considered;

#	HEATING PROFILE (Θ_g [°C] ,t [min])	START INSTANTS OF THE COOLING PROCESSES [s]				
1	**ISO834** ***(paragraph 6.4.3.1.1)*****:** $\Theta_g = 20 + 345 \cdot \log_{10}(8 \cdot t + 1)$	600				
2	**SLOW – minimum opening coefficient –** ***(paragraph 6.4.3.1.2)*****:** $\Theta_g = 20 + 1.325 \cdot (1 - 0{,}324 \cdot e^{-0{,}0152 \cdot t} - 0{,}204 \cdot e^{-0{,}1292 \cdot t} - 0{,}472 \cdot e^{-1{,}444 \cdot t})$	1.260	1.800	2.400	3.000	3.360
3	**EXTREMELY SLOW** ***(paragraph 6.4.3.1.3)*****:** $\Theta_g = 20 + 1.325 \cdot (1 - 0{,}324 \cdot e^{-0{,}0077 \cdot t} - 0{,}204 \cdot e^{-0{,}06545 \cdot t} - 0{,}472 \cdot e^{-0{,}7315 \cdot t})$	4.800				

Table 6-29. *Start instants of the extinguishing actions.*

6.5 RESULTS

6.5.1 Atlas of the analyzed cases

As the amount of cases analyzed is huge, the first task to accomplish is to collect again in a single table all of the combinations analyzed of the model described on the previous paragraphs:

COOLING START TIME (s)	COOLING TYPE	COOLING SUBTYPE	CODE	Combination	PC1 (RH) [%]			PC2 (K) [m²]			PC3 (TH) [cm]	PC4 (Heating curve)			PC5 (Mat)	
					40	50	60	10^{-19}	10^{-18}	10^{-17}	12	PAR1	PAR2	PAR4	C60	C90
600	SURF	FIRST COOL	1SFC	TH12K017RH40PAR1C60	X					X	X	X			X	
600	SURF	FIRST COOL	2SFC	TH12K018RH40PAR1C60	X				X		X	X			X	
600	SURF	FIRST COOL*	3SFC	TH12K019RH40PAR1C60	X			X			X	X			X	
600	SURF	FIRST COOL	4SFC	TH12K017RH50PAR1C60		X				X	X	X			X	
600	ENV	SLOW	5ES	TH12K018RH50PAR1C60		X			X		X	X			X	
		MEDIUM	5EM													
		FAST	5EF													
	SURF	HEAT	5SH													
		KEEP	5SK													
		REPEAT	5SR													
		FIRST COOL	5SFC													
--/--	--/--	--/--	5NC													
600	SURF	FIRST COOL	6SFC	TH12K019RH50PAR1C60		X		X			X	X			X	
600	SURF	FIRST COOL	7SFC	TH12K017RH60PAR1C60			X			X	X	X			X	
600	SURF	FIRST COOL	8SFC	TH12K018RH60PAR1C60			X		X		X	X			X	
600	SURF	FIRST COOL*	9SFC	TH12K019RH60PAR1C60			X	X			X	X			X	
3360	SURF	FIRST COOL	10SFC	TH12K017RH40PAR2C60	X					X	X		X		X	
3360	SURF	FIRST COOL	11SFC	TH12K018RH40PAR2C60	X				X		X		X		X	
3360	SURF	FIRST COOL	12SFC	TH12K019RH40PAR2C60	X			X			X		X		X	

Table 6-30. *Atlas of the analyzed cases.*

COOLING START TIME (s)	COOLING TYPE	COOLING SUBTYPE	CODE	Combination	PC1 (RH) [%]			PC2 (K) [m^2]			PC3 (TH) [cm]	PC4 (Heating curve)			PC5 (Mat)	
					40	50	60	10^{-19}	10^{-18}	10^{-17}	12	PAR1	PAR2	PAR4	C60	C90
3360	SURF	FIRST COOL	13SFC	TH12K017RH50PAR2C60		X				X	X		X		X	
1800	ENV	SLOW	14ES	TH12K018RH50PAR2C60		X			X		X		X		X	
		MEDIUM	14EM													
		FAST	14EF													
	SURF	HEAT	14SH													
		KEEP	14SK													
		REPEAT	14SR													
		FIRST COOL	14SFC													
2400	ENV	SLOW	14ES													
		MEDIUM	14EM													
		FAST	14EF													
	SURF	FIRST COOL (10K/s)	14SFC													
		FIRST COOL (15K/s)	14SFC													
3000	ENV	SLOW	14ES													
		MEDIUM	14EM													
		FAST	14EF													
	SURF	KEEP	14SK													
3360	ENV	SLOW	14ES													
		MEDIUM	14EM													
		FAST	14EF													
3360	SURF	HEAT	14SH													
		KEEP	14SK													
		REPEAT	14SR													
--/--	--/--	--/--	14NC													
1260	SURF	FIRST COOL	15SFC	TH12K019RH50PAR2C60		X		X			X		X		X	
3360	SURF	FIRST COOL	15SFC													
3360	SURF	FIRST COOL	16SFC	TH12K017RH60PAR2C60			X			X	X		X		X	
3360	SURF	FIRST COOL	17SFC	TH12K018RH60PAR2C60			X		X		X		X		X	
3360	SURF	FIRST COOL	18SFC	TH12K019RH60PAR2C60			X	X			X		X		X	
600	SURF	FIRST COOL	37SFC	TH12K017RH40PAR1C90	X					X	X	X				X
600	SURF	FIRST COOL	38SFC	TH12K018RH40PAR1C90	X				X		X	X				X
600	SURF	FIRST COOL	39SFC	TH12K019RH40PAR1C90	X			X			X	X				X
600	SURF	FIRST COOL	40SFC	TH12K017RH50PAR1C90		X				X	X	X				X
600	SURF	FIRST COOL	41SFC	TH12K018RH50PAR1C90		X			X		X	X				X
600	SURF	FIRST COOL*	42SFC	TH12K019RH50PAR1C90		X		X			X	X				X
600	SURF	FIRST COOL	43SFC	TH12K017RH60PAR1C90			X			X	X	X				X
600	SURF	FIRST COOL	44SFC	TH12K018RH60PAR1C90			X		X		X	X				X
600	SURF	FIRST COOL	45SFC	TH12K019RH60PAR1C90			X	X			X	X				X
3360	SURF	FIRST COOL	46SFC	TH12K017RH40PAR2C90	X					X	X		X			X
3360	SURF	FIRST COOL	47SFC	TH12K018RH40PAR2C90	X				X		X		X			X
3360	SURF	FIRST COOL	48SFC	TH12K019RH40PAR2C90	X			X			X		X			X
3360	SURF	FIRST COOL	49SFC	TH12K017RH50PAR2C90		X				X	X		X			X

Table 6-30 (continued). *Atlas of the analyzed cases.*

COOLING START TIME (s)	COOLING TYPE	COOLING SUBTYPE	CODE	Combination	PC1 (RH) [%]			PC2 (K) [m²]			PC3 (TH) [cm]	PC4 (Heating curve)			PC5 (Mat)	
					40	50	60	10^{-19}	10^{-18}	10^{-17}	12	PAR1	PAR2	PAR4	C60	C90
1800	SURF	FIRST COOL	50SFC	TH12K018RH50PAR2C90		X			X		X		X			X
3360	SURF	FIRST COOL	50SFC													
1260	SURF	FIRST COOL	51SFC	TH12K019RH50PAR2C90		X		X			X		X			X
1560	SURF	FIRST COOL	51SFC													
3360	SURF	FIRST COOL	51SFC													
3360	SURF	FIRST COOL	52SFC	TH12K017RH60PAR2C90			X			X	X		X			X
3360	SURF	FIRST COOL	53SFC	TH12K018RH60PAR2C90			X		X		X		X			X
3360	SURF	FIRST COOL	54SFC	TH12K019RH60PAR2C90			X	X			X		X			X
4800	SURF	FIRST COOL	100SFC	TH12K019RH50PAR3C90		X		X			X			X		X
--/--	--/--	--/--	100NC													

Remark 1: See the details about cooling process in the paragraph corresponding to each case.
Remark 2: The cases rounded by a thick blue line will be adopted as *Reference Cases* to be analyzed in a deeper detail.

Table 6-30 (continued). *Atlas of the analyzed cases.*

By apart from these combinations, two cases more are analyzed in order to discern the effect of the extremely high cooling rates of the surface that arise when using high-pressure hose nozzles, as it was deducted from the results of the Computational Fluid Dynamics simulations developed in paragraph 6.4.3.2.4.3. (-32,36 K/s as its mean value and -136,6 K/s as its absolute maximum value):

COOLING START TIME (s)	COOLING TYPE	COOLING SUBTYPE	CODE	Combination	PC1 (RH) [%]			PC2 (K) [m²]			PC3 (TH) [cm]	PC4 (Heating curve)			PC5 (Mat)	
					40	50	60	10^{-19}	10^{-18}	10^{-17}	12	PAR1	PAR2	PAR4	C60	C90
3360	SURF	KEEP (32,36K/s)	200SK	TH12K018RH50PAR2C60		X			X		X		X		X	
		KEEP (136,6K/s)	200SK													

Table 6-31. *Cases analyzed with extremely high cooling rates.*

Remark: For a better understanding and identification of the values characterizing each combination, the type of notation used to describe each of these seventy three combinations is the following one:

TH**K***RH**PAR*C**, where,

TH** indicates the value of the thickness of the model (in cm) used in the computation – Parameter 3 –

K*** indicates the value of the intrinsic permeability (in m^2) – Parameter 2 –,

RH** indicates the value of the initial saturation degree (in %) – Parameter 1 –,

PAR* indicates the parametric heating curve taken into account in the computation, – Parameter 4 –

C** indicates the material considered in the computation – Parameter 5 –.

Hence, for example, the combination TH12K018RH50PAR1C60 stands for a case characterised by a *thickness*=12 cm, $k=10^{-18}$ m^2, S_{init}*=50%, Parametric curve*=ISO Curve (Par1) and C60 material.

6.5.2 Cooling Phenomenological and Mechanistic Analysis

Within next paragraphs, the hygro-thermo-chemo-mechanical phenomena occurred during the cooling processes already described, for the reference cases, are analyzed in detail. The analyzed cases are, therefore, the following ones:

Reference case analyzed	***Related Paragraph***
Reference case # 05 – TH12K018RH50PAR1C60 – Start of cooling: 600 seconds	6.5.2.1.
Reference case # 14 – TH12K018RH50PAR2C60 – Start of cooling 1.800s	6.5.2.2.
Reference case # 14 – TH12K018RH50PAR2C60 – Start of cooling 2.400s	6.5.2.3.
Reference case # 14 – TH12K018RH50PAR2C60 – Start of cooling 3.000s	6.5.2.4.
Reference case # 14 – TH12K018RH50PAR2C60 – Start of cooling 3.360s	6.5.2.5.
Reference case # 14 – TH12K018RH50PAR2C60 – Start of cooling 3.360s with extremely high cooling rates	6.5.2.6.
Reference case # 100 – TH12K019RH50PAR4C90 – Start of cooling 4.800s	6.5.2.7.

Table 6-32. *Reference Cases analyzed within the Cooling Phenomenological and Mechanistic Analysis.*

Each analysis is done for each of the subtypes of cooling already mentioned and it includes, beyond the phenomenological and mechanistic analysis, a collection of the main results of the reference case for each stage of the cooling process as well as the main graphic results of the case in the Time-Space domain. Cases referred to in paragraphs 6.5.2.1, 6.5.2.5, 6.5.2.6 and 6.5.2.7 are especially deeply analyzed in those paragraphs. Related to the rest of cases, included in paragraphs 6.5.2.2, 6.5.2.3 and 6.5.2.4, on these paragraphs are exposed the main results but they are dealt in depth on paragraph 6.5.3.2 cause they are particularly focused on the analysis of the effect of the start instant of cooling processes (which is the only difference with respect to the case analyzed deeply on paragraph 6.5.2.5). The stated collection of the main results includes, for each of the cases, the following results for each heating/cooling stage:

I_{s4max} is the maximum value of the spalling index selected for this thesis and already described [-],
X_{IS4max} is the position [cm] corresponding to the maximum value of I_{S4},
t_{IS4max} is the absolute time [s]corresponding to the maximum value of I_{S4},

v_{max} is the maximum value – at any position and time (during the considered stage) – of the average velocity of spalled pieces considering both the energy contribution by the elastic strain energy and by the compressed gas [m/s] (it appears as a zero value when ΔE_k is negative and spalling is not possible),
X_{vmax} is the position [cm] corresponding to the maximum value of *v*,
t_{vmax} is the absolute time [s]corresponding to the maximum value of *v*,

v^*_{max} is the maximum value of the average velocity of spalled pieces [m/s]. It is calculated taking account all the instants (during the considered stage) but only those positions where mechanical damage presents values equal or higher than 0,10 (10 per cent). It appears as a zero value when spalling is not energetically possible or where mechanical damage has not reached a 10 per cent value,
X_{v*max} is the position [cm] corresponding to the maximum value of *v**,
t_{v*max} is the absolute time [s]corresponding to the maximum value of *v**,

d_{max} is the maximum value of the mechanical damage [-] at any position and time (during the considered stage),
X_{dmax} is the position [cm] corresponding to the maximum value of *d*,
t_{dmax} is the absolute time [s]corresponding to the maximum value of *d*,

T_{max} is the maximum value of the temperature [K] at any position and time (during the considered stage),
X_{Tmax} is the position [cm] corresponding to the maximum value of *T*,
t_{Tmax} is the absolute time [s]corresponding to the maximum value of *T*,

$P_{g,max}$ is the maximum value of the gas pressure [Pa] achieved at any position and time (during the considered stage),
$X_{Pg,max}$ is the position [cm] corresponding to the maximum value of P_g,
$t_{Pg,max}$ is the absolute time [s]corresponding to the maximum value of P_g,

The collection of the main graphic results of the case in the Time-Space domain is then included with the graphical representation form described in paragraph 6.2.3. (see figure 6-5).

6.5.2.1 REFERENCE CASE # 05 – TH12K018RH50PAR1C60 – START OF COOLING: 600S

The main features of this reference case are the following ones:

		PC1 (RH) [%]			PC2 (K) [m^2]			PC3 (TH) [cm]			PC4 (Heating curve)			PC5 (Mat)	
#	**Combination**	**40**	**50**	**60**	10^{-19}	10^{-18}	10^{-17}	**12**	**24**	**50**	**PAR1**	**PAR2**	**PAR4**	**C60**	**C90**
5	TH12K018RH50PAR1C60		X			X		X			X			X	

Table 6-33. *Main Features of the Reference Case #05 – TH12K018RH50PAR1C60.*

with an starting instant of the first cooling process at 600 seconds. The types and subtypes of cooling processes analyzed in this reference case are the following ones:

Type of Cooling	***Subtype of Cooling*** (***Remark:*** *See each Paragraph for more details on the features of the Cooling Processes.)*	***Related Paragraph***	***Figures numbers***
Environmental	Slow Cooling	6.5.2.1.1	6-48 to 6-57
Environmental	Medium Cooling	6.5.2.1.2	6-58 to 6-64
Environmental	Fast Cooling	6.5.2.1.3	6-65 to 6-66
Surface	Followed by Heating	6.5.2.1.4	6-67 to 6-76
Surface	Followed by an imposed constant Surface Temperature	6.5.2.1.5	6-77 to 6-81
Surface	Divided into Two Periods	6.5.2.1.6	6-82 to 6-87
Environment Heating up to three hours (10.800 seconds) without any cooling		6.5.2.1.7	6-88 to 6-89

Table 6-34. *Types and Subtypes of Cooling Processes Analyzed in the Reference Case #05 – TH12K018RH50PAR1C60*

6.5.2.1.1 Environmental Slow Cooling

6.5.2.1.1.1 Phenomenological and Mechanistic analysis of the Heating Stage

As it was explained on previous chapters the surface of the concrete element is initially heated both by a convective flux and by a radiation flux, what results in a gradual increase of the element temperature, starting from the surface zone (see figures 6-57 i) and 6-48 in more detail).

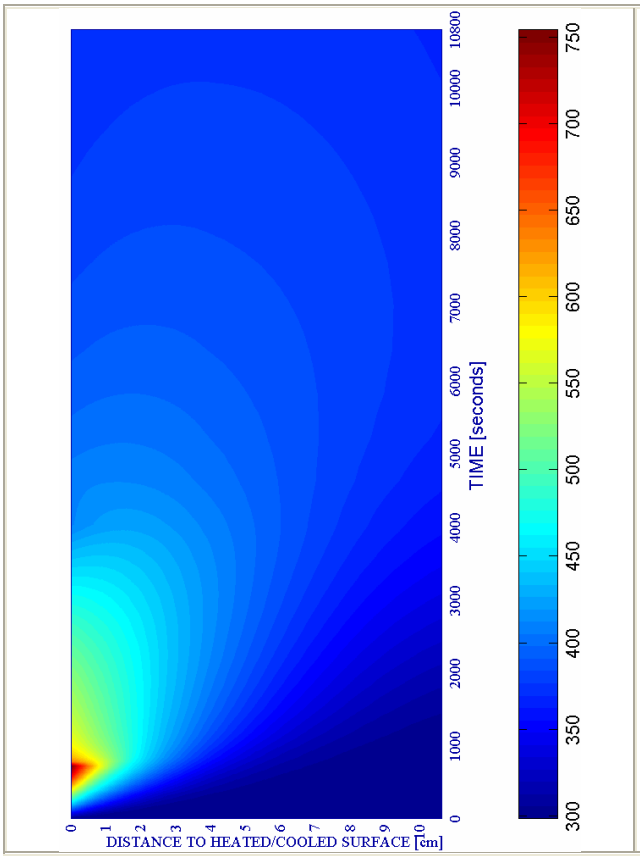

Figure 6-48. *Temperature T [K] during the 3 first hours*

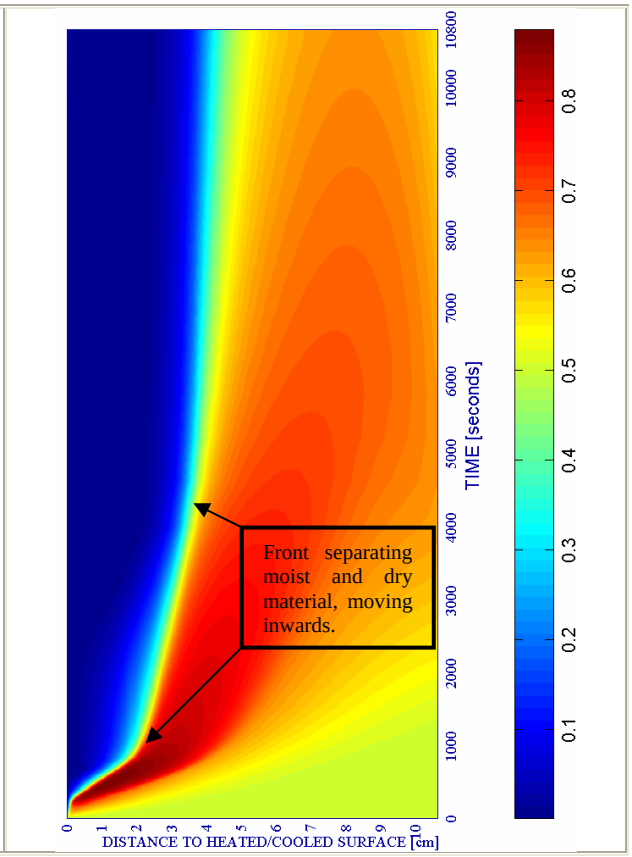

Figure 6-49. *Relative Humidity [-] during the 3 first hours*

The temperature gradients appear, in part, because almost all moisture must evaporate in the temperature range of 100-200ºC before a further temperature increase, what requires a considerable amount of energy (as it is shown on next table, the maximum temperature reached during this heating stage is 754,18 K, clearly above these values). Due to moisture evaporation, the relative humidity in the surface zone (initially 50% for this case) decreases to a very low value, figures 6-57 h) and 6-49 in more detail, and an initially sharp front, separating the moist and dry material, moves inwards. At this front intensive evaporation takes place, increasing considerably the vapour pressure (up to 1,25 MPa). The maximum values of vapour and gas pressures (figures 6-57 f) and 6-57 e) respectively) increase initially, then they remain almost constant as the surface temperature increases and the front moves inwards (as it is shown on next table, the absolute maximum value of gas pressure is achieved during this heating stage).

The maximum value of gas pressure usually coincides with the position where the temperature of approximately 200ºC occurs. In the regions with lower temperature, below about 130ºC, the gas pressure increase is caused mainly by a growth of the dry air pressure due to heating, achieving the maximum value of 0,25 – 0,4 MPa at the position with a temperature of about 100ºC. In the regions with higher temperature, the effect of a rapid increase of vapour pressure due to heating and temperature-dependence of the saturation vapour pressure predominate. At temperatures 200-300 ºC the gas in the material pores consists mainly of water vapour and the gradients of vapour pressure cause the vapour flow both towards the surface and inwards. The latter mass flow results in vapour condensation when the hot vapour inflows colder – internal layers of the concrete element – and in an increase of the relative humidity close to the 85 per cent (see figure 6-49) clearly above the initial value, often referred to as “moisture clog” or “saturation plug” [1]. An additional increase of the liquid water volume in the material pores is due to the water thermal dilatation, which is particularly important above the temperature of about 160ºC. A significant decrease of the gas permeability may be observed due to these effects, resulting in a decrease of the pore space available for the gas phase.

Increasing temperature causes the material dilatation of the aggregate which in part is due to concrete dehydration (products of the chemical reactions have greater volume than the initial volume of a concrete), in part due to material cracking and progressive crack opening, and finally due to “normal” thermal dilatation of the material skeleton. The concrete cracking during heating is caused by an incompatibility of thermal dilatation of the aggregate and the cement paste, resulting in high traction stresses in the Inter-Phase Transition Zones and development of local micro-cracks. Due to these cracks and chemical transformations of concrete (dehydration), the concrete strength properties and Young’s modulus degrade gradually, what can be expressed [53] in terms of the so-called thermo-chemical damage parameter (see figure 6-50).

A thermal dilatation of the external layers of a heated element is constrained by the core material which has lower temperature (figure 6-48). This causes macro-stresses in the external layers of the element, compression in the direction parallel to the surface (figure 6-57 l)) and traction in the direction perpendicular to it (figure 6-57 k)), as well as accumulation of the elastic strain energy (figure 6-57 j)). The tensile stresses may cause further development of cracks and fractures, parallel to the element surface, resulting in subsequent degradation of the material strength properties in the surface zone (see on figure 6-50 the increasing values of Thermo-Chemical damage and on figures 6-57 b) and 6-51 those corresponding to mechanical damage). An additional, external compressive load parallel to the element surface can intensify the aforementioned phenomena. Development of the cracks, both of thermo-chemical origin and the macro-stresses induced ones, causes a considerable increase of the material intrinsic permeability, and thereupon gas pressure decreases in the external layers where high temperatures are observed (see figure 6-52).

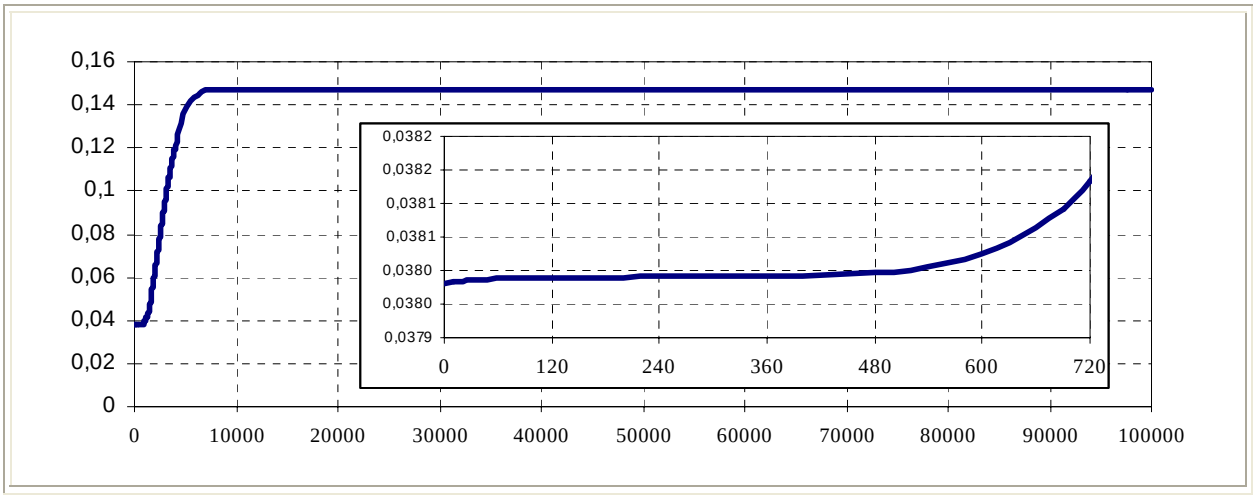

Figure 6-50. *Thermo-Chemical damage V [-] evolution at surface during the whole process with detail on heating stage.*

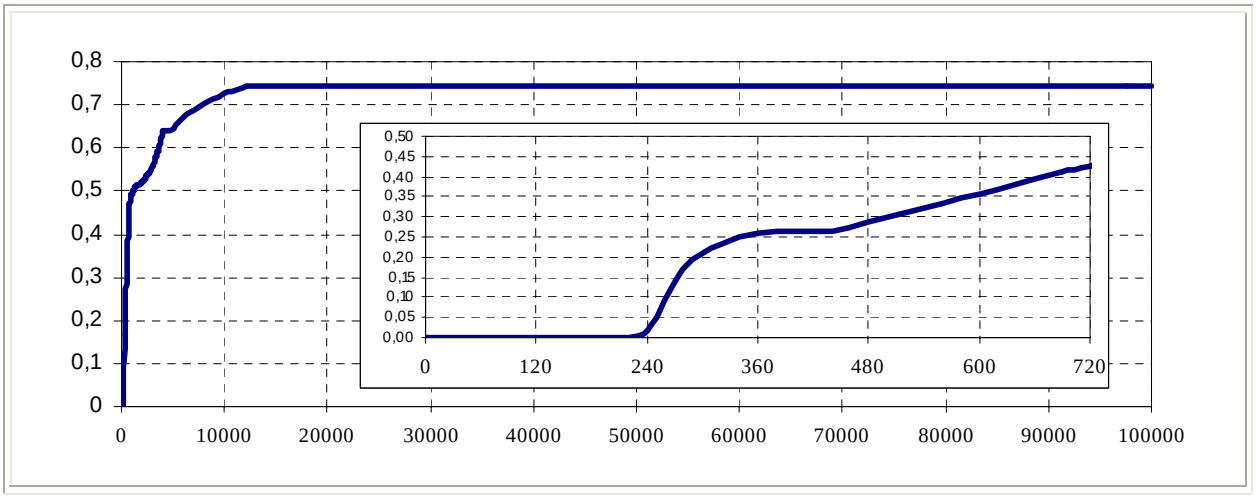

Figure 6-51 *Mechanical damage d [-] evolution at surface during the whole process with detail on heating stage.*

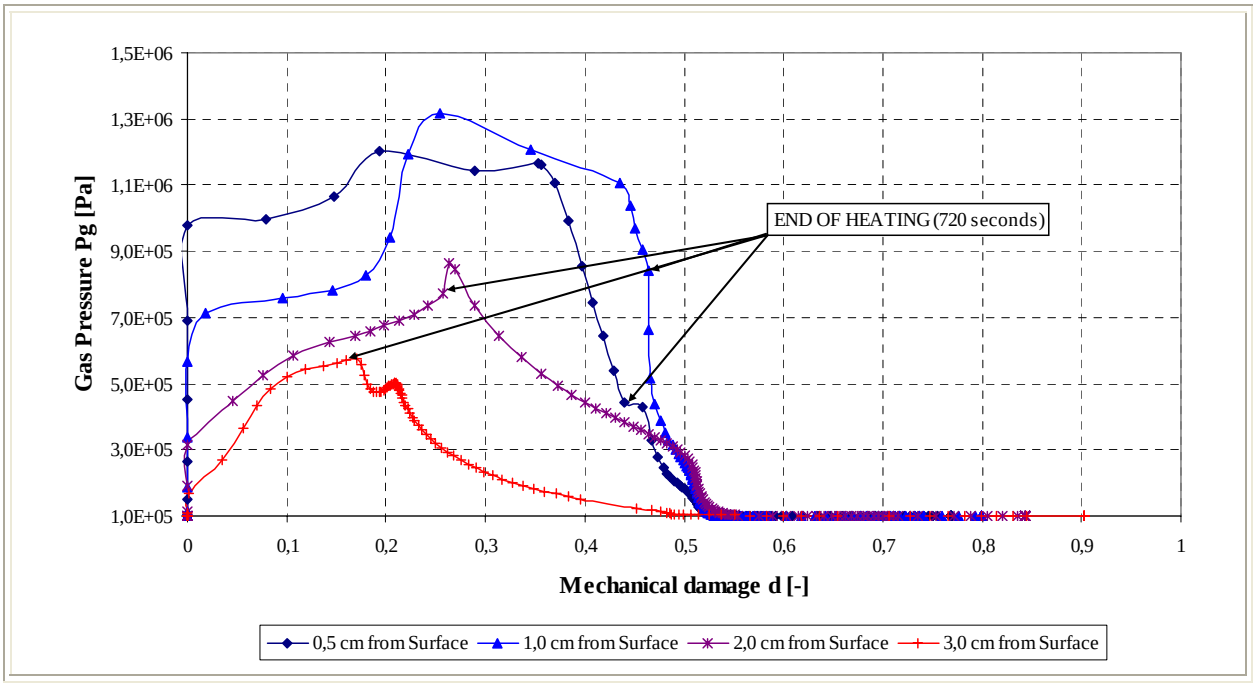

Figure 6-52. *Gas Pressure [Pa] versus Mechanical damage d [-] at several distances from the heated surface.*

The highest values of gas pressure usually correspond to the temperature 150-250 ºC, and this is also the range where the so-called thermal spalling of concrete usually occurs (when

elastic strain energy of constrained thermal dilatation, accumulated in the surface layer and then rapidly released after concrete fracture is considerable, the thermal spalling can be violent and explosive in nature as it was observed during the experimental tests developed).

6.5.2.1.1.2 Phenomenological and Mechanistic analysis of the Environment Cooling Stage

At the start instant of the cooling process (720 seconds from the beginning of heating), the maximum temperature is reached at the heated surface, being the zones close to the surface almost completely dry. The 'moisture clog' is situated 2 centimetres away from the surface (figure 6-54 b) and c)) matching this position with that corresponding to the maximum value of the vapour pressure caused by intensive water evaporation in the temperature range 100-200 ºC. The zone between the surface and the moisture clog shows the highest values of mechanical damage (0,4824 at 1,3 centimetres from surface, as shown at the next table and on figure 6-55 a)) being the longitudinal stresses in this layer tensile stress (figure 6-54 b), as it occurs in the rest of the layers at this instant) while transversal stresses achieve high levels of compression (figure 6-56). At this instant, the elastic energy is mostly accumulated close to the surface (figure 6-55 c)), precisely in the abovementioned layer – what leads to an unquestionable energetic viability of spalling occurrence of the layers close to the surface, clearly of explosive nature with velocities of the spalled pieces ranging from about 12,35 m/s at just 4 minutes from the beginning of the heating to 8,48 m/s at the start instant of the cooling process –. Besides this, at this start instant the heat flux moves inwards from the surface, while water vapour fluxes are addressed, from the moisture clog, both towards the heated surface and inwards due to the gradients of vapour pressure. The latter flux means vapour condensation when it reaches colder layers.

As the cooling process starts (beyond 720 seconds), the heat flux continues initially addressed only inwards from the surface – since the maximum temperature is still at the surface, figure 6-54 a) –, so the inner layers keep increasing their temperature, being at each instant the maximum value of vapour pressure progressively farther from the surface and at the depth where the temperature is of approximately 200ºC (figure 6-54 b)). Besides this, it is observed that the value corresponding to the peak of vapour pressure is progressively reduced during the environment cooling; this sharp decrease of the vapour pressure values (together with a decrease in the elastic strain energy that will be explained next) leads to a progressive decrease of the Spalling Index IS_4 values despite mechanical damage values increase during cooling until a really late stage.

As the cooling process continues, the temperature gradients in the structural element become lower since the surface temperature decreases while the inner temperatures increase (figure 6-54 a)). In this way, before the end of the environment cooling (at 4.020 seconds) the range of layers with enough temperature to become their liquid water evaporated has been extended from the initial 0-0,033 metres at 720 seconds up to the range 0-0,080 metres at 4.020 seconds. This means that 2/3 of the layer may present water vapour at the end of the environment cooling. At this instant, from which the environment temperature is assumed constant and equal to the initial ambient temperature (25 ºC), the zone with the maximum mechanical damage has grown until a depth of 0,025 metres with a maximum value of 0,6406, while longitudinal stresses – still being tensile at all the depths – are lower at the surface and higher at the inner layers. The maximum value of the elastic strain energy (figure 6-55 c)), considerably lower than at the beginning of the cooling process, does not appear any more at the surface but at 0,035 metres inwards. Once the environment cooling has finished, since its temperature is still considerably lower than the structural element temperature at all of its depths, two heat fluxes arise (directed each towards opposite surfaces). In this way, at almost 3 hours (10.620 seconds) from the beginning of the heating (9.900 seconds from the start of environment cooling or 6.200 seconds from its end) the temperature in the structural element is mostly uniform (about 100ºC according to figure 6-54 a)) and therefore low enough to condensate all of the evaporated vapour.

From this point, the gradient in water content is progressively cancelled through its diffusion and while a singular phenomenon is observed at both surfaces: although it will be studied in a more detail on paragraph 6.5.2.8.2., it shall be observed that there is an infiltration – across both surfaces – of the relative humidity of the environment towards the inner layers. This effect happens since a constant vapour pressure of the environment has been imposed at both sides of the structural element – see the paragraph explaining the boundary conditions used in the calculations – and, hence, as the temperature in the environment decreases its relative humidity increases (being approximately the 50% at ambient temperature) so, from the end of environment cooling (at 4.020 seconds) its relative humidity is considerably higher than the relative humidity in the layers close to the surface so it infiltrates inside them. The final state of the structural element, once it has reached a maximum temperature below the ambient temperature + 10ºC, shows a relative humidity mostly constant and of about the 30 per cent.

It is also remarkable that at approximately 3 hours (10.620 seconds) from the beginning of the heating (6.200 seconds from the environment cooling end), there arise compressive longitudinal (xx) stresses, first in the inner zones and later close to the surface where compressions achieve really high values at the end of the process. Due to this effect, elastic strain energy is accumulated again close to the surface (see figure 6-55 c)) at the end of the structural element process, appearing a second 'bag' of zones from 3 to 7 centimetres away from the surface where spalling would be again energetically viable at a stage as late as 27 hours after the start of the heating and more than 26 hours after the fire is supposed to be extinguished (see figure 6-57 d)). However, this spalling phenomenon is avoided herein due to the compressive nature of longitudinal stresses at these instants. In the meantime, mechanical damage keeps increasing its values at all depths (despite having finished the environment cooling process) until it arises values of about the 88 per cent (0,8773 in the next table) three centimetres away from the surface at 42.420 seconds (see figures 6-57 b) and 6-53 for more detail). From this instant up to the end where ambient temperature is achieved everywhere in the structural element, mechanical damage will not increase any more.

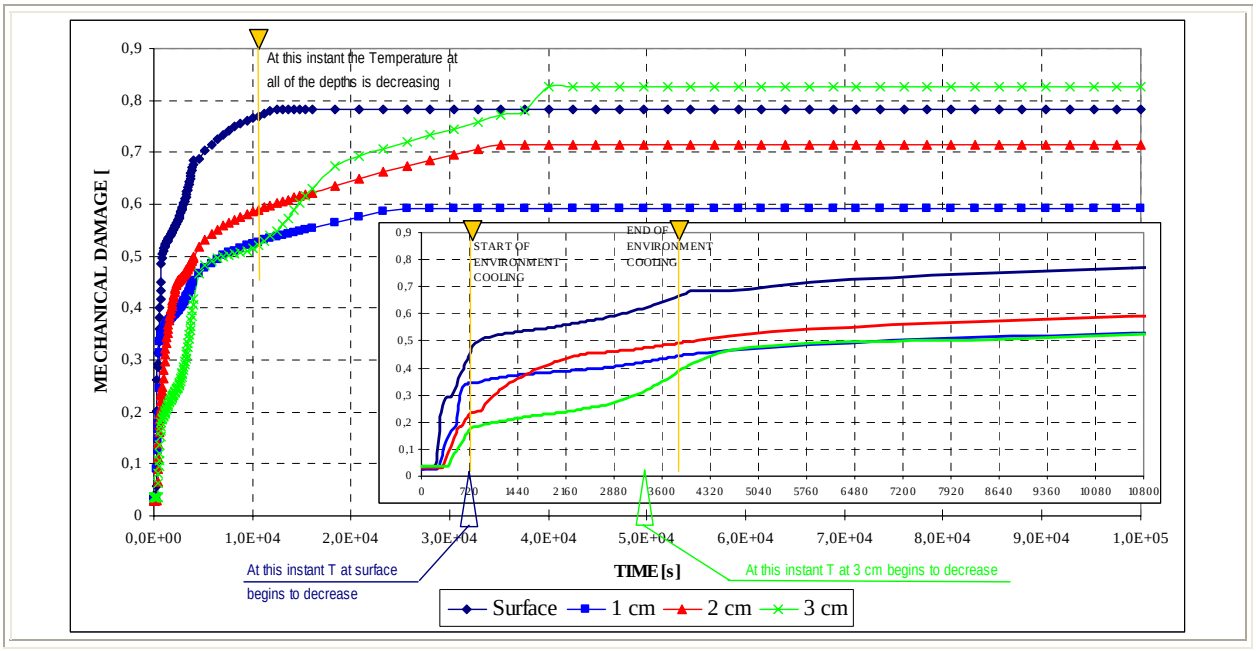

Figure 6-53. *Mechanical damage d [-] evolution during all of the heating and cooling stages, with detail on the environment cooling stage (from 720 s to 4.020 s).*

Finally, the thermo-chemical damage parameter achieves maximum values of about the 15 per cent, increasing hence the maximum value of Total Damage up to the 94 per cent at a depth of 3 centimetres from heated surface.

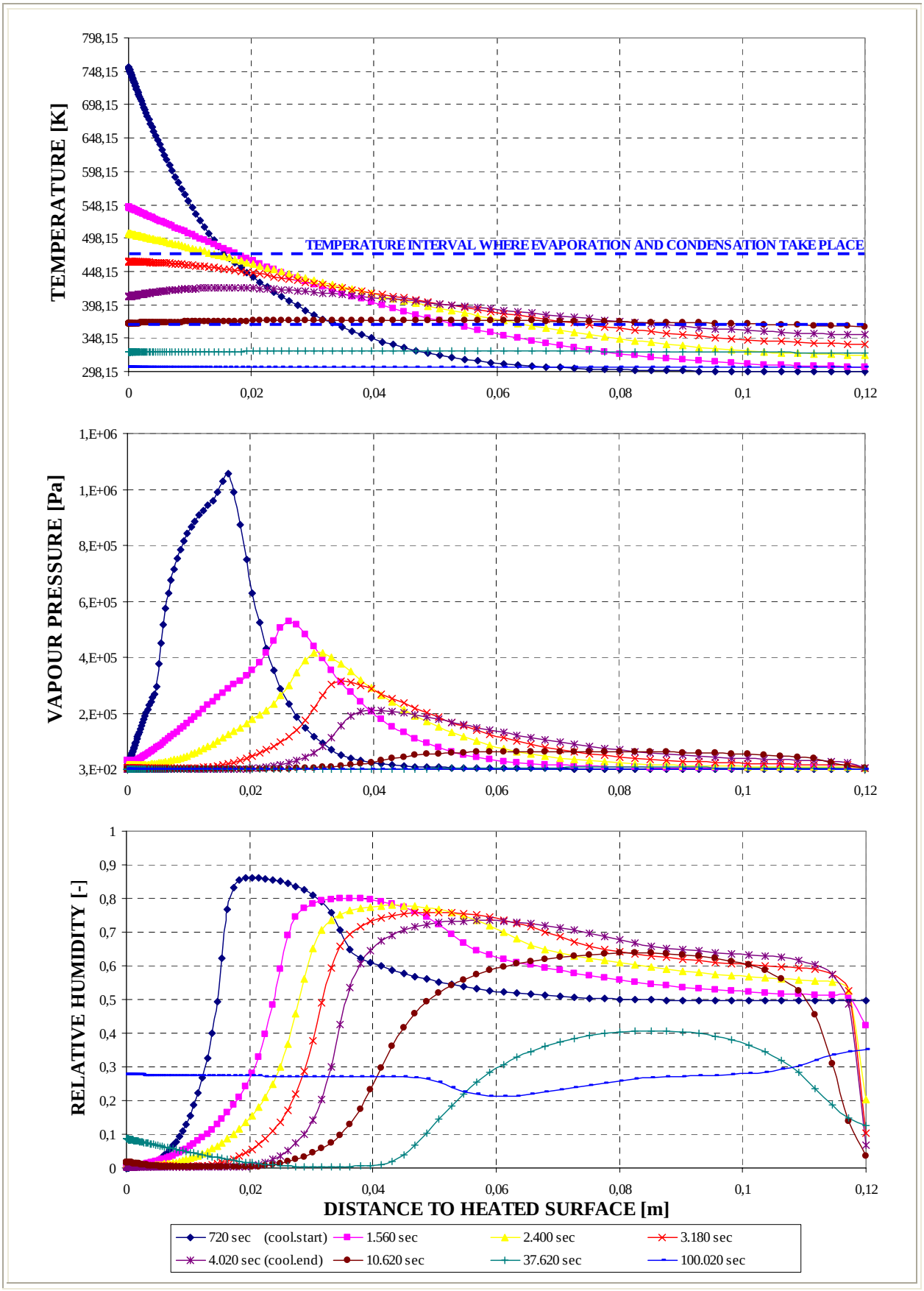

Figure 6-54. *a) Temperature, b) Vapour Pressure and c) Relative Humidity at several distances from the heated surface during Environment cooling process.*

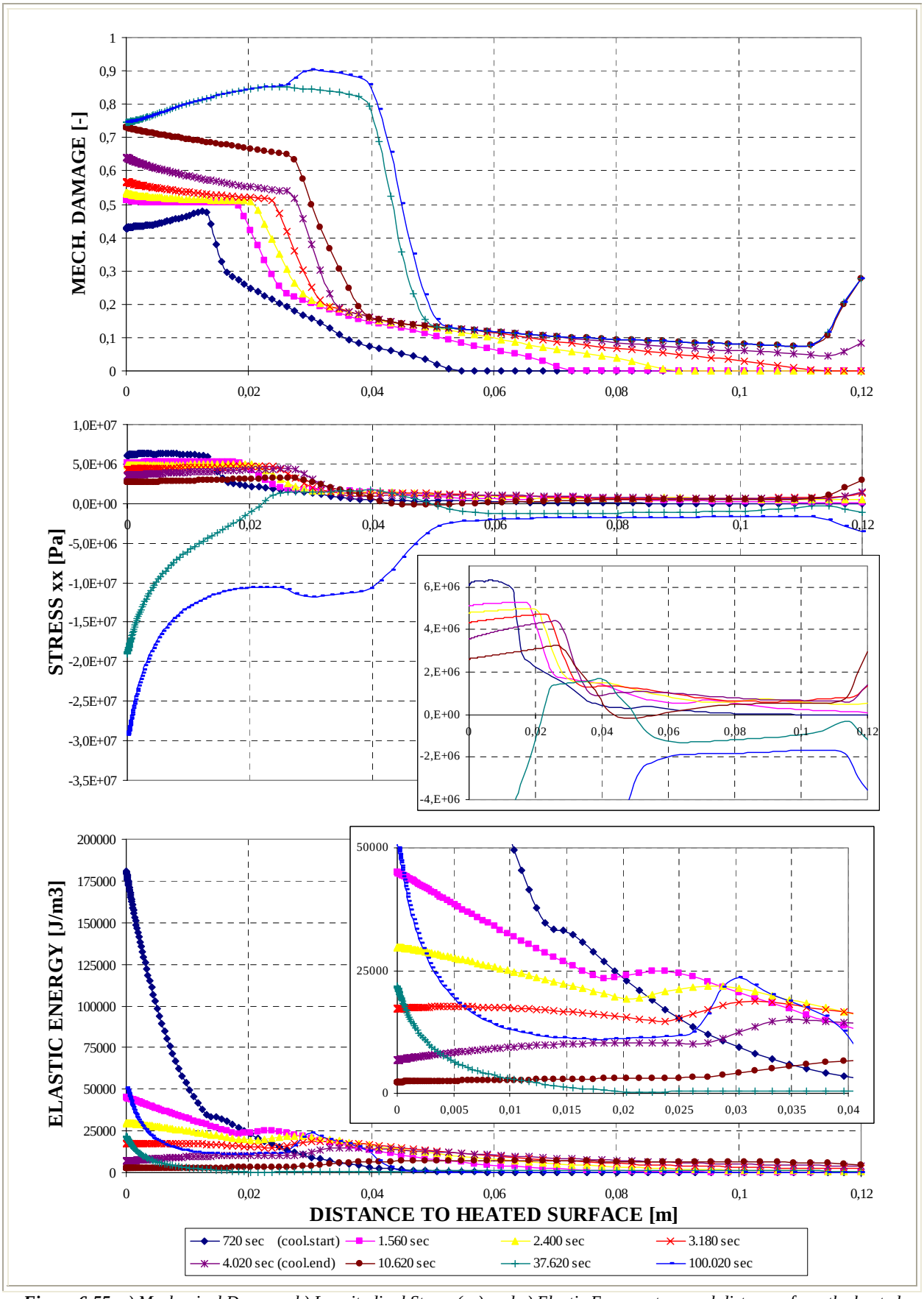

Figure 6-55. *a) Mechanical Damage, b) Longitudinal Stress (xx) and c) Elastic Energy at several distances from the heated surface during Environment cooling process.*

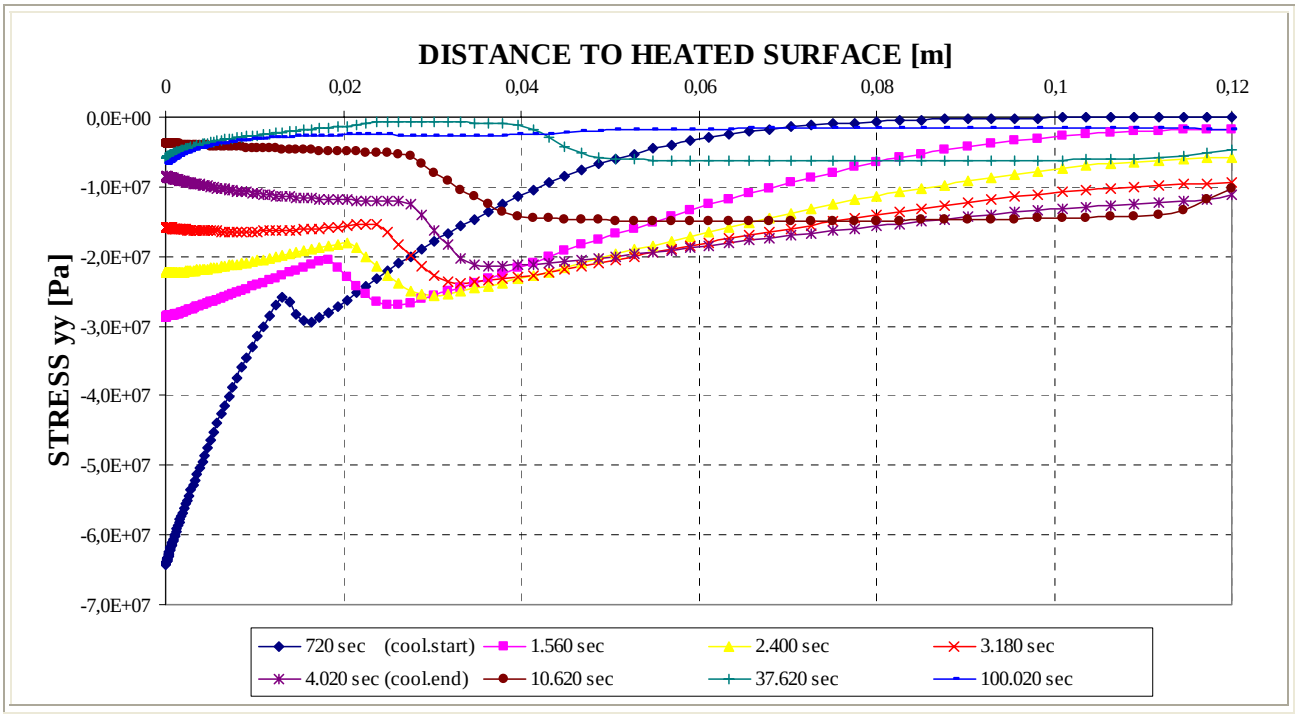

Figure 6-56. *Transversal Stress (yy) at several distances from the heated surface during Environment cooling process.*

6.5.2.1.1.3 Collection of the Main Results of this Case for each Stage of the Cooling Process

Next it is shown a collection of the main results cited in the last subparagraph, as well as a description of each of the stages that compose the heating and cooling processes analyzed herein. Highlighted in red are the maximum values achieved by each parameter.

Table 6-35. *Description of the Cooling Process Stages and Collection of the Main Results related to Spalling Index and velocity*

Stage description	Absolute Time Start [s]	Absolute Time End [s]	$IS4_{max}$ [-]	X_{IS4max} [cm]	t_{IS4max} [s]	v_{max} [m/s]	X_{vmax} [cm]	t_{vmax} [s]	v_{max}* [m/s]	X_{vmax*} [cm]	t_{vmax*} [s]
First Heating	0	600+120	0,3688	0,582	600	12,349	0,152	240	9,521	0,245	280
Environment cooling	720	4.020	0,3239	0,860	720	8,479	0,916	720	8,479	0,916	720
Environment constant Temperature up to an absolute time 10.800s	4.020	10.800	0,0013	3,796	4.020	1,697	10,632	4.020	1,521	7,034	4.020
Environment Constant Temperature for t > 10.800s	10.800	100.020	0,0001	3,964	10.800	1,561	4,314	100.020	1,561	4,314	100.020
Maximum for t ≤ 10.800s†	0	10.800	0,3688	0,582	600	12,349	0,152	240	9,521	0,245	280
Absolute Maximum	0	100.020	0,3688	0,582	600	12,349	0,152	240	9,521	0,245	280

Remark †: *These results are included for the Comparative Analysis developed on Paragraph 6.5.3*

Stage description	Absolute Time Start [s]	Absolute Time End [s]	d_{max} [-]	X_{dmax} [cm]	t_{dmax} [s]	T_{max} [K]	X_{Tmax} [cm]	t_{Tmax} [s]	p^g_{max} [MPa]	X_{pgmax} [cm]	t_{pgmax} [s]
First Heating	0	600+120	0,4824	1,312	720	754,18	0,000	720	1,3276	0,860	480
Environment cooling	720	4.020	0,6406	0,000	4.020	754,18	0,000	720	1,056	1,644	720
Environment constant Temperature up to an absolute time 10.800s	4.020	10.800	0,7304	0,000	10.800	423,68	1,555	4.020	0,344	3,964	4.020
Environment Constant Temperature for t > 10.800s	10.800	100.020	0,8773	3,028	42.420	373,15	4,314	10.800	0,248	8,286	10.800
Maximum for t ≤ 10.800s†	0	10.800	0,7304	0,000	10.800	754,18	0,000	720	1,3276	0,860	480
Absolute Maximum	0	100.020	0,8773	3,028	42.420	754,18	0,000	720	1,3276	0,860	480

Table 6-36. *Description of the Cooling Process Stages and Collection of the Main Results related to mechanical damage, Temperature and Gas Pressure*

6.5.2.1.1.4 Main Graphic Results of this Case in the Time-Space domain.

a) Spalling Index IS4 [-]

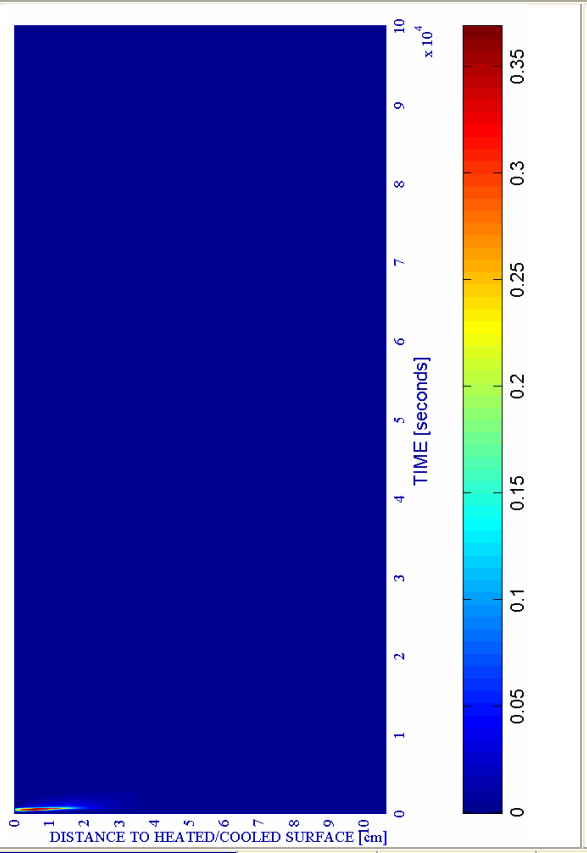

b) Mechanical damage d [-]

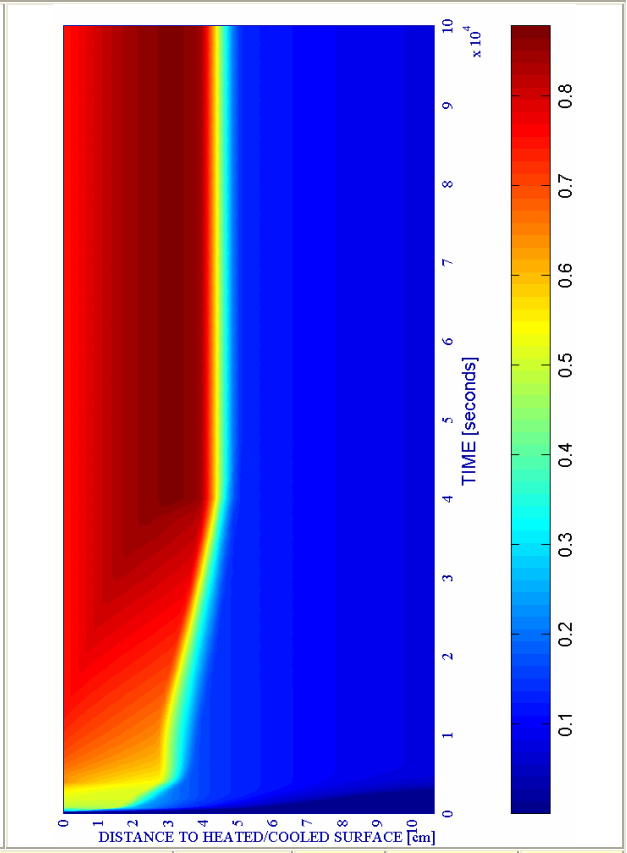

ENVIRONMENTAL - SLOW		PC1 - RH [%]			PC2 - K_0 [m^2]			PC4 - Heating curve			PC5 – Mat.		Cooling length[s]	Start of cooling [s]	End of cooling [s]
#	Combination	40	50	60	10^{-19}	10^{-18}	10^{-17}	PAR1	PAR2	PAR4	C60	C90			
05	TH12K018RH50PAR1C60		X			X		X			X		3.300	600+120	4.020

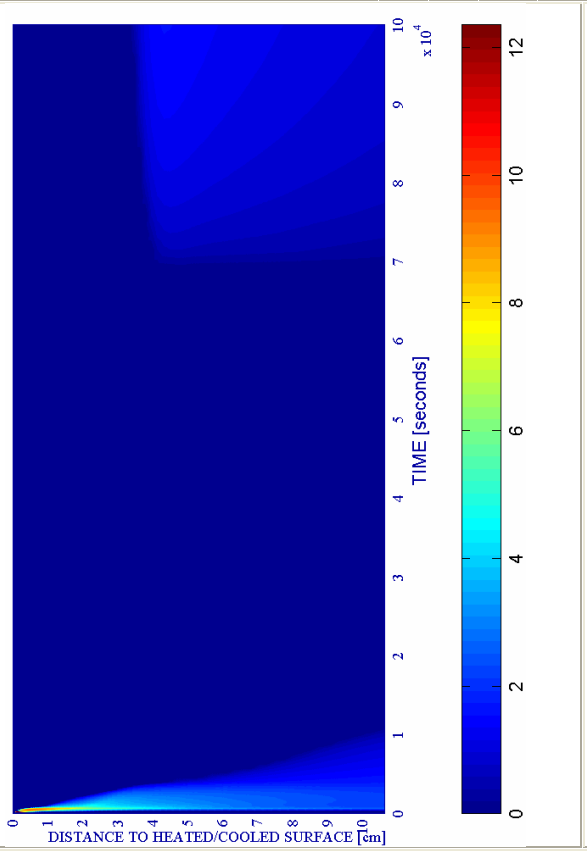

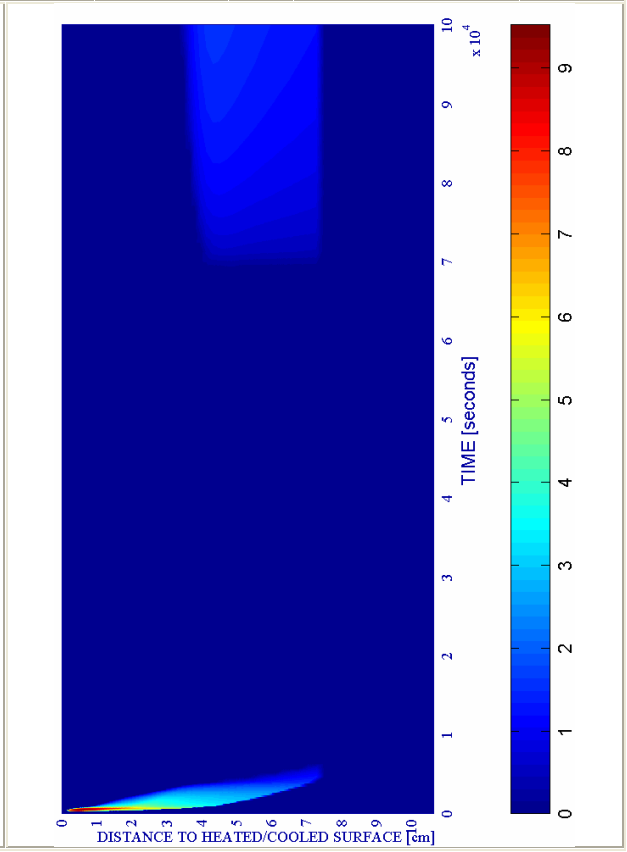

c) Velocity of spalled pieces v [m/s]

Figure 6-57.

d) Velocity [m/s] where d ≥ 0,10

e) Gas pressure $p^g \cdot 10^{-5}$ [Pa]

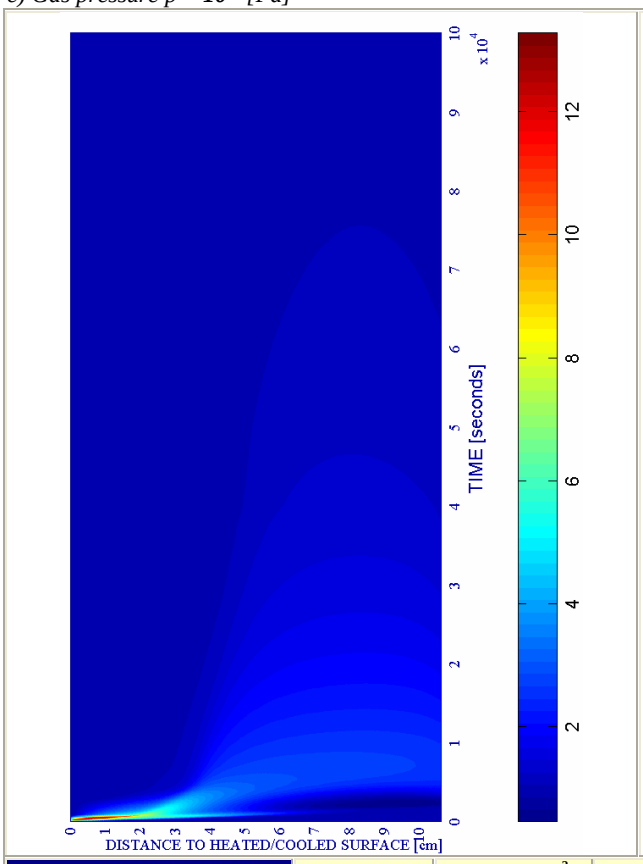

f) Vapour pressure $p^v \cdot 10^{-5}$ [Pa]

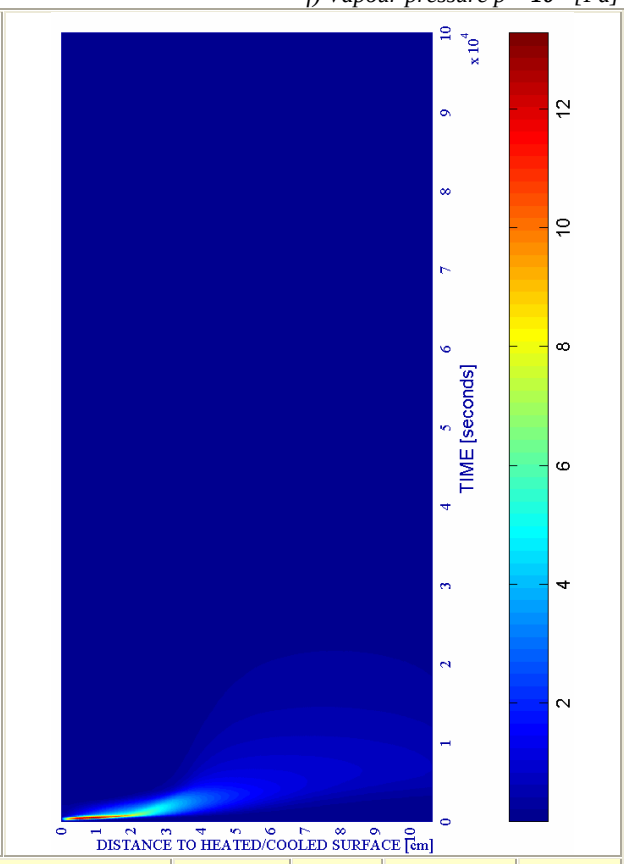

ENVIRONMENTAL - SLOW	PC1 - RH [%]			PC2 - K_0 [m^2]			PC4 - Heating curve			PC5 – Mat.		Cooling length[s]	Start of cooling [s]	End of cooling [s]
#	Combination	40	50	60	10^{-19}	10^{-18}	10^{-17}	PAR1	PAR2	PAR4	C60	C90			
05	TH12K018RH50PAR1C60		X			X		X			X		3.300	600+120	4.020

g) Saturation Degree S [-]

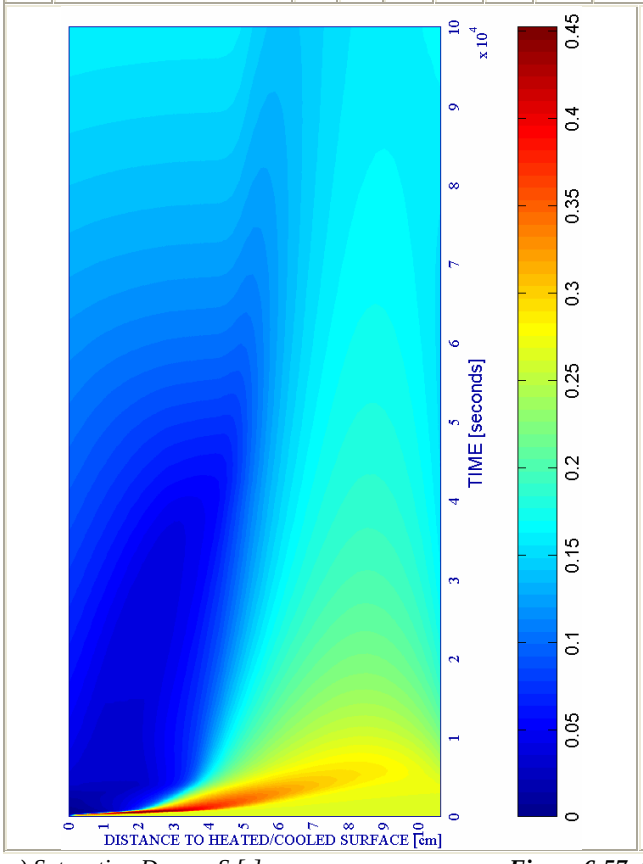

h) Relative Humidity RH [-]

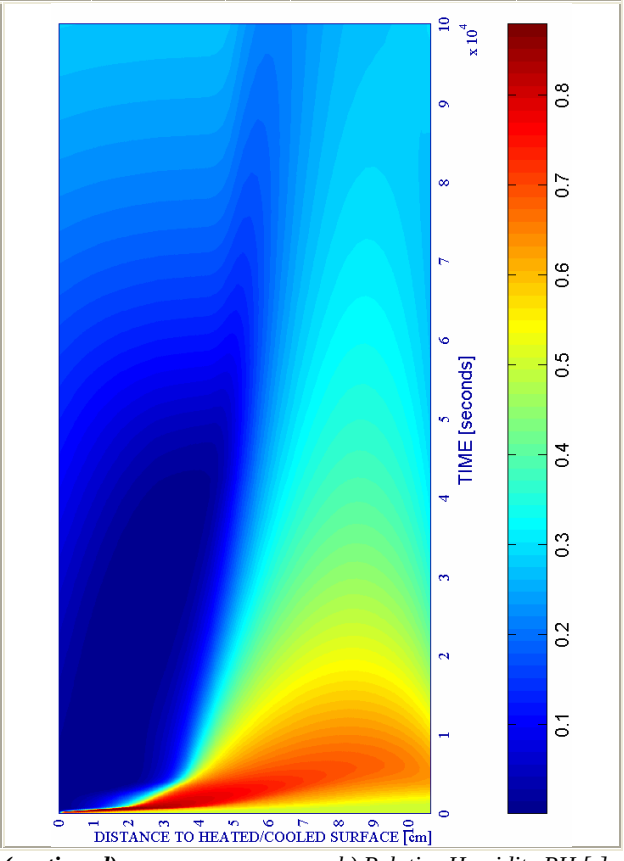

Figure 6-57. (continued)

i) Temperature [K]

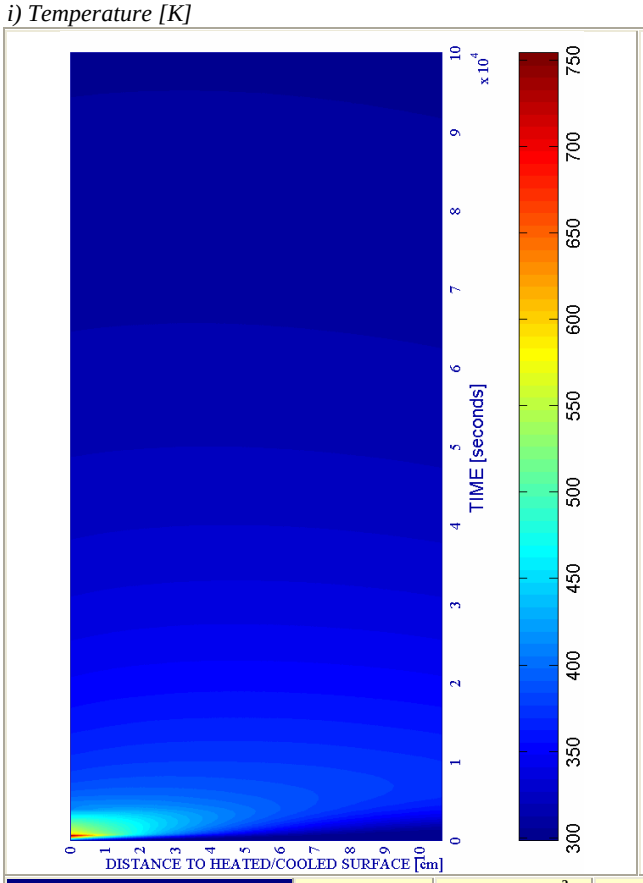

*j) Elastic Energy U · **10**$^{-4}$ [J/m^3]*

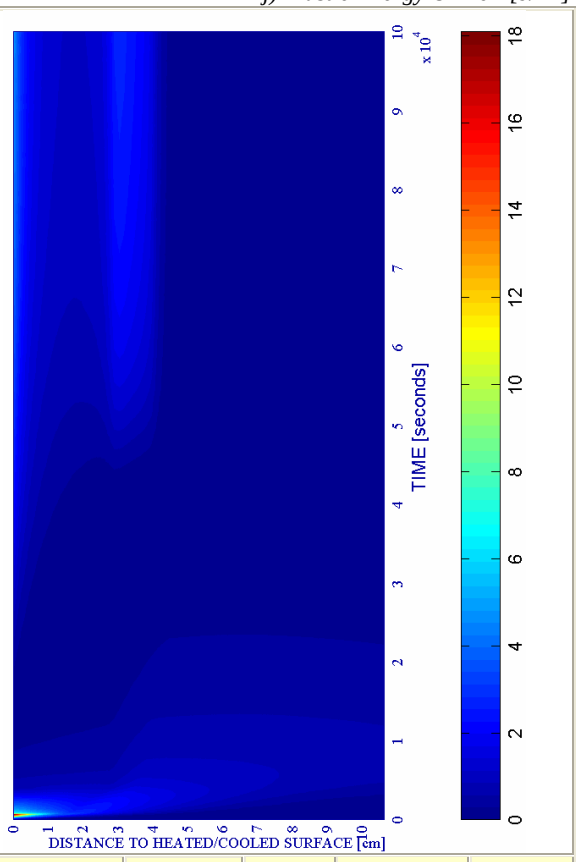

ENVIRONMENTAL - SLOW		PC1 - RH [%]			PC2 - K_0 [m^2]			PC4 - Heating curve			PC5 – Mat.		Cooling length[s]	Start of cooling [s]	End of cooling [s]
#	Combination	40	50	60	10^{-19}	10^{-18}	10^{-17}	PAR1	PAR2	PAR4	C60	C90			
05	TH12K018RH50PAR1C60		X			X		X			X		3.300	600+120	4.020

*k) Stress in longitudinal (xx) direction · **10**$^{-7}$ [Pa]*

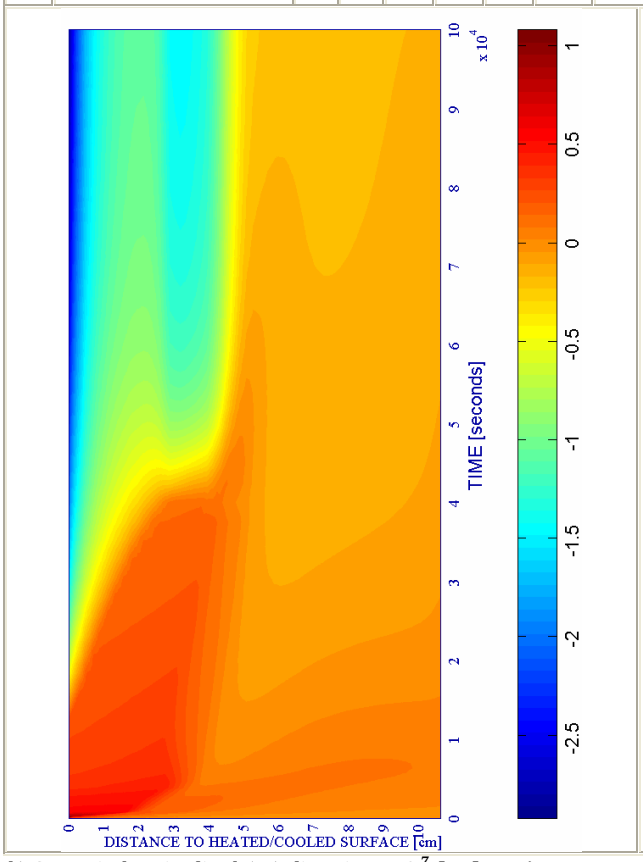

Figure 6-57. (continued)

*l) Stress in transversal (yy) direction · **10**$^{-7}$ [Pa]*

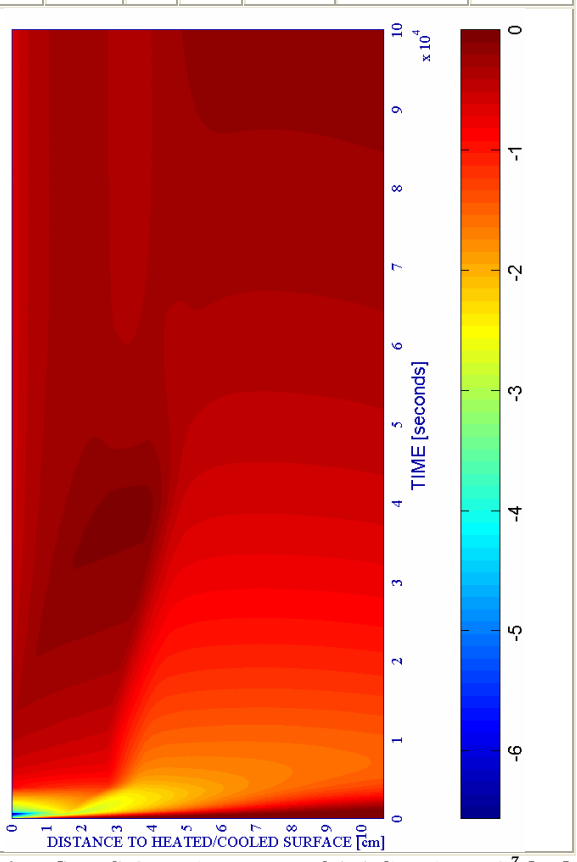

6.5.2.1.2 Environmental Medium Cooling

The phenomenological and mechanistic analysis of this case, where the only difference in the calculation conditions is a higher rate of cooling of the environment, is in general analogous to what was developed in the previous paragraph (corresponding to a 'slow' rate). However, there are some slight differences in the phenomena features that will be briefly exposed next.

First, as it can be observed in figure 6-59, the front separating moist and dry material does not reach a depth as far from the surface as in the case corresponding to a 'slow' cooling, mainly due to the fact that the condensation of the water vapour starts sooner (see figure 6-60).

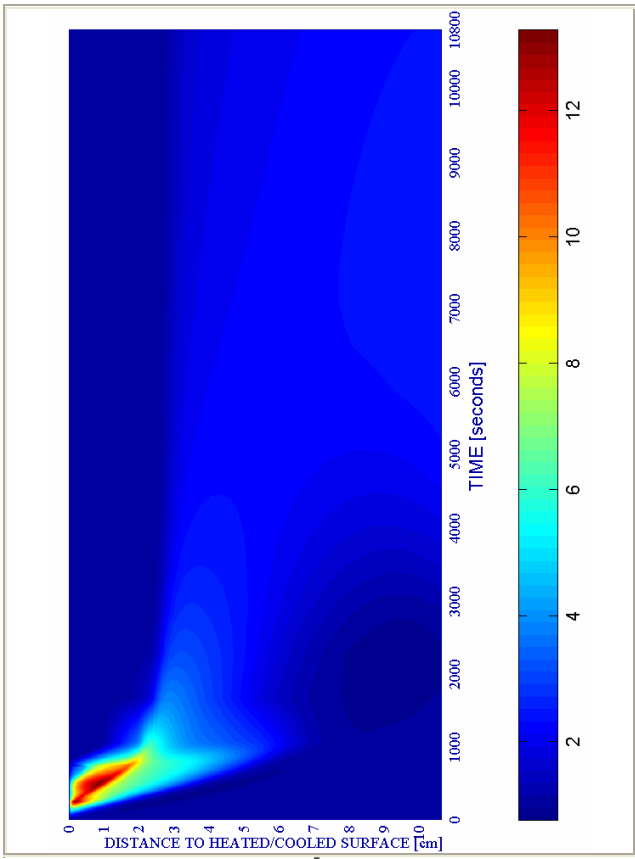

Figure 6-58. *Gas pressure · 10^{-5} [Pa] during the 3 first hours*

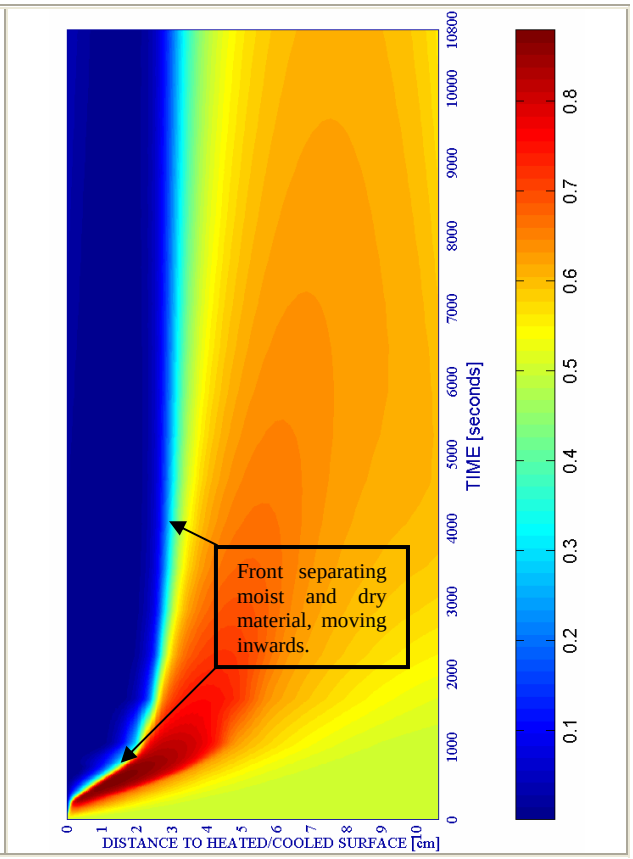

Figure 6-59. *Relative Humidity [-] during the 3 first hours*

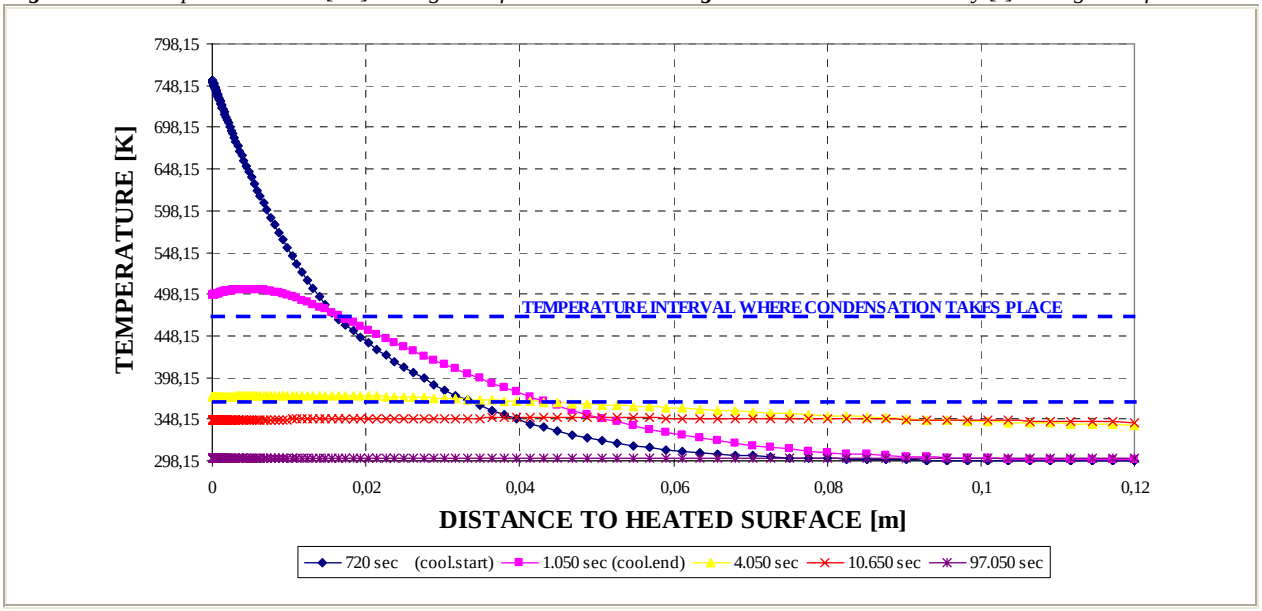

Figure 6-60. *Temperature at several distances from the heated/cooled surface during Environment cooling process.*

The increase of mechanical damage during the Environment cooling process stops also sooner than in the previous case (see figure 6-61), showing a maximum value of 0,8041 at 1,389 centimetres from the surface and at only 17.850 seconds (while in the 'slow' cooling case this increase stopped almost seven hours later).

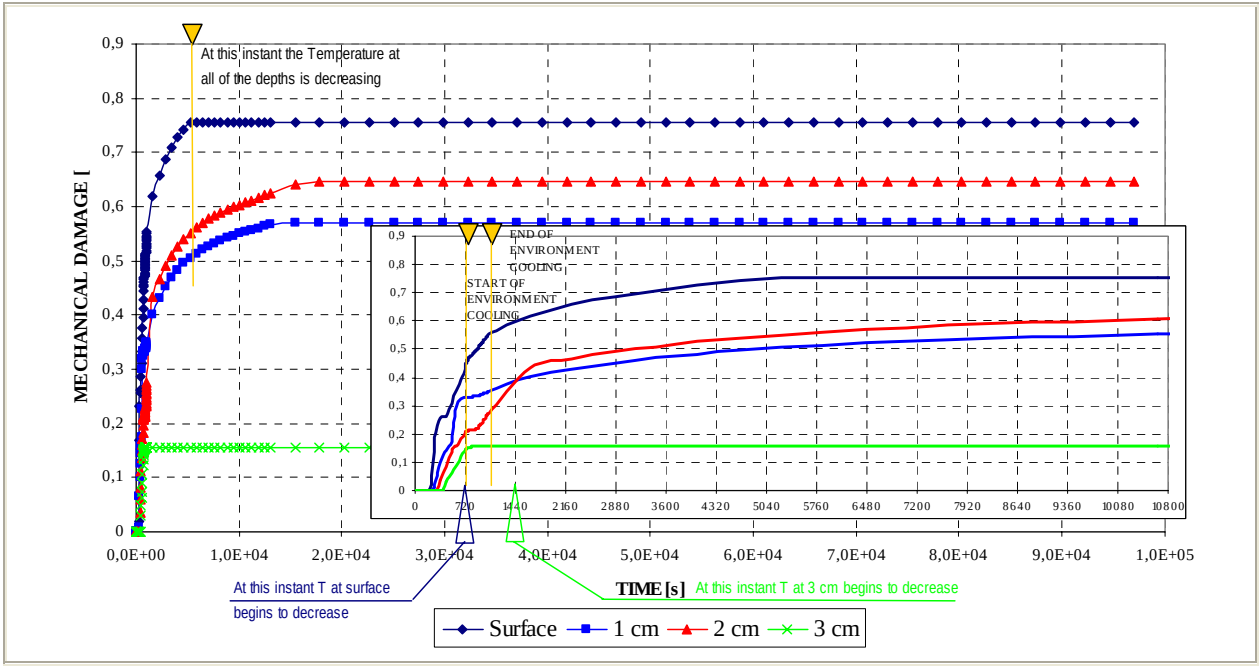

Figure 6-61. *Mechanical damage d [-] evolution, with detail on the environment cooling stage (from 720 s to 1.050 s).*

Besides this, at it can be observed in figure 6-62, the depth affected by high values of mechanical damage (and therefore cracking) has been reduced to the three first centimetres instead of the five centimetres shown in the case with 'slow' cooling (and the final maximum level of cracking is about a 7 per cent lower).

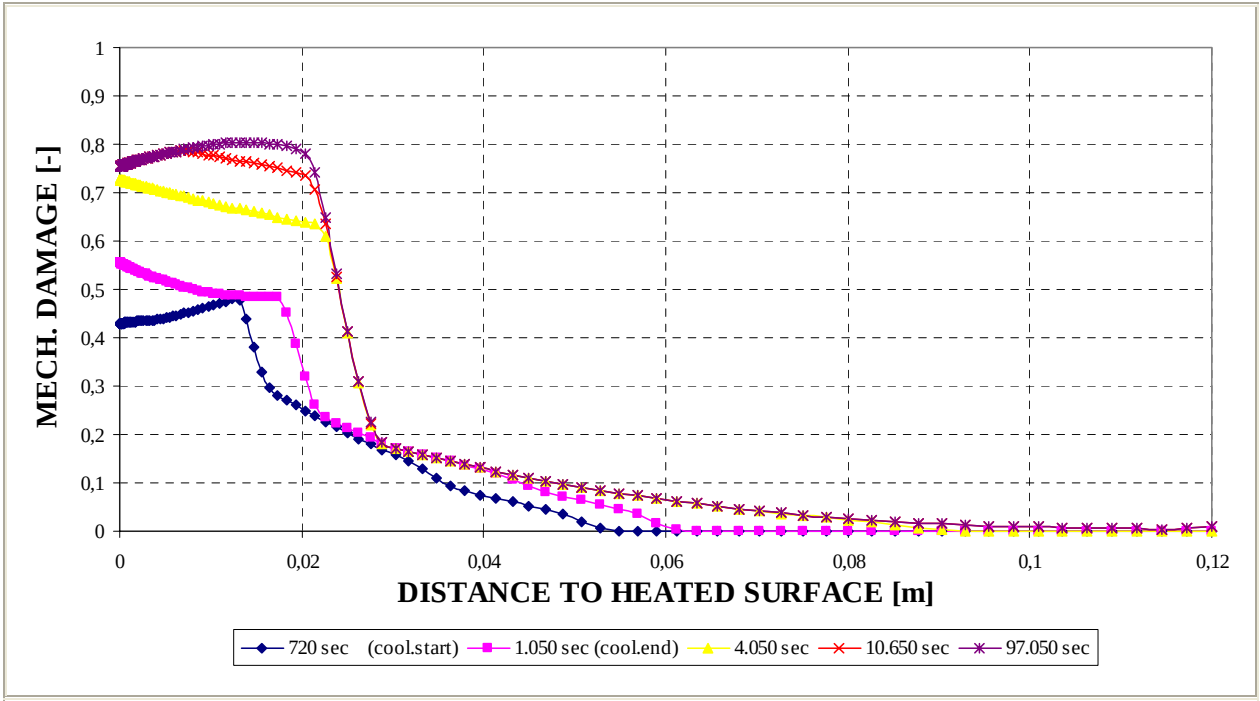

Figure 6-62. *Mechanical damage d [-] at several distances from the heated/cooled surface during Environment cooling process.*

On the contrary than the previous case, here does not appear a second 'bag' of zones where spalling would be again energetically viable at a late stage in the extinguishing process (see figure 6-64 d)). Finally, the compressive stress level arisen at the end of the structural element cooling process is at some locations higher than in the case corresponding to a 'slow' cooling.

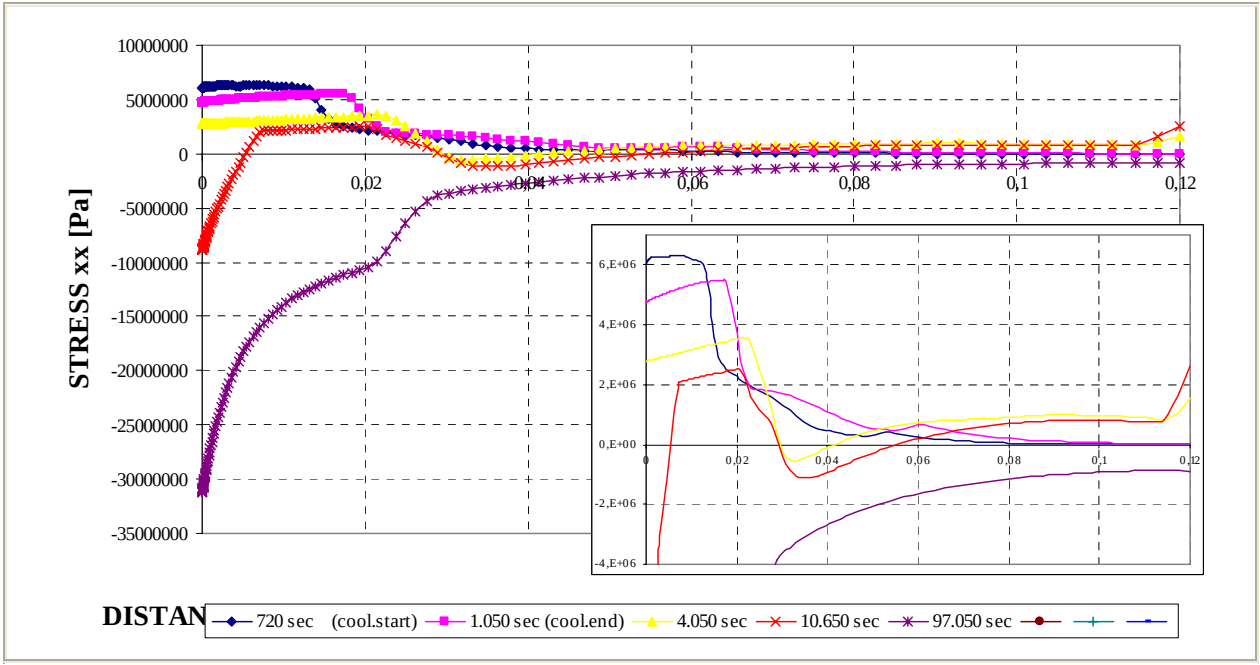

Figure 6-63. *Longitudinal Stress (xx) at several distances from the heated/cooled surface during Environment cooling process.*

Next it is shown a collection of the main results cited in the last subparagraph, as well as a description of each of the stages that compose the heating and cooling processes analyzed herein.

Table 6-37. *Description of the Cooling Process Stages and Collection of the Main Results related to Spalling Index and velocity*

Stage description	Absolute Time Start [s]	Absolute Time End [s]	$IS4_{max}$ [-]	X_{IS4max} [cm]	t_{IS4max} [s]	v_{max} [m/s]	X_{vmax} [cm]	t_{vmax} [s]	v_{max}* [m/s]	X_{vmax*} [cm]	t_{vmax*} [s]
First Heating	0	600+120	0,3688	0,582	600	12,349	0,152	240	9,521	0,245	280
Environment cooling	720	1.050	0,3239	0,860	720	8,479	0,916	720	8,479	0,916	720
Environment constant Temperature up to an absolute time 10.800s	1.050	10.800	0,0156	1,832	1.050	3,351	2,375	1.050	3,351	2,375	1.050
Environment Constant Temperature for t > 10.800s	10.800	97.050	0,0000	---	---	0,000	---	---	0,000	---	---
Maximum for t ≤ 10.800s†	0	10.800	0,3688	0,582	600	12,349	0,152	240	9,521	0,245	280
Absolute Maximum	0	97.050	0,3688	0,582	600	12,349	0,152	240	9,521	0,245	280

Remark †: *These results are included for the Comparative Analysis developed on Paragraph 6.5.3*

Stage description	Absolute Time Start [s]	Absolute Time End [s]	d_{max} [-]	X_{dmax} [cm]	t_{dmax} [s]	T_{max} [K]	X_{Tmax} [cm]	t_{Tmax} [s]	p^g_{max} [MPa]	X_{pgmax} [cm]	t_{pgmax} [s]
First Heating	0	600+120	0,4824	1,312	720	754,18	0,000	720	1,3276	0,860	480
Environment cooling	720	1.050	0,5545	0,000	1.050	754,18	0,000	720	1,0557	1,644	720
Environment constant Temperature up to an absolute time 10.800s	1.050	10.800	0,7889	0,710	10.800	503,79	0,442	1.050	0,5890	2,375	1.050
Environment Constant Temperature for t > 10.800s	10.800	97.050	0,8041	1,389	17.850	348,48	4,683	10.800	0,2308	10,361	11.250
Maximum for t ≤ 10.800s†	0	10.800	0,7889	0,710	10.800	754,18	0,000	720	1,3276	0,860	480
Absolute Maximum	0	97.050	0,8041	1,389	17.850	754,18	0,000	720	1,3276	0,860	480

Table 6-38. *Description of the Cooling Process Stages and Collection of the Main Results related to mechanical damage, Temperature and Gas Pressure*

a) Spalling Index IS4 [-] *b) Mechanical damage d [-]*

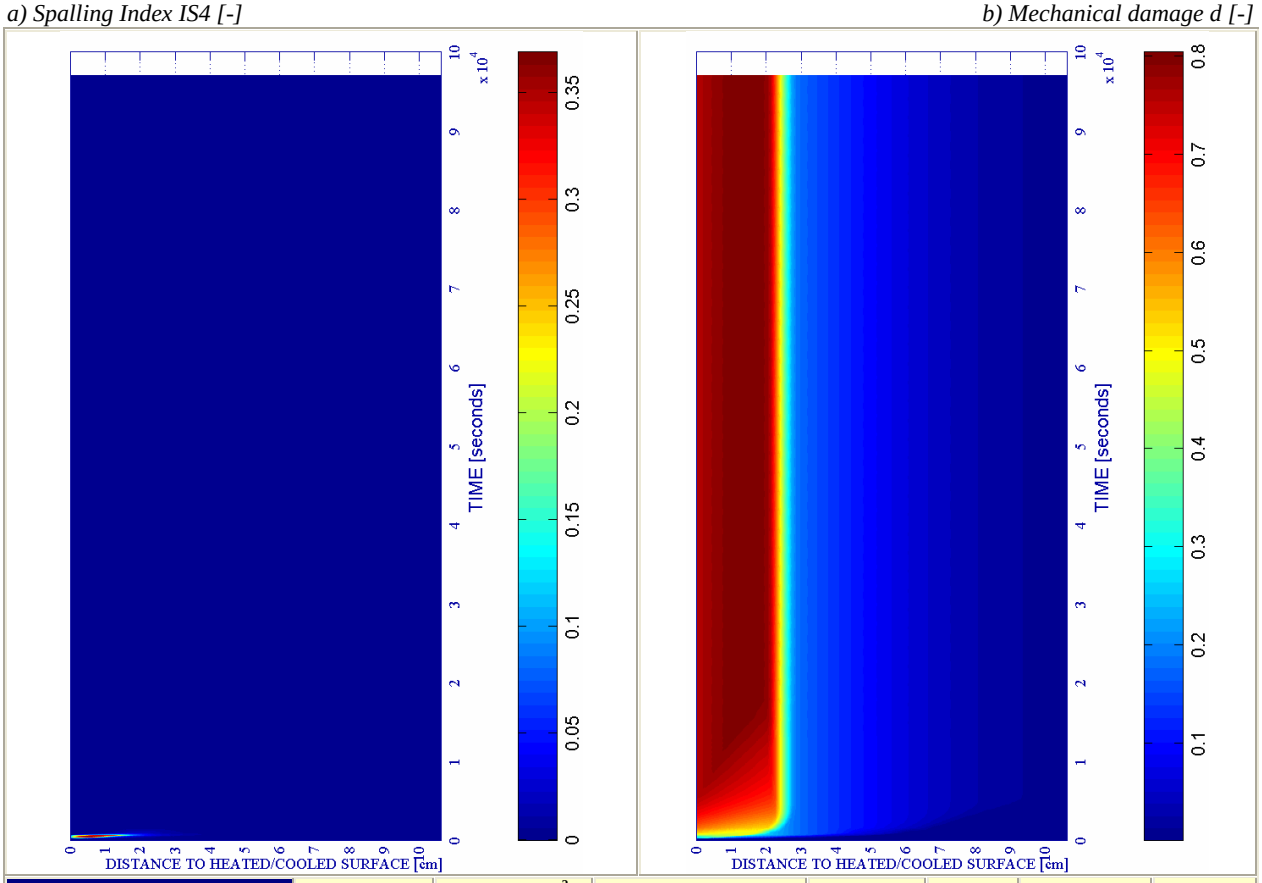

ENVIRONMENTAL - MED.		PC1 - RH [%]			PC2 - K_0 [m^2]			PC4 - Heating curve			PC5 – Mat.		Cooling length[s]	Start of cooling [s]	End of cooling [s]
#	Combination	40	50	60	10^{-19}	10^{-18}	10^{-17}	PAR1	PAR2	PAR4	C60	C90			
05	TH12K018RH50PAR1C60		X			X		X			X		330	600+120	1.050

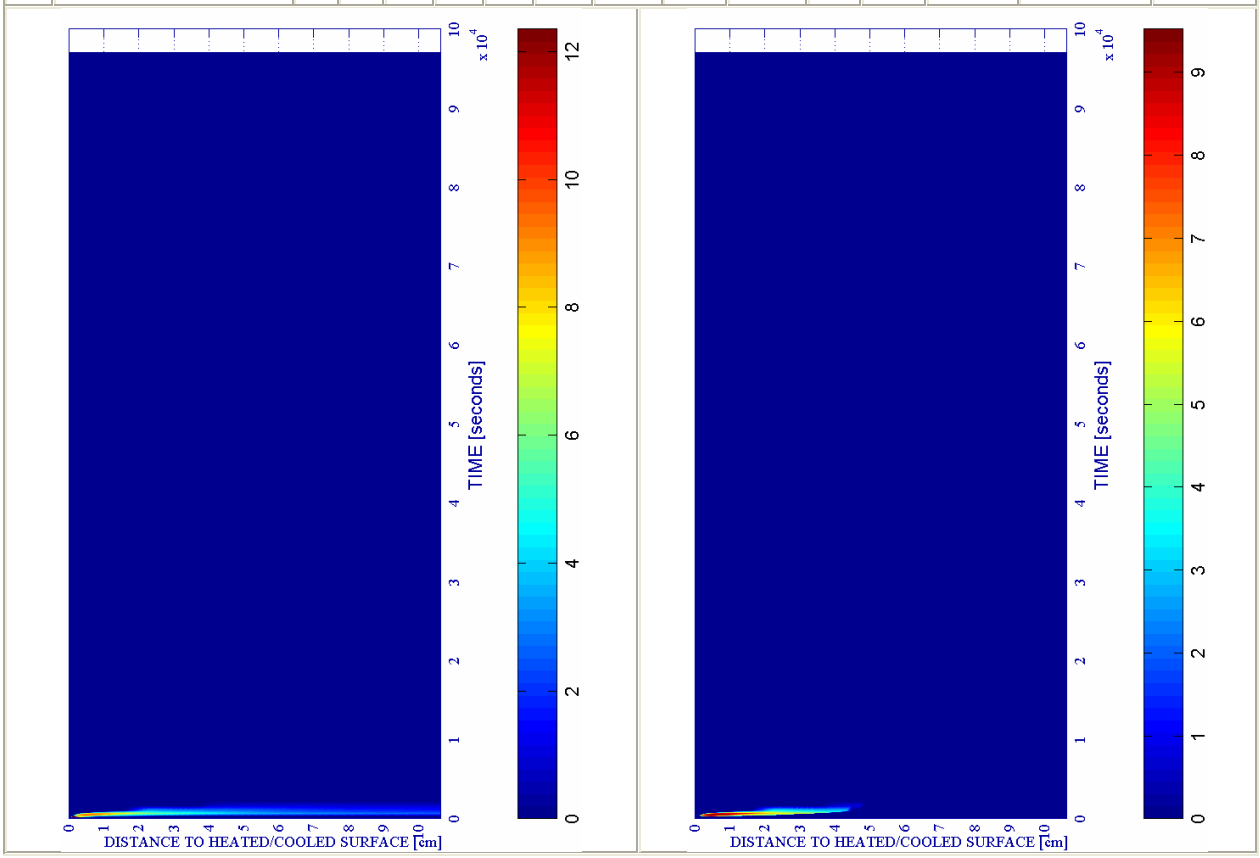

c) Velocity of spalled pieces v [m/s] ***Figure 6-64.*** *d) Velocity [m/s] where d ≥ 0,10*

e) Gas pressure $p^g \cdot 10^{-5}$ [Pa]

f) Vapour pressure $p^v \cdot 10^{-5}$ [Pa]

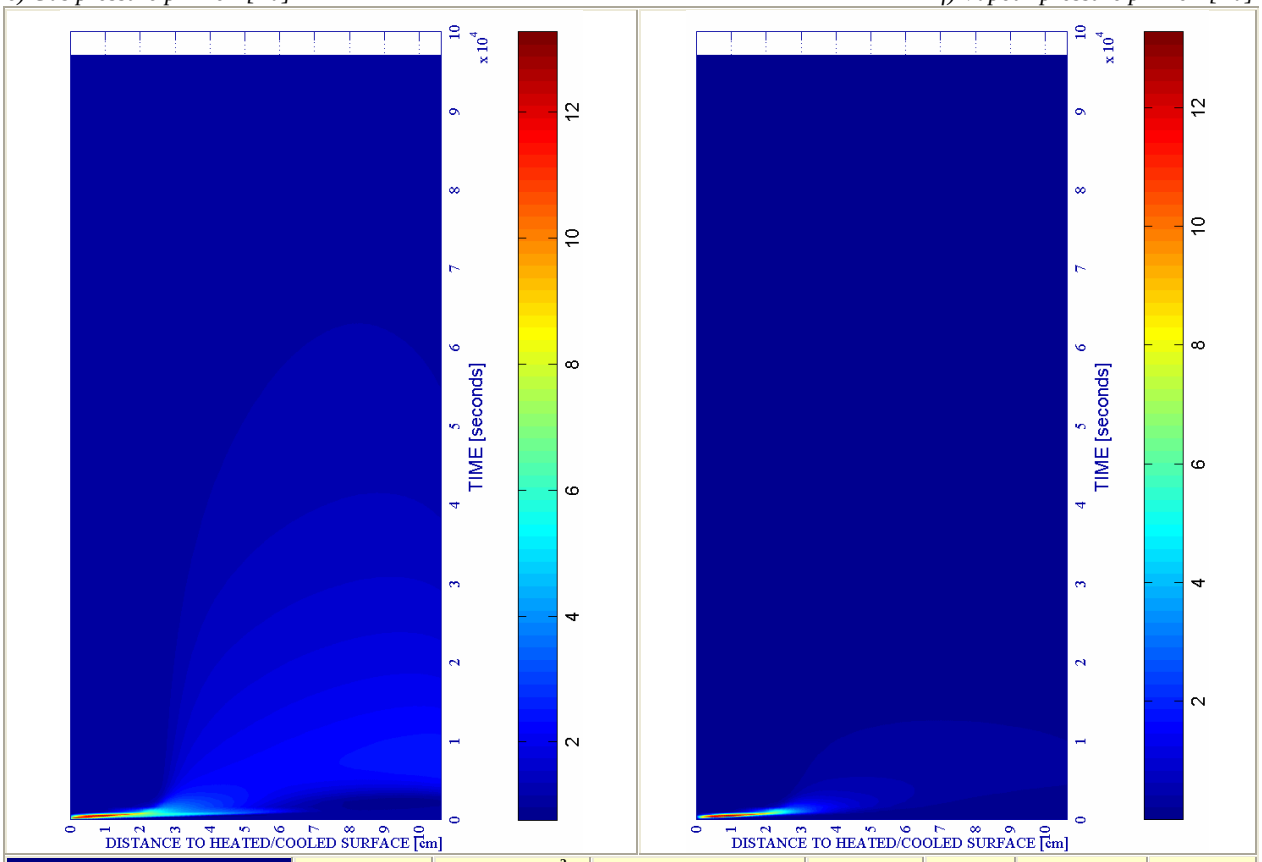

ENVIRONMENTAL - MED.		PC1 - RH [%]			PC2 - K_0 [m^2]			PC4 - Heating curve			PC5 – Mat.		Cooling length[s]	Start of cooling [s]	End of cooling [s]
#	Combination	40	50	60	10^{-19}	10^{-18}	10^{-17}	PAR1	PAR2	PAR4	C60	C90			
05	TH12K018RH50PAR1C60		X			X		X			X		330	600+120	1.050

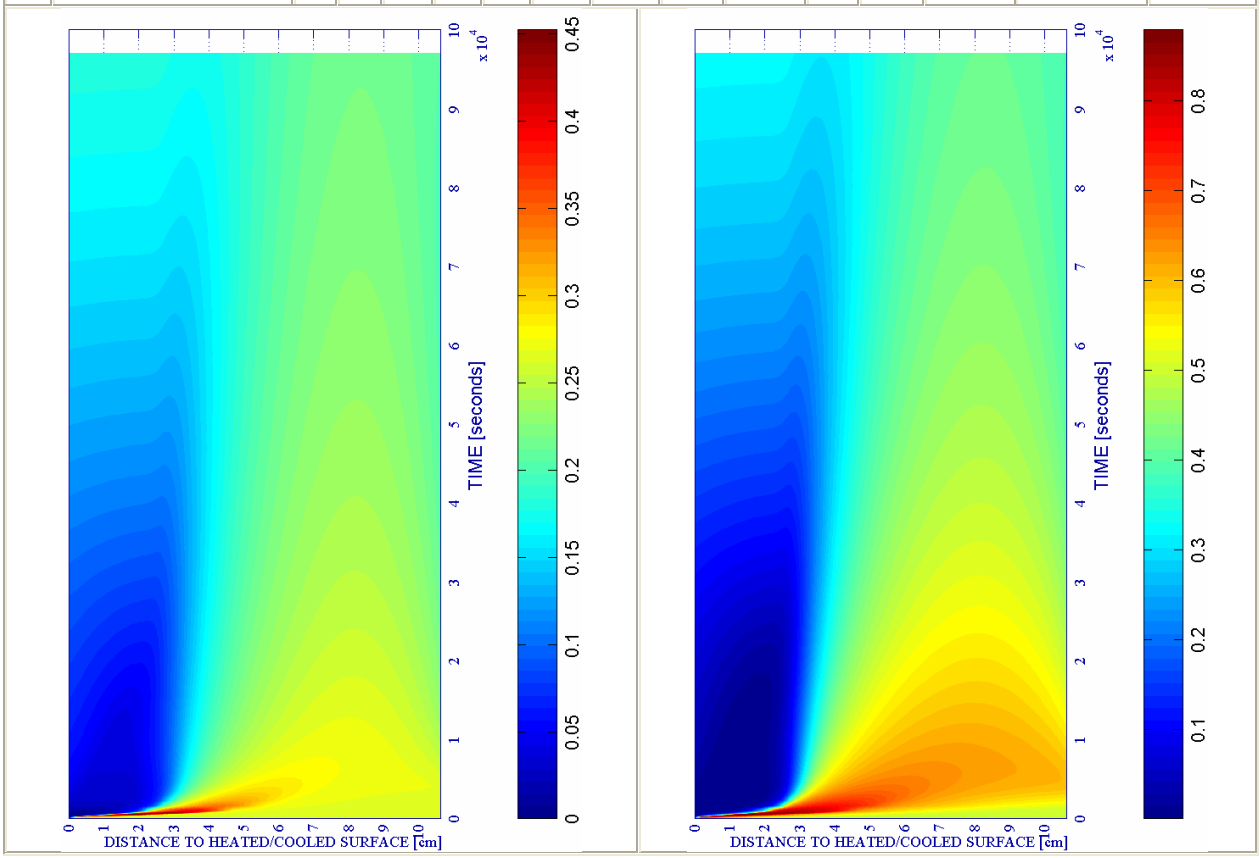

g) Saturation Degree S [-]

Figure 6-64. (continued)

h) Relative Humidity RH [-]

i) Temperature [K]

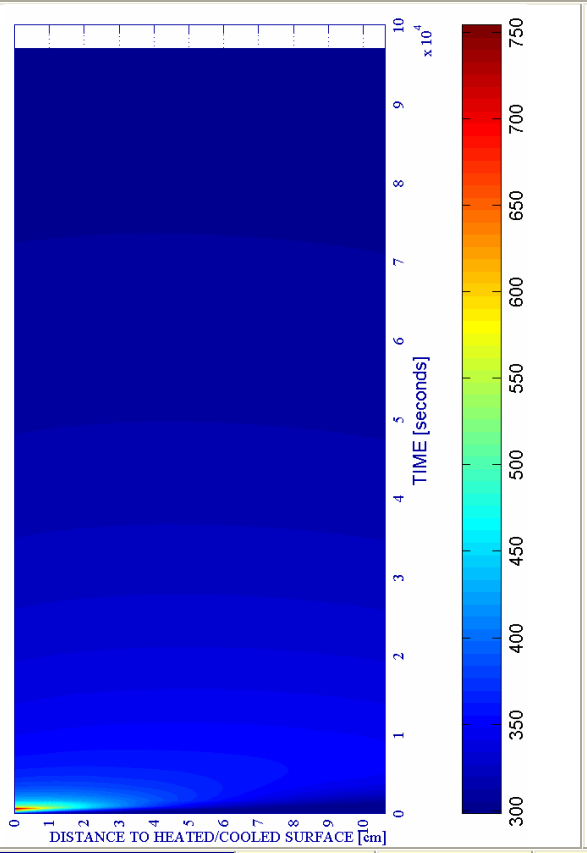

*j) Elastic Energy U · **10**$^{-4}$ [J/m^3]*

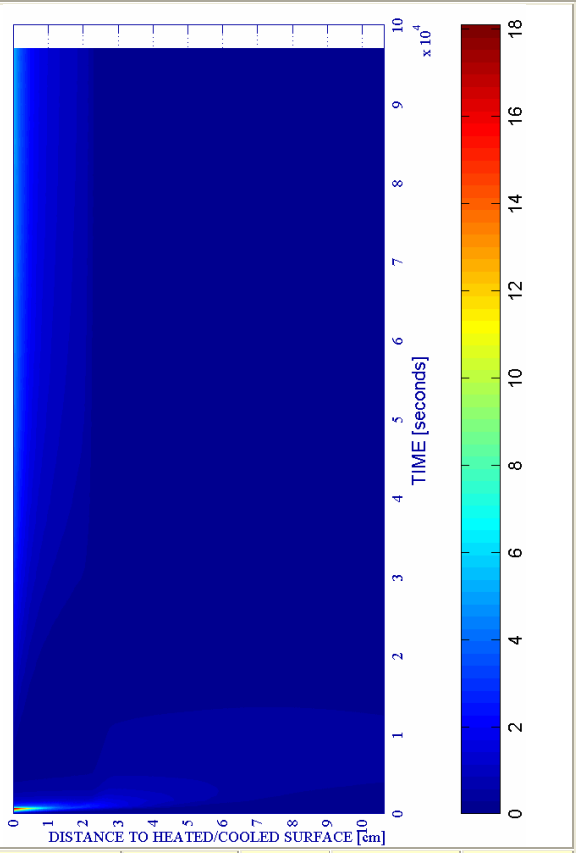

ENVIRONMENTAL - MED.		PC1 - RH [%]			PC2 - K_0 [m^2]			PC4 - Heating curve			PC5 – Mat.		Cooling length[s]	Start of cooling [s]	End of cooling [s]
#	Combination	40	50	60	10^{-19}	10^{-18}	10^{-17}	PAR1	PAR2	PAR4	C60	C90			
05	TH12K018RH50PAR1C60		X			X		X			X		330	600+120	1.050

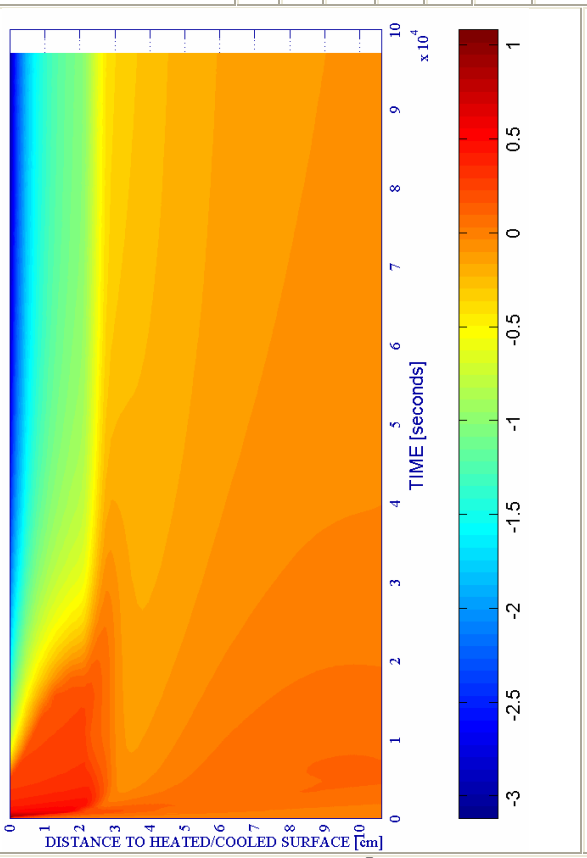

*k) Stress in longitudinal (xx) direction · **10**$^{-7}$ [Pa]*

Figure 6-64. (continued)

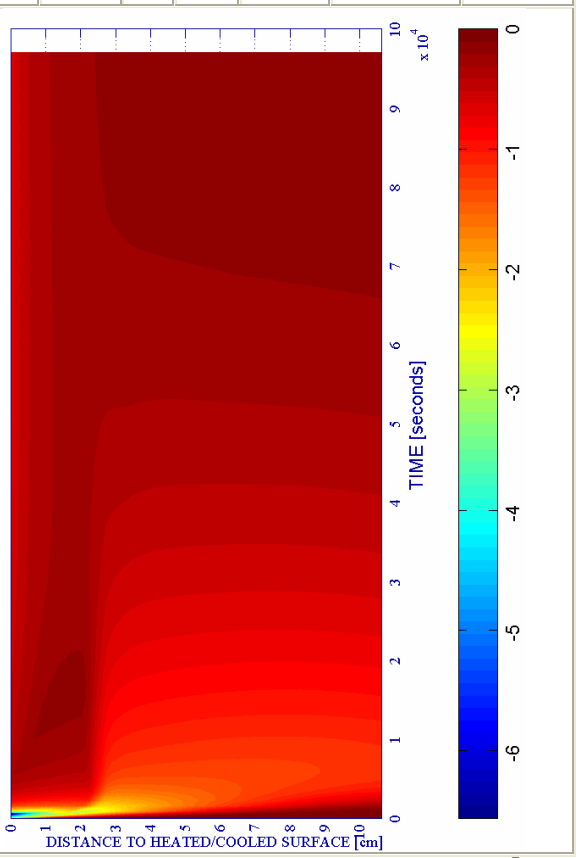

*l) Stress in transversal (yy) direction · **10**$^{-7}$ [Pa]*

6.5.2.1.3 Environmental Fast Cooling

The phenomena analysis to develop from the results obtained for the 'fast' cooling case are, in general, very similar to those obtained from the 'medium' rate of cooling case (described in previous paragraph) but also qualitative and quantitatively different from those corresponding to the 'slow' cooling case (see figure 6-66 a) to l)). For instance, referring to the mechanical damage the only difference is that the depth with high values is even slightly smaller than in the 'medium' cooling case (see figure 6-65). A deeper comparison of these cases will be developed later in paragraph 6.5.3.1.1. Next it is shown a collection of the main results corresponding to this subparagraph.

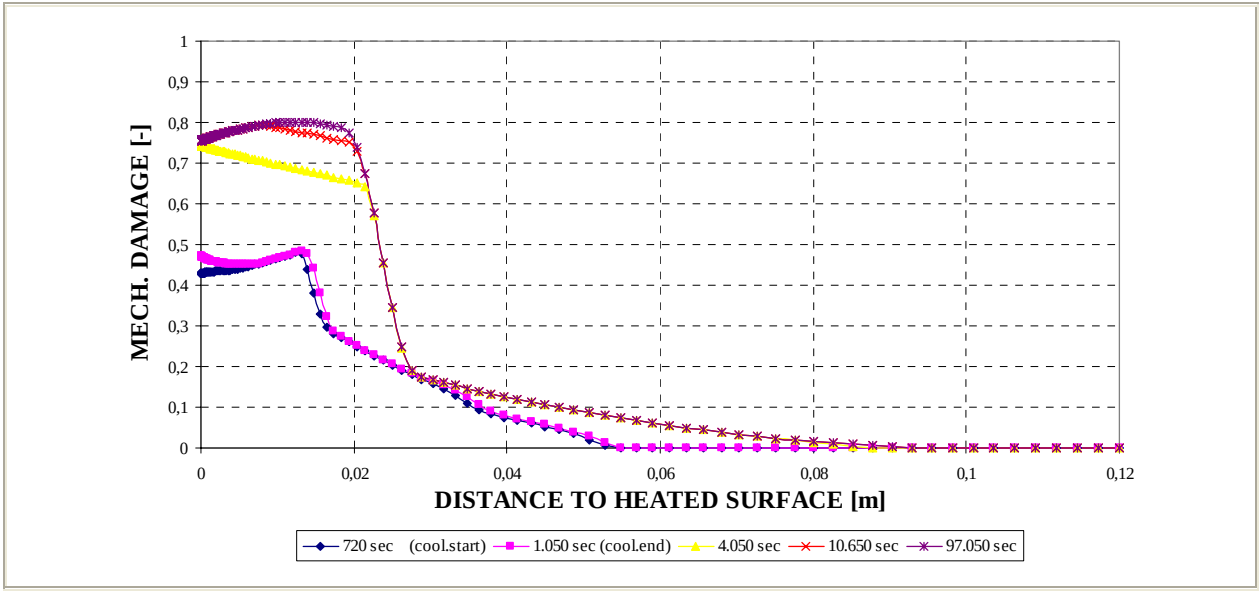

Figure 6-65. *Mechanical damage d [-] at several distances from the heated surface during Environment cooling process.*

Table 6-39. *Description of the Cooling Process Stages and Collection of the Main Results related to Spalling Index and velocity*

Stage description	**Absolute Time Start [s]**	**Absolute Time End [s]**	**$IS4_{max}$ [-]**	**X_{IS4max} [cm]**	**t_{IS4max} [s]**	**v_{max} [m/s]**	**X_{vmax} [cm]**	**t_{vmax} [s]**	**v_{max}* [m/s]**	**X_{vmax*} [cm]**	**t_{vmax*} [s]**
First Heating	0	600+120	0,3688	0,582	600	12,349	0,152	240	9,521	0,245	280
Environment cooling	720	753	0,3239	0,860	720	8,479	0,916	720	8,479	0,916	720
Environment constant Temperature up to an absolute time 10.800s	753	10.800	0,1817	1,238	753	6,881	1,736	753	6,881	1,736	753
Environment Constant Temperature for t > 10.800s	10.800	96.753	0,0000	---	---	0,000	---	---	0,000	---	---
Maximum for t ≤ 10.800s†	0	10.800	0,3688	0,582	600	12,349	0,152	240	9,521	0,245	280
Absolute Maximum	0	96.753	0,3688	0,582	600	12,349	0,152	240	9,521	0,245	280

Remark †: *These results are included for the Comparative Analysis developed on Paragraph 6.5.3*

Stage description	**Absolute Time Start [s]**	**Absolute Time End [s]**	**d_{max} [-]**	**X_{dmax} [cm]**	**t_{dmax} [s]**	**T_{max} [K]**	**X_{Tmax} [cm]**	**t_{Tmax} [s]**	**p^g_{max} [MPa]**	**X_{pgmax} [cm]**	**t_{pgmax} [s]**
First Heating	0	600+120	0,4824	1,312	720	754,18	0,000	720	1,3276	0,860	480
Environment cooling	720	753	0,4851	1,312	738	754,18	0,000	720	1,0557	1,644	720
Environment constant Temperature up to an absolute time 10.800s	753	10.800	0,7925	0,758	10.800	632,00	0,140	753	1,0041	1,736	753
Environment Constant Temperature for t > 10.800s	10.800	96.753	0,8021	1,167	15.153	347,27	4,683	10.800	0,2305	10,361	10.800
Maximum for t ≤ 10.800s†	0	10.800	0,7925	0,758	10.800	754,18	0,000	720	1,3276	0,860	480
Absolute Maximum	0	96.753	0,8021	1,167	15.153	754,18	0,000	720	1,3276	0,860	480

Table 6-40. *Description of the Cooling Process Stages and Collection of the Main Results related to mechanical damage, Temperature and Gas Pressure*

a) Spalling Index IS4 [-] *b) Mechanical damage d [-]*

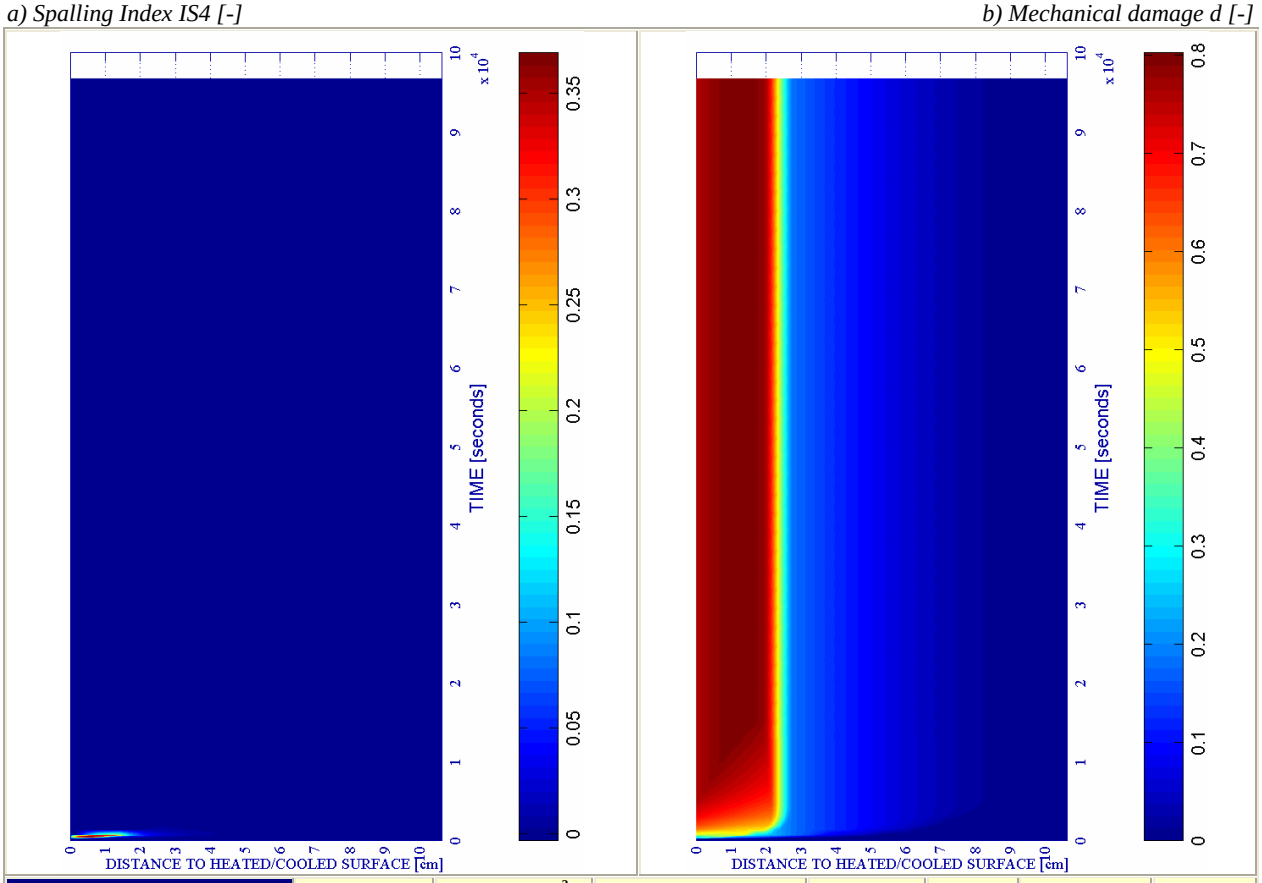

ENVIRONMENTAL - FAST		PC1 - RH [%]			PC2 - K_0 [m^2]			PC4 - Heating curve			PC5 – Mat.		Cooling length[s]	Start of cooling [s]	End of cooling [s]
#	Combination	40	50	60	10^{-19}	10^{-18}	10^{-17}	PAR1	PAR2	PAR4	C60	C90			
05	TH12K018RH50PAR1C60		X			X		X			X		33	600+120	753

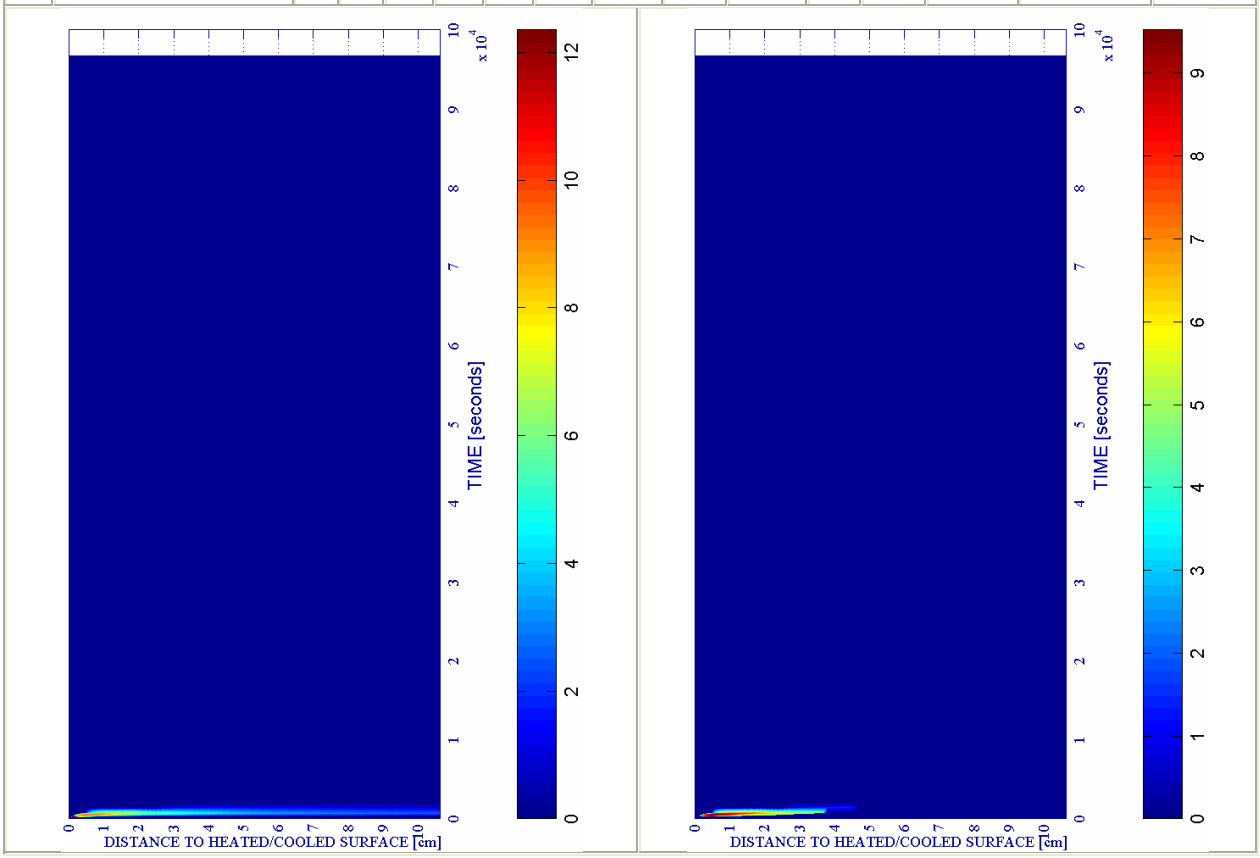

c) Velocity of spalled pieces v [m/s] ***Figure 6-66.*** *d) Velocity [m/s] where d ≥ 0,10*

e) Gas pressure $p^g \cdot 10^{-5}$ [Pa]

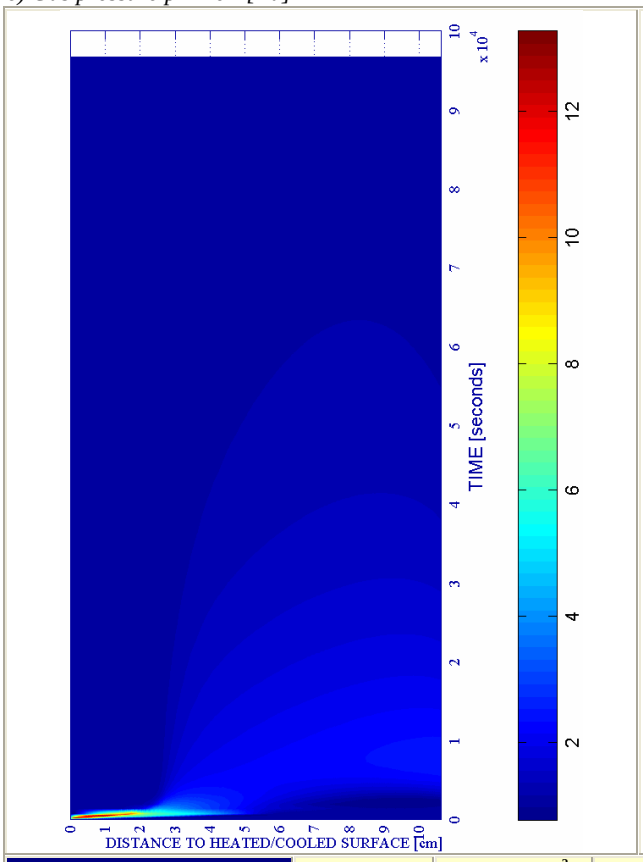

f) Vapour pressure $p^v \cdot 10^{-5}$ [Pa]

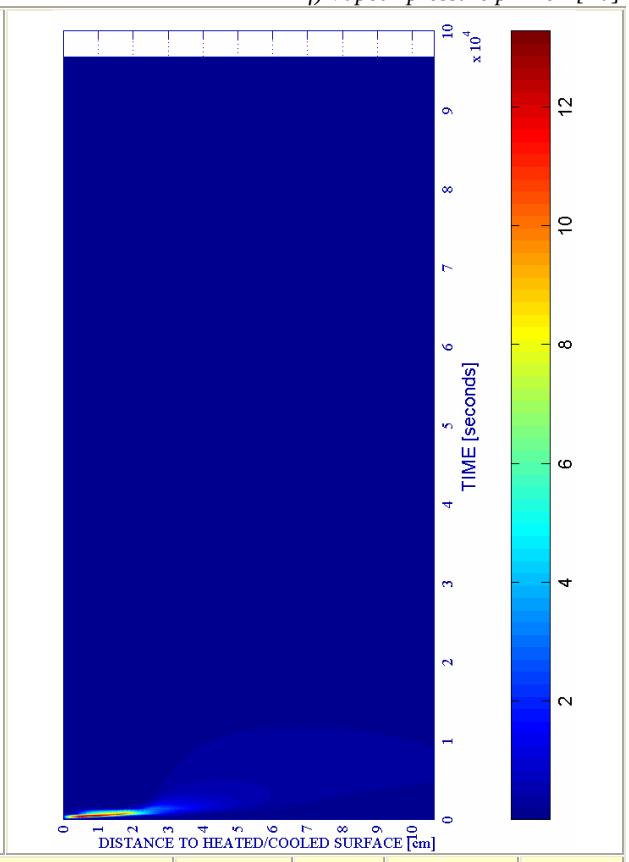

ENVIRONMENTAL - FAST	PC1 - RH [%]			PC2 - K_0 [m^2]			PC4 - Heating curve			PC5 – Mat.		Cooling length[s]	Start of cooling [s]	End of cooling [s]
#	Combination	40	50	60	10^{-19}	10^{-18}	10^{-17}	PAR1	PAR2	PAR4	C60	C90			
05	TH12K018RH50PAR1C60		X			X		X			X		33	600+120	753

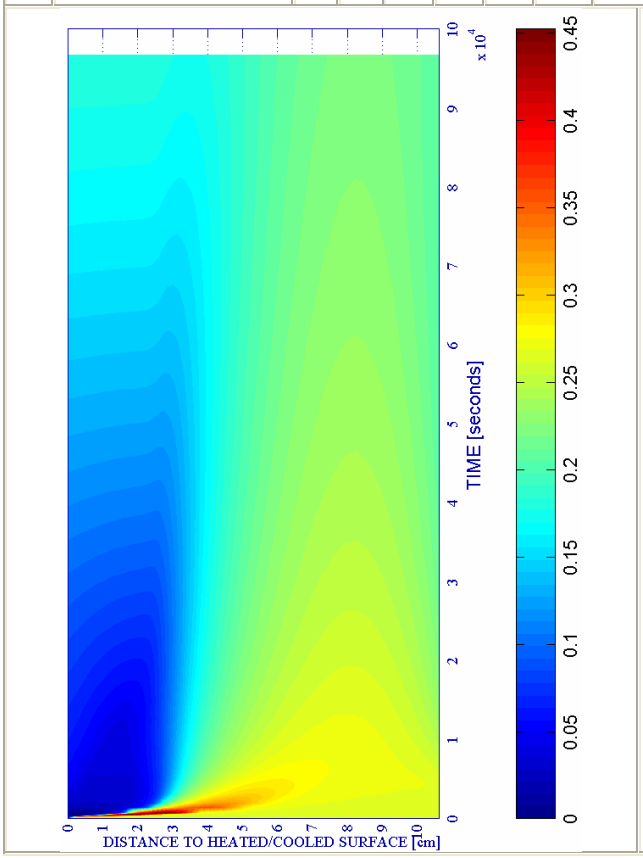

g) Saturation Degree S [-]

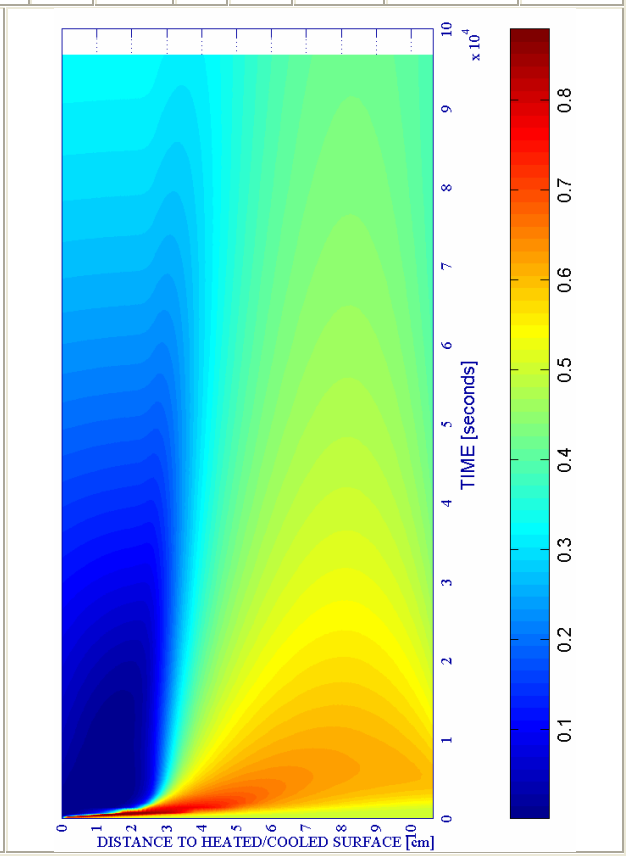

h) Relative Humidity RH [-]

Figure 6-66. (continued)

i) Temperature [K]

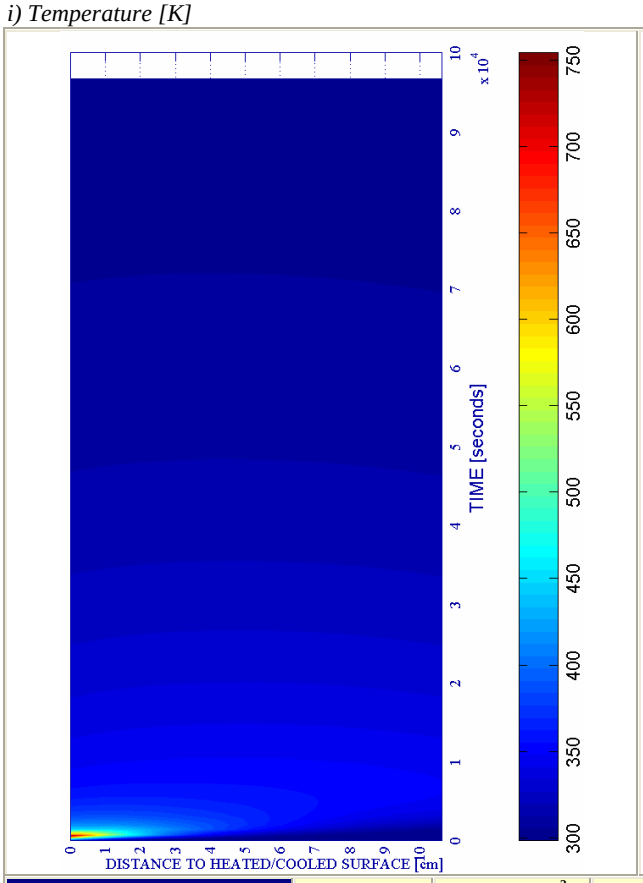

*j) Elastic Energy U · **10**$^{-4}$ [J/m^3]*

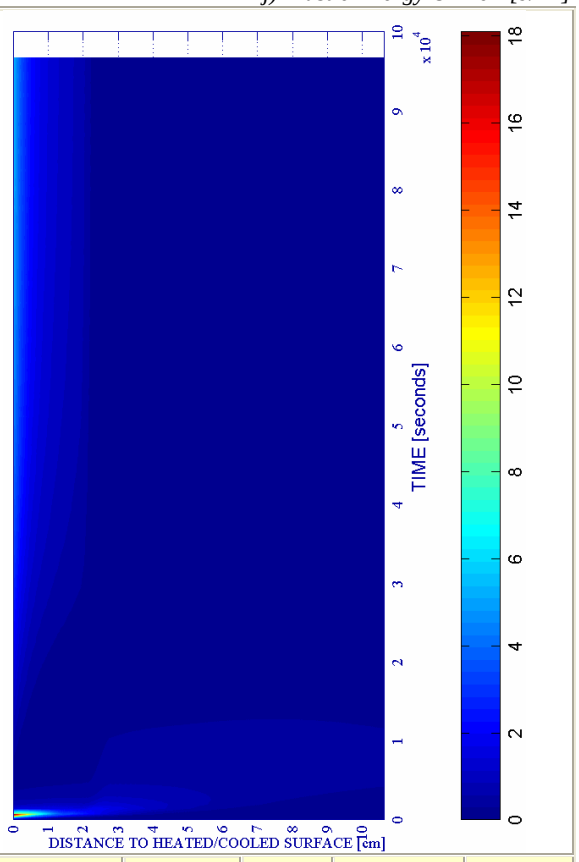

ENVIRONMENTAL - FAST	PC1 - RH [%]			PC2 - K_0 [m^2]			PC4 - Heating curve			PC5 – Mat.		Cooling length[s]	Start of cooling [s]	End of cooling [s]
#	Combination	40	50	60	10^{-19}	10^{-18}	10^{-17}	PAR1	PAR2	PAR4	C60	C90			
05	TH12K018RH50PAR1C60		X			X		X			X		33	600+120	753

*k) Stress in longitudinal (xx) direction · **10**$^{-7}$ [Pa]*

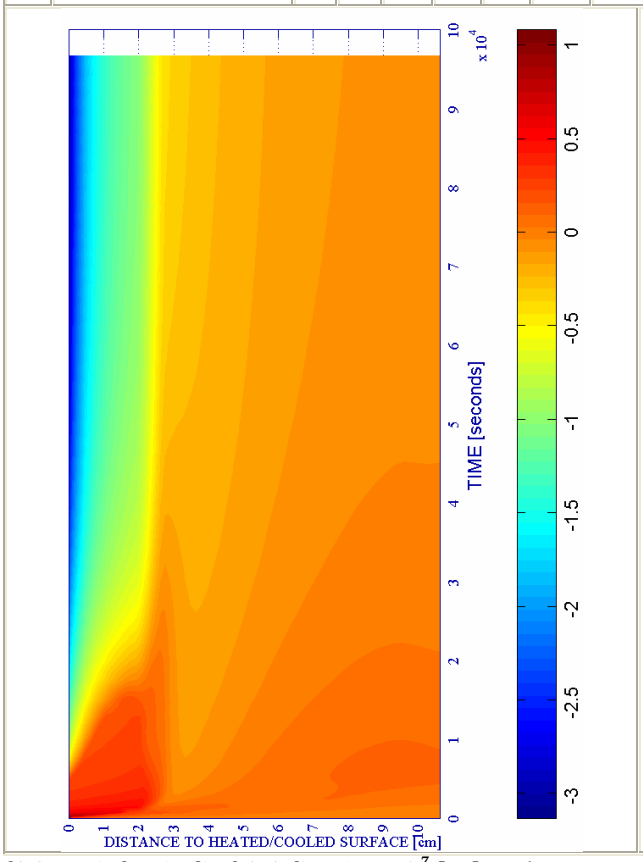

Figure 6-66. (continued)

*l) Stress in transversal (yy) direction · **10**$^{-7}$ [Pa]*

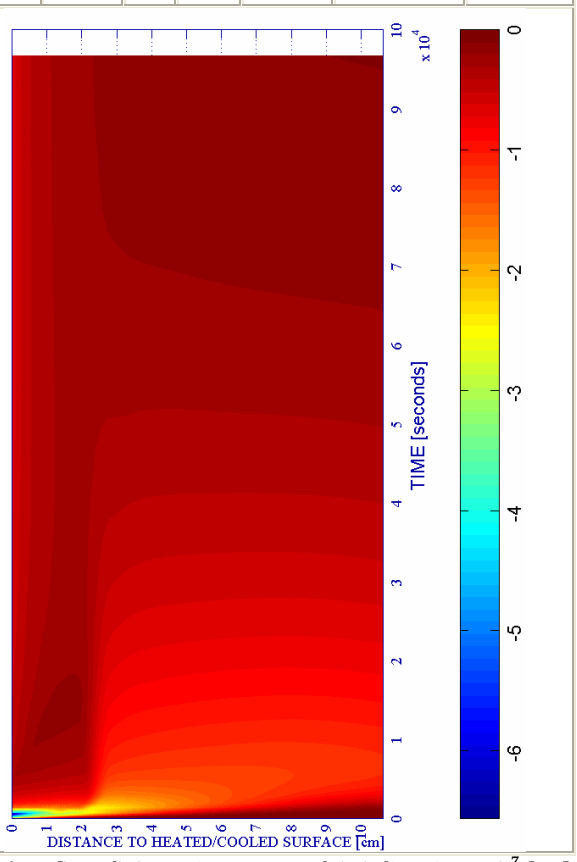

6.5.2.1.4 Surface Cooling followed by a Heating phase

6.5.2.1.4.1 Phenomenological and Mechanistic analysis of the Surface Cooling Stage

In the case analyzed herein, the phenomena occurred during the first heating stage (up to 720 seconds) are exactly those explained in previous paragraphs. However, at 720 seconds starts a cooling process of the surface of the structural element featured by a cooling rate (see figure 6-71) much higher than that observed during the Environment cooling. Indeed if, for instance, in the Fast Environment cooling case the temperature in the surface decreased 126,03 K in 33 seconds (the length of the environment cooling process, what means a cooling rate of the surface of 3,82 K/s), in this case in only 40 seconds (just 7 seconds more) the temperature in the surface decreases as much as 407,93 K (more than 10 K per second).

During the Surface Cooling stage, defined by the time range from 720 to 760 seconds, the Total Damage D rises in the layers next to the surface from an initial value of 0,4495 up to a high final value of 0,8359 (see figure 6-70). This means that in only forty seconds of surface cooling, Total Damage close to the surface increases in about a 100 per cent, reaching a quite high level and approaching to an almost complete destruction of the superficial layer (more precisely, of a depth corresponding to the first centimetre). This phenomenon will leave the structural element – and, hence, the steel reinforcing bars – considerably more exposed to the fire effect after the surface cooling has finished, since the first centimetre layer will have spalled-off (see tables 6-41 and 6-42 and figures 6-76 c) and d)).

In the meantime, during this cooling period of forty seconds gas pressure decreases considerably, especially in the first centimetre layer, due in part to the abovementioned cracking and in a smaller part due to condensation of the slightly remaining water vapour (see figures 6-72 and 6-76 e)).

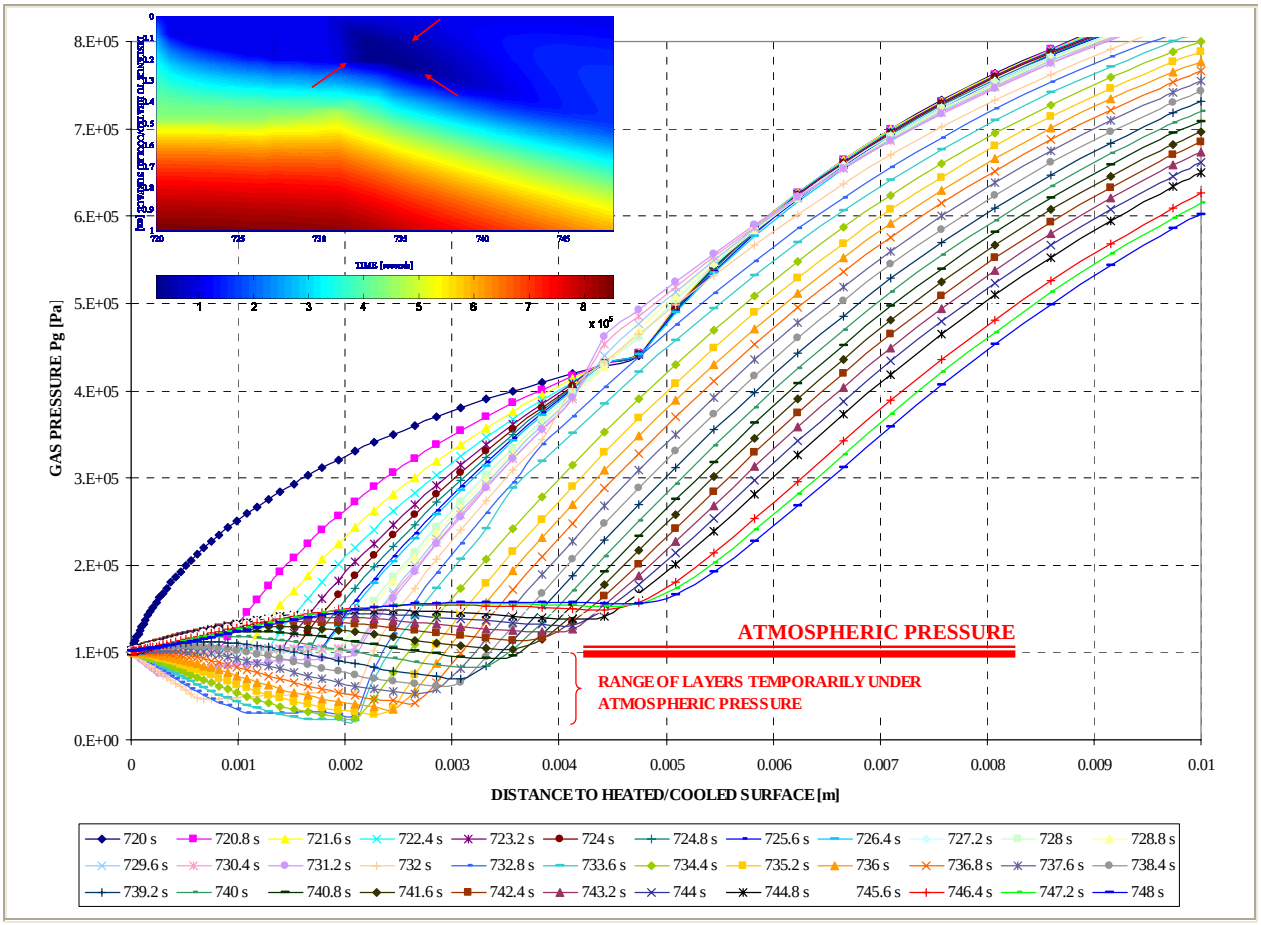

Figure 6-67. *Detail of the Gas Pressure Pg [Pa] evolution during the first 28 seconds of the Surface cooling process.*

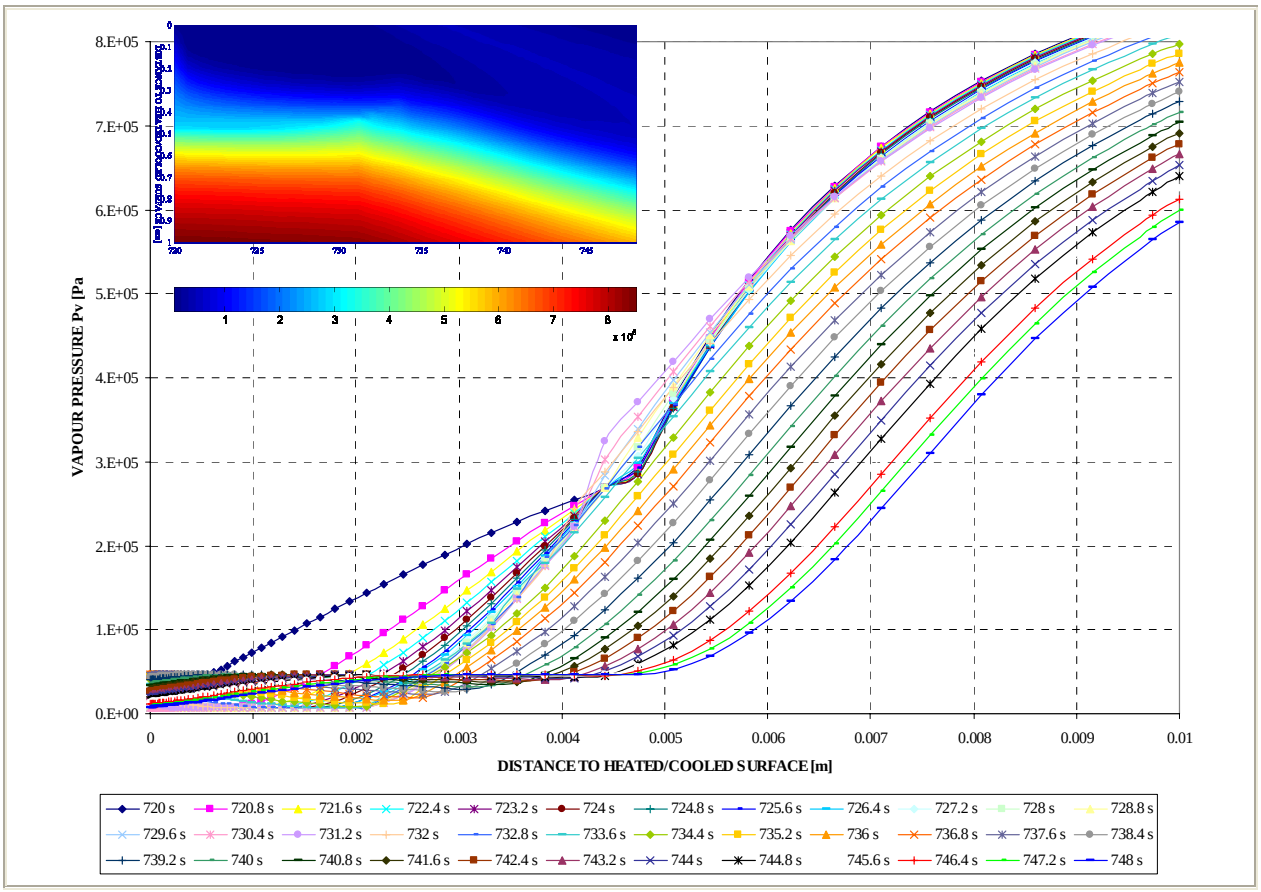

Figure 6-68. *Detail of the Vapour Pressure Pg [Pa] evolution during the first 28 seconds of the Surface cooling process.*

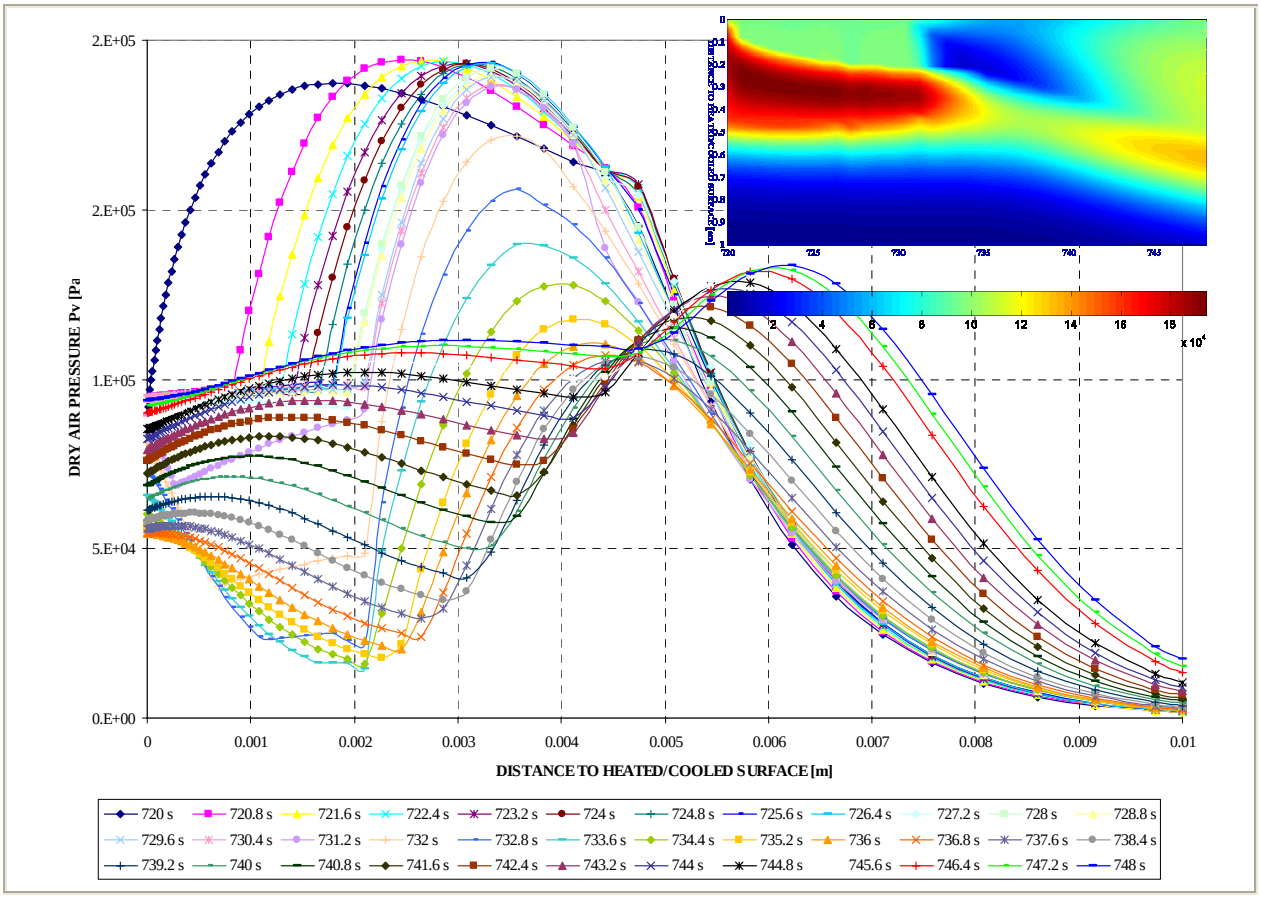

Figure 6-69. *Detail of the Dry Air Pressure Pg [Pa] evolution during the first 28 seconds of the Surface cooling process.*

Specifically, in the first 5 millimetres gas pressure undergoes atmospheric pressure in the time range from 730 to 740 seconds (see figures 6-67 and 6-76 e)), occurring this phenomenon simultaneously with the interval of time where water vapour reaches – in a descending process – the critical temperature of water (647,3 K). In figures 6-68 and 6-69 are observed both components of gas pressure: water vapour pressure and dry air pressure.

Related to the rest of parameters with influence on the Spalling Index I_{s4} values, it is remarkable to observe that although the relative humidity values (see figures 6-73 and 6-76 h)) suffer big oscillations in the first 5 millimetres layer – having increased at the surface, for instance, in a 1000 per cent magnitude from an initial value of 0,0537 per cent up to a final value of 0,5376 per cent at the end of cooling process – this fact does not appear to be relevant in the overall phenomenological and mechanistic analysis since at this zone material keeps almost completely dried.

On the other hand, as it was expectable tensile longitudinal stresses (xx) decrease significantly in the first centimetre during the cooling process (see figures 6-75 and 6-76 k)) from an initial value at the surface of 6,07 MPa down to a final value of 1,93 MPa at the end of cooling process. Nevertheless, as a difference with the case where the Environment was cooled, no compressive longitudinal stresses arise at any depth – although observing the trend in their evolution, it would be expectable that compressive longitudinal stresses would appear if the cooling process would have been longer –. Beyond the first centimetre close to the surface, no significant variations of longitudinal stresses have been noticed. This decrease in material stress state is one of the consequences of the material intensive cracking close to the surface, leading this phenomenon also to the Elastic Strain Energy accumulated within this zone being released during cooling process and, hence, decreasing its values close to zero (see figure 6-74 and 6-76 j)).

Due to all of these trends, Spalling Index I_{s4} values decrease during the whole cooling process (see Table 6-41 and figure 6-76 a)), reducing therefore the thermal spalling risk. Besides this fact, the energy available to promote an explosive spalling is also reduced considerably during cooling from a maximum value of 8,479 m/s at a depth of 0,916 centimetres at the start of cooling process – being the first layer where spalling is energetically viable at this instant at a depth of 0,3 centimetres from surface and the last at a depth of 3,47 centimetres – down to a maximum value of 5,119 m/s at a depth of 1,832 centimetres at the end of cooling – being the first layer where spalling is energetically viable at this instant at a depth of 1,03 centimetres from surface and the last at a depth of 3,63 centimetres – (see figures 6-76 c) and 6-76 d)). However, it is noticeable that since the decrease of elastic energy previously mentioned occurs mainly in the first centimetre close to the surface, thermal spalling keeps being energetically viable in the stated range during the whole cooling process.

6.5.2.1.4.2 Phenomenological and Mechanistic analysis of the Second Heating Stage

In the subsequent heating stage, once the surface cooling process has finished (760 seconds) and up to an absolute time of three hours, Total Damage continues increasing but always keeping the most damaged zones close to the surface due to the already explained phenomena occurred during cooling and on the contrary to what happened during the first cooling stage – where the most damaged zones were from 1 to 2 centimetres away from surface – (see figures 6-70 and 6-76 b)). An analysis of the final state of the structural element (after that three hours) reveals that more than the 60 per cent of the structural element would be completely destroyed (cracked) and the remaining 40 per cent would be with a damaging level above the 80 per cent.

A comparative analysis with the case where no cooling is applied during the first three hours (see paragraph 6.5.3.1.3) will show that these remaining conditions are worse than in the case where no cooling action on the surface is applied.

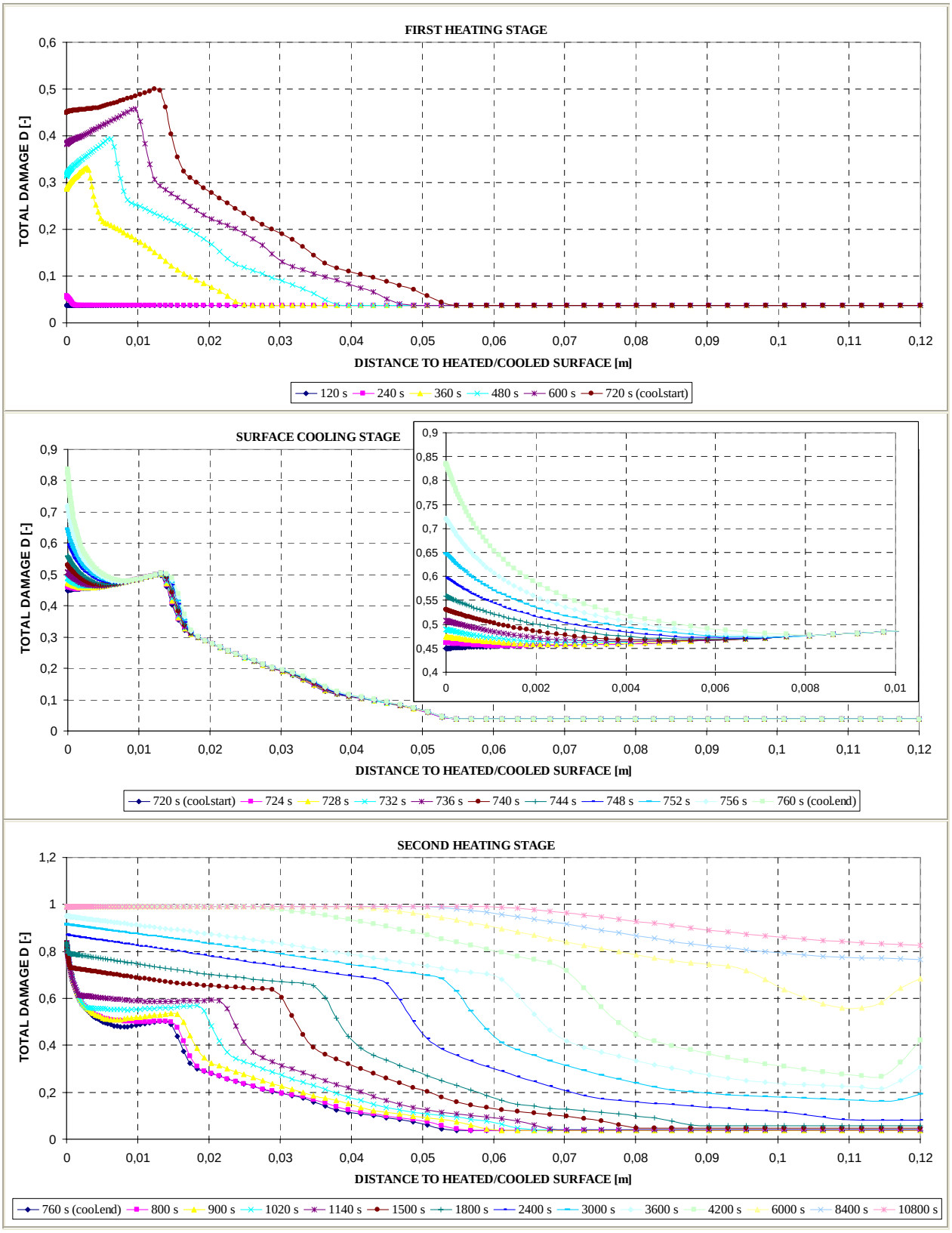

Figure 6-70. *Total damage D [-] at several distances from the heated/cooled surface during each stage of the Surface cooling processes*

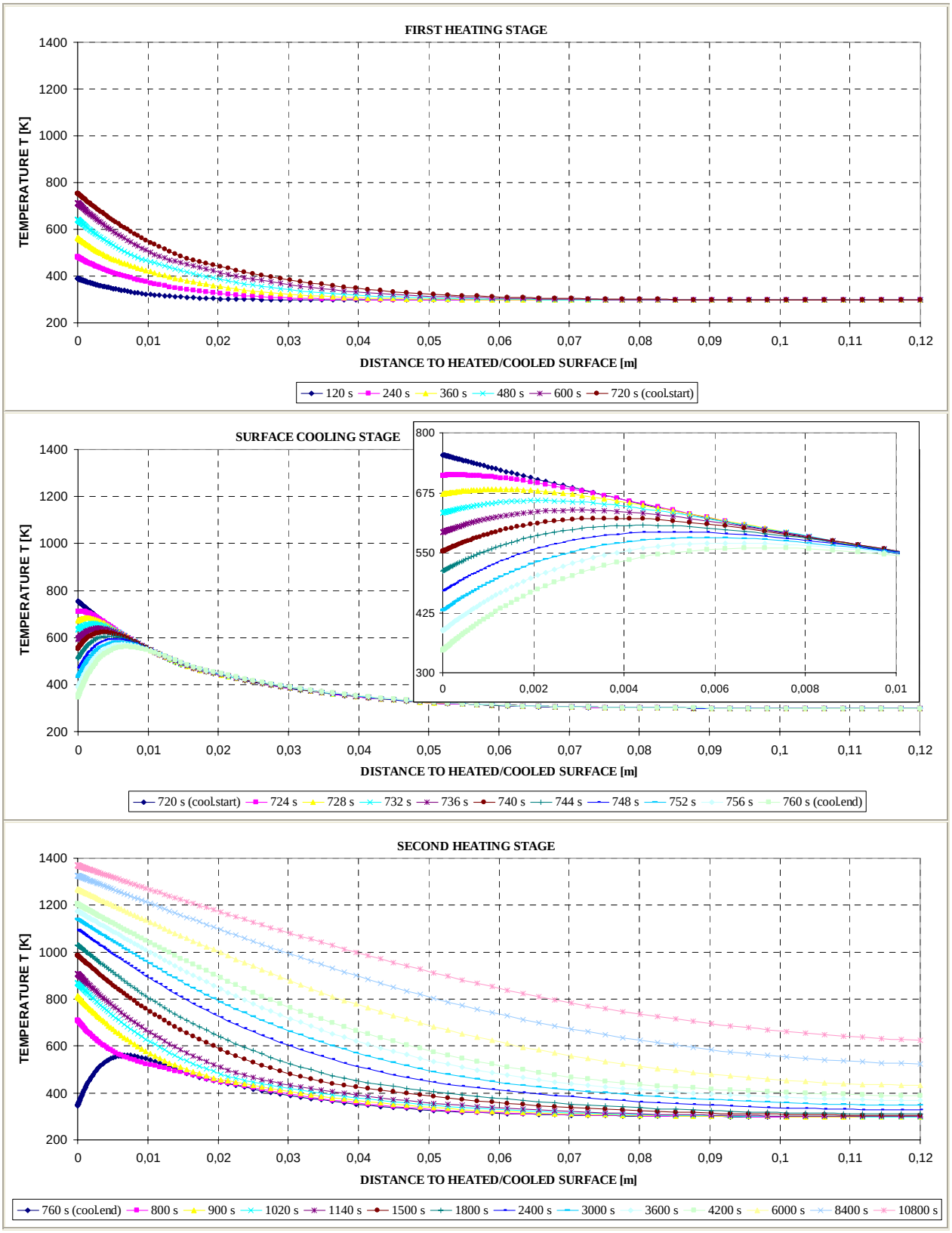

Figure 6-71. *Temperature T [K] at several distances from the heated/cooled surface during each stage of the Surface cooling processes*

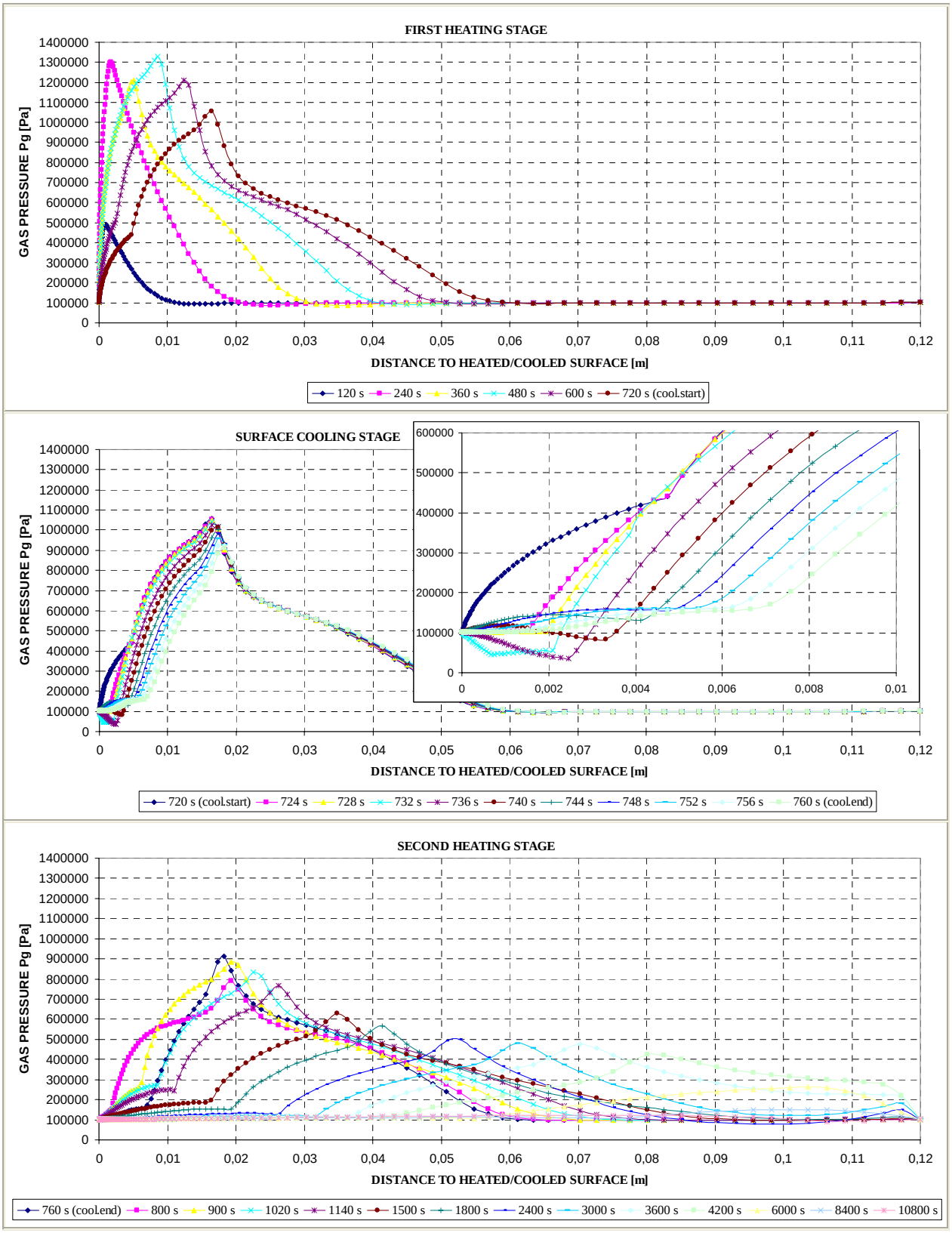

Figure 6-72. *Gas Pressure Pg [Pa] at several distances from the heated/cooled surface during each stage of the Surface cooling processes*

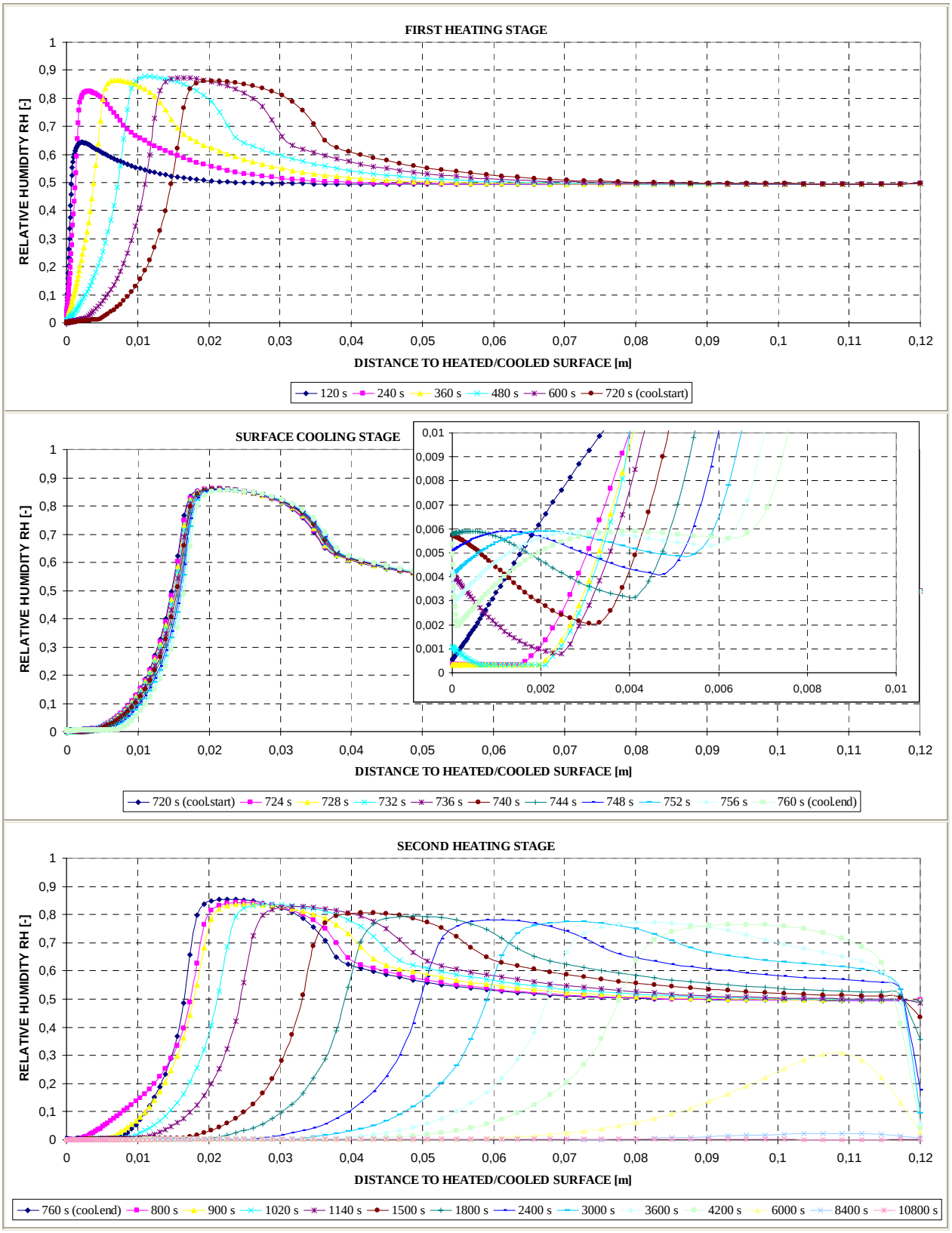

Figure 6-73. *Relative Humidity RH [-] at several distances from the heated/cooled surface during each stage of the Surface cooling processes*

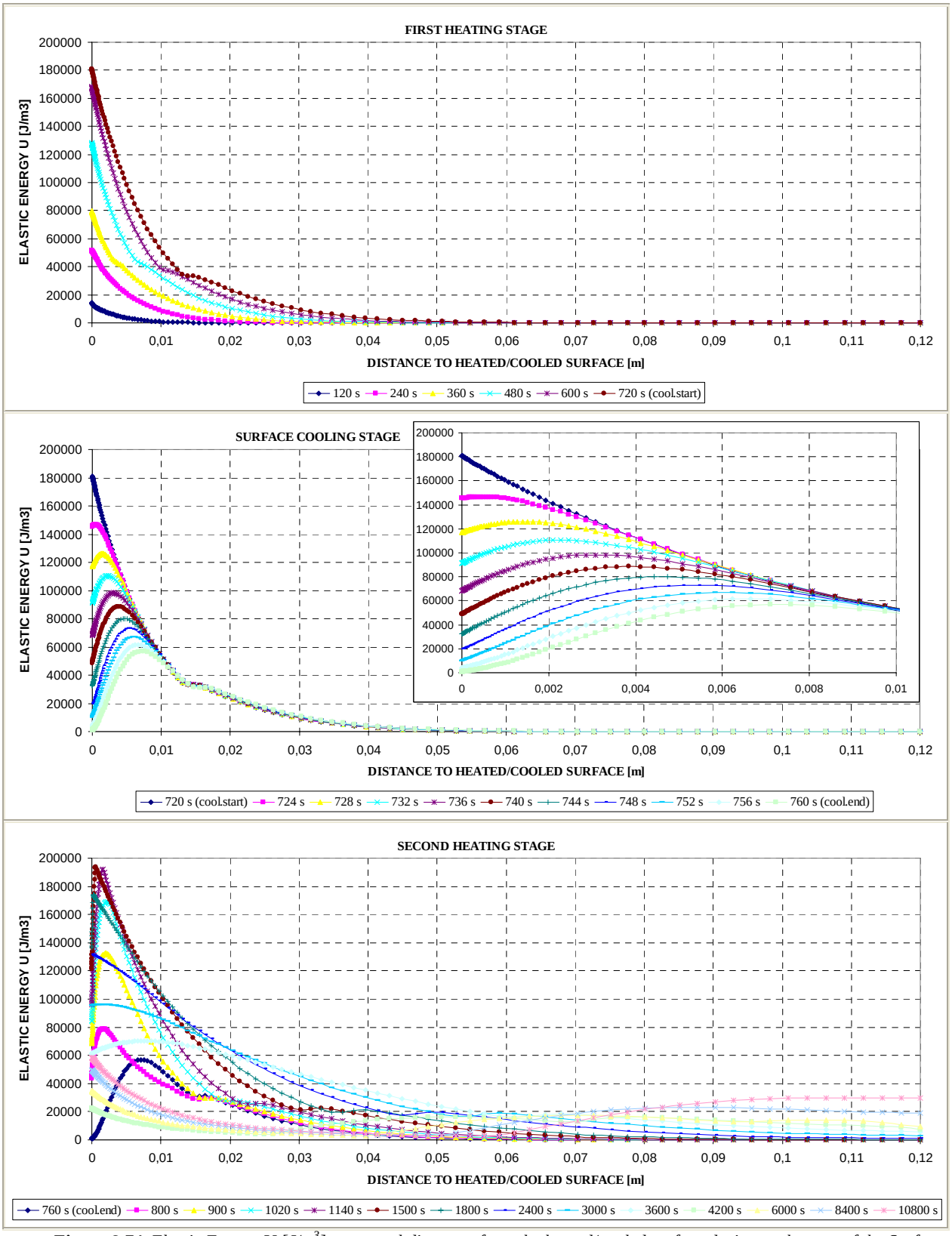

Figure 6-74. *Elastic Energy U [J/m^3] at several distances from the heated/cooled surface during each stage of the Surface cooling processes*

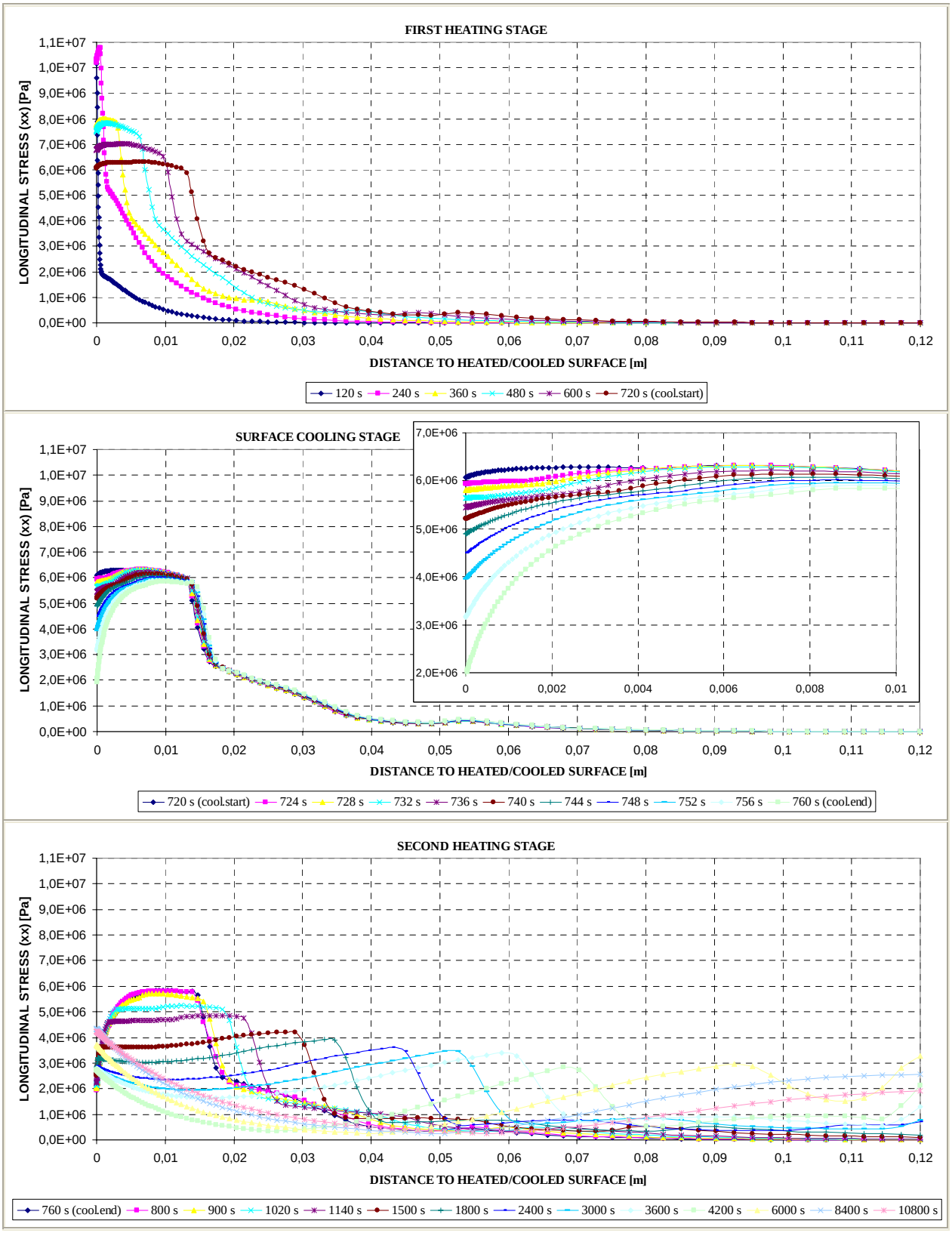

Figure 6-75. *Longitudinal stress (xx) [Pa] at several distances from the heated/cooled surface during each stage of the Surface cooling processes*

As it occurred during the first heating, the maximum value of the gas pressure (significantly lower now than in the first heating despite the temperatures reached are much higher) moves progressively away from the surface up to a distance of 11 centimetres from the heated surface (see figures 6-72 and 6-76 e)) and then softening the gas pressure gradients until a uniform gas pressure value equal to atmospheric pressure is observed at the whole structural element.

Meanwhile, the front separating dry and moist material also moves inwards being progressively less sharp (see figures 6-73 and 6-76 h)) and achieving a relative humidity of about the 80% at a range of a quarter of the depth. At the end of the cooling process both the relative humidity and the saturation degree are null (see figure 6-76 g)), since the structural element has been completely 'boiled' (as it is colloquially said in the trade jargon) due to the extreme temperatures profile (with a maximum temperature of 1.369,20 K and more than the 90 per cent of the structural element above the critical point of water at the end of the second heating stage – 10.800 seconds –).

Tensile longitudinal (xx) stresses tend to decrease next to the surface – where the higher levels of damage are found – while they raise up progressively at the farther zones (see figures 6-75 and 6-76 k)). At the end of the overall three hours process the most longitudinally tensioned zones are those close to the surface. The Elastic Strain Energy accumulated next to the surface increases at the beginning of the heating stage and later – as damage increases – it decreases again to really low values.

6.5.2.1.4.3 Collection of the Main Results of this Case for each Stage of the Cooling Process

Next it is shown a collection of the main results cited in the last subparagraph, as well as a description of each of the stages that compose the heating and cooling processes analyzed herein. Highlighted in red are the maximum values achieved by each parameter.

Table 6-41. *Description of the Cooling Process Stages and Collection of the Main Results related to Spalling Index and velocity*

Stage description	**Absolute Time Start [s]**	**Absolute Time End [s]**	$IS4_{max}$ [-]	X_{IS4max} [cm]	t_{IS4max} [s]	v_{max} [m/s]	X_{vmax} [cm]	t_{vmax} [s]	v_{max}* [m/s]	X_{vmax*} [cm]	t_{vmax*} [s]
First Heating	0	600+120	0,3688	0,582	600	12,349	0,152	240	9,521	0,245	280
Surface cooling	720	760	0,3239	0,860	720	8,479	0,916	720	8,479	0,916	720
Second Heating up to 10.800s	760	10.800	0,2411	1,389	1.020	8,311	1,389	1.200	8,311	1,389	1.200
Absolute Maximum	0	10.800	0,3688	0,582	600	12,349	0,152	240	9,521	0,245	280

Remark † ***:*** *These results are included for the Comparative Analysis developed on Paragraph 6.5.3*

Stage description	**Absolute Time Start [s]**	**Absolute Time End [s]**	d_{max} [-]	X_{dmax} [cm]	t_{dmax} [s]	T_{max} [K]	X_{Tmax} [cm]	t_{Tmax} [s]	p^g_{max} [MPa]	X_{pgmax} [cm]	t_{pgmax} [s]
First Heating	0	600+120	0,4824	1,312	720	754,18	0,000	720	1,3276	0,860	480
Surface cooling	720	760	0,8299	0,000	760	754,18	0,000	720	1,0557	1,644	720
Second Heating up to 10.800s	760	10.800	0,9900	0 - 2,497	4.200	1.369,20	0,000	10.800	0,9127	1,832	760
Absolute Maximum	0	10.800	0,9900	0 - 2,497	4.200	1.369,20	0,000	10.800	1,3276	0,860	480

Table 6-42. *Description of the Cooling Process Stages and Collection of the Main Results related to mechanical damage, Temperature and Gas Pressure*

6.5.2.1.4.4 Main Graphic Results of this Case in the Time-Space Domain

Next it is shown a collection of twelve Time-Space graphics representing the evolution of all of the parameters cited in the last subparagraph and for all of the stages that compose the heating and cooling processes analyzed herein.

a) Spalling Index IS4 [-] *b) Mechanical damage d [-]*

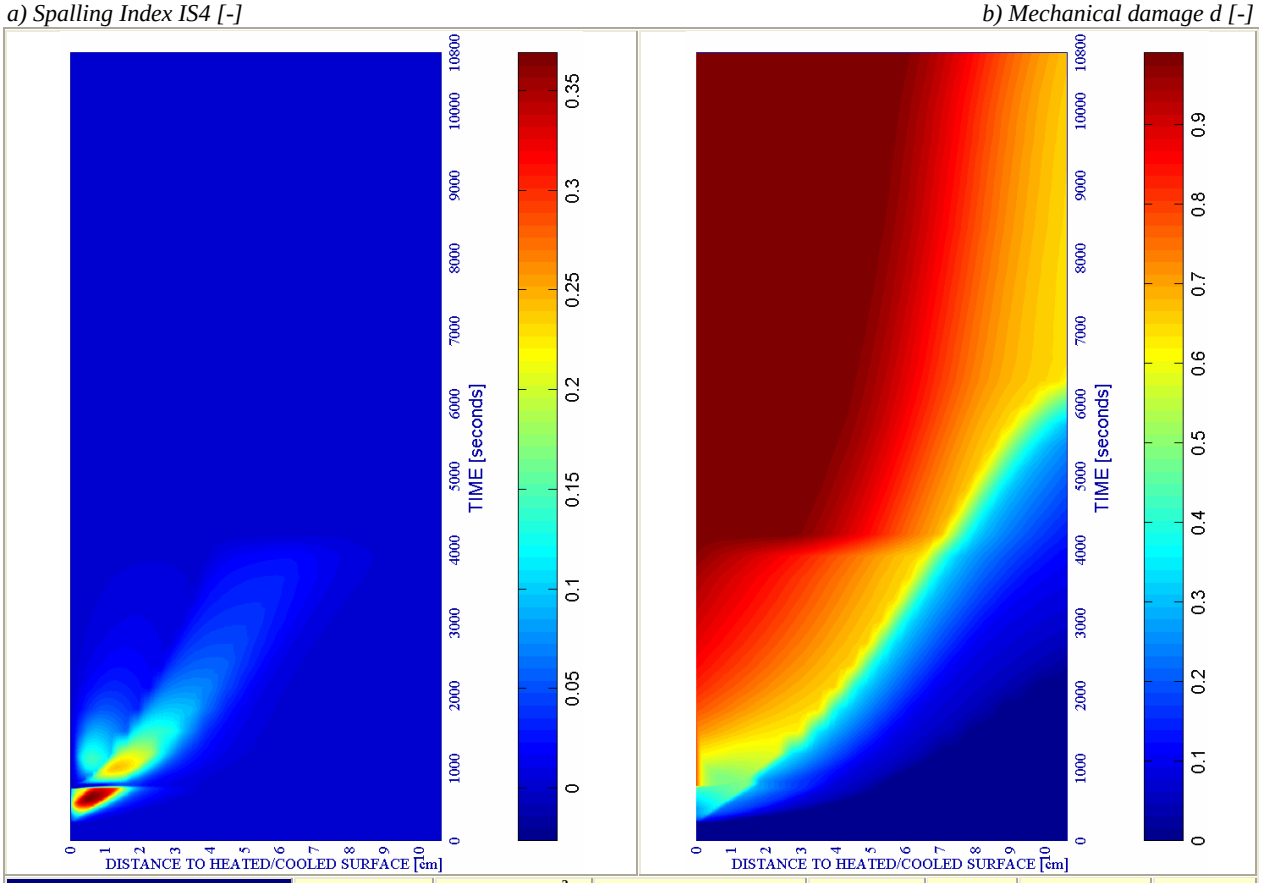

SURFACE COOL+HEAT		PC1 - RH [%]			PC2 - K_0 [m^2]			PC4 - Heating curve			PC5 – Mat.		Cooling length[s]	Start of cooling [s]	End of cooling [s]
#	Combination	40	50	60	10^{-19}	10^{-18}	10^{-17}	PAR1	PAR2	PAR4	C60	C90			
05	TH12K018RH50PAR1C60		X			X		X			X		40	600+120	760

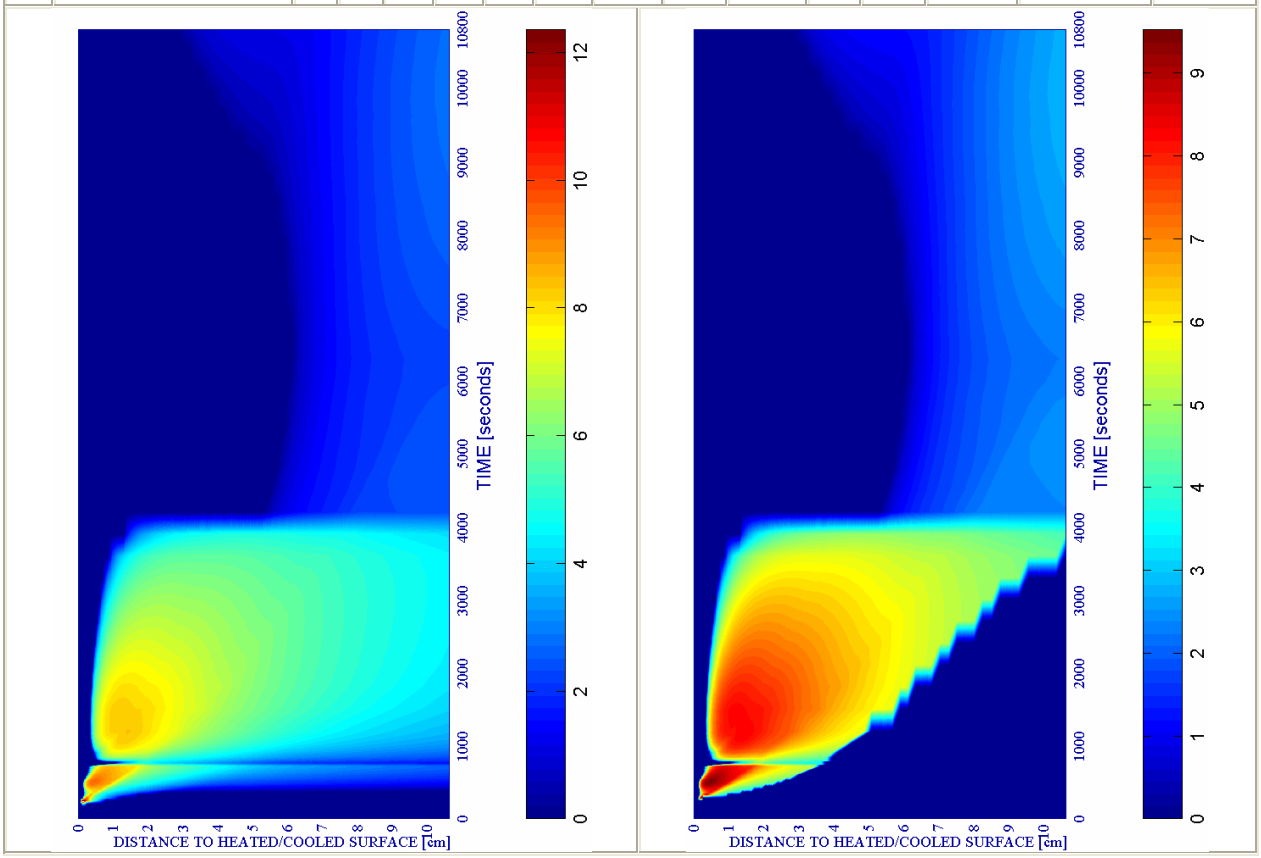

c) Velocity of spalled pieces v [m/s] ***Figure 6-76.*** *d) Velocity [m/s] where d ≥ 0,10*

e) Gas pressure $p^g \cdot 10^{-5}$ [Pa]

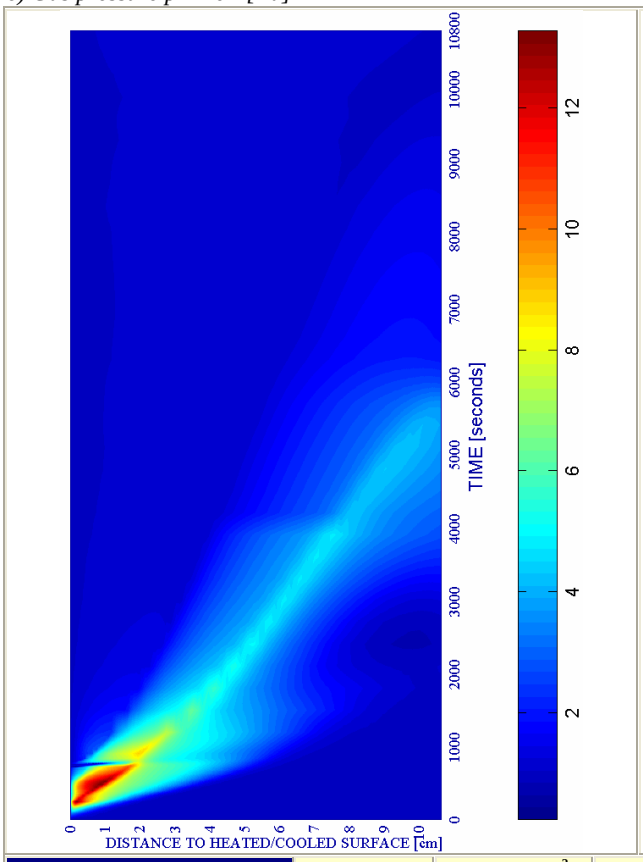

f) Vapour pressure $p^v \cdot 10^{-5}$ [Pa]

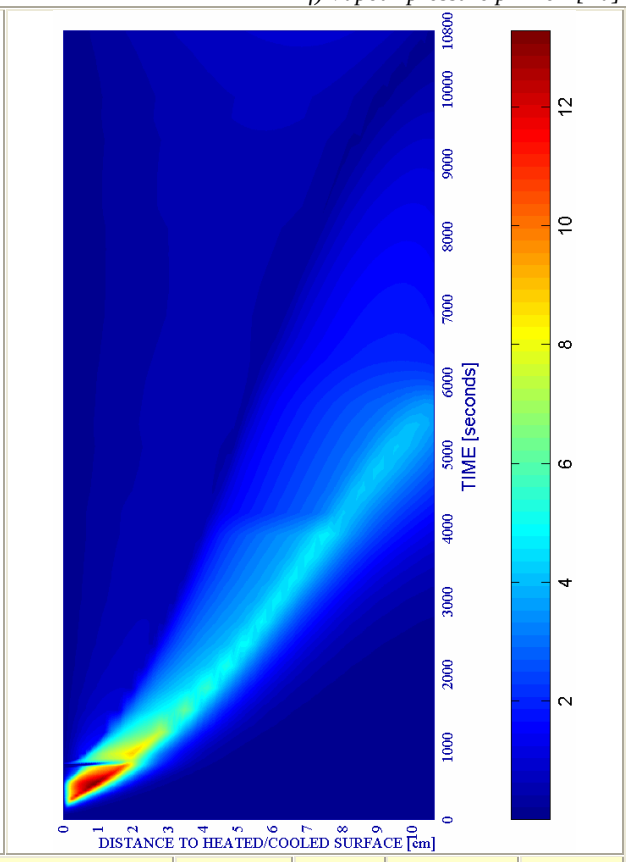

SURFACE COOL+HEAT		PC1 - RH [%]			PC2 - K_0 [m^2]			PC4 - Heating curve			PC5 – Mat.		Cooling length[s]	Start of cooling [s]	End of cooling [s]
#	Combination	40	50	60	10^{-19}	10^{-18}	10^{-17}	PAR1	PAR2	PAR4	C60	C90			
05	TH12K018RH50PAR1C60		X			X		X			X		40	600+120	760

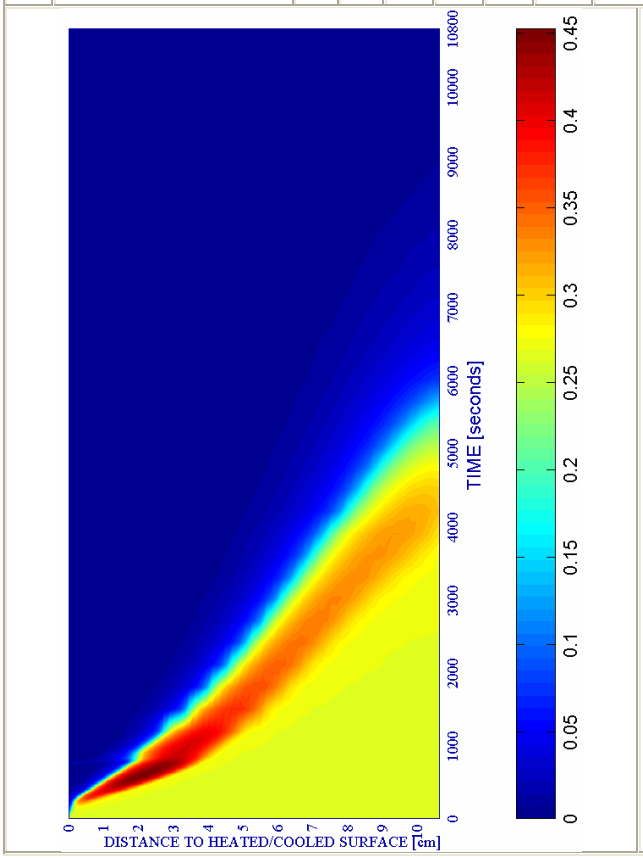

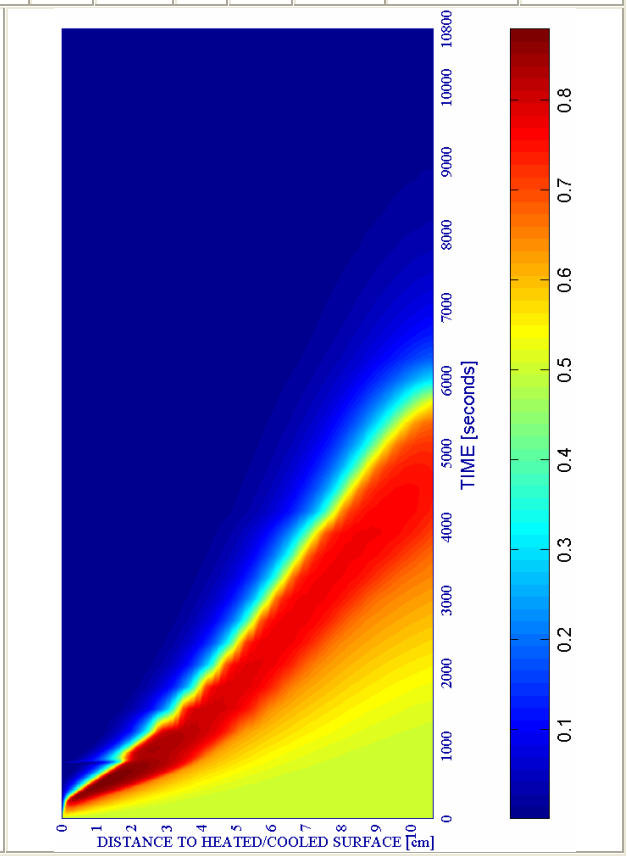

g) Saturation Degree S [-]

Figure 6-76. (continued)

h) Relative Humidity RH [-]

i) Temperature [K] *j) Elastic Energy U · **10^{-4}** [J/m^3]*

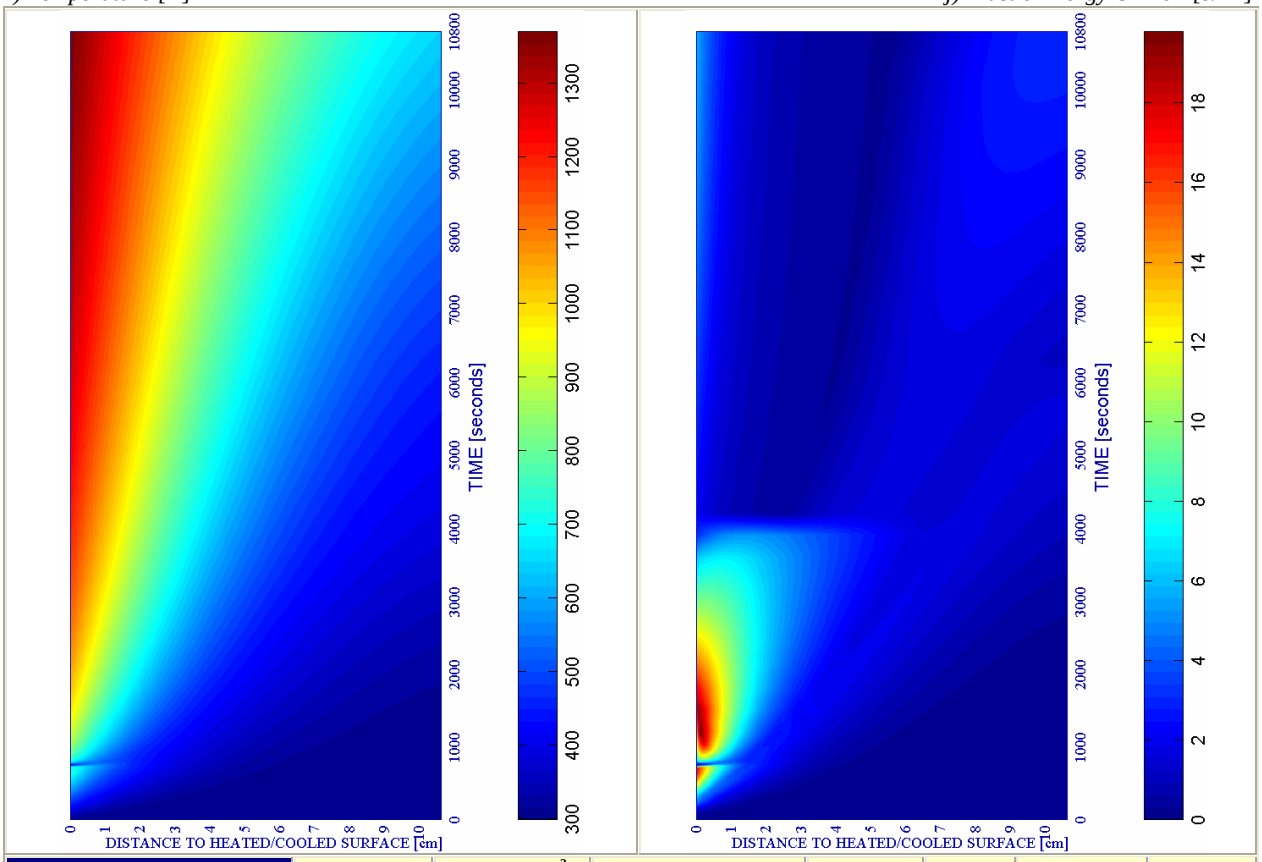

SURFACE COOL+HEAT		PC1 - RH [%]			PC2 - K_0 [m^2]			PC4 - Heating curve			PC5 – Mat.		Cooling length[s]	Start of cooling [s]	End of cooling [s]
#	Combination	40	50	60	10^{-19}	10^{-18}	10^{-17}	PAR1	PAR2	PAR4	C60	C90			
05	TH12K018RH50PAR1C60		X			X		X			X		40	600+120	760

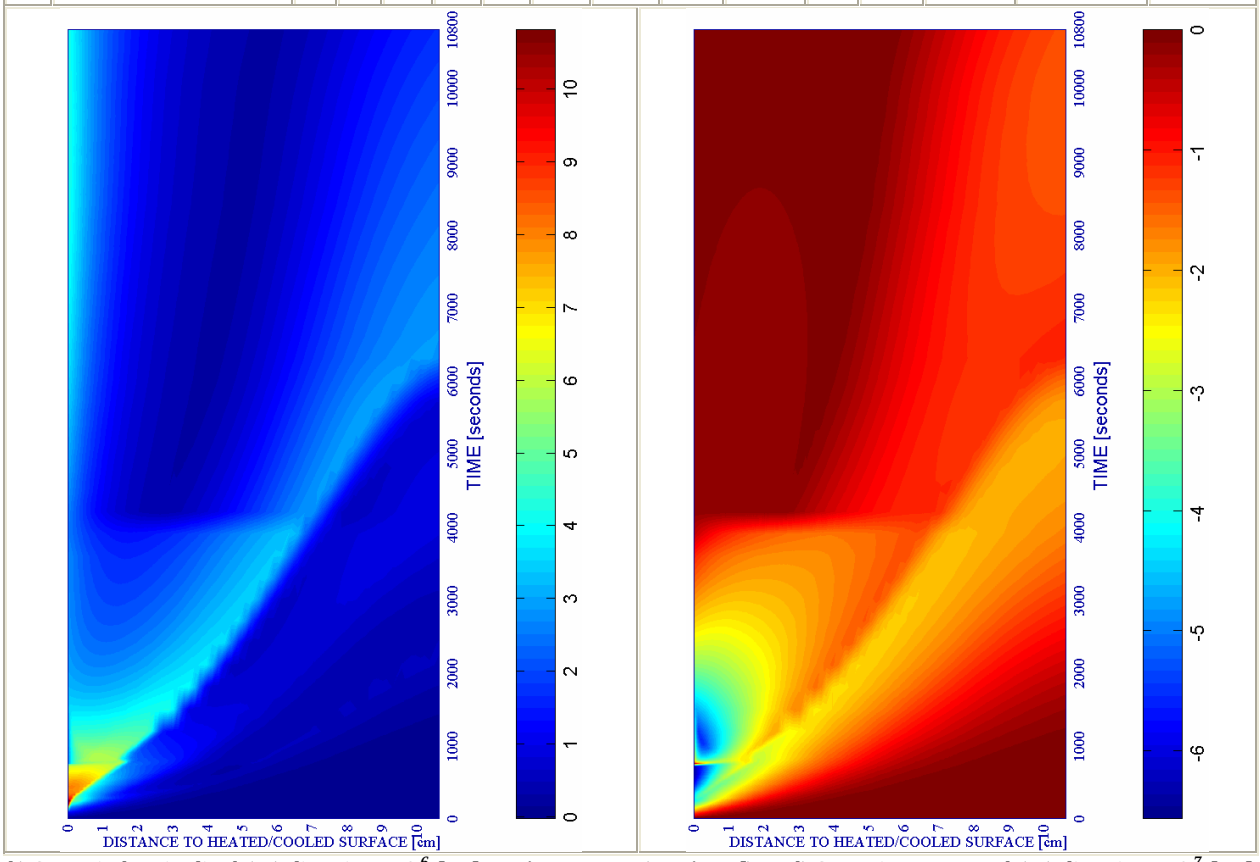

*k) Stress in longitudinal (xx) direction · **10^{-6}** [Pa]* ***Figure 6-76. (continued)*** *l) Stress in transversal (yy) direction · **10^{-7}** [Pa]*

6.5.2.1.5 Surface Cooling followed by an imposed Constant Surface Temperature

After the Surface Cooling stage, defined by the time range from 720 to 760 seconds, despite having finished the cooling boundary conditions, keeping Surface Temperature Constant, the Total Damage D keeps increasing especially in the 2 centimetres layers next to the surface. Hence, between 760 and 1.163 seconds the Total Damage D increase at the following values (see figure 6-79):

TIME [s] \ DISTANCE TO SURFACE [cm]	0,5 centimetres	1,0 centimetres	2,0 centimetres
760 seconds	0,5003	0,4916	0,2791
1.163 seconds	0,8728	0,7588	0,6068

Table 6-43. *Total Damage D [-] values at different depths*

The values shown on last table denote an increase of Total Damage, as Surface Temperature is kept constant, from about a 74 per cent at 0,5 centimetres from surface up to an increase of about a 117 per cent at 2,0 centimetres from surface., reaching a quite high level and approaching to an almost complete destruction of the superficial layer. As it is observed on figure 6-81 b), this increase is due to increases both in mechanical and thermo-chemical damages.

The significant decrease in the gas pressure values observed during cooling process continues during this constant surface temperature (see figure 6-81 e)), showing its maximum values progressively farther from the surface, while the environment relative humidity infiltration is now observed in the 5 millimetres contiguous to the surface, as it is shown on figure 6-77, starting precisely when surface constant temperature period starts:

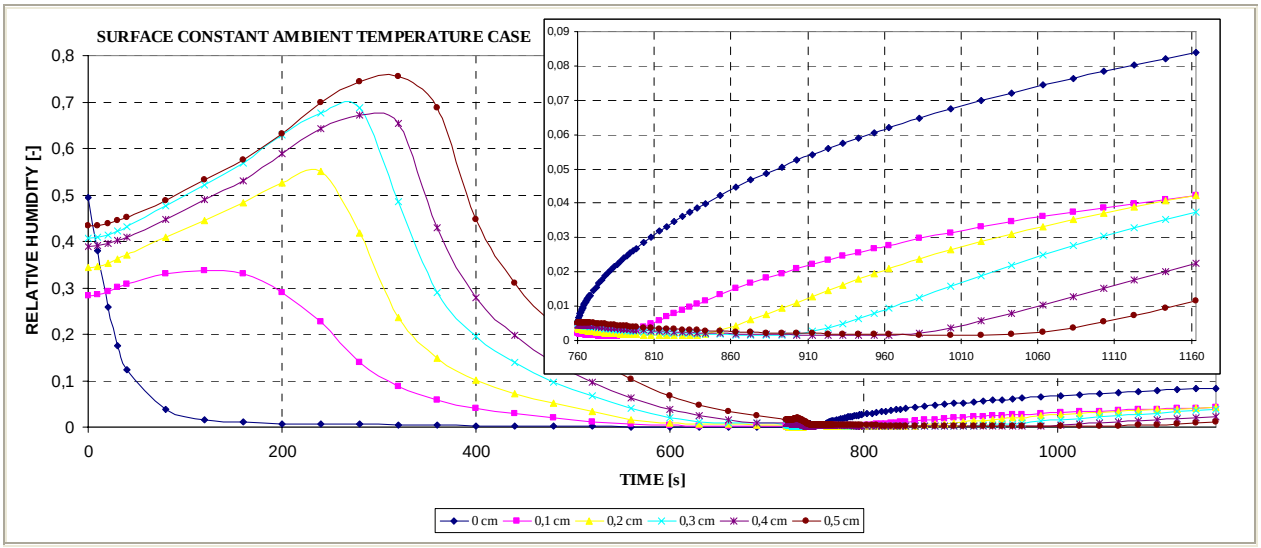

Figure 6-77. *Relative Humidity RH [-] evolution in the 0,5 cm layer contiguous to the heated/cooled surface during each stage of the Surface cooling processes*

Related to the rest of parameters with influence on the Spalling Index I_{s4} values, it is remarkable to observe that as it was expectable tensile longitudinal stresses (xx) decrease significantly in the first centimetre during the constant surface temperature process (see figures 6-80 and 6-81 k)) from an initial tensile value at the surface of 2,00 MPa down to a final compressive value of -2,8 MPa at the end of constant surface temperature process.

Hence, as a difference with the case where the Surface was heated again after cooling, high compressive longitudinal stresses arise at the first centimetre contiguous to the surface. Beyond the three centimetres close to the surface, no significant variations of longitudinal stresses have been noticed. This increase in material (compressive) stress state leads to the Elastic Strain Energy accumulation within the 5 millimetres layer close to surface (see figure 6-78 and 6-81 j)).

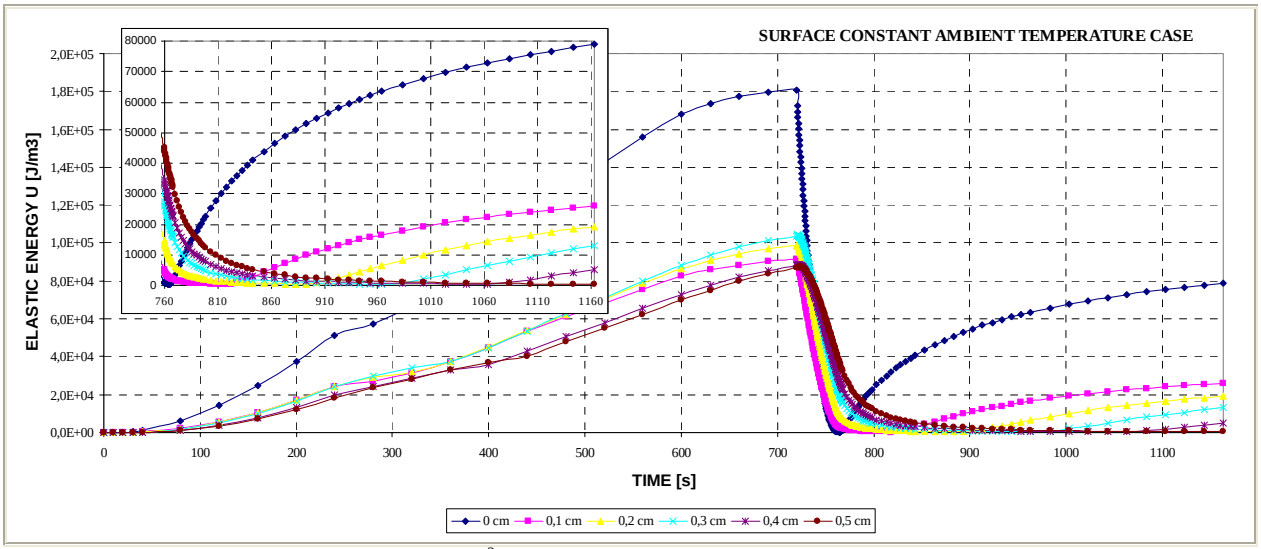

Figure 6-78. *Elastic Strain Energy U [J/m^3] evolution in the 0,5 cm layer contiguous to the heated/cooled surface during each stage of the Surface cooling processes*

Due to all of these trends, Spalling Index I_{s4} values decrease during the whole surface constant ambient temperature process (see Table 6-44 and figure 6-81 a)), reducing therefore the thermal spalling risk. Besides this fact, beyond 893 seconds (133 seconds after the start of the surface constant temperature process) thermal spalling is not viable any longer, mainly due precisely to the fact that the only zones with accumulated Elastic Strain Energy present compressive – not tensile – stresses.

Next it is shown a collection of the main results cited in the last subparagraph, as well as a description of each of the stages that compose the heating and cooling processes analyzed herein. Highlighted in red are the maximum values achieved by each parameter.

Table 6-44. *Description of the Cooling Process Stages and Collection of the Main Results related to Spalling Index and velocity*

Stage description	**Absolute Time Start [s]**	**Absolute Time End [s]**	**$IS4_{max}$ [-]**	**X_{IS4max} [cm]**	**t_{IS4max} [s]**	**v_{max} [m/s]**	**X_{vmax} [cm]**	**t_{vmax} [s]**	**v_{max}* [m/s]**	**X_{vmax*} [cm]**	**t_{vmax*} [s]**
First Heating	0	600+120	0,3688	0,582	600	12,349	0,152	240	9,521	0,245	280
Surface cooling	720	760	0,3239	0,860	720	8,479	0,916	720	8,479	0,916	720
Surface Constant T	760	1.163	0,0615	1.470	760	5,119	1,832	760	5,119	1,832	760
Absolute Maximum	0	1.163	0,3688	0,582	600	12,349	0,152	240	9,521	0,245	280

Remark † ***:*** *These results are included for the Comparative Analysis developed on Paragraph 6.5.3*

Stage description	**Absolute Time Start [s]**	**Absolute Time End [s]**	**d_{max} [-]**	**X_{dmax} [cm]**	**t_{dmax} [s]**	**T_{max} [K]**	**X_{Tmax} [cm]**	**t_{Tmax} [s]**	**p^g_{max} [MPa]**	**X_{pgmax} [cm]**	**t_{pgmax} [s]**
First Heating	0	600+120	0,4824	1,312	720	754,18	0,000	720	1,3276	0,860	480
Surface cooling	720	760	0,8299	0,000	760	754,18	0,000	720	1,0557	1,644	720
Surface Constant T	760	1.163	0,8721	0,544	1.163	560,27	0,710	760	0,9127	1,832	760
Absolute Maximum	0	1.163	0,8721	0,544	1.163	754,18	0,000	720	1,3276	0,860	480

Table 6-45. *Description of the Cooling Process Stages and Collection of the Main Results related to mechanical damage, Temperature and Gas Pressure*

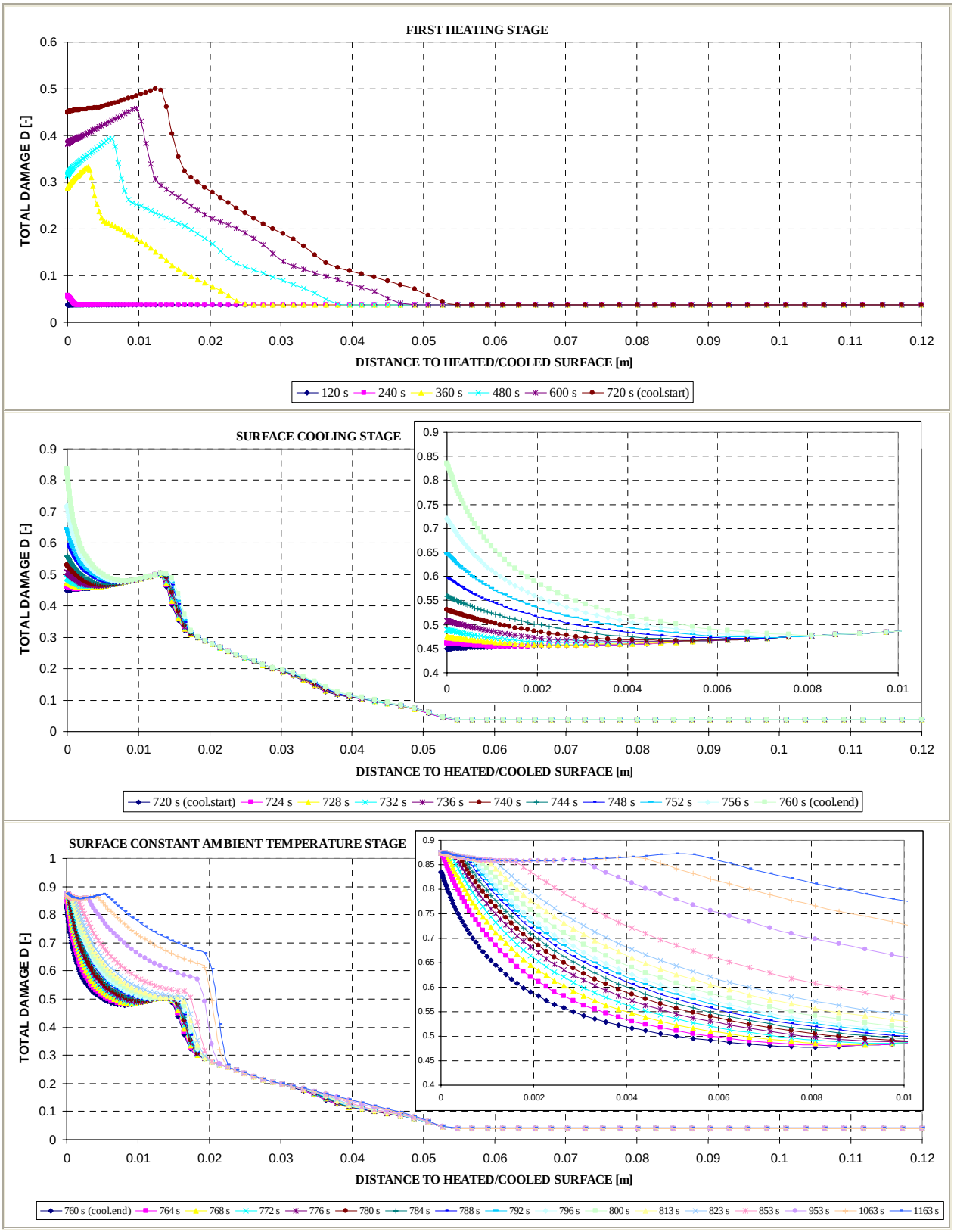

Figure 6-79. *Total Damage D [-] at several distances from the heated/cooled surface during each stage of the Surface cooling processes*

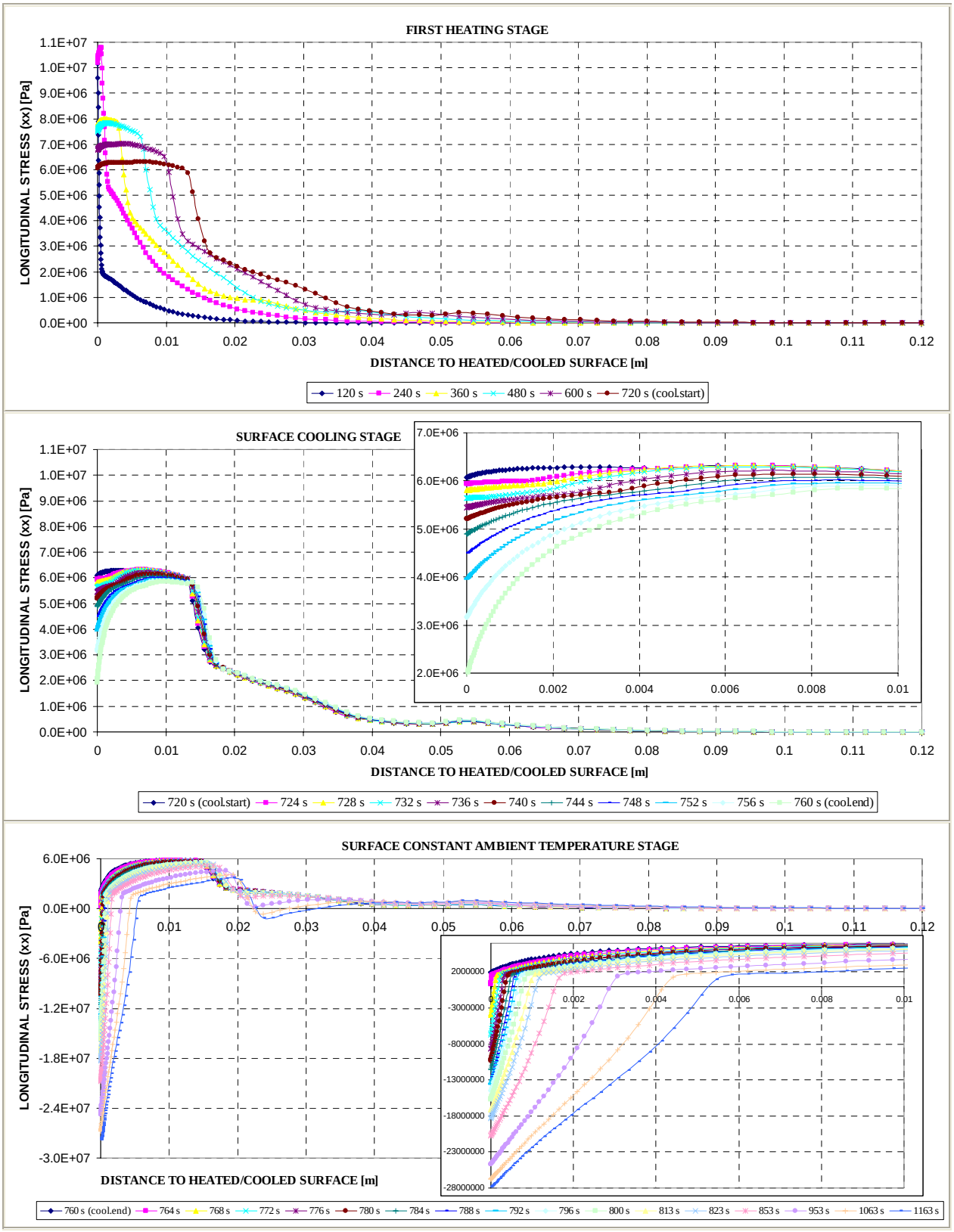

Figure 6-80. *Longitudinal stress (xx) [Pa] at several distances from the heated/cooled surface during each stage of the Surface cooling processes*

Next it is shown a collection of twelve Time-Space graphics representing the evolution of all of the parameters cited in the last subparagraph and for all of the stages that compose the heating and cooling processes analyzed herein.

a) Spalling Index IS4 [-] *b) Mechanical damage d [-]*

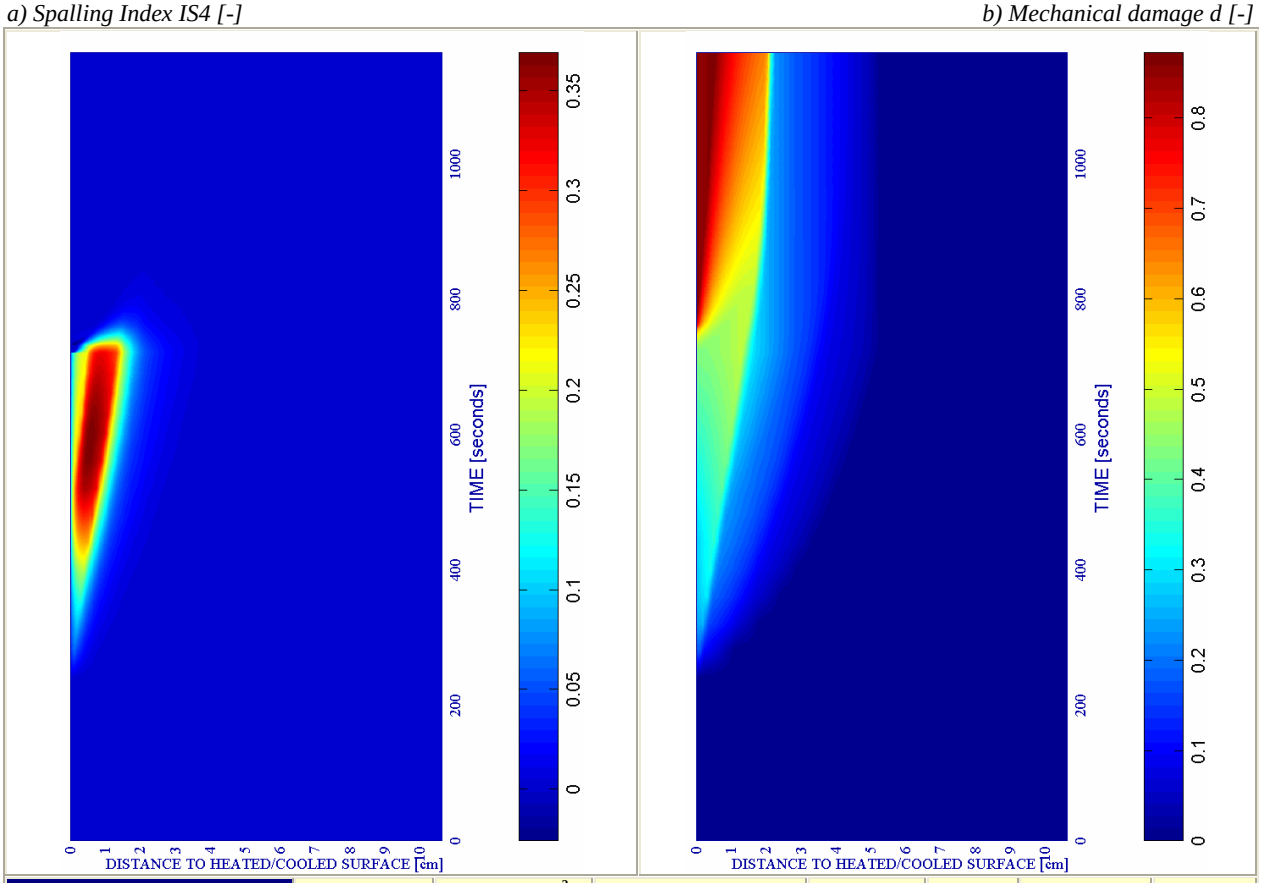

SURFACE COOL+KEEP		PC1 - RH [%]			PC2 - K_0 [m^2]			PC4 - Heating curve			PC5 – Mat.		Cooling length[s]	Start of cooling [s]	End of cooling [s]
#	Combination	40	50	60	10^{-19}	10^{-18}	10^{-17}	PAR1	PAR2	PAR4	C60	C90			
05	TH12K018RH50PAR1C60		X			X		X			X		423	600+120	1.163

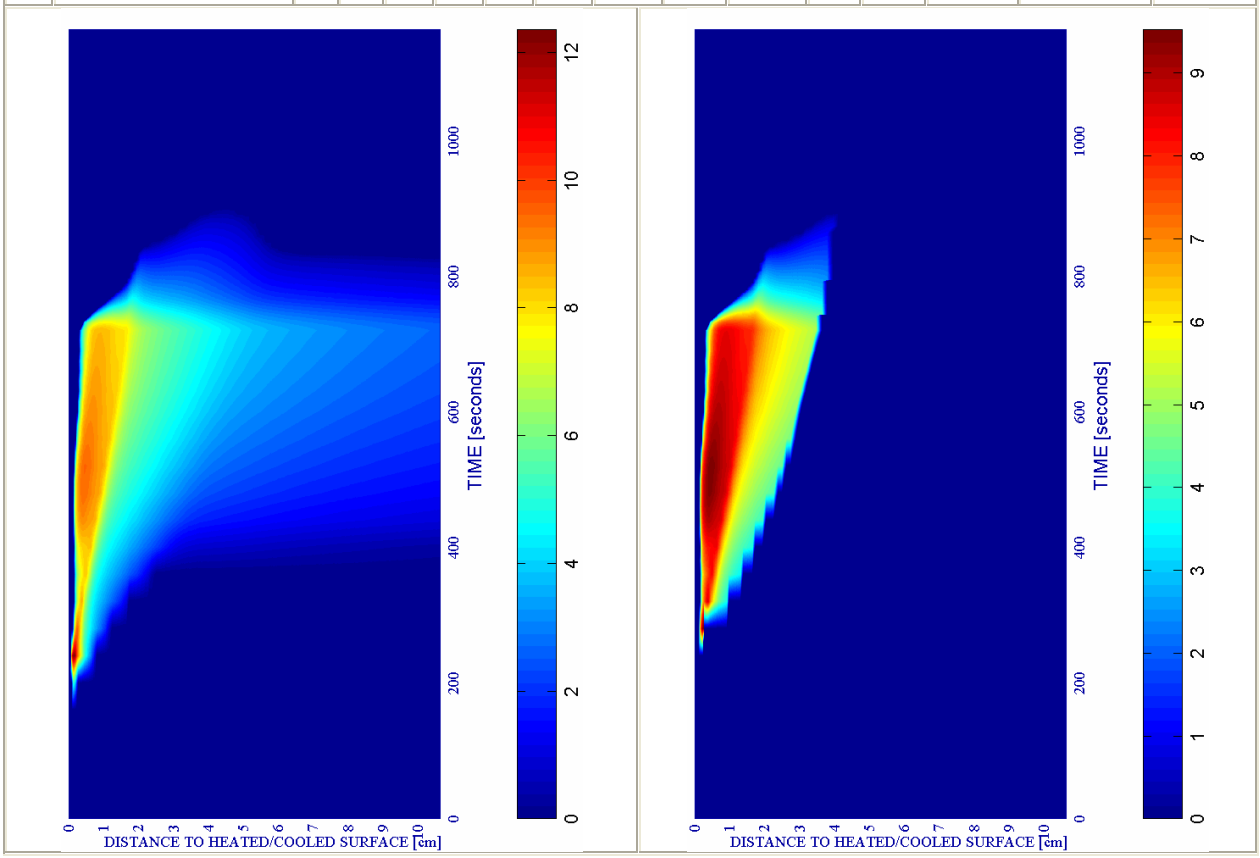

c) Velocity of spalled pieces v [m/s] ***Figure 6-81.*** *d) Velocity [m/s] where d ≥ 0,10*

e) Gas pressure $p^g \cdot 10^{-5}$ [Pa]

f) Vapour pressure $p^v \cdot 10^{-5}$ [Pa]

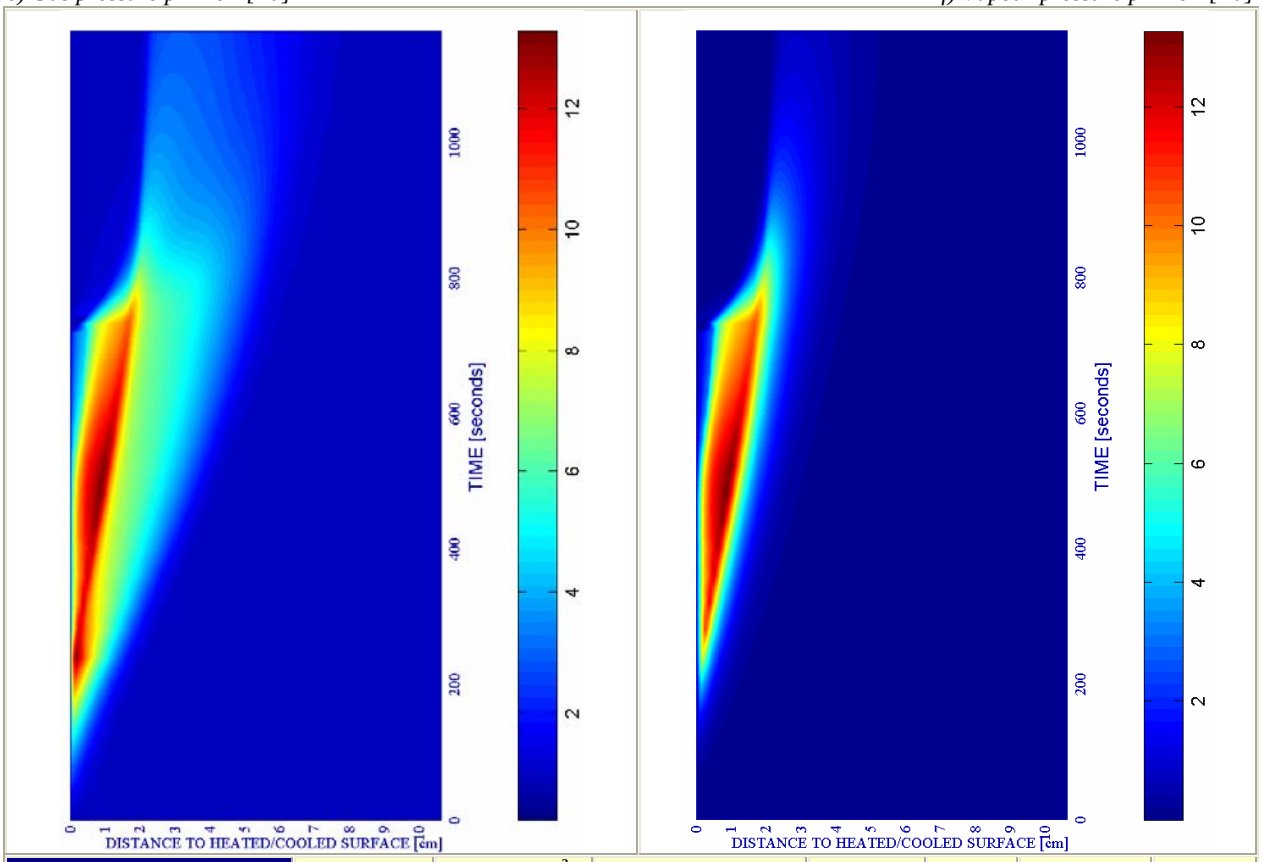

SURFACE COOL+KEEP		PC1 - RH [%]			PC2 - K_0 [m^2]			PC4 - Heating curve			PC5 – Mat.		Cooling length[s]	Start of cooling [s]	End of cooling [s]
#	Combination	40	50	60	10^{-19}	10^{-18}	10^{-17}	PAR1	PAR2	PAR4	C60	C90			
05	TH12K018RH50PAR1C60		X			X		X			X		423	600+120	1.163

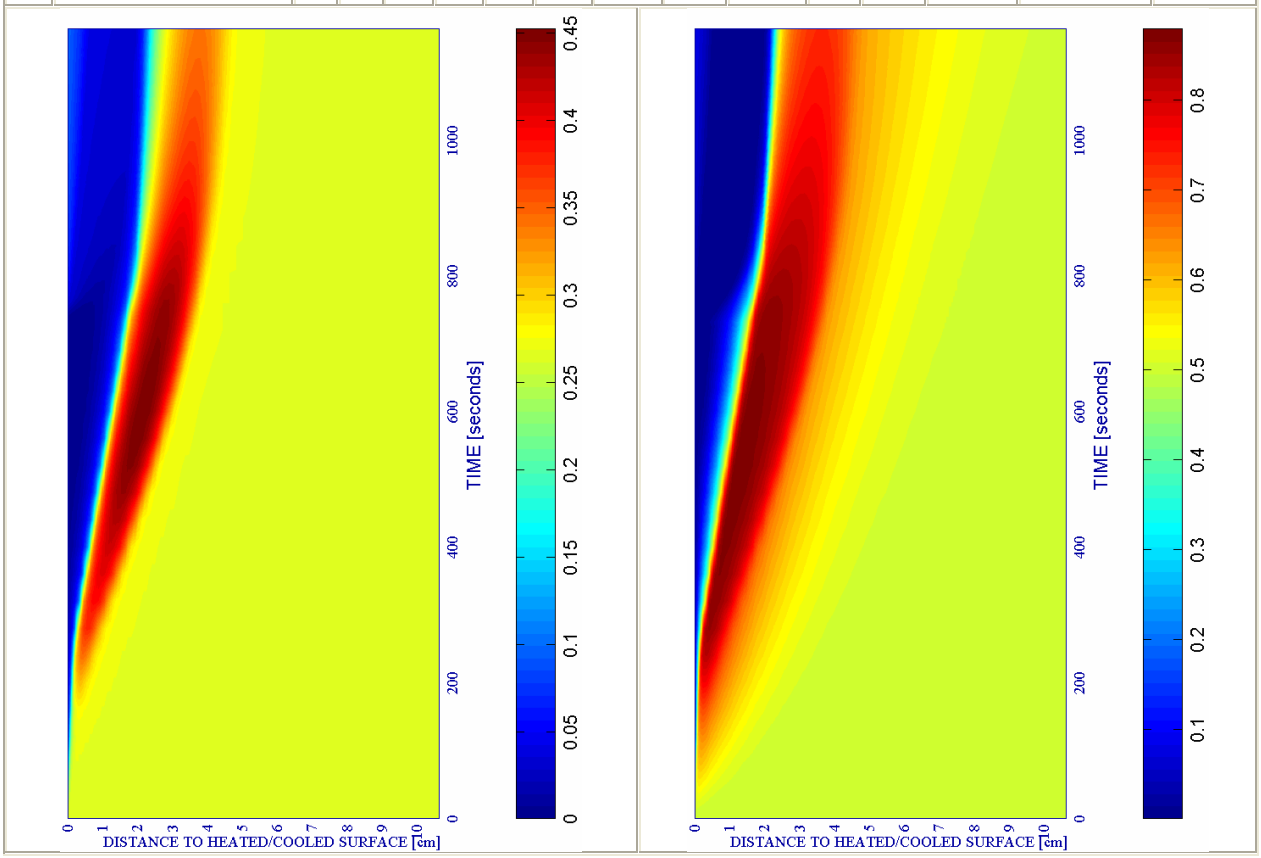

g) Saturation Degree S [-]

Figure 6-81. (continued)

h) Relative Humidity RH [-]

i) Temperature [K]

*j) Elastic Energy U · **10**$^{-4}$ [J/m^3]*

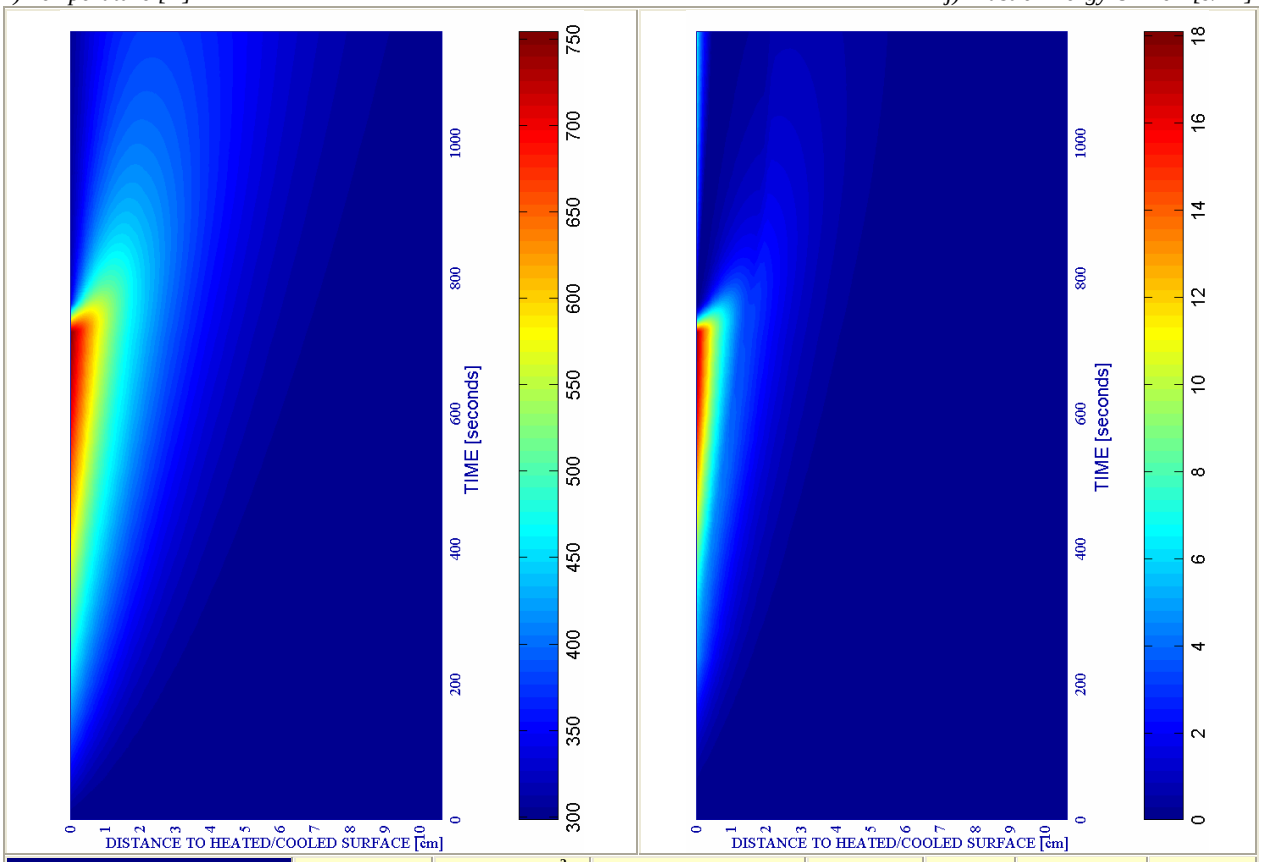

SURFACE COOL+KEEP		PC1 - RH [%]			PC2 - K_0 [m^2]			PC4 - Heating curve			PC5 – Mat.		Cooling length[s]	Start of cooling [s]	End of cooling [s]
#	Combination	40	50	60	10^{-19}	10^{-18}	10^{-17}	PAR1	PAR2	PAR4	C60	C90			
05	TH12K018RH50PAR1C60		X			X		X			X		423	600+120	1.163

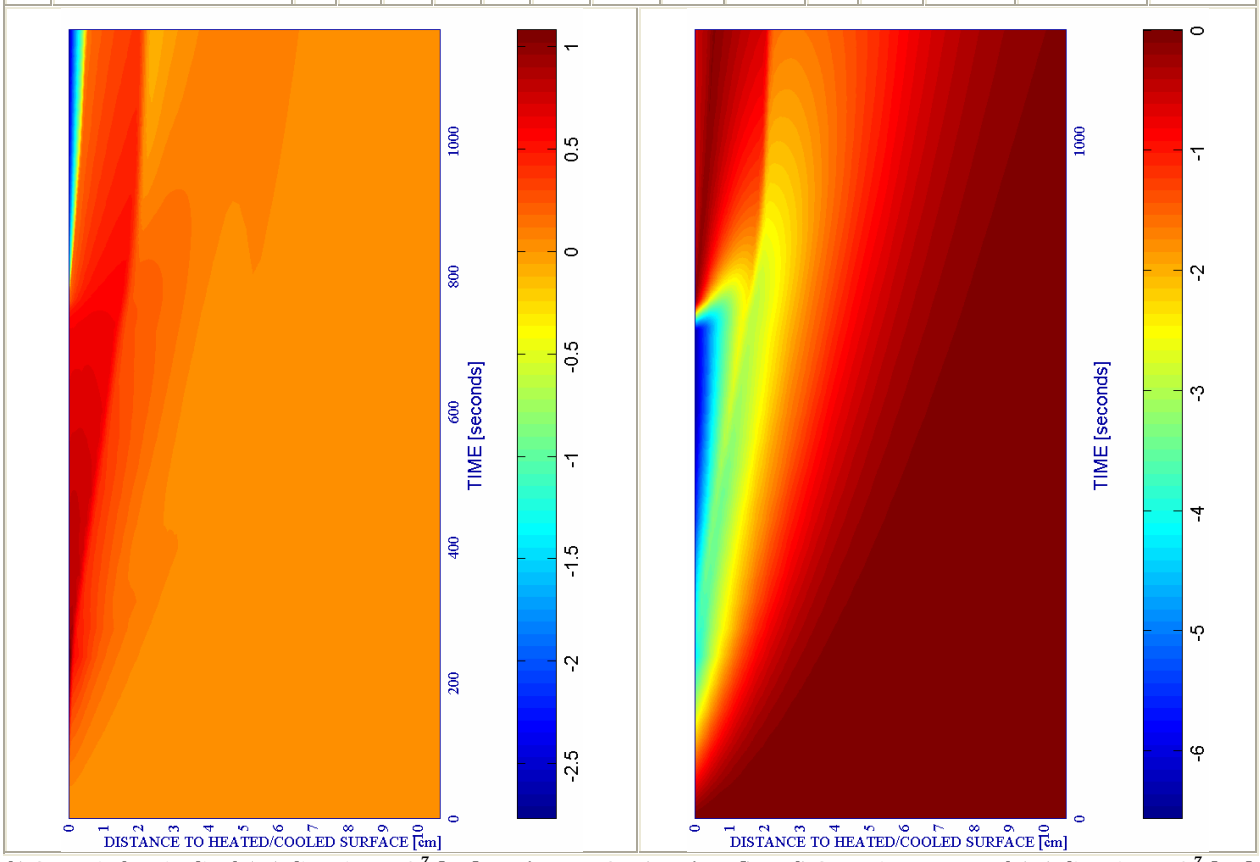

*k) Stress in longitudinal (xx) direction · **10**$^{-7}$ [Pa]*

Figure 6-81. (continued)

*l) Stress in transversal (yy) direction · **10**$^{-7}$ [Pa]*

6.5.2.1.6 Surface Cooling in Two Periods

The especial issue of the phenomenological and mechanistic analysis of this case is to discern if the hygro-thermo-chemo-mechanical processes involved in repeated heating-cooling solicitations present cyclic tendencies or lead each of them to different final states of the structural element. On the other hand, on paragraph 6.5.3.1.2 there is included a comparison of the final state of the structural element – after three hours from the start of the fire – for 1, 2 and 3 consecutive heating-cooling cycles.

In order to ease the understanding of the explanation exposed in this paragraph, the tables 6-46 and 6-47 show a description of each of the stages that compose the heating and cooling processes analyzed herein, as well as a collection of the main results cited in this subparagraph. Highlighted in red are the maximum values achieved by each parameter.

Table 6-46. *Description of the Cooling Process Stages and Collection of the Main Results related to Spalling Index and velocity*

Stage description	Absolute Time Start [s]	Absolute Time End [s]	$IS4_{max}$ [-]	X_{IS4max} [cm]	t_{IS4max} [s]	v_{max} [m/s]	X_{vmax} [cm]	t_{vmax} [s]	v_{max}* [m/s]	X_{vmax*} [cm]	t_{vmax*} [s]
First Heating	0	600+120	0,3688	0,582	600	12,349	0,152	240	9,521	0,245	280
First Surface cooling	720	760	0,3239	0,860	720	8,479	0,916	720	8,479	0,916	720
Second Heating	760	840	0,1536	1,035	840	6,466	1,167	840	6,466	1,167	840
Second Surface cool.	840	886	0,1538	1,035	842	6,473	1,167	842	6,473	1,167	842
Heating up to 10.800s	886	10.800	0,2259	1,470	1.140	8,304	1,167	1.500	8,304	1,167	1.500
Absolute Maximum	0	10.800	0,3688	0,582	600	12,349	0,152	240	9,521	0,245	280

Remark [†]***:*** *These results are included for the Comparative Analysis developed on Paragraph 6.5.3*

Stage description	Absolute Time Start [s]	Absolute Time End [s]	d_{max} [-]	X_{dmax} [cm]	t_{dmax} [s]	T_{max} [K]	X_{Tmax} [cm]	t_{Tmax} [s]	p^g_{max} [MPa]	X_{pgmax} [cm]	t_{pgmax} [s]
First Heating	0	600+120	0,4824	1,312	720	754,18	0,000	720	1,3276	0,860	480
First Surface cooling	720	760	0,8299	0,000	760	754,18	0,000	720	1,0557	1,644	720
Second Heating	760	840	0,8299	0,000	760	765,68	0,000	840	0,9127	1,832	760
Second Surface cool.	840	886	0,8488	0,000	886	765,68	0,000	840	0,8510	1,932	862
Heating up to 10.800s	886	10.800	0,9900	0 – 2,497	4.200	1.369,10	0,000	10.800	0,8316	2,145	1.020
Absolute Maximum	0	10.800	0,9900	0 – 2,497	4.200	1.369,10	0,000	10.800	1,3276	0,860	480

Table 6-47. *Description of the Cooling Process Stages and Collection of the Main Results related to mechanical damage, Temperature and Gas Pressure*

As it can be observed on figures 6-84 and 6-87 b) during the Second Heating stage Total Damage remains mostly unchanged at all of the depths of the structural element. This fact is due to the shortness of this heating period (only eighty seconds) what leads to maximum temperatures not so high as those corresponding to the start instant of the first cooling stage and to a longitudinal stress state with just slight variations (see figure 6-86 and 6-87 k)) during this period. On the contrary, gas pressure values experiment significant increases in the layers close to the surface during this heating stage (see figure 6-85 and 6-87 e)).

Within the subsequent 'Second surface cooling' stage, again the differences in Total Damage and the longitudinal stress state are non significant (in figures 6-84 and 6-86 all the graphs corresponding to the period between 840 and 886 seconds are superposed). The tendency with gas pressure values is analogue to that corresponding to the first surface cooling stage, decreasing slightly its maximum and moving inwards the structural element (as it happened during the first surface cooling stage gas pressure values under atmospheric pressure appear within the 4 millimetres contiguous to the cooled surface). It is only remarkable that the maximum value of gas pressure during this cooling stage appears at mid-stage (862 seconds) and not at its start.

All these facts mean that, in terms of Total Damage and longitudinal stress the amplitude of the thermal cycles is not high enough to affect the mechanical state of the structural element (neither the Elastic Strain Energy, since as it is shown on figures 6-82 and 6-87 j) its values follow qualitatively identical cycles during the heating-cooling ones.

Moreover, as it can be observed on figures 6-83 and 6-87 h) the hygral behaviour is also qualitatively repetitive (see for example on figure 6-83 the relative humidity at several positions close to the surface corresponding to the start instants of the second and third heating processes, 760 and 886 seconds respectively).

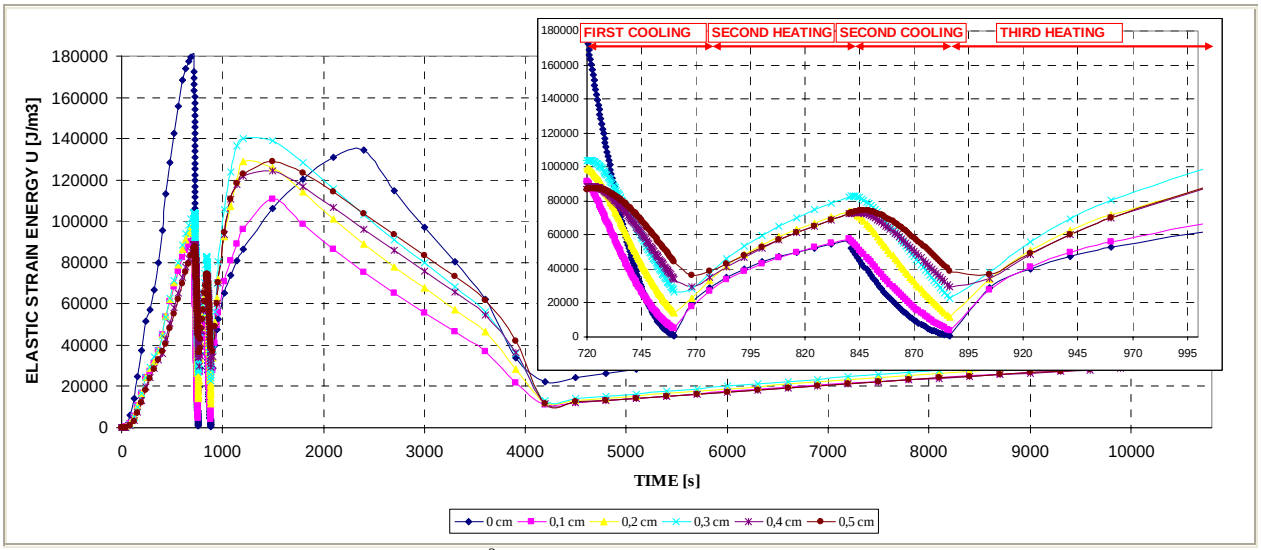

Figure 6-82. *Elastic Strain Energy U [J/m^3] at several distances from the heated/cooled surface during each stage of the Surface cooling processes*

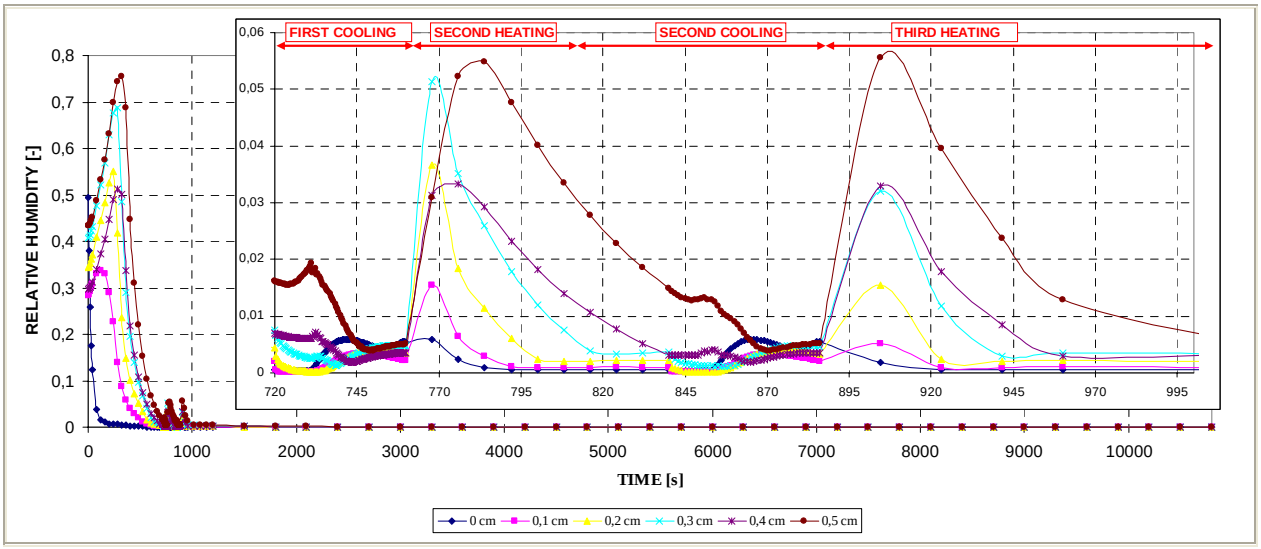

Figure 6-83. *Relative Humidity RH [-] at several distances from the heated/cooled surface during each stage of the Surface cooling processes*

During the third heating stage it is remarkable that at approximately 4.000 seconds from the start of the fire it is observed a sharp increase of Total Damage (more precisely, of Mechanical Damage – see figure 6-87 b)) and of the longitudinal stress (see figures 6-86 and 6-87 k)), a sharp decrease in the gas pressure and elastic strain energy values (see figures 6-87 e) and 6-82 respectively) and, consequently, both the Spalling Index values and the energy available for thermal spalling decrease significantly (see figures 6-87 a), 6-87 c) and 6-87 d)), although thermal spalling is still energetically viable until the end of the 3 hours overall heating-cooling process at really important depths (see specifically figure 6-87 d)).

After figures 6-84 to 86, it is shown a collection of twelve Time-Space graphics representing the evolution of all of the parameters cited in the last subparagraph and for all of the stages that compose the heating and cooling processes analyzed herein.

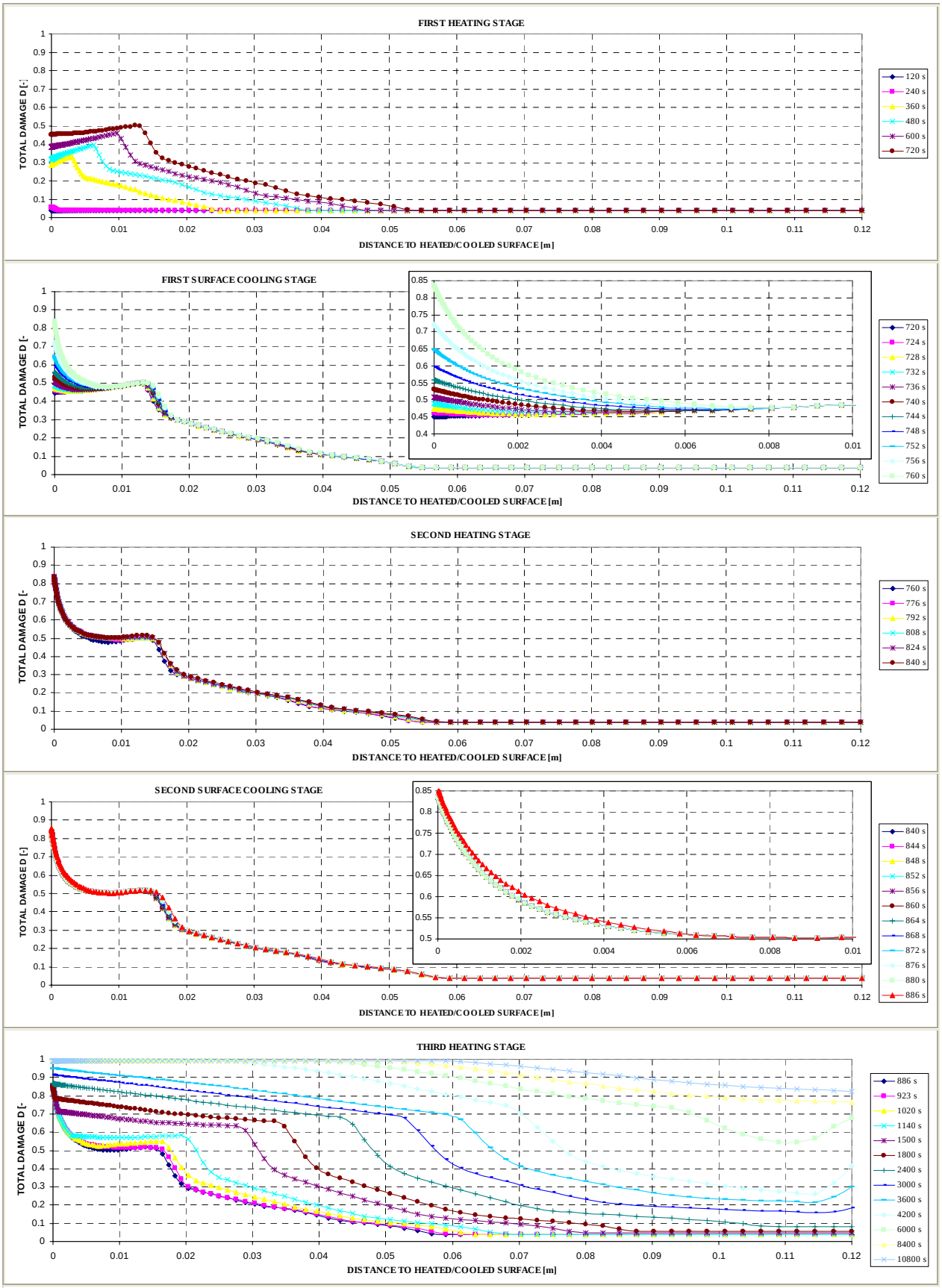

Figure 6-84. *Total Damage D [-] at several distances from the heated/cooled surface during each stage of the Surface cooling processes*

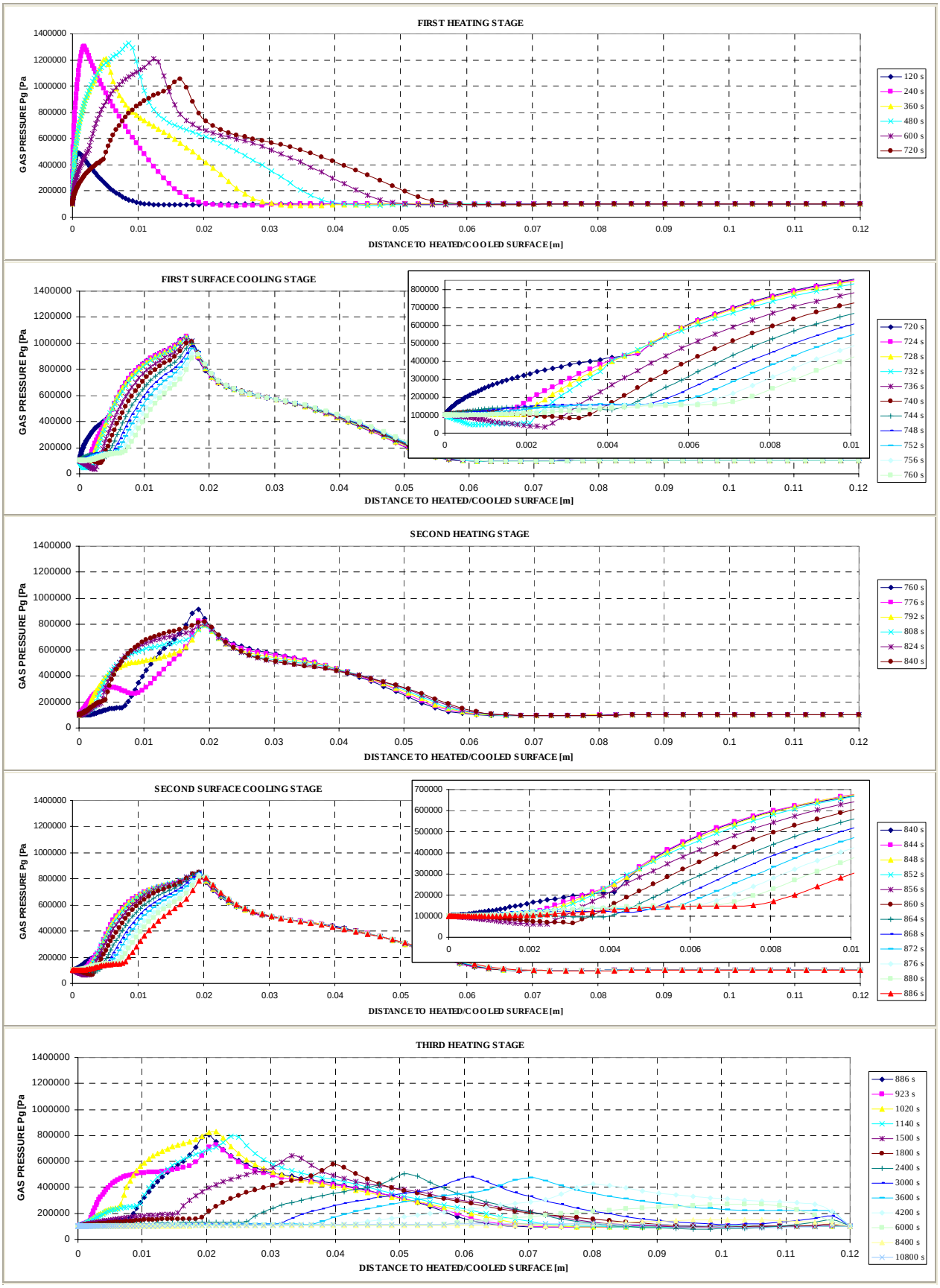

Figure 6-85. *Gas Pressure Pg [Pa] at several distances from the heated/cooled surface during each stage of the Surface cooling processes*

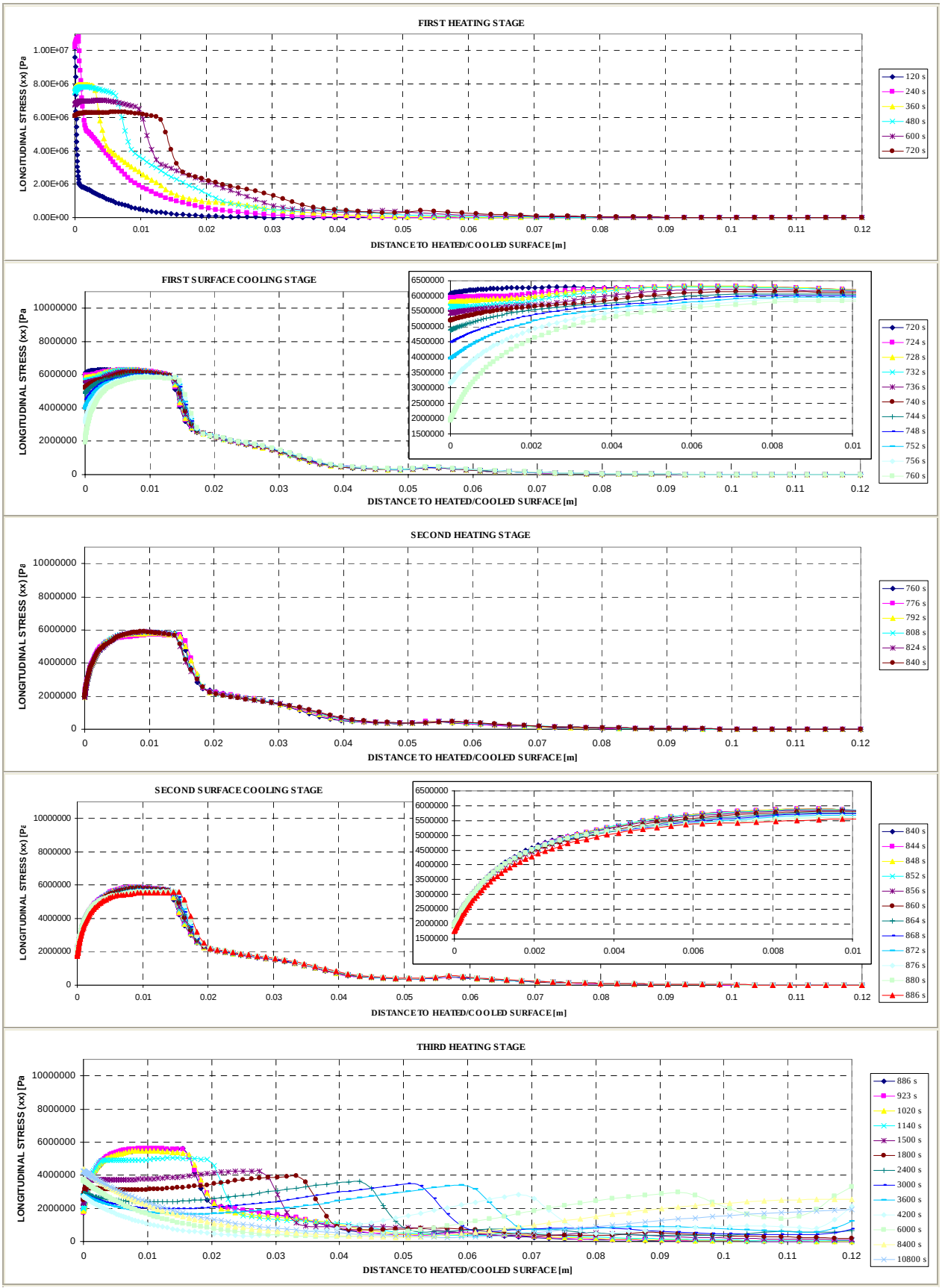

Figure 6-86. *Longitudinal stress (xx) [Pa] at several distances from the heated/cooled surface during each stage of the Surface cooling processes*

a) Spalling Index IS4 [-]

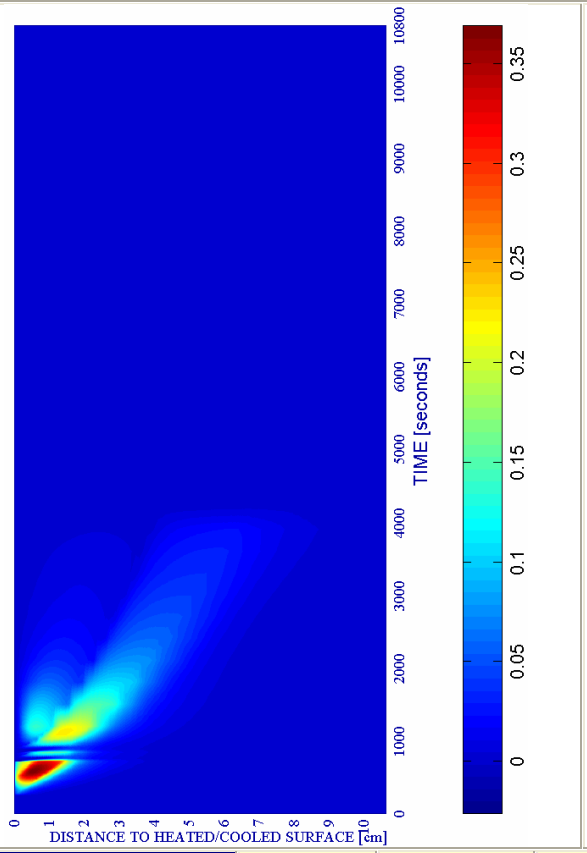

b) Mechanical damage d [-]

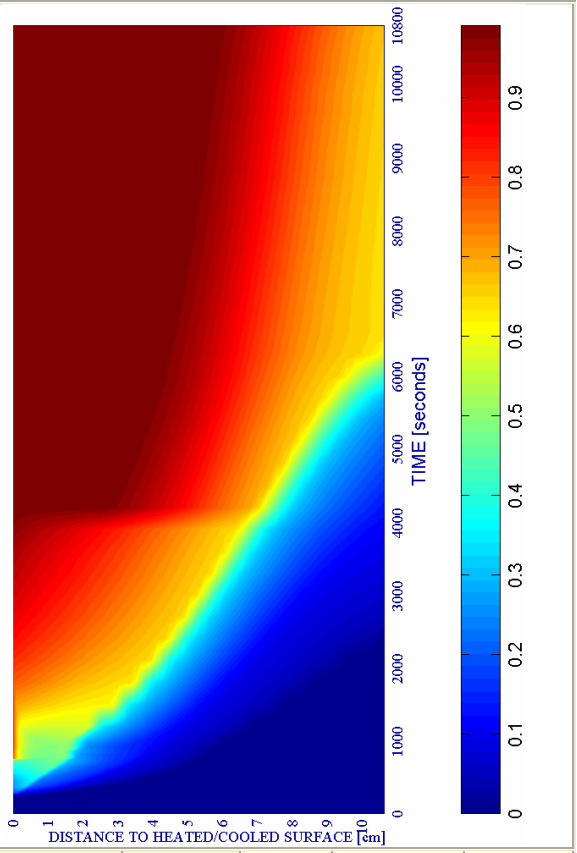

SURFACE COOL+REPEAT		PC1 - RH [%]			PC2 - K_0 [m^2]			PC4 - Heating curve			PC5 – Mat.		Cooling length[s]	Start of cooling [s]	End of cooling [s]
#	Combination	40	50	60	10^{-19}	10^{-18}	10^{-17}	PAR1	PAR2	PAR4	C60	C90			
05	TH12K018RH50PAR1C60		X			X		X			X		40 / 46	600+120 / 840	760 / 886

c) Velocity of spalled pieces v [m/s]

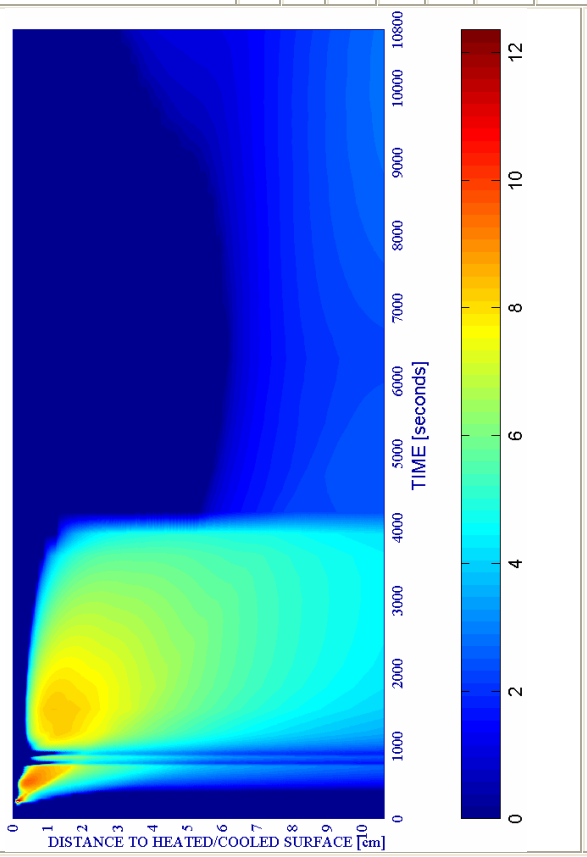

Figure 6-87.

d) Velocity [m/s] where d ≥ 0,10

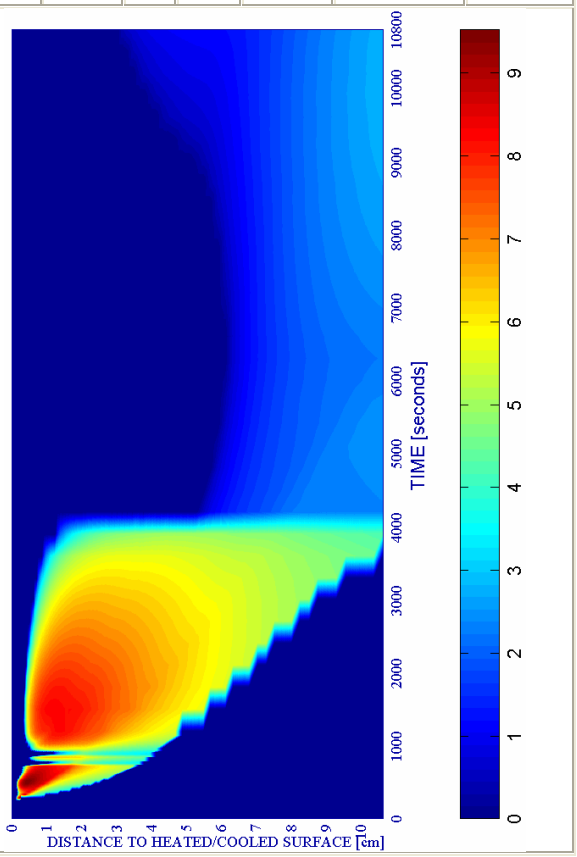

e) Gas pressure $p^g \cdot 10^{-5}$ [Pa]

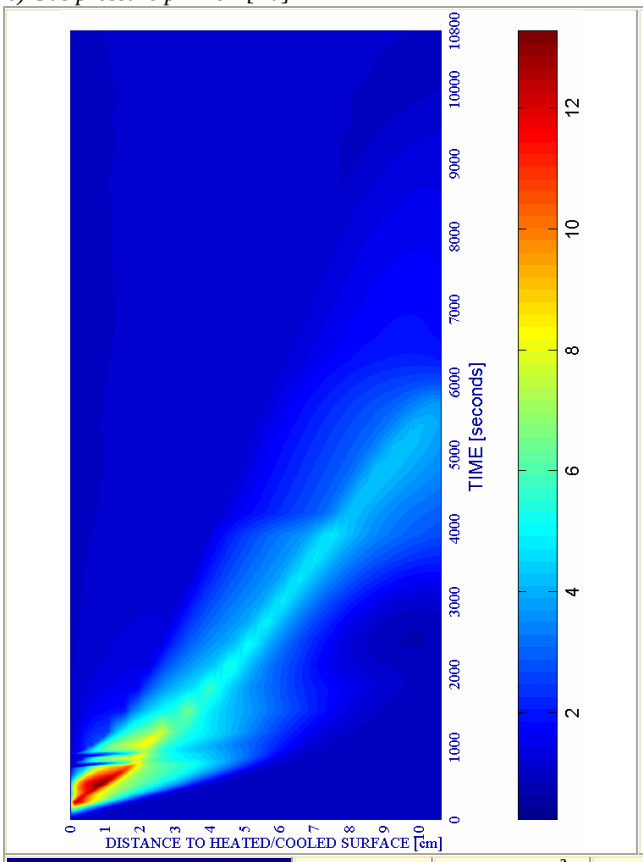

f) Vapour pressure $p^v \cdot 10^{-5}$ [Pa]

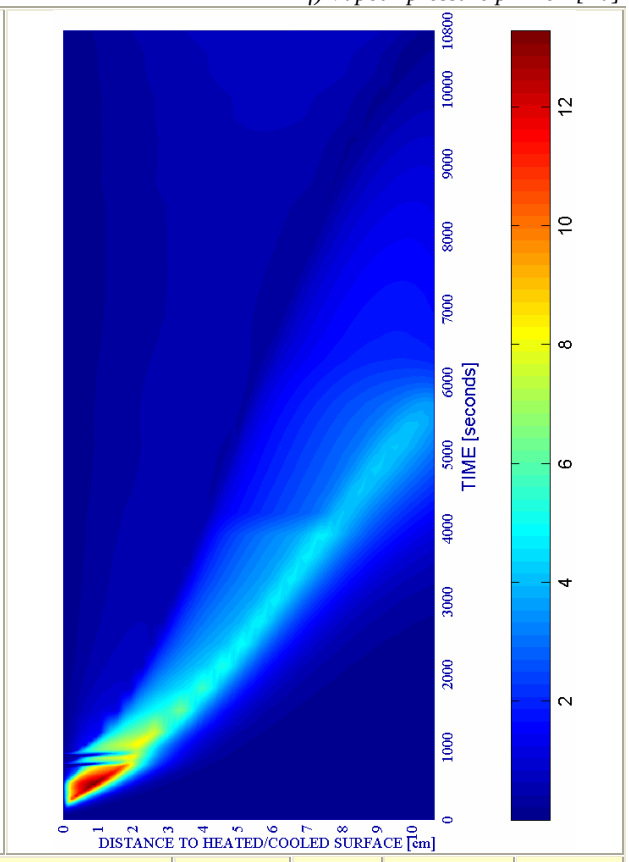

SURFACE COOL+REPEAT		PC1 - RH [%]			PC2 - K_0 [m^2]			PC4 - Heating curve			PC5 – Mat.		Cooling length[s]	Start of cooling [s]	End of cooling [s]
#	Combination	40	50	60	10^{-19}	10^{-18}	10^{-17}	PAR1	PAR2	PAR4	C60	C90			
05	TH12K018RH50PAR1C60		X			X		X			X		40 / 46	600+120 / 840	760 / 886

g) Saturation Degree S [-]

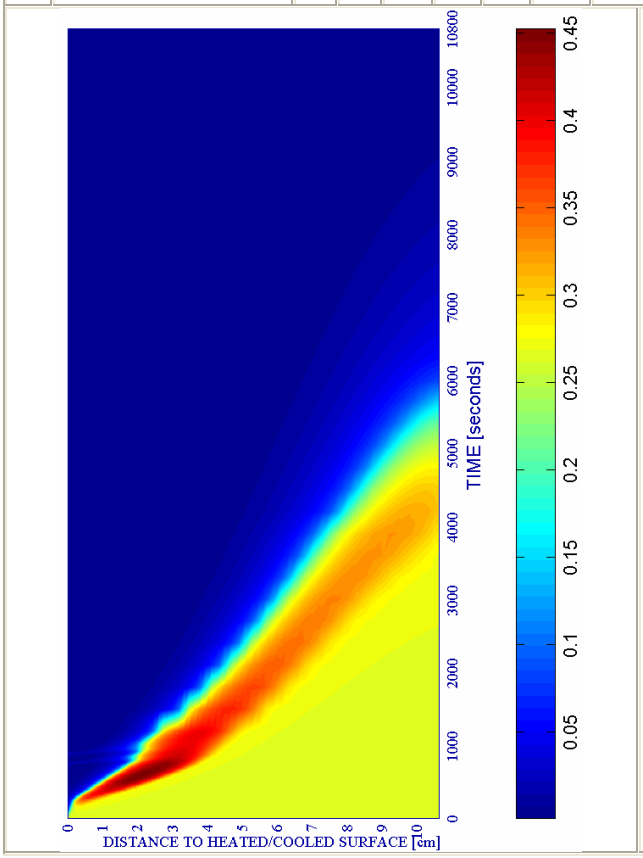

Figure 6-87. (continued)

h) Relative Humidity RH [-]

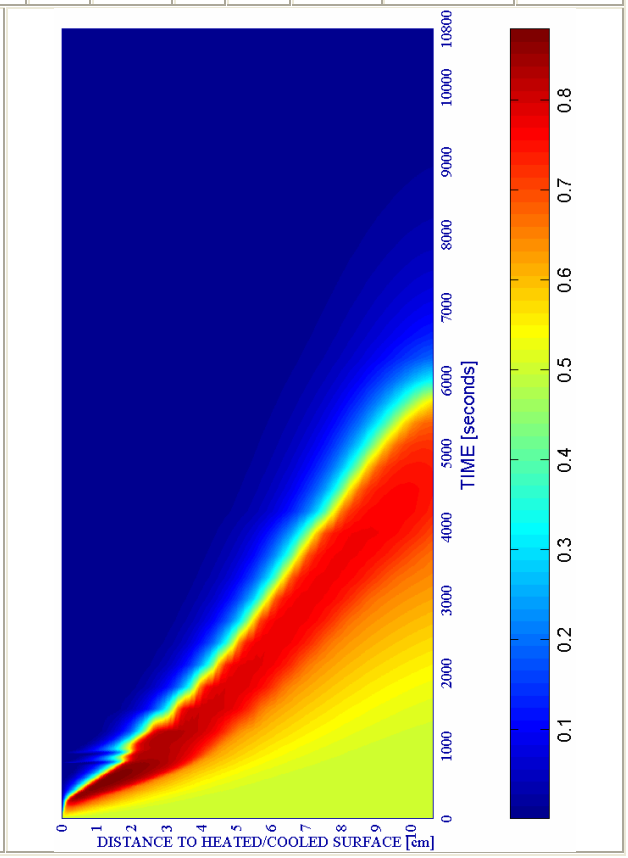

i) Temperature [K]

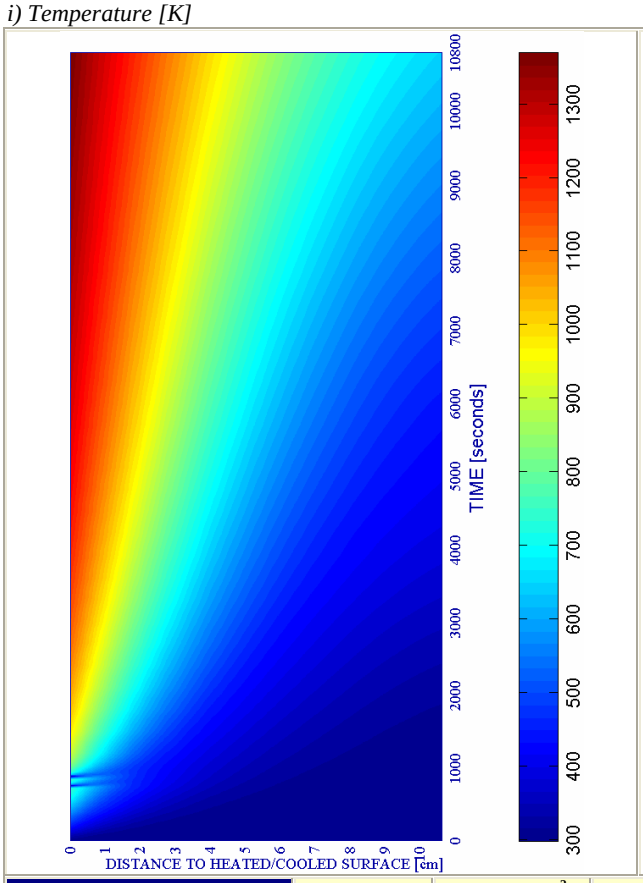

*j) Elastic Energy U · **10^{-4}** [J/m^3]*

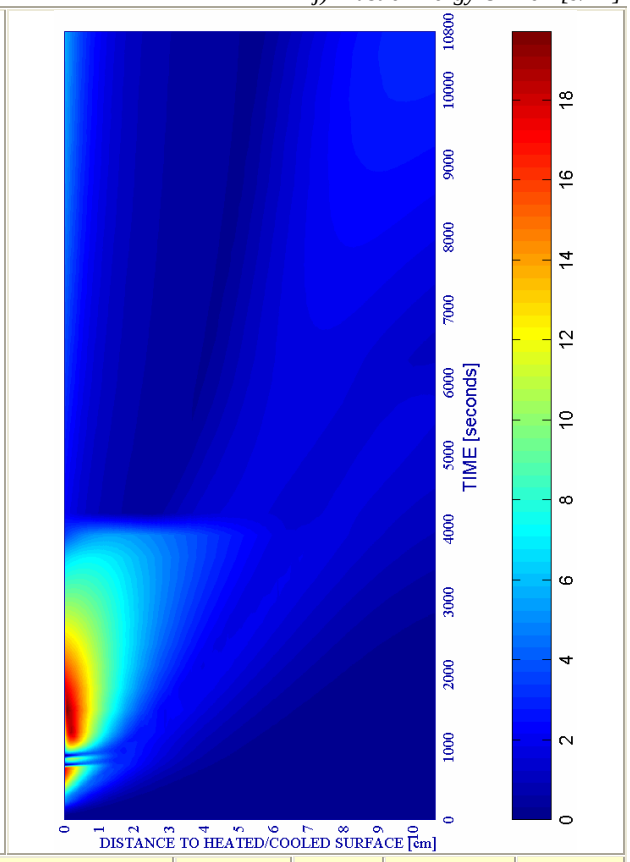

SURFACE COOL+REPEAT		PC1 - RH [%]			PC2 - K_0 [m^2]			PC4 - Heating curve			PC5 – Mat.		Cooling length[s]	Start of cooling [s]	End of cooling [s]
#	Combination	40	50	60	10^{-19}	10^{-18}	10^{-17}	PAR1	PAR2	PAR4	C60	C90			
05	TH12K018RH50PAR1C60		X			X		X			X		40 / 46	600+120 / 840	760 / 886

*k) Stress in longitudinal (xx) direction · **10^{-6}** [Pa]*

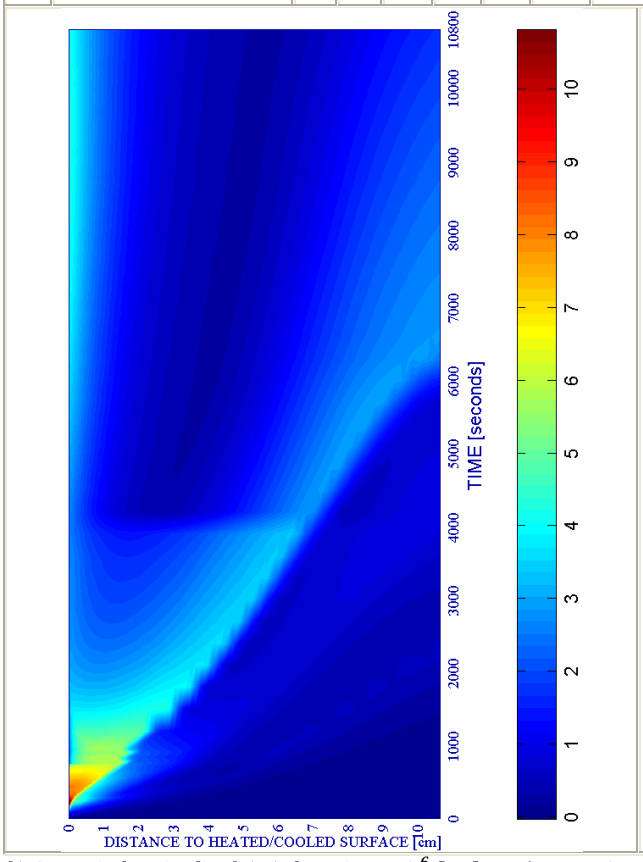

Figure 6-87. (continued)

*l) Stress in transversal (yy) direction · **10^{-7}** [Pa]*

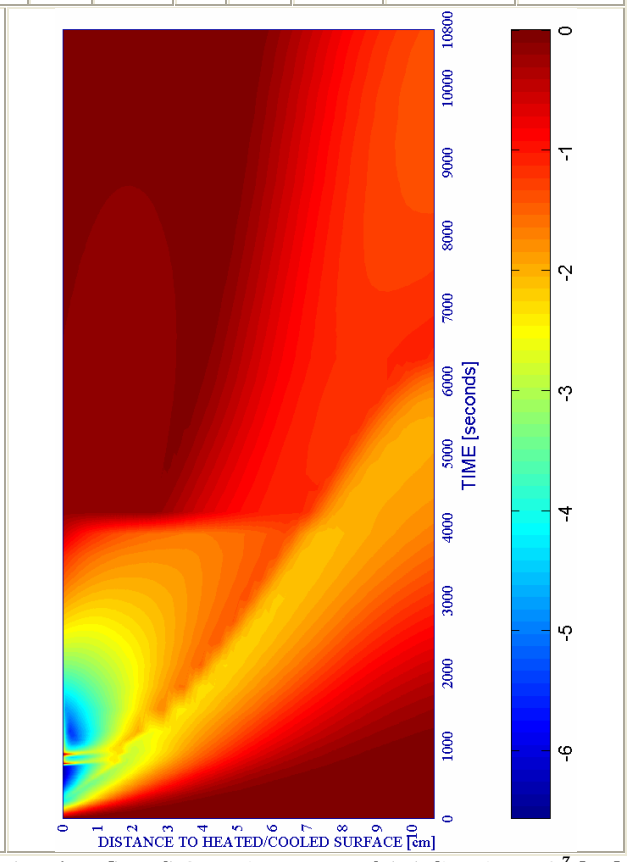

6.5.2.1.7 Environmental Heating up to Three Hours Without any Cooling

Phenomenological and mechanistic analysis of this case is not qualitatively different from those corresponding to the heating stages analyzed within last paragraphs. However, the results exposed herein will be extremely useful for comparison purposes as it is detailed and dealt in depth on paragraph 6.5.3 of this chapter.

Next it is shown a collection of the main results cited in this subparagraph, as well as a description of each of the stages that compose the heating process analyzed herein.

Table 6-48. *Description of the Cooling Process Stages and Collection of the Main Results related to Spalling Index and velocity*

Stage description	Absolute Time Start [s]	Absolute Time End [s]	$IS4_{max}$ [-]	X_{IS4max} [cm]	t_{IS4max} [s]	v_{max} [m/s]	X_{vmax} [cm]	t_{vmax} [s]	v_{max}* [m/s]	X_{vmax*} [cm]	t_{vmax*} [s]
Heating up to 10.800s	0	10.800	0,3688	0,582	600	12,349	0,152	240	9,521	0,245	280

Remark †***:*** *These results are included for the Comparative Analysis developed on Paragraph 6.5.3*

Stage description	Absolute Time Start [s]	Absolute Time End [s]	d_{max} [-]	X_{dmax} [cm]	t_{dmax} [s]	T_{max} [K]	X_{Tmax} [cm]	t_{Tmax} [s]	p^g_{max} [MPa]	X_{pgmax} [cm]	t_{pgmax} [s]
Heating up to 10.800s	0	10.800	0,9908	0 – 2,258	4.000	1.369,20	0,000	10.800	1,3276	0,860	480

Table 6-49. *Description of the Cooling Process Stages and Collection of the Main Results related to mechanical damage, Temperature and Gas Pressure*

As it is shown on figure 6-88, beyond the Mechanical Damage maximum – values that appear on last table at depths up to 2,258 centimetres – Total Damage values are increased by Thermo-Chemical Damage (which reaches values higher than 0,53) so Total Damage at the end of the three hours heating process has reached the maximum possible value – 0,99 – at a layer corresponding exactly to half the total thickness of the structural element – 6 centimetres from 12 – so half the structural element will be completely destroyed exposing reinforcing bars to fire action. The other half of the structural element will also present extremely high values of the Total Damage, above the 82 per cent.

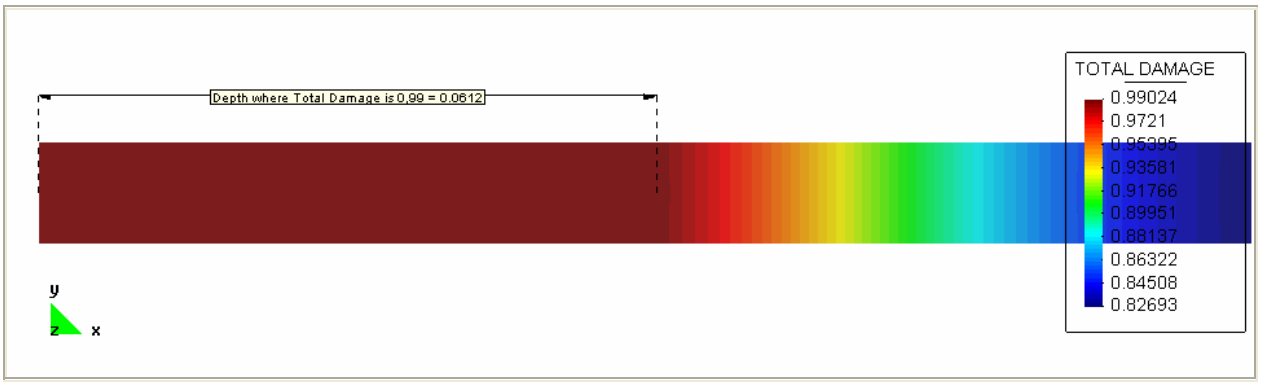

Figure 6-88. *Total Damage D [-] at the structural element at the end of the heating process without any cooling (time: 10.800 seconds)*

It is also remarkable that the maximum temperature achieved in this process (1.369,2 K) matches that corresponding to the process including one or two surface cooling intermediate stages. This fact initially suggests a rather local effect of the surface cooling processes considered in this chapter.

On figures 6-89 a) to l) it is shown a collection of twelve Time-Space graphics representing the evolution of all of the parameters cited in the last subparagraph and for all of the stages that compose the heating and cooling processes analyzed herein.

a) Spalling Index IS4 [-] *b) Mechanical damage d [-]*

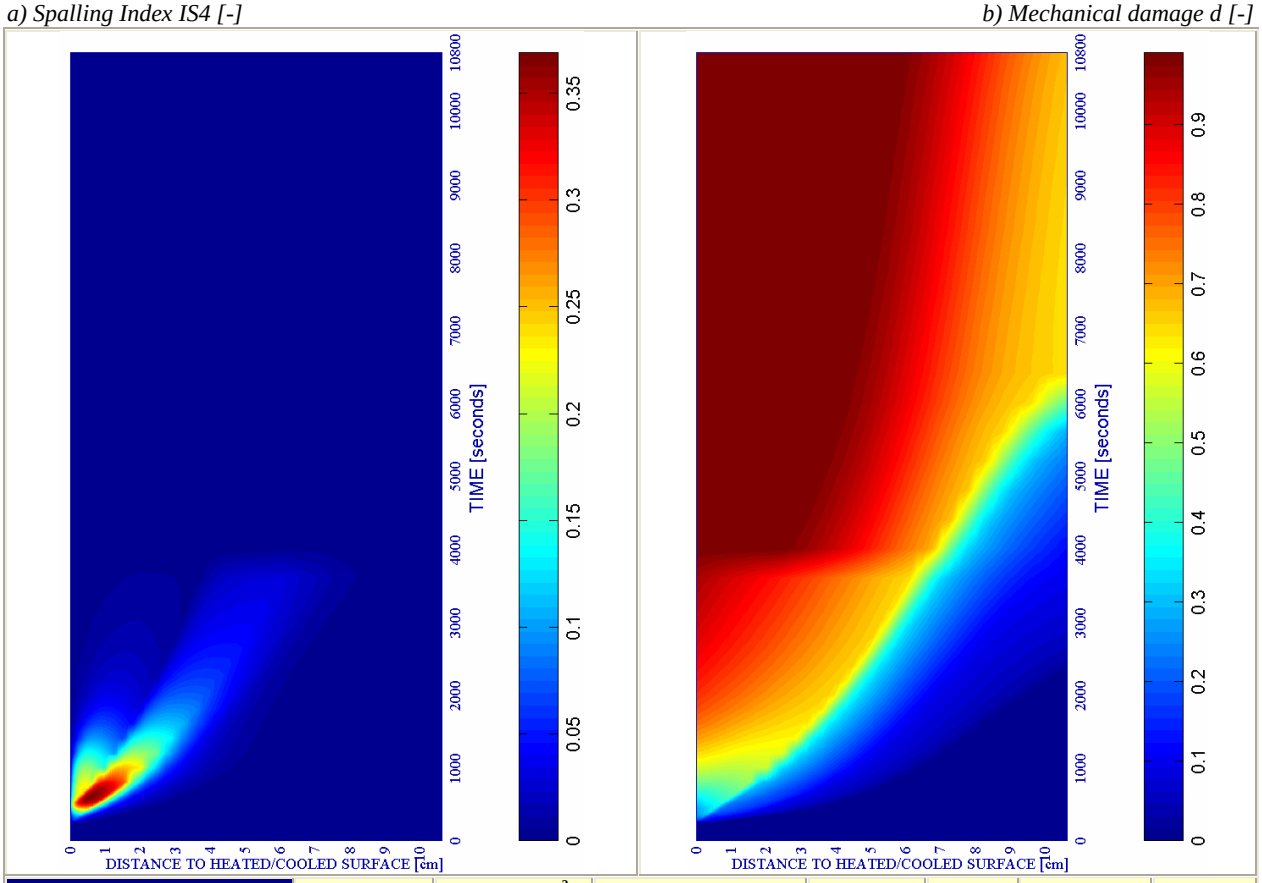

WITHOUT COOLING		PC1 - RH [%]			PC2 - K_0 [m^2]			PC4 - Heating curve			PC5 – Mat.		Cooling length[s]	Start of cooling [s]	End of cooling [s]
#	Combination	40	50	60	10^{-19}	10^{-18}	10^{-17}	PAR1	PAR2	PAR4	C60	C90			
05	TH12K018RH50PAR1C60		X			X		X			X		---	---	---

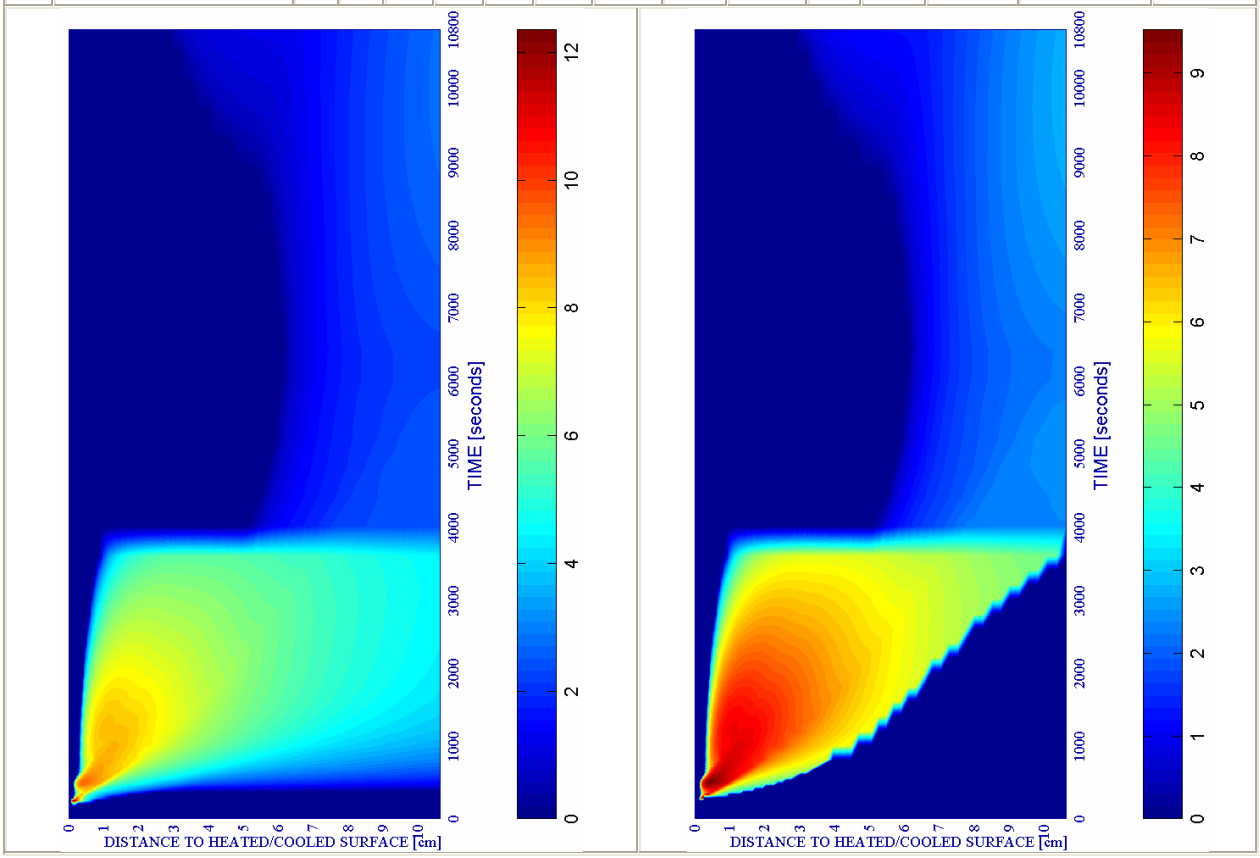

c) Velocity of spalled pieces v [m/s] ***Figure 6-89.*** *d) Velocity [m/s] where d ≥ 0,10*

e) Gas pressure $p^g \cdot 10^{-5}$ [Pa]

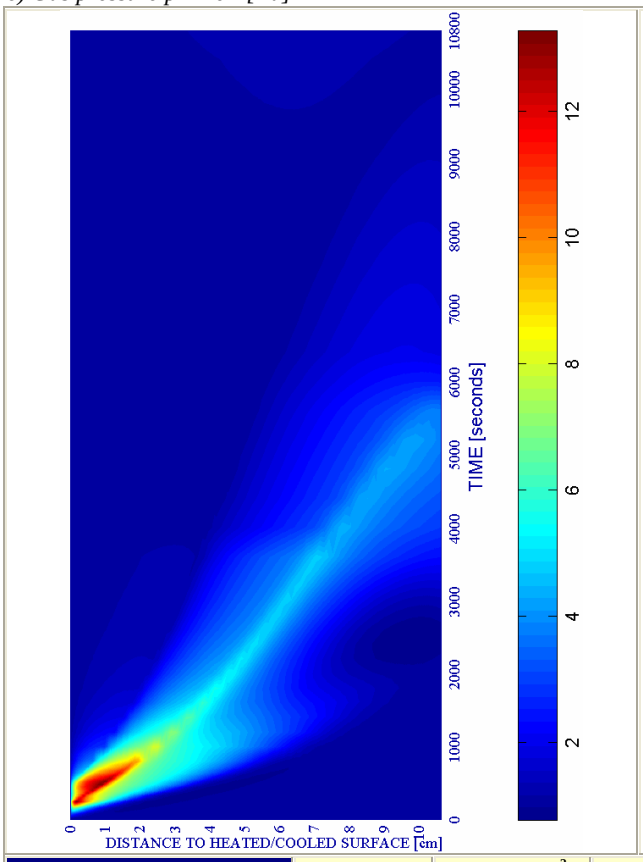

f) Vapour pressure $p^v \cdot 10^{-5}$ [Pa]

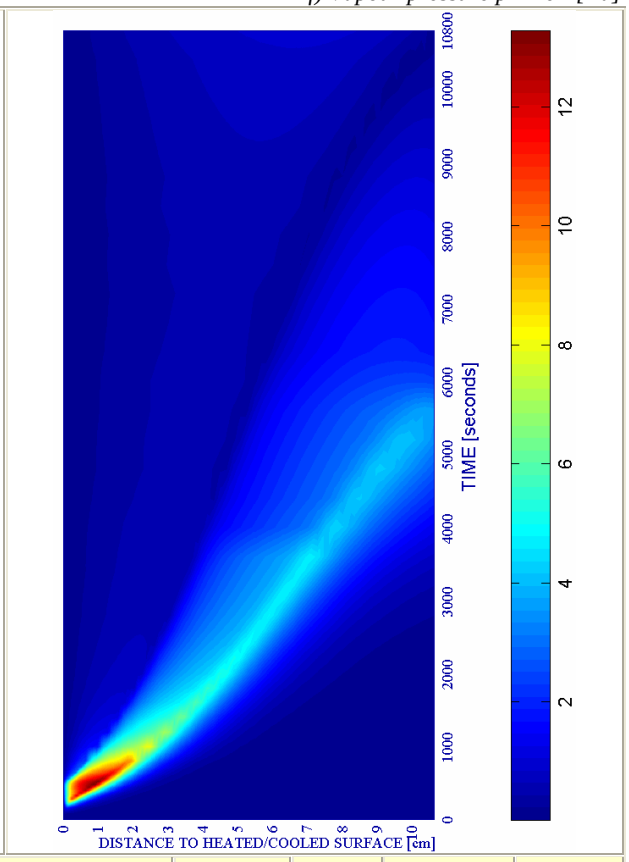

WITHOUT COOLING		PC1 - RH [%]			PC2 - K_0 [m^2]			PC4 - Heating curve			PC5 – Mat.		Cooling length[s]	Start of cooling [s]	End of cooling [s]
#	Combination	40	50	60	10^{-19}	10^{-18}	10^{-17}	PAR1	PAR2	PAR4	C60	C90			
05	TH12K018RH50PAR1C60		X			X		X			X		---	---	---

g) Saturation Degree S [-]

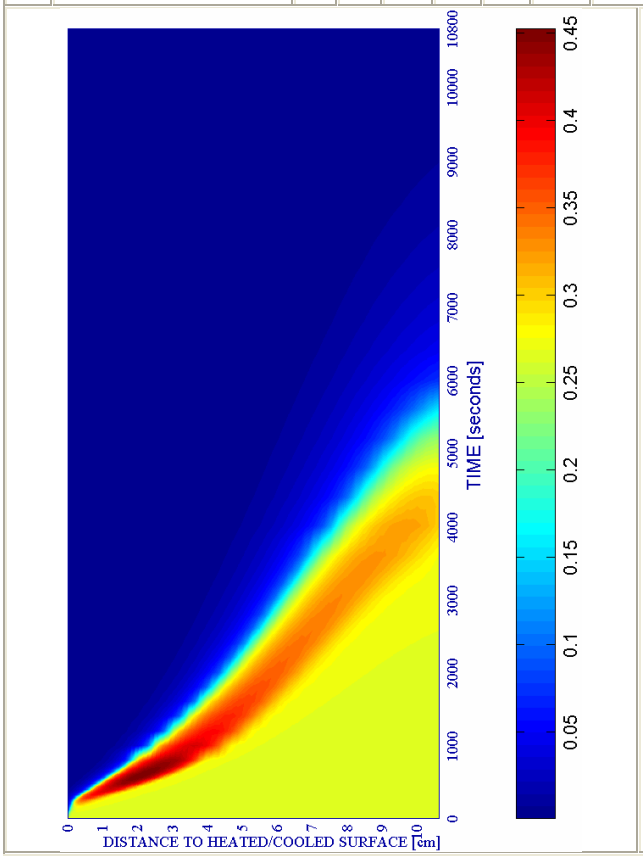

Figure 6-89. (continued)

h) Relative Humidity RH [-]

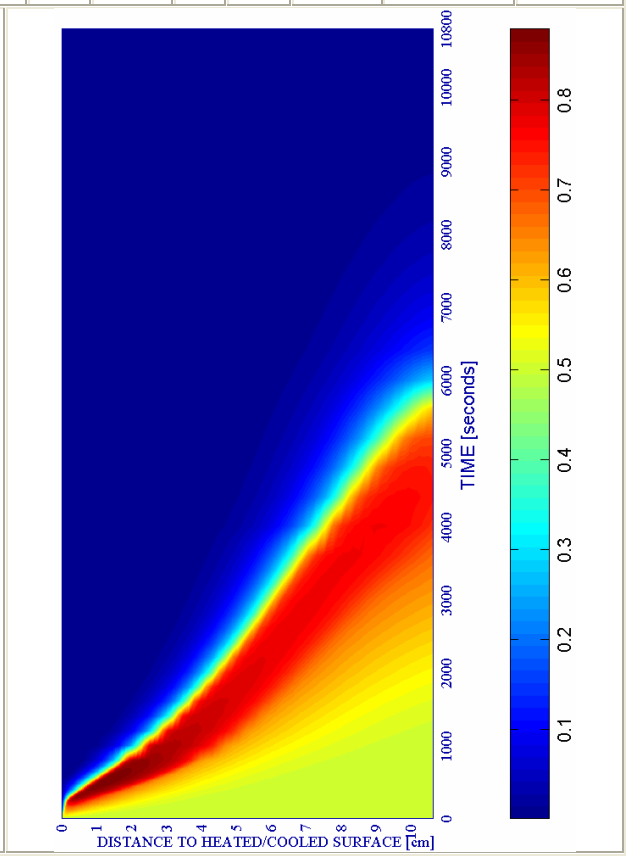

i) Temperature [K]

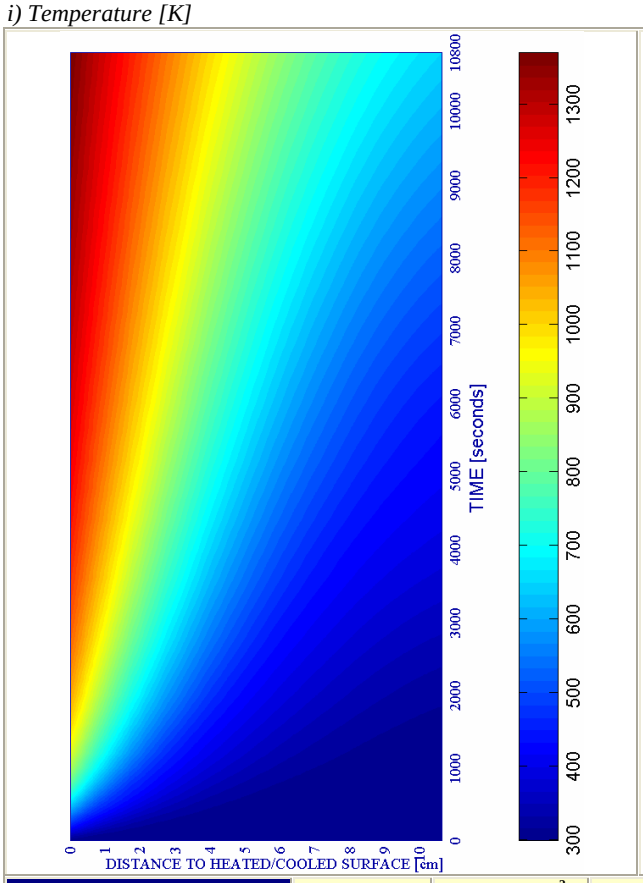

*j) Elastic Energy U · **10**$^{-4}$ [J/m^3]*

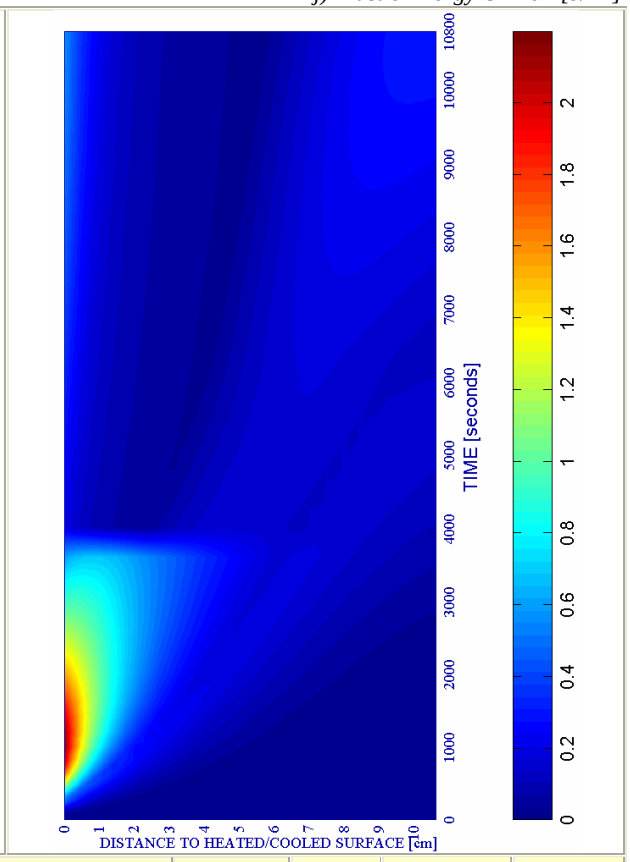

WITHOUT COOLING		PC1 - RH [%]			PC2 - K_0 [m^2]			PC4 - Heating curve			PC5 – Mat.		Cooling length[s]	Start of cooling [s]	End of cooling [s]
#	Combination	40	50	60	10^{-19}	10^{-18}	10^{-17}	PAR1	PAR2	PAR4	C60	C90			
05	TH12K018RH50PAR1C60		X			X		X			X		---	---	---

*k) Stress in longitudinal (xx) direction · **10**$^{-6}$ [Pa]*

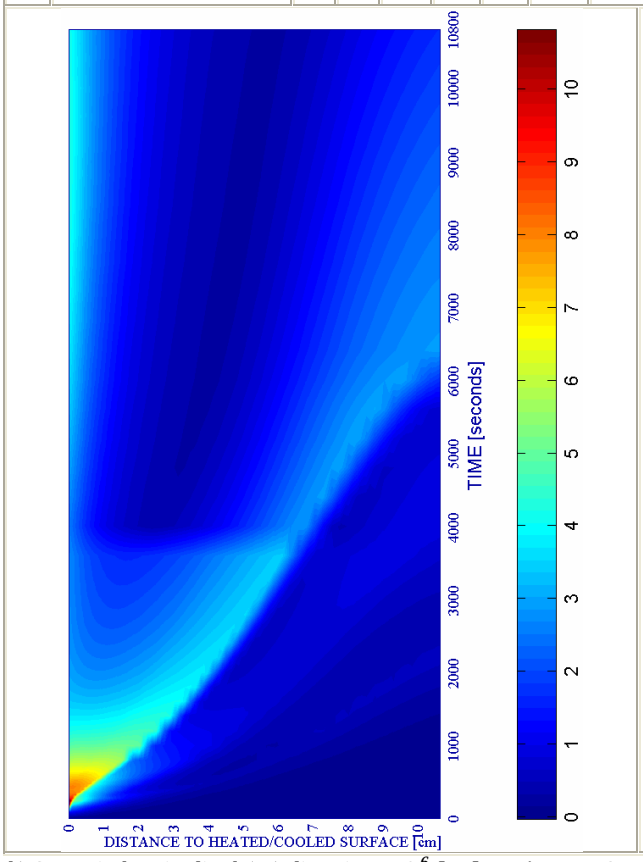

Figure 6-89. (continued)

*l) Stress in transversal (yy) direction · **10**$^{-7}$ [Pa]*

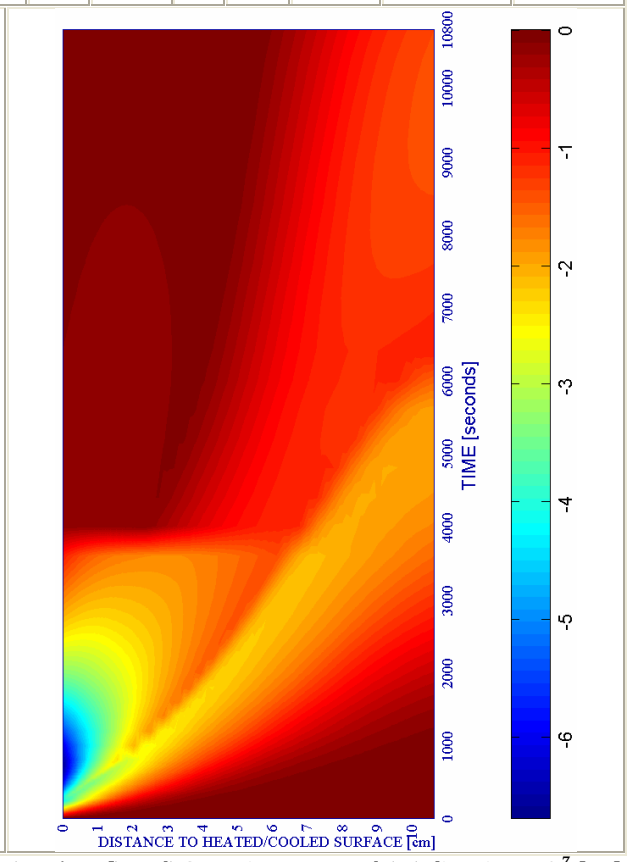

6.5.2.2 REFERENCE CASE # 14 – TH12K018RH50PAR2C60 – START OF COOLING: 1.800S

The main features of this reference case are the following ones:

		PC1 (RH) [%]			PC2 (K) [m^2]			PC3 (TH) [cm]			PC4 (Heating curve)			PC5 (Mat)	
#	**Combination**	**40**	**50**	**60**	10^{-19}	10^{-18}	10^{-17}	**12**	**24**	**50**	**PAR1**	**PAR2**	**PAR3**	**C60**	**C90**
14	TH12K018RH50PAR2C60		X			X		X				X		X	

Table 6-50. *Main Features of the Reference Case #14 – TH12K018RH50PAR2C60.*

with an starting instant of the first cooling process at 1.800 seconds. The types and subtypes of cooling processes analyzed in this reference case are the following ones:

Type of Cooling	***Subtype of Cooling***	***Related Paragraph***	***Figures numbers***
Environmental	Slow Cooling	6.5.2.2.1	6-90 a) to l)
Environmental	Medium Cooling	6.5.2.2.2	6-91 a) to l)
Environmental	Fast Cooling	6.5.2.2.3	6-92 a) to l)
Surface	Followed by Heating	6.5.2.2.4	6-93 a) to l)
Surface	Followed by an imposed constant Surface Temperature	6.5.2.2.5	6-94 a) to l)
Surface	Divided into Two Periods	6.5.2.2.6	6-95 a) to l)

Remark: *See each Paragraph for more details on the features of the Cooling Processes.*

Table 6-51. *Types and Subtypes of Cooling Processes Analyzed in the Reference Case #14 – TH12K018RH50PAR2C60 with the Start of Cooling Process at 1.800 seconds*

As it was explained on paragraph 6.5.2 this case shows the start instant of cooling processes as the only input difference with respect to the case analyzed deeply on paragraph 6.5.2.5. Therefore, herein are exposed the main results of this case but they are dealt in depth on *paragraph 6.5.3.2 – Analysis of the Effect of the Cooling Start Instant.*

6.5.2.2.1 Environmental Slow Cooling

Table 6-52. *Description of the Cooling Process Stages and Collection of the Main Results related to Spalling Index and velocity.*

Stage description - figure 6-90 a) to l) -	**Absolute Time Start [s]**	**Absolute Time End [s]**	$IS4_{max}$ [-]	X_{IS4max} [cm]	t_{IS4max} [s]	v_{max} [m/s]	X_{vmax} [cm]	t_{vmax} [s]	v_{max}* [m/s]	X_{vmax*} [cm]	t_{vmax*} [s]
First Heating	0	1.800+120	0,0129	0,227	1.920	0,000	---	---	0,000	---	---
Environment cooling	1.920	2.760	0,0129	0,227	1.920	0,000	---	---	0,000	---	---
Environment constant Temperature up to an absolute time 10.800s	2.760	10.800	0,0003	1,099	2.760	0,000	---	---	0,000	---	---
Environment Constant Temperature for t > 10.800s	10.800	74.760	0,0000	---	---	0,000	---	---	0,000	---	---
Maximum for $t \leq 10.800s^{\dagger}$	0	10.800	0,0129	0,227	1.920	0,000	---	---	0,000	---	---
Absolute Maximum	0	74.760	0,0129	0,227	1.920	0,000	---	---	0,000	---	---

Remark †***:*** *These results are included for the Comparative Analysis developed on Paragraph 6.5.3*

Stage description - figure 6-90 a) to l) -	**Absolute Time Start [s]**	**Absolute Time End [s]**	d_{max} [-]	X_{dmax} [cm]	t_{dmax} [s]	T_{max} [K]	X_{Tmax} [cm]	t_{Tmax} [s]	p^g_{max} [MPa]	X_{pgmax} [cm]	t_{pgmax} [s]
First Heating	0	1.800+120	0,3718	0,210	1.920	467,16	0,000	1.920	0,5967	0,582	1.920
Environment cooling	1.920	2.760	0,5606	0,000	2.760	467,16	0,000	1.920	0,5967	0,582	1.920
Environment constant Temperature up to an absolute time 10.800s	2.760	10.800	0,6634	0,412	6.360	372,05	0,808	2.760	0,2821	1,644	2.760
Environment Constant Temperature for t > 10.800s	10.800	74.760	0,6634	0,412	10.800	328,00	4,683	10.800	0,1807	10,092	10.800
Maximum for $t \leq 10.800s^{\dagger}$	0	10.800	0,6634	0,412	6.360	467,16	0,000	1.920	0,5967	0,582	1.920
Absolute Maximum	0	74.760	0,6634	0,412	6.360	467,16	0,000	1.920	0,5967	0,582	1.920

Table 6-53. *Description of the Cooling Process Stages and Collection of the Main Results related to mechanical damage, Temperature and Gas Pressure.*

*a) Spalling Index IS4 · **10**^{3} [-]* *b) Mechanical damage d [-]*

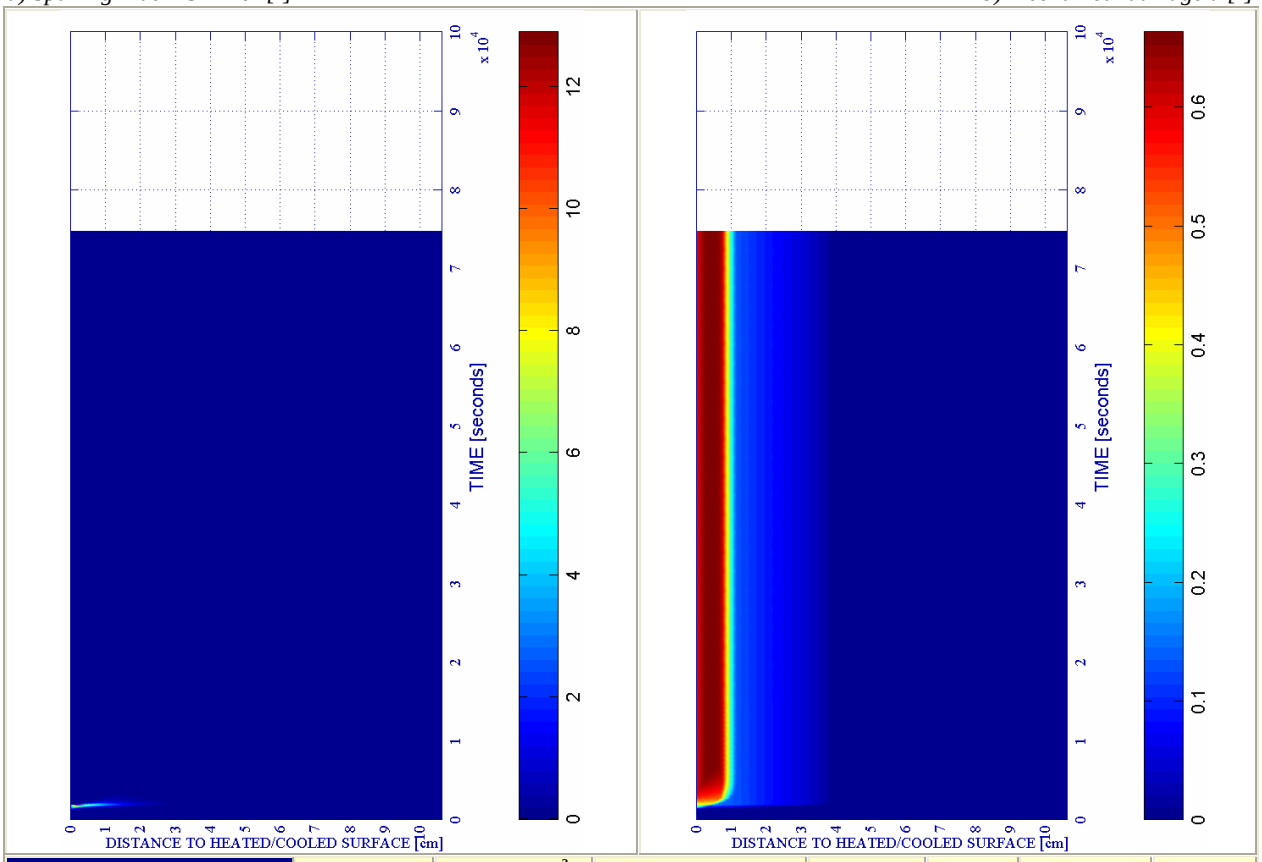

ENVIRONMENTAL - SLOW		PC1 - RH [%]			PC2 - K_0 [m^2]			PC4 - Heating curve			PC5 – Mat.		Cooling length[s]	Start of cooling [s]	End of cooling [s]
#	Combination	40	50	60	10^{-19}	10^{-18}	10^{-17}	PAR1	PAR2	PAR4	C60	C90			
14	TH12K018RH50PAR2C60		X			X			X		X		840	1.800+120	2.760

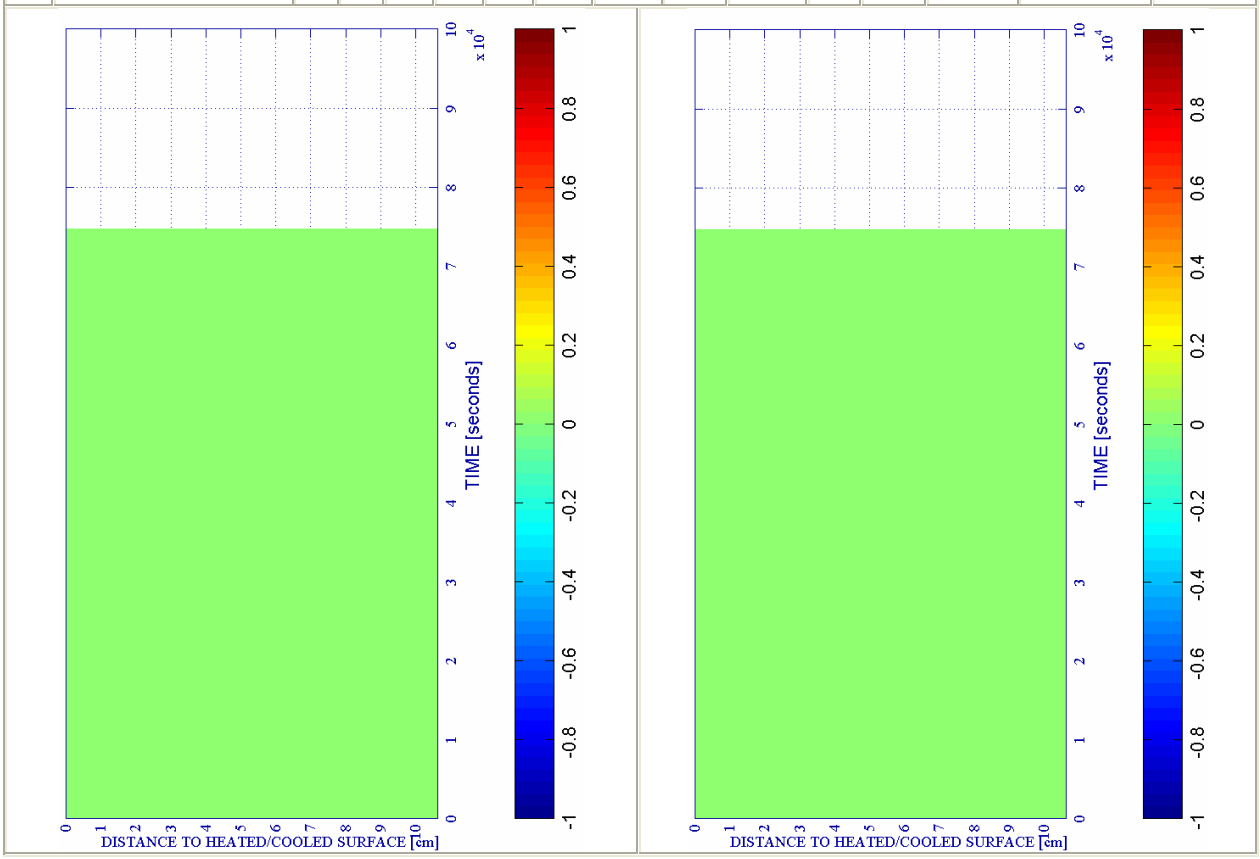

c) Velocity of spalled pieces v [m/s] ***Figure 6-90.*** *d) Velocity [m/s] where d ≥ 0,10*

e) Gas pressure $p^g \cdot 10^{-5}$ [Pa]

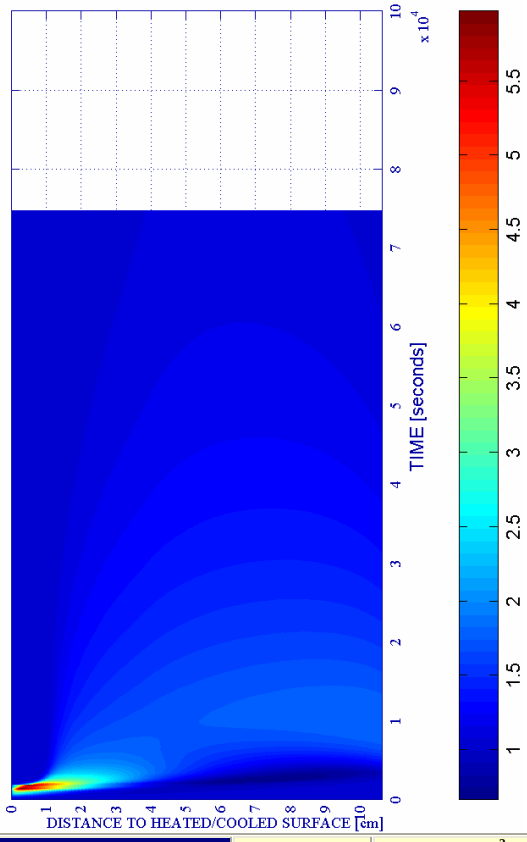

f) Vapour pressure $p^v \cdot 10^{-5}$ [Pa]

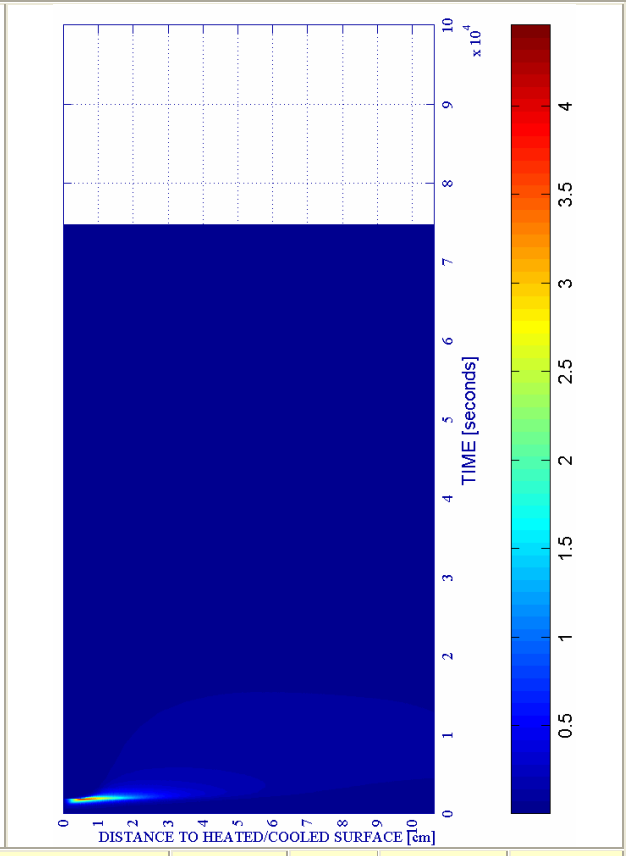

ENVIRONMENTAL - SLOW	PC1 - RH [%]			PC2 - K_0 [m^2]			PC4 - Heating curve			PC5 – Mat.		Cooling length[s]	Start of cooling [s]	End of cooling [s]
#	Combination	40	50	60	10^{-19}	10^{-18}	10^{-17}	PAR1	PAR2	PAR4	C60	C90			
14	TH12K018RH50PAR2C60		X			X			X		X		840	1.800+120	2.760

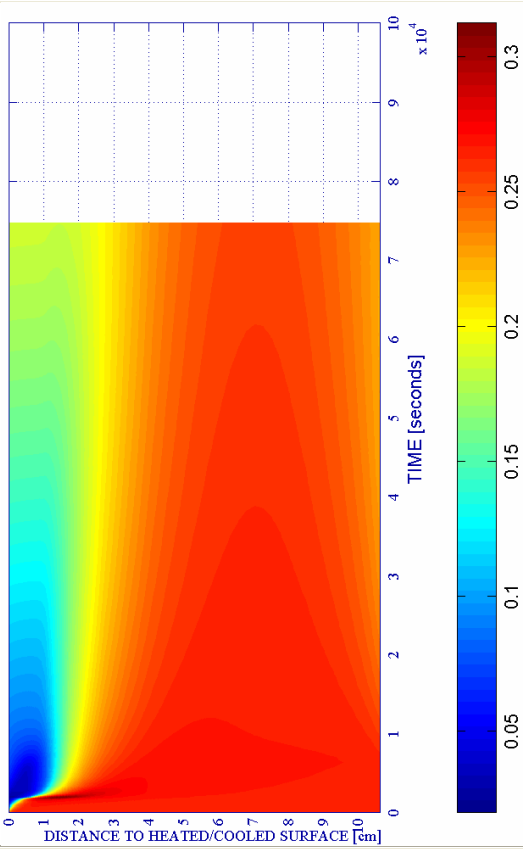

g) Saturation Degree S [-]

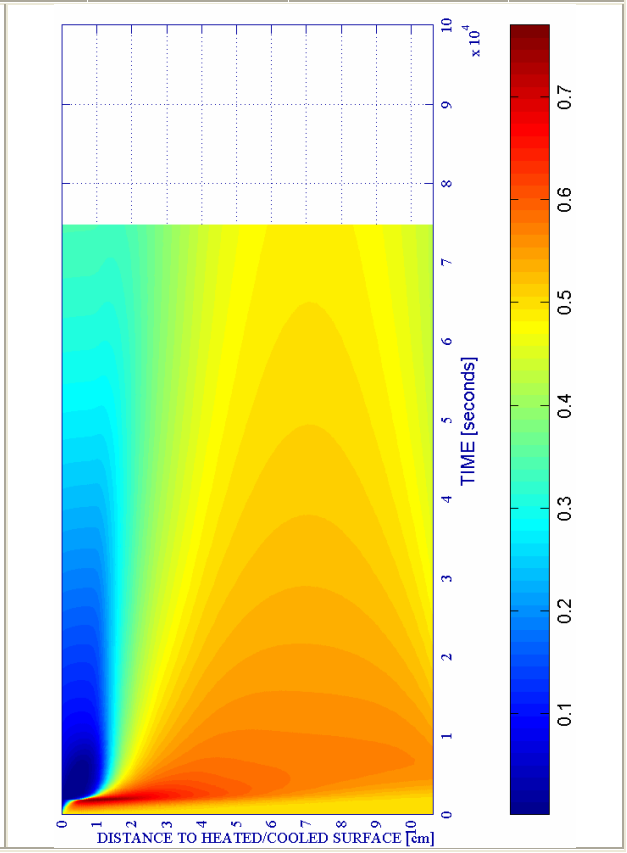

h) Relative Humidity RH [-]

Figure 6-90. (continued)

i) Temperature [K]

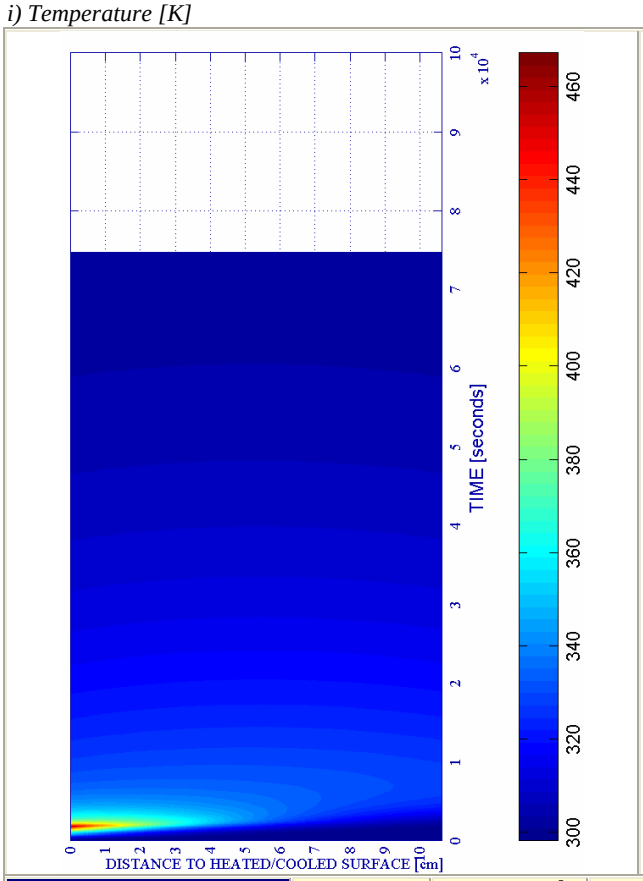

*j) Elastic Energy U · **10**$^{-4}$ [J/m^3]*

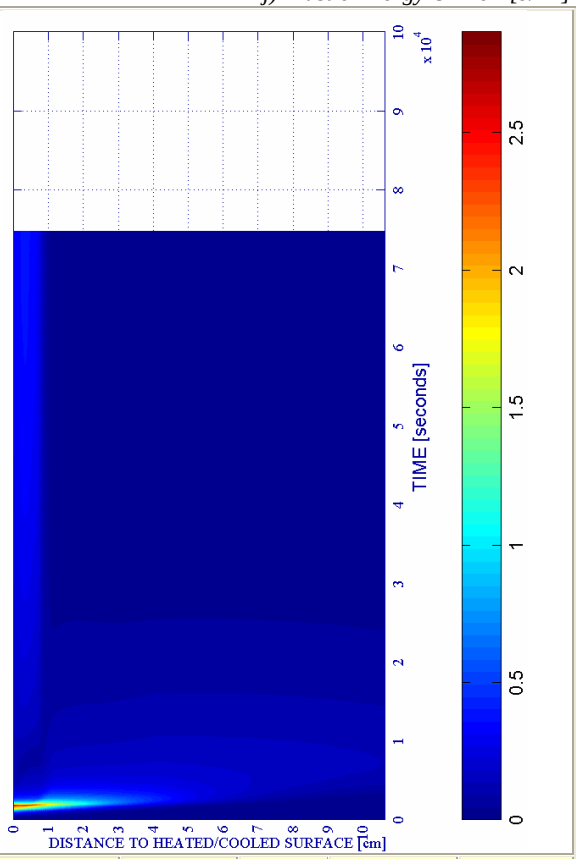

ENVIRONMENTAL - SLOW	PC1 - RH [%]			PC2 - K_0 [m^2]			PC4 - Heating curve			PC5 – Mat.		Cooling length[s]	Start of cooling [s]	End of cooling [s]
#	Combination	40	50	60	10^{-19}	10^{-18}	10^{-17}	PAR1	PAR2	PAR4	C60	C90			
14	TH12K018RH50PAR2C60		X			X			X		X		840	1.800+120	2.760

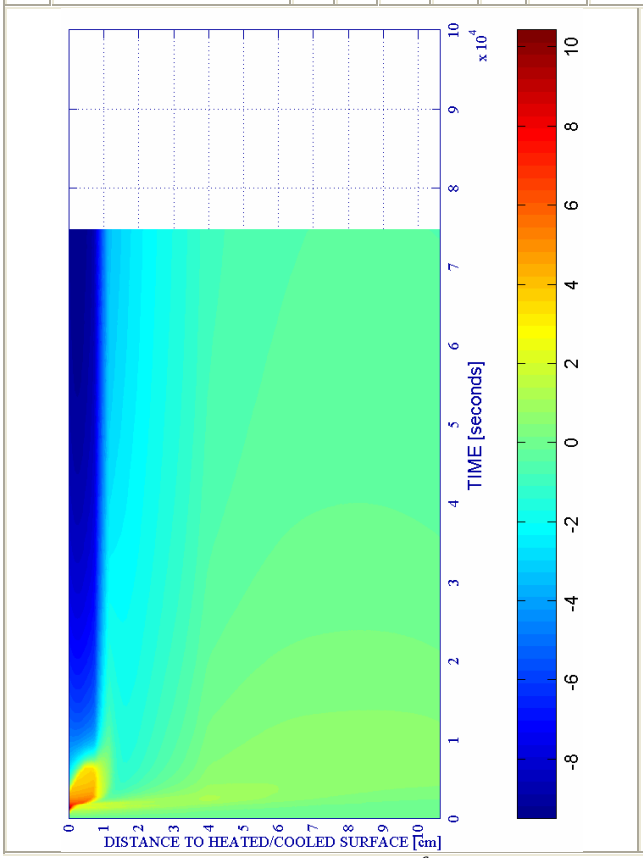

*k) Stress in longitudinal (xx) direction · **10**$^{-6}$ [Pa]*

Figure 6-90. (continued)

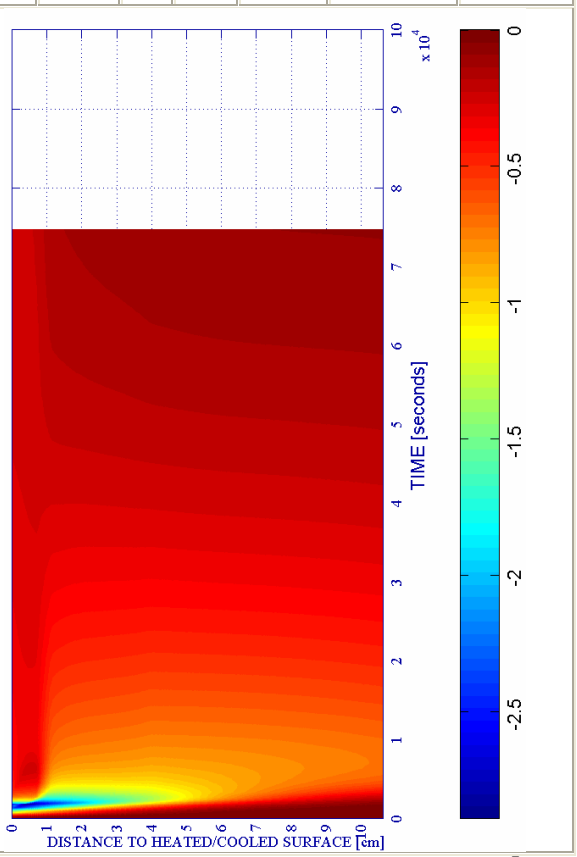

*l) Stress in transversal (yy) direction · **10**$^{-7}$ [Pa]*

6.5.2.2.2 Environmental Medium Cooling

Table 6-54. *Description of the Cooling Process Stages and Collection of the Main Results related to Spalling Index and velocity*

Stage description - figure 6-91 a) to l) -	**Absolute Time Start [s]**	**Absolute Time End [s]**	**$IS4_{max}$ [-]**	**X_{IS4max} [cm]**	**t_{IS4max} [s]**	**v_{max} [m/s]**	**X_{vmax} [cm]**	**t_{vmax} [s]**	**v_{max}* [m/s]**	**X_{vmax*} [cm]**	**t_{vmax*} [s]**
First Heating	0	1.800+120	0,0129	0,227	1.920	0,000	---	---	0,000	---	---
Environment cooling	1.920	2.004	0,0129	0,227	1.920	0,000	---	---	0,000	---	---
Environment constant Temperature up to an absolute time 10.800s	2.004	10.800	0,0034	0,710	2.004	0,000	---	---	0,000	---	---
Environment Constant Temperature for t > 10.800s	10.800	74.004	0,0000	---	---	0,000	---	---	0,000	---	---
Maximum for t ≤ 10.800s†	0	10.800	0,0129	0,227	1.920	0,000	---	---	0,000	---	---
Absolute Maximum	0	74.004	0,0129	0,227	1.920	0,000	---	---	0,000	---	---

Remark †: *These results are included for the Comparative Analysis developed on Paragraph 6.5.3*

Stage description - figure 6-91 a) to l) -	**Absolute Time Start [s]**	**Absolute Time End [s]**	**d_{max} [-]**	**X_{dmax} [cm]**	**t_{dmax} [s]**	**T_{max} [K]**	**X_{Tmax} [cm]**	**t_{Tmax} [s]**	**p^g_{max} [MPa]**	**X_{pgmax} [cm]**	**t_{pgmax} [s]**
First Heating	0	1.800+120	0,3718	0,210	1.920	467,16	0,000	1.920	0,5967	0,582	1.920
Environment cooling	1.920	2.004	0,4323	0,000	2.004	467,16	0,000	1.920	0,5970	0,623	1.924
Environment constant Temperature up to an absolute time 10.800s	2.004	10.800	0,6641	0,412	10.800	422,59	0,245	2.004	0,4845	0,860	2.004
Environment Constant Temperature for t > 10.800s	10.800	74.004	0,6641	0,412	10.800	327,74	4,683	10.800	0,1796	10,092	10.800
Maximum for t ≤ 10.800s†	0	10.800	0,6641	0,412	6.360	467,16	0,000	1.920	0,5970	0,623	1.924
Absolute Maximum	0	74.004	0,6641	0,412	6.360	467,16	0,000	1.920	0,5970	0,623	1.924

Table 6-55. *Description of the Cooling Process Stages and Collection of the Main Results related to mechanical damage, Temperature and Gas Pressure*

6.5.2.2.3 Environmental Fast Cooling

Table 6-56. *Description of the Cooling Process Stages and Collection of the Main Results related to Spalling Index and velocity*

Stage description - figure 6-92 a) to l) -	**Absolute Time Start [s]**	**Absolute Time End [s]**	**$IS4_{max}$ [-]**	**X_{IS4max} [cm]**	**t_{IS4max} [s]**	**v_{max} [m/s]**	**X_{vmax} [cm]**	**t_{vmax} [s]**	**v_{max}* [m/s]**	**X_{vmax*} [cm]**	**t_{vmax*} [s]**
First Heating	0	1.800+120	0,0129	0,227	1.920	0,000	---	---	0,000	---	---
Environment cooling	1.920	1.928	0,0129	0,227	1.920	0,000	---	---	0,000	---	---
Environment constant Temperature up to an absolute time 10.800s	1.928	10.800	0,0089	0,357	1.928	0,000	---	---	0,000	---	---
Environment Constant Temperature for t > 10.800s	10.800	73.928	0,0000	---	---	0,000	---	---	0,000	---	---
Maximum for t ≤ 10.800s†	0	10.800	0,0129	0,227	1.920	0,000	---	---	0,000	---	---
Absolute Maximum	0	73.928	0,0129	0,227	1.920	0,000	---	---	0,000	---	---

Remark †: *These results are included for the Comparative Analysis developed on Paragraph 6.5.3*

Stage description - figure 6-92 a) to l) -	**Absolute Time Start [s]**	**Absolute Time End [s]**	**d_{max} [-]**	**X_{dmax} [cm]**	**t_{dmax} [s]**	**T_{max} [K]**	**X_{Tmax} [cm]**	**t_{Tmax} [s]**	**p^g_{max} [MPa]**	**X_{pgmax} [cm]**	**t_{pgmax} [s]**
First Heating	0	1.800+120	0,3718	0,210	1.920	467,16	0,000	1.920	0,5967	0,582	1.920
Environment cooling	1.920	1.928	0,3810	0,000	1.928	467,16	0,000	1.920	0,5967	0,582	1.920
Environment constant Temperature up to an absolute time 10.800s	1.928	10.800	0,6634	0,412	6.728	451,45	0,075	1.928	0,5952	0,623	1.928
Environment Constant Temperature for t > 10.800s	10.800	73.928	0,6634	0,412	10.800	327,90	4,875	10.800	0,1799	10,092	10.800
Maximum for t ≤ 10.800s†	0	10.800	0,6634	0,412	6.728	467,16	0,000	1.920	0,5967	0,582	1.920
Absolute Maximum	0	73.928	0,6634	0,412	6.728	467,16	0,000	1.920	0,5967	0,582	1.920

Table 6-57. *Description of the Cooling Process Stages and Collection of the Main Results related to mechanical damage, Temperature and Gas Pressure*

*a) Spalling Index IS4 · **10**^{3} [-]*

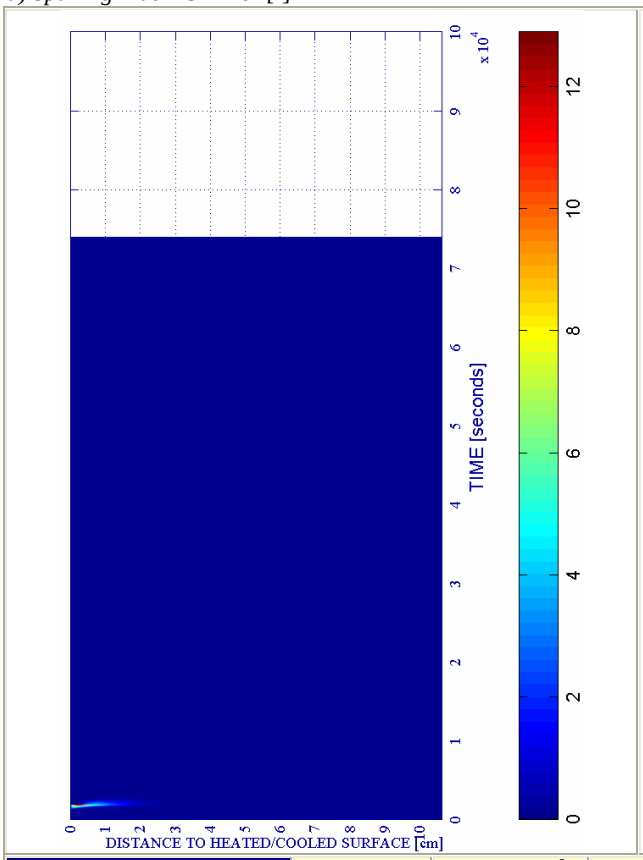

b) Mechanical damage d [-]

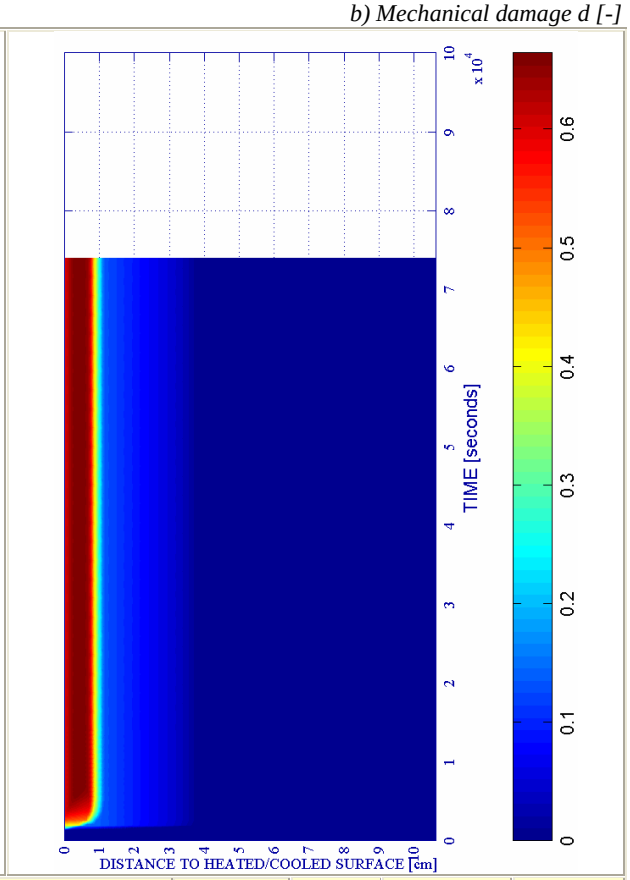

ENVIRONMENTAL - MED.		PC1 - RH [%]			PC2 - K_0 [m^2]			PC4 - Heating curve			PC5 – Mat.		Cooling length[s]	Start of cooling [s]	End of cooling [s]
#	Combination	40	50	60	10^{-19}	10^{-18}	10^{-17}	PAR1	PAR2	PAR4	C60	C90			
14	TH12K018RH50PAR2C60		X			X			X		X		84	1.800+120	2.004

c) Velocity of spalled pieces v [m/s]

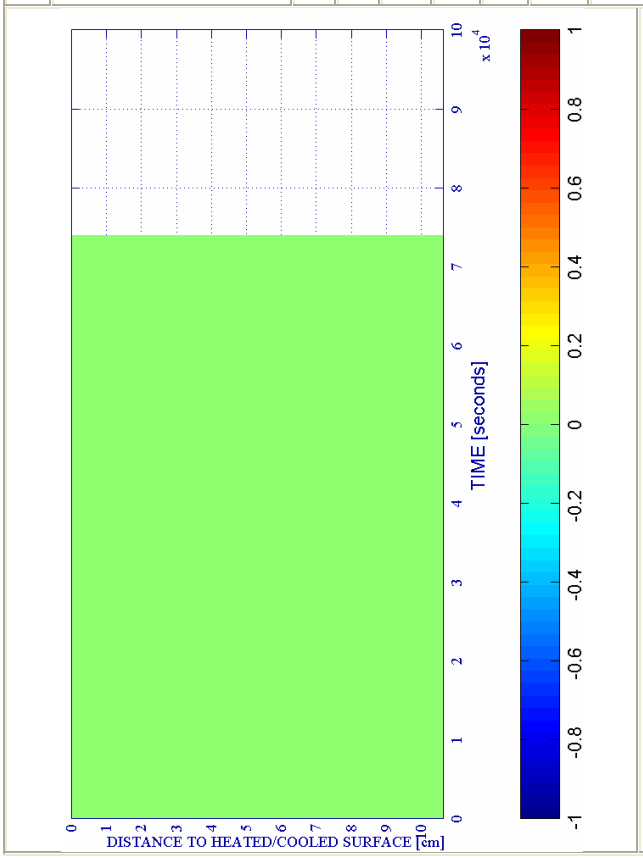

d) Velocity [m/s] where d ≥ 0,10

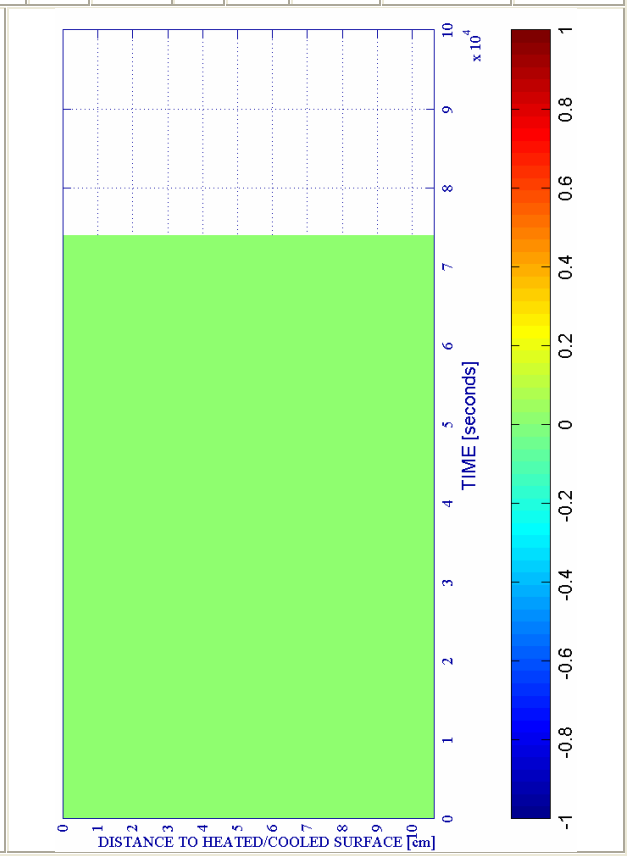

Figure 6-91.

e) Gas pressure $p^g \cdot 10^{-5}$ [Pa]

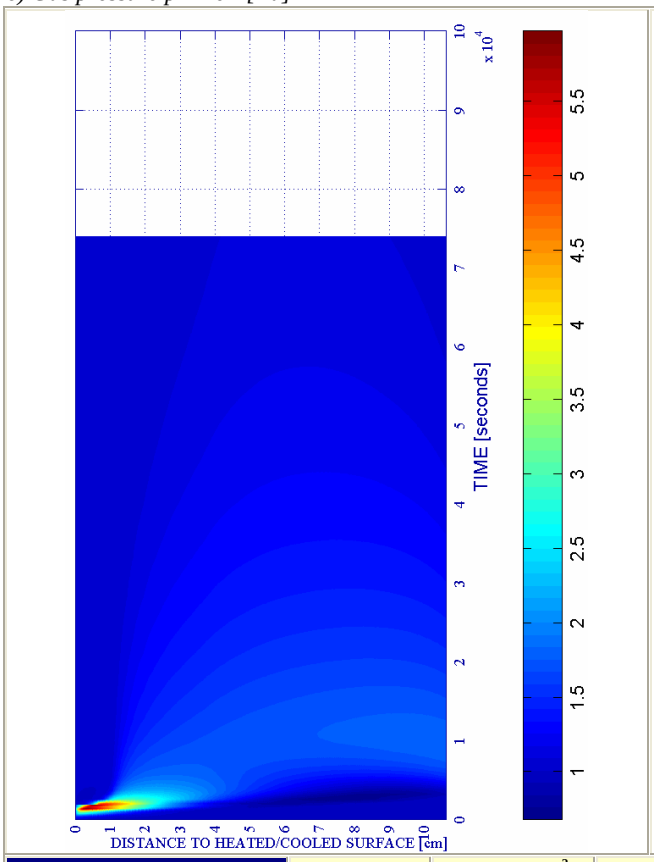

f) Vapour pressure $p^v \cdot 10^{-5}$ [Pa]

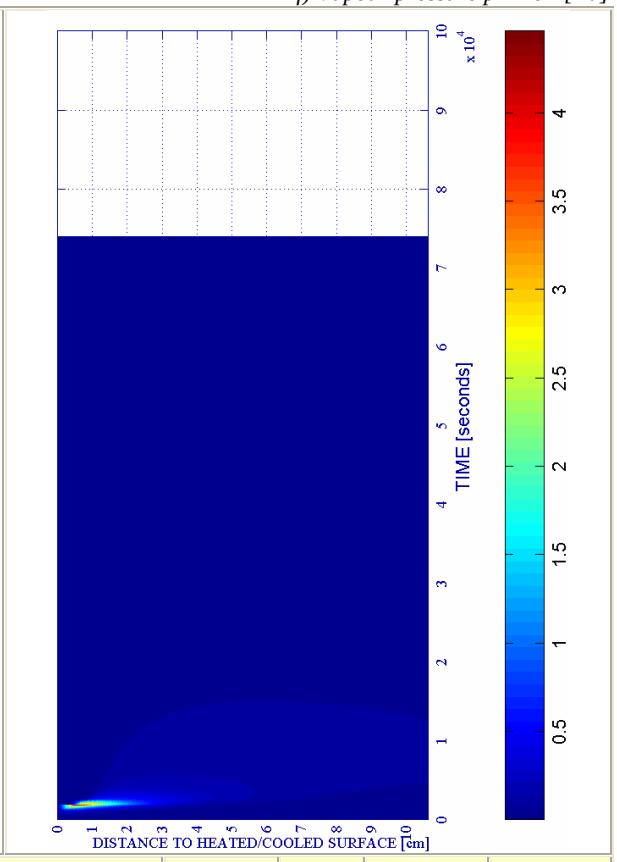

ENVIRONMENTAL - MED.		PC1 - RH [%]			PC2 - K_0 [m^2]			PC4 - Heating curve			PC5 – Mat.		Cooling length[s]	Start of cooling [s]	End of cooling [s]
#	Combination	40	50	60	10^{-19}	10^{-18}	10^{-17}	PAR1	PAR2	PAR4	C60	C90			
14	TH12K018RH50PAR2C60		X			X			X		X		84	1.800+120	2.004

g) Saturation Degree S [-]

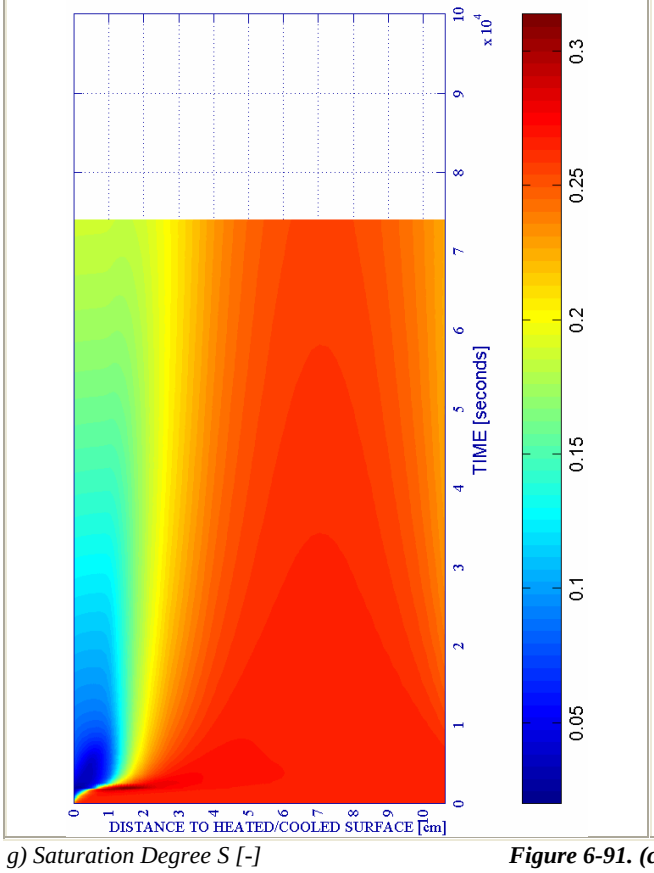

h) Relative Humidity RH [-]

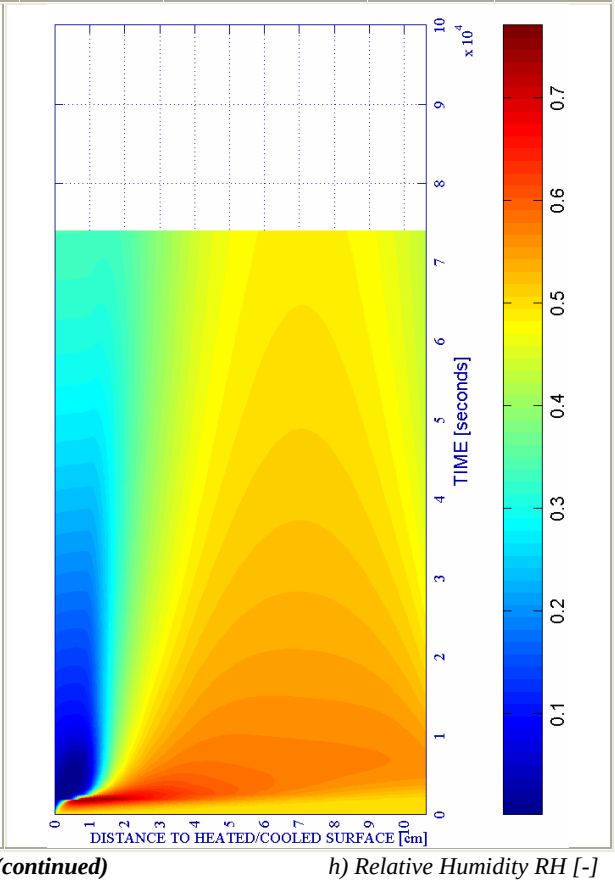

Figure 6-91. (continued)

i) Temperature [K]

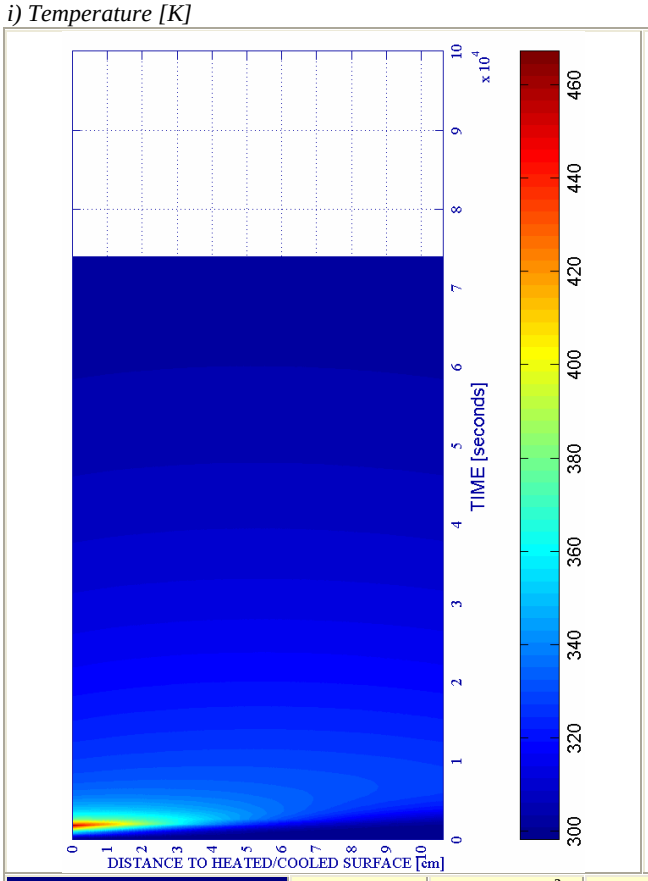

*j) Elastic Energy U · **10**$^{-4}$ [J/m^3]*

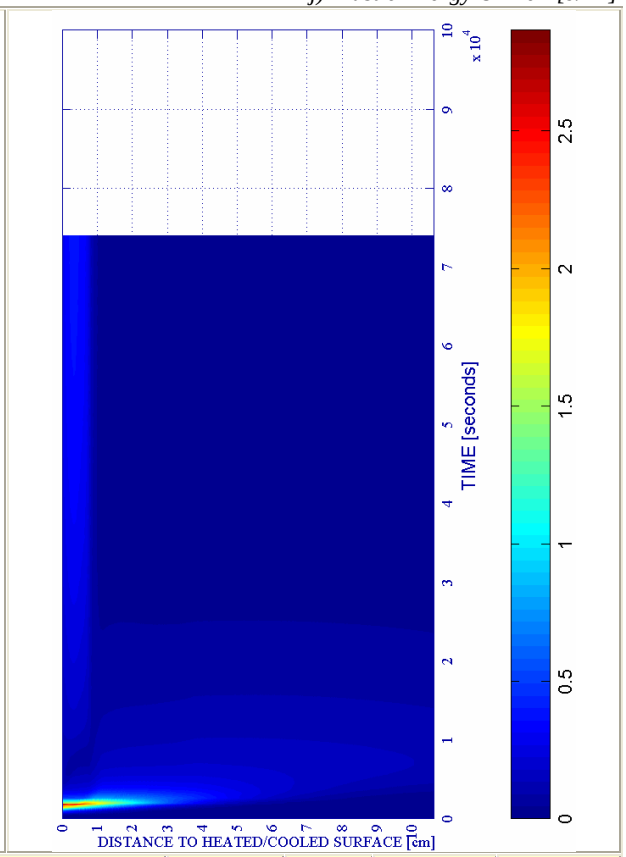

ENVIRONMENTAL - MED.		PC1 - RH [%]			PC2 - K_0 [m^2]			PC4 - Heating curve			PC5 – Mat.		Cooling length[s]	Start of cooling [s]	End of cooling [s]
#	Combination	40	50	60	10^{-19}	10^{-18}	10^{-17}	PAR1	PAR2	PAR4	C60	C90			
14	TH12K018RH50PAR2C60		X			X			X		X		84	1.800+120	2.004

*k) Stress in longitudinal (xx) direction · **10**$^{-6}$ [Pa]*

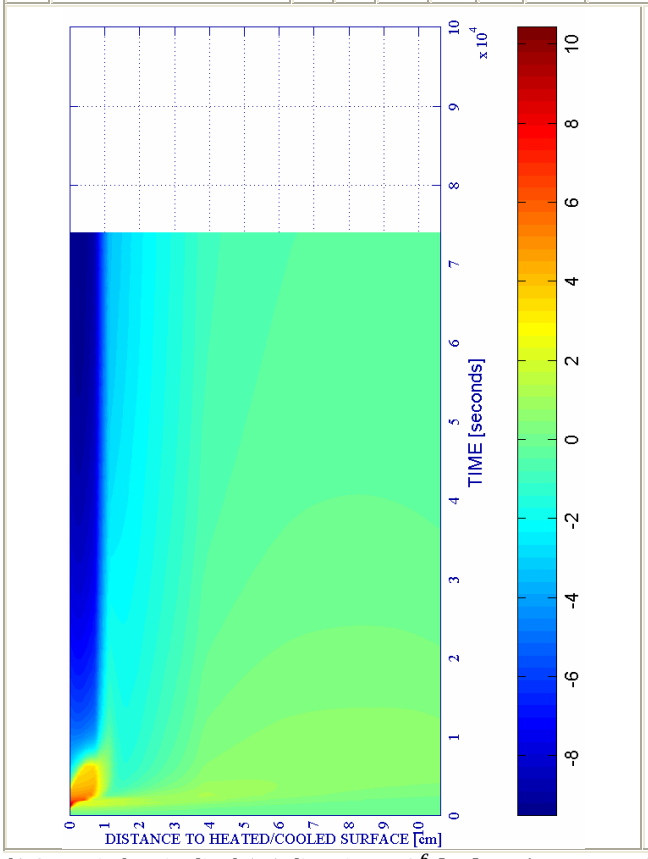

Figure 6-91. (continued)

*l) Stress in transversal (yy) direction · **10**$^{-7}$ [Pa]*

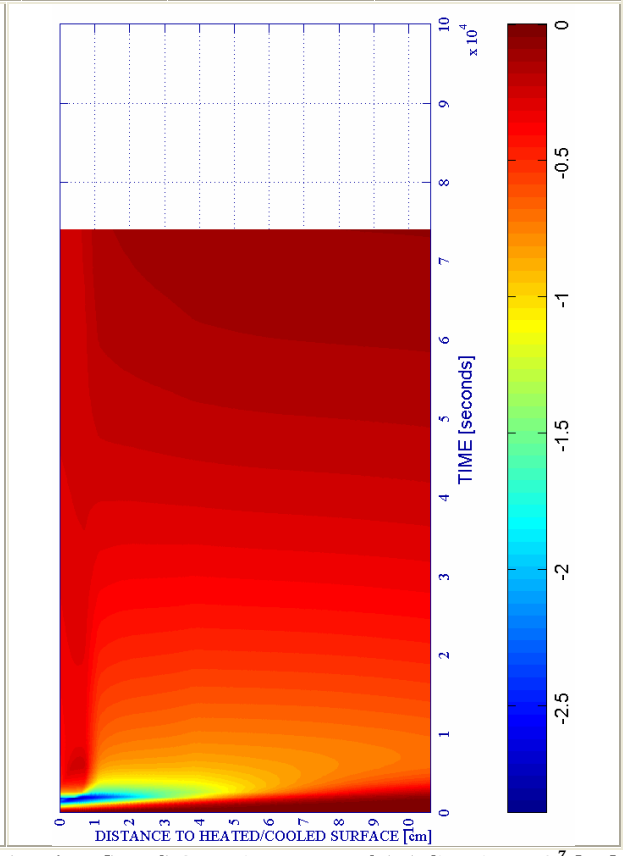

*a) Spalling Index IS4 · **10**^{3} [-]* *b) Mechanical damage d [-]*

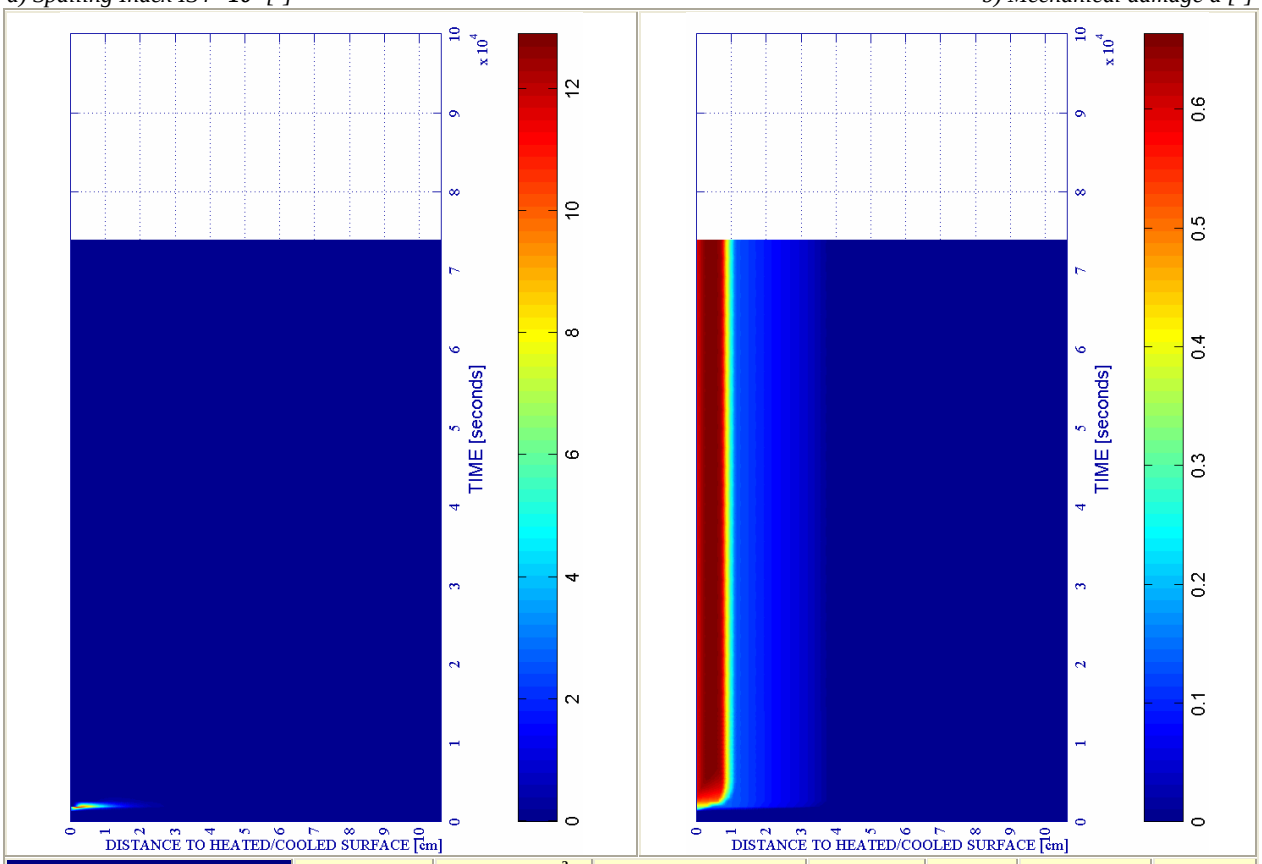

ENVIRONMENTAL - FAST		PC1 - RH [%]			PC2 - K_0 [m^2]			PC4 - Heating curve			PC5 – Mat.		Cooling length[s]	Start of cooling [s]	End of cooling [s]
#	Combination	40	50	60	10^{-19}	10^{-18}	10^{-17}	PAR1	PAR2	PAR4	C60	C90			
14	TH12K018RH50PAR2C60		X			X			X		X		8	1.800+120	1.928

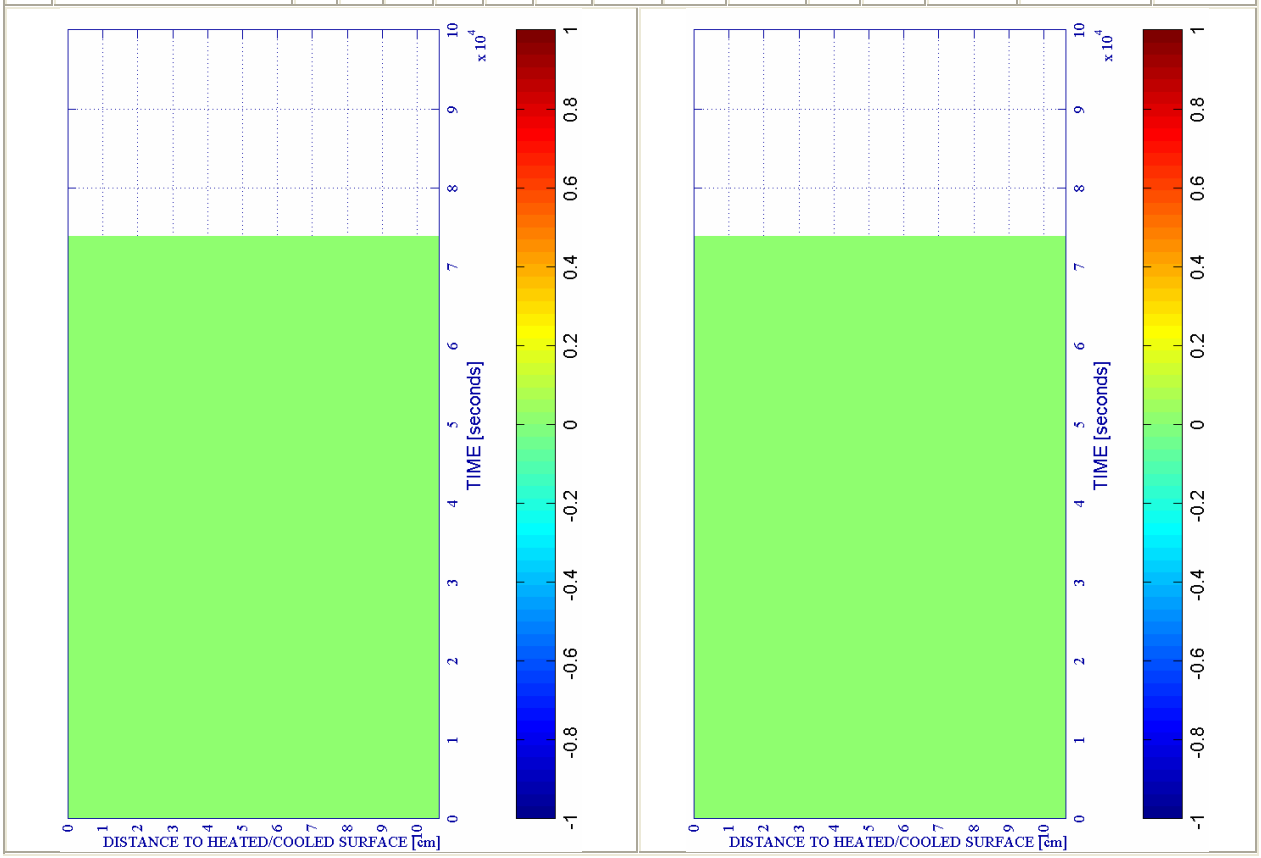

c) Velocity of spalled pieces v [m/s] ***Figure 6-92.*** *d) Velocity [m/s] where d ≥ 0,10*

e) Gas pressure $p^g \cdot 10^{-5}$ [Pa]

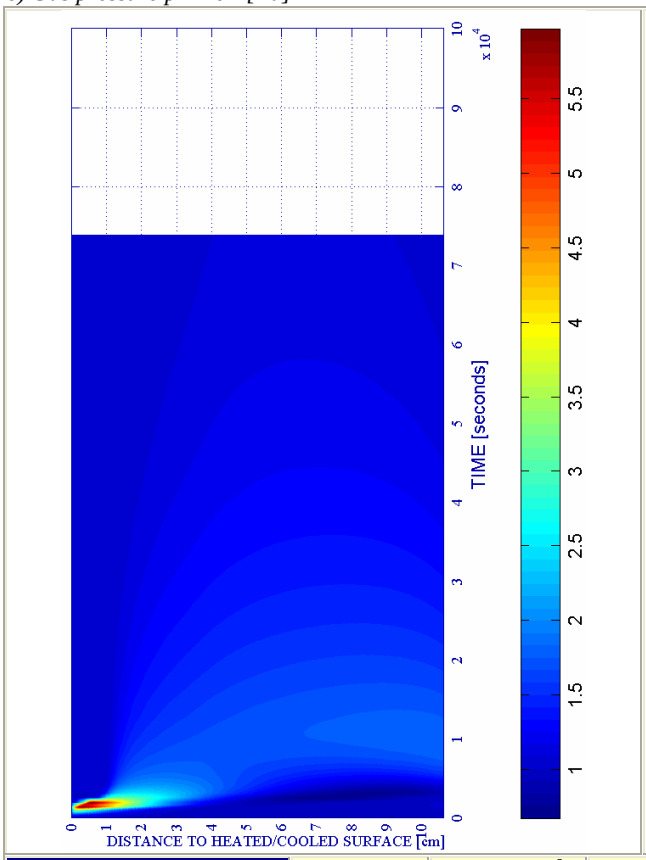

f) Vapour pressure $p^v \cdot 10^{-5}$ [Pa]

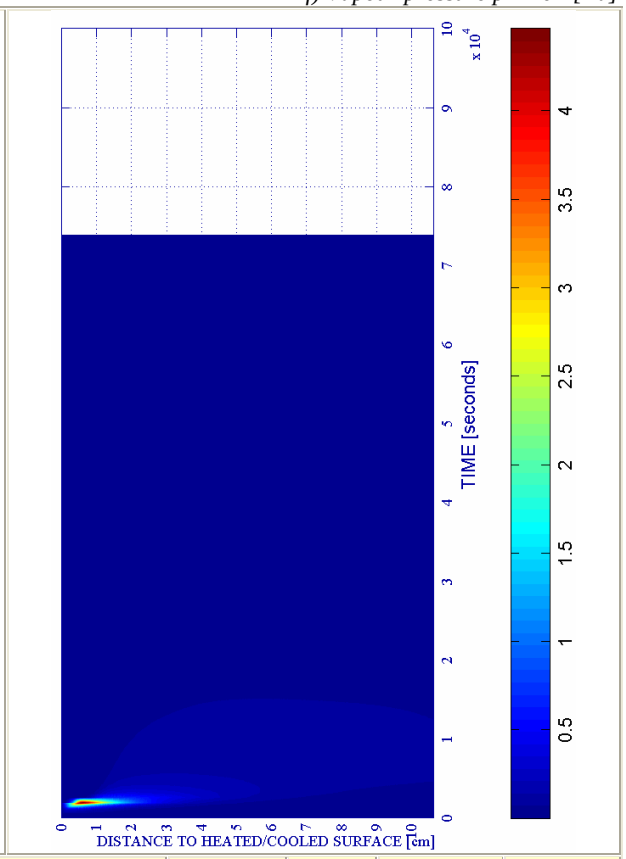

ENVIRONMENTAL - FAST	PC1 - RH [%]			PC2 - K_0 [m^2]			PC4 - Heating curve			PC5 – Mat.		Cooling length[s]	Start of cooling [s]	End of cooling [s]
# Combination	40	50	60	10^{-19}	10^{-18}	10^{-17}	PAR1	PAR2	PAR4	C60	C90			
14 TH12K018RH50PAR2C60		X			X			X		X		8	1.800+120	1.928

g) Saturation Degree S [-]

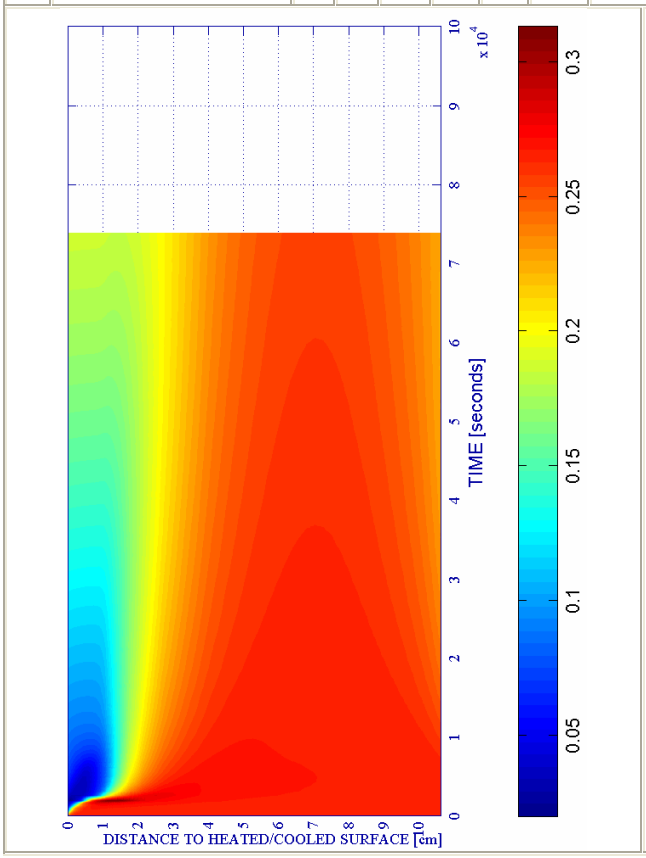

Figure 6-92. (continued)

h) Relative Humidity RH [-]

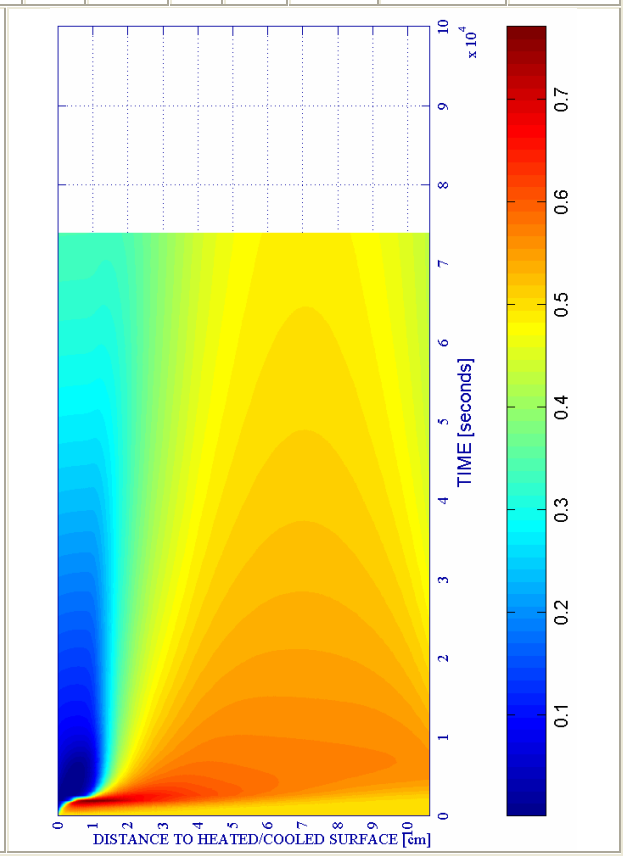

i) Temperature [K] *j) Elastic Energy U · **10^{-4}** [J/m^3]*

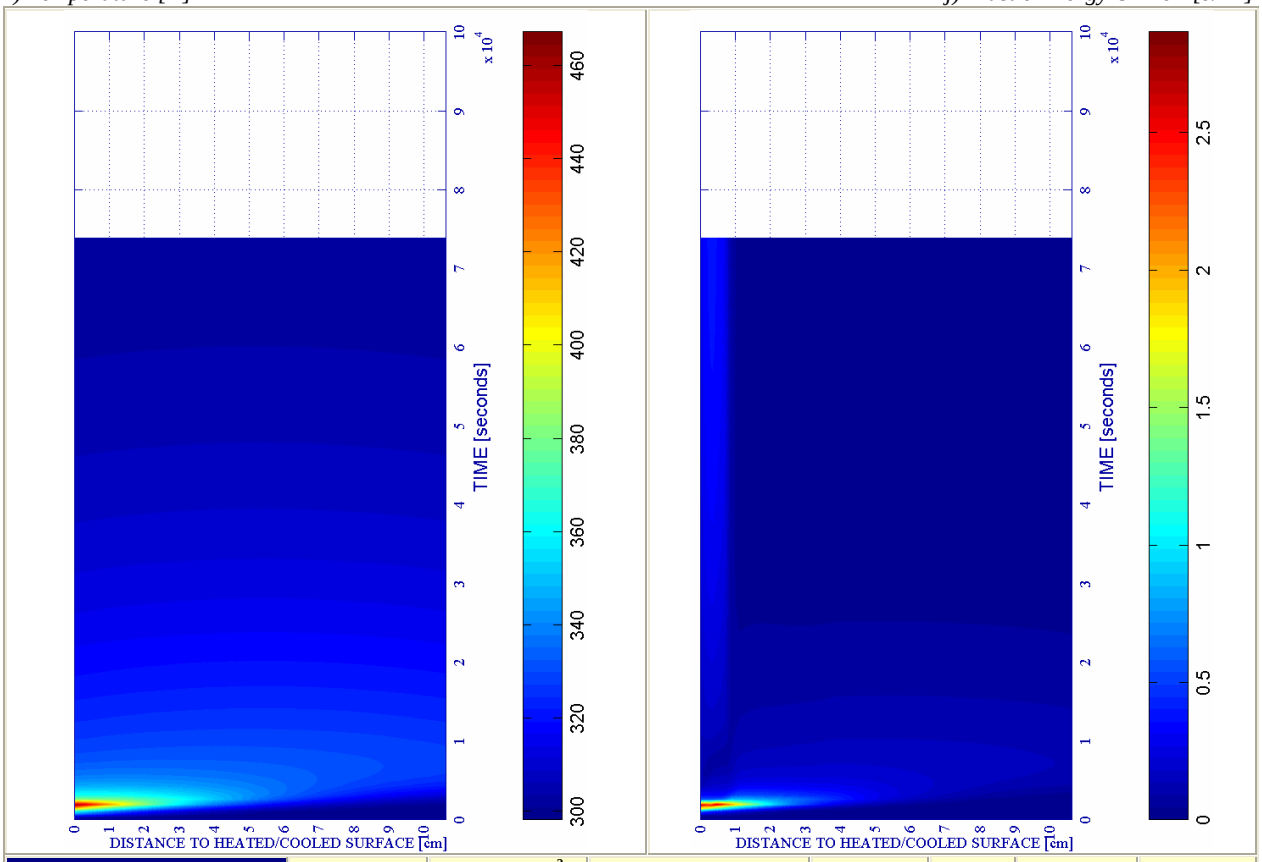

ENVIRONMENTAL - FAST	PC1 - RH [%]			PC2 - K_0 [m^2]			PC4 - Heating curve			PC5 – Mat.		Cooling length[s]	Start of cooling [s]	End of cooling [s]
#	Combination	40	50	60	10^{-19}	10^{-18}	10^{-17}	PAR1	PAR2	PAR4	C60	C90			
14	TH12K018RH50PAR2C60		X			X			X		X		8	1.800+120	1.928

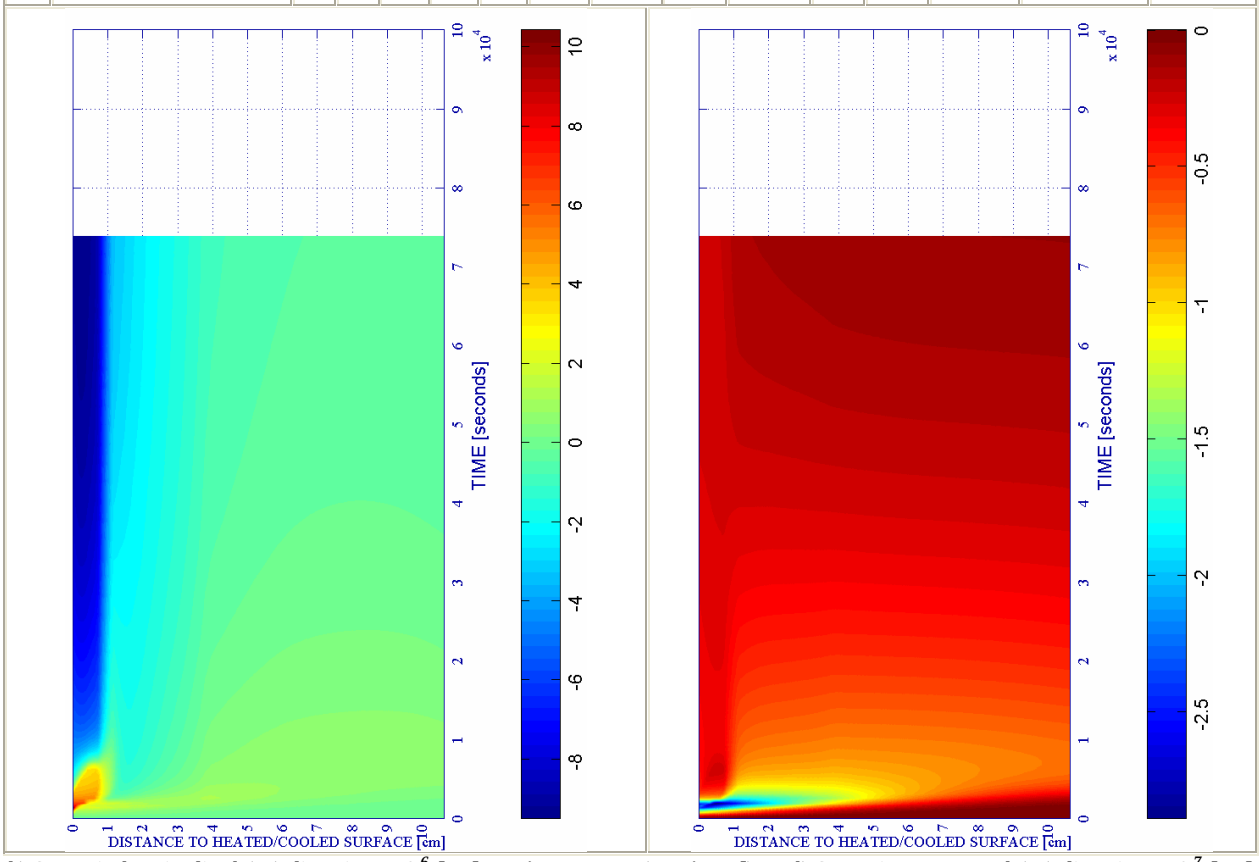

*k) Stress in longitudinal (xx) direction · **10^{-6}** [Pa]* ***Figure 6-92. (continued)*** *l) Stress in transversal (yy) direction · **10^{-7}** [Pa]*

6.5.2.2.4 Surface Cooling followed by a Heating phase

Table 6-58. *Description of the Cooling Process Stages and Collection of the Main Results related to Spalling Index and velocity*

Stage description - figure 6-93 a) to l) -	**Absolute Time Start [s]**	**Absolute Time End [s]**	**$IS4_{max}$ [-]**	**X_{IS4max} [cm]**	**t_{IS4max} [s]**	**v_{max} [m/s]**	**X_{vmax} [cm]**	**t_{vmax} [s]**	**v_{max}^* [m/s]**	**X_{vmax*} [cm]**	**t_{vmax*} [s]**
First Heating	0	1.800+120	0,0129	0,227	1.920	0,000	---	---	0,000	---	---
Surface cooling	1.920	1.936	0,0129	0,227	1.920	0,000	---	---	0,000	---	---
Second Heating up to 10.800s	1.936	10.800	0,0977	1,099	3.478	6,637	3,172	10.800	6,637	3,172	10.800
Absolute Maximum	0	10.800	0,0977	1,099	3.478	6,637	3,172	10.800	6,637	3,172	10.800

Stage description - figure 6-93 a) to l) -	**Absolute Time Start [s]**	**Absolute Time End [s]**	**d_{max} [-]**	**X_{dmax} [cm]**	**t_{dmax} [s]**	**T_{max} [K]**	**X_{Tmax} [cm]**	**t_{Tmax} [s]**	**p^g_{max} [MPa]**	**X_{pgmax} [cm]**	**t_{pgmax} [s]**
First Heating	0	1.800+120	0,3718	0,210	1.920	467,16	0,000	1.920	0,5967	0,582	1.920
Surface cooling	1.920	1.936	0,6806	0,000	1.936	467,16	0,000	1.920	0,5975	0,623	1.924,8
Second Heating up to 10.800s	1.936	10.800	0,8115	0,000	10.800	982,85	0,000	10.800	0,8057	1,736	2.878
Absolute Maximum	0	10.800	0,8115	0,000	10.800	982,85	0,000	10.800	0,8057	1,736	2.878

Table 6-59. *Description of the Cooling Process Stages and Collection of the Main Results related to mechanical damage, Temperature and Gas Pressure*

6.5.2.2.5 Surface Cooling followed by an imposed Constant Surface Temperature

Table 6-60. *Description of the Cooling Process Stages and Collection of the Main Results related to Spalling Index and velocity*

Stage description - figure 6-94 a) to l) -	**Absolute Time Start [s]**	**Absolute Time End [s]**	**$IS4_{max}$ [-]**	**X_{IS4max} [cm]**	**t_{IS4max} [s]**	**v_{max} [m/s]**	**X_{vmax} [cm]**	**t_{vmax} [s]**	**v_{max}^* [m/s]**	**X_{vmax*} [cm]**	**t_{vmax*} [s]**
First Heating	0	1.800+120	0,0129	0,227	1.920	0,000	---	---	0,000	---	---
Surface cooling	1.920	1.936	0,0129	0,227	1.920	0,000	---	---	0,000	---	---
Surface Constant T	1.936	2.239	0,0034	0,665	1.936	0,000	---	---	0,000	---	---
Absolute Maximum	0	2.239	0,0129	0,227	1.920	0,000	---	---	0,000	---	---

Stage description - figure 6-94 a) to l) -	**Absolute Time Start [s]**	**Absolute Time End [s]**	**d_{max} [-]**	**X_{dmax} [cm]**	**t_{dmax} [s]**	**T_{max} [K]**	**X_{Tmax} [cm]**	**t_{Tmax} [s]**	**p^g_{max} [MPa]**	**X_{pgmax} [cm]**	**t_{pgmax} [s]**
First Heating	0	1.800+120	0,3718	0,210	1.920	467,16	0,000	1.920	0,5967	0,582	1.920
Surface cooling	1.920	1.936	0,6806	0,000	1.936	467,16	0,000	1.920	0,5975	0,623	1.924,8
Surface Constant T	1.936	2.239	0,7863	0,265	2.129	427,69	0,544	1.936	0,5599	0,710	1.936
Absolute Maximum	0	2.239	0,7863	0,265	2.129	467,16	0,000	1.920	0,5599	0,710	1.936

Table 6-61. *Description of the Cooling Process Stages and Collection of the Main Results related to mechanical damage, Temperature and Gas Pressure*

6.5.2.2.6 Surface Cooling in Two Periods

Table 6-62. *Description of the Cooling Process Stages and Collection of the Main Results related to Spalling Index and velocity*

Stage description - figure 6-95 a) to l) -	**Absolute Time Start [s]**	**Absolute Time End [s]**	**$IS4_{max}$ [-]**	**X_{IS4max} [cm]**	**t_{IS4max} [s]**	**v_{max} [m/s]**	**X_{vmax} [cm]**	**t_{vmax} [s]**	**v_{max}^* [m/s]**	**X_{vmax*} [cm]**	**t_{vmax*} [s]**
First Heating	0	1.800+120	0,0129	0,227	1.920	0,000	---	---	0,000	---	---
First Surface cooling	1.920	1.936	0,0129	0,227	1.920	0,000	---	---	0,000	---	---
Second Heating	1.936	2.278	0,0170	0,474	2.278	0,877	5,687	2.278	0,869	0,974	2.278
Second Surface cool.	2.278	2.298	0,0170	0,474	2.278	0,877	5,687	2.278	0,871	0,974	2.278,5
Heating up to 10.800s	2.298	2.307‡	0,0079	0.916	2.298	0,000	---	---	0,000	---	---
Absolute Maximum	0	2.307‡	0,0170	0,474	2.278	0,877	5,687	2.278	0,871	0,974	2.278,5

Remark ‡: *Results are available only up to this instant due to a lack of numerical convergence*

Stage description - figure 6-95 a) to l) -	**Absolute Time Start [s]**	**Absolute Time End [s]**	**d_{max} [-]**	**X_{dmax} [cm]**	**t_{dmax} [s]**	**T_{max} [K]**	**X_{Tmax} [cm]**	**t_{Tmax} [s]**	**p^g_{max} [MPa]**	**X_{pgmax} [cm]**	**t_{pgmax} [s]**
First Heating	0	1.800+120	0,3718	0,210	1.920	467,16	0,000	1.920	0,5967	0,582	1.920
First Surface cooling	1.920	1.936	0,6806	0,000	1.936	467,16	0,000	1.920	0,5975	0,623	1.924,8
Second Heating	1.936	2.278	0,6806	0,000	1.936	506,97	0,000	2.278	0,6653	0,860	2.278
Second Surface cool.	2.278	2.298	0,7445	0,000	2.298	506,97	0,000	2.278	0,6796	0,916	2.289,5
Heating up to 10.800s	2.298	2.307‡	0,7445	0,000	2.298	454,16	0,582	2.298	0,6581	0,974	2.298
Absolute Maximum	0	2.307‡	0,7445	0,000	2.298	506,97	0,000	2.278	0,6796	0,916	2.289,5

Table 6-63. *Description of the Cooling Process Stages and Collection of the Main Results related to mechanical damage, Temperature and Gas Pressure*

a) Spalling Index IS4 [-]

b) Mechanical damage d [-]

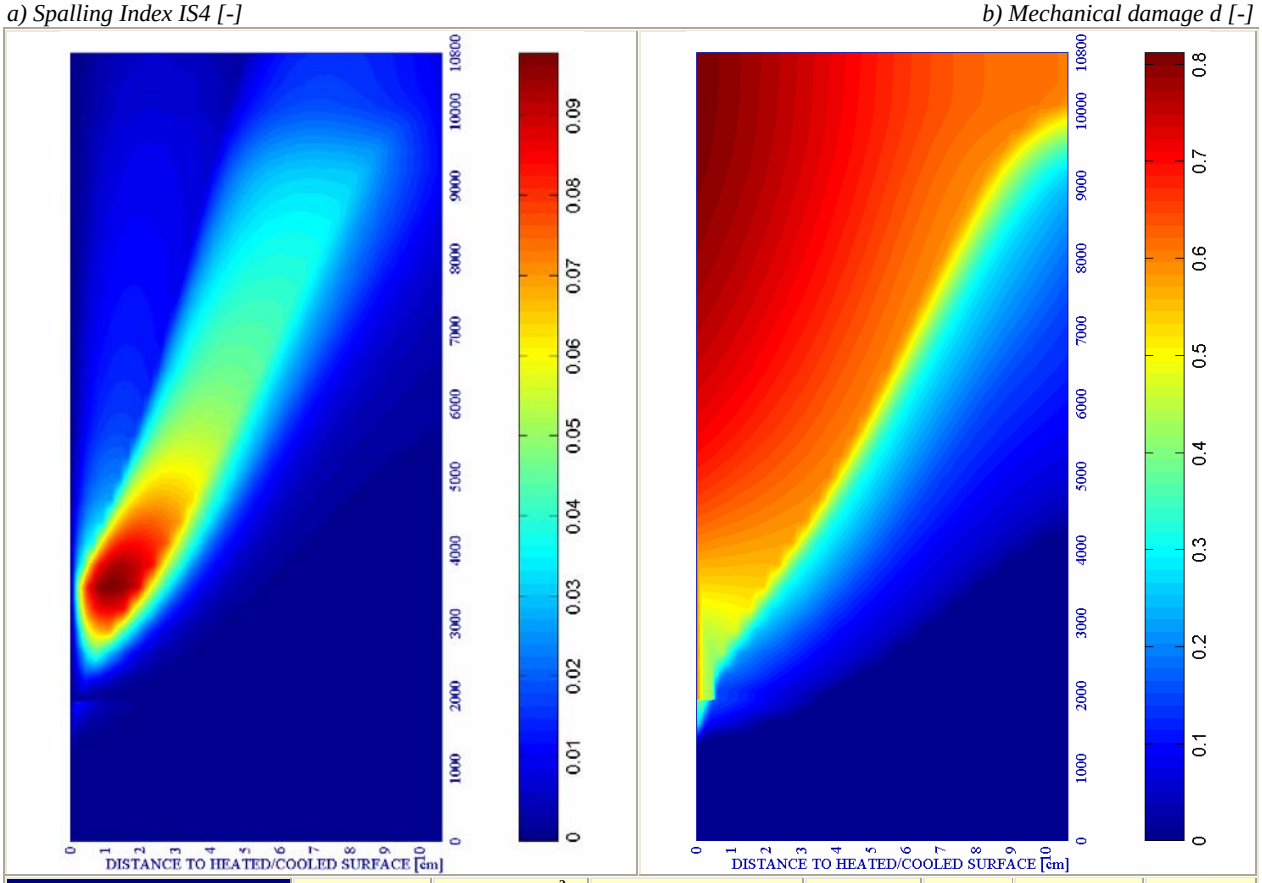

SURFACE COOL+HEAT		PC1 - RH [%]			PC2 - K_0 [m^2]			PC4 - Heating curve			PC5 – Mat.		Cooling length[s]	Start of cooling [s]	End of cooling [s]
#	Combination	40	50	60	10^{-19}	10^{-18}	10^{-17}	PAR1	PAR2	PAR4	C60	C90			
14	TH12K018RH50PAR2C60		X			X			X		X		16	1.800+120	1.936

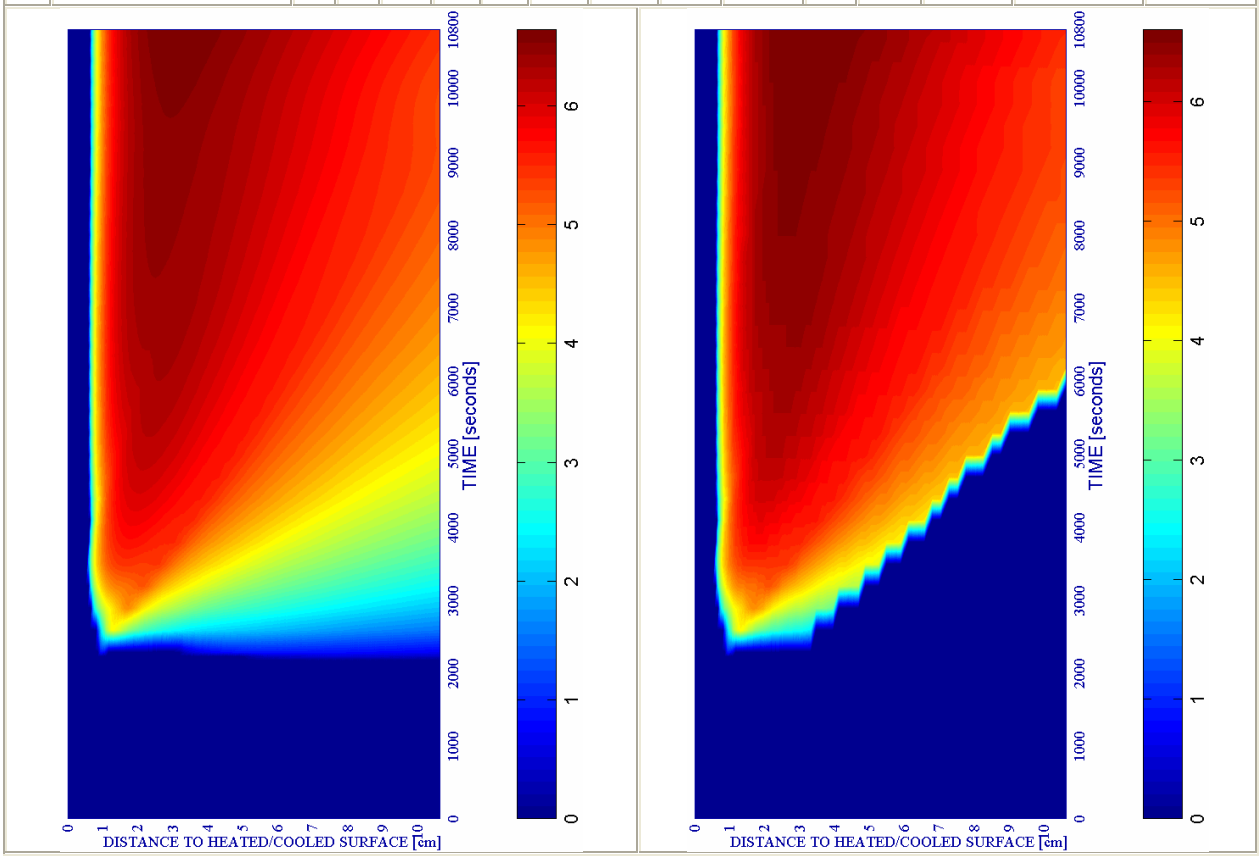

c) Velocity of spalled pieces v [m/s]

Figure 6-93.

d) Velocity [m/s] where d ≥ 0,10

e) Gas pressure $p^g \cdot 10^{-5}$ [Pa]

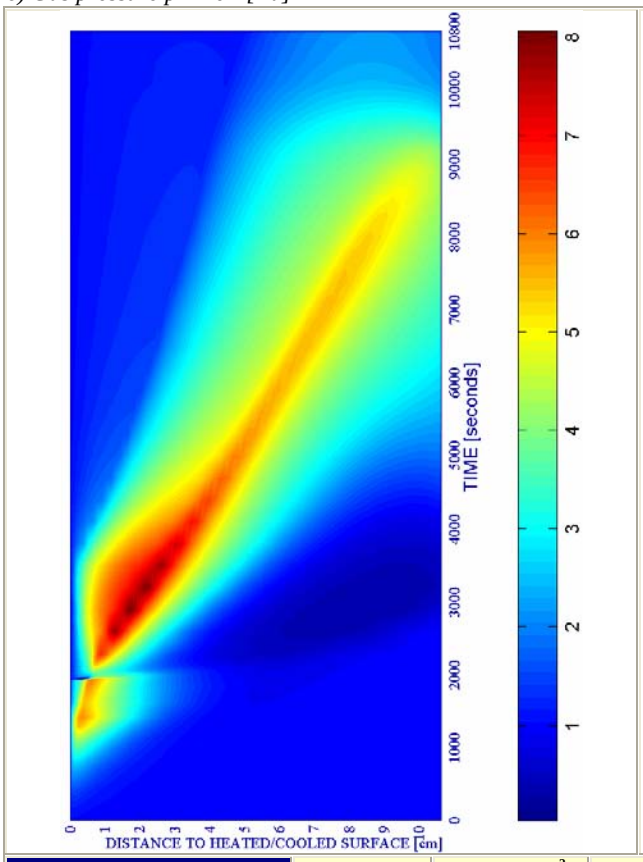

f) Vapour pressure $p^v \cdot 10^{-5}$ [Pa]

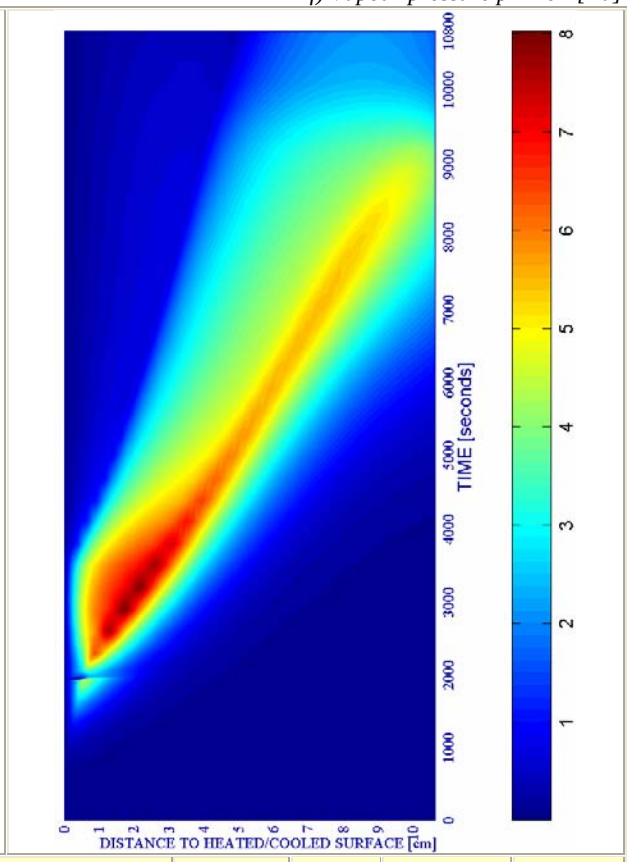

SURFACE COOL+HEAT		PC1 - RH [%]			PC2 - K_0 [m^2]			PC4 - Heating curve			PC5 – Mat.		Cooling length[s]	Start of cooling [s]	End of cooling [s]
#	Combination	40	50	60	10^{-19}	10^{-18}	10^{-17}	PAR1	PAR2	PAR4	C60	C90			
14	TH12K018RH50PAR2C60		X			X			X		X		16	1.800+120	1.936

g) Saturation Degree S [-]

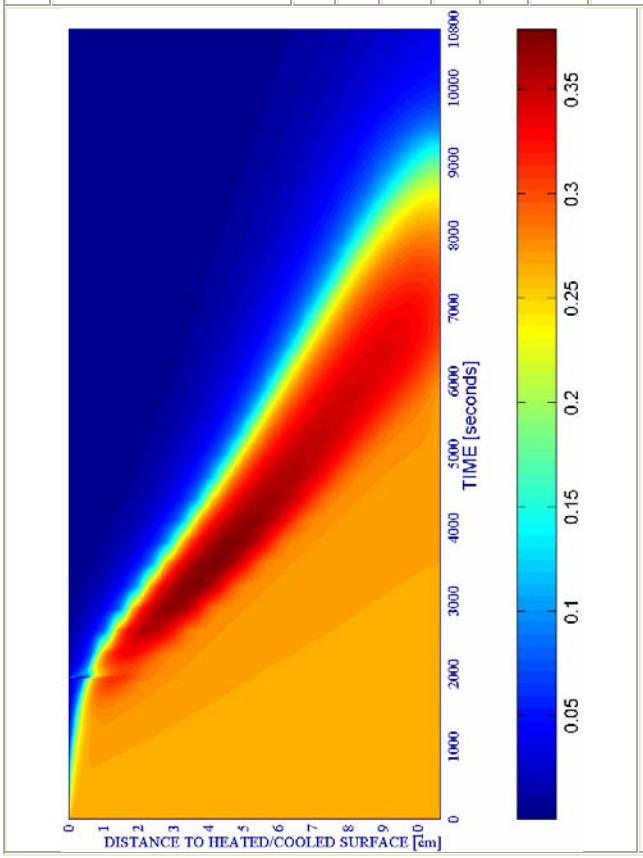

h) Relative Humidity RH [-]

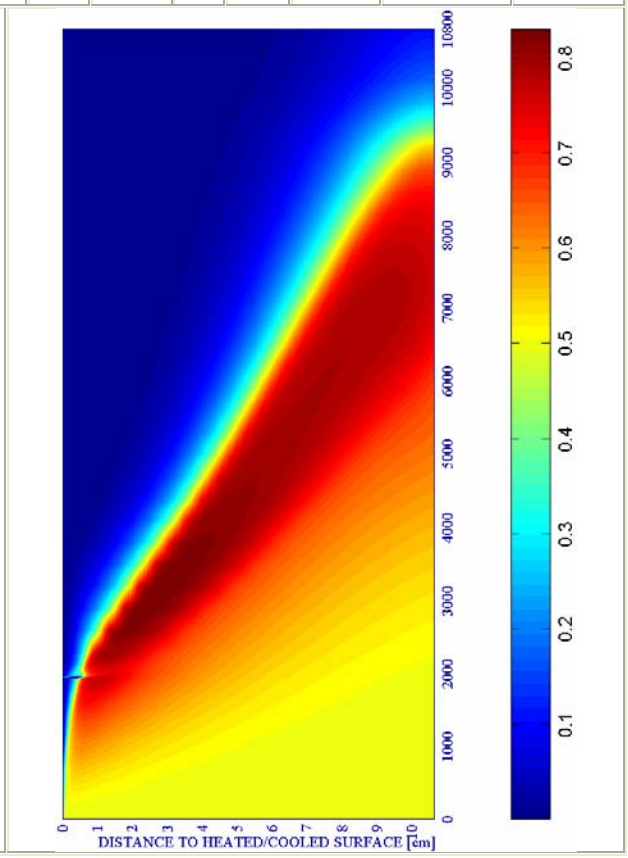

Figure 6-93. (continued)

i) Temperature [K] *j) Elastic Energy U · **10^{-4}** [J/m^3]*

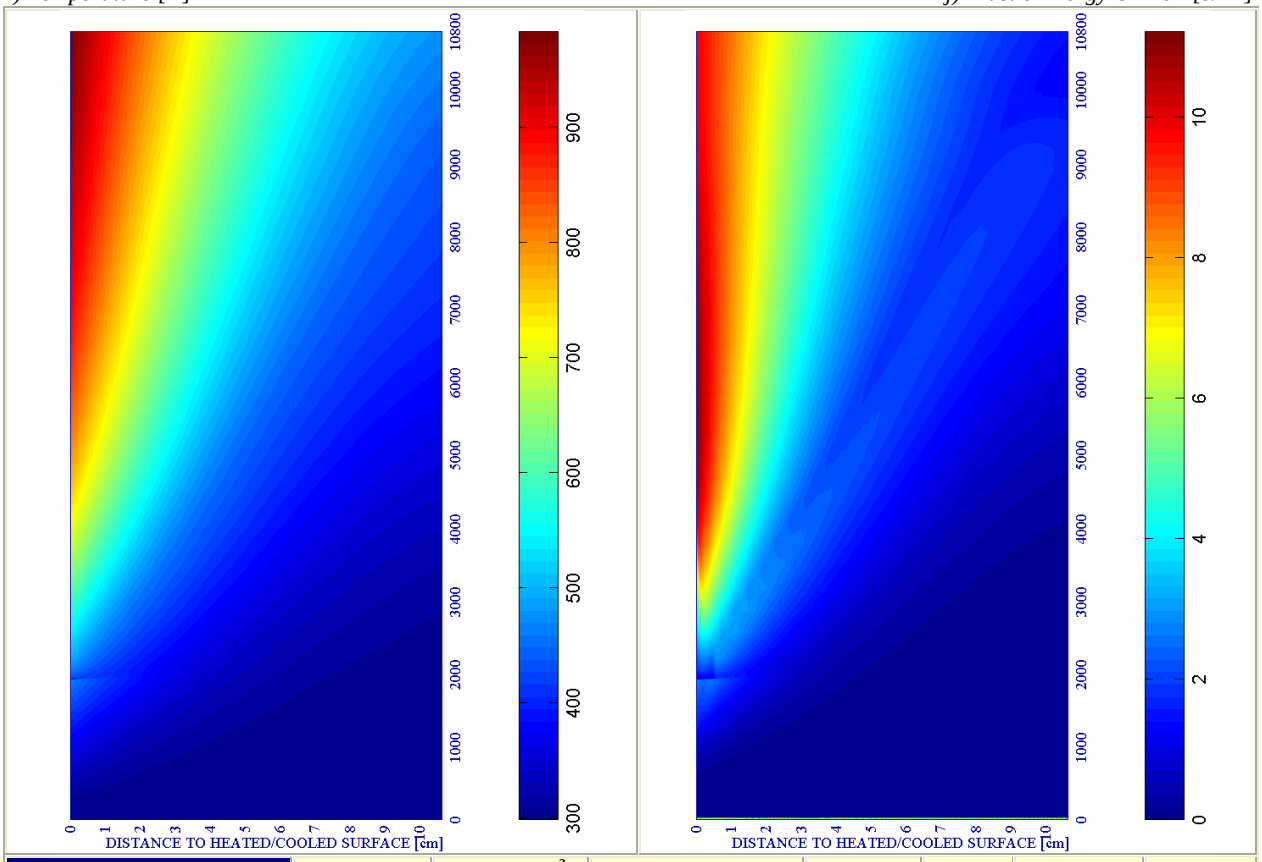

SURFACE COOL+HEAT		PC1 - RH [%]			PC2 - K_0 [m^2]			PC4 - Heating curve			PC5 – Mat.		Cooling length[s]	Start of cooling [s]	End of cooling [s]
#	Combination	40	50	60	10^{-19}	10^{-18}	10^{-17}	PAR1	PAR2	PAR4	C60	C90			
14	TH12K018RH50PAR2C60		X			X			X		X		16	1.800+120	1.936

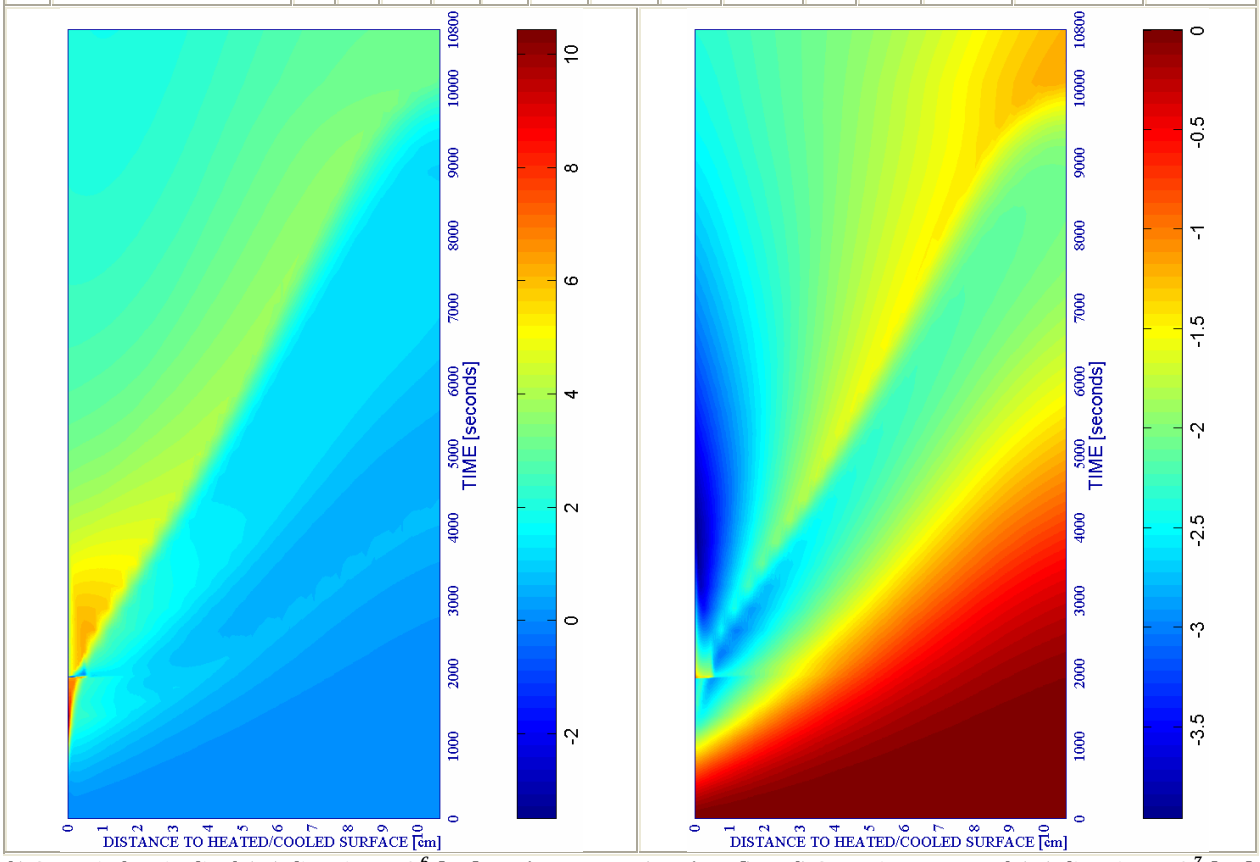

*k) Stress in longitudinal (xx) direction · **10^{-6}** [Pa]* ***Figure 6-93. (continued)*** *l) Stress in transversal (yy) direction · **10^{-7}** [Pa]*

*a) Spalling Index IS4 · **10**^{3} [-]* *b) Mechanical damage d [-]*

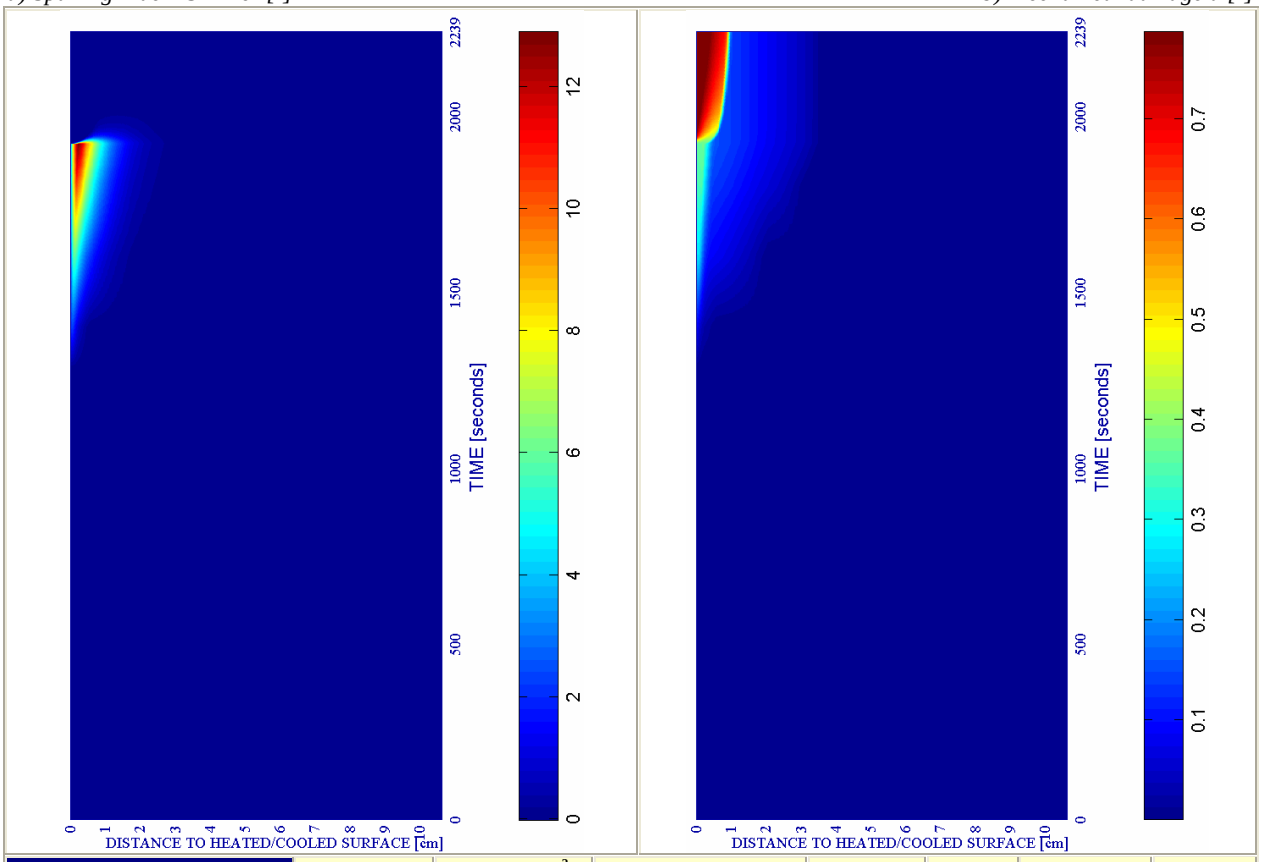

SURFACE COOL+KEEP		PC1 - RH [%]			PC2 - K_0 [m^2]			PC4 - Heating curve			PC5 – Mat.		Cooling length[s]	Start of cooling [s]	End of cooling [s]
#	Combination	40	50	60	10^{-19}	10^{-18}	10^{-17}	PAR1	PAR2	PAR4	C60	C90			
14	TH12K018RH50PAR2C60		X			X			X		X		319	1.800+120	2.239

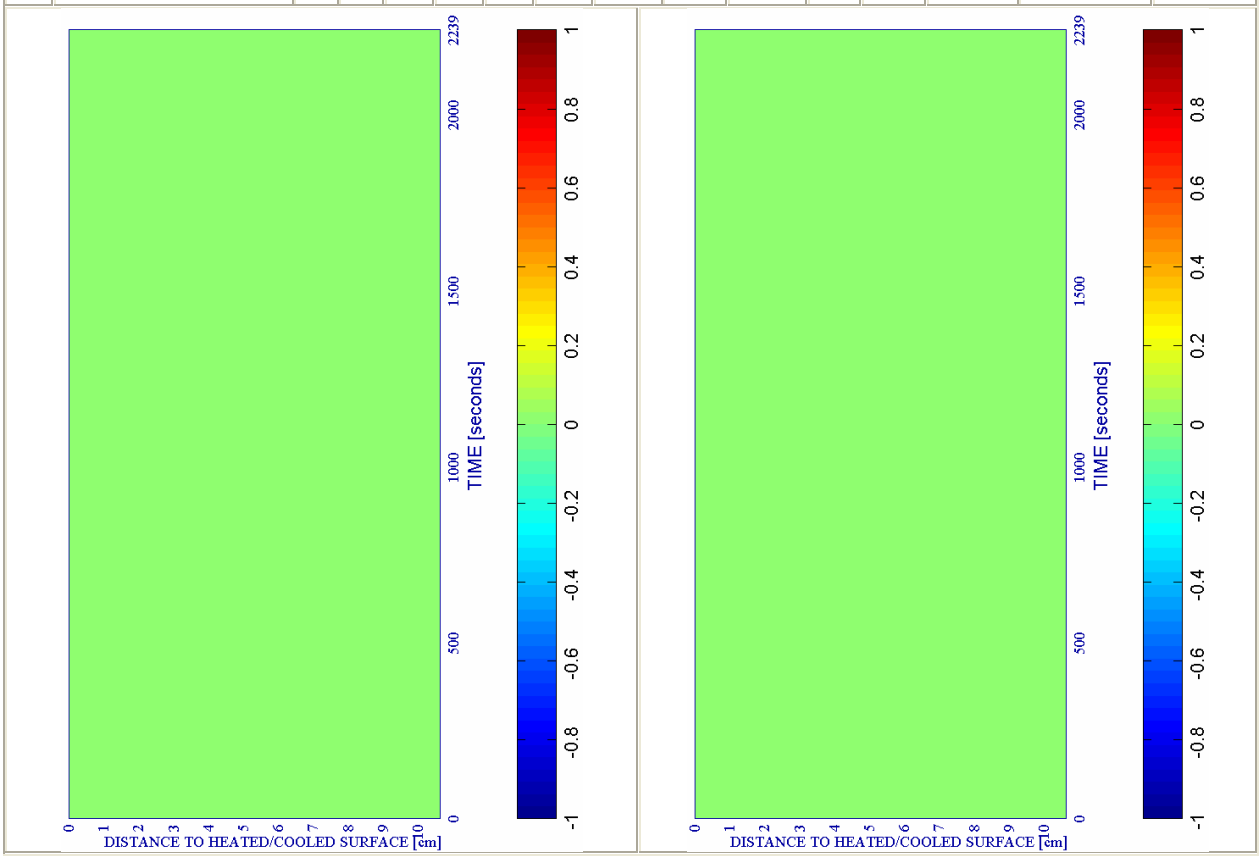

c) Velocity of spalled pieces v [m/s] ***Figure 6-94.*** *d) Velocity [m/s] where d ≥ 0,10*

e) Gas pressure $p^g \cdot 10^{-5}$ [Pa]

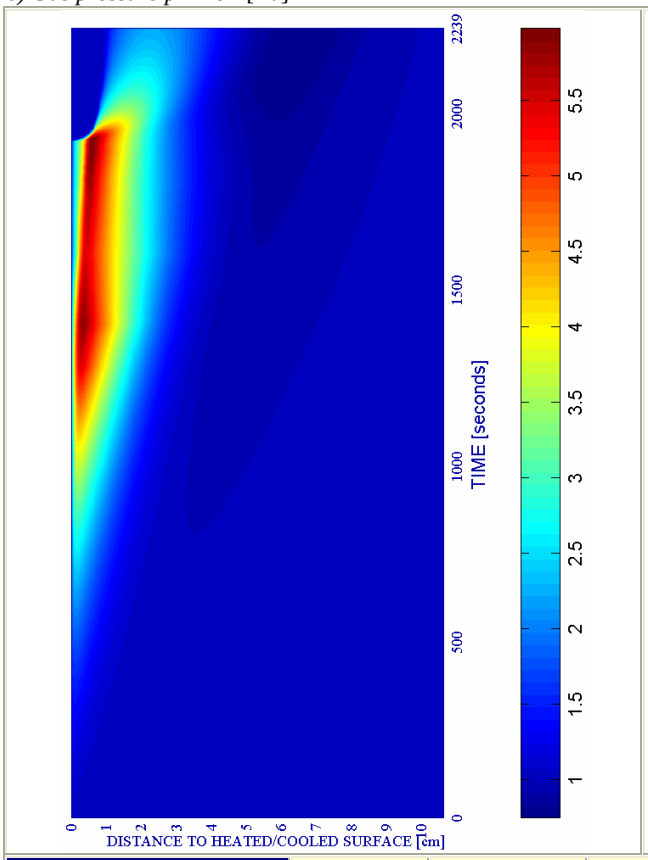

f) Vapour pressure $p^v \cdot 10^{-5}$ [Pa]

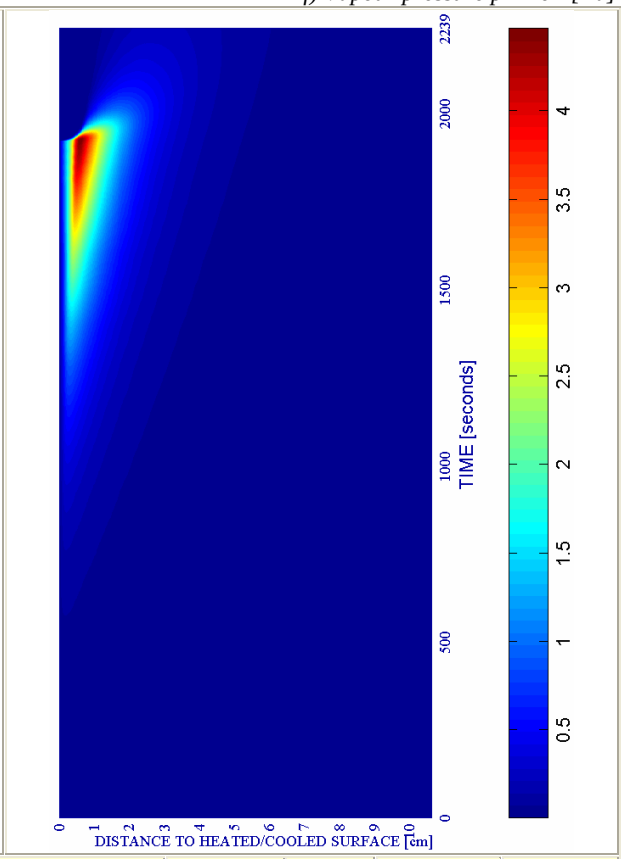

SURFACE COOL+KEEP		PC1 - RH [%]			PC2 - K_0 [m^2]			PC4 - Heating curve			PC5 – Mat.		Cooling length[s]	Start of cooling [s]	End of cooling [s]
#	Combination	40	50	60	10^{-19}	10^{-18}	10^{-17}	PAR1	PAR2	PAR4	C60	C90			
14	TH12K018RH50PAR2C60		X			X			X		X		319	1.800+120	2.239

g) Saturation Degree S [-]

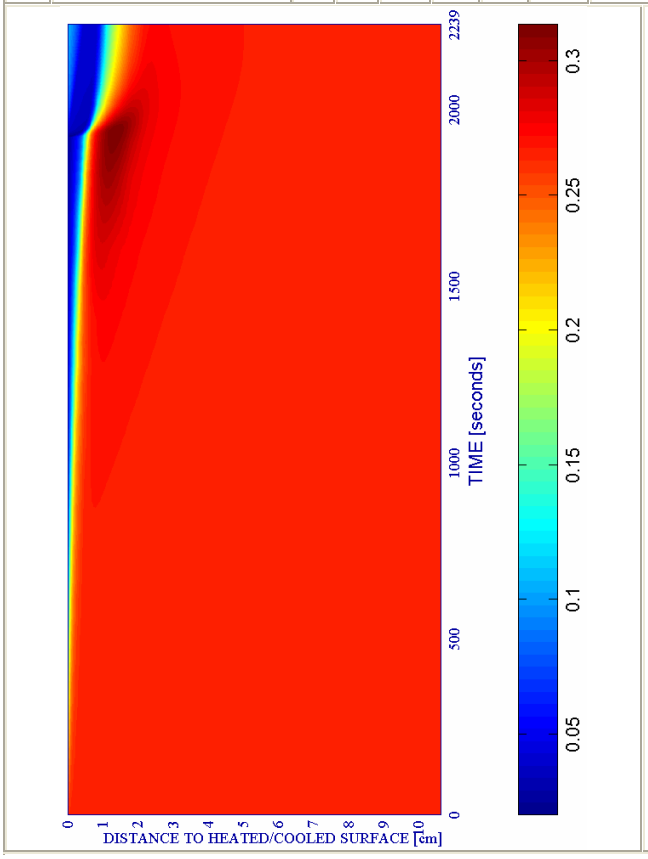

Figure 6-94. (continued)

h) Relative Humidity RH [-]

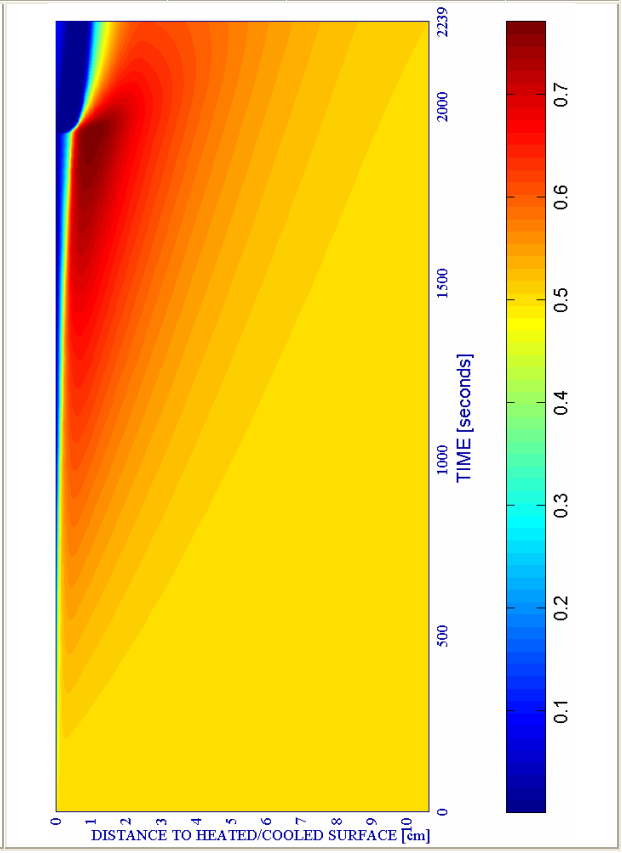

i) Temperature [K]

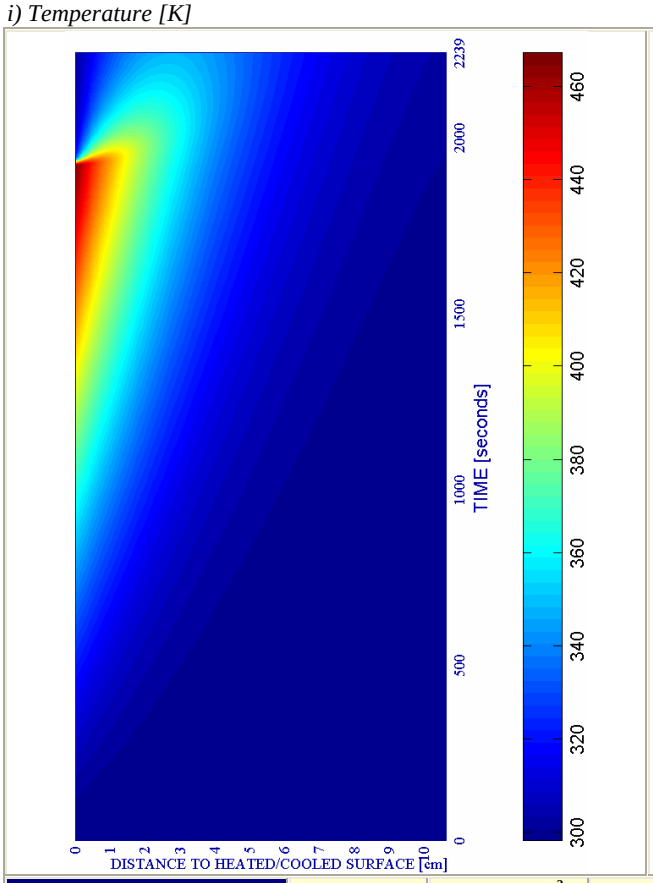

*j) Elastic Energy U · **10**$^{-4}$ [J/m^3]*

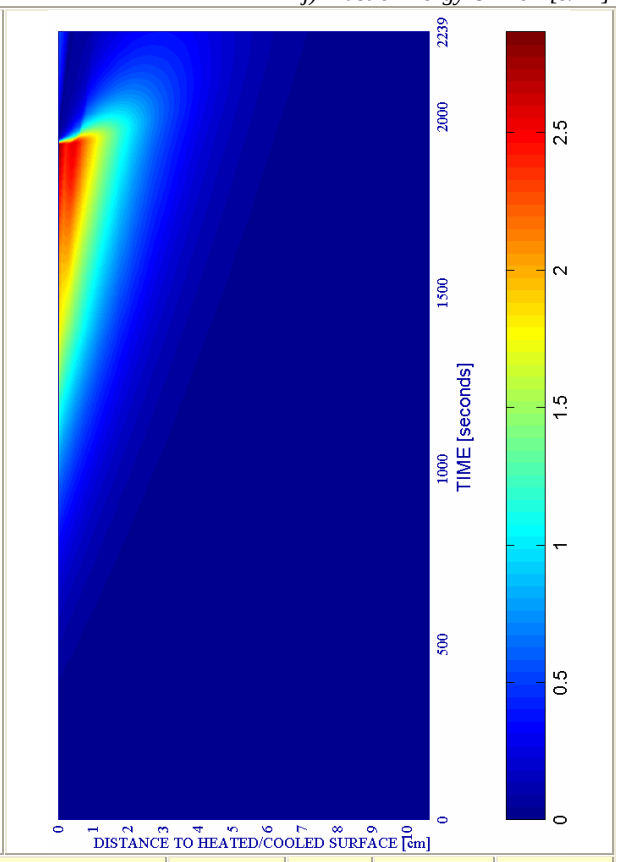

SURFACE COOL+KEEP		PC1 - RH [%]			PC2 - K_0 [m^2]			PC4 - Heating curve			PC5 – Mat.		Cooling length[s]	Start of cooling [s]	End of cooling [s]
#	Combination	40	50	60	10^{-19}	10^{-18}	10^{-17}	PAR1	PAR2	PAR4	C60	C90			
14	TH12K018RH50PAR2C60		X			X			X		X		319	1.800+120	2.239

*k) Stress in longitudinal (xx) direction · **10**$^{-6}$ [Pa]*

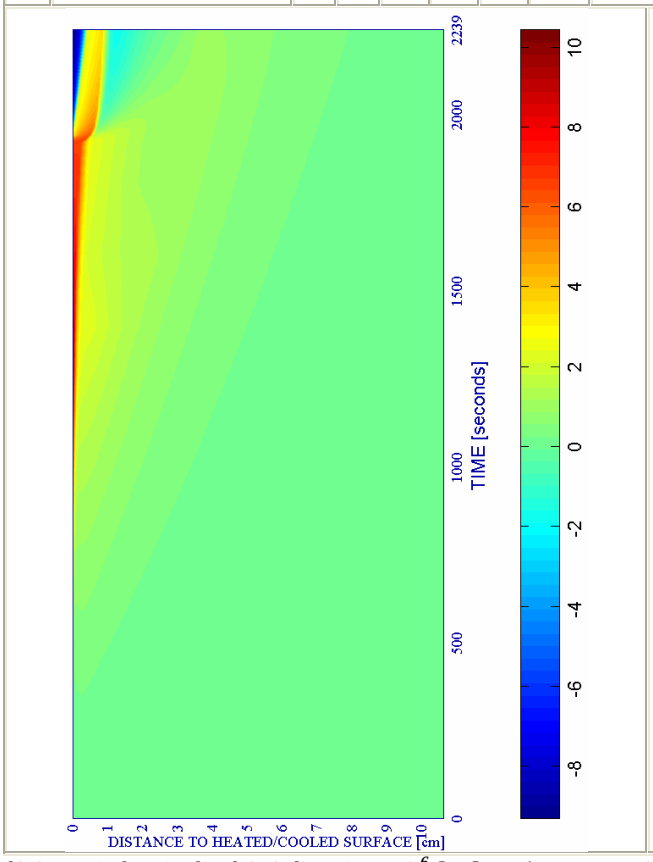

Figure 6-94. (continued)

*l) Stress in transversal (yy) direction · **10**$^{-7}$ [Pa]*

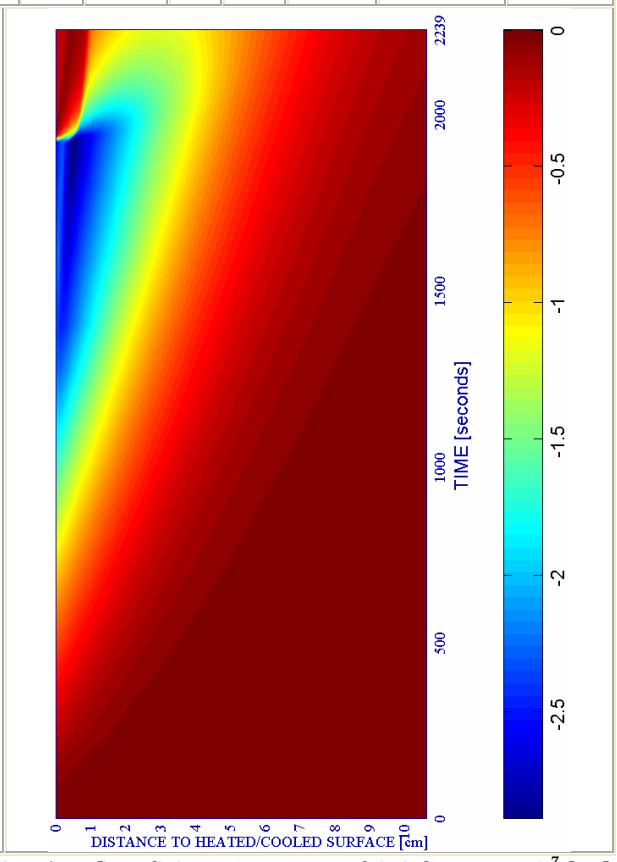

*a) Spalling Index IS4 · **10**^{3} [-]* *b) Mechanical damage d [-]*

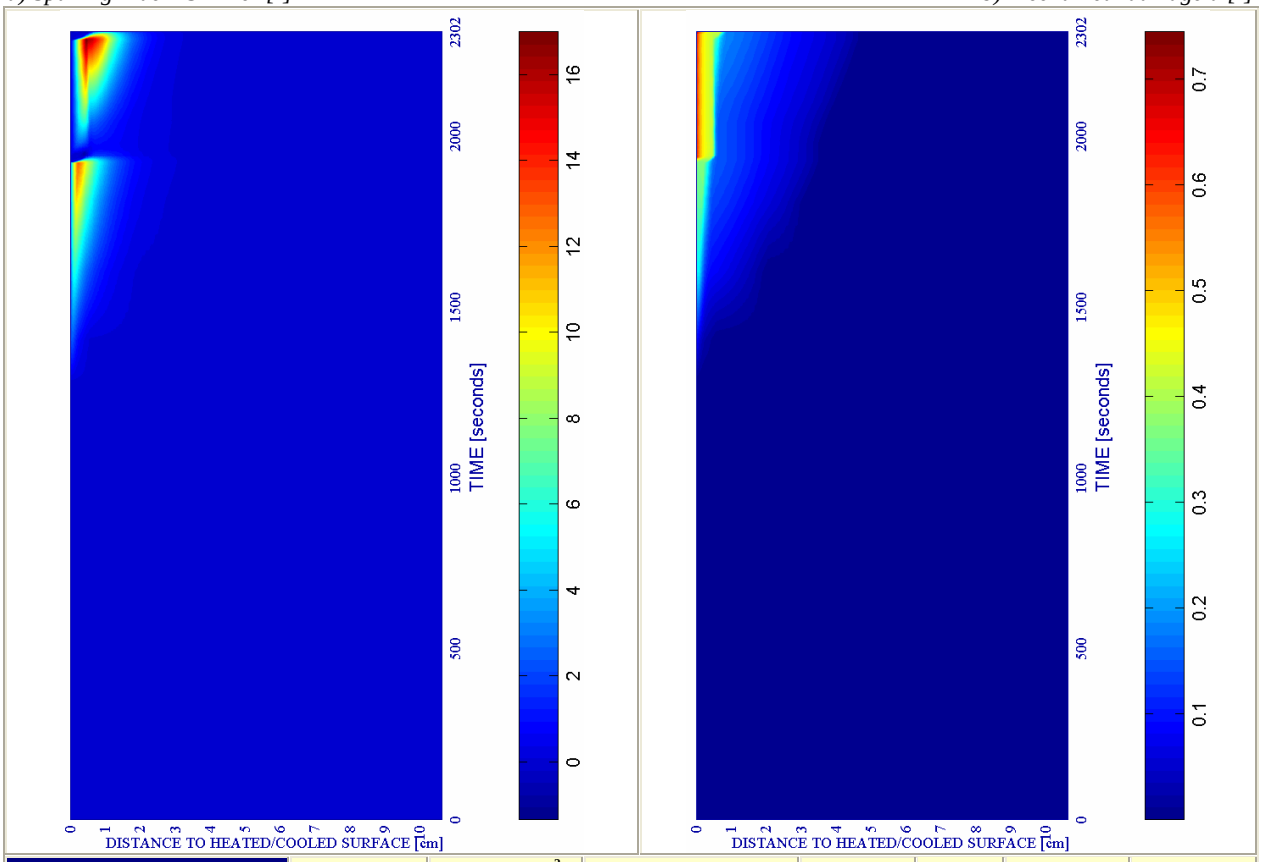

SURFACE COOL+REPEAT		PC1 - RH [%]			PC2 - K_0 [m^2]			PC4 - Heating curve			PC5 – Mat.		Cooling length[s]	Start of cooling [s]	End of cooling [s]
#	Combination	40	50	60	10^{-19}	10^{-18}	10^{-17}	PAR1	PAR2	PAR4	C60	C90			
14	TH12K018RH50PAR2C60		X			X			X		X		16 / 20	1.920 / 2.278	1.936 / 2.298

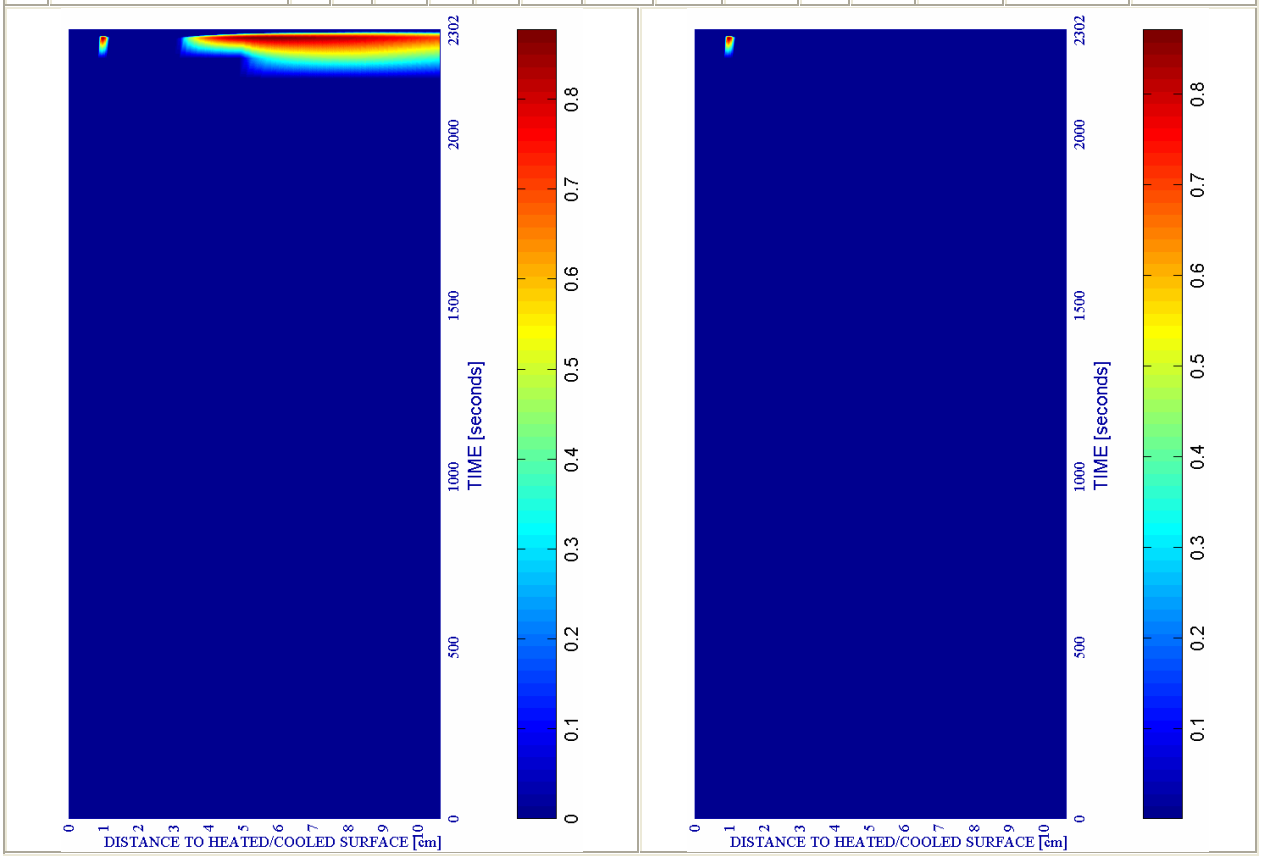

c) Velocity of spalled pieces v [m/s] ***Figure 6-95.*** *d) Velocity [m/s] where d ≥ 0,10*

e) Gas pressure $p^g \cdot 10^{-5}$ [Pa]

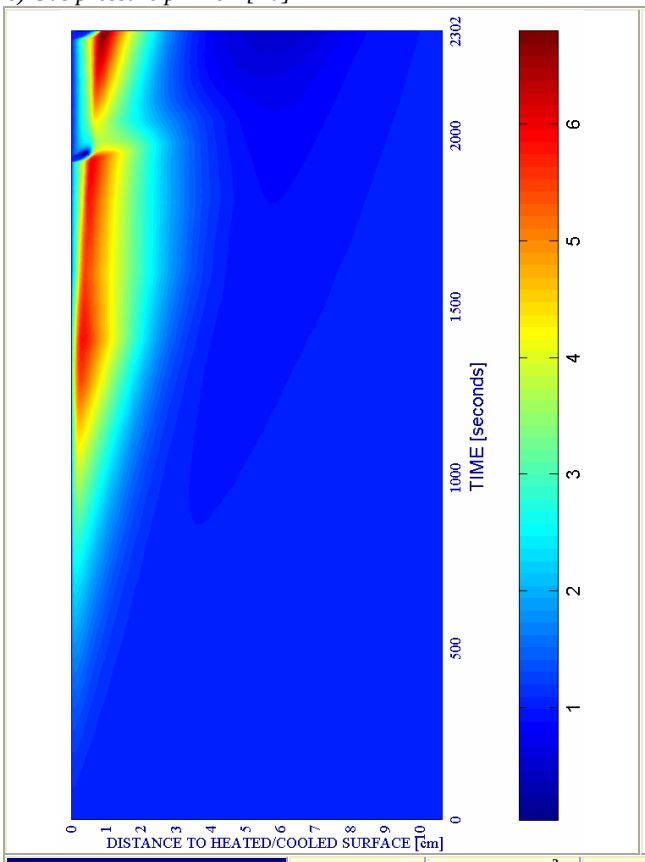

f) Vapour pressure $p^v \cdot 10^{-5}$ [Pa]

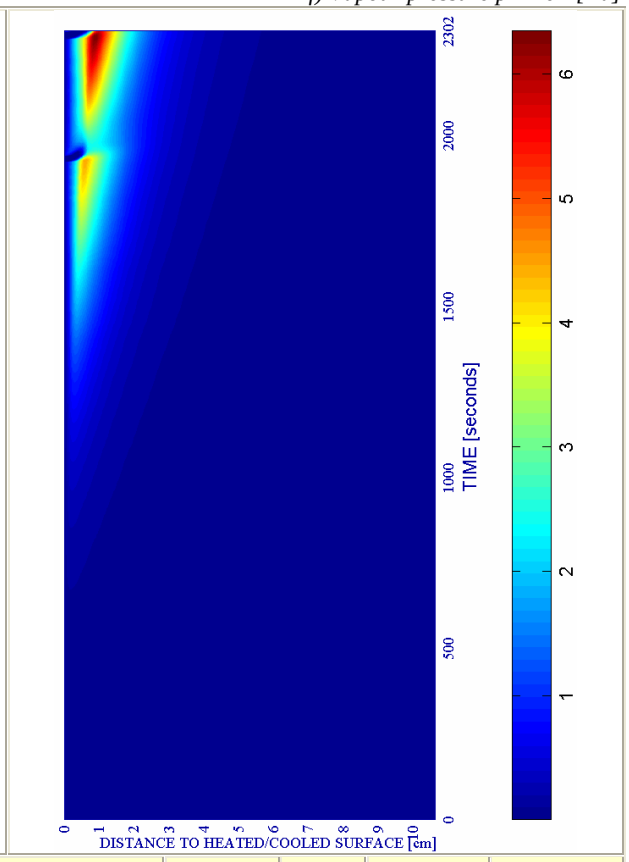

SURFACE COOL+REPEAT		PC1 - RH [%]			PC2 - K_0 [m^2]			PC4 - Heating curve			PC5 – Mat.		Cooling length[s]	Start of cooling [s]	End of cooling [s]
#	Combination	40	50	60	10^{-19}	10^{-18}	10^{-17}	PAR1	PAR2	PAR4	C60	C90			
14	TH12K018RH50PAR2C60		X			X			X		X		16 / 20	1.920 / 2.278	1.936 / 2.298

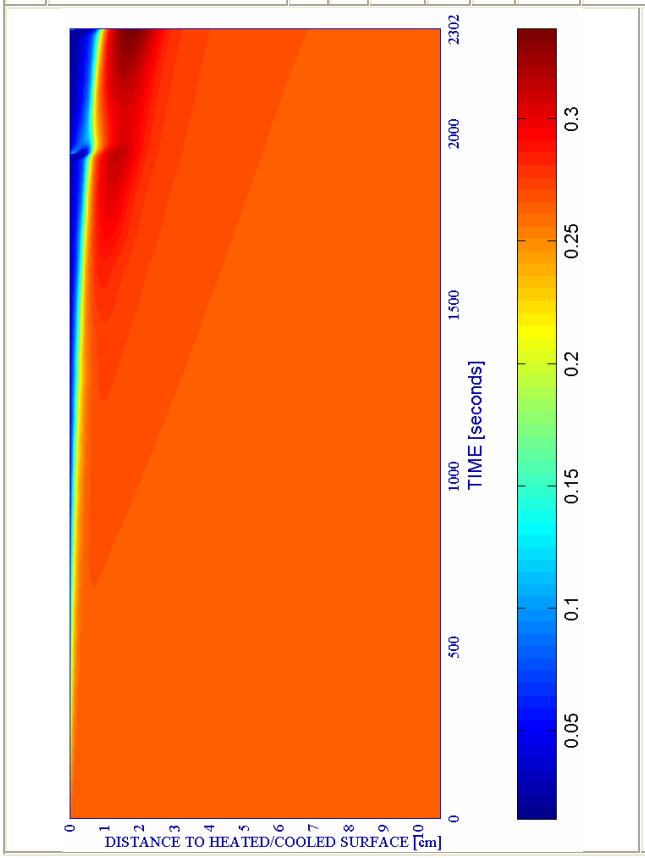

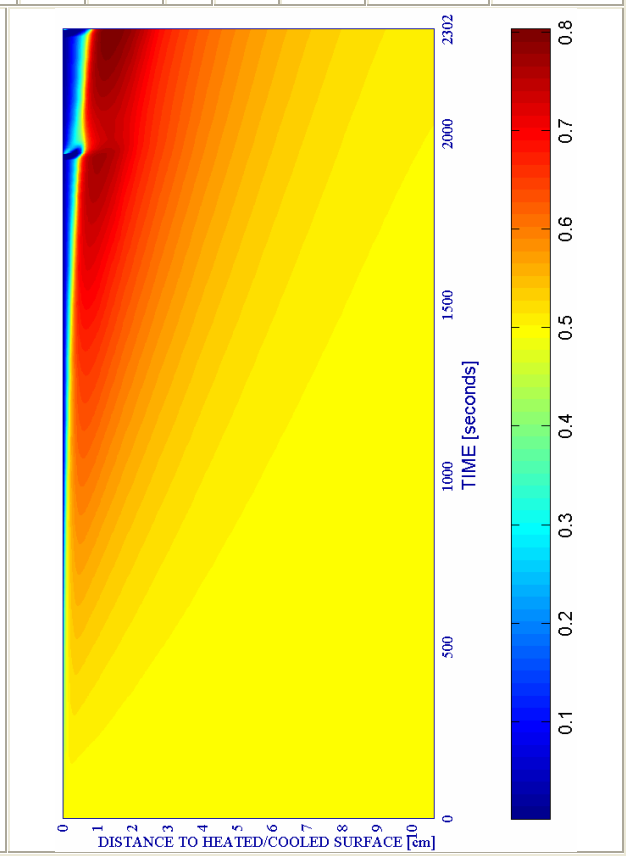

g) Saturation Degree S [-]

Figure 6-95. (continued)

h) Relative Humidity RH [-]

i) Temperature [K]

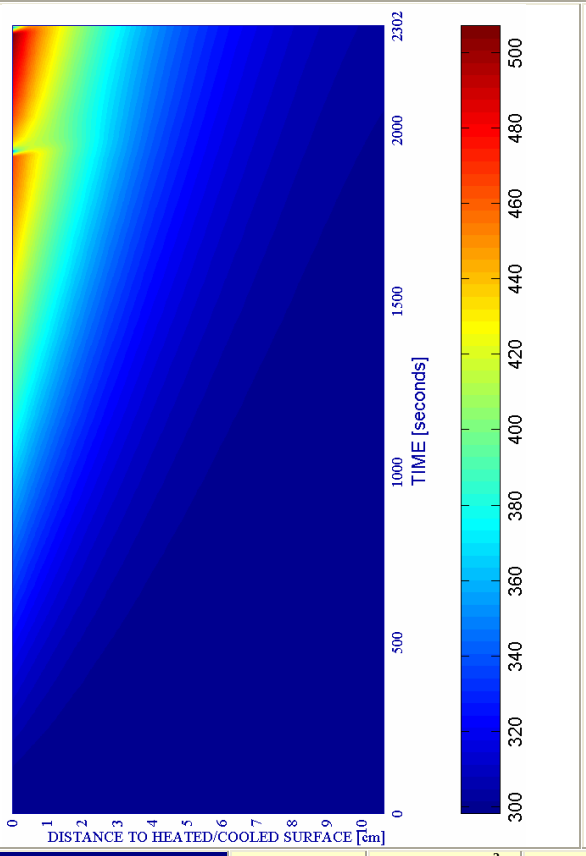

j) Elastic Energy U · 10^{-4} [J/m^3]

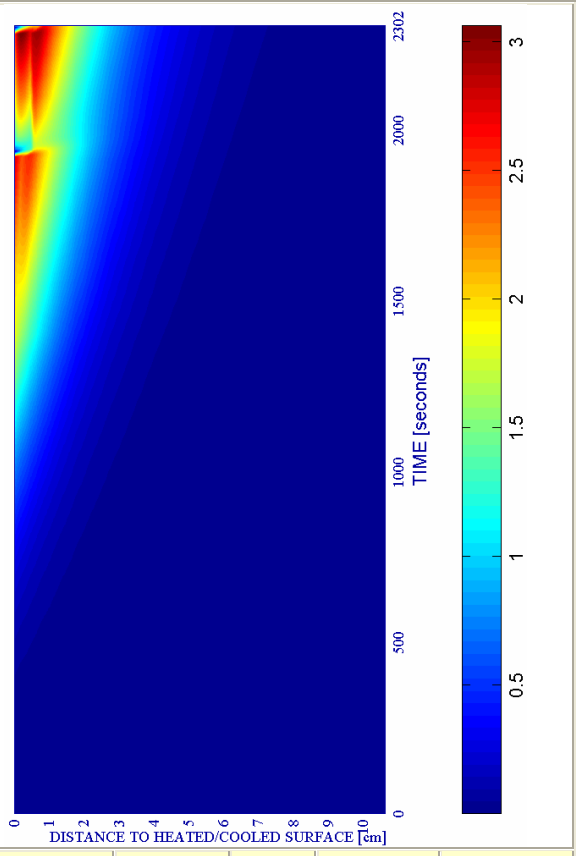

SURFACE COOL+REPEAT		PC1 - RH [%]			PC2 - K_0 [m^2]			PC4 - Heating curve			PC5 – Mat.		Cooling length[s]	Start of cooling [s]	End of cooling [s]
#	Combination	40	50	60	10^{-19}	10^{-18}	10^{-17}	PAR1	PAR2	PAR4	C60	C90			
14	TH12K018RH50PAR2C60		X			X			X		X		16 / 20	1.920 / 2.278	1.936 / 2.298

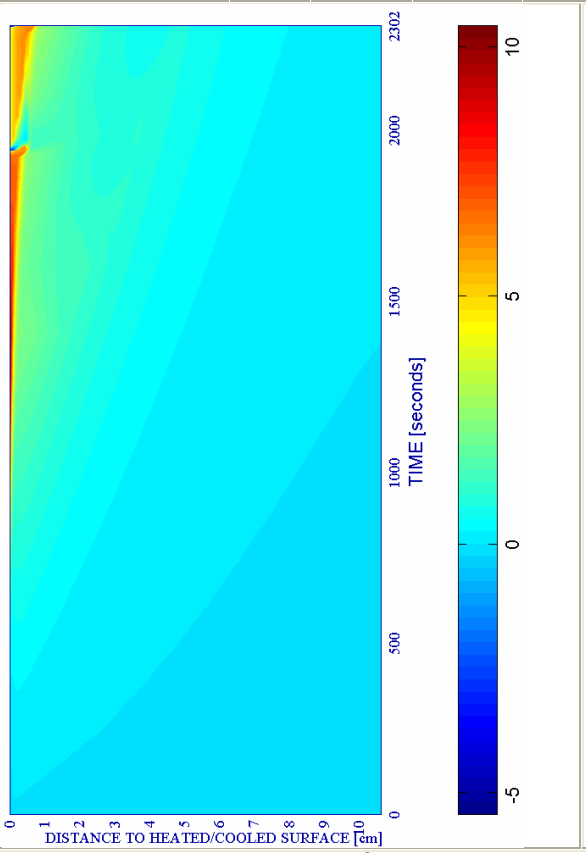

k) Stress in longitudinal (xx) direction · 10^{-6} [Pa]

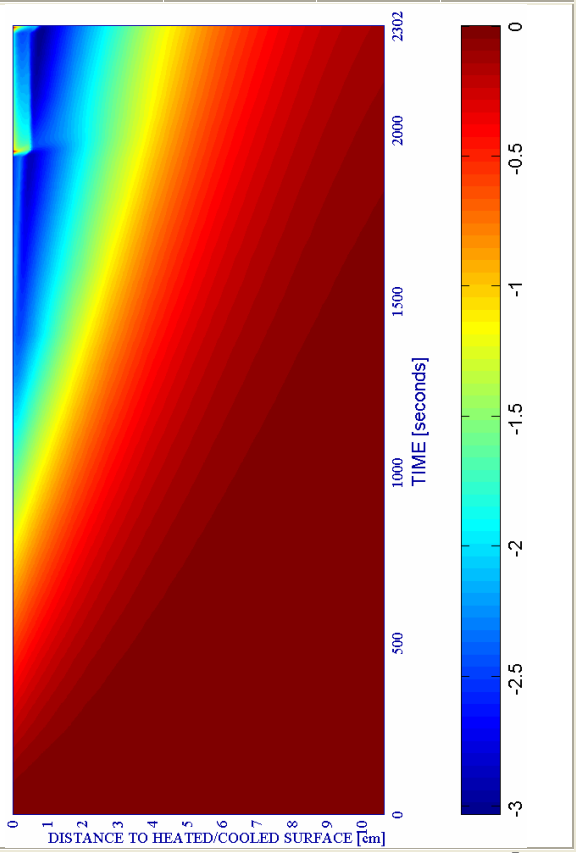

l) Stress in transversal (yy) direction · 10^{-7} [Pa]

Figure 6-95. (continued)

6.5.2.3 REFERENCE CASE # 14 – TH12K018RH50PAR2C60 – START OF COOLING: 2.400S

The main features of this reference case are the following ones:

		PC1 (RH) [%]			PC2 (K) [m^2]			PC3 (TH) [cm]			PC4 (Heating curve)			PC5 (Mat)	
#	**Combination**	**40**	**50**	**60**	10^{-19}	10^{-18}	10^{-17}	**12**	**24**	**50**	**PAR1**	**PAR2**	**PAR3**	**C60**	**C90**
14	TH12K018RH50PAR2C60		X			X		X				X		X	

Table 6-64. *Main Features of the Reference Case #14 – TH12K018RH50PAR2C60.*

with an starting instant of the first cooling process at 2.400 seconds. The types and subtypes of cooling processes analyzed in this reference case are the following ones:

Type of Cooling	***Subtype of Cooling***	***Related Paragraph***	***Figures numbers***
Environmental	Slow Cooling	6.5.2.3.1	6-96 a) to d)
Environmental	Medium Cooling	6.5.2.3.2	6-97 a) to d)
Environmental	Fast Cooling	6.5.2.3.3	6-98 a) to d)

Remark: *See each Paragraph for more details on the features of the Cooling Processes.*

Table 6-65. *Types and Subtypes of Cooling Processes Analyzed in the Reference Case #14 – TH12K018RH50PAR2C60 with the Start of Cooling Process at 2.400 seconds*

As it was explained on paragraph 6.5.2 this case shows the start instant of cooling processes as the only input difference with respect to the case analyzed deeply on paragraph 6.5.2.5. Therefore, herein are exposed the main results of this case but they are dealt in depth on *paragraph 6.5.3.2 – Analysis of the Effect of the Cooling Start Instant.*

6.5.2.3.1 Environmental Slow Cooling

Table 6-66. *Description of the Cooling Process Stages and Collection of the Main Results related to Spalling Index and velocity*

Stage description - figure 6-96 a) to d) -	**Absolute Time Start [s]**	**Absolute Time End [s]**	$IS4_{max}$ [-]	X_{IS4max} [cm]	t_{IS4max} [s]	v_{max} [m/s]	X_{vmax} [cm]	t_{vmax} [s]	v_{max}* [m/s]	X_{vmax*} [cm]	t_{vmax*} [s]
First Heating	0	2.400+120	0,0569	0,700	2.520	4,380	1,300	2.520	4,380	1,300	2.520
Environment cooling	2.520	4.560	0,0569	0,700	2.520	4,380	1,300	2.520	4,380	1,300	2.520
Environment constant Temperature up to an absolute time 10.800s	4.560	10.800	0,0008	2,600	4.560	0,932	11,500	4.560	0,000	---	---
Environment Constant Temperature for t > 10.800s	10.800	106.560	0,0000	---	---	0,000	---	---	0,000	---	---
Maximum for t ≤ 10.800s†	0	10.800	0,0569	0,700	2.520	4,380	1,300	2.520	4,380	1,300	2.520
Absolute Maximum	0	106.560	0,0569	0,700	2.520	4,380	1,300	2.520	4,380	1,300	2.520

Remark †: *These results are included for the Comparative Analysis developed on Paragraph 6.5.3*

Stage description - figure 6-96 a) to d) -	**Absolute Time Start [s]**	**Absolute Time End [s]**	d_{max} [-]	X_{dmax} [cm]	t_{dmax} [s]	T_{max} [K]	X_{Tmax} [cm]	t_{Tmax} [s]	p^g_{max} [MPa]	X_{pgmax} [cm]	t_{pgmax} [s]
First Heating	0	2.400+120	0,4324	0,700	2.520	542,44	0,000	2.520	0,8079	1,200	2.490
Environment cooling	2.520	4.560	0,5977	0,000	4.560	542,44	0,000	2.520	0,8027	1,200	2.520
Environment constant Temperature up to an absolute time 10.800s	4.560	10.800	0,7158	0,200	10.800	403,42	1,200	4.560	0,3232	2,900	4.560
Environment Constant Temperature for t > 10.800s	10.800	106.560	0,7901	1,300	23.760	358,03	4,100	10.800	0,2403	9,600	10.800
Maximum for t ≤ 10.800s†	0	10.800	0,7158	0,200	10.800	542,44	0,000	2.520	0,8079	1,200	2.490
Absolute Maximum	0	106.560	0,7901	1,300	23.760	542,44	0,000	2.520	0,8079	1,200	2.490

Table 6-67. *Description of the Cooling Process Stages and Collection of the Main Results related to mechanical damage, Temperature and Gas Pressure*

a) Spalling Index IS4 [-]

b) Mechanical damage d [-]

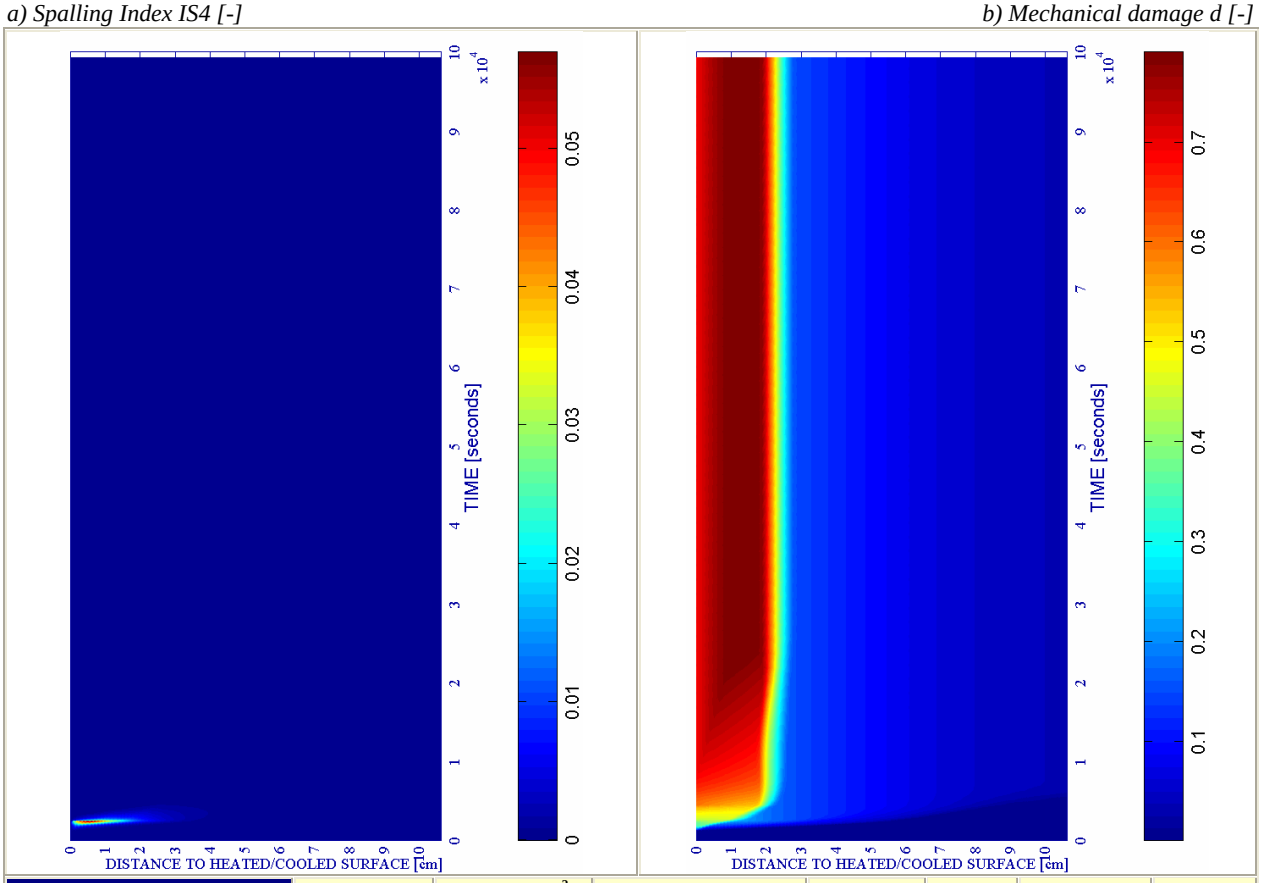

ENVIRONMENTAL - SLOW		PC1 - RH [%]			PC2 - K_0 [m^2]			PC4 - Heating curve			PC5 – Mat.		Cooling length[s]	Start of cooling [s]	End of cooling [s]
#	Combination	40	50	60	10^{-19}	10^{-18}	10^{-17}	PAR1	PAR2	PAR4	C60	C90			
14	TH12K018RH50PAR2C60		X			X			X		X		2.040	2.400+120	4.560

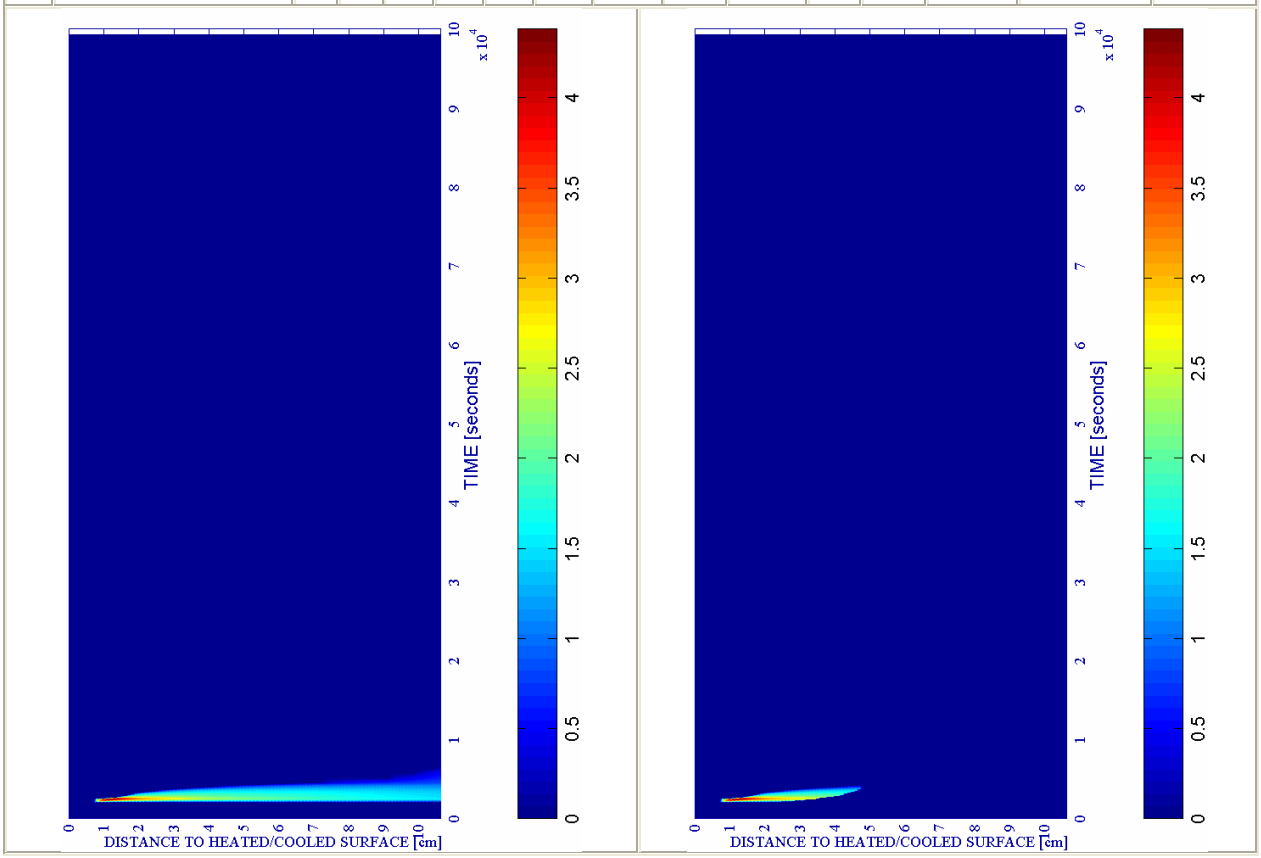

c) Velocity of spalled pieces v [m/s]

Figure 6-96.

d) Velocity [m/s] where d ≥ 0,10

6.5.2.3.2 Environmental Medium Cooling

Table 6-68. *Description of the Cooling Process Stages and Collection of the Main Results related to Spalling Index and velocity*

Stage description - figure 6-97 a) to d) -	**Absolute Time Start [s]**	**Absolute Time End [s]**	**$IS4_{max}$ [-]**	**X_{IS4max} [cm]**	**t_{IS4max} [s]**	**v_{max} [m/s]**	**X_{vmax} [cm]**	**t_{vmax} [s]**	**v_{max}^* [m/s]**	**X_{vmax*} [cm]**	**t_{vmax*} [s]**
First Heating	0	2.400+120	0,0569	0,700	2.520	4,380	1,300	2.520	4,380	1,300	2.520
Environment cooling	2.520	2.720	0,0569	0,700	2.520	4,380	1,300	2.520	4,380	1,300	2.520
Environment constant Temperature up to an absolute time 10.800s	2.720	10.800	0,0095	1,600	2.720	1,906	2,400	2.720	1,906	2,400	2.720
Environment Constant Temperature for t > 10.800s	10.800	104.720	0,0000	---	---	0,000	---	---	0,000	---	---
Maximum for t ≤ 10.800s†	0	10.800	0,0569	0,700	2.520	4,380	1,300	2.520	4,380	1,300	2.520
Absolute Maximum	0	104.720	0,0569	0,700	2.520	4,380	1,300	2.520	4,380	1,300	2.520

Remark †: *These results are included for the Comparative Analysis developed on Paragraph 6.5.3*

Stage description - figure 6-97 a) to d) -	**Absolute Time Start [s]**	**Absolute Time End [s]**	**d_{max} [-]**	**X_{dmax} [cm]**	**t_{dmax} [s]**	**T_{max} [K]**	**X_{Tmax} [cm]**	**t_{Tmax} [s]**	**p^g_{max} [MPa]**	**X_{pgmax} [cm]**	**t_{pgmax} [s]**
First Heating	0	2.400+120	0,4324	0,700	2.520	542,44	0,000	2.520	0,8079	1,200	2.490
Environment cooling	2.520	2.720	0,4843	0,000	2.720	542,44	0,000	2.520	0,8027	1,200	2.520
Environment constant Temperature up to an absolute time 10.800s	2.720	10.800	0,7470	0,400	10.800	464,62	0,400	2.720	0,5786	1,700	2.720
Environment Constant Temperature for t > 10.800s	10.800	104.720	0,7773	1,000	18.320	349,21	4,200	10.800	0,2375	10,300	10.800
Maximum for t ≤ 10.800s†	0	10.800	0,7470	0,400	10.800	542,44	0,000	2.520	0,8079	1,200	2.490
Absolute Maximum	0	104.720	0,7773	1,000	18.320	542,44	0,000	2.520	0,8079	1,200	2.490

Table 6-69. *Description of the Cooling Process Stages and Collection of the Main Results related to mechanical damage, Temperature and Gas Pressure*

6.5.2.3.3 Environmental Fast Cooling

Table 6-70. *Description of the Cooling Process Stages and Collection of the Main Results related to Spalling Index and velocity*

Stage description - figure 6-98 a) to d) -	**Absolute Time Start [s]**	**Absolute Time End [s]**	**$IS4_{max}$ [-]**	**X_{IS4max} [cm]**	**t_{IS4max} [s]**	**v_{max} [m/s]**	**X_{vmax} [cm]**	**t_{vmax} [s]**	**v_{max}^* [m/s]**	**X_{vmax*} [cm]**	**t_{vmax*} [s]**
First Heating	0	2.400+120	0,0569	0,700	2.520	4,380	1,300	2.520	4,380	1,300	2.520
Environment cooling	2.520	2.540	0,0569	0,700	2.520	4,380	1,300	2.520	4,380	1,300	2.520
Environment constant Temperature up to an absolute time 10.800s	2.540	10.800	0,0383	0,800	2.540	4,095	1,300	2.540	4,095	1,300	2.540
Environment Constant Temperature for t > 10.800s	10.800	99.836	0,0000	---	---	0,000	---	---	0,000	---	---
Maximum for t ≤ 10.800s†	0	10.800	0,0569	0,700	2.520	4,380	1,300	2.520	4,380	1,300	2.520
Absolute Maximum	0	99.836	0,0569	0,700	2.520	4,380	1,300	2.520	4,380	1,300	2.520

Remark †: *These results are included for the Comparative Analysis developed on Paragraph 6.5.3*

Stage description - figure 6-98 a) to d) -	**Absolute Time Start [s]**	**Absolute Time End [s]**	**d_{max} [-]**	**X_{dmax} [cm]**	**t_{dmax} [s]**	**T_{max} [K]**	**X_{Tmax} [cm]**	**t_{Tmax} [s]**	**p^g_{max} [MPa]**	**X_{pgmax} [cm]**	**t_{pgmax} [s]**
First Heating	0	2.400+120	0,4324	0,700	2.520	542,44	0,000	2.520	0,8079	1,200	2.490
Environment cooling	2.520	2.540	0,4363	0,700	2.535,5	542,44	0,000	2.520	0,8027	1,200	2.520
Environment constant Temperature up to an absolute time 10.800s	2.540	10.800	0,7481	0,400	10.800	511,81	0,100	2.540	0,7933	1,300	2.540
Environment Constant Temperature for t > 10.800s	10.800	99.836	0,7754	0,900	16.436	348,79	4,300	10.800	0,2364	10,300	10.800
Maximum for t ≤ 10.800s†	0	10.800	0,7481	0,400	10.800	542,44	0,000	2.520	0,8079	1,200	2.490
Absolute Maximum	0	99.836	0,7754	0,900	16.436	542,44	0,000	2.520	0,8079	1,200	2.490

Table 6-71. *Description of the Cooling Process Stages and Collection of the Main Results related to mechanical damage, Temperature and Gas Pressure*

a) Spalling Index IS4 [-] *b) Mechanical damage d [-]*

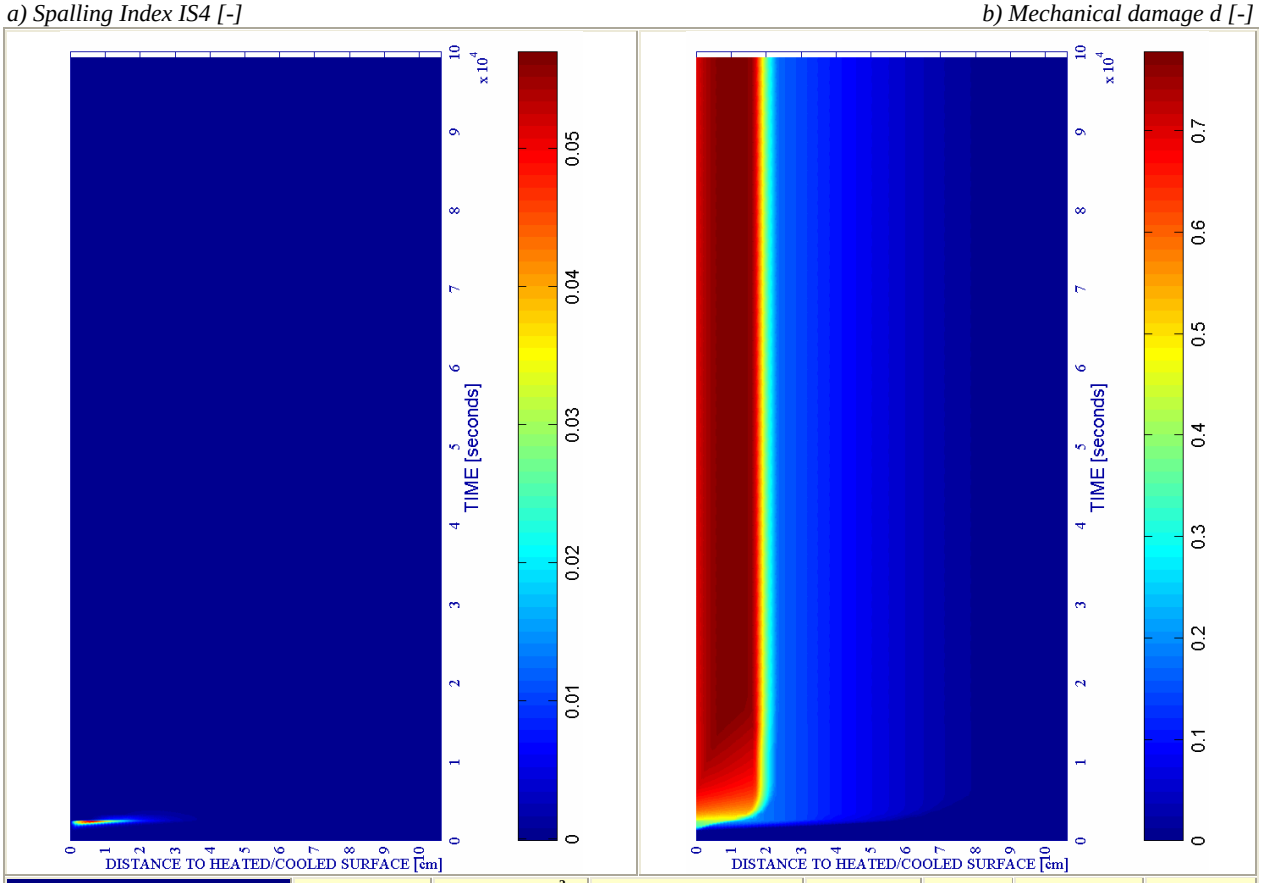

ENVIRONMENTAL - MED.	PC1 - RH [%]			PC2 - K_0 [m^2]			PC4 - Heating curve			PC5 – Mat.		Cooling length[s]	Start of cooling [s]	End of cooling [s]
#	Combination	40	50	60	10^{-19}	10^{-18}	10^{-17}	PAR1	PAR2	PAR4	C60	C90			
14	TH12K018RH50PAR2C60		X			X			X		X		200	2.400+120	2.720

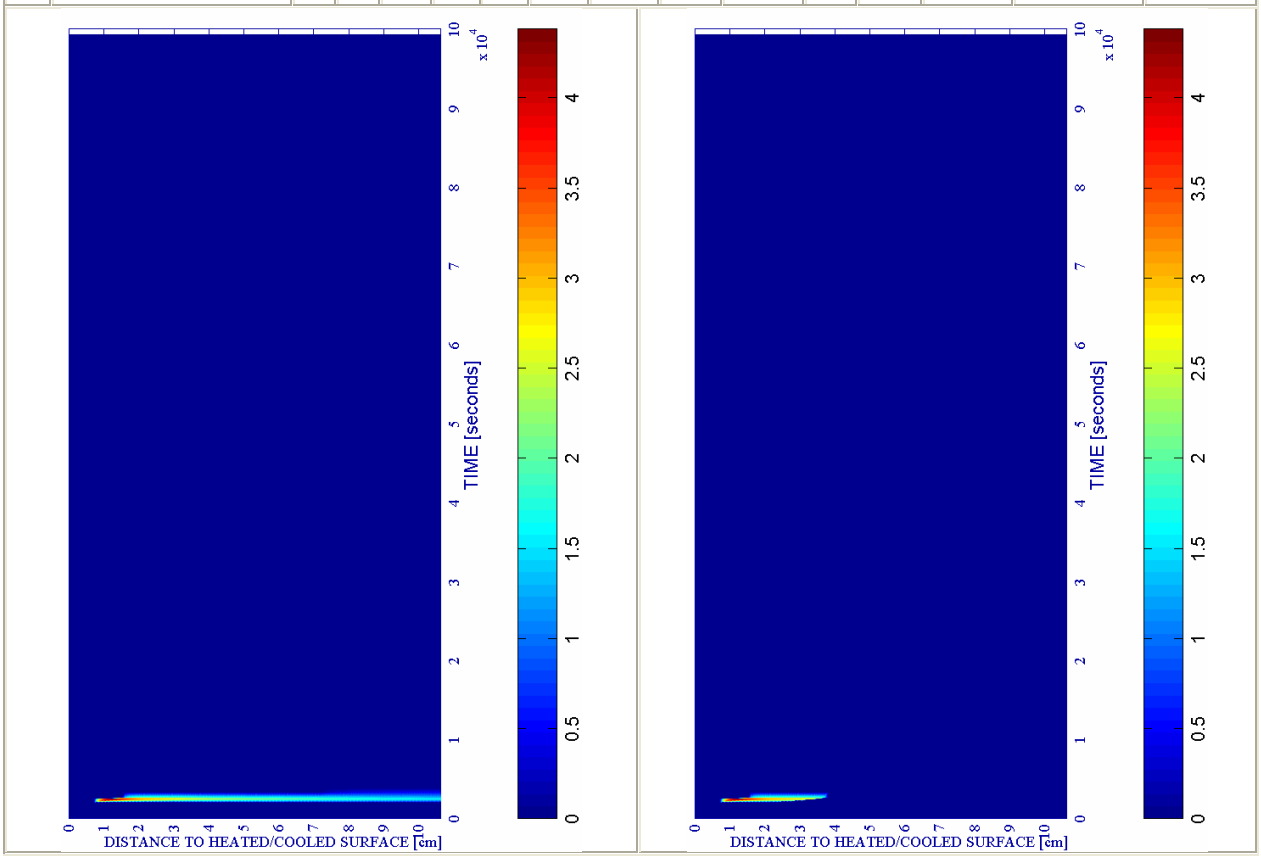

c) Velocity of spalled pieces v [m/s] ***Figure 6-97.*** *d) Velocity [m/s] where d ≥ 0,10*

a) Spalling Index IS4 [-] *b) Mechanical damage d [-]*

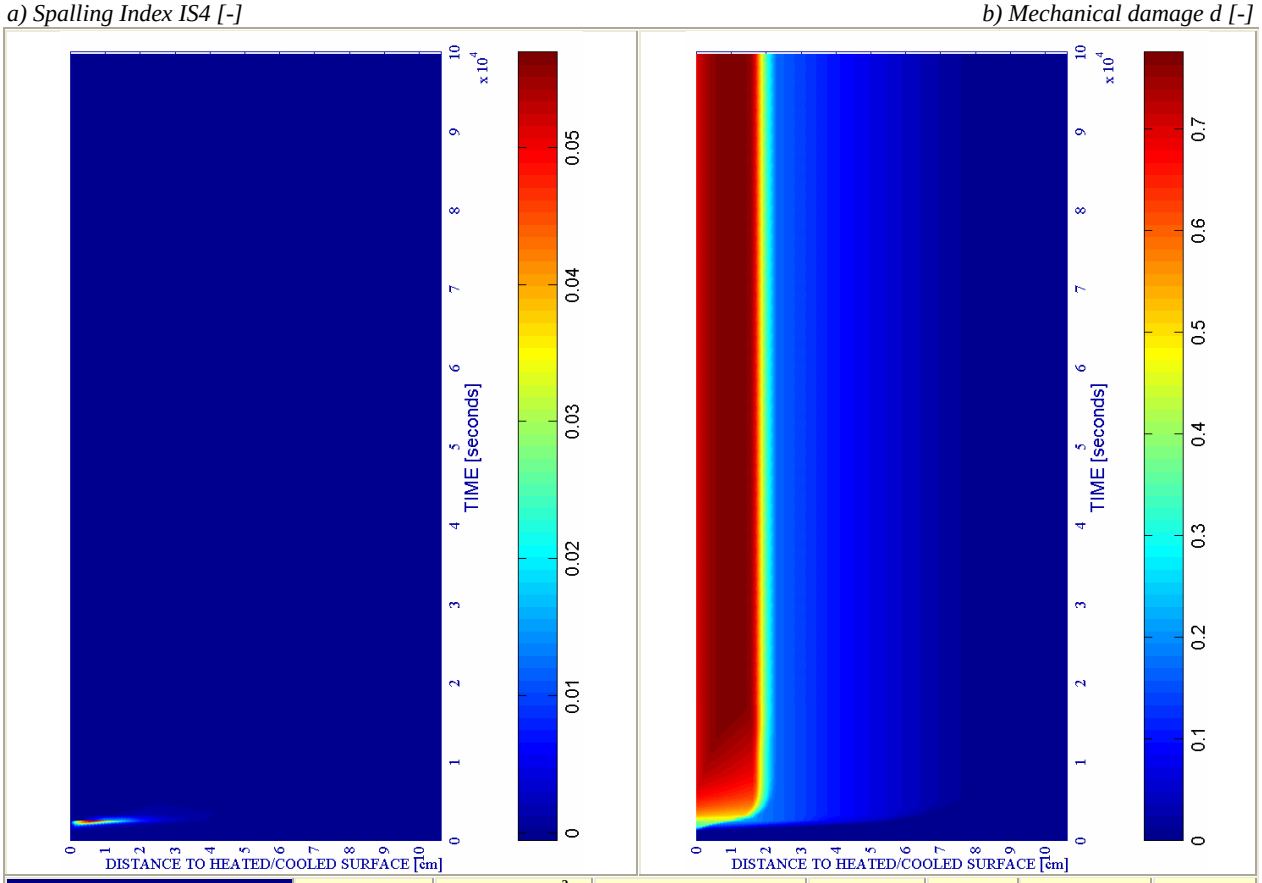

ENVIRONMENTAL - FAST	PC1 - RH [%]			PC2 - K_0 [m^2]			PC4 - Heating curve			PC5 – Mat.		Cooling length[s]	Start of cooling [s]	End of cooling [s]
#	Combination	40	50	60	10^{-19}	10^{-18}	10^{-17}	PAR1	PAR2	PAR4	C60	C90			
14	TH12K018RH50PAR2C60		X			X			X		X		20	2.400+120	2.540

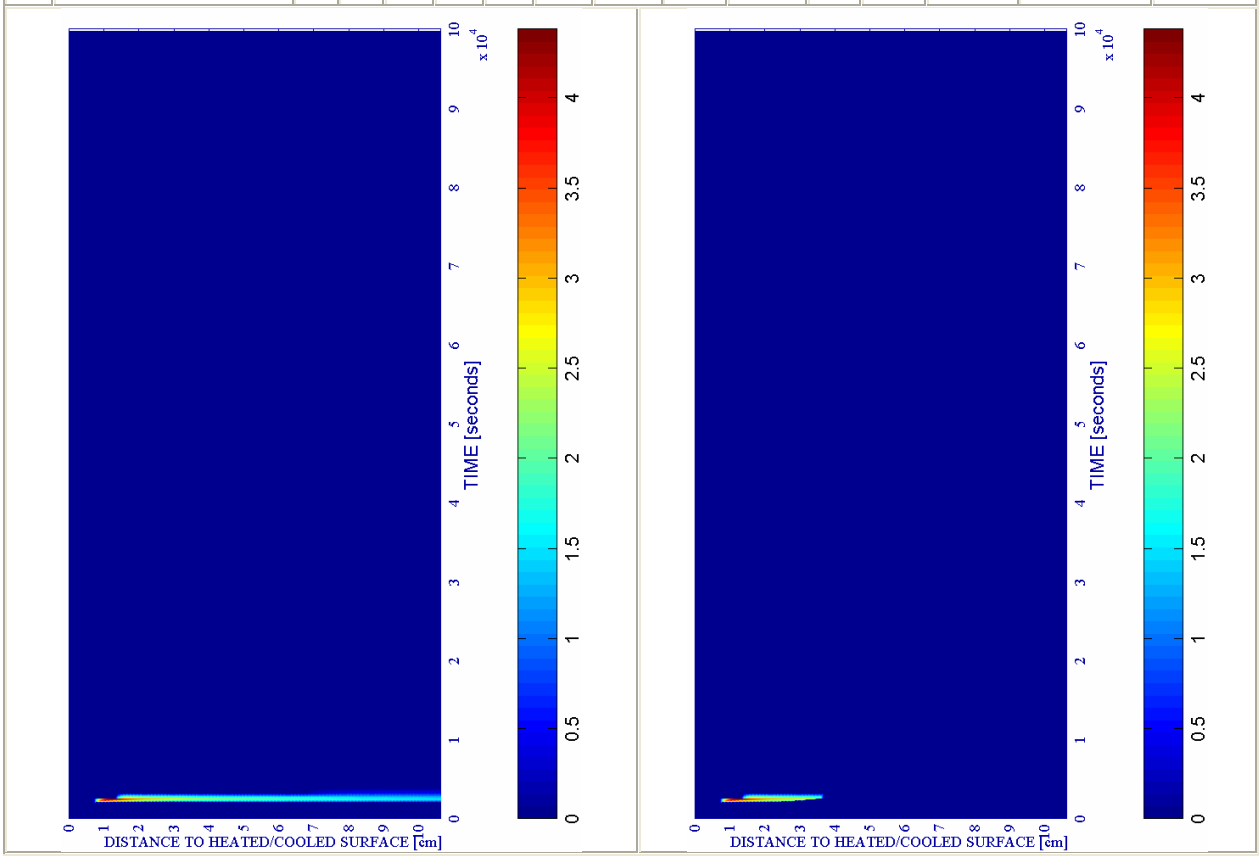

c) Velocity of spalled pieces v [m/s] ***Figure 6-98.*** *d) Velocity [m/s] where d ≥ 0,10*

6.5.2.4 REFERENCE CASE # 14 – TH12K018RH50PAR2C60 – START OF COOLING: 3.000S

The main features of this reference case are the following ones:

		PC1 (RH) [%]			PC2 (K) [m^2]			PC3 (TH) [cm]			PC4 (Heating curve)			PC5 (Mat)	
#	**Combination**	**40**	**50**	**60**	10^{-19}	10^{-18}	10^{-17}	**12**	**24**	**50**	**PAR1**	**PAR2**	**PAR3**	**C60**	**C90**
14	TH12K018RH50PAR2C60		X			X		X				X		X	

Table 6-72. *Main Features of the Reference Case #14 – TH12K018RH50PAR2C60.*

with an starting instant of the first cooling process at 3.000 seconds. The types and subtypes of cooling processes analyzed in this reference case are the following ones:

Type of Cooling	***Subtype of Cooling***	***Related Paragraph***	***Figures numbers***
Environmental	Slow Cooling	6.5.2.4.1	6-99 a) to d)
Environmental	Medium Cooling	6.5.2.4.2	6-100 a) to d)
Environmental	Fast Cooling	6.5.2.4.3	6-101 a) to d)
Surface	Followed by an imposed constant Surface Temperature	6.5.2.4.4	6-102 a) to d)

Remark: *See each Paragraph for more details on the features of the Cooling Processes.*

Table 6-73. *Types and Subtypes of Cooling Processes Analyzed in the Reference Case #14 – TH12K018RH50PAR2C60 with the Start of Cooling Process at 3.000 seconds*

As it was explained o paragraph 6.5.2 this case shows the start instant of cooling processes as the only input difference with respect to the case analyzed deeply on paragraph 6.5.2.5. Therefore, herein are exposed the main results of this case but they are dealt in depth on *paragraph 6.5.3.2 – Analysis of the Effect of the Cooling Start Instant*.

6.5.2.4.1 Environmental Slow Cooling

Table 6-74. *Description of the Cooling Process Stages and Collection of the Main Results related to Spalling Index and velocity*

Stage description - figure 6-99 a) to d) -	**Absolute Time Start [s]**	**Absolute Time End [s]**	**$IS4_{max}$ [-]**	**X_{IS4max} [cm]**	**t_{IS4max} [s]**	**v_{max} [m/s]**	**X_{vmax} [cm]**	**t_{vmax} [s]**	**v_{max}* [m/s]**	**X_{vmax*} [cm]**	**t_{vmax*} [s]**
First Heating	0	3.000+120	0,0894	0,974	3.090	5,228	2,037	3.090	5,228	2,037	3.090
Environment cooling	3.120	5.460	0,0893	0,974	3.120	5,224	2,037	3.120	5,224	2,037	3.120
Environment constant Temperature up to an absolute time 10.800s	5.460	10.800	0,0015	0,633	5.460	1,806	10,632	5.460	1,695	7,272	5.460
Environment Constant Temperature for t > 10.800s	10.800	101.460	0,0002	4,314	10.800	1,902	4,496	101.460	1,902	4,496	101.460
Maximum for t ≤ 10.800s†	0	10.800	0,0894	0,974	3.090	5,228	2,037	3.090	5,228	2,037	3.090
Absolute Maximum	0	101.460	0,0894	0,974	3.090	5,228	2,037	3.090	5,228	2,037	3.090

Remark †: *These results are included for the Comparative Analysis developed on Paragraph 6.5.3*

Stage description - figure 6-99 a) to d) -	**Absolute Time Start [s]**	**Absolute Time End [s]**	**d_{max} [-]**	**X_{dmax} [cm]**	**t_{dmax} [s]**	**T_{max} [K]**	**X_{Tmax} [cm]**	**t_{Tmax} [s]**	**p^g_{max} [MPa]**	**X_{pgmax} [cm]**	**t_{pgmax} [s]**
First Heating	0	3.000+120	0,5079	1,470	3.120	614,64	0,000	3.120	0,8256	1,555	2.760
Environment cooling	3.120	5.460	0,6335	0,000	5.460	614,64	0,000	3.120	0,8087	2,145	3.120
Environment constant Temperature up to an absolute time 10.800s	5.460	10.800	0,7105	0,000	10.800	428.31	1,555	5.460	0,3530	4,137	5.460
Environment Constant Temperature for t > 10.800s	10.800	101.460	0,8823	2,258	41.460	381,74	3,321	10.800	0,2660	8,007	10.800
Maximum for t ≤ 10.800s†	0	10.800	0,7105	0,000	10.800	614,64	0,000	3.120	0,8256	1,555	2.760
Absolute Maximum	0	101.460	0,8823	2,258	41.460	614,64	0,000	3.120	0,8256	1,555	2.760

Table 6-75. *Description of the Cooling Process Stages and Collection of the Main Results related to mechanical damage, Temperature and Gas Pressure*

a) Spalling Index IS4 [-] *b) Mechanical damage d [-]*

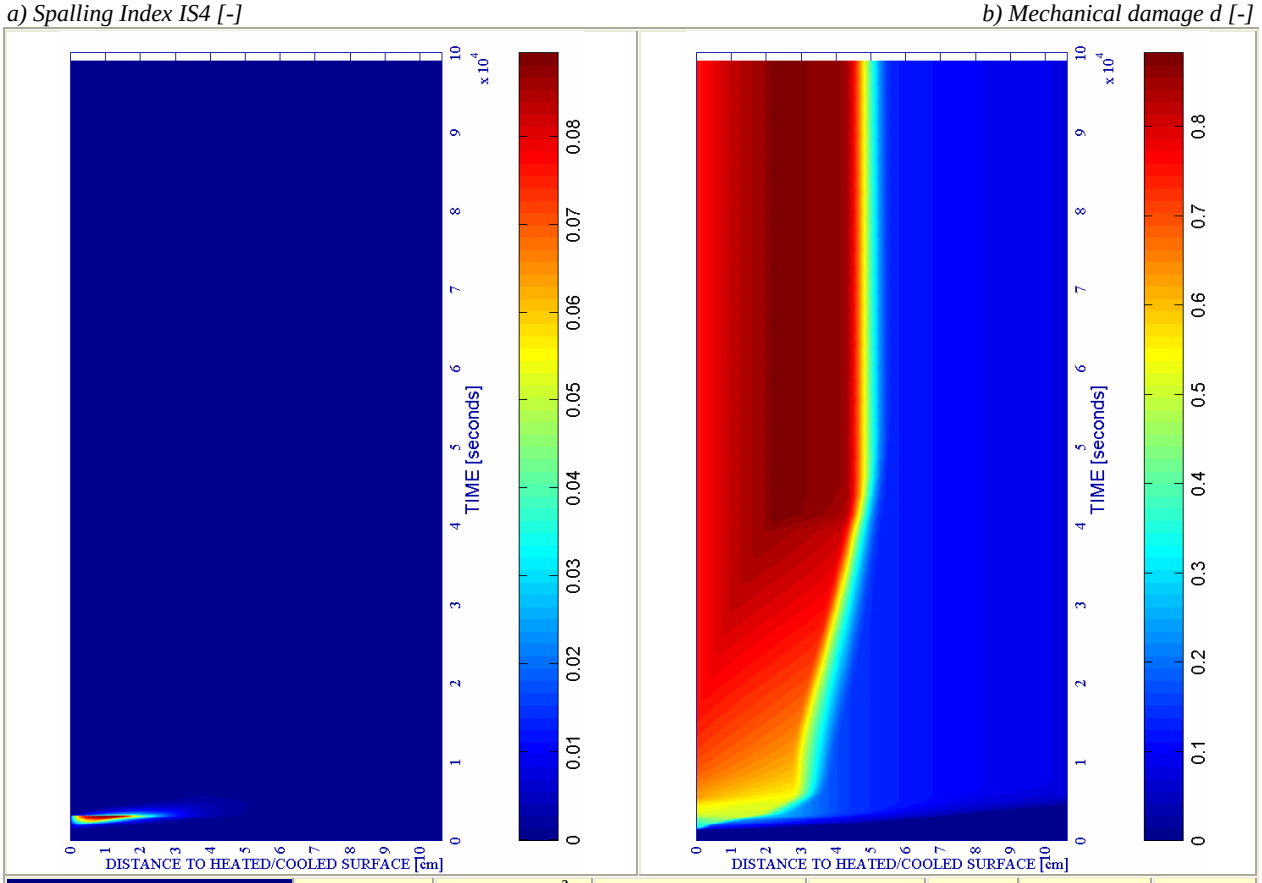

ENVIRONMENTAL - SLOW		PC1 - RH [%]			PC2 - K_0 [m^2]			PC4 - Heating curve			PC5 – Mat.		Cooling length[s]	Start of cooling [s]	End of cooling [s]
#	Combination	40	50	60	10^{-19}	10^{-18}	10^{-17}	PAR1	PAR2	PAR4	C60	C90			
14	TH12K018RH50PAR2C60		X			X			X		X		2.340	3.000+120	5.460

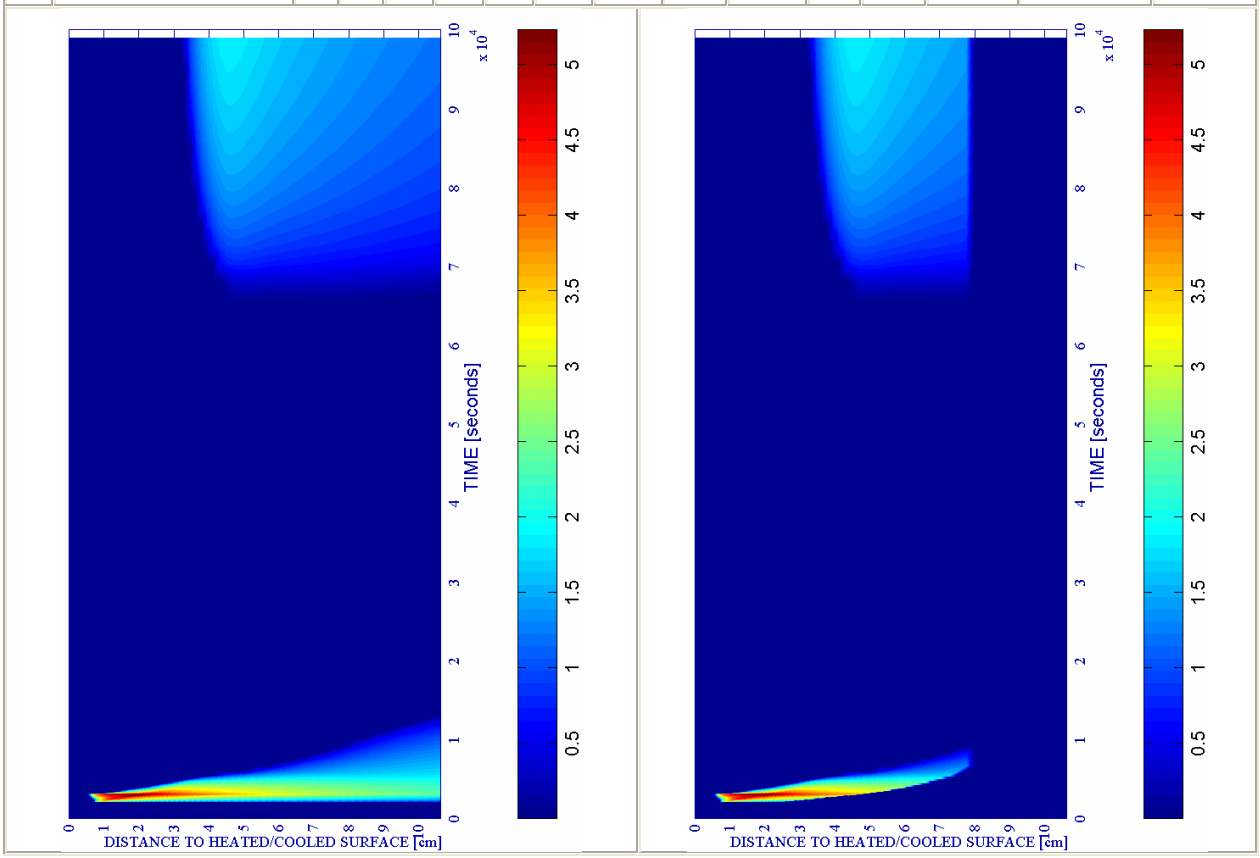

c) Velocity of spalled pieces v [m/s] ***Figure 6-99.*** *d) Velocity [m/s] where d ≥ 0,10*

6.5.2.4.2 Environmental Medium Cooling

Table 6-76. *Description of the Cooling Process Stages and Collection of the Main Results related to Spalling Index and velocity*

Stage description -figure 6-100 a) to d)-	**Absolute Time Start [s]**	**Absolute Time End [s]**	**$IS4_{max}$ [-]**	**X_{IS4max} [cm]**	**t_{IS4max} [s]**	**v_{max} [m/s]**	**X_{vmax} [cm]**	**t_{vmax} [s]**	**v_{max}* [m/s]**	**X_{vmax*} [cm]**	**t_{vmax*} [s]**
First Heating	0	3.000+120	0,0894	0,974	3.090	5,228	2,037	3.090	5,228	2,037	3.090
Environment cooling	3.120	3.360	0,0893	0,974	3.120	5,224	2,037	3.120	5,224	2,037	3.120
Environment constant Temperature up to an absolute time 10.800s	3.360	10.800	0,0180	1,932	3.360	3,564	2,623	3.360	3,564	2,623	3.360
Environment Constant Temperature for t > 10.800s	10.800	99.360	0,0001	3,633	10.800	0,000	---	---	0,000	---	---
Maximum for t ≤ 10.800s†	0	10.800	0,0894	0,974	3.090	5,228	2,037	3.090	5,228	2,037	3.090
Absolute Maximum	0	99.360	0,0894	0,974	3.090	5,228	2,037	3.090	5,228	2,037	3.090

Remark †: *These results are included for the Comparative Analysis developed on Paragraph 6.5.3*

Stage description -figure 6-100 a) to d)-	**Absolute Time Start [s]**	**Absolute Time End [s]**	**d_{max} [-]**	**X_{dmax} [cm]**	**t_{dmax} [s]**	**T_{max} [K]**	**X_{Tmax} [cm]**	**t_{Tmax} [s]**	**p^g_{max} [MPa]**	**X_{pgmax} [cm]**	**t_{pgmax} [s]**
First Heating	0	3.000+120	0,5079	1,470	3.120	614,64	0,000	3.120	0,8256	1,555	2.760
Environment cooling	3.120	3.360	0,5496	0,000	3.360	614,64	0,000	3.120	0,8087	2,145	3.120
Environment constant Temperature up to an absolute time 10.800s	3.360	10.800	0,7376	0,000	10.800	507,56	0,474	3.360	0,6234	2,623	3.360
Environment Constant Temperature for t > 10.800s	10.800	99.360	0,8543	2,258	36.960	370,57	3,321	10.800	0,2486	8,771	10.800
Maximum for t ≤ 10.800s†	0	10.800	0,7376	0,000	10.800	614,64	0,000	3.120	0,8256	1,555	2.760
Absolute Maximum	0	99.360	0,8543	2,258	36.960	614,64	0,000	3.120	0,8256	1,555	2.760

Table 6-77. *Description of the Cooling Process Stages and Collection of the Main Results related to mechanical damage, Temperature and Gas Pressure*

6.5.2.4.3 Environmental Fast Cooling

Table 6-78. *Description of the Cooling Process Stages and Collection of the Main Results related to Spalling Index and velocity*

Stage description -figure 6-101 a) to d)-	**Absolute Time Start [s]**	**Absolute Time End [s]**	**$IS4_{max}$ [-]**	**X_{IS4max} [cm]**	**t_{IS4max} [s]**	**v_{max} [m/s]**	**X_{vmax} [cm]**	**t_{vmax} [s]**	**v_{max}* [m/s]**	**X_{vmax*} [cm]**	**t_{vmax*} [s]**
First Heating	0	3.000+120	0,0894	0,974	3.090	5,228	2,037	3.090	5,228	2,037	3.090
Environment cooling	3.120	3.144	0,0893	0,974	3.120	5,224	2,037	3.120	5,224	2,037	3.120
Environment constant Temperature up to an absolute time 10.800s	3.144	10.800	0,0664	1,470	3.144	4,982	2,145	3.144	4,982	2,145	3.144
Environment Constant Temperature for t > 10.800s	10.800	99.144	0,0001	3,633	10.800	0,000	---	---	0,000	---	---
Maximum for t ≤ 10.800s†	0	10.800	0,0894	0,974	3.090	5,228	2,037	3.090	5,228	2,037	3.090
Absolute Maximum	0	99.144	0,0894	0,974	3.090	5,228	2,037	3.090	5,228	2,037	3.090

Remark †: *These results are included for the Comparative Analysis developed on Paragraph 6.5.3*

Stage description -figure 6-101 a) to d)-	**Absolute Time Start [s]**	**Absolute Time End [s]**	**d_{max} [-]**	**X_{dmax} [cm]**	**t_{dmax} [s]**	**T_{max} [K]**	**X_{Tmax} [cm]**	**t_{Tmax} [s]**	**p^g_{max} [MPa]**	**X_{pgmax} [cm]**	**t_{pgmax} [s]**
First Heating	0	3.000+120	0,5079	1,470	3.120	614,64	0,000	3.120	0,8256	1,555	2.760
Environment cooling	3.120	3.144	0,5091	1,470	3.135	614,64	0,000	3.120	0,8087	2,145	3.120
Environment constant Temperature up to an absolute time 10.800s	3.144	10.800	0,7372	0,000	10.800	572,00	0,152	3.144	0,7899	2,145	3.144
Environment Constant Temperature for t > 10.800s	10.800	99.144	0,8529	2,145	36.744	370,67	3,475	10.800	0,2493	8,771	10.800
Maximum for t ≤ 10.800s†	0	10.800	0,7372	0,000	10.800	614,64	0,000	3.120	0,8256	1,555	2.760
Absolute Maximum	0	99.144	0,8529	2,145	36.744	614,64	0,000	3.120	0,8256	1,555	2.760

Table 6-79. *Description of the Cooling Process Stages and Collection of the Main Results related to mechanical damage, Temperature and Gas Pressure*

a) Spalling Index IS4 [-] *b) Mechanical damage d [-]*

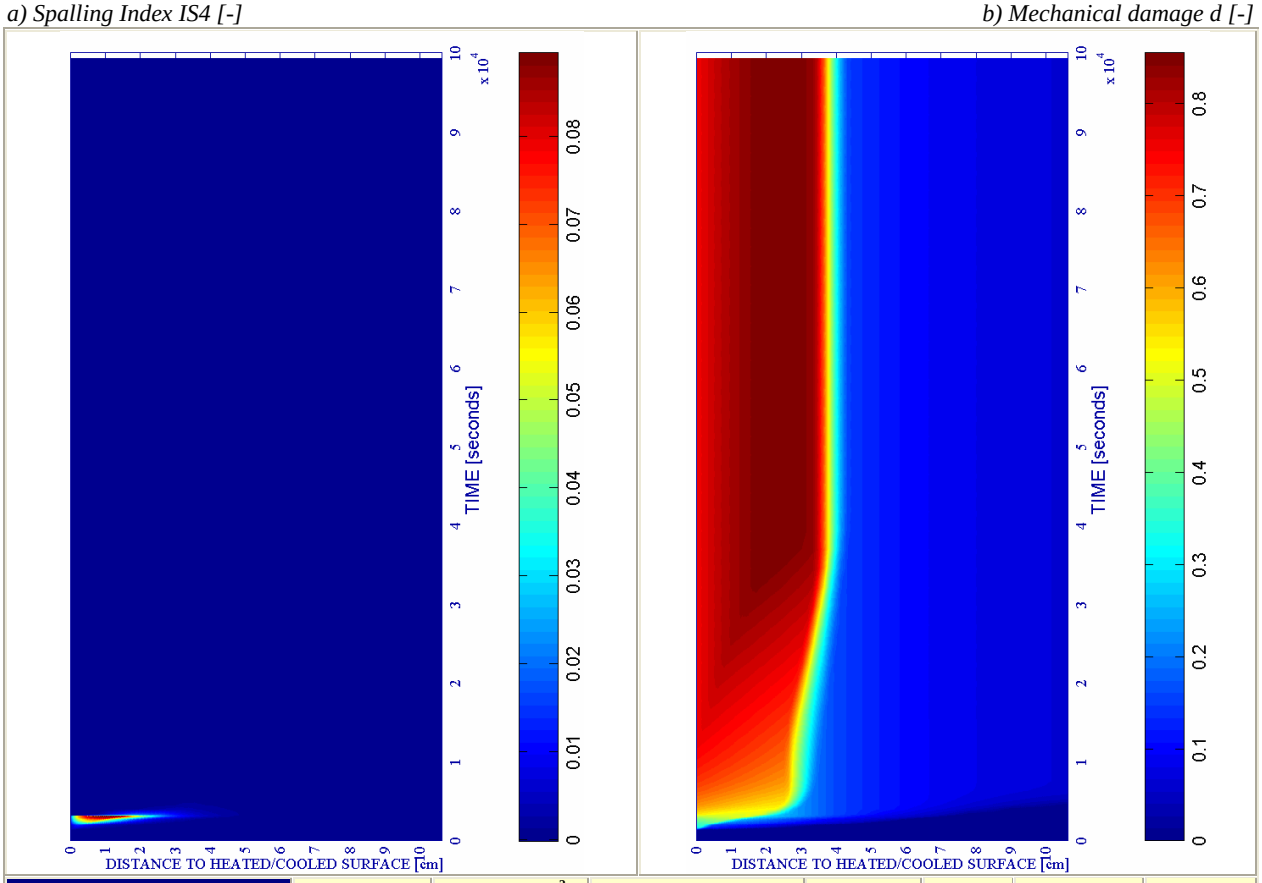

ENVIRONMENTAL - MED.		PC1 - RH [%]			PC2 - K_0 [m^2]			PC4 - Heating curve			PC5 – Mat.		Cooling length[s]	Start of cooling [s]	End of cooling [s]
#	Combination	40	50	60	10^{-19}	10^{-18}	10^{-17}	PAR1	PAR2	PAR4	C60	C90			
14	TH12K018RH50PAR2C60		X			X			X		X		240	3.000+120	3.360

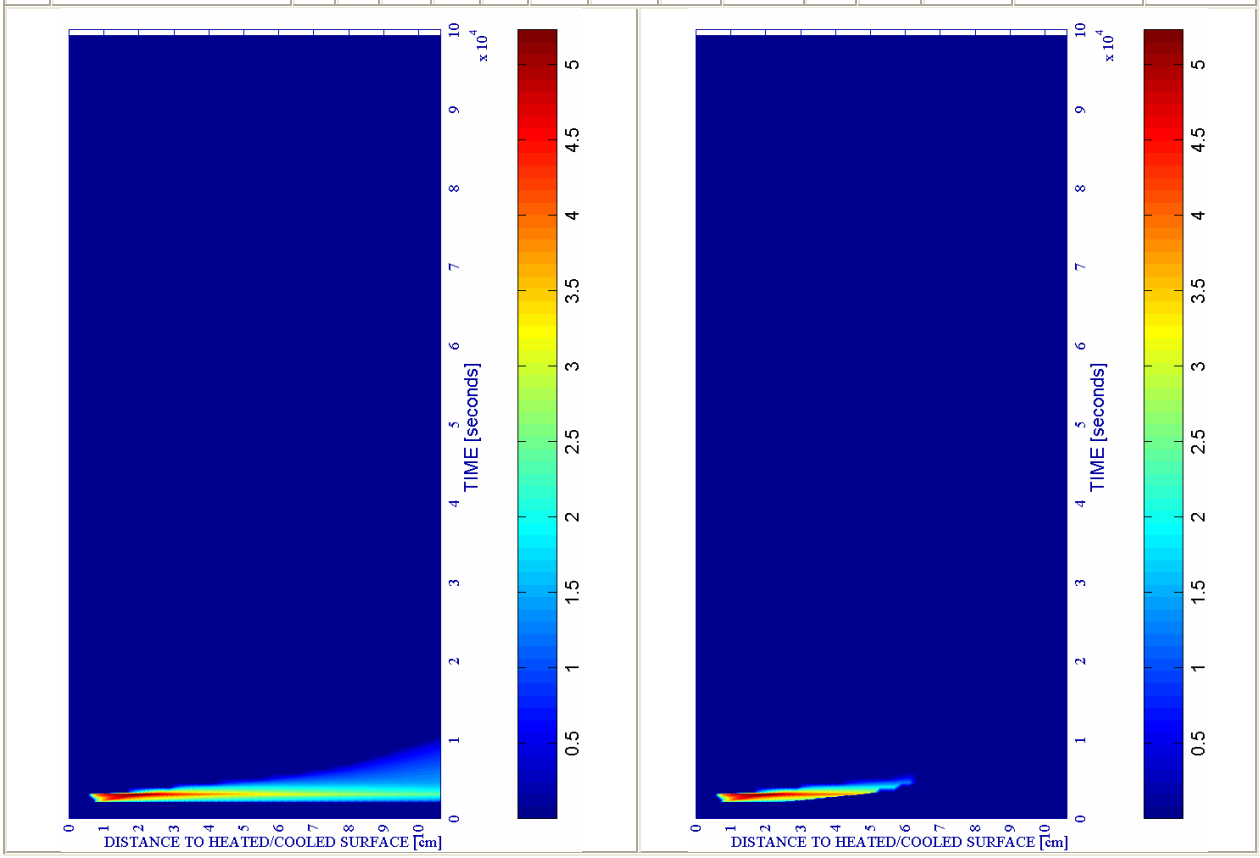

c) Velocity of spalled pieces v [m/s] ***Figure 6-100.*** *d) Velocity [m/s] where d ≥ 0,10*

a) Spalling Index IS4 [-] *b) Mechanical damage d [-]*

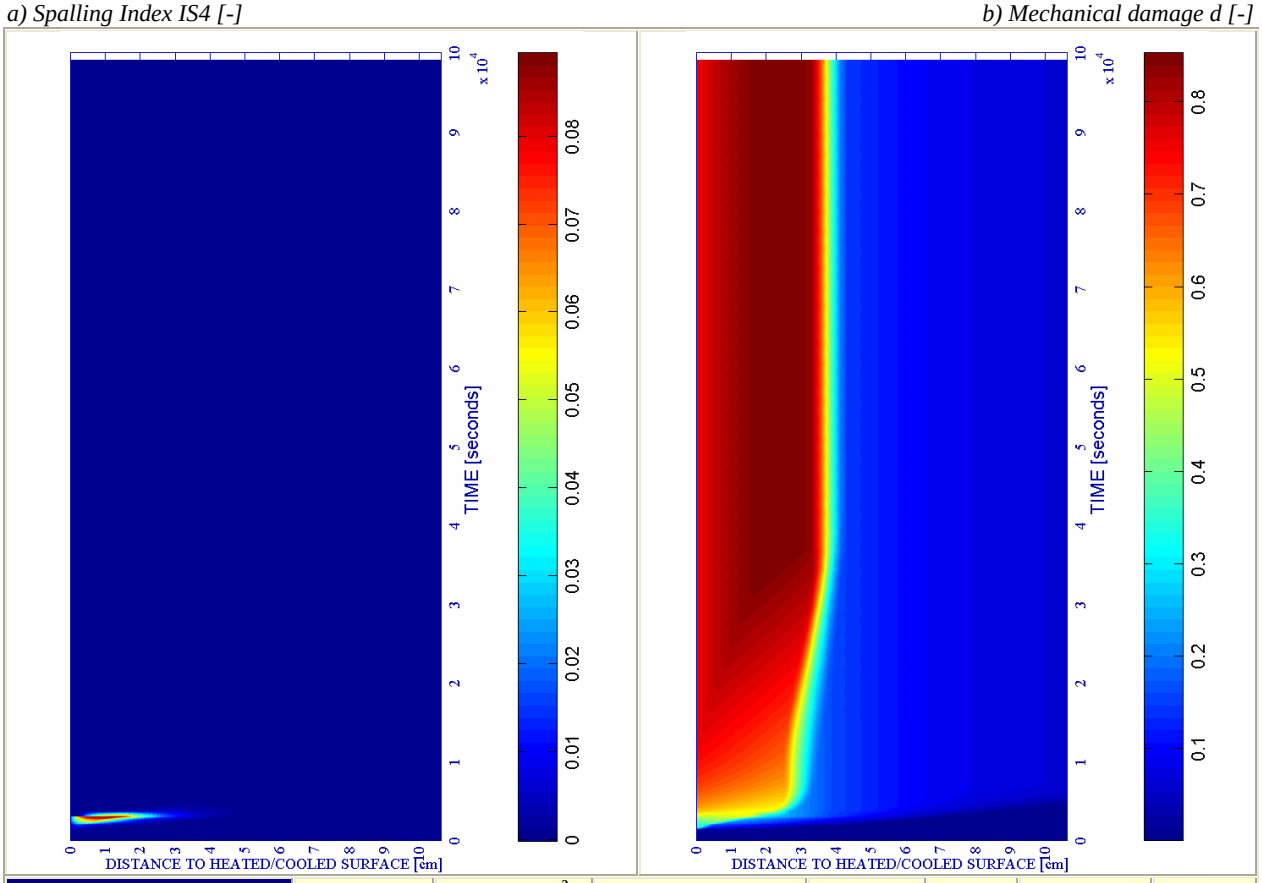

ENVIRONMENTAL - FAST	PC1 - RH [%]			PC2 - K_0 [m^2]			PC4 - Heating curve			PC5 – Mat.		Cooling length[s]	Start of cooling [s]	End of cooling [s]
#	Combination	40	50	60	10^{-19}	10^{-18}	10^{-17}	PAR1	PAR2	PAR4	C60	C90			
14	TH12K018RH50PAR2C60		X			X			X		X		24	3.000+120	3.144

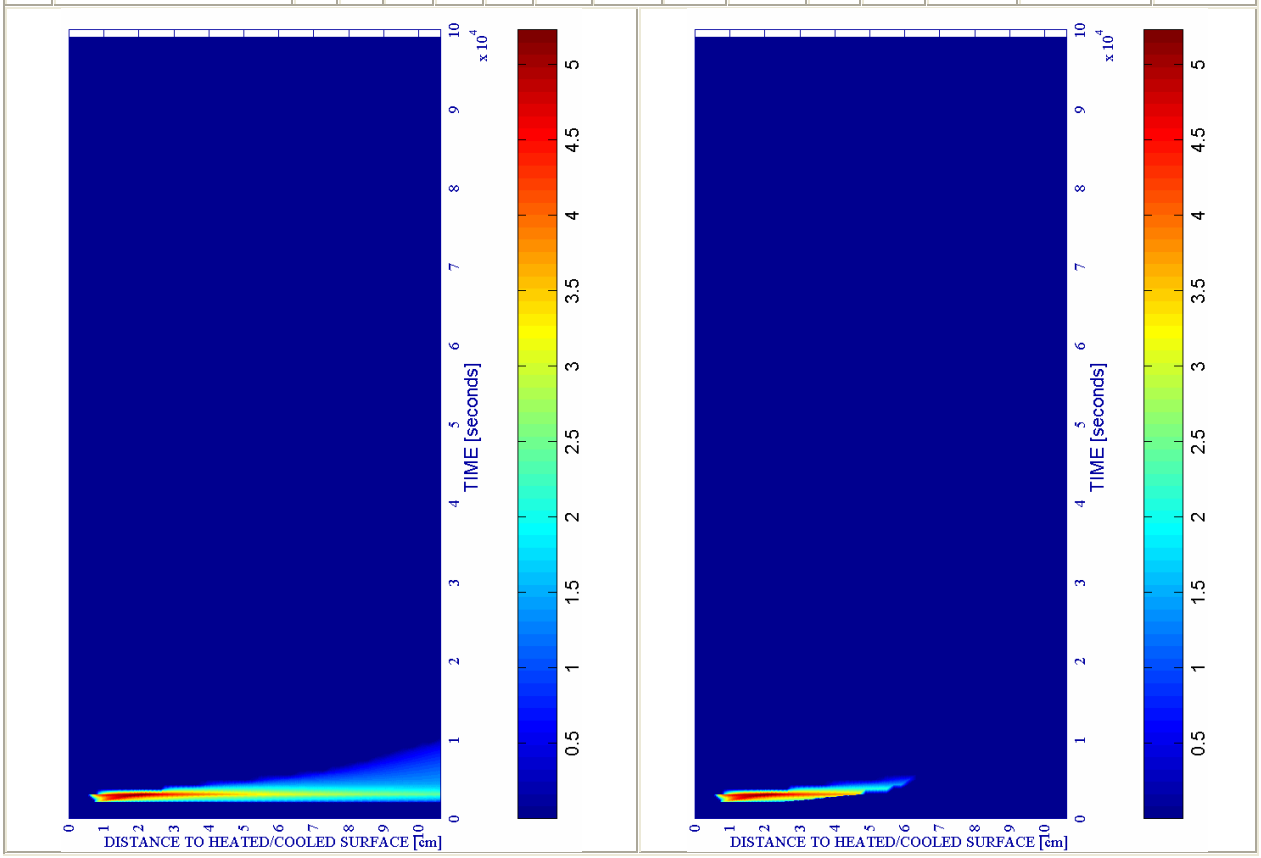

c) Velocity of spalled pieces v [m/s] ***Figure 6-101.*** *d) Velocity [m/s] where d ≥ 0,10*

a) Spalling Index IS4 [-] *b) Mechanical damage d [-]*

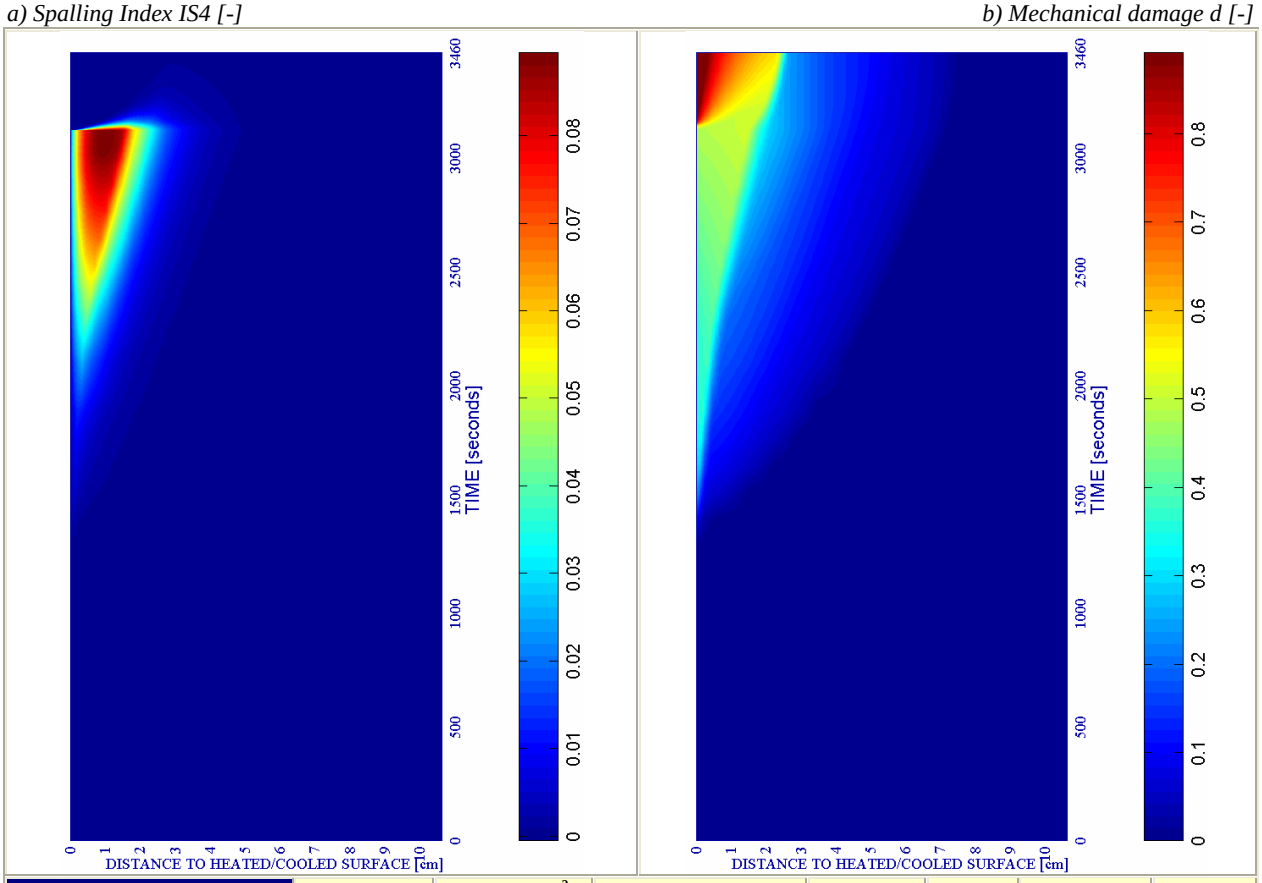

SURFACE COOL+KEEP		PC1 - RH [%]			PC2 - K_0 [m^2]			PC4 - Heating curve			PC5 – Mat.		Cooling length[s]	Start of cooling [s]	End of cooling [s]
#	Combination	40	50	60	10^{-19}	10^{-18}	10^{-17}	PAR1	PAR2	PAR4	C60	C90			
14	TH12K018RH50PAR2C60		X			X			X		X		340	3.000+120	3.460

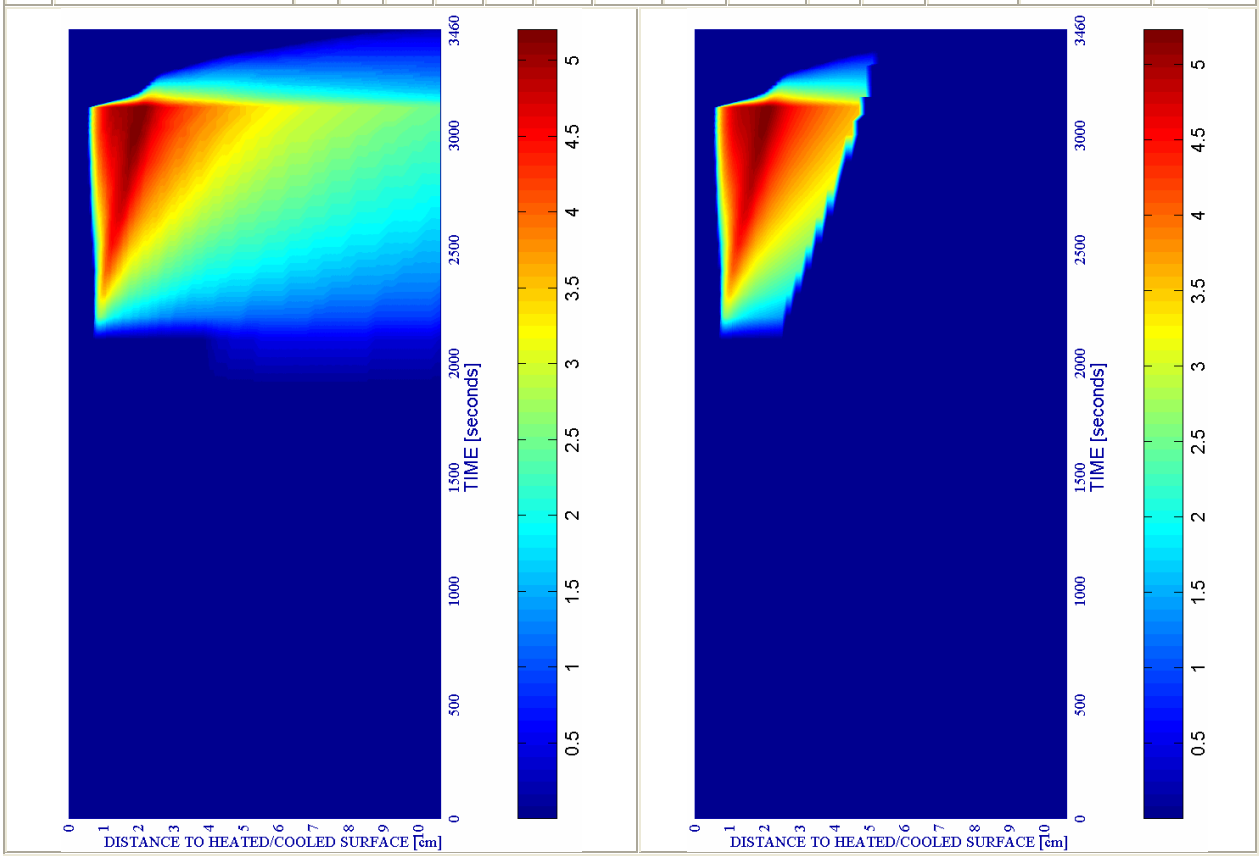

c) Velocity of spalled pieces v [m/s] ***Figure 6-102.*** *d) Velocity [m/s] where d ≥ 0,10*

6.5.2.4.4 Surface Cooling followed by an imposed Constant Surface Temperature

Table 6-80. *Description of the Cooling Process Stages and Collection of the Main Results related to Spalling Index and velocity*

Stage description -figure 6-102 a) to d)-	Absolute Time Start [s]	Absolute Time End [s]	$IS4_{max}$ [-]	X_{IS4max} [cm]	t_{IS4max} [s]	v_{max} [m/s]	X_{vmax} [cm]	t_{vmax} [s]	v_{max}* [m/s]	X_{vmax*} [cm]	t_{vmax*} [s]
First Heating	0	3.000+120	0,0894	0,974	3.090	5,228	2,037	3.090	5,228	2,037	3.090
Surface cooling	3.120	3.152	0,0893	0,974	3.120	5,228	2,037	3.090	5,228	2,037	3.090
Surface Constant T	3.152	3.460	0,0313	1,644	3.152	4,034	2,258	3.152	4,034	2,258	3.152
Absolute Maximum	0	3.460	0,0894	0,974	3.090	5,228	2,037	3.090	5,228	2,037	3.090

Remark [†]***:*** *These results are included for the Comparative Analysis developed on Paragraph 6.5.3*

Stage description -figure 6-102 a) to d)-	Absolute Time Start [s]	Absolute Time End [s]	d_{max} [-]	X_{dmax} [cm]	t_{dmax} [s]	T_{max} [K]	X_{Tmax} [cm]	t_{Tmax} [s]	p^g_{max} [MPa]	X_{pgmax} [cm]	t_{pgmax} [s]
First Heating	0	3.000+120	0,5079	1,470	3.120	614,64	0,000	3.120	0,8256	1,555	2.760
Surface cooling	3.120	3.152	0,8256	0,000	3.152	614,64	0,000	3.120	0,8087	2,145	3.120
Surface Constant T	3.152	3.460	0,8911	0,033	3.182	530,58	0,7576	3.152	0,7664	2,258	3.152
Absolute Maximum	0	3.460	0,8911	0,033	3.182	614,64	0,000	3.120	0,8256	1,555	2.760

Table 6-81. *Description of the Cooling Process Stages and Collection of the Main Results related to mechanical damage, Temperature and Gas Pressure*

6.5.2.5 REFERENCE CASE # 14 – TH12K018RH50PAR2C60 – START OF COOLING: 3.360S

The main features of this reference case are the following ones:

		PC1 (RH) [%]			PC2 (K) [m^2]			PC3 (TH) [cm]			PC4 (Heating curve)			PC5 (Mat)	
#	Combination	40	50	60	10^{-19}	10^{-18}	10^{-17}	12	24	50	PAR1	PAR2	PAR3	C60	C90
14	TH12K018RH50PAR2C60		X			X		X			X	X		X	

Table 6-82. *Main Features of the Reference Case #14 – TH12K018RH50PAR2C60.*

with an starting instant of the first cooling process at 3.360 seconds. The types and subtypes of cooling processes analyzed in this reference case are the following ones:

Type of Cooling	*Subtype of Cooling*	*Related Paragraph*	*Figures numbers*
Environmental	Slow Cooling	6.5.2.5.1	6-103 to 6-112
Environmental	Medium Cooling	6.5.2.5.2	6-113 to 6-119
Environmental	Fast Cooling	6.5.2.5.3	6-120 to 6-121
Surface	Followed by Heating	6.5.2.5.4	6-122 to 6-129
Surface	Followed by an imposed constant Surface Temperature	6.5.2.5.5	6-130 to 6-134
Surface	Divided into Three Periods	6.5.2.5.6	6-135 to 6-140
Environment Heating up to three hours (10.800 seconds) without any cooling		6.5.2.5.7	6-141 to 6-142

Remark: *See each Paragraph for more details on the features of the Cooling Processes.*

Table 6-83. *Types and Subtypes of Cooling Processes Analyzed in the Reference Case #14 – TH12K018RH50PAR2C60 with the Start of Cooling Process at 3.360 seconds*

6.5.2.5.1 Environmental Slow Cooling

6.5.2.5.1.1 Phenomenological and Mechanistic analysis of the Heating Stage

As it occurred with the case corresponding to an ISO834 heating curve (see paragraph 6.5.2.1.1) the surface of the concrete element is initially heated both by a convective flux and by a radiation flux, what results in a rather more gradual increase of the element temperature starting from the surface zone than in the ISO834 case (see figures 6-112 i) and 6-103 in more detail).

Due to the slower heating process, although the maximum temperatures reached during the heating stage (656,65 K) are lower than in the ISO heating curve case (754,18 K) the temperature gradients in the structural element are smaller herein, leading to greater depths of the element (5,4 centimetres instead of 3,2 centimetres of the ISO case) where temperature has risen

beyond the evaporation conditions of water (see figure 109 a)) what leads, in the meantime, to higher vapour pressure values at deep layers).

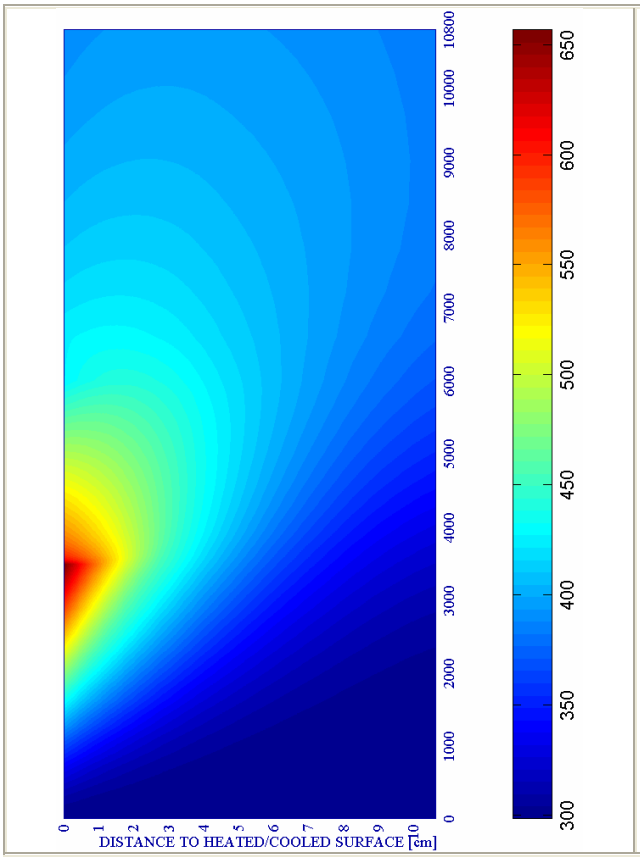

Figure 6-103. *Temperature T [K] during the 3 first hours*

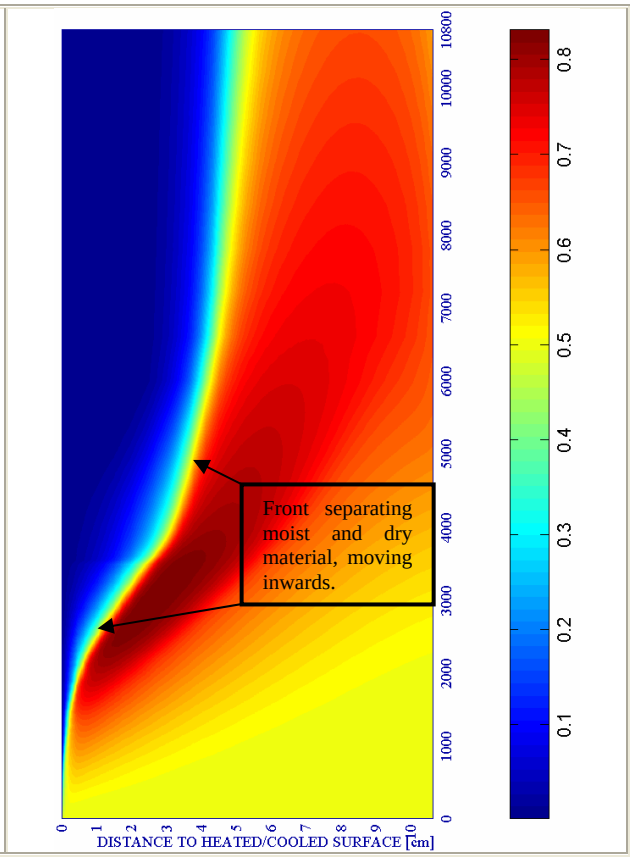

Figure 6-104. *Relative Humidity [-] during the 3 first hours*

Due to moisture evaporation, the relative humidity in the surface zone (initially 50% for this case) decreases to a very low value, figures 6-112 h) and 6-109 c) and 6-104 in more detail, and an initially sharp front, separating the moist and dry material, moves inwards to a depth, at the end instant of the heating stage (3.480 seconds), of 3 centimetres. At this front intensive evaporation takes place, increasing considerably the vapour pressure (up to 7,80 MPa). The maximum values of vapour and gas pressures (figures 6-109 b), 6-112 f) and 6-105, 6-112 e) respectively) increase initially, then they remain almost constant as the surface temperature increases and the front moves inwards (as it is shown on Table 6-85, the absolute maximum value of gas pressure is achieved during this heating stage).

The maximum value of gas pressure usually coincides with the position where the temperature of approximately 200ºC occurs. In the regions with lower temperature, below about 130ºC, the gas pressure increase is caused mainly by a growth of the dry air pressure due to heating, achieving the maximum value of 0,25 – 0,4 MPa at the position with a temperature of about 100ºC. In the regions with higher temperature, the effect of a rapid increase of vapour pressure due to heating and temperature-dependence of the saturation vapour pressure predominate. At temperatures 200-300 ºC the gas in the material pores consists mainly of water vapour and the gradients of vapour pressure cause the vapour flow both towards the surface and inwards. The latter mass flow results in vapour condensation when the hot vapour inflows colder – internal layers of the concrete element – and in an increase of the relative humidity close to the 85 per cent (see figure 6-104) clearly above the initial value, often referred to as “moisture clog” or “saturation plug” [1]. An additional increase of the liquid water volume in the material pores is due to the water thermal dilatation, which is particularly important above the temperature of

about 160ºC. A significant decrease of the gas permeability may be observed due to these effects, resulting in a decrease of the pore space available for the gas phase.

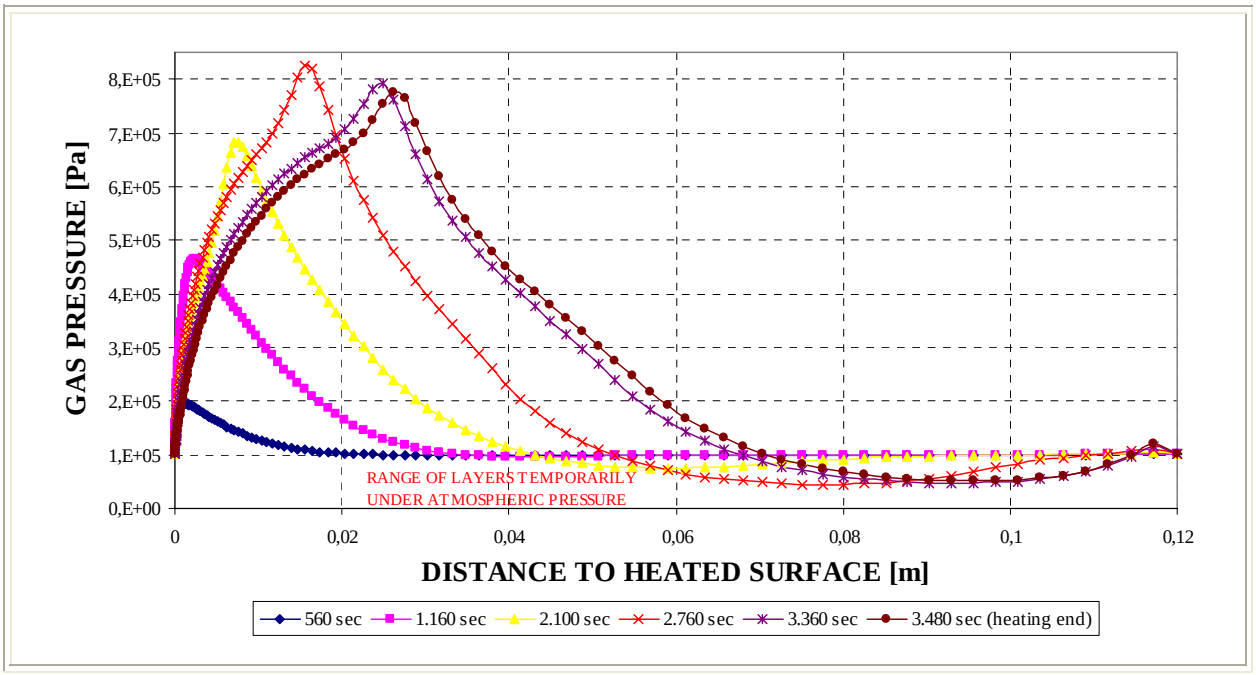

Figure 6-105. *Gas pressure at all the depths during the heating stage.*

Analogously to what was observed in ISO834 heating curve case, increasing temperature causes the material dilatation of the aggregate which in part is due to concrete dehydration (products of the chemical reactions have greater volume than the initial volume of a concrete), in part due to material cracking and progressive crack opening, and finally due to "normal" thermal dilatation of the material skeleton. The concrete cracking during heating is caused by an incompatibility of thermal dilatation of the aggregate and the cement paste, resulting in high traction stresses in the Inter-Phase Transition Zones and development of local micro-cracks. Due to these cracks and chemical transformations of concrete (dehydration), the concrete strength properties and Young's modulus degrade gradually, what can be expressed [53] in terms of the so-called thermo-chemical damage parameter.

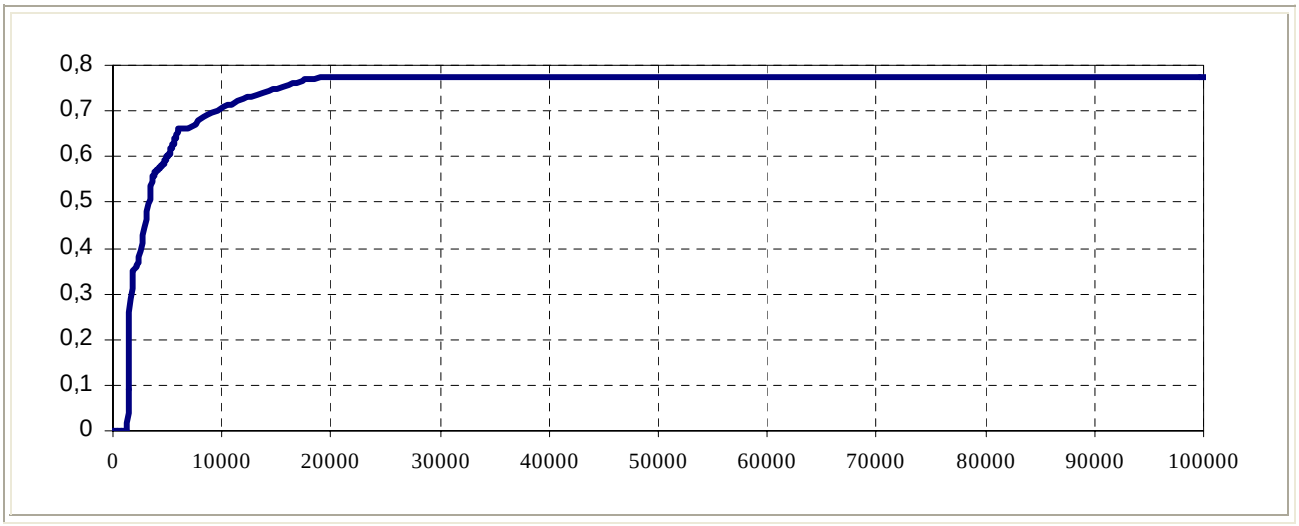

Figure 6-106. *Mechanical damage d [-] evolution at surface during the whole process with detail on heating stage.*

Again, a thermal dilatation of the external layers of a heated element is constrained by the core material which has lower temperature (figure 6-103). This causes macro-stresses in the external layers of the element, compression in the direction parallel to the surface (figure 6-112

l)) and traction in the direction perpendicular to it (figure 6-112 k)), as well as accumulation of the elastic strain energy (figure 6-112 j)). The tensile stresses may cause further development of cracks and fractures, parallel to the element surface, resulting in subsequent degradation of the material strength properties in the surface zone (see on figures 6-112 b) and 6-106 the increasing values corresponding to mechanical damage). An additional, external compressive load parallel to the element surface can intensify the aforementioned phenomena. Development of the cracks, both of thermo-chemical origin and the macro-stresses induced ones, causes a considerable increase of the material intrinsic permeability, and thereupon gas pressure decreases in the external layers where high temperatures are observed (see figure 6-107).

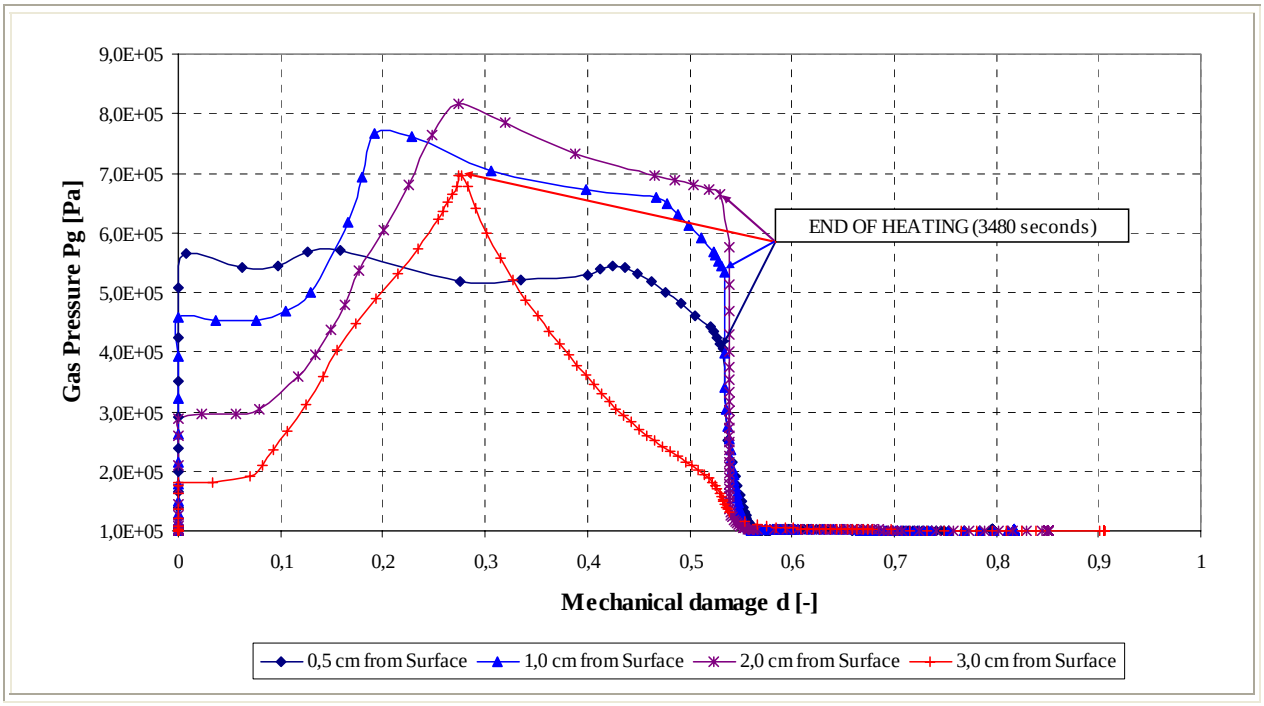

Figure 6-107. *Gas Pressure [Pa] versus Mechanical damage d [-] at several distances from the heated surface.*

The highest values of gas pressure usually correspond to the temperature 150-250 ºC, and this is also the range where the so-called thermal spalling of concrete usually occurs (when elastic strain energy of constrained thermal dilatation (figure 6-112 j)), accumulated in the surface layer and then rapidly released after concrete fracture is considerable, the thermal spalling can be violent and explosive in nature as it was observed during the experimental tests developed).

As it was explained on the Chapter concerning the Spalling Nomograms (Chapter 4) the maximum value of the Spalling Index I_{s4} reached during the heating stage analyzed herein (0,1004 at 1,035 centimetres from surface and 3.390 seconds from the beginning of the fire, according to Table 6-84) is considerably lower to that corresponding to the ISO834 heating curve (0,3688 at 0,582 centimetres from surface and 600 seconds from the beginning of the fire, see paragraph 6.5.2.1.1 and Table 6-36), being however in this case the expected spalling less explosive in nature but much more massive than in the ISO834 case (the maximum value of the velocity of spalled-off pieces – 5,453 m/s – is herein located 1,644 centimetres away from the heated surface – Table 6-84 – while it was of only 0,152 centimetres in the ISO834 case).

6.5.2.5.1.2 Phenomenological and Mechanistic analysis of the Environment Cooling Stage

At the start instant of the cooling process (3.480 seconds from the beginning of heating), the maximum temperature is reached at the heated surface, being the zones close to the surface almost completely dry. The ‘moisture clog’ is situated 3 centimetres away from the surface (figure 6-109 b) and c)) matching this position with that corresponding to the maximum value of

the vapour pressure caused by intensive water evaporation in the temperature range 100-200 ºC. The zone between the surface and the moisture clog shows the highest values of mechanical damage (0,5401 at 1,932 centimetres from surface, as shown at the next table and on figure 6-110 a)) being the longitudinal stresses in this layer tensile stress (figure 6-110 b), as it occurs in the rest of the layers at this instant) while transversal stresses achieve high levels of compression (figure 6-111). At this instant, the elastic energy is mostly accumulated close to the surface (figure 6-110 c)), precisely in the abovementioned layer – what leads to an unquestionable energetic viability of spalling occurrence of the layers close to the surface, of relatively explosive nature with velocities of the spalled pieces of about 5,45 m/s at the start instant of the cooling process –. Besides this, at this start instant the heat flux moves inwards from the surface, while water vapour fluxes are addressed, from the moisture clog, both towards the heated surface and inwards due to the gradients of vapour pressure. The latter flux means vapour condensation when it reaches colder layers.

As the cooling process starts (beyond 3.480 seconds), the heat flux continues initially addressed only inwards from the surface – since the maximum temperature is still at the surface, figure 6-109 a) –, so the inner layers keep increasing their temperature, being at each instant the maximum value of vapour pressure progressively farther from the surface and at the depth where the temperature is of approximately 200ºC (figure 6-109 b)). Besides this, it is observed that the value corresponding to the peak of vapour pressure is progressively reduced during the environment cooling; this sharp decrease of the vapour pressure values (together with a decrease in the elastic strain energy that will be explained next) leads to a progressive decrease of the Spalling Index IS_4 values despite mechanical damage values increase during cooling until a really late stage (in fact, until the end of the structural element temperature decrease down to the ambient temperature).

As the cooling process continues, the temperature gradients in the structural element become lower since the surface temperature decreases while the inner temperatures increase (figure 6-109 a)). In this way, before the end of the environment cooling (at 6.000 seconds) the range of layers with enough temperature to become their liquid water evaporated has been extended from the initial 0-0,042 metres at 3.480 seconds up to the range 0-0,092 metres at 6.000 seconds. This means that 3/4 of the layer may present water vapour at the end of the environment cooling. At this instant, from which the environment temperature is assumed constant and equal to the initial ambient temperature (25 ºC), the zone with the maximum mechanical damage has grown until a depth of 0,032 metres with a maximum value of 0,6595 located at the surface, while longitudinal stresses – still being tensile at all the depths – are lower at the surface and higher at the inner layers. The maximum value of the elastic strain energy (figure 6-110 c)), considerably lower than at the beginning of the cooling process, does not appear any more at the surface but at 0,042 metres inwards. Once the environment cooling has finished, since its temperature is still considerably lower than the structural element temperature at all of its depths, two heat fluxes arise (directed each towards opposite surfaces). In this way, at 3 hours (10.800 seconds) from the beginning of the heating (7.320 seconds from the start of environment cooling or 4.800 seconds from its end) the temperature in the structural element is mostly uniform (about 100ºC according to figure 6-110 a)) and therefore low enough to condensate all of the evaporated vapour.

From this point, the gradient in water content is progressively cancelled through its diffusion and while a singular phenomenon is observed at both surfaces: although it will be studied in a more detail on paragraph 6.5.2.8.2., it shall be observed that there is an infiltration – across both surfaces – of the relative humidity of the environment towards the inner layers. This effect happens since a constant vapour pressure of the environment has been imposed at both sides of the structural element – see the paragraph explaining the boundary conditions used in the calculations –, and, hence, as the temperature in the environment decreases its relative humidity

increases (being approximately the 50% at ambient temperature) so, from the end of environment cooling (at 6.000 seconds) its relative humidity is considerably higher than the relative humidity in the layers close to the surface so it infiltrates inside them. The final state of the structural element, once it has reached a maximum temperature below the ambient temperature + 10ºC, shows a relative humidity mostly constant and of about the 25 per cent.

It is also remarkable that, approximately, at 3 hours (10.800 seconds) from the beginning of the heating (4.800 seconds from the environment cooling end), there arise compressive longitudinal (xx) stresses, first in the inner zones and later close to the surface where compressions achieve really high values at the end of the process. Due to this effect, elastic strain energy is accumulated again close to the surface (see figure 6-110 c)) at the end of the structural element cooling process, appearing a second 'bag' of zones from 3 to 12 centimetres away from the surface where spalling would be again energetically viable at a stage as late as 18,6 hours after the start of the heating and more than 17 hours after the fire is supposed to be extinguished (see figure 6-112 d)). However, this spalling phenomenon is avoided hitherto due to the compressive nature of longitudinal stresses at these instants. In the meantime, mechanical damage keeps increasing its values at all depths (despite having finished the environment cooling process) until it arises values of about the 92 per cent (0,9204 in Table 6-85) 4 centimetres away from the surface at the end, where ambient temperature is achieved everywhere in the structural element (see figures 6-112 b) and 6-108 for more detail). It is also remarkable that the mechanical damage values at the surface opposite to where heating and cooling processes have been imposed are significant and much higher than in several of the inner zones (see figure 6-110 a)).

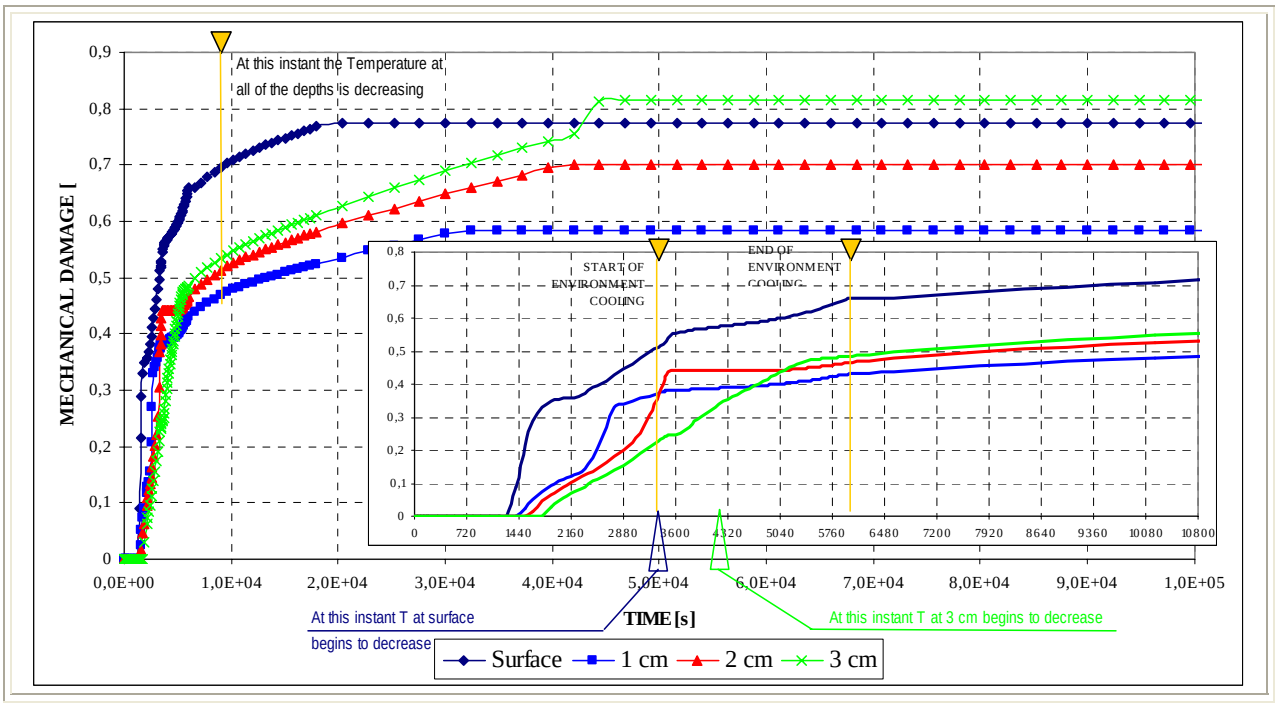

Figure 6-108. *Mechanical damage d [-] evolution during all of the heating and cooling stages, with detail on the three first hours (up to 10.800 seconds).*

Finally, the thermo-chemical damage parameter achieves maximum values of about the 16 per cent, increasing hence the maximum value of Total Damage up to the 96 per cent at a depth of 3,8 centimetres from heated surface.

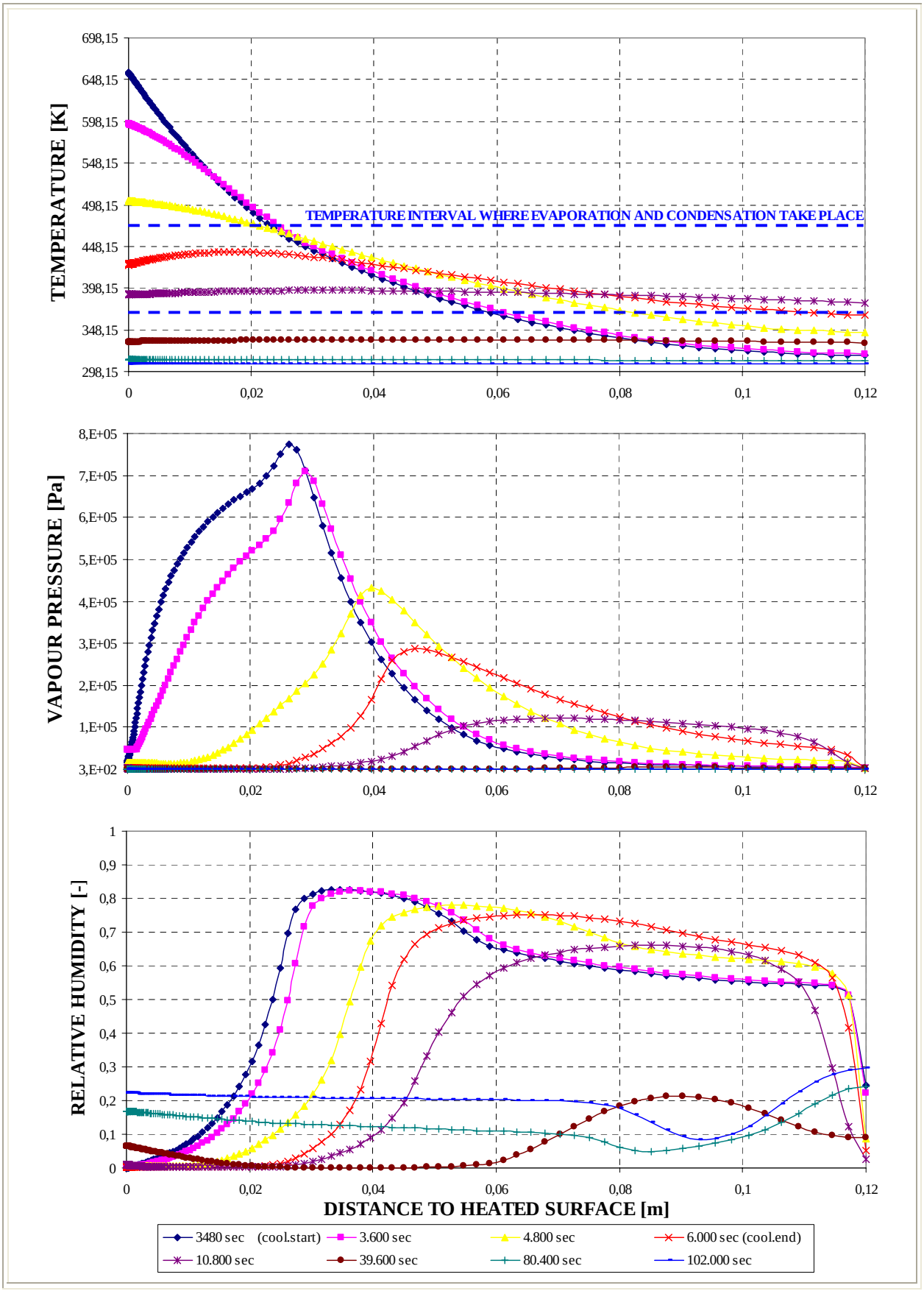

Figure 6-109. *a) Temperature, b) Vapour Pressure and c) Relative Humidity at several distances from the heated surface during Environment cooling process.*

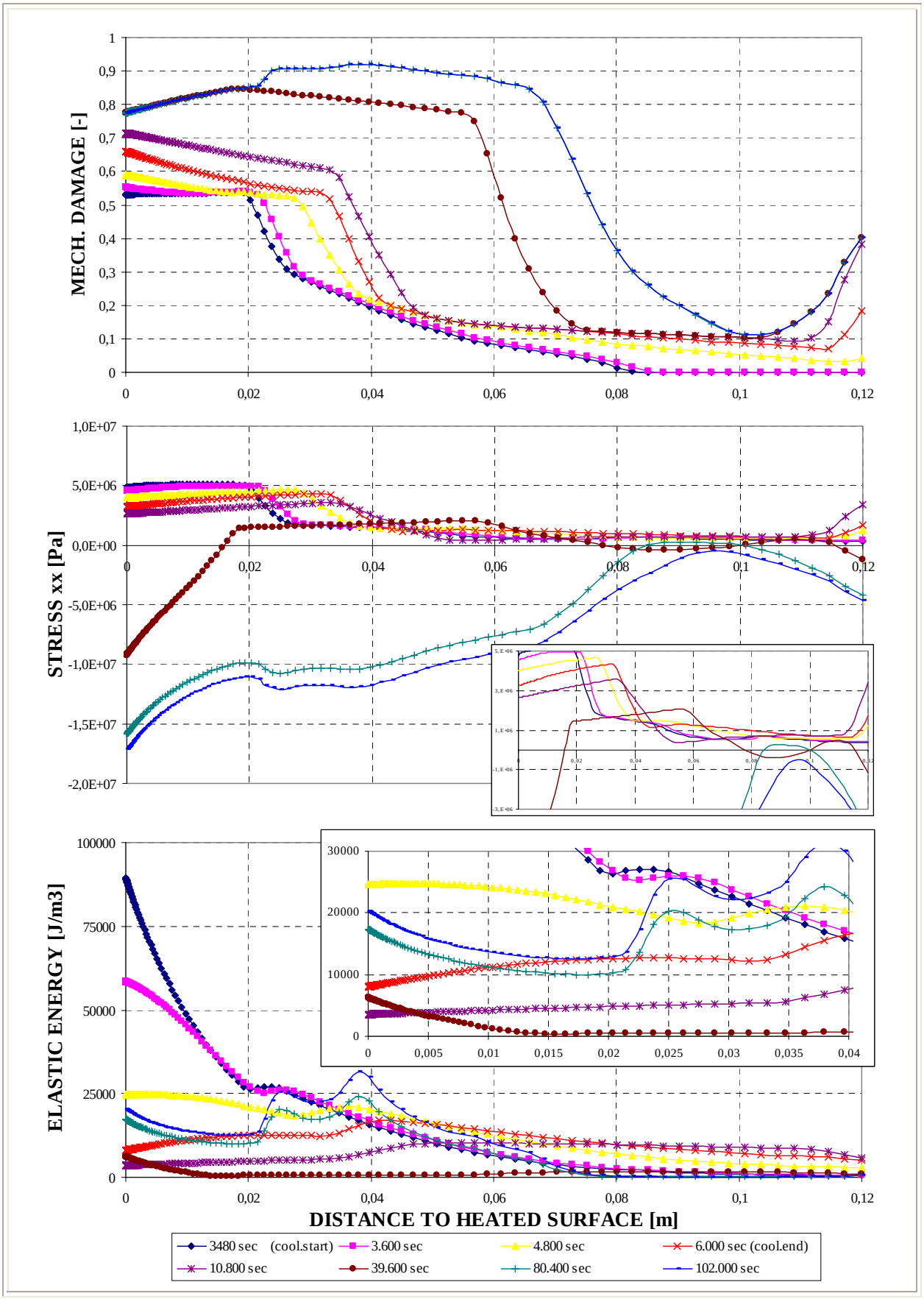

Figure 6-110. *a) Mechanical Damage, b) Longitudinal Stress (xx) and c) Elastic Energy at several distances from the heated surface during Environment cooling process.*

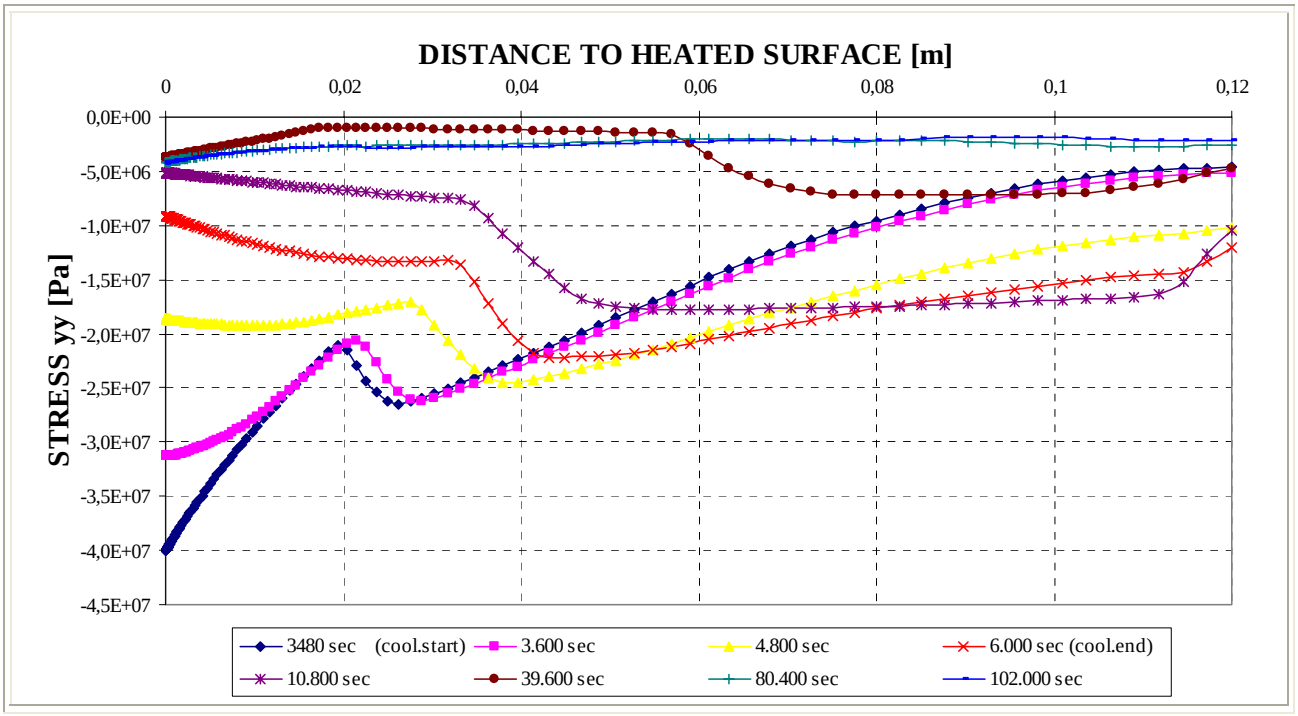

Figure 6-111. *Transversal Stress (yy) at several distances from the heated surface during Environment cooling process.*

6.5.2.5.1.3 Collection of the Main Results of this Case for each Stage of the Cooling Process

Next it is shown a collection of the main results cited in the last subparagraph, as well as a description of each of the stages that compose the heating and cooling processes analyzed herein. Highlighted in red are the maximum values achieved by each parameter.

Table 6-84. *Description of the Cooling Process Stages and Collection of the Main Results related to Spalling Index and velocity*

Stage description	Absolute Time Start [s]	Absolute Time End [s]	$IS4_{max}$ [-]	X_{IS4max} [cm]	t_{IS4max} [s]	v_{max} [m/s]	X_{vmax} [cm]	t_{vmax} [s]	v_{max}^* [m/s]	X_{vmax*} [cm]	t_{vmax*} [s]
First Heating	0	3.360+120	0,1004	1,035	3.390	5,453	1,644	3.480	5,453	1,644	3.480
Environment cooling	3.480	6.000	0,0982	1,099	3.480	5,453	1,644	3.480	5,453	1,644	3.480
Environment constant Temperature up to an absolute time 10.800s	6.000	10.800	0,0019	4,496	6.000	2,167	10,632	6.000	2,148	8,771	6.000
Environment Constant Temperature for t > 10.800s	10.800	102.000	0,0003	5,272	10.800	2,961	5,901	102.000	2,961	5,901	102.000
Maximum for t ≤ 10.800s†	0	10.800	0,1004	1,035	3.390	5,453	1,644	3.480	5,453	1,644	3.480
Absolute Maximum	0	102.000	0,1004	1,035	3.390	5,453	1,644	3.480	5,453	1,644	3.480

Remark †: *These results are included for the Comparative Analysis developed on Paragraph 6.5.3*

Stage description	Absolute Time Start [s]	Absolute Time End [s]	d_{max} [-]	X_{dmax} [cm]	t_{dmax} [s]	T_{max} [K]	X_{Tmax} [cm]	t_{Tmax} [s]	p^g_{max} [MPa]	X_{pgmax} [cm]	t_{pgmax} [s]
First Heating	0	3.360+120	0,5401	1,932	3.480	656,65	0,000	3.480	0,8256	1,555	2.760
Environment cooling	3.480	6.000	0,6595	0,000	6.000	656,65	0,000	3.480	0,7757	2,623	3.480
Environment constant Temperature up to an absolute time 10.800s	6.000	10.800	0,7149	0,000	10.800	441,42	1,736	6.000	0,3723	4,683	6.000
Environment Constant Temperature for t > 10.800s	10.800	102.000	0,9204	3,964	102.000	395,41	3,172	10.800	0,2867	7,759	10.800
Maximum for t ≤ 10.800s†	0	10.800	0,7149	0,000	10.800	656,65	0,000	3.480	0,8256	1,555	2.760
Absolute Maximum	0	102.000	0,9204	3,964	102.000	656,65	0,000	3.480	0,8256	1,555	2.760

Table 6-85. *Description of the Cooling Process Stages and Collection of the Main Results related to mechanical damage, Temperature and Gas Pressure*

6.5.2.5.1.4 Main Graphic Results of this Case in the Time-Space domain.

a) Spalling Index IS4 [-]

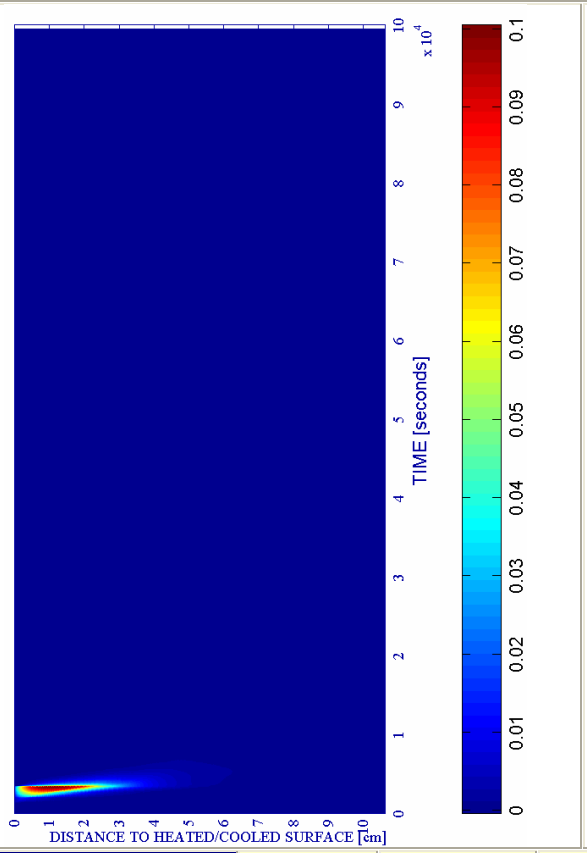

b) Mechanical damage d [-]

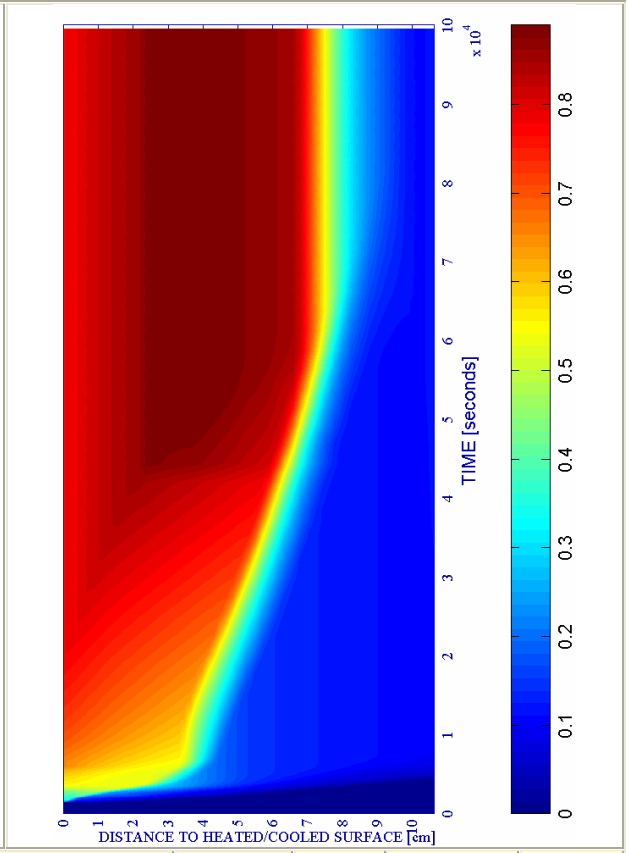

ENVIRONMENTAL - SLOW	PC1 - RH [%]			PC2 - K_0 [m^2]			PC4 - Heating curve			PC5 – Mat.		Cooling length[s]	Start of cooling [s]	End of cooling [s]
#	Combination	40	50	60	10^{-19}	10^{-18}	10^{-17}	PAR1	PAR2	PAR4	C60	C90			
14	TH12K018RH50PAR2C60		X			X			X		X		2.520	3.360+120	6.000

c) Velocity of spalled pieces v [m/s]

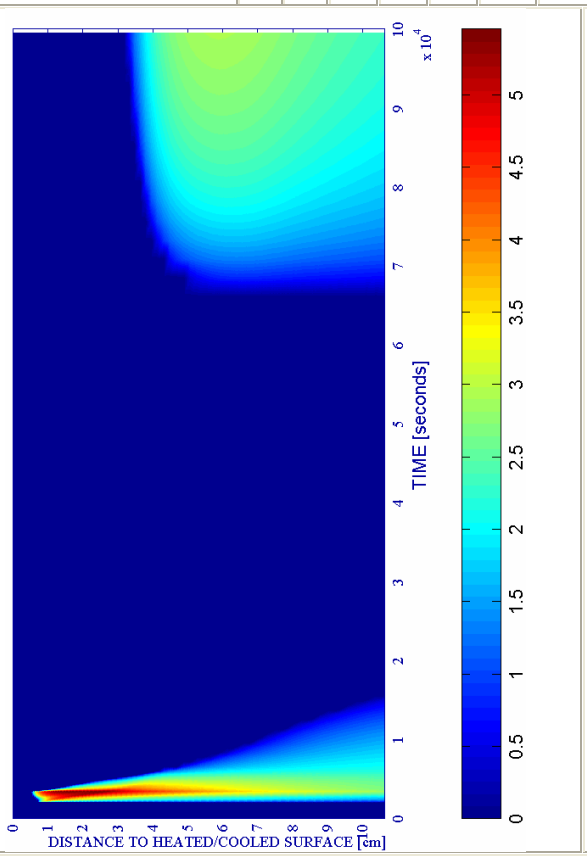

Figure 6-112.

d) Velocity [m/s] where d ≥ 0,10

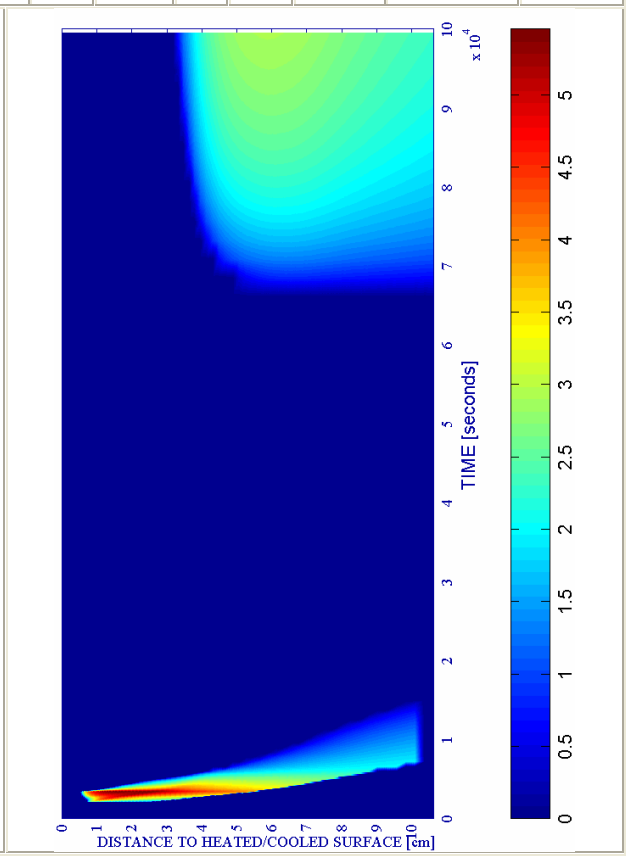

e) Gas pressure $p^g \cdot 10^{-5}$ [Pa]

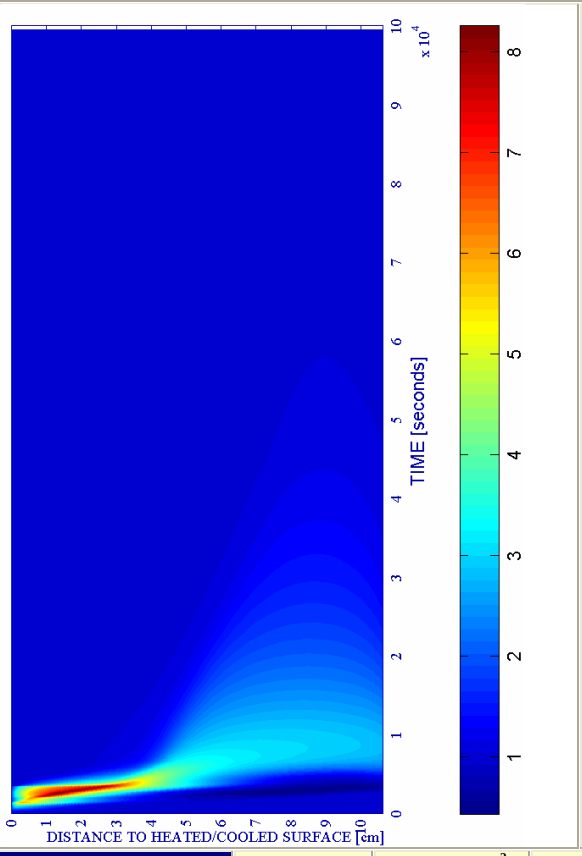

f) Vapour pressure $p^v \cdot 10^{-5}$ [Pa]

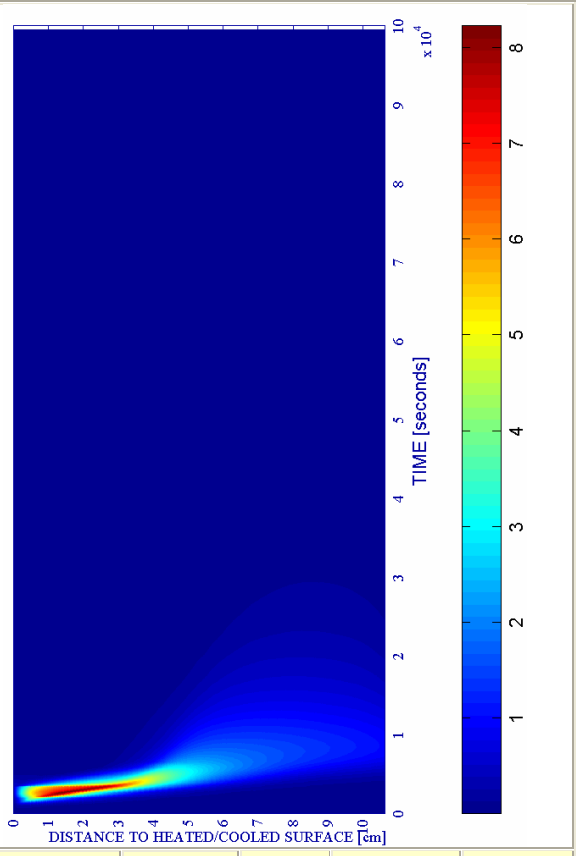

ENVIRONMENTAL - SLOW		PC1 - RH [%]			PC2 - K_0 [m^2]			PC4 - Heating curve			PC5 – Mat.		Cooling length[s]	Start of cooling [s]	End of cooling [s]
#	Combination	40	50	60	10^{-19}	10^{-18}	10^{-17}	PAR1	PAR2	PAR4	C60	C90			
14	TH12K018RH50PAR2C60		X			X			X		X		2.520	3.360+120	6.000

g) Saturation Degree S [-]

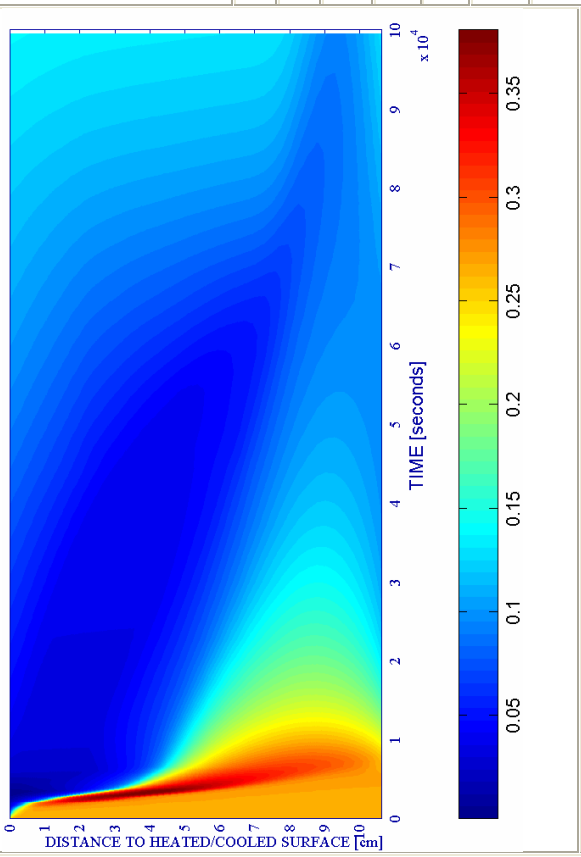

Figure 6-112. (continued)

h) Relative Humidity RH [-]

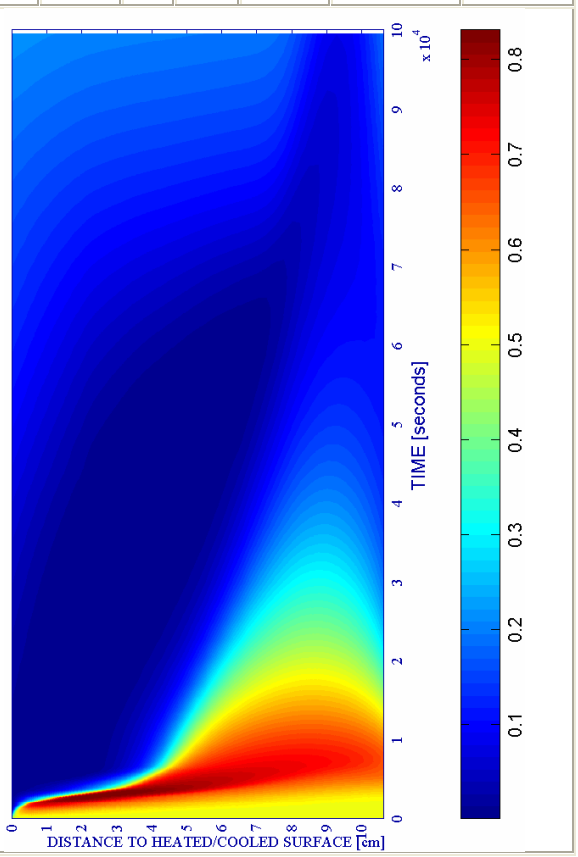

i) Temperature [K]

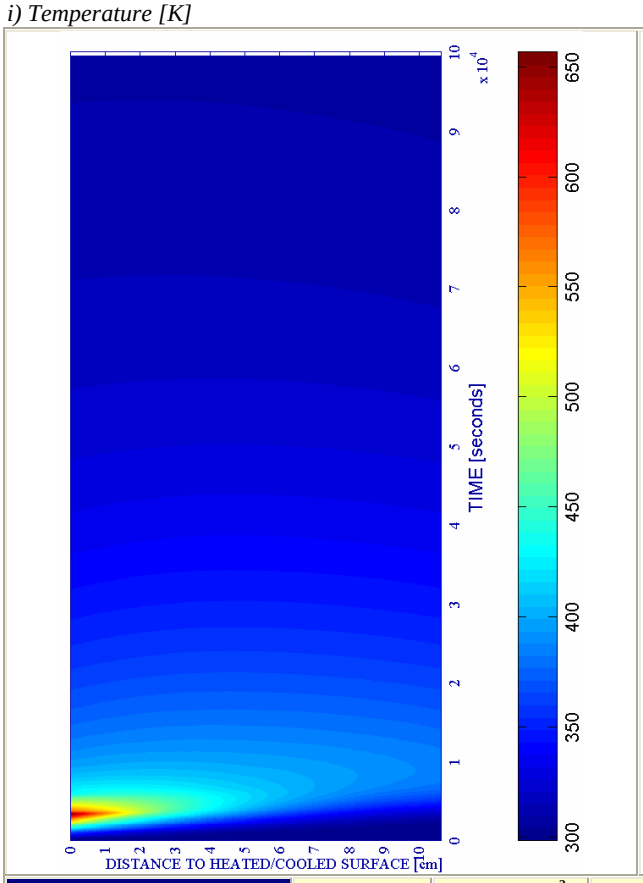

*j) Elastic Energy U · **10**$^{-4}$ [J/m^3]*

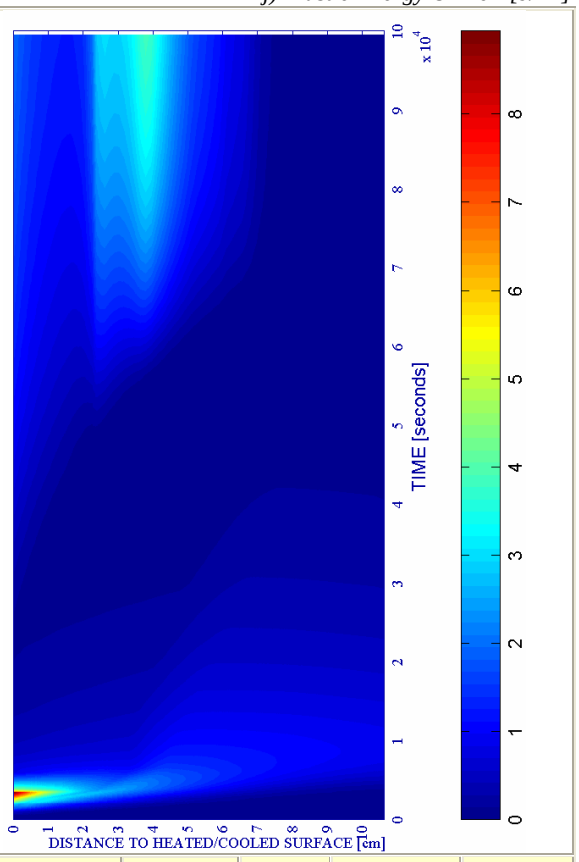

ENVIRONMENTAL - SLOW		PC1 - RH [%]			PC2 - K_0 [m^2]			PC4 - Heating curve			PC5 – Mat.		Cooling length[s]	Start of cooling [s]	End of cooling [s]
#	Combination	40	50	60	10^{-19}	10^{-18}	10^{-17}	PAR1	PAR2	PAR4	C60	C90			
14	TH12K018RH50PAR2C60		X			X			X		X		2.520	3.360+120	6.000

*k) Stress in longitudinal (xx) direction · **10**$^{-7}$ [Pa]*

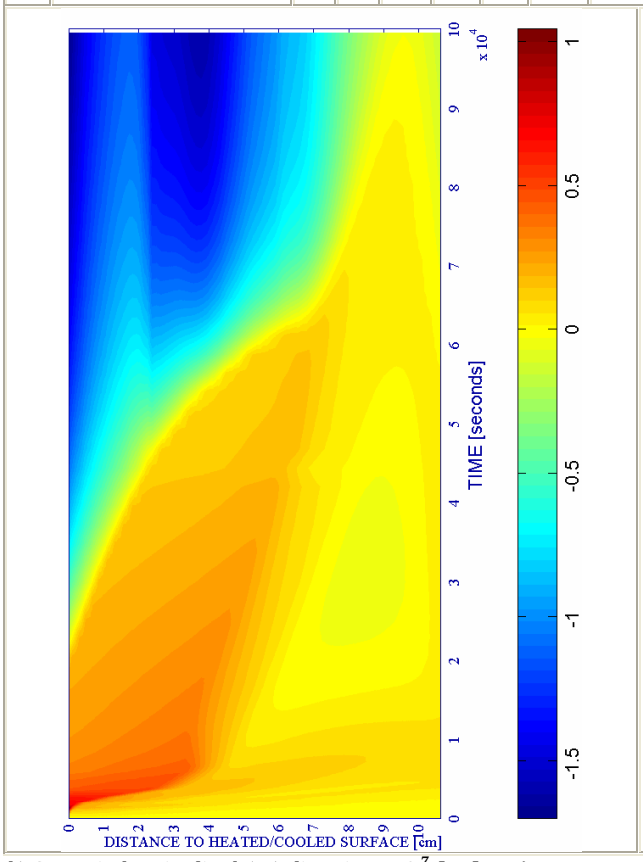

Figure 6-112. (continued)

*l) Stress in transversal (yy) direction · **10**$^{-7}$ [Pa]*

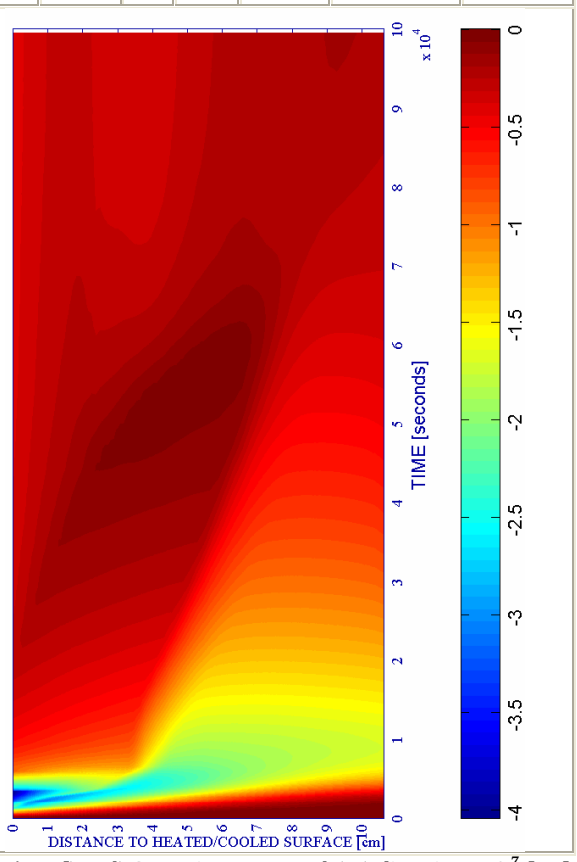

6.5.2.5.2 Environmental Medium Cooling

The phenomenological and mechanistic analysis of this case, where the only difference in the calculation conditions is a higher rate of cooling of the environment, is in general analogous to what was developed in the previous paragraph (corresponding to a 'slow' rate). However, there are some slight differences in the phenomena features that will be briefly exposed next.

First, as it can be observed in figure 6-114, the front separating moist and dry material does not reach a depth as far from the surface as in the case corresponding to a 'slow' cooling, mainly due to the fact that the condensation of the water vapour starts sooner (see figure 6-115).

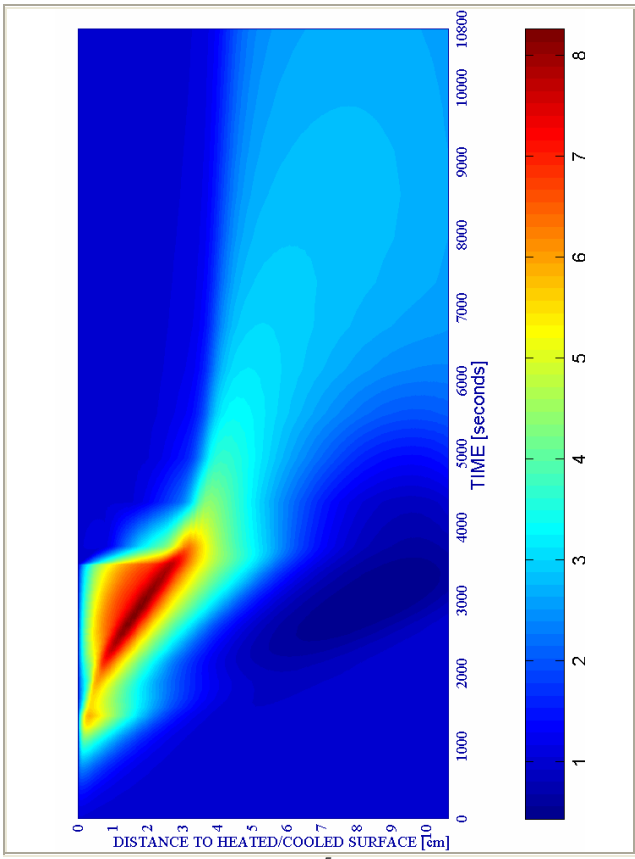

Figure 6-113. *Gas pressure · 10^{-5} [Pa] during the 3 first hours*

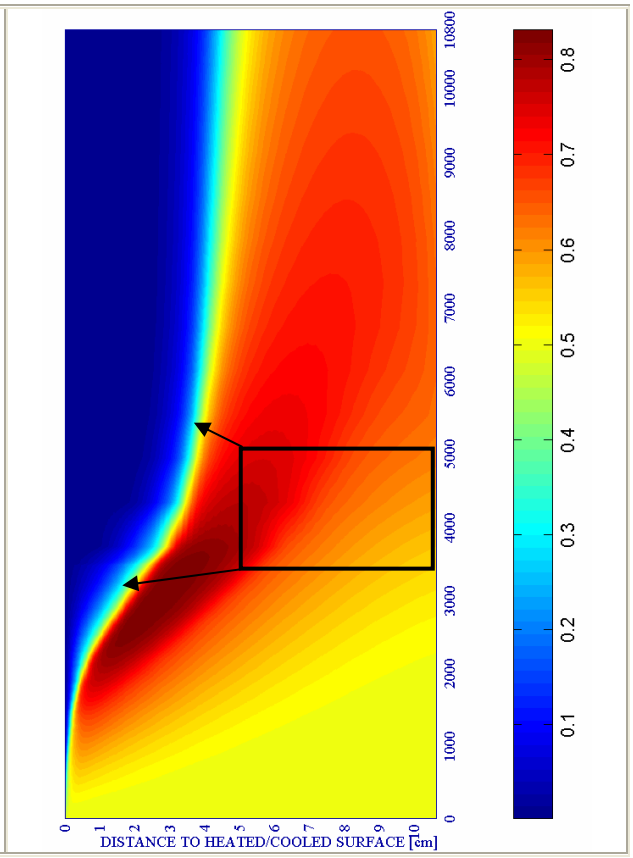

Figure 6-114. *Relative Humidity [-] during the 3 first hours*

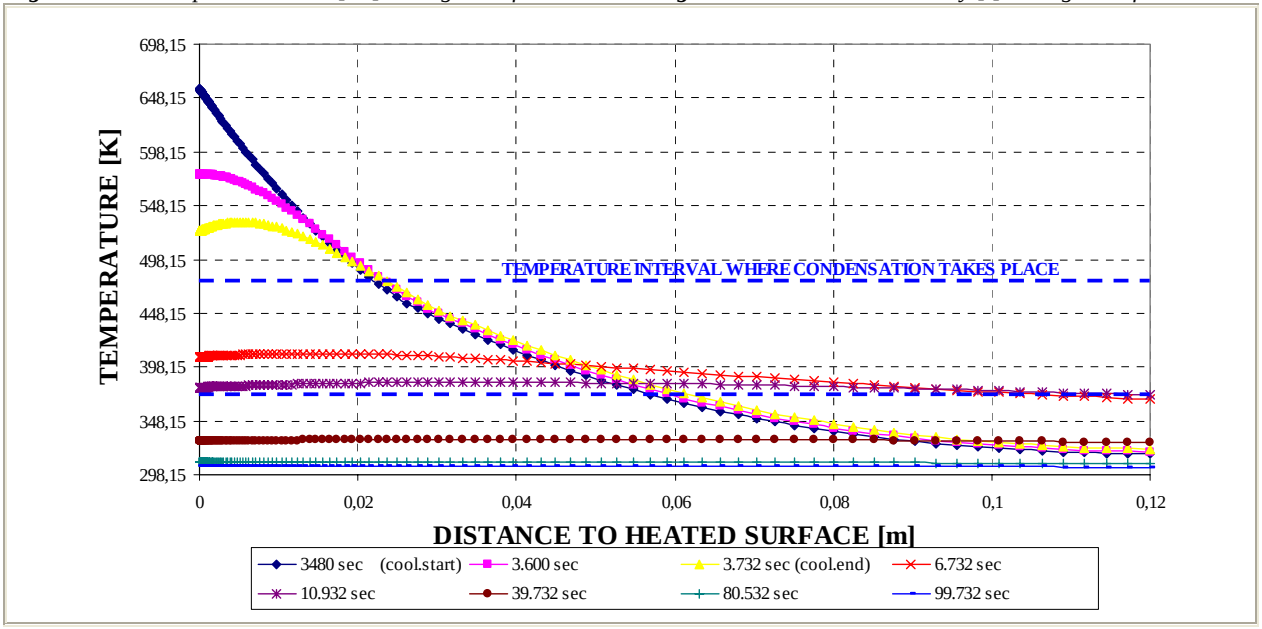

Figure 6-115. *Temperature at several distances from the heated/cooled surface during Environment cooling process.*

The increase of mechanical damage during the Environment cooling process stops also sooner than in the previous case (see figure 6-116), showing a maximum value of 0,898 at 3,321 centimetres from the surface and at 46.932 seconds (while in the 'slow' cooling case this increase did not stop during the whole environment cooling and constant ambient temperature processes).

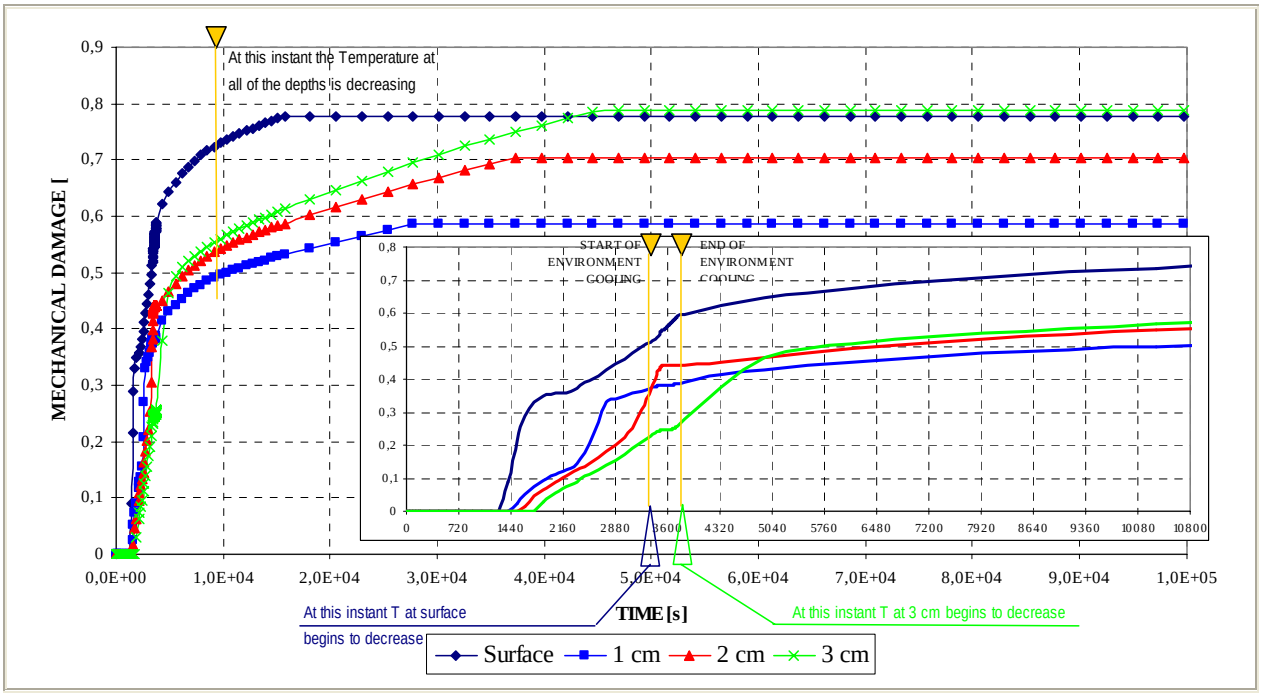

Figure 6-116. *Mechanical damage d [-] evolution, with detail on the environment cooling stage (from 720 s to 1.050 s).*

Besides this, at it can be observed in figure 6-117, the depth affected by high values of mechanical damage (and therefore cracking) has been reduced to the 3,321 first centimetres instead of the 3,964 centimetres shown in the case with 'slow' cooling (and the final maximum level of cracking is about a 2,2 per cent lower).

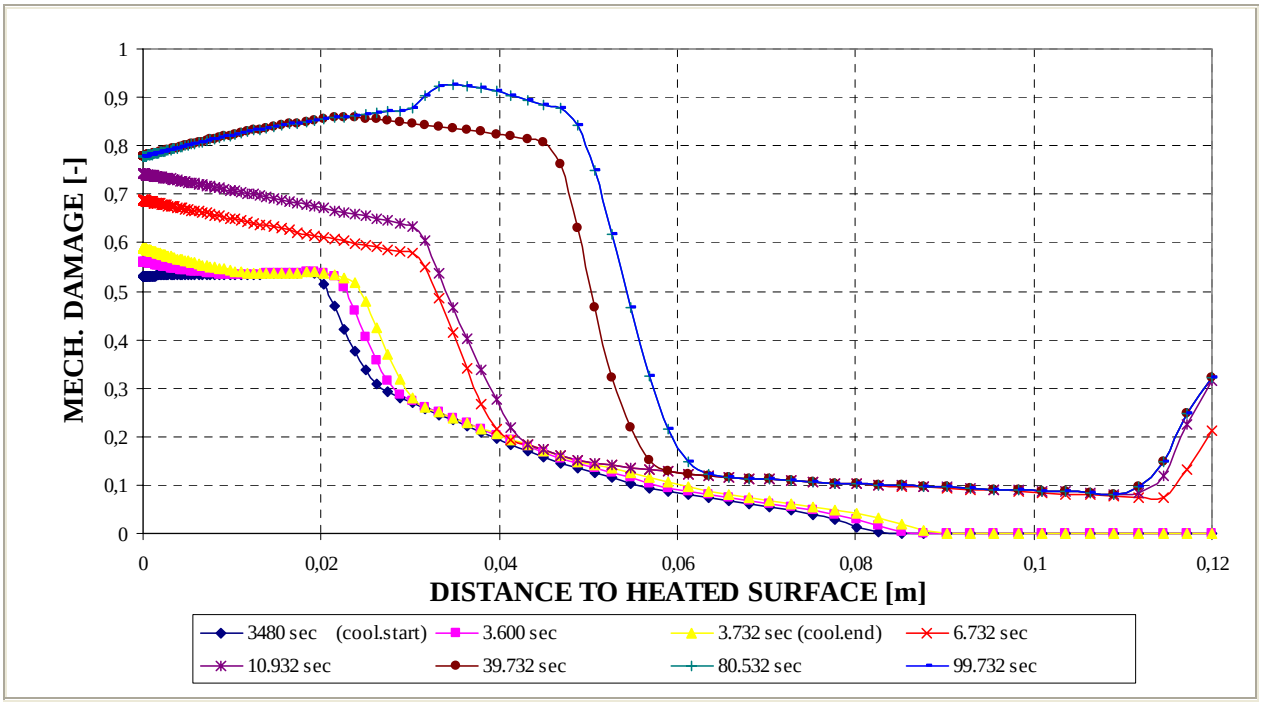

Figure 6-117. *Mechanical damage d [-] at several distances from the heated/cooled surface during Environment cooling process.*

As it occurred in the previous case, here appear again a second 'bag' of zones where spalling would be again energetically viable at a late stage in the extinguishing process (see figure 6-119 d)). However the compressive stress level arisen at the end of the structural element cooling process, higher at some locations than in the case corresponding to a 'slow' cooling, avoids the possibility of suffering thermal spalling at late stages.

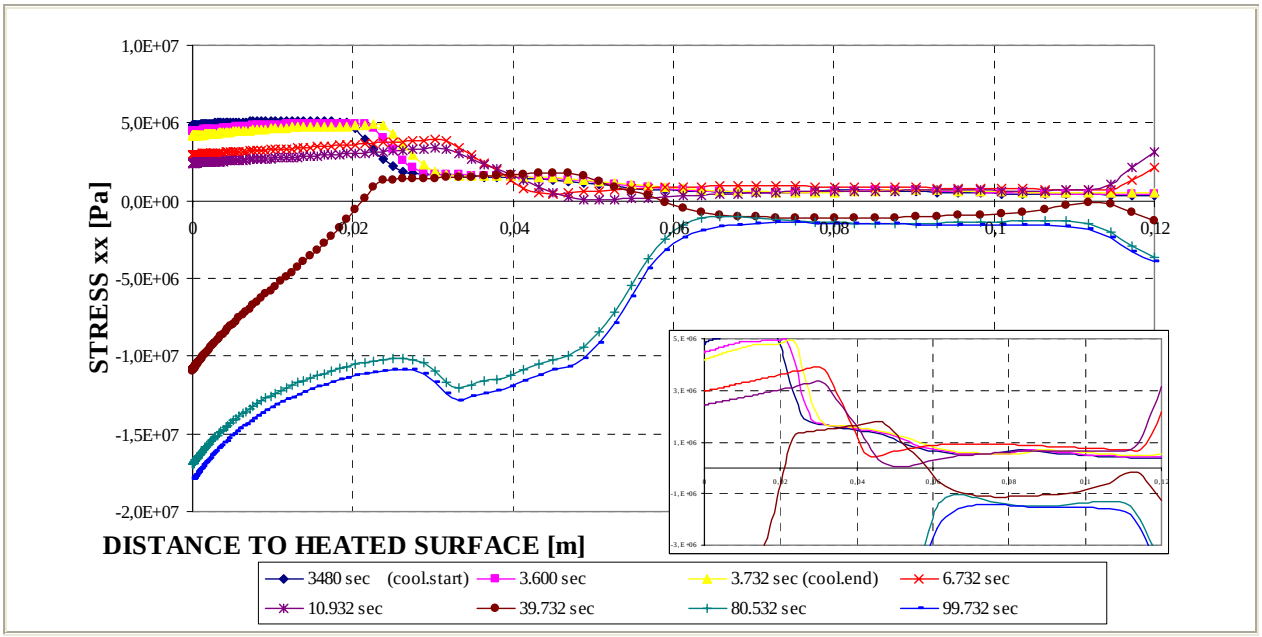

Figure 6-118. *Longitudinal Stress (xx) at several distances from the heated/cooled surface during Environment cooling process.*

Next it is shown a collection of the main results cited in the last subparagraph, as well as a description of each of the stages that compose the heating and cooling processes analyzed herein.

Table 6-86. *Description of the Cooling Process Stages and Collection of the Main Results related to Spalling Index and velocity*

Stage description	Absolute Time Start [s]	Absolute Time End [s]	$IS4_{max}$ [-]	X_{IS4max} [cm]	t_{IS4max} [s]	v_{max} [m/s]	X_{vmax} [cm]	t_{vmax} [s]	v_{max}* [m/s]	X_{vmax*} [cm]	t_{vmax*} [s]
First Heating	0	3.360+120	0,1004	1,035	3.390	5,453	1,644	3.480	5,453	1,644	3.480
Environment cooling	3.480	3.732	0,0982	1,099	3.480	5,453	1,644	3.480	5,453	1,644	3.480
Environment constant Temperature up to an absolute time 10.800s	3.732	10.800	0,0234	2,375	3.732	3,987	3,172	3.732	3,987	3,172	3.732
Environment Constant Temperature for t > 10.800s	10.800	99.732	0,0002	5,071	10.800	2,606	5,071	99.732	2,606	5,071	99.732
Maximum for t ≤ 10.800s†	0	10.800	0,1004	1,035	3.390	5,453	1,644	3.480	5,453	1,644	3.480
Absolute Maximum	0	99.732	0,1004	1,035	3.390	5,453	1,644	3.480	5,453	1,644	3.480

Remark †: *These results are included for the Comparative Analysis developed on Paragraph 6.5.3*

Stage description	Absolute Time Start [s]	Absolute Time End [s]	d_{max} [-]	X_{dmax} [cm]	t_{dmax} [s]	T_{max} [K]	X_{Tmax} [cm]	t_{Tmax} [s]	p^g_{max} [MPa]	X_{pgmax} [cm]	t_{pgmax} [s]
First Heating	0	3.360+120	0,5401	1,932	3.480	656,65	0,000	3.480	0,8256	1,555	2.760
Environment cooling	3.480	3.732	0,5892	0,000	3.732	656,65	0,000	3.480	0,7757	2,623	3.480
Environment constant Temperature up to an absolute time 10.800s	3.732	10.800	0,7365	0,000	10.800	533,02	0,508	3.732	0,6281	3,172	3.732
Environment Constant Temperature for t > 10.800s	10.800	99.732	0,8980	3,321	46.932	384,08	3,321	10.800	0,2669	8,259	10.800
Maximum for t ≤ 10.800s†	0	10.800	0,7365	0,000	10.800	656,65	0,000	3.480	0,8256	1,555	2.760
Absolute Maximum	0	99.732	0,8980	3,321	46.932	656,65	0,000	3.480	0,8256	1,555	2.760

Table 6-87. *Description of the Cooling Process Stages and Collection of the Main Results related to mechanical damage, Temperature and Gas Pressure*

a) Spalling Index IS4 [-]

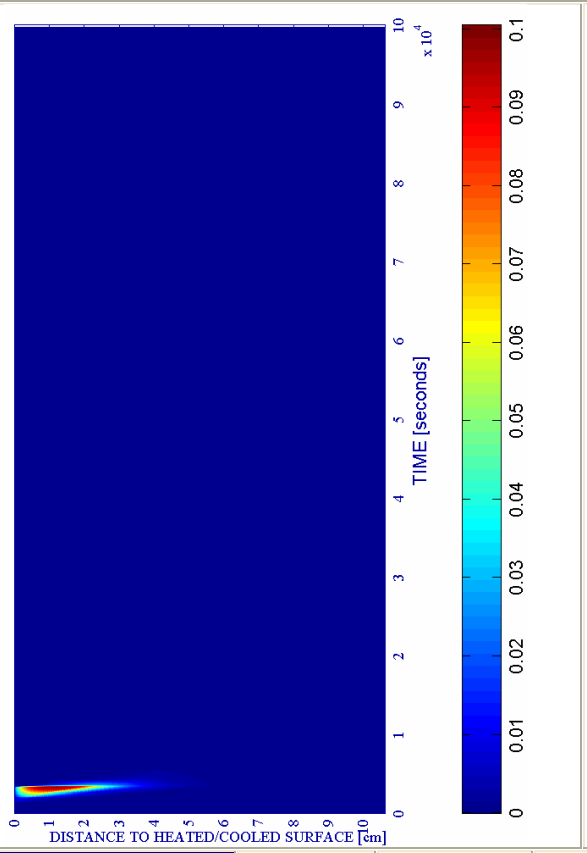

b) Mechanical damage d [-]

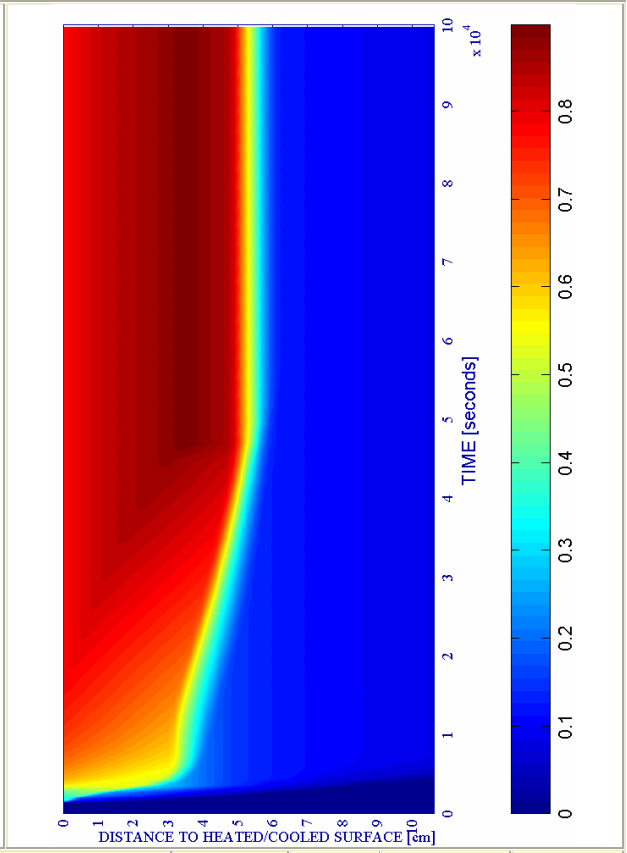

ENVIRONMENTAL - MED.		PC1 - RH [%]			PC2 - K_0 [m^2]			PC4 - Heating curve			PC5 – Mat.		Cooling length[s]	Start of cooling [s]	End of cooling [s]
#	Combination	40	50	60	10^{-19}	10^{-18}	10^{-17}	PAR1	PAR2	PAR4	C60	C90			
14	TH12K018RH50PAR2C60		X			X			X		X		252	3.360+120	3.732

c) Velocity of spalled pieces v [m/s]

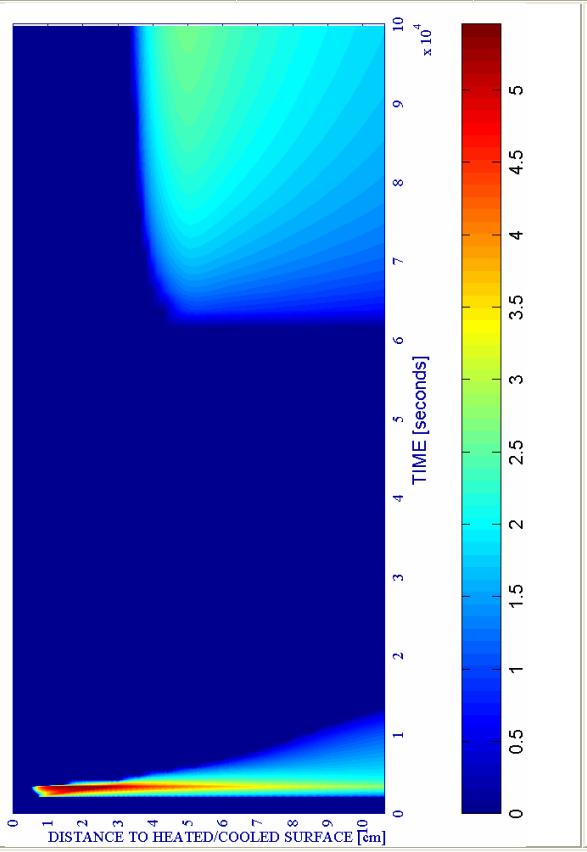

d) Velocity [m/s] where d ≥ 0,10

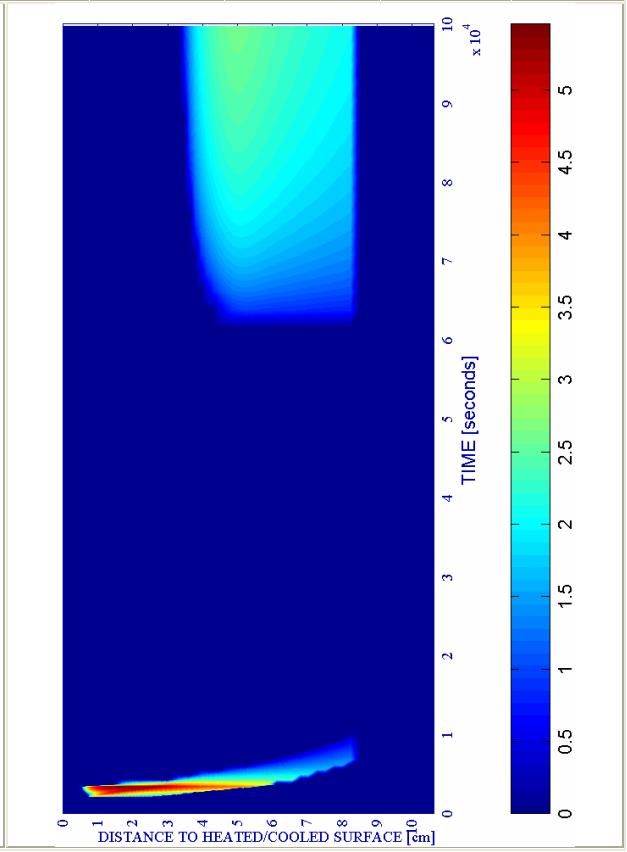

Figure 6-119.

e) Gas pressure $p^g \cdot 10^{-5}$ [Pa]

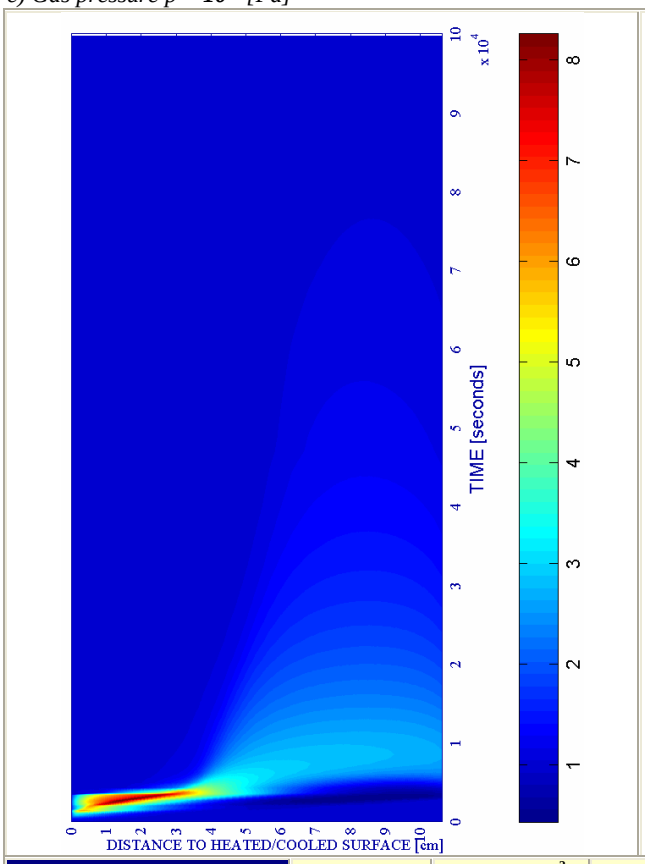

f) Vapour pressure $p^v \cdot 10^{-5}$ [Pa]

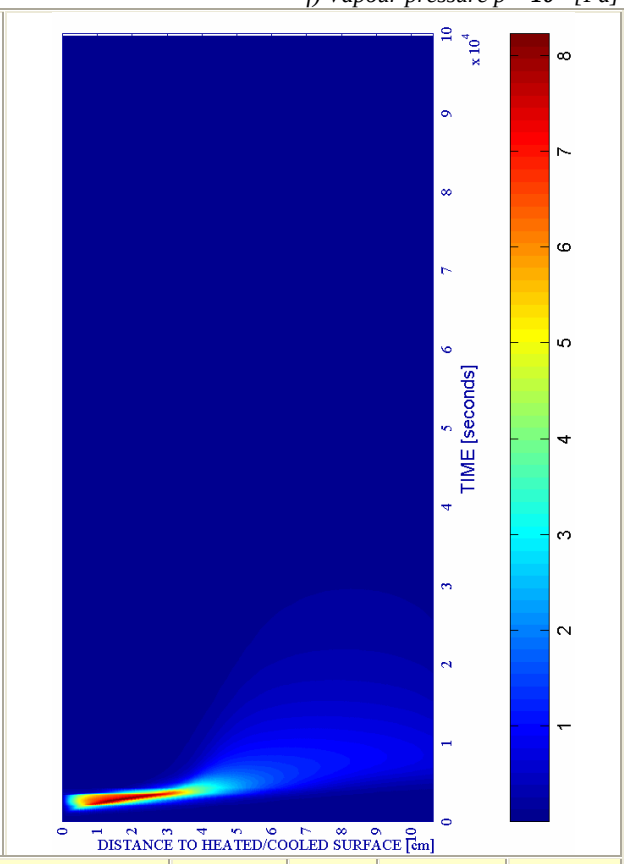

ENVIRONMENTAL - MED.		PC1 - RH [%]			PC2 - K_0 [m^2]			PC4 - Heating curve			PC5 – Mat.		Cooling length[s]	Start of cooling [s]	End of cooling [s]
#	Combination	40	50	60	10^{-19}	10^{-18}	10^{-17}	PAR1	PAR2	PAR4	C60	C90			
14	TH12K018RH50PAR2C60		X			X			X		X		252	3.360+120	3.732

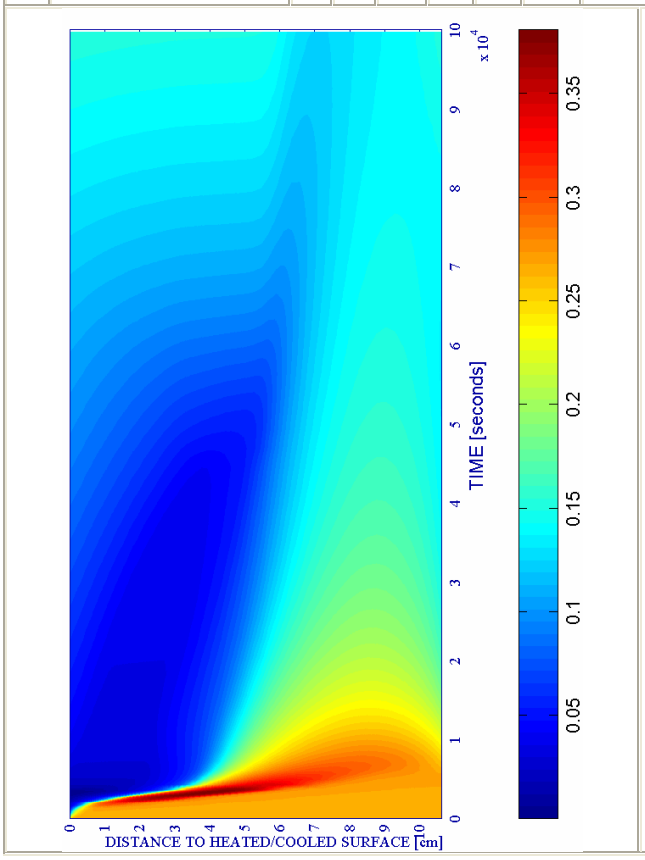

g) Saturation Degree S [-]

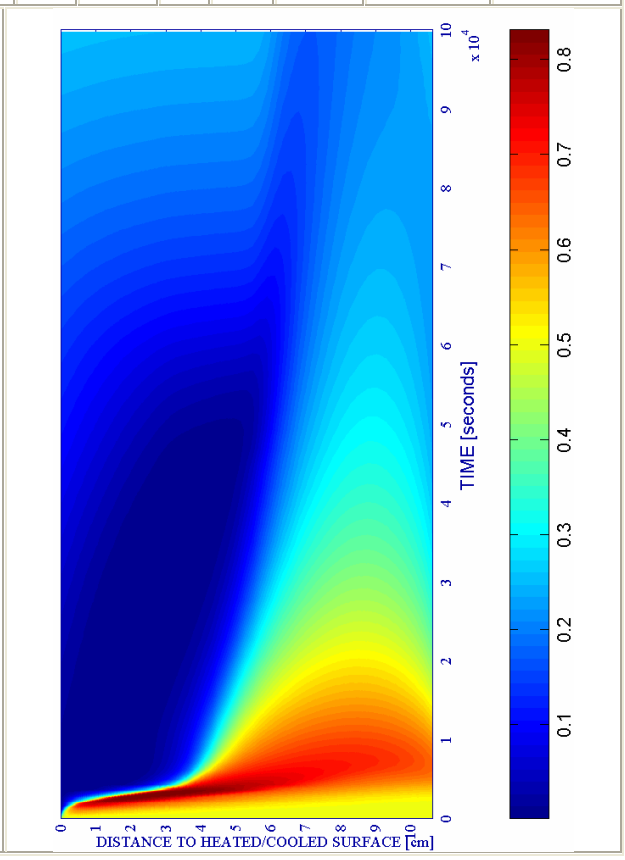

h) Relative Humidity RH [-]

Figure 6-119. (continued)

i) Temperature [K]

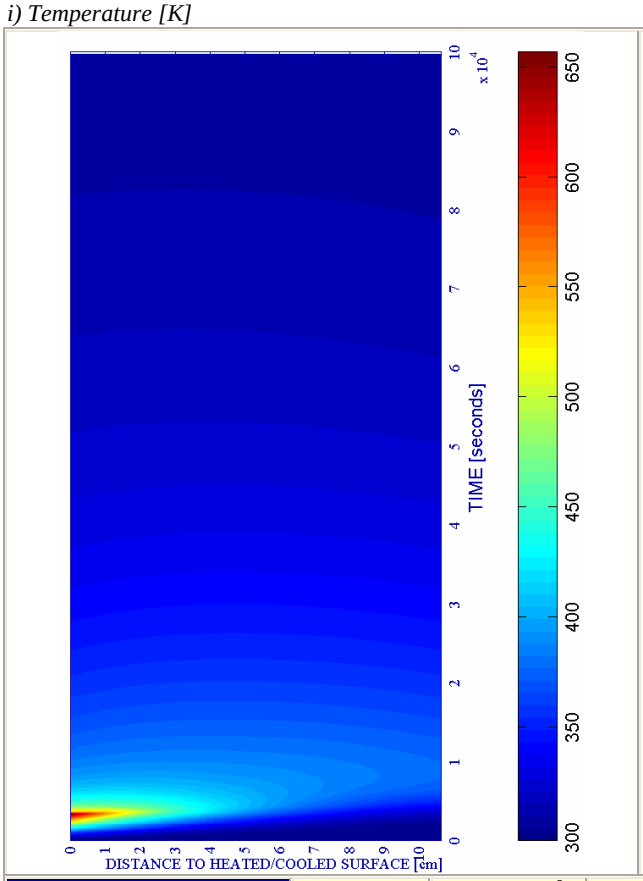

*j) Elastic Energy U · **10**$^{-4}$ [J/m^3]*

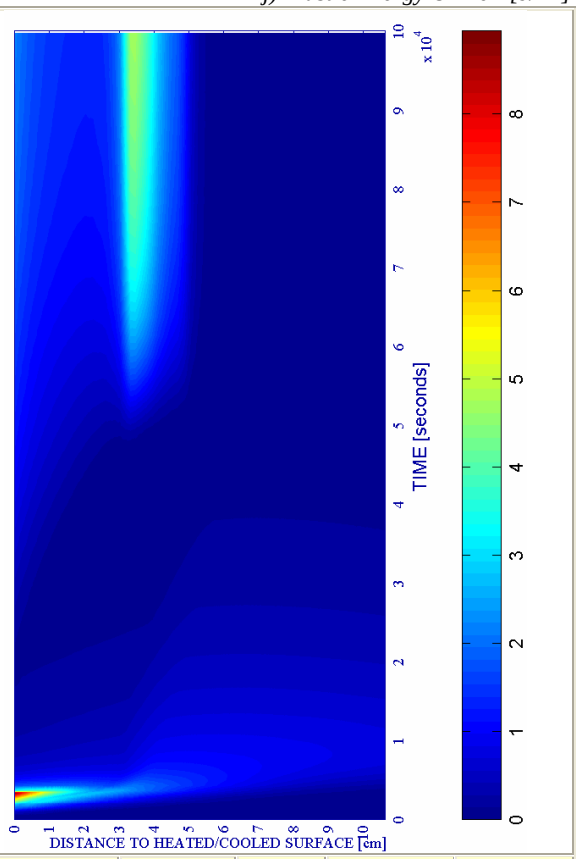

ENVIRONMENTAL - MED.	PC1 - RH [%]			PC2 - K_0 [m^2]			PC4 - Heating curve			PC5 – Mat.		Cooling length[s]	Start of cooling [s]	End of cooling [s]
#	Combination	40	50	60	10^{-19}	10^{-18}	10^{-17}	PAR1	PAR2	PAR4	C60	C90			
14	TH12K018RH50PAR2C60		X			X			X		X		252	3.360+120	3.732

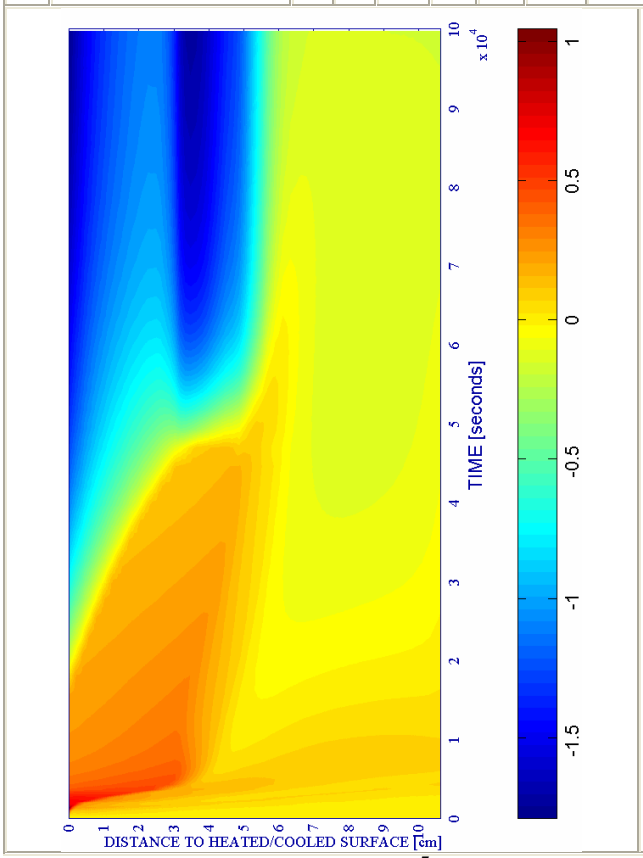

*k) Stress in longitudinal (xx) direction · **10**$^{-7}$ [Pa]*

Figure 6-119. (continued)

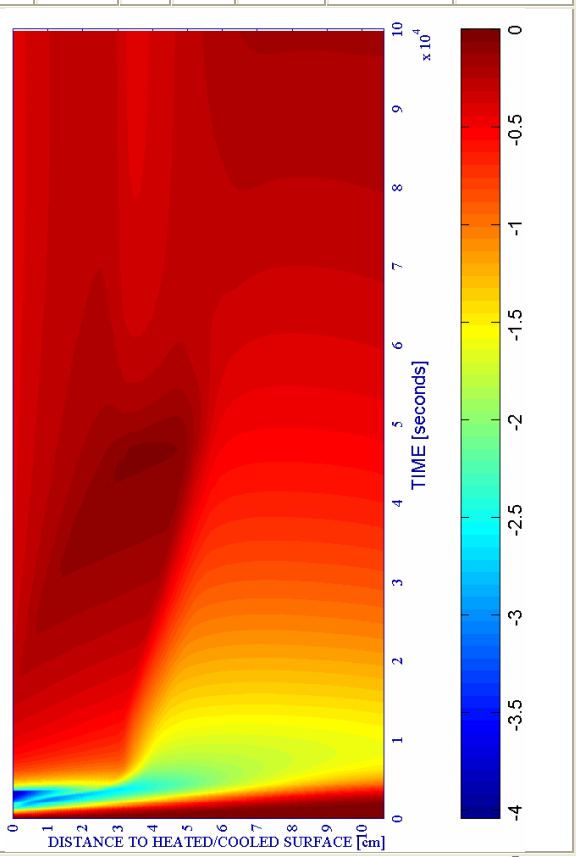

*l) Stress in transversal (yy) direction · **10**$^{-7}$ [Pa]*

6.5.2.5.3 Environmental Fast Cooling

The phenomena analysis to develop from the results obtained for the 'fast' cooling case are, in general, very similar to those obtained from the 'medium' rate of cooling case (described in previous paragraph) so also qualitative and quantitatively different from those corresponding to the 'slow' cooling case (see figure 6-121 a) to l)). For instance, referring to the mechanical damage the only difference is that the depth with high values is even slightly smaller than in the 'medium' cooling case (see figure 6-120). A deeper comparison of these cases will be developed later in paragraph 6.5.3.1.1. Next it is shown a collection of the main results corresponding to this subparagraph.

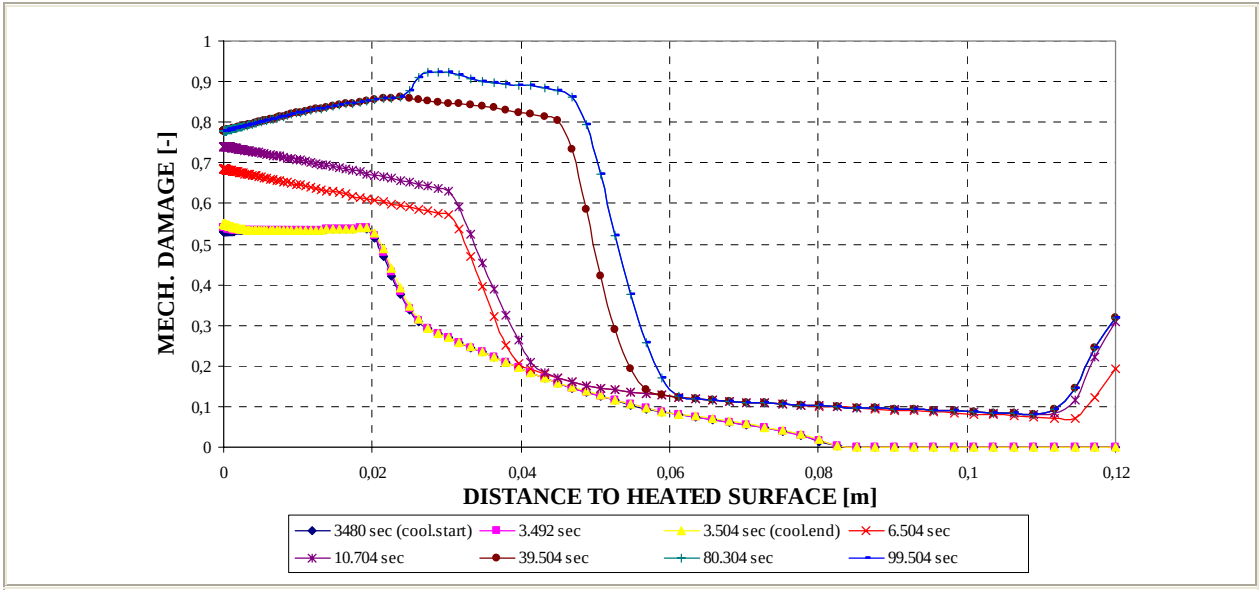

Figure 6-120. *Mechanical damage d [-] at several distances from the heated surface during Environment cooling process.*

Table 6-88. *Description of the Cooling Process Stages and Collection of the Main Results related to Spalling Index and velocity*

Stage description	Absolute Time Start [s]	Absolute Time End [s]	$IS4_{max}$ [-]	X_{IS4max} [cm]	t_{IS4max} [s]	v_{max} [m/s]	X_{vmax} [cm]	t_{vmax} [s]	v_{max}* [m/s]	X_{vmax*} [cm]	t_{vmax*} [s]
First Heating	0	3.360+120	0,1004	1,035	3.390	5,453	1,644	3.480	5,453	1,644	3.480
Environment cooling	3.480	3.504	0,0982	1,099	3.480	5,453	1,644	3.480	5,453	1,644	3.480
Environment constant Temperature up to an absolute time 10.800s	3.504	10.800	0,0742	1,736	3.504	5,209	2,623	3.504	5,209	2,623	3.504
Environment Constant Temperature for t > 10.800s	10.800	99.504	0,0002	5,071	10.800	2,724	4,875	99.504	2,724	4,875	99.504
Maximum for t ≤ 10.800s†	0	10.800	0,1004	1,035	3.390	5,453	1,644	3.480	5,453	1,644	3.480
Absolute Maximum	0	99.504	0,1004	1,035	3.390	5,453	1,644	3.480	5,453	1,644	3.480

Remark †: *These results are included for the Comparative Analysis developed on Paragraph 6.5.3*

Stage description	Absolute Time Start [s]	Absolute Time End [s]	d_{max} [-]	X_{dmax} [cm]	t_{dmax} [s]	T_{max} [K]	X_{Tmax} [cm]	t_{Tmax} [s]	p^g_{max} [MPa]	X_{pgmax} [cm]	t_{pgmax} [s]
First Heating	0	3.360+120	0,5401	1,932	3.480	656,65	0,000	3.480	0,8256	1,555	2.760
Environment cooling	3.480	3.504	0,5493	0,000	3.504	656,65	0,000	3.480	0,7757	2,623	3.480
Environment constant Temperature up to an absolute time 10.800s	3.504	10.800	0,7411	0,000	10.800	608,23	0,165	3.504	0,7613	2,753	3.504
Environment Constant Temperature for t > 10.800s	10.800	99.504	0,8995	2,753	44.304	382,32	3,475	10.800	0,2635	8,259	10.800
Maximum for t ≤ 10.800s†	0	10.800	0,7411	0,000	10.800	656,65	0,000	3.480	0,8256	1,555	2.760
Absolute Maximum	0	99.504	0,8995	2,753	44.304	656,65	0,000	3.480	0,8256	1,555	2.760

Table 6-89. *Description of the Cooling Process Stages and Collection of the Main Results related to mechanical damage, Temperature and Gas Pressure*

a) Spalling Index IS4 [-]

b) Mechanical damage d [-]

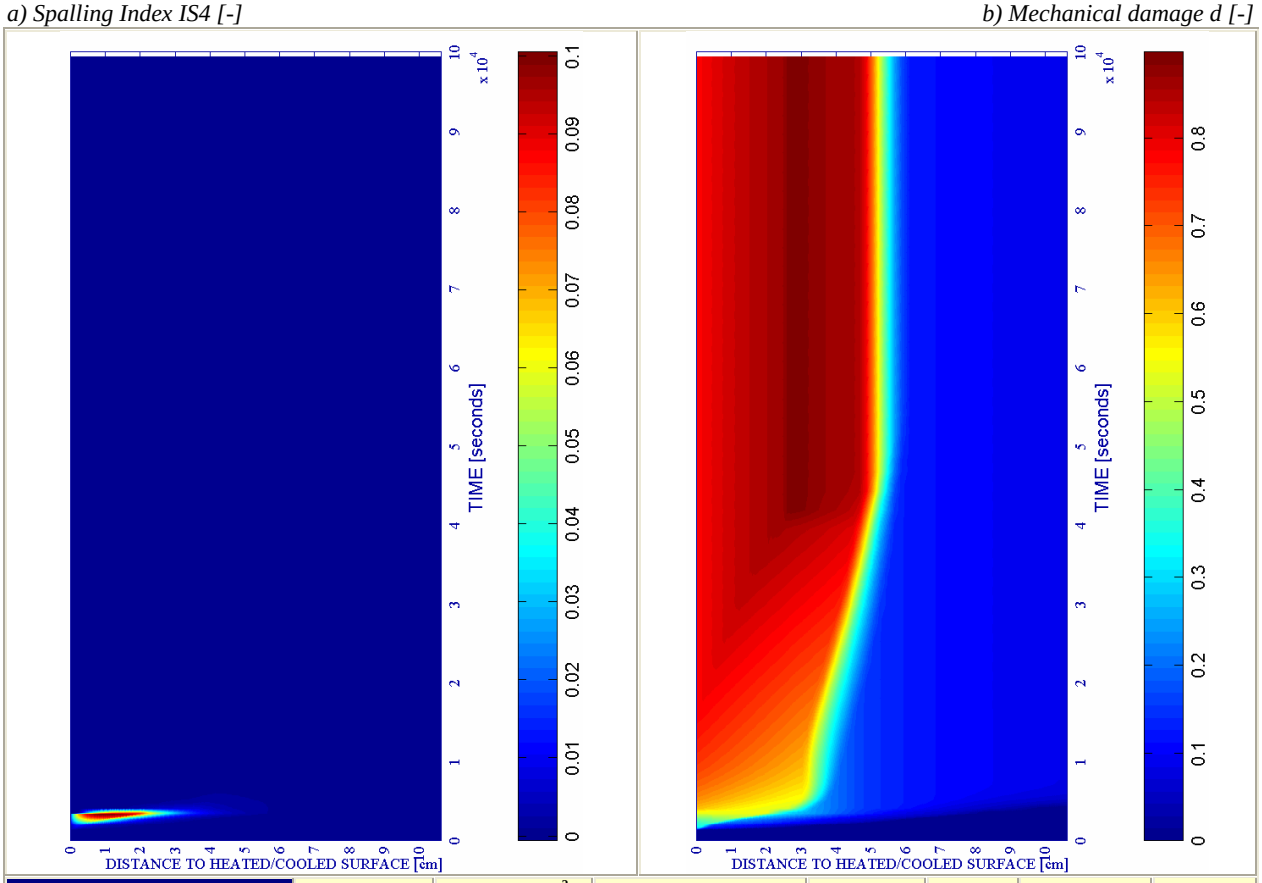

ENVIRONMENTAL - FAST		PC1 - RH [%]			PC2 - K_0 [m^2]			PC4 - Heating curve			PC5 – Mat.		Cooling length[s]	Start of cooling [s]	End of cooling [s]
#	Combination	40	50	60	10^{-19}	10^{-18}	10^{-17}	PAR1	PAR2	PAR4	C60	C90			
14	TH12K018RH50PAR2C60		X			X			X		X		24	3.360+120	3.504

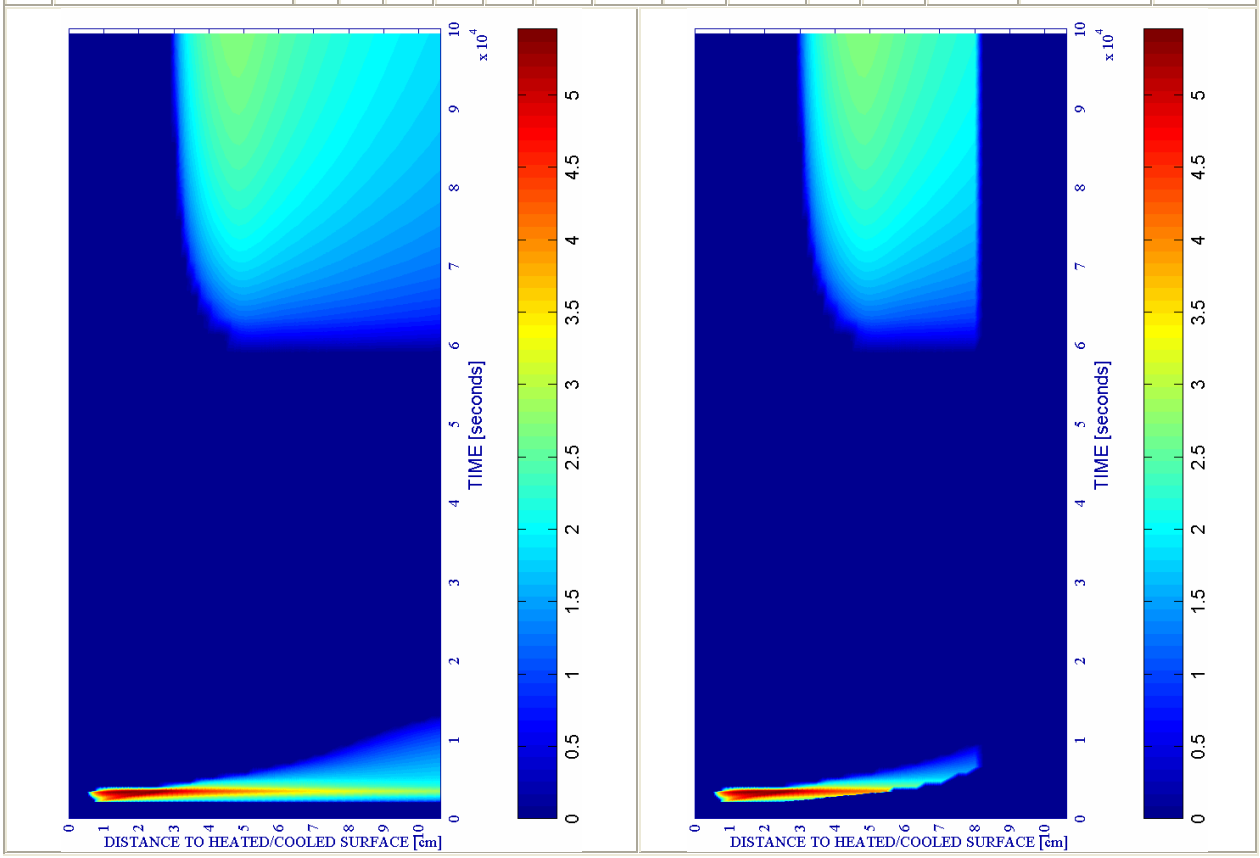

c) Velocity of spalled pieces v [m/s]

Figure 6-121.

d) Velocity [m/s] where d ≥ 0,10

e) Gas pressure $p^g \cdot 10^{-5}$ [Pa]

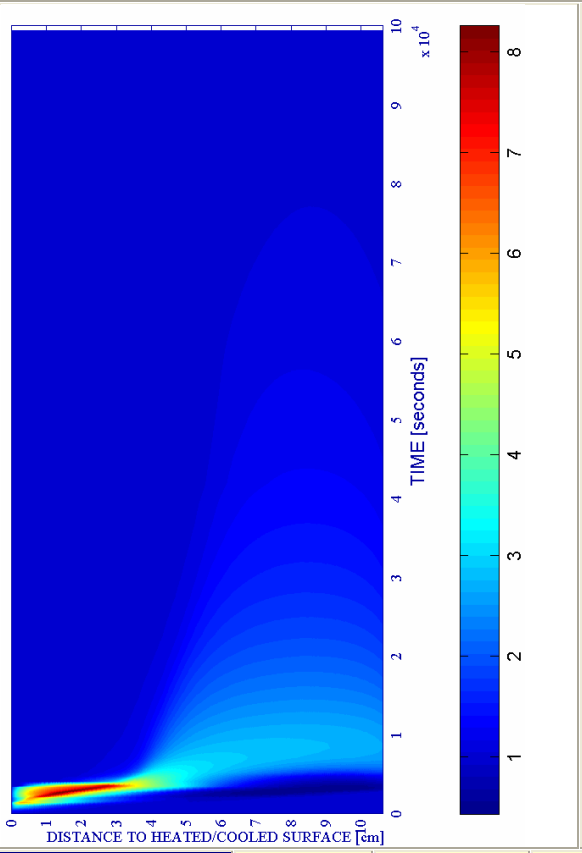

f) Vapour pressure $p^v \cdot 10^{-5}$ [Pa]

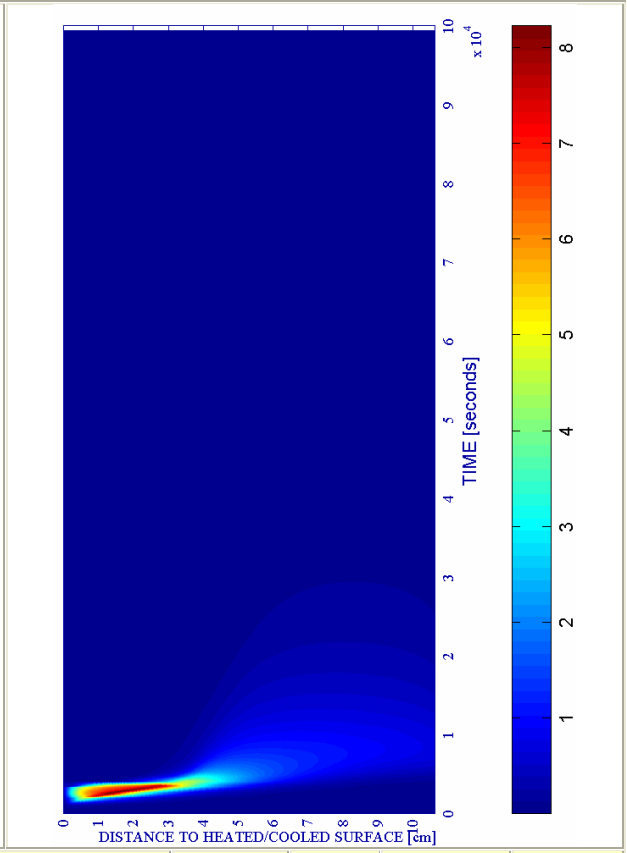

ENVIRONMENTAL - FAST	PC1 - RH [%]			PC2 - K_0 [m^2]			PC4 - Heating curve			PC5 – Mat.		Cooling length[s]	Start of cooling [s]	End of cooling [s]
#	Combination	40	50	60	10^{-19}	10^{-18}	10^{-17}	PAR1	PAR2	PAR4	C60	C90			
14	TH12K018RH50PAR2C60		X			X			X		X		24	3.360+120	3.504

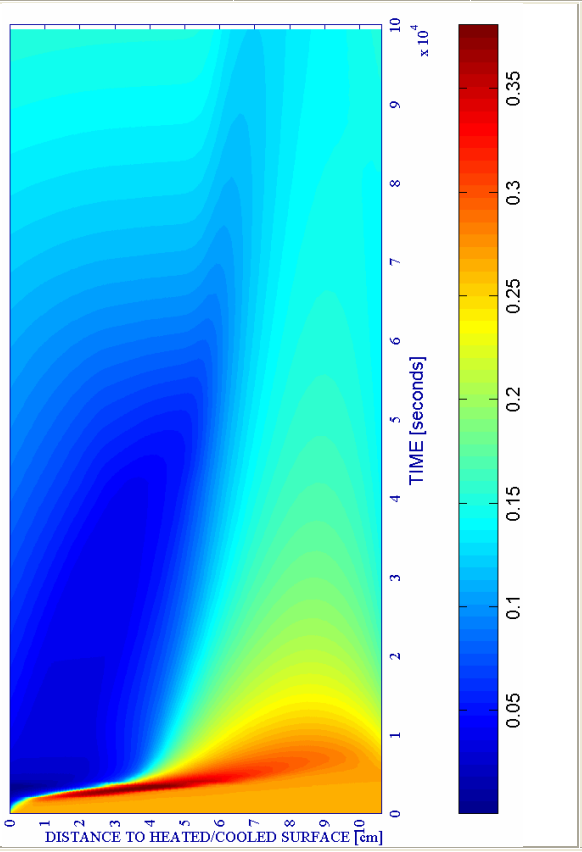

g) Saturation Degree S [-]

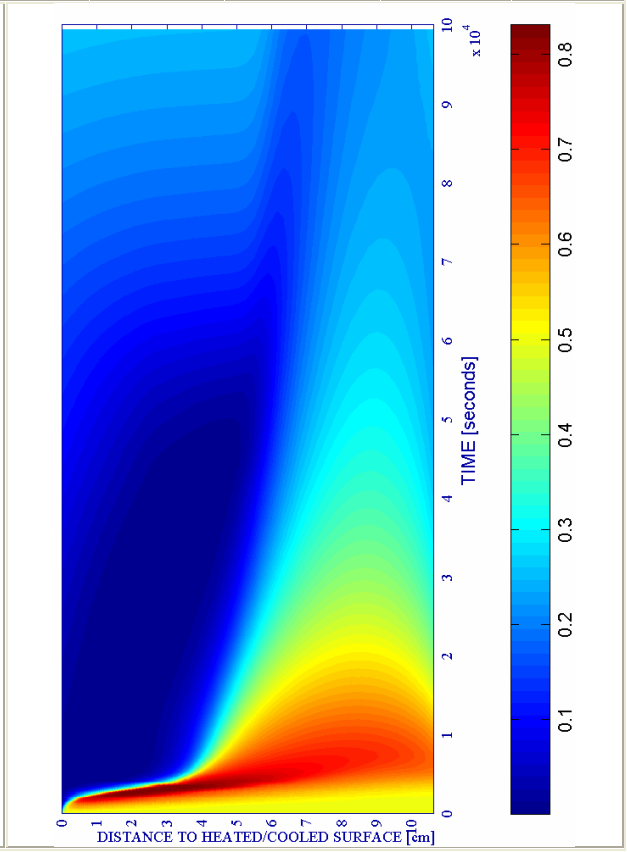

h) Relative Humidity RH [-]

Figure 6-121. (continued)

i) Temperature [K]

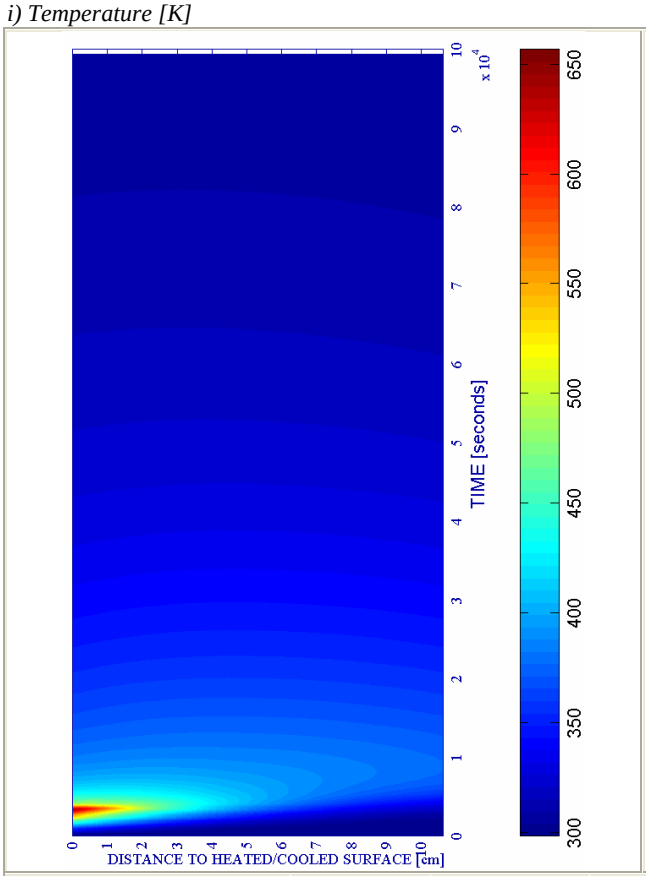

*j) Elastic Energy U · **10**$^{-4}$ [J/m^3]*

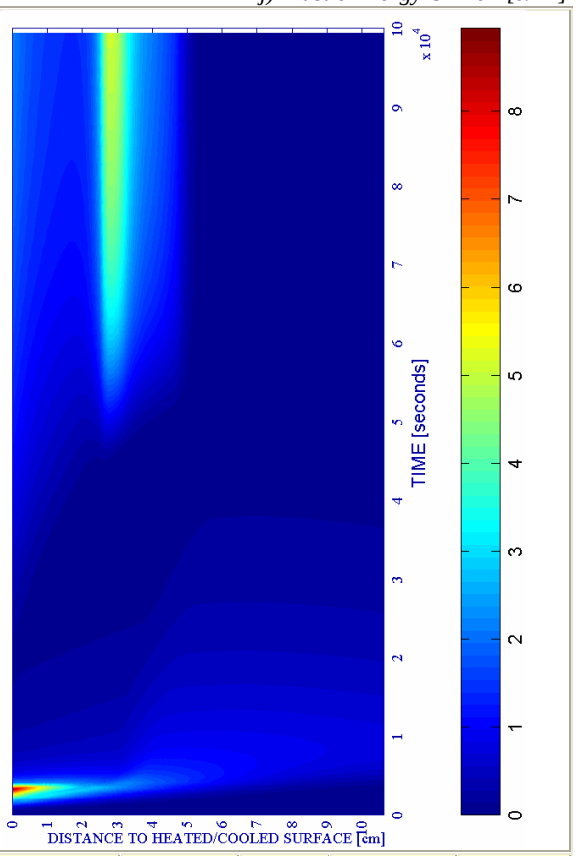

ENVIRONMENTAL - FAST	PC1 - RH [%]			PC2 - K_0 [m^2]			PC4 - Heating curve			PC5 – Mat.		Cooling length[s]	Start of cooling [s]	End of cooling [s]
#	Combination	40	50	60	10^{-19}	10^{-18}	10^{-17}	PAR1	PAR2	PAR4	C60	C90			
14	TH12K018RH50PAR2C60		X			X			X		X		24	3.360+120	3.504

*k) Stress in longitudinal (xx) direction · **10**$^{-7}$ [Pa]*

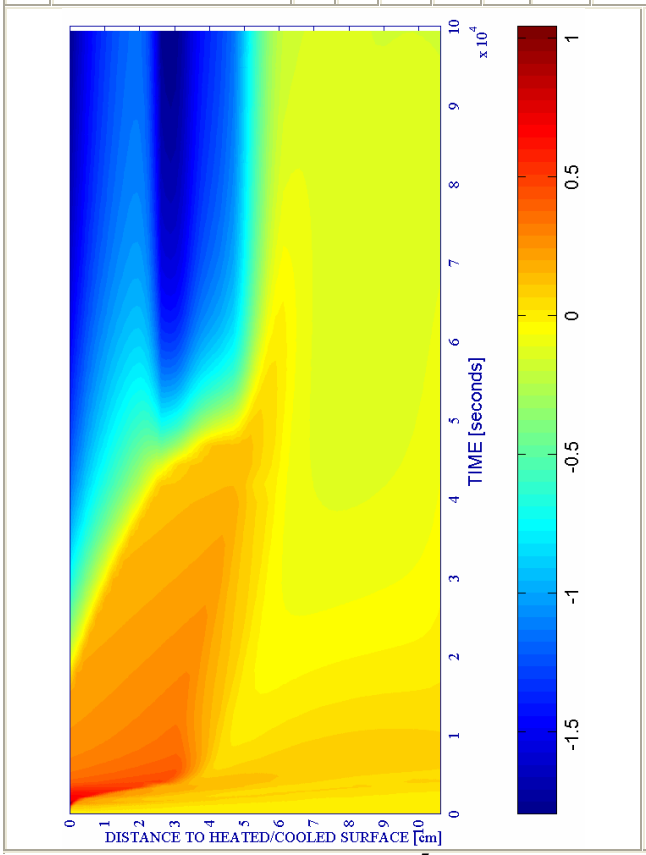

Figure 6-121. (continued)

*l) Stress in transversal (yy) direction · **10**$^{-7}$ [Pa]*

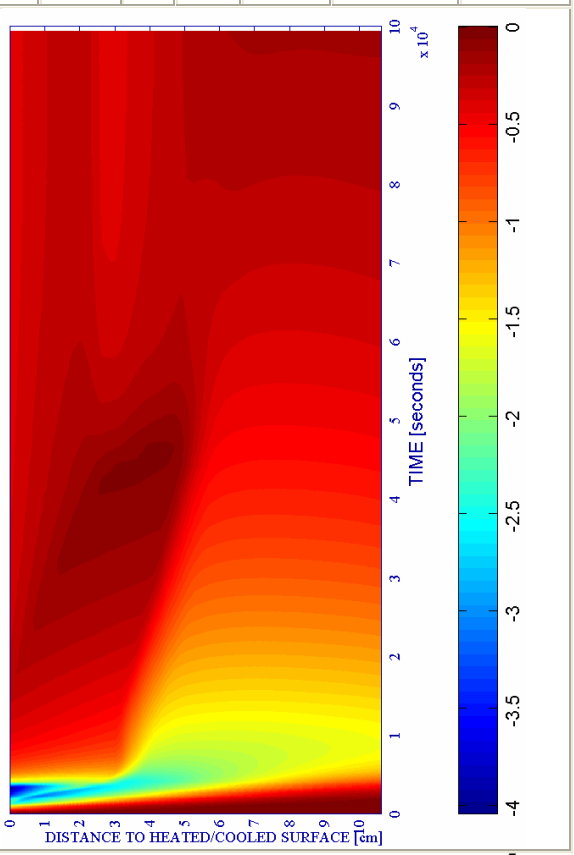

6.5.2.5.4 Surface Cooling followed by a Heating phase

6.5.2.5.4.1 Phenomenological and Mechanistic analysis of the Surface Cooling Stage

In the case analyzed herein, the phenomena occurred during the first heating stage (up to 3.480 seconds) are exactly those explained in previous paragraphs. However, at 3.480 seconds starts a cooling process of the surface of the structural element featured by a cooling rate (see figure 6-124) much higher than that observed during the Environment cooling. Indeed if, for instance, in the Fast Environment cooling case the temperature in the surface decreased only 52,18 K during the first 24 seconds (the length of the environment cooling process, what means a cooling rate of the surface of 2,17 K/s), in this case in only 36 seconds (just 12 seconds more) the temperature in the surface decreases as much as 309,86 K (close to 10 K per second).

During the Surface Cooling stage, defined by the time range from 3.480 to 3.516 seconds, the Total Damage D rises in the layers next to the surface from an initial value of 0,5613 up to a high final value of 0,8578 (see figure 6-123). This means that in only 36 seconds of surface cooling, Total Damage close to the surface increases in about a 53 per cent, reaching a quite high level and approaching to an almost complete destruction of the superficial layer (more precisely, of a depth corresponding to the first centimetre). This phenomenon will leave the structural element – and, hence, the steel reinforcing bars – considerably more exposed to the fire effect after the surface cooling has finished, since the first centimetre layer will have spalled-off (see tables 6-90 and 6-91 and figures 6-129 c) and d)).

In the meantime, during this cooling period of forty seconds gas pressure decreases considerably, especially in the first centimetre layer, due in part to the abovementioned cracking and in a smaller part due to condensation of the slightly remaining water vapour (see figures 6-125 and 6-129 e)).

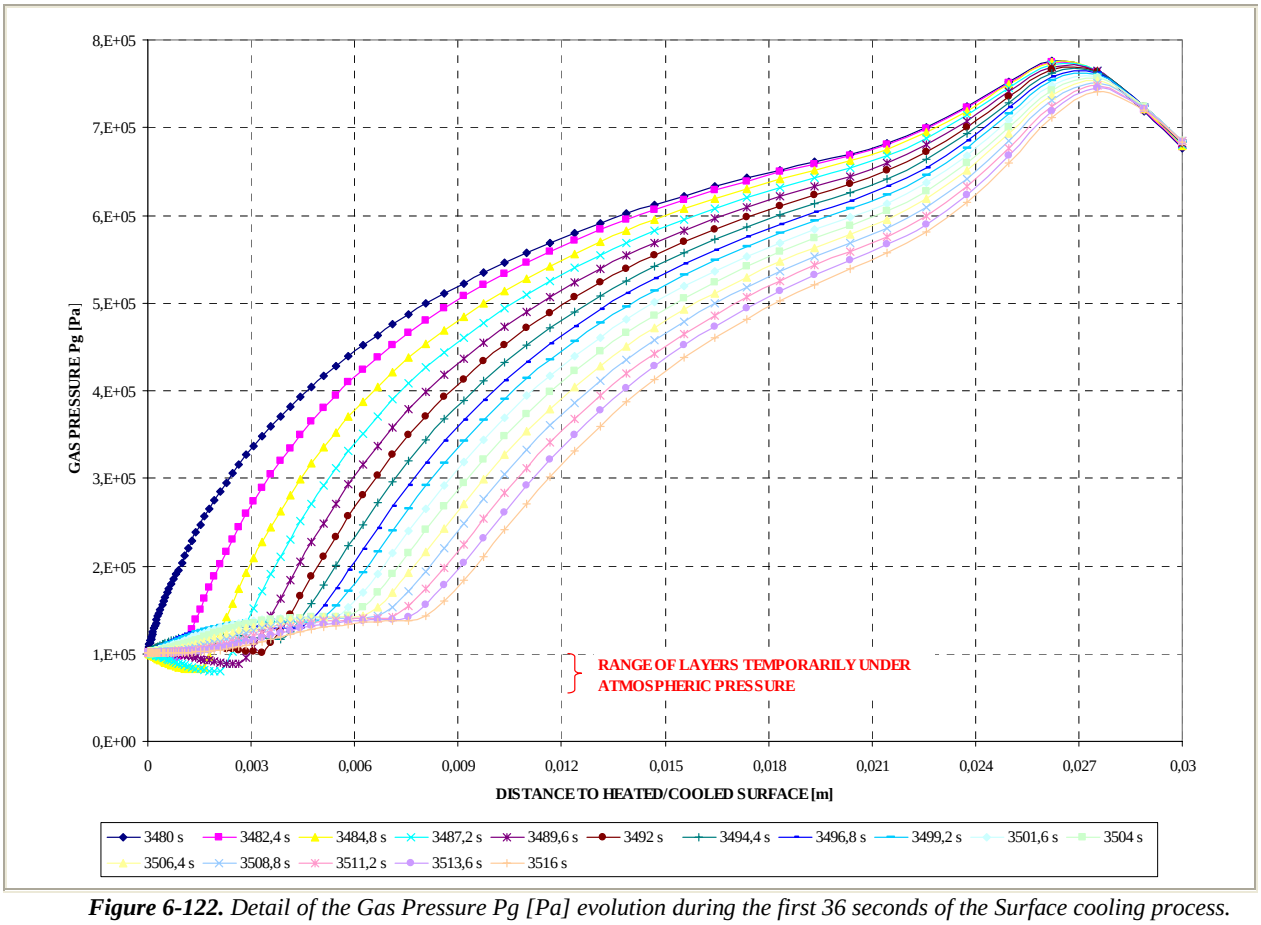

Figure 6-122. *Detail of the Gas Pressure Pg [Pa] evolution during the first 36 seconds of the Surface cooling process.*

Specifically, in the first 3 millimetres gas pressure undergoes atmospheric pressure in the time range from 3.482 to 3.492 seconds (see figures 6-122 and 6-129 e)), occurring this phenomenon simultaneously with the interval of time where water vapour reaches – in a descending process – the critical temperature of water (647,3 K).

Related to the rest of parameters with influence on the Spalling Index I_{s4} values, it is remarkable to observe that although the relative humidity values (see figures 6-126 and 6-129 h)) suffer big oscillations in the first 5 millimetres layer – having increased at the surface, for instance, in a 400 per cent magnitude from an initial value of 0,08 per cent up to a final value of 0,4 per cent at the end of cooling process – this fact does not appear to be relevant in the overall phenomenological and mechanistic analysis since at this zone material keeps almost completely dried.

On the other hand, as it was expectable tensile longitudinal stresses (xx) decrease significantly in the first centimetre during the cooling process (see figures 6-128 and 6-129 k)) from an initial value at the surface of 4,90 MPa down to a final value of 1,60 MPa at the end of cooling process. Nevertheless, as a difference with the case where the Environment was cooled, no compressive longitudinal stresses arise at any depth – although observing the trend in their evolution, it would be expectable that compressive longitudinal stresses would appear if the cooling process would have been longer –. Beyond the first two centimetres close to the surface, no significant variations of longitudinal stresses have been noticed. This decrease in material stress state is one of the consequences of the material intensive cracking close to the surface, leading this phenomenon also to the Elastic Strain Energy accumulated within this zone being released during cooling process and, hence, decreasing its values close to zero (see figure 6-127 and 6-129 j)).

Due to all of these trends, Spalling Index I_{s4} values decrease during the whole cooling process (see Table 6-90 and figure 6-129 a)), reducing therefore the thermal spalling risk. Besides this fact, the energy available to promote an explosive spalling is also reduced considerably during cooling from a maximum value of 5,453 m/s at a depth of 1,644 centimetres at the start of cooling process – being the first layer where spalling is energetically viable at this instant at a depth of 0,58 centimetres from surface and the last at a depth of 5,48 centimetres – down to a maximum value of 4.310 m/s at a depth of 2,730 centimetres at the end of cooling – being the first layer where spalling is energetically viable at this instant at a depth of 1,39 centimetres from surface and the last at a depth of 5,48 centimetres – (see figures 6-129 c) and 6-129 d)). However, it is noticeable that since the decrease of elastic energy previously mentioned occurs mainly in the first centimetre close to the surface, thermal spalling keeps being energetically viable in the stated range during the whole cooling process.

6.5.2.5.4.2 Phenomenological and Mechanistic analysis of the Second Heating Stage

In the subsequent heating stage, once the surface cooling process has finished (3.516 seconds) and up to an absolute time of three hours, Total Damage continues increasing but always keeping the most damaged zones close to the surface due to the already explained phenomena occurred during cooling and on the contrary to what happened during the first cooling stage – where the most damaged zones were from 1 to 2 centimetres away from surface – (see figures 6-123 and 6-129 b)). An analysis of the final state of the structural element (after that three hours) reveals that more than the 33 per cent of the structural element would be completely destroyed (cracked) and the remaining 67 per cent would be with a damaging level above the 70 per cent.

A comparative analysis with the case where no cooling is applied during the first three hours (see paragraph 6.5.3.1.3) will show that these remaining conditions are worse than in the case where no cooling action on the surface is applied.

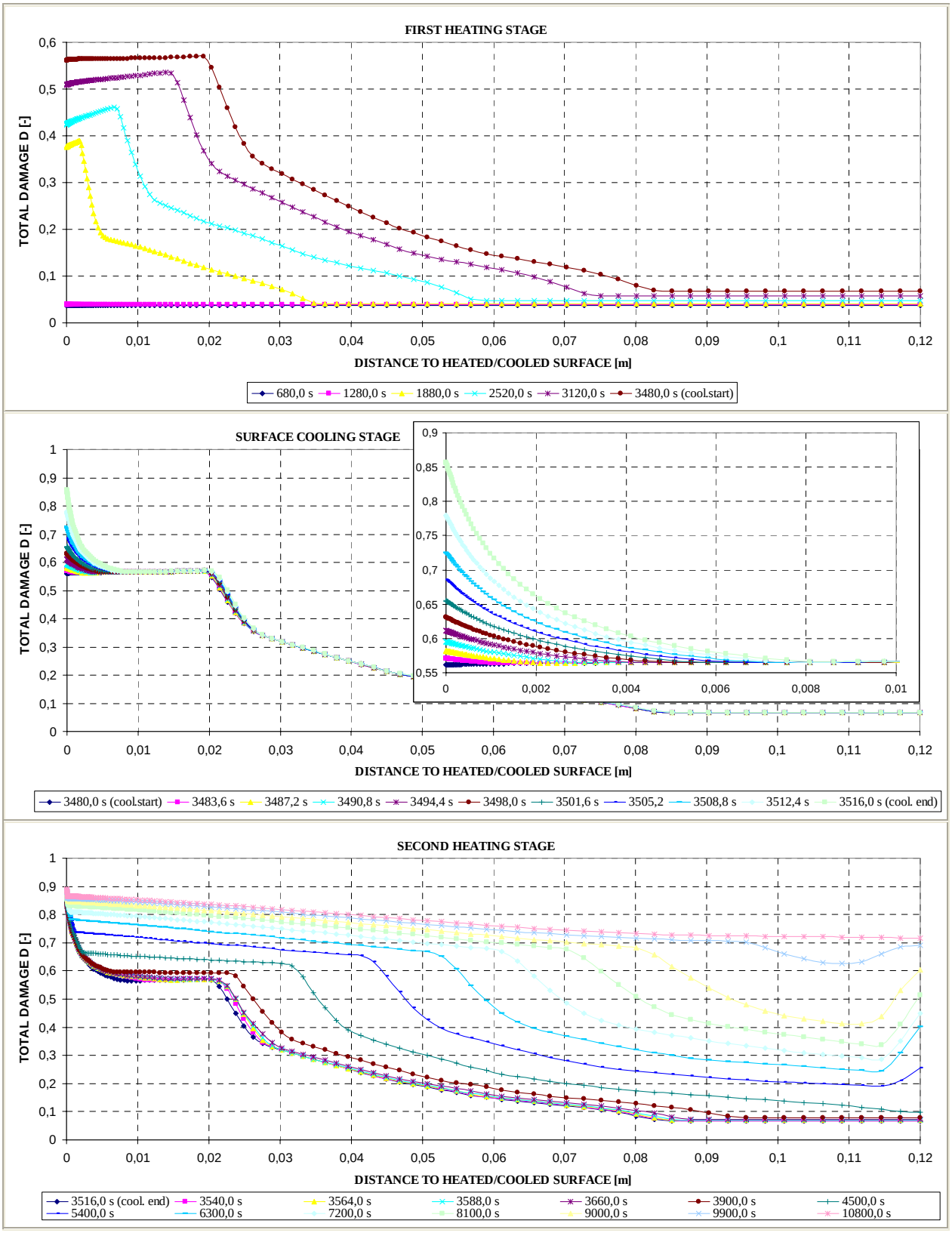

Figure 6-123. *Total damage D [-] at several distances from the heated/cooled surface during each stage of the Surface heating and cooling processes*

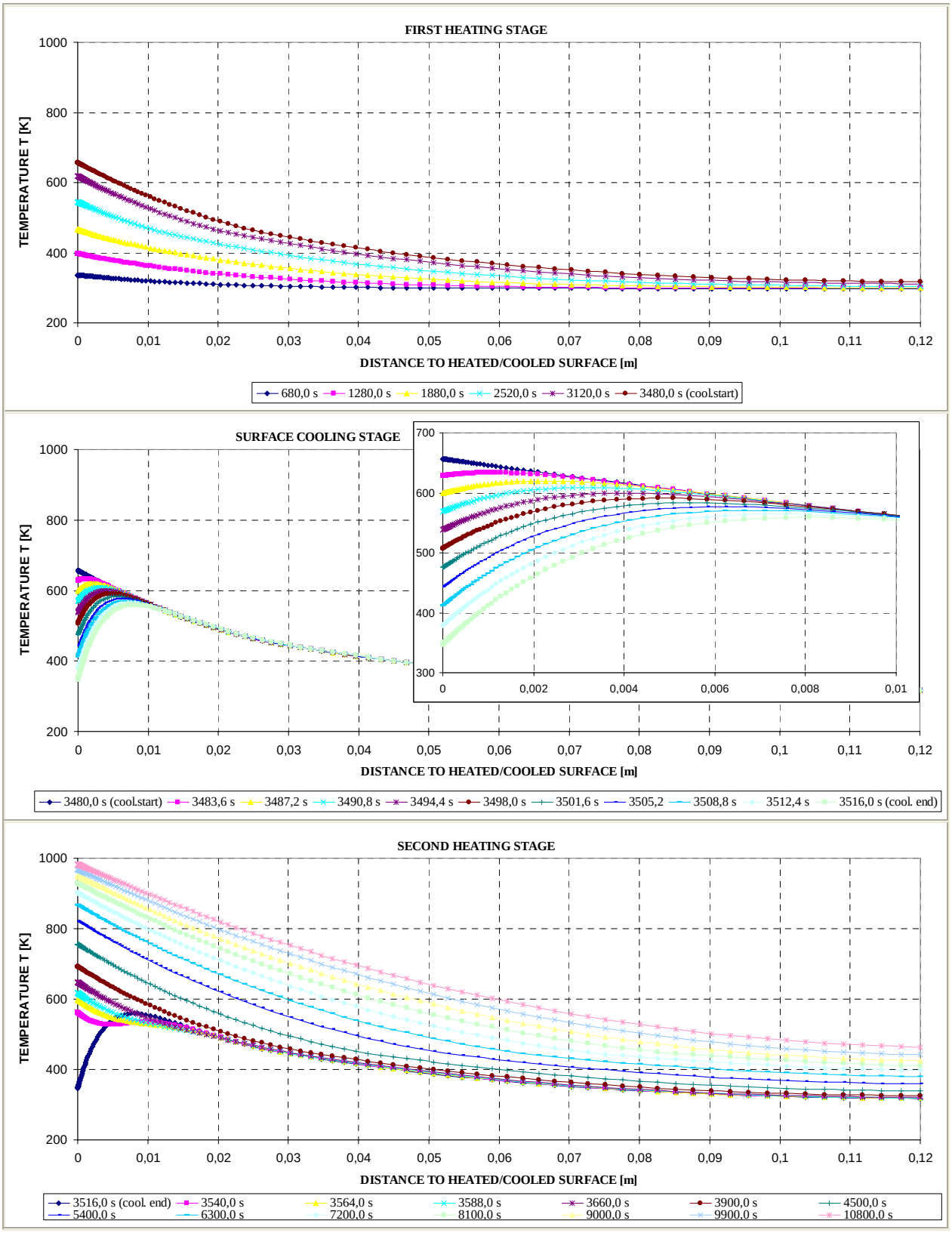

Figure 6-124. *Temperature T [K] at several distances from the heated/cooled surface during each stage of the Surface heating and cooling processes*

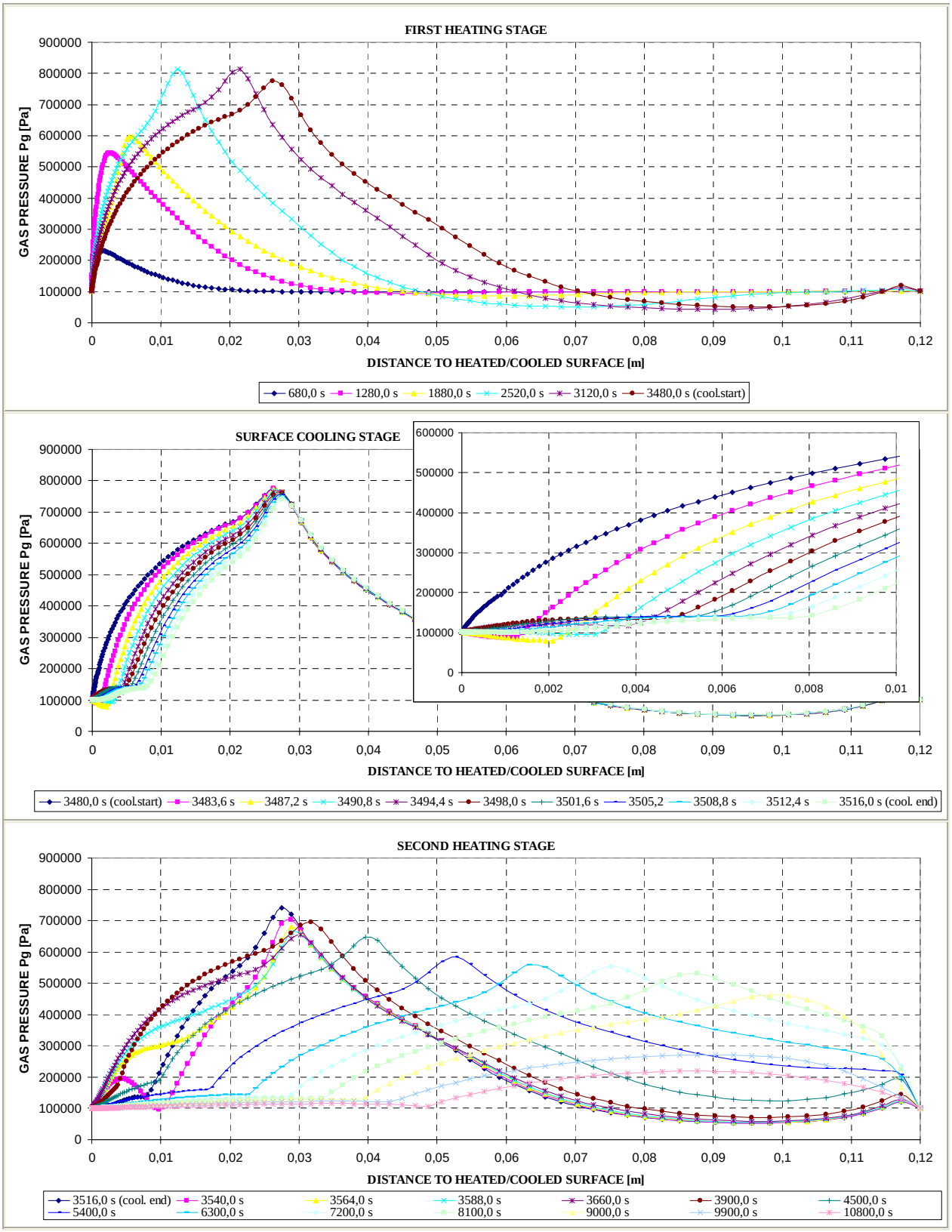

Figure 6-125. *Gas Pressure Pg [Pa] at several distances from the heated/cooled surface during each stage of the Surface heating and cooling processes*

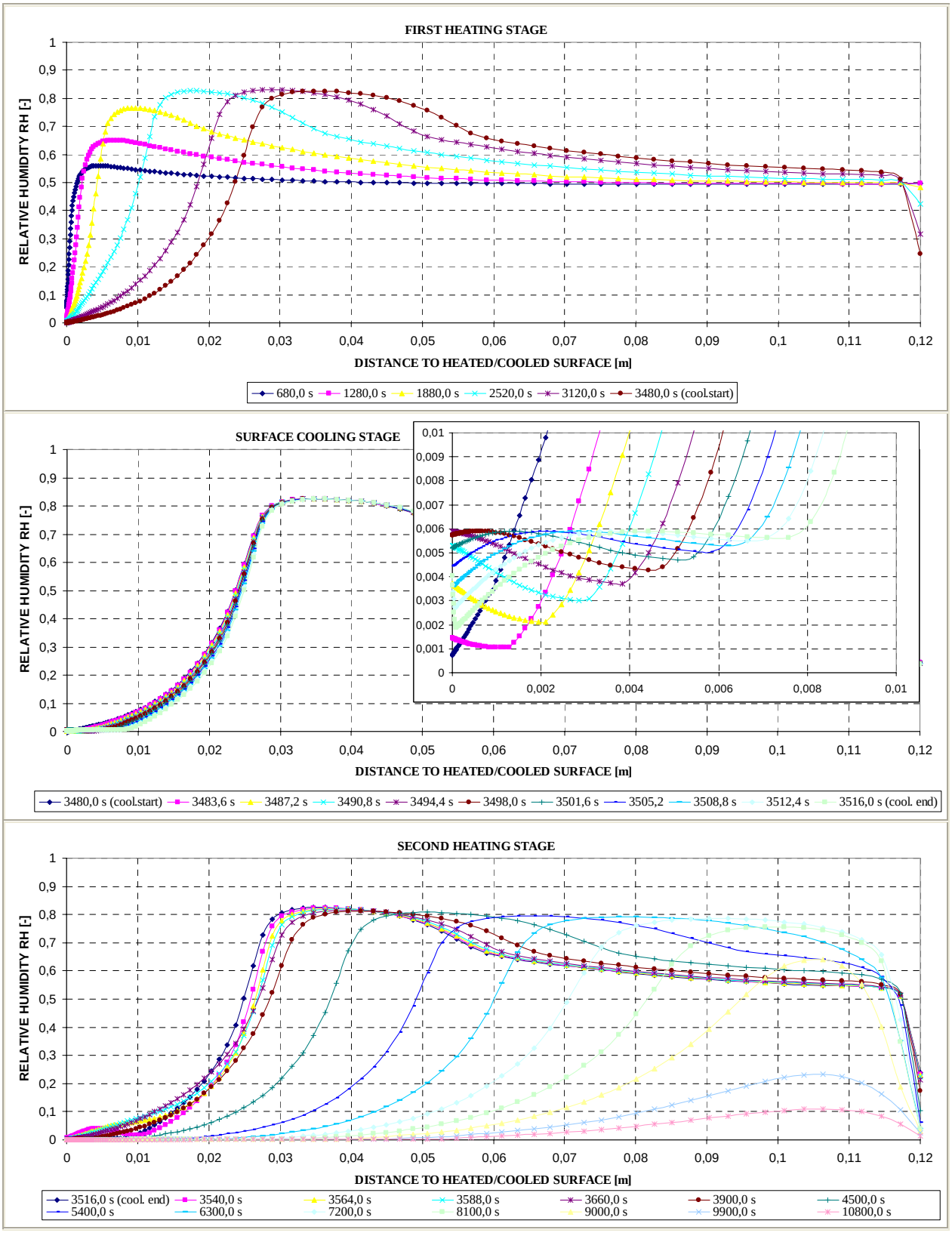

Figure 6-126. *Relative Humidity RH [-] at several distances from the heated/cooled surface during each stage of the Surface heating and cooling processes*

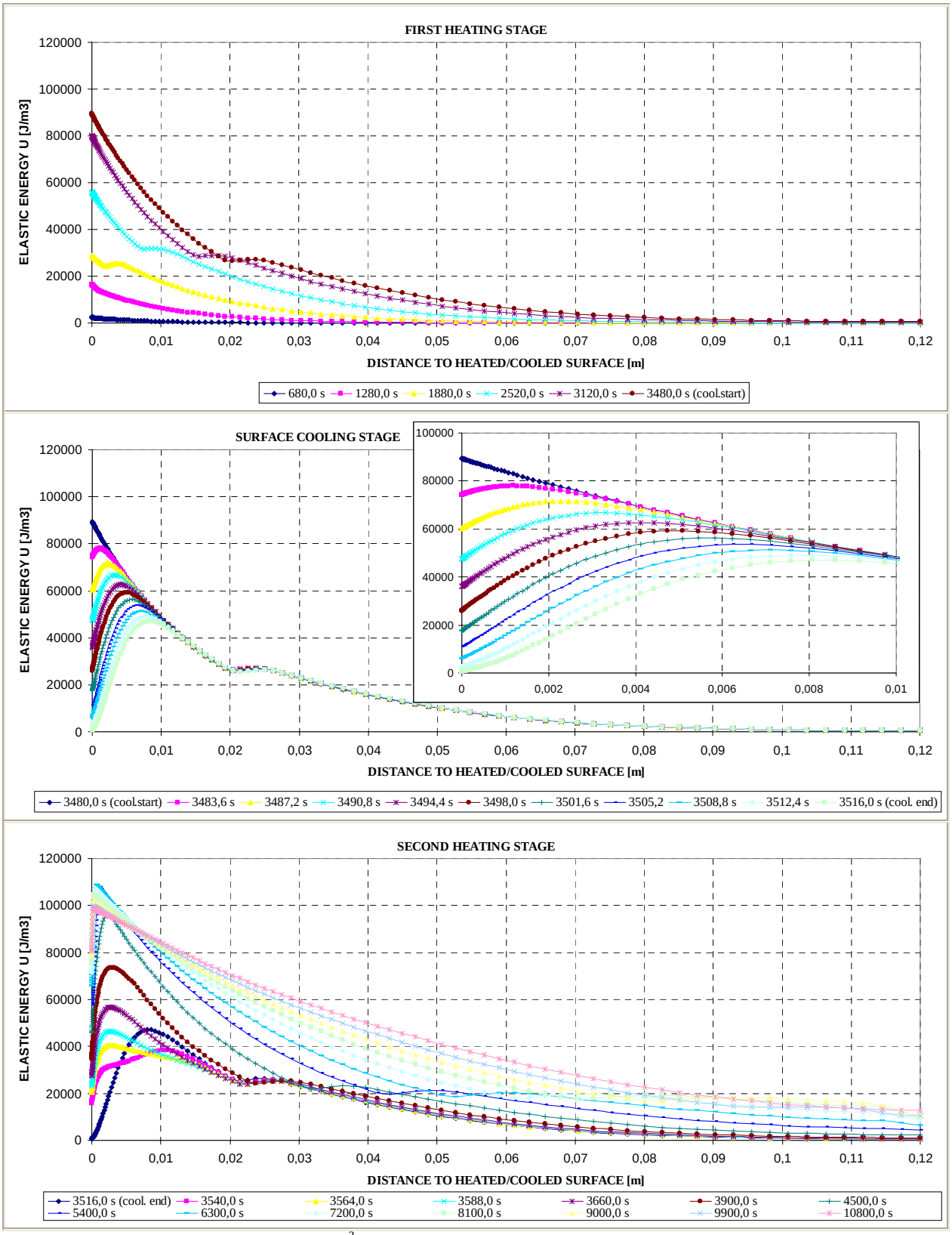

Figure 6-127. *Elastic Energy U [J/m^3] at several distances from the heated/cooled surface during each stage of the Surface heating and cooling processes*

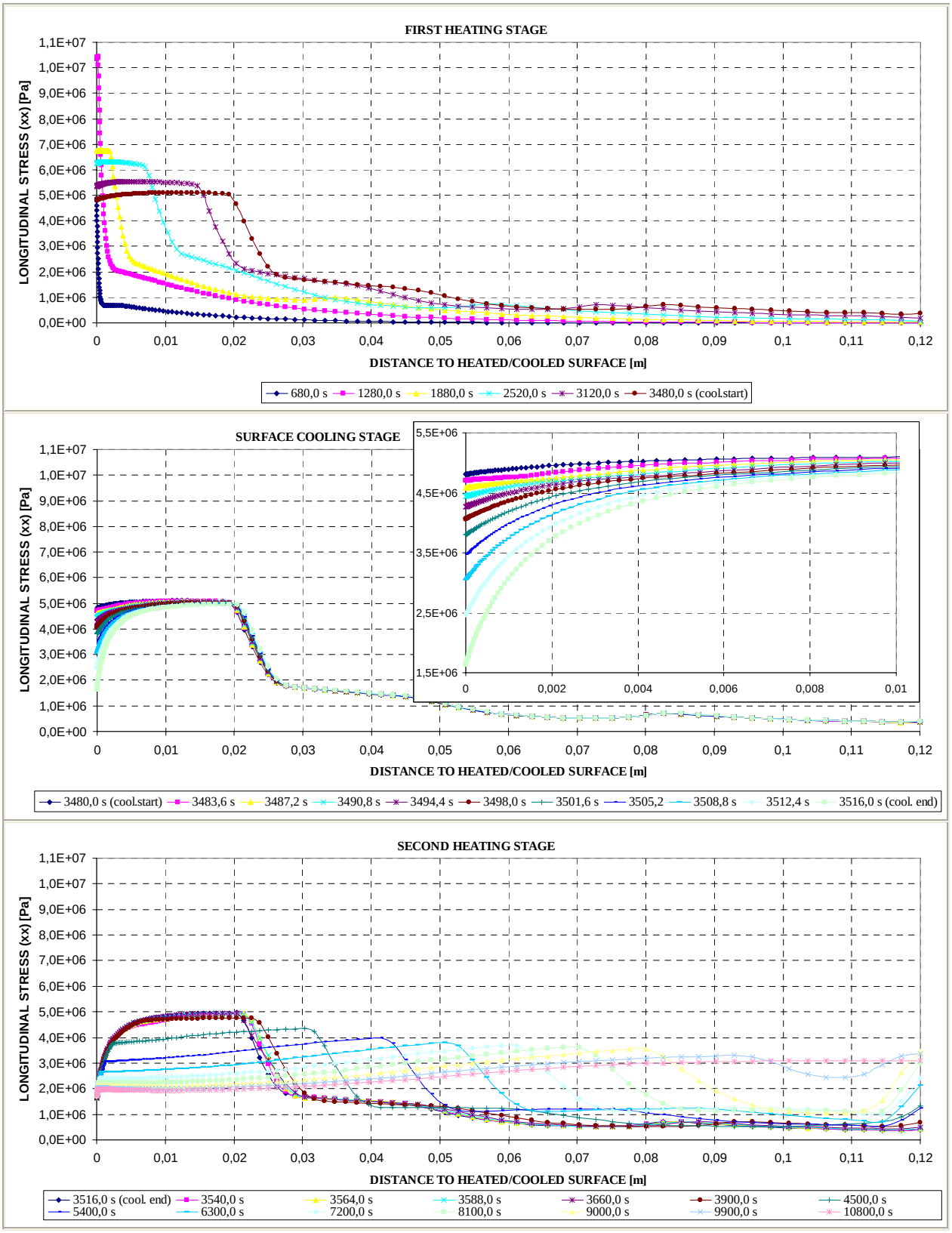

Figure 6-128. *Longitudinal stress (xx) [Pa] at several distances from the heated/cooled surface during each stage of the Surface heating and cooling processes*

As it occurred during the first heating, the maximum value of the gas pressure (significantly lower now than in the first heating despite the temperatures reached are much higher) moves progressively away from the surface up to a distance of 9 centimetres from the heated surface (see figures 6-125 and 6-129 e)) and then softening the gas pressure gradients (but without reaching a uniform gas pressure value equal to atmospheric pressure at the whole structural element).

Meanwhile, the front separating dry and moist material also moves inwards being progressively less sharp (see figures 6-126 and 6-129 h)) and achieving a relative humidity of about the 80% at a range of a quarter of the depth. At the end of the cooling process both the relative humidity and the saturation degree are almost null (see figure 6-129 g)), since half the layers next to the structural element surface have been completely 'boiled' (as it is colloquially said in the trade jargon) due to the high temperatures profile (with a maximum temperature of 982,75 K and more than the 50 per cent of the structural element above the critical point of water at the end of the second heating stage – 10.800 seconds –). However, the second half of the thickness of the structural element (that farther from the heated surface) remains with non-null relative humidity (of about the 10 per cent) at the end of the second heating stage.

Tensile longitudinal (xx) stresses tend to decrease next to the surface – where the higher levels of damage are found – while they raise up progressively at the farther zones (see figures 6-128 and 6-129 k)). At the end of the overall three hours process the most longitudinally tensioned zones are those farthest from the surface. The Elastic Strain Energy accumulated next to the surface increases at the beginning of the heating stage and later – as damage increases – it decreases (slightly because the increase of mechanical damage at the layers next to the surface is low during the second heating stage).

6.5.2.5.4.3 Collection of the Main Results of this Case for each Stage of the Cooling Process

Next it is shown a collection of the main results cited in the last subparagraph, as well as a description of each of the stages that compose the heating and cooling processes analyzed herein. Highlighted in red are the maximum values achieved by each parameter.

Table 6-90. *Description of the Cooling Process Stages and Collection of the Main Results related to Spalling Index and velocity*

Stage description	**Absolute Time Start [s]**	**Absolute Time End [s]**	**$IS4_{max}$** [-]	**X_{IS4max}** [cm]	**t_{IS4max}** [s]	**v_{max}** [m/s]	**X_{vmax}** [cm]	**t_{vmax}** [s]	**v_{max}*** [m/s]	**X_{vmax*}** [cm]	**t_{vmax*}** [s]
First Heating	0	3.360+120	0,1004	1,035	3.390	5,453	1,644	3.480	5,453	1,644	3.480
Surface cooling	3.480	3.516	0,0982	1,099	3.480	5,453	1,644	3.480	5,453	1,644	3.480
Second Heating up to 10.800s	3.516	10.800	0,0760	1,932	4.200	6,631	3,172	10.800	6,631	3,172	10.800
Absolute Maximum	0	10.800	0,1004	1,035	3.390	6,631	3,172	10.800	6,631	3,172	10.800

Remark [†]***:*** *These results are included for the Comparative Analysis developed on Paragraph 6.5.3*

Stage description	**Absolute Time Start [s]**	**Absolute Time End [s]**	**d_{max}** [-]	**X_{dmax}** [cm]	**t_{dmax}** [s]	**T_{max}** [K]	**X_{Tmax}** [cm]	**t_{Tmax}** [s]	**p^g_{max}** [MPa]	**X_{pgmax}** [cm]	**t_{pgmax}** [s]
First Heating	0	3.360+120	0,5401	1,932	3.480	656,65	0,000	3.480	0,8256	1,555	2.760
Surface cooling	3.480	3.516	0,8475	0,000	3.516	656,65	0,000	3.480	0,7757	2,623	3.480
Second Heating up to 10.800s	3.516	10.800	0,8475	0,000	3.516	982,75	0,000	10.800	0,7412	2,753	3.516
Absolute Maximum	0	10.800	0,8475	0,000	3.516	982,75	0,000	10.800	0,8256	1,555	2.760

Table 6-91. *Description of the Cooling Process Stages and Collection of the Main Results related to mechanical damage, Temperature and Gas Pressure*

a) Spalling Index IS4 [-] *b) Mechanical damage d [-]*

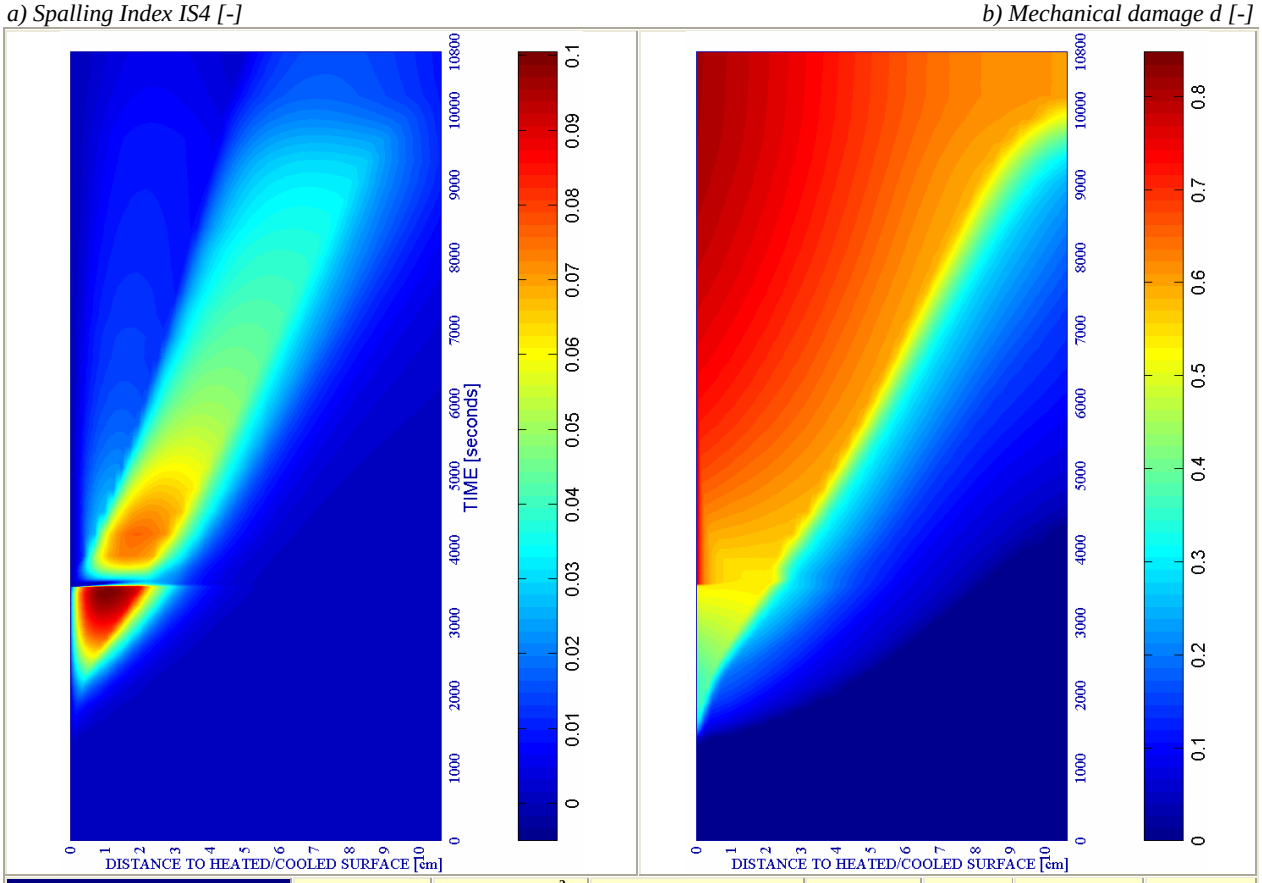

SURFACE COOL+HEAT		PC1 - RH [%]			PC2 - K_0 [m^2]			PC4 - Heating curve			PC5 – Mat.		Cooling length[s]	Start of cooling [s]	End of cooling [s]
#	Combination	40	50	60	10^{-19}	10^{-18}	10^{-17}	PAR1	PAR2	PAR4	C60	C90			
14	TH12K018RH50PAR2C60		X			X			X		X		36	3.360+120	3.516

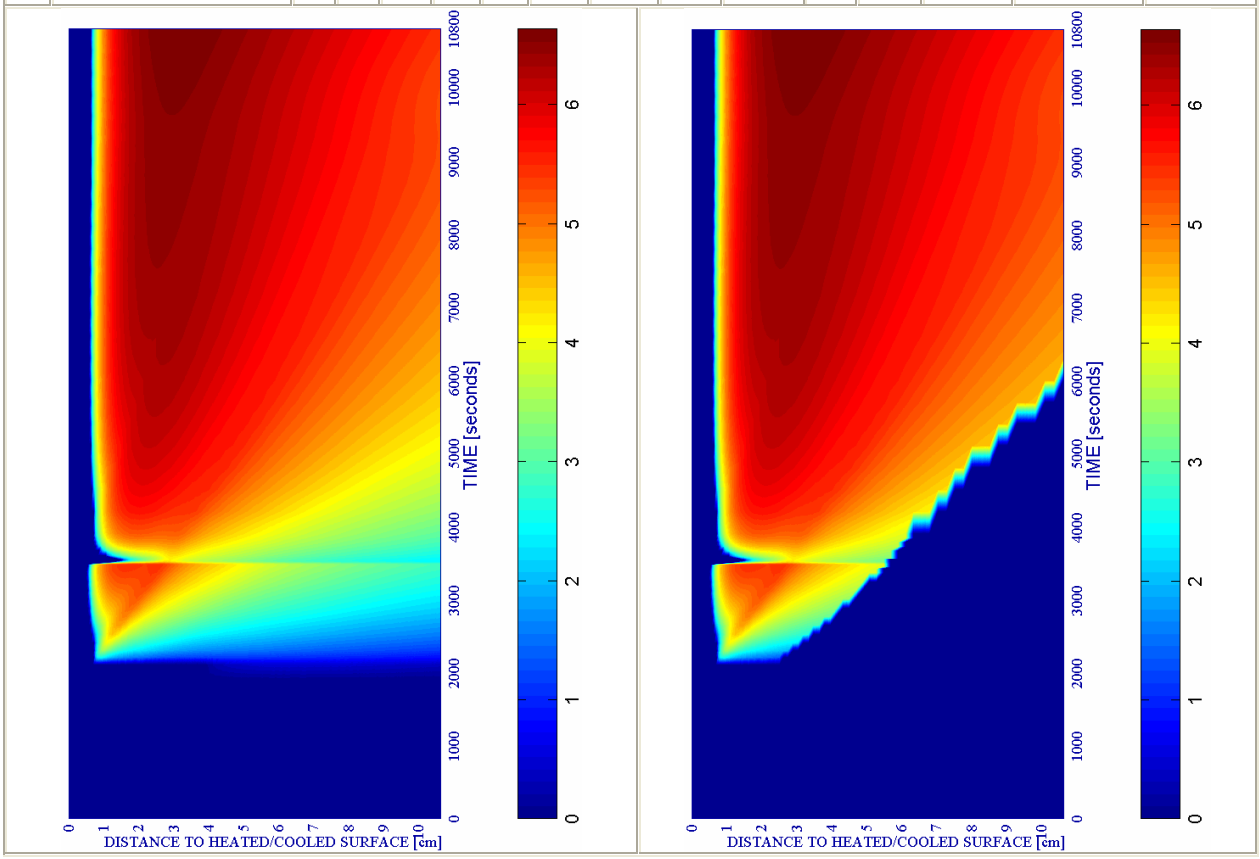

c) Velocity of spalled pieces v [m/s] ***Figure 6-129.*** *d) Velocity [m/s] where d ≥ 0,10*

e) Gas pressure $p^g \cdot 10^{-5}$ [Pa]

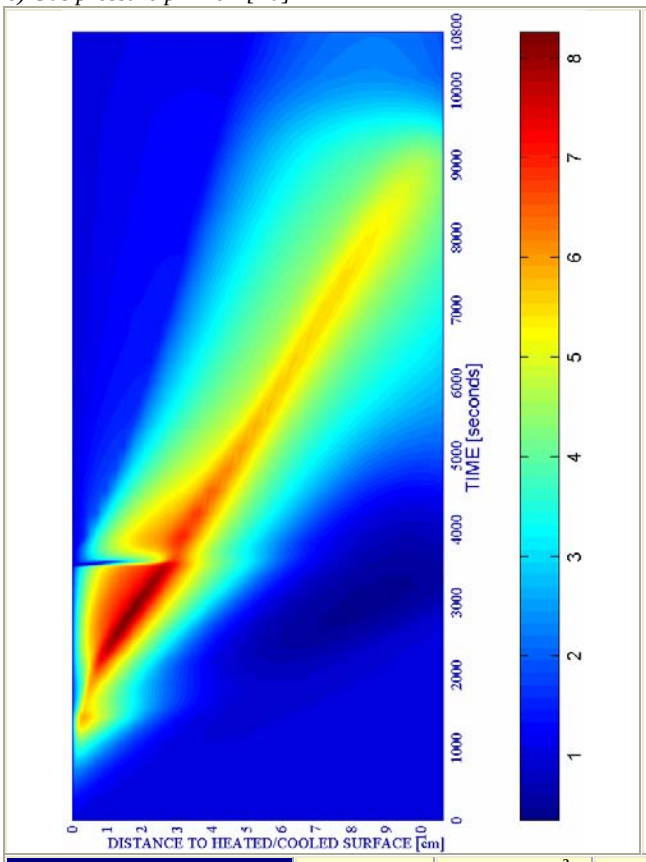

f) Vapour pressure $p^v \cdot 10^{-5}$ [Pa]

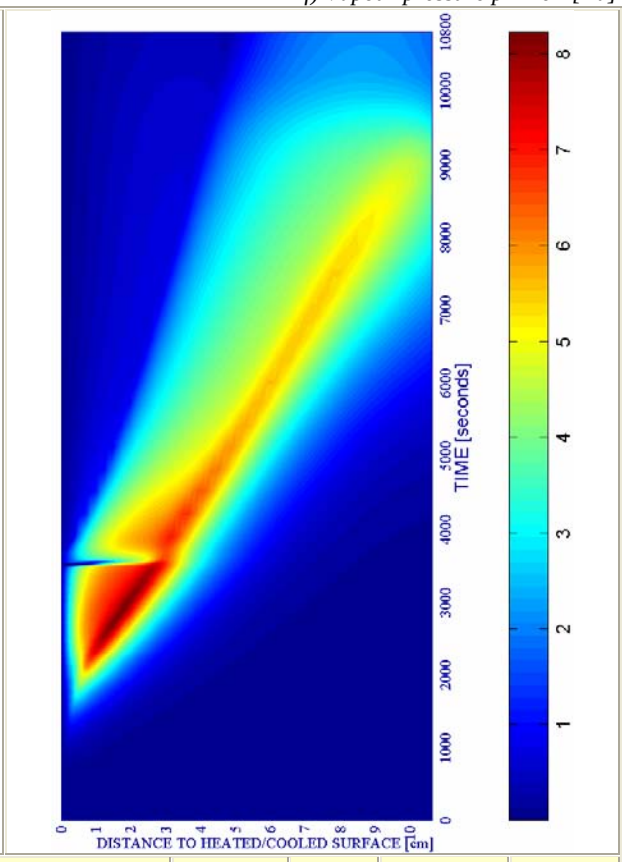

SURFACE COOL+HEAT		PC1 - RH [%]			PC2 - K_0 [m^2]			PC4 - Heating curve			PC5 – Mat.		Cooling length[s]	Start of cooling [s]	End of cooling [s]
#	Combination	40	50	60	10^{-19}	10^{-18}	10^{-17}	PAR1	PAR2	PAR4	C60	C90			
14	TH12K018RH50PAR2C60		X			X			X		X		36	3.360+120	3.516

g) Saturation Degree S [-]

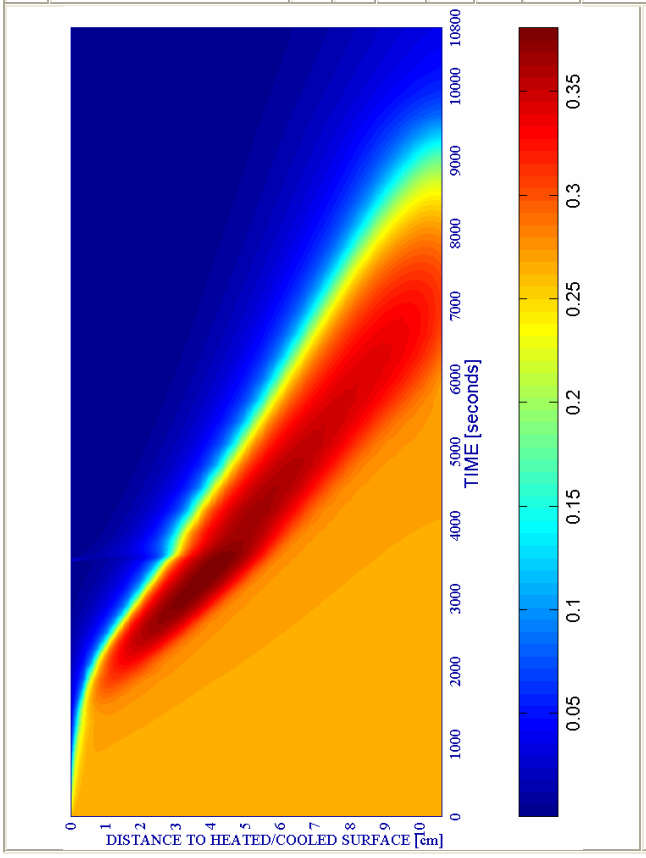

Figure 6-129. (continued)

h) Relative Humidity RH [-]

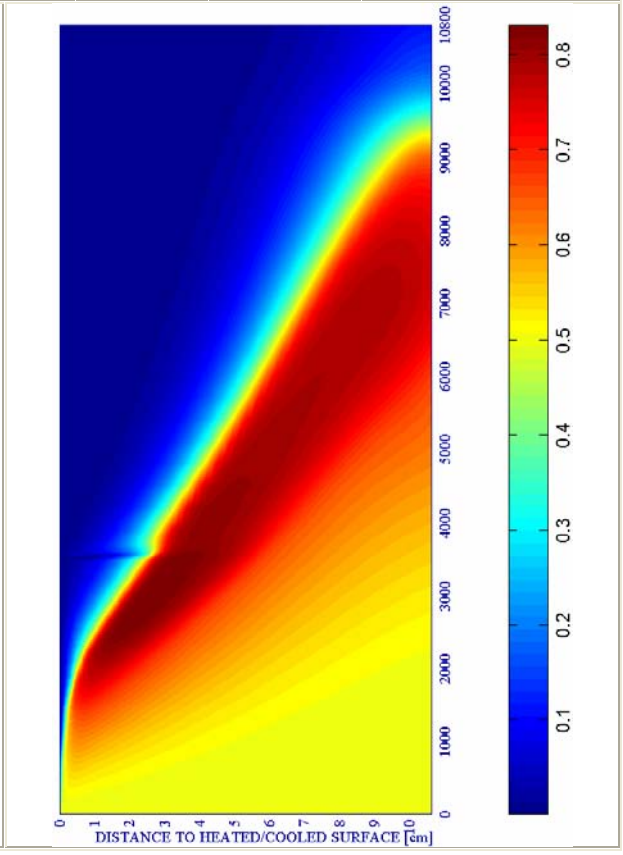

i) Temperature [K] *j) Elastic Energy U · **10^{-4}** [J/m^3]*

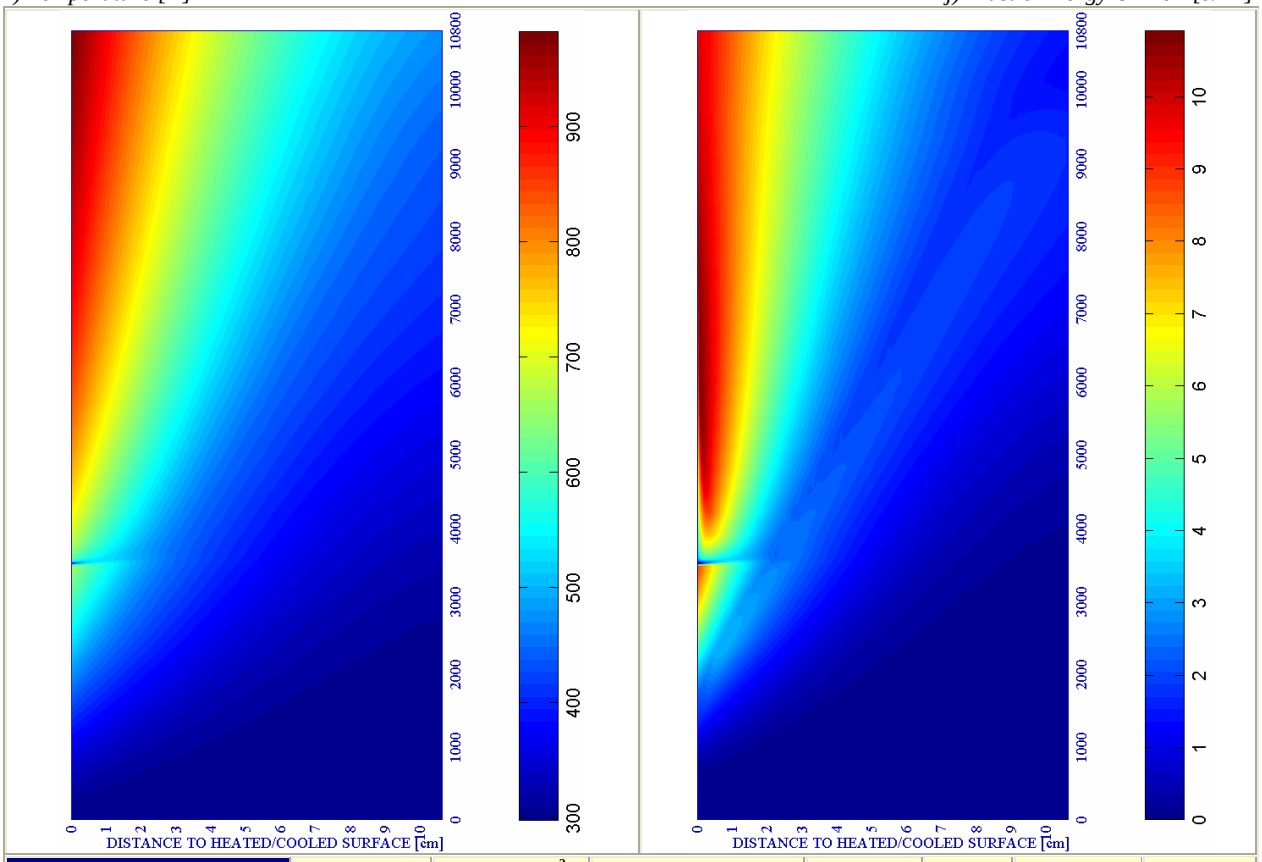

SURFACE COOL+HEAT		PC1 - RH [%]			PC2 - K_0 [m^2]			PC4 - Heating curve			PC5 – Mat.		Cooling length[s]	Start of cooling [s]	End of cooling [s]
#	Combination	40	50	60	10^{-19}	10^{-18}	10^{-17}	PAR1	PAR2	PAR4	C60	C90			
14	TH12K018RH50PAR2C60		X			X			X		X		36	3.360+120	3.516

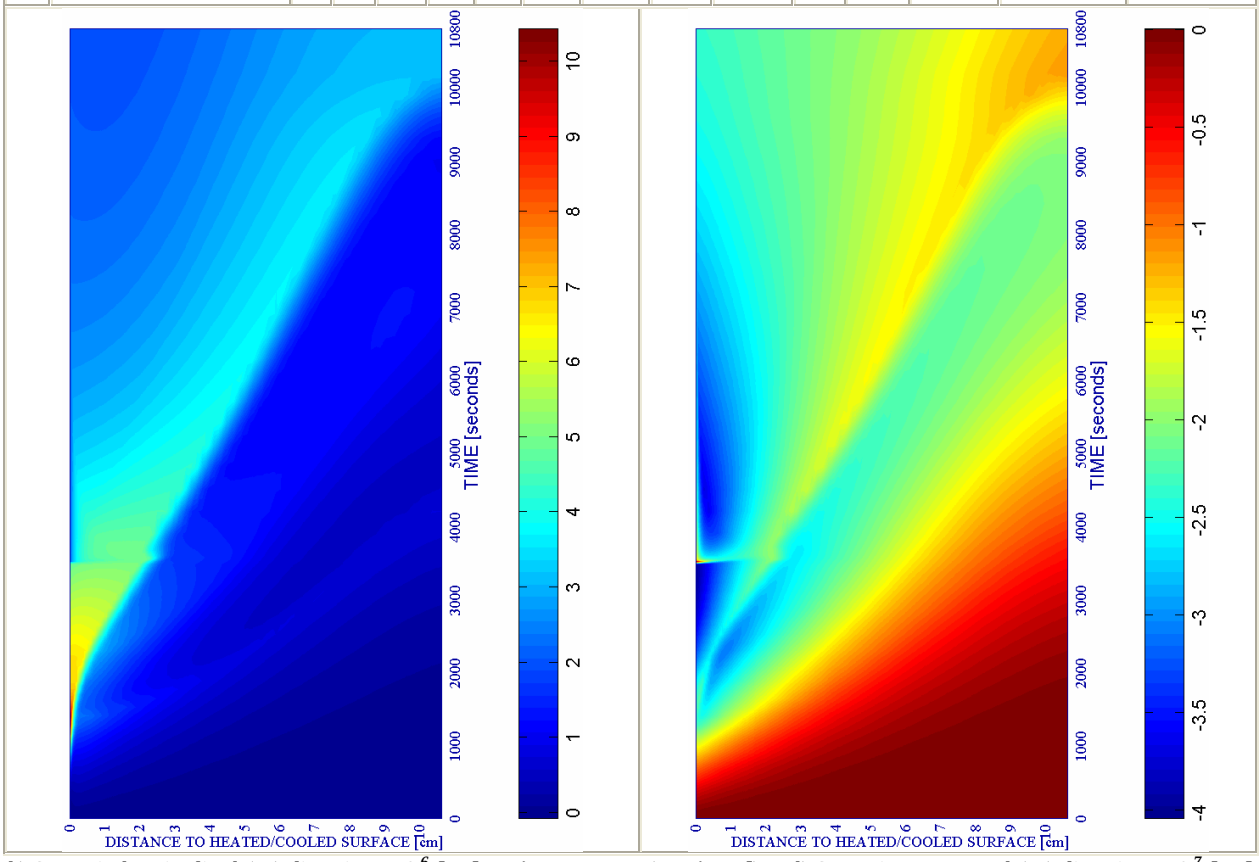

*k) Stress in longitudinal (xx) direction · **10^{-6}** [Pa]* ***Figure 6-129. (continued)*** *l) Stress in transversal (yy) direction · **10^{-7}** [Pa]*

6.5.2.5.5 Surface Cooling followed by an imposed Constant Surface Temperature

After the Surface Cooling stage, defined by the time range from 3.480 to 3.516 seconds, despite having finished the cooling boundary conditions, keeping Surface Temperature Constant, the Total Damage D keeps increasing especially in the 2 centimetres layers next to the surface. Hence, between 3.516 and 3.839 seconds the Total Damage D increase at the following values (see figure 6-132):

TIME [s] \ DISTANCE TO SURFACE [cm]	0,5 centimetres	1,0 centimetres	2,0 centimetres
3.516 seconds	0,5892	0,5660	0,5963
3.839 seconds	0,8461	0,7401	0,6339

Table 6-92. *Total Damage D [-] values at different depths*

The values shown on last table denote an increase of Total Damage, as Surface Temperature is kept constant, from about a 44 per cent at 0,5 centimetres from surface down to an increase of about a 6 per cent at 2,0 centimetres from surface., reaching a quite high level and approaching to an almost complete destruction of the superficial layer. As it is observed on figure 6-134 b), this increase is due to increases both in mechanical and thermo-chemical damages.

The significant decrease in the gas pressure values observed during cooling process continues during this constant surface temperature (see figure 6-134 e)), showing its maximum values progressively farther from the surface, while the environment relative humidity infiltration is now observed in the 5 millimetres contiguous to the surface, as it is shown on figure 6-130, starting precisely when surface constant temperature period starts:

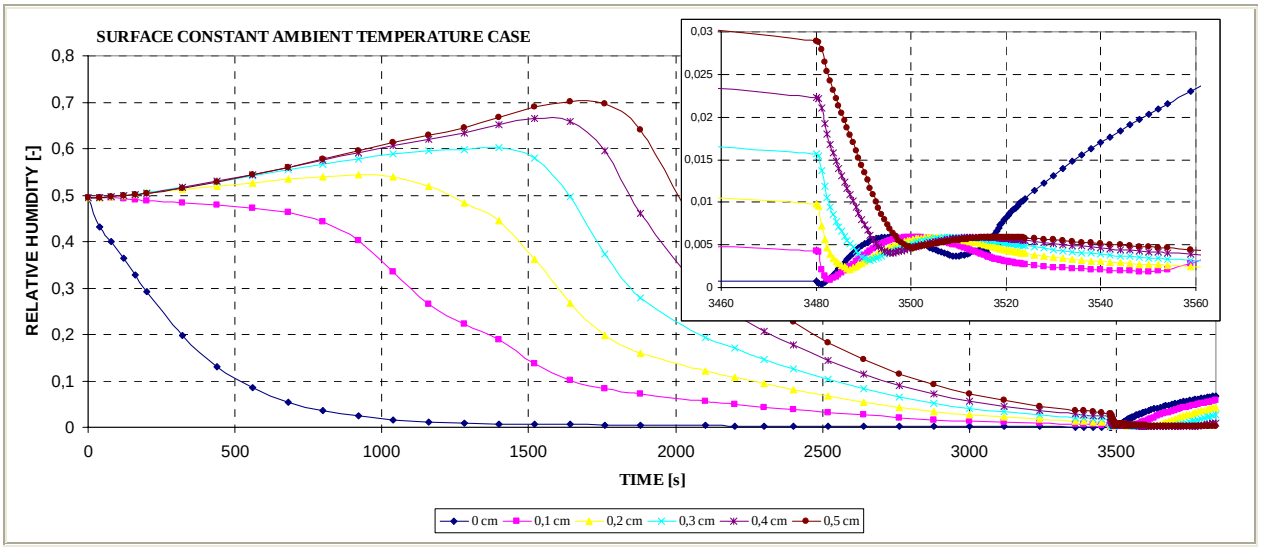

Figure 6-130. *Relative Humidity RH [-] evolution in the 0,5 cm layer contiguous to the heated/cooled surface during each stage of the Surface cooling processes*

Related to the rest of parameters with influence on the Spalling Index I_{s4} values, it is remarkable to observe that as it was expectable tensile longitudinal stresses (xx) decrease significantly in the first centimetre during the constant surface temperature process (see figures 6-133 and 6-134 k)) from an initial tensile value at the surface of 1,64 MPa down to a final compressive value of -1,58 MPa at the end of constant surface temperature process.

Hence, as a difference with the case where the Surface was heated again after cooling, high compressive longitudinal stresses arise at the first centimetre contiguous to the surface. Beyond the four centimetres close to the surface, no significant variations of longitudinal stresses have been noticed. This increase in material (compressive) stress state leads to the Elastic Strain Energy accumulation within the 5 millimetres layer close to surface (see figure 6-131 and 6-134 j)).

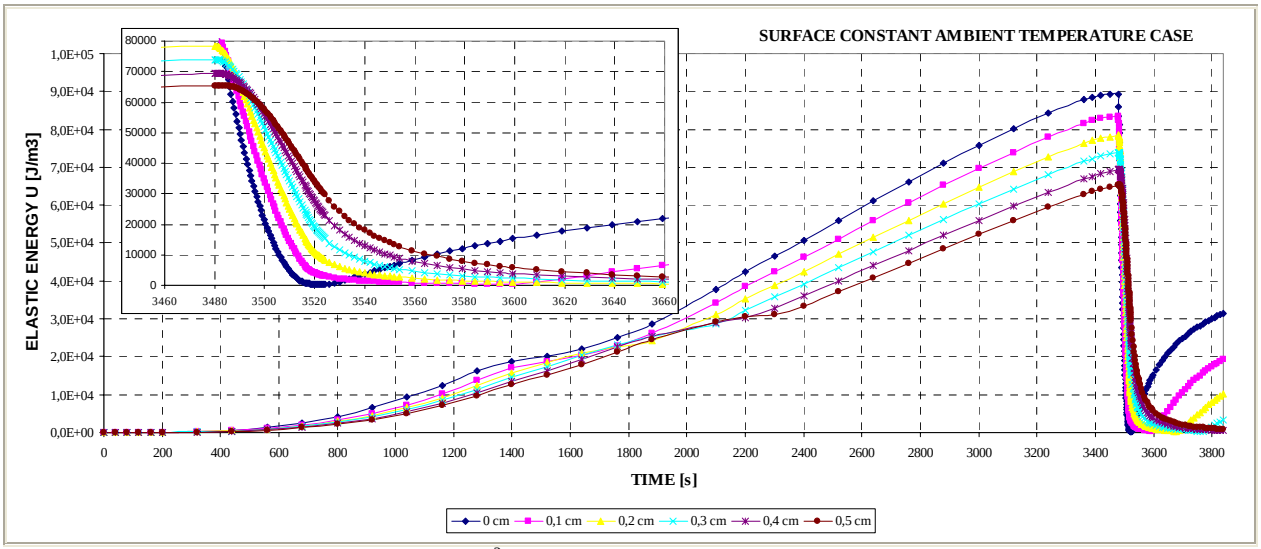

Figure 6-131. *Elastic Strain Energy U [J/m^3] evolution in the 0,5 cm layer contiguous to the heated/cooled surface during each stage of the Surface cooling processes*

Due to all of these trends, Spalling Index I_{s4} values decrease during the whole surface constant ambient temperature process (see Table 6-93 and figure 6-134 a)), reducing therefore the thermal spalling risk. However, thermal spalling is energetically viable until the end of the time interval considered (despite compressive stresses appear close to the surface, tensile stresses keep present at the inner layers, where both the constrained energy and the gas pressure are still high enough to make thermal spalling viable).

Next it is shown a collection of the main results cited in the last subparagraph, as well as a description of each of the stages that compose the heating and cooling processes analyzed herein. Highlighted in red are the maximum values achieved by each parameter.

Table 6-93. *Description of the Cooling Process Stages and Collection of the Main Results related to Spalling Index and velocity*

Stage description	Absolute Time Start [s]	Absolute Time End [s]	$IS4_{max}$ [-]	X_{IS4max} [cm]	t_{IS4max} [s]	v_{max} [m/s]	X_{vmax} [cm]	t_{vmax} [s]	v_{max}* [m/s]	X_{vmax*} [cm]	t_{vmax*} [s]
First Heating	0	3.360+120	0,1004	1,035	3.390	5,453	1,644	3.480	5,453	1,644	3.480
Surface cooling	3.480	3.516	0,0982	1,099	3.480	5,453	1,644	3.480	5,453	1,644	3.480
Surface Constant T	3.516	3.839	0,0374	0,084	3.516	4,306	2,753	3.516	4,306	2,753	3.516
Absolute Maximum	0	3.839	0,1004	1,035	3.390	5,453	1,644	3.480	5,453	1,644	3.480

Remark † ***:*** *These results are included for the Comparative Analysis developed on Paragraph 6.5.3*

Stage description	Absolute Time Start [s]	Absolute Time End [s]	d_{max} [-]	X_{dmax} [cm]	t_{dmax} [s]	T_{max} [K]	X_{Tmax} [cm]	t_{Tmax} [s]	p^g_{max} [MPa]	X_{pgmax} [cm]	t_{pgmax} [s]
First Heating	0	3.360+120	0,5401	1,932	3.480	656,65	0,000	3.480	0,8256	1,555	2.760
Surface cooling	3.480	3.516	0,8475	0,000	3.516	656,65	0,000	3.480	0,7757	2,623	3.480
Surface Constant T	3.516	3.839	0,8923	0,010	3.528	559,06	0,808	3.516	0,7412	2,753	3.516
Absolute Maximum	0	3.839	0,8923	0,010	3.528	656,65	0,000	3.480	0,8256	1,555	2.760

Table 6-94. *Description of the Cooling Process Stages and Collection of the Main Results related to mechanical damage, Temperature and Gas Pressure*

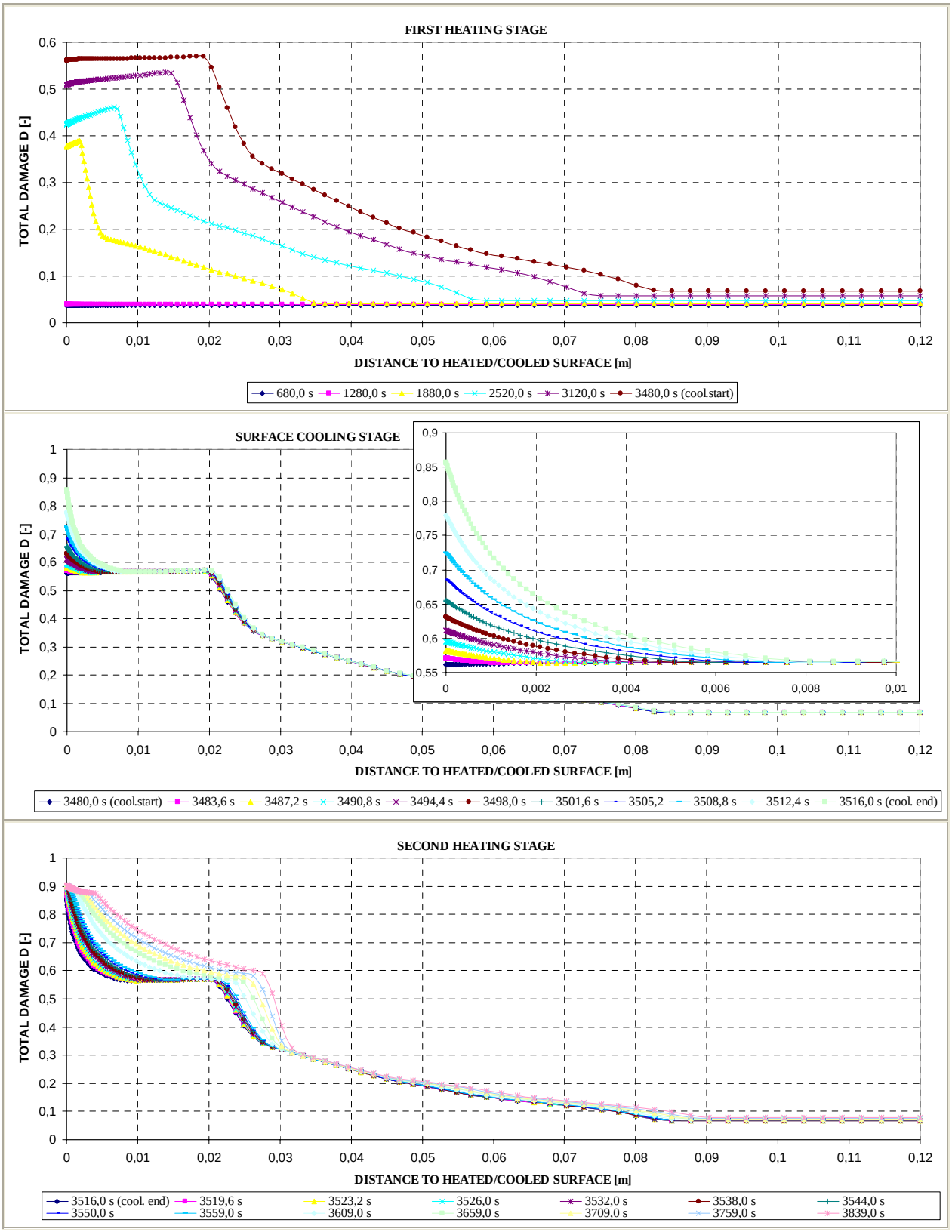

Figure 6-132. *Total Damage D [-] at several distances from the heated/cooled surface during each stage of the Surface cooling processes*

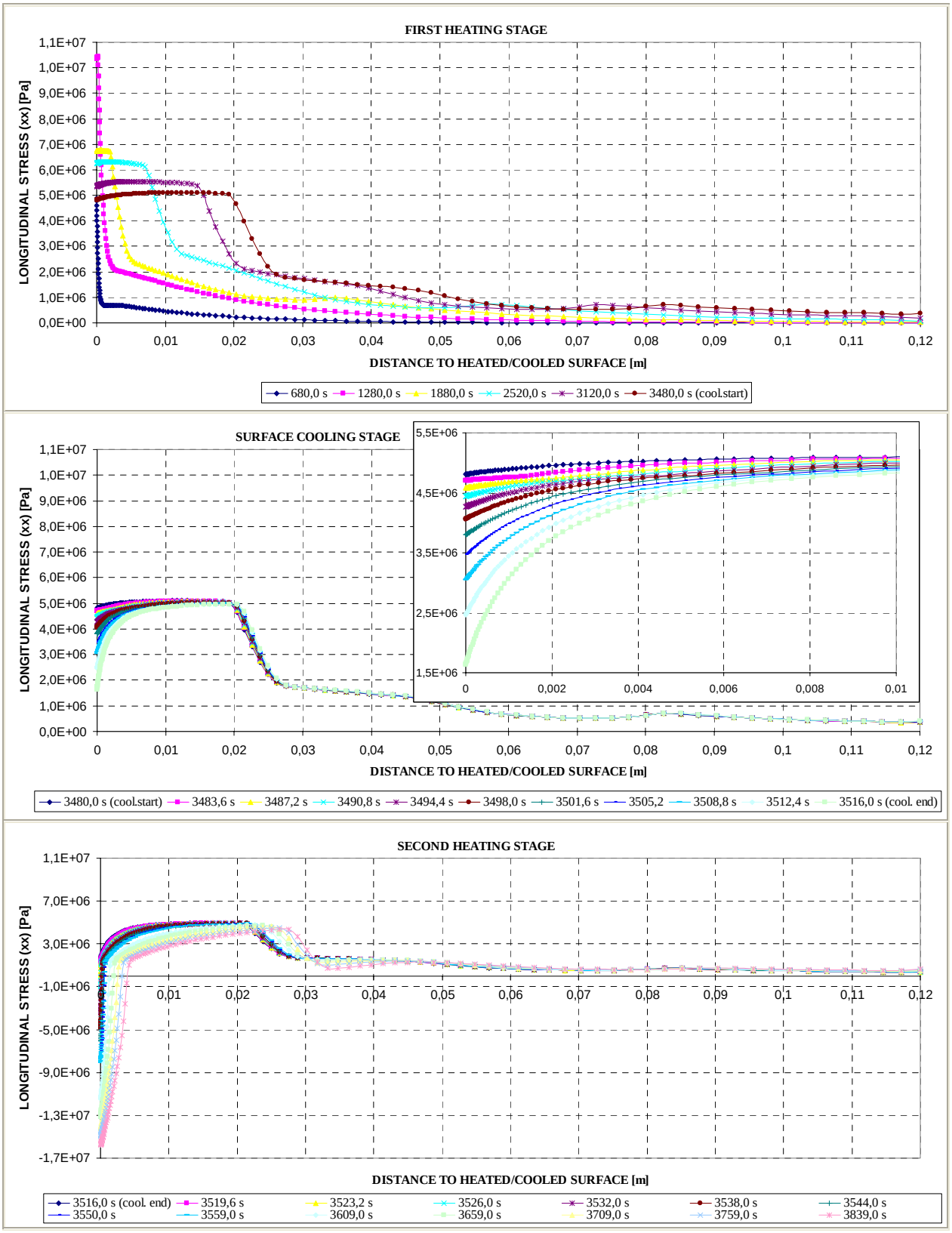

Figure 6-133. *Longitudinal stress (xx) [Pa] at several distances from the heated/cooled surface during each stage of the Surface cooling processes*

Next it is shown a collection of twelve Time-Space graphics representing the evolution of all of the parameters cited in the last subparagraph and for all of the stages that compose the heating and cooling processes analyzed herein.

a) Spalling Index IS4 [-] *b) Mechanical damage d [-]*

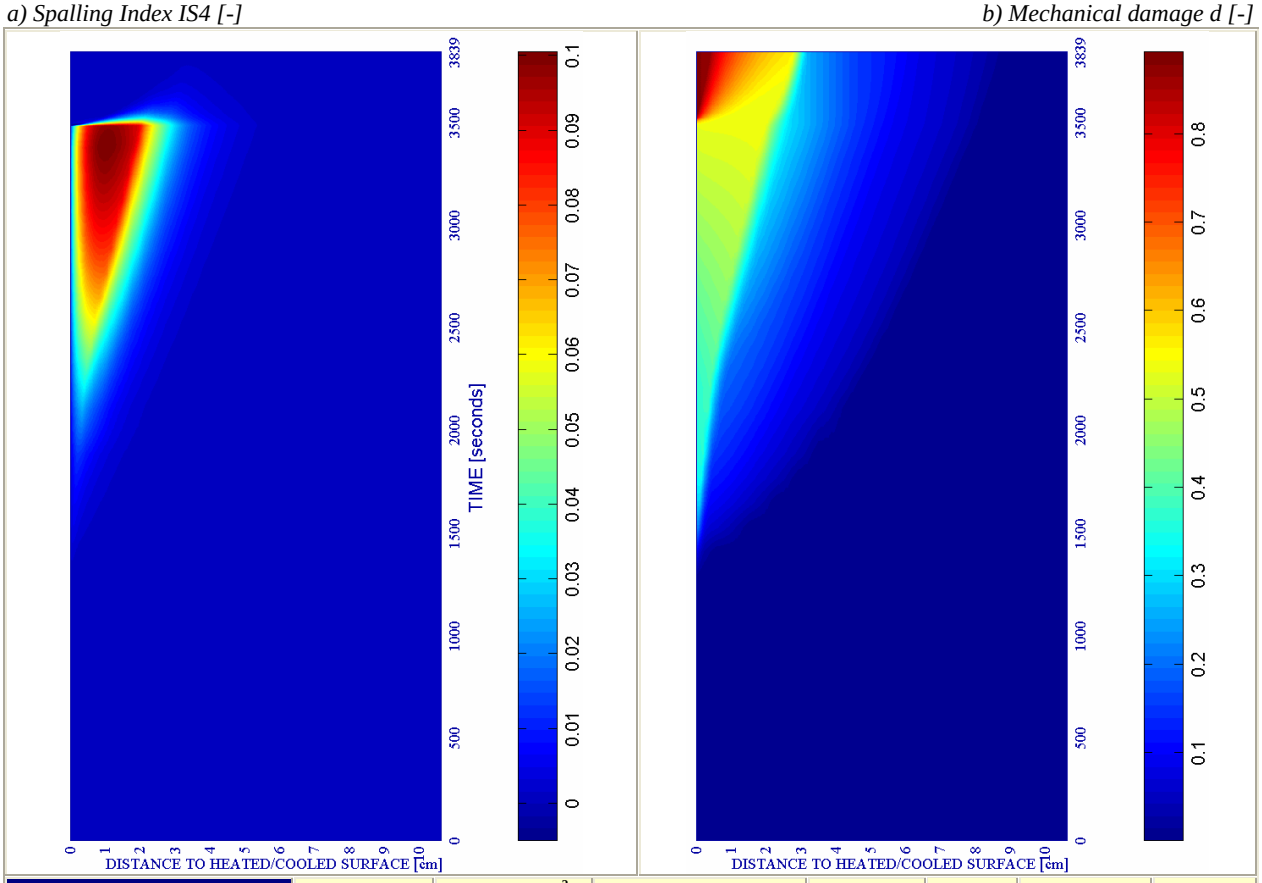

SURFACE COOL+KEEP		PC1 - RH [%]			PC2 - K_0 [m^2]			PC4 - Heating curve			PC5 – Mat.		Cooling length[s]	Start of cooling [s]	End of cooling [s]
#	Combination	40	50	60	10^{-19}	10^{-18}	10^{-17}	PAR1	PAR2	PAR4	C60	C90			
14	TH12K018RH50PAR2C60		X			X			X		X		359	3.360+120	3.839

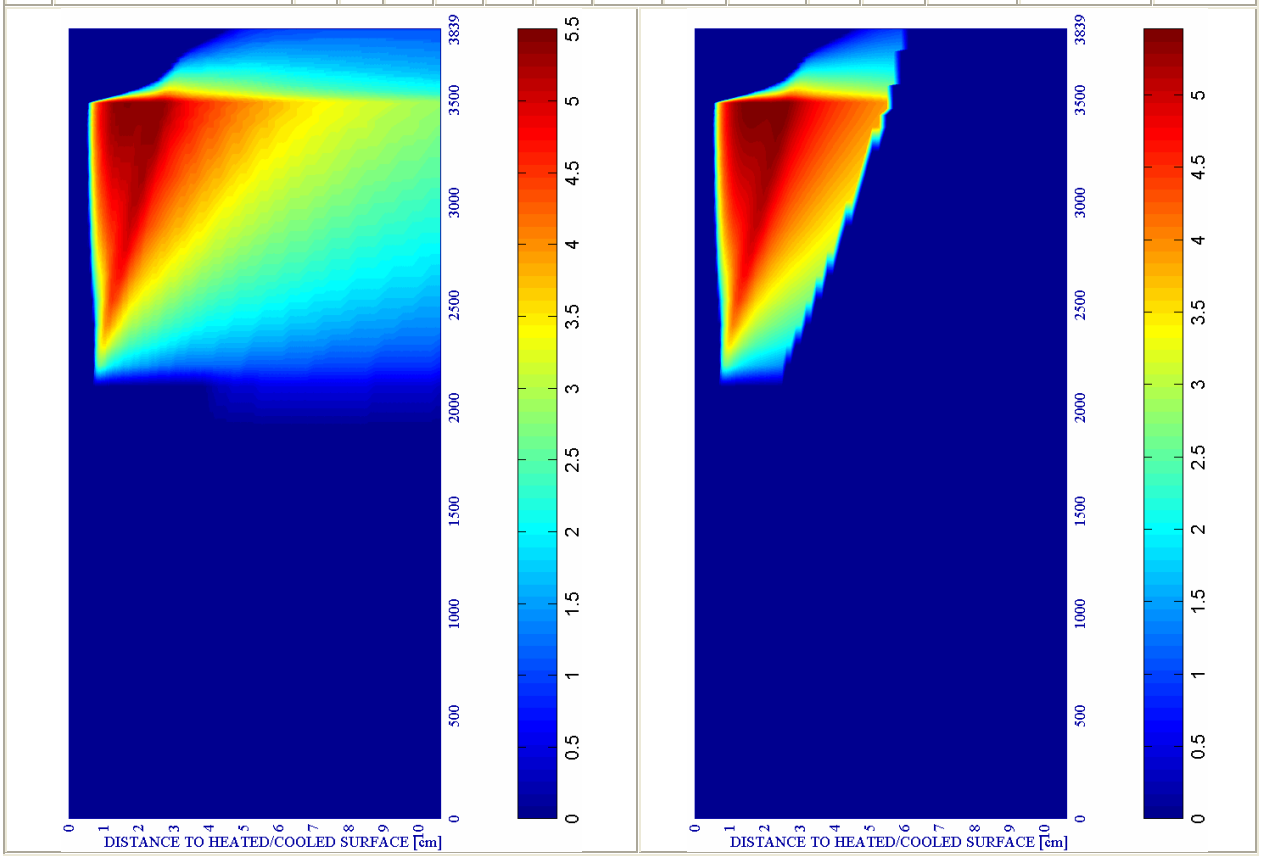

c) Velocity of spalled pieces v [m/s] ***Figure 6-134.*** *d) Velocity [m/s] where d ≥ 0,10*

e) Gas pressure $p^g \cdot 10^{-5}$ [Pa]

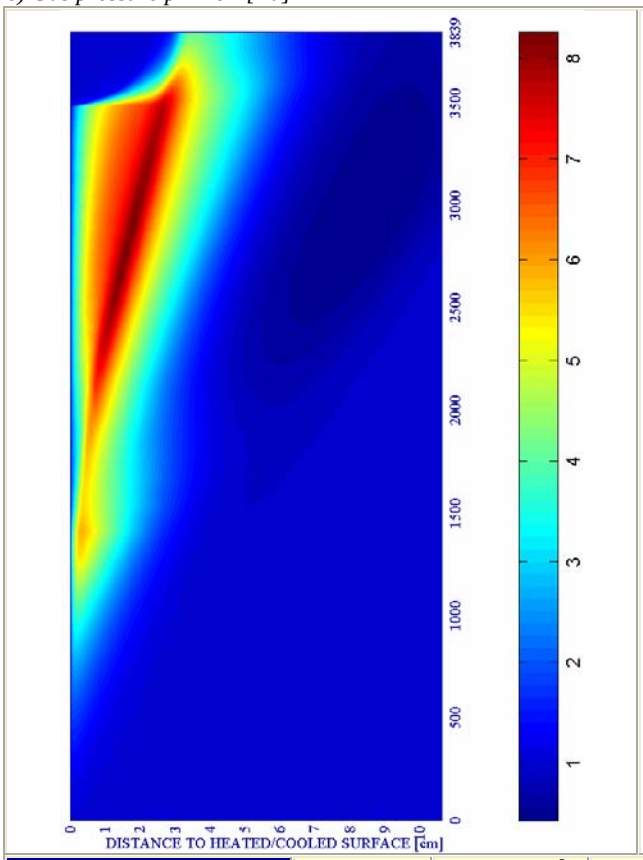

f) Vapour pressure $p^v \cdot 10^{-5}$ [Pa]

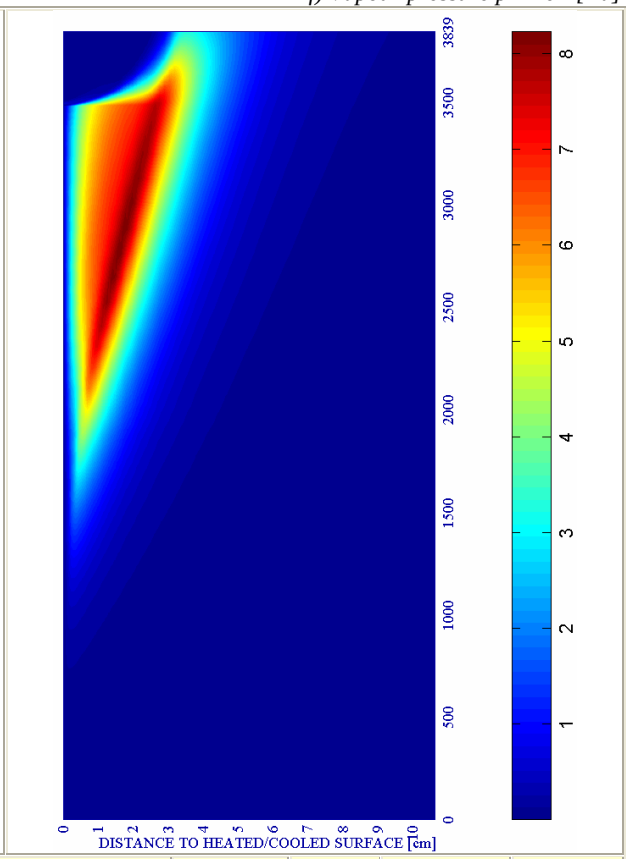

SURFACE COOL+KEEP		PC1 - RH [%]			PC2 - K_0 [m^2]			PC4 - Heating curve			PC5 – Mat.		Cooling length[s]	Start of cooling [s]	End of cooling [s]
#	Combination	40	50	60	10^{-19}	10^{-18}	10^{-17}	PAR1	PAR2	PAR4	C60	C90			
14	TH12K018RH50PAR2C60		X			X			X		X		359	3.360+120	3.839

g) Saturation Degree S [-]

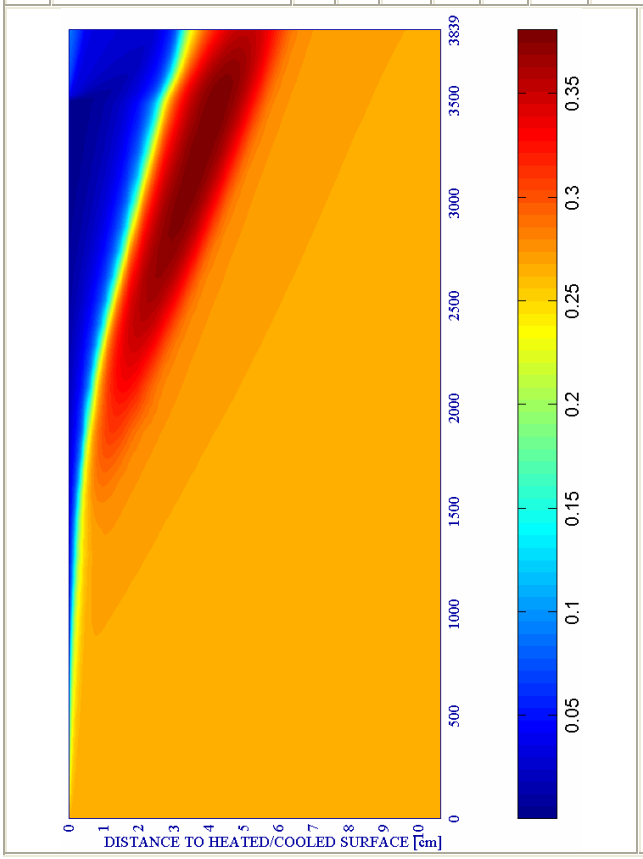

Figure 6-134. (continued)

h) Relative Humidity RH [-]

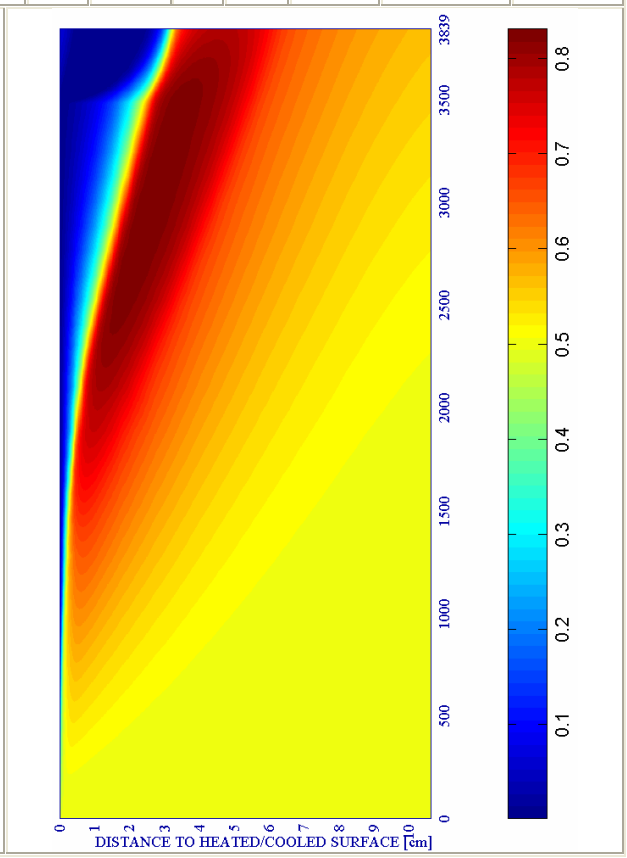

i) Temperature [K] *j) Elastic Energy U · **10^{-4}** [J/m^3]*

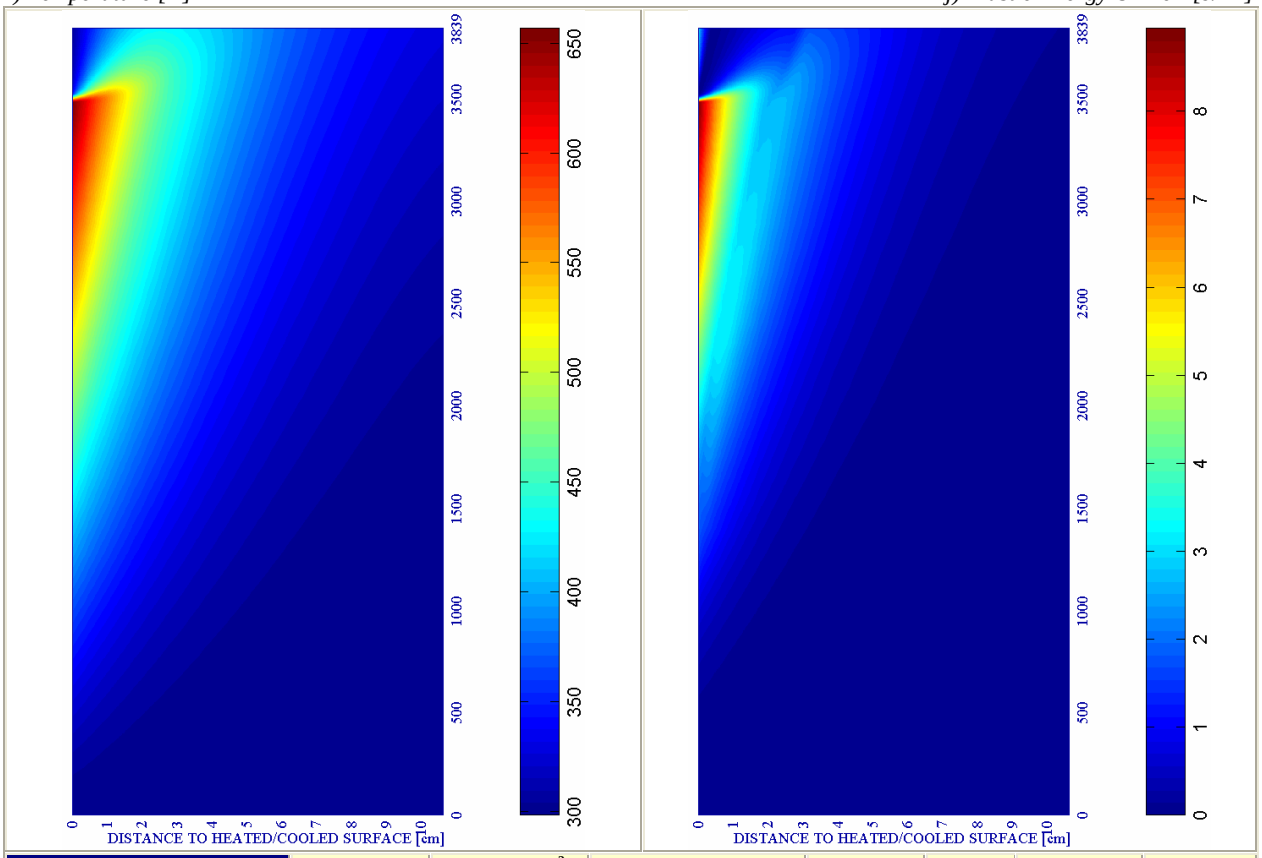

SURFACE COOL+KEEP		PC1 - RH [%]			PC2 - K_0 [m^2]			PC4 - Heating curve			PC5 – Mat.		Cooling length[s]	Start of cooling [s]	End of cooling [s]
#	Combination	40	50	60	10^{-19}	10^{-18}	10^{-17}	PAR1	PAR2	PAR4	C60	C90			
14	TH12K018RH50PAR2C60		X			X			X		X		359	3.360+120	3.839

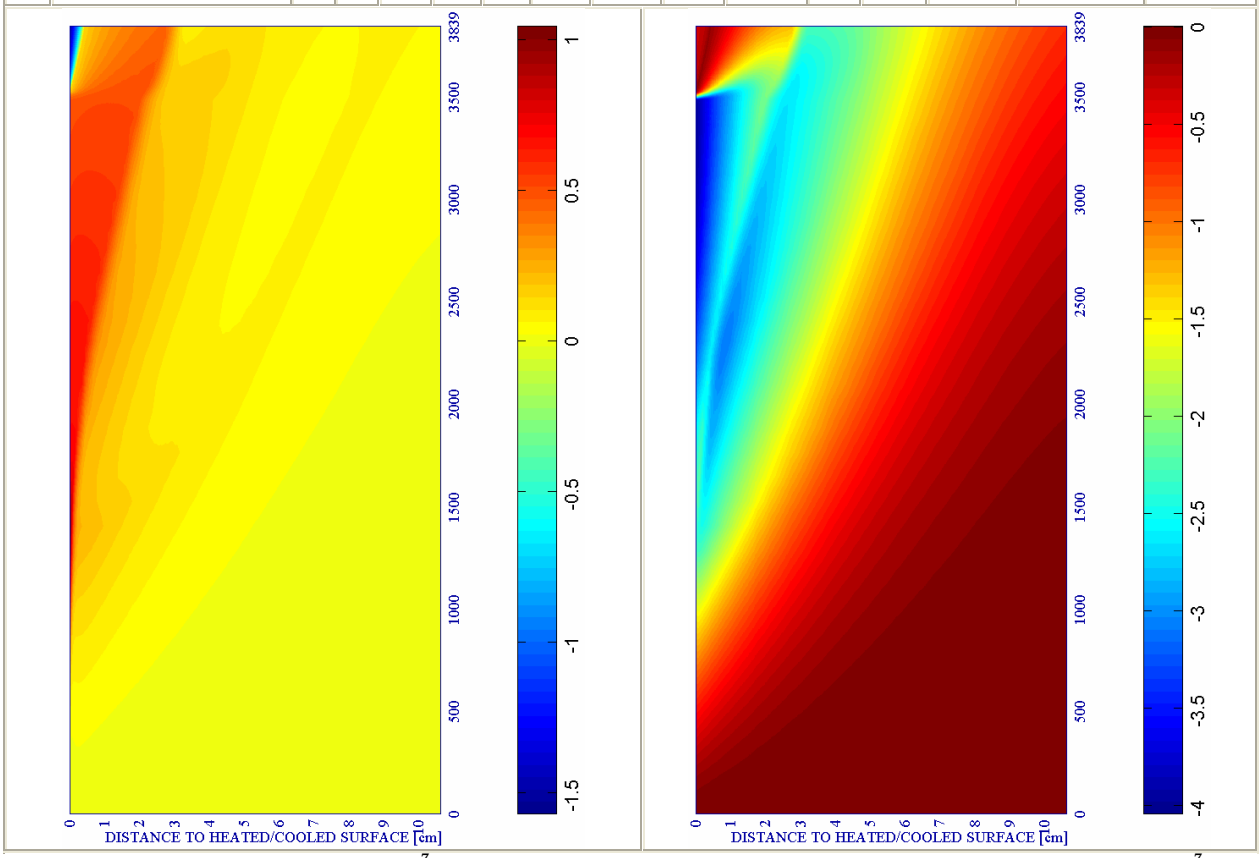

*k) Stress in longitudinal (xx) direction · **10^{-7}** [Pa]* ***Figure 6-134. (continued)*** *l) Stress in transversal (yy) direction · **10^{-7}** [Pa]*

6.5.2.5.6 Surface Cooling in Three Periods

The especial issue of the analysis of the phenomena involved in this case is to discern if the hygro-thermo-chemo-mechanical processes appearing in repeated heating-cooling solicitations present cyclic tendencies or lead each of them to different final states of the structural element.

On the other hand, on paragraph 6.5.3.1.2 there is included a comparison of the final state of the structural element – after three hours from the start of the fire – for 1, 2 and 3 consecutive heating-cooling cycles.

In order to ease the understanding of the explanation exposed in this paragraph, the tables 6-95 and 6-96 show a description of each of the stages that compose the heating and cooling processes analyzed herein, as well as a collection of the main results cited in this subparagraph. Highlighted in red are the maximum values achieved by each parameter.

Table 6-95. *Description of the Cooling Process Stages and Collection of the Main Results related to Spalling Index and velocity*

Stage description	**Absolute Time Start [s]**	**Absolute Time End [s]**	$IS4_{max}$ [-]	X_{IS4max} [cm]	t_{IS4max} [s]	v_{max} [m/s]	X_{vmax} [cm]	t_{vmax} [s]	v_{max}* [m/s]	X_{vmax*} [cm]	t_{vmax*} [s]
First Heating	0	3.360+120	0,1004	1,035	3.390	5,453	1,644	3.480	5,453	1,644	3.480
First Surface cooling	3.480	3.516	0,0982	1,099	3.480	5,453	1,644	3.480	5,453	1,644	3.480
Second Heating	3.516	3.600	0,0374	2,037	3.516	4,306	2,753	3.516	4,306	2,753	3.516
Second Surface cool.	3.600	3.633	0,0355	2,037	3.601,8	4,289	3,028	3.600	4,289	3,028	3.600
Third Heating	3.633	3.717	0,0255	1,167	3.717	3,910	3,172	3.717	3,910	3,172	3.717
Third Surface cool.	3.717	3.750	0,0256	1,167	3.717	3,910	3,172	3.717	3,910	3,172	3.717
Heating up to 10.800s	3.750	10.800	0,0747	2,037	4.500	6,622	3,172	10.800	6,622	3,172	10.800
Absolute Maximum	0	10.800	0,1004	1,035	3.390	6,622	3,172	10.800	6,622	3,172	10.800

Remark [†]***:*** *These results are included for the Comparative Analysis developed on Paragraph 6.5.3*

Stage description	**Absolute Time Start [s]**	**Absolute Time End [s]**	d_{max} [-]	X_{dmax} [cm]	t_{dmax} [s]	T_{max} [K]	X_{Tmax} [cm]	t_{Tmax} [s]	p^g_{max} [MPa]	X_{pgmax} [cm]	t_{pgmax} [s]
First Heating	0	3.360+120	0,5401	1,932	3.480	656,65	0,000	3.480	0,8256	1,555	2.760
First Surface cooling	3.480	3.516	0,8475	0,000	3.516	656,65	0,000	3.480	0,7757	2,623	3.480
Second Heating	3.516	3.600	0,8475	0,000	3.516	624,88	0,000	3.600	0,7412	2,753	3.516
Second Surface cool.	3.600	3.633	0,8566	0,000	3.633	624,88	0,000	3.600	0,6561	3,028	3.600
Third Heating	3.633	3.717	0,8566	0,000	3.633	617,99	0,000	3.717	0,6477	3,028	3.633
Third Surface cool.	3.717	3.750	0,8606	0,000	3.750	617,99	0,000	3.717	0,5968	3,172	3.717
Heating up to 10.800s	3.750	10.800	0,8606	0,000	3.750	982,48	0,000	10.800	0,6748	3,321	4.200
Absolute Maximum	0	10.800	0,8606	0,000	3.750	982,48	0,000	10.800	0,8256	1,555	2.760

Table 6-96. *Description of the Cooling Process Stages and Collection of the Main Results related to mechanical damage, Temperature and Gas Pressure*

As it can be observed on figures 6-137 and 6-139 b) during the Second Heating stage Total Damage remains mostly unchanged at all of the depths of the structural element. This fact is due to the shortness of this heating period what leads to maximum temperatures not so high as those corresponding to the start instant of the first cooling stage and to a longitudinal stress state with just slight variations (see figure 6-139 and 6-140 k)) during this period.

On the contrary, gas pressure values experiment significant increases especially in the layers close to the surface during these heating stage (see figure 6-138 and 6-140 e)).

Within the subsequent 'Second surface cooling' stage, again the differences in Total Damage and the longitudinal stress state are non significant (in figures 6-137 and 6-139 all the graphs corresponding to the period between 3.600 and 3.633 seconds are superposed).The tendency with gas pressure values is analogue to that corresponding to the first surface cooling stage, decreasing slightly its maximum and moving inwards the structural element.

The third heating and surface cooling stages show qualitatively identical phenomena.

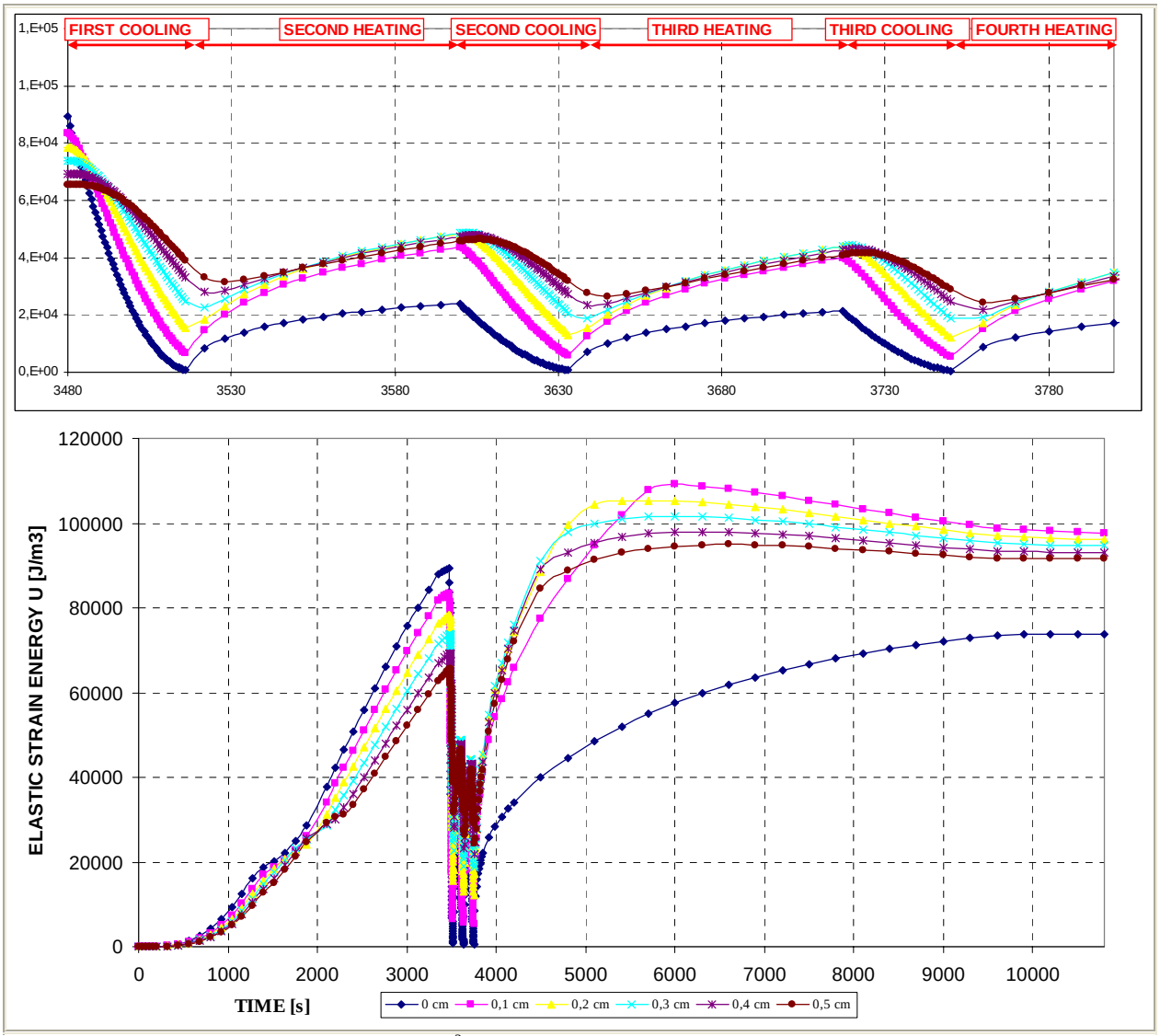

Figure 6-135. *Elastic Strain Energy U [J/m^3] at several distances from the heated/cooled surface during each stage of the Surface cooling processes*

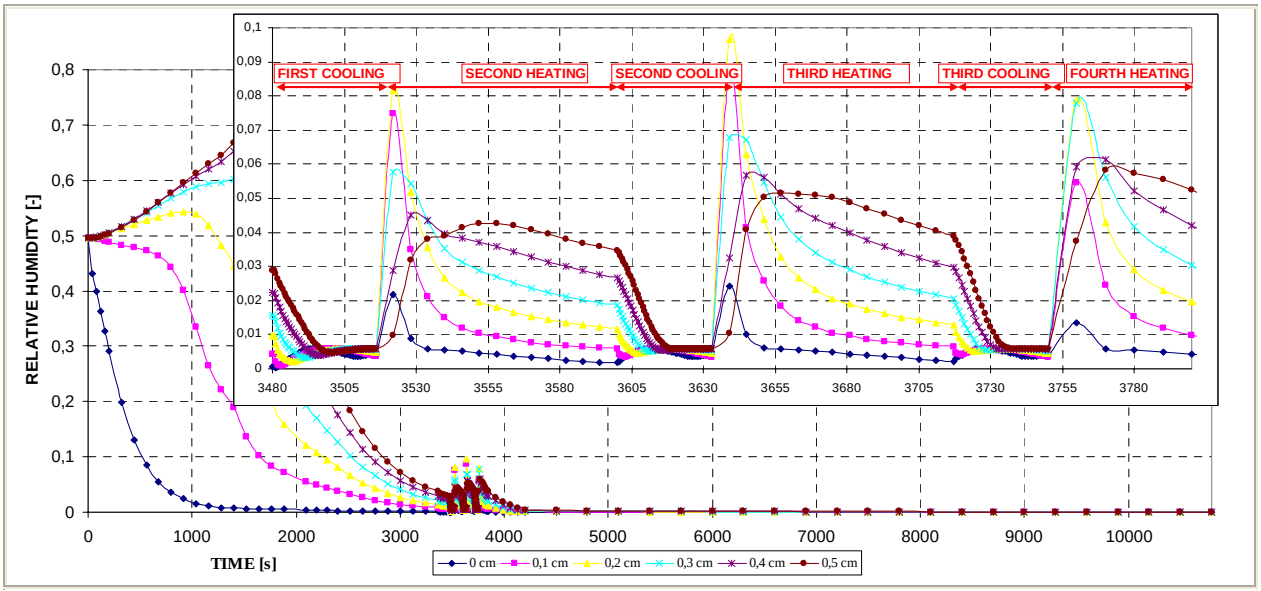

Figure 6-136. *Relative Humidity RH [-] at several distances from the heated/cooled surface during each stage of the Surface cooling processes*

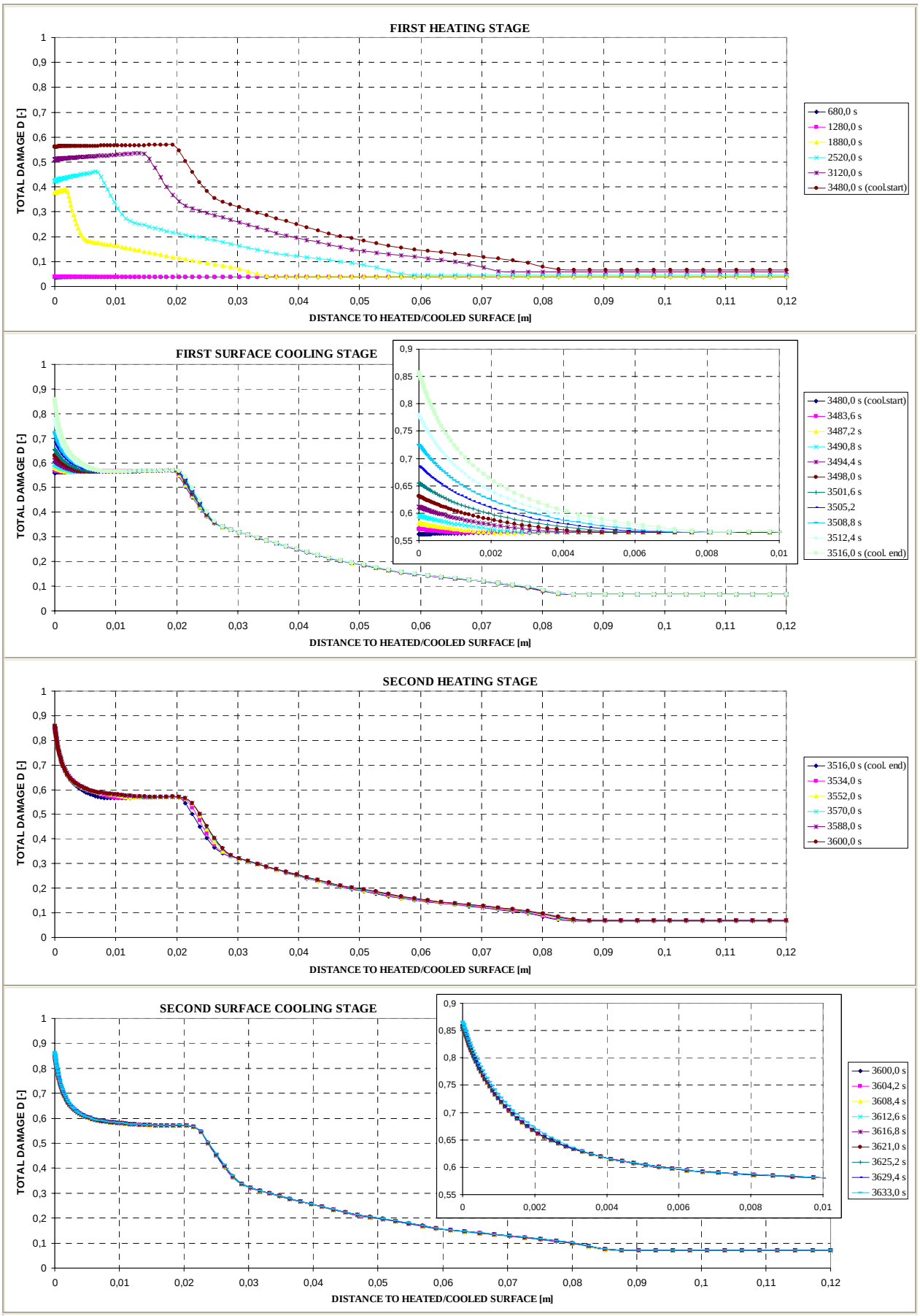

Figure 6-137 (first part). *Total Damage D [-] at several distances from the heated/cooled surface during each stage of the Surface cooling processes*

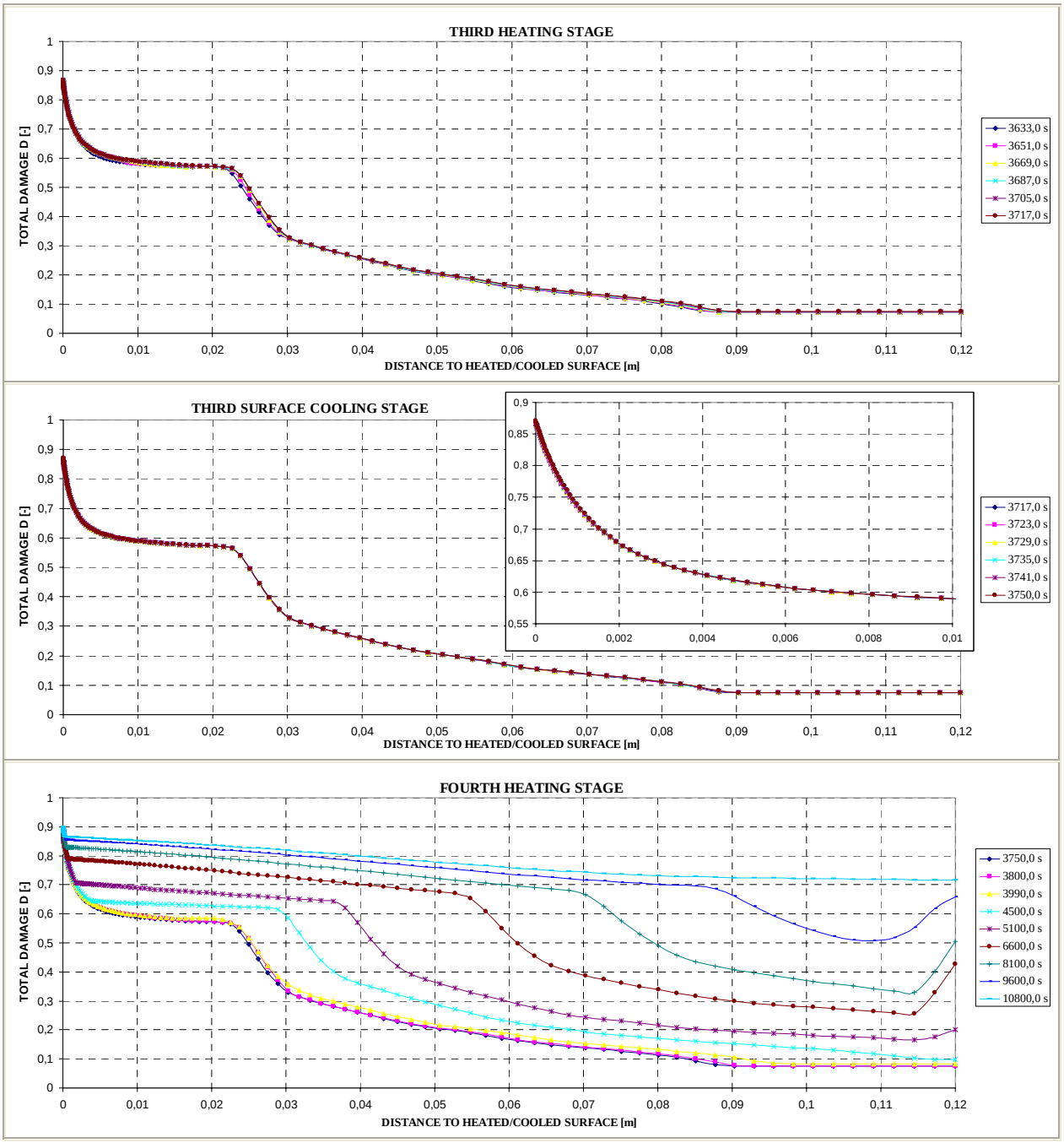

Figure 6-137 (continued). *Total Damage D [-] at several distances from the heated/cooled surface during each stage of the Surface cooling processes*

All these facts mean that, in terms of Total Damage and longitudinal stress the amplitude of the thermal cycles is not high enough to affect the mechanical state of the structural element (neither the Elastic Strain Energy, since as it is shown on figures 6-135 and 6-140 j) its values follow qualitatively identical cycles during the heating-cooling ones.

Moreover, as it can be observed on figures 6-136 and 6-140 h) the hygral behaviour is also qualitatively repetitive (see for example on figure 6-136 the relative humidity at several positions close to the surface corresponding to the start instants of the second, third and fourth heating processes, 3.516, 3.633 and 3.750 seconds respectively).

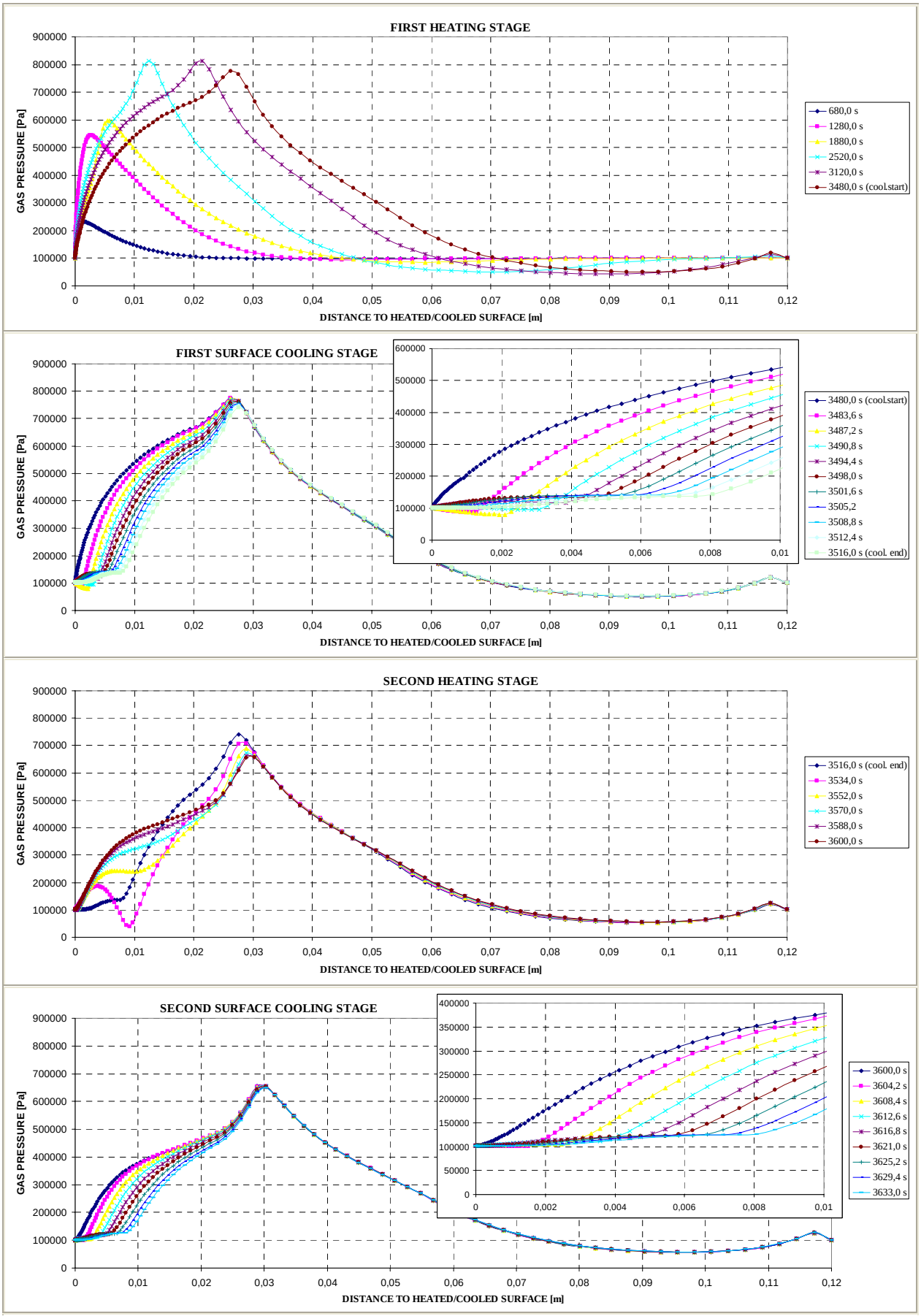

Figure 6-138 (first part). *Gas Pressure Pg [Pa] at several distances from the heated/cooled surface during each stage of the Surface cooling processes*

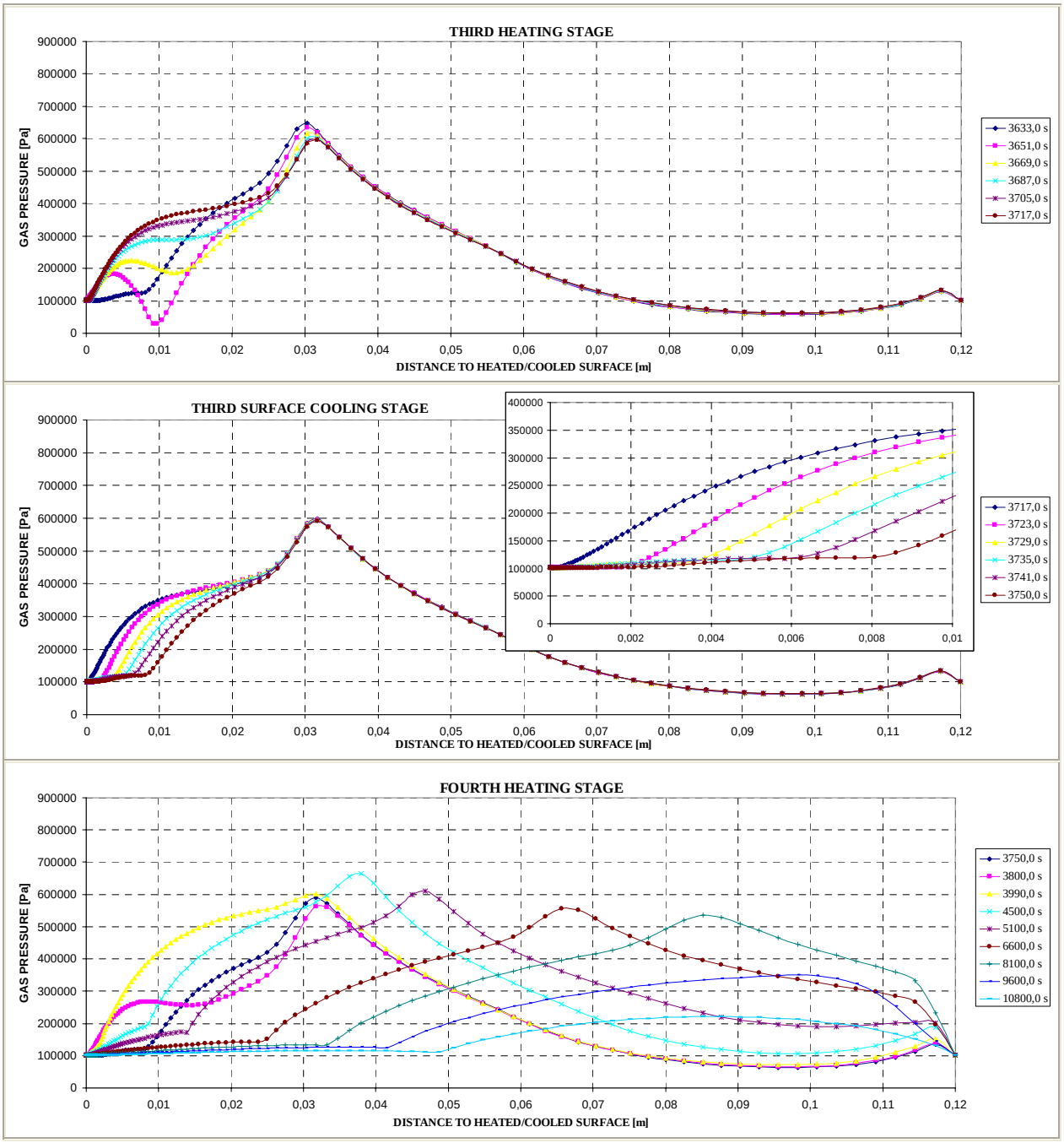

Figure 6-138 (continued). *Gas Pressure Pg [Pa] at several distances from the heated/cooled surface during each stage of the Surface cooling processes*

During the fourth heating stage it is remarkable that at approximately 5.000 seconds from the start of the fire it is observed a sharp increase of Total Damage (more precisely, of Mechanical Damage – see figure 6-140 b)), a sharp decrease of the longitudinal tensile stress close to the surface – and increase in the inner layers – (see figures 6-139 and 6-140 k)) and of the gas pressure and elastic strain energy values (see figures 6-138 e) and 6-135 respectively) and, consequently, both the Spalling Index values and the energy available for thermal spalling close to the surface decrease significantly – the energy available for thermal spalling in the inner layers keeps increasing up to the end of the fourth heating – (see figures 6-140 a), 6-140 c) and 6-140 d)), so thermal spalling is still energetically viable until the end of the 3 hours overall heating-cooling process at really important depths (see specifically figure 6-140 d)).

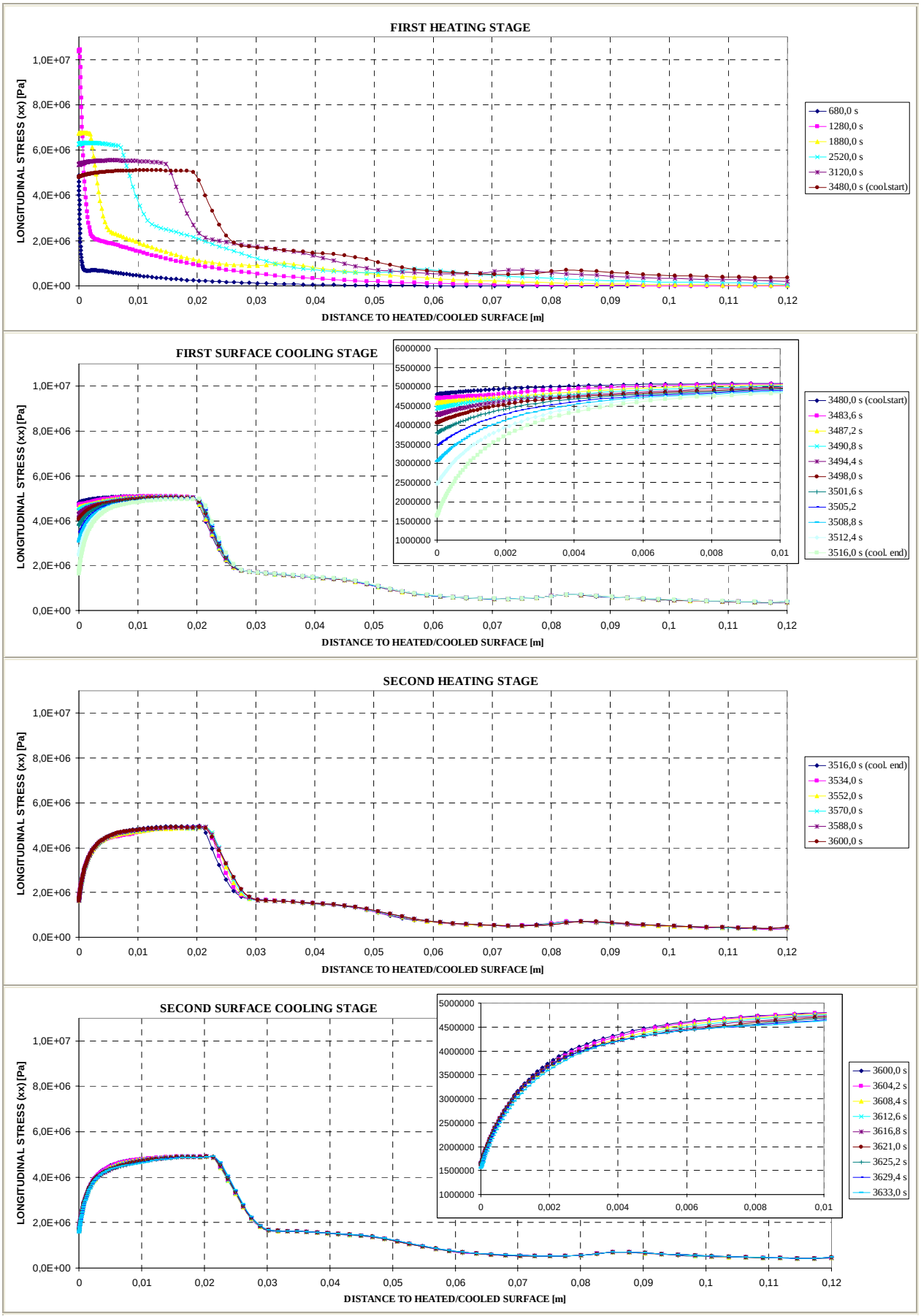

Figure 6-139 (first part). *Longitudinal stress (xx) [Pa] at several distances from the heated/cooled surface during each stage of the Surface cooling processes*

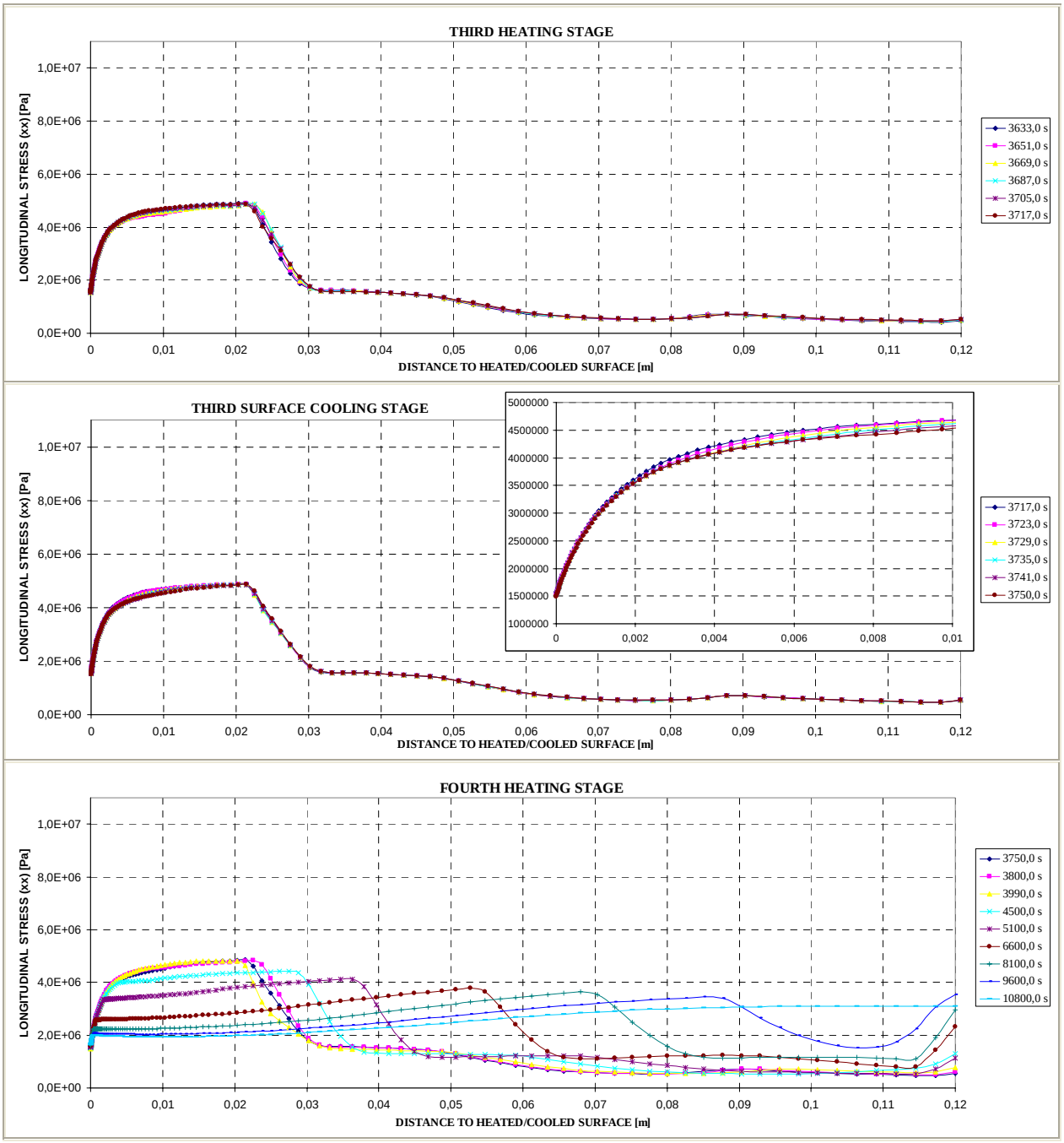

Figure 6-139 (continued). *Longitudinal stress (xx) [Pa] at several distances from the heated/cooled surface during each stage of the Surface cooling processes*

After figures 6-137 to 139, it is shown a collection of twelve Time-Space graphics representing the evolution of all of the parameters cited in the last subparagraph and for all of the stages that compose the heating and cooling processes analyzed herein.

a) Spalling Index IS4 [-]

b) Mechanical damage d [-]

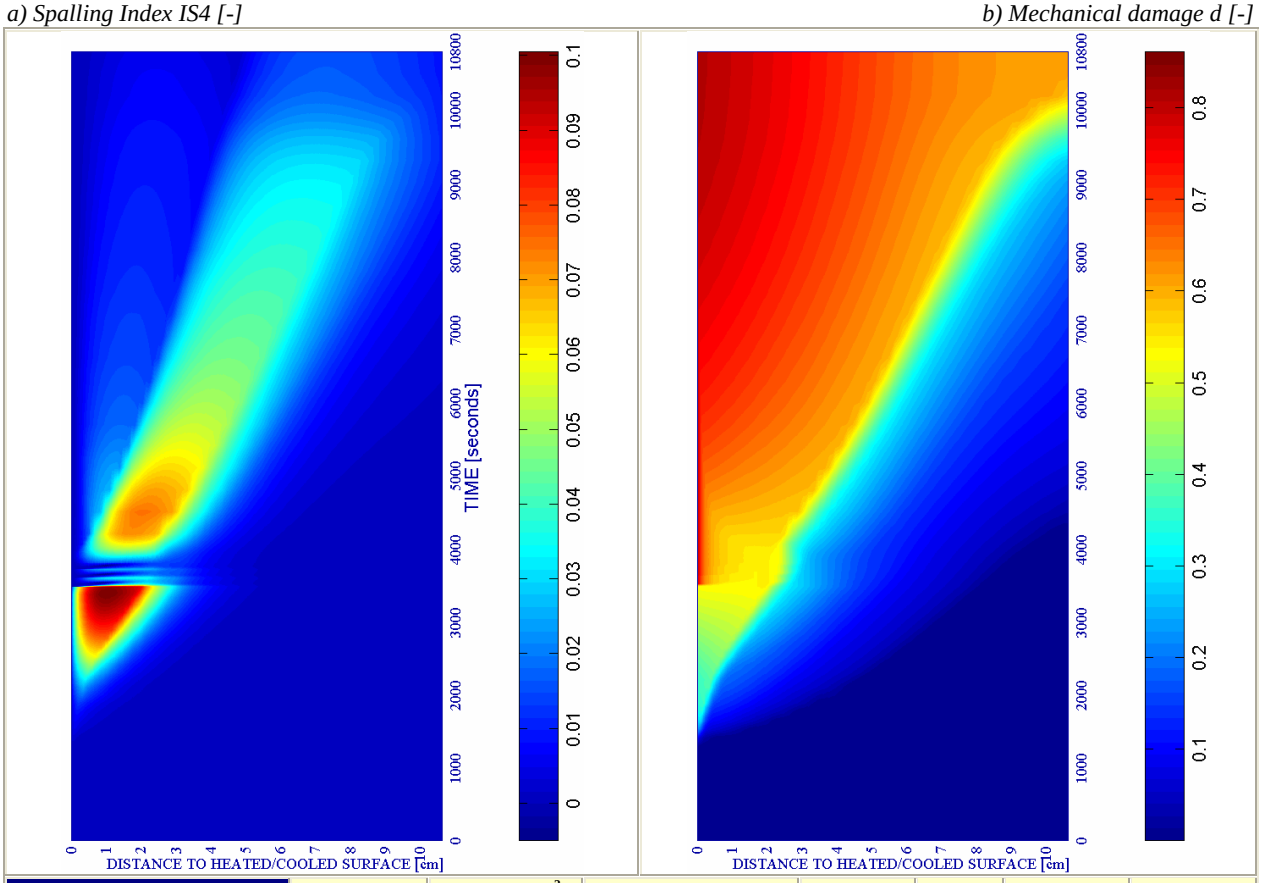

SURFACE COOL+REPEAT	PC1 - RH [%]			PC2 - K_0 [m^2]			PC4 - Heating curve			PC5 – Mat.		Cooling length[s]	Start of cooling [s]	End of cooling [s]
#	Combination	40	50	60	10^{-19}	10^{-18}	10^{-17}	PAR1	PAR2	PAR4	C60	C90			
14	TH12K018RH50PAR2C60		X			X			X		X		36 /33 / 33	3.480/3.600/3.717	3.516/3.633 /3.750

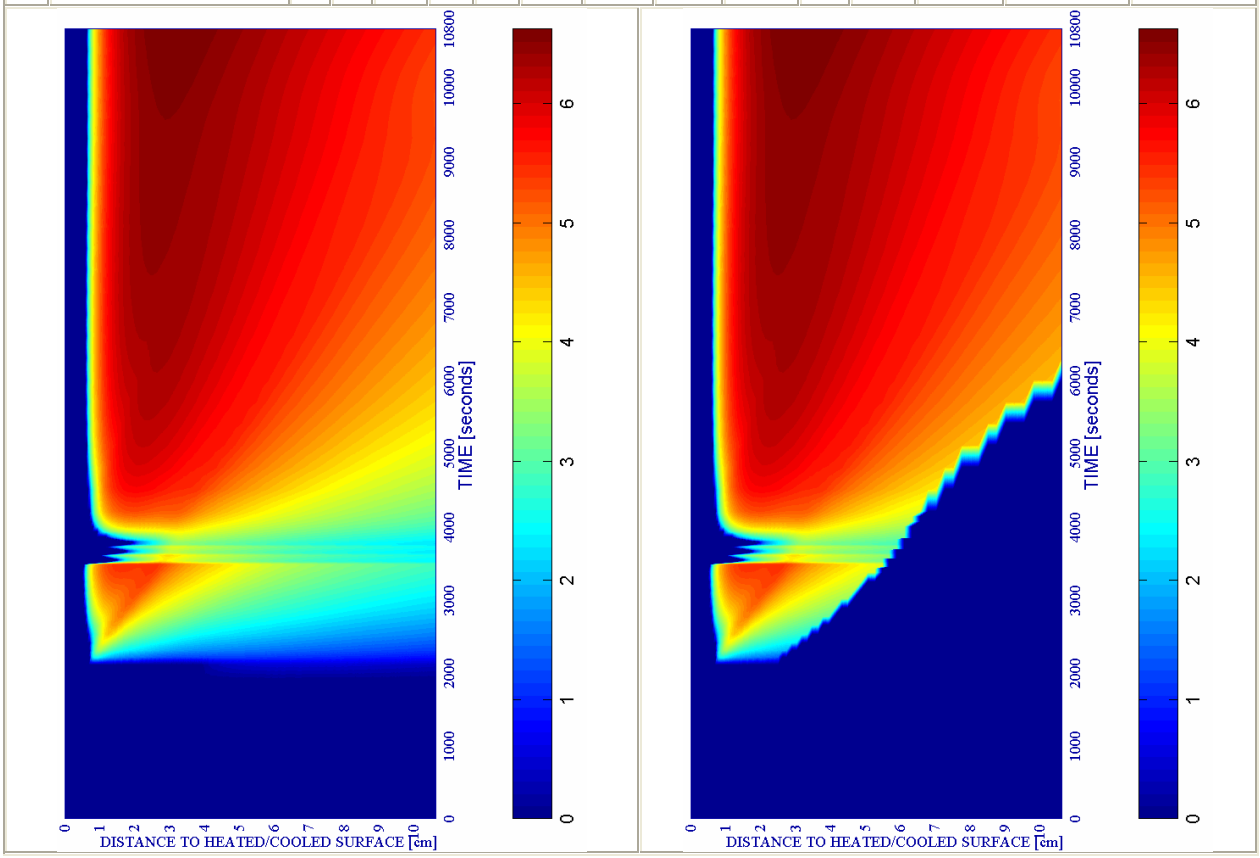

c) Velocity of spalled pieces v [m/s]

Figure 6-140.

d) Velocity [m/s] where d ≥ 0,10

e) Gas pressure $p^g \cdot 10^{-5}$ [Pa]

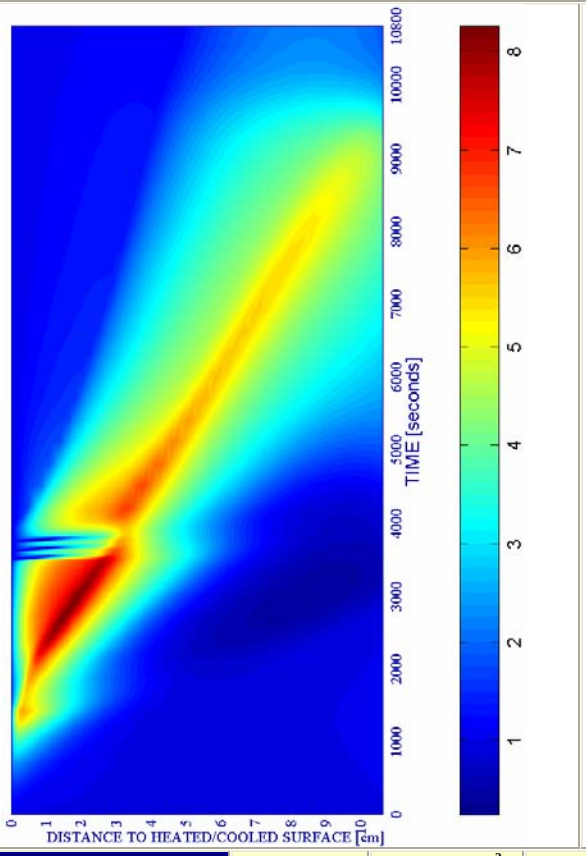

f) Vapour pressure $p^v \cdot 10^{-5}$ [Pa]

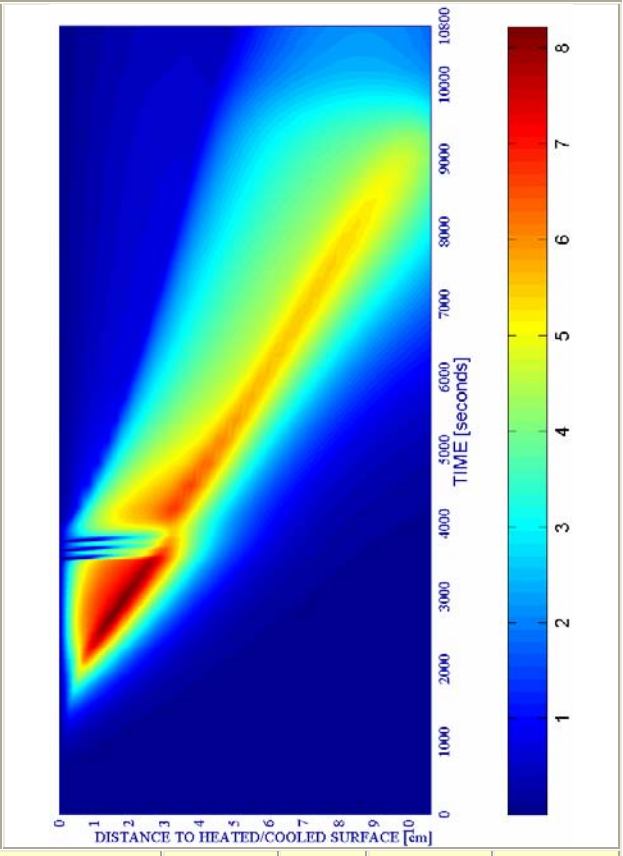

SURFACE COOL+REPEAT		PC1 - RH [%]			PC2 - K_0 [m^2]			PC4 - Heating curve			PC5 – Mat.		Cooling length[s]	Start of cooling [s]	End of cooling [s]
#	Combination	40	50	60	10^{-19}	10^{-18}	10^{-17}	PAR1	PAR2	PAR4	C60	C90			
14	TH12K018RH50PAR2C60		X			X			X		X		36 /33 / 33	3.480/3.600/3.717	3.516/3.633 /3.750

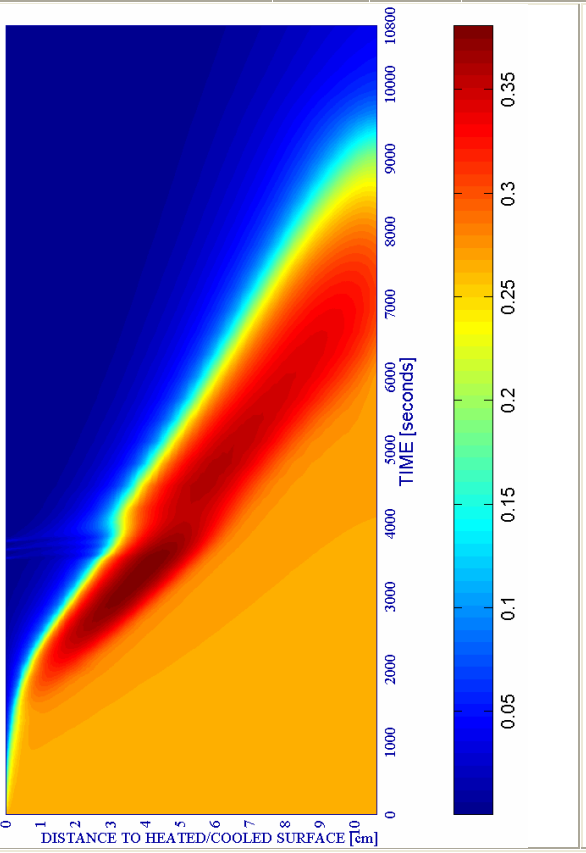

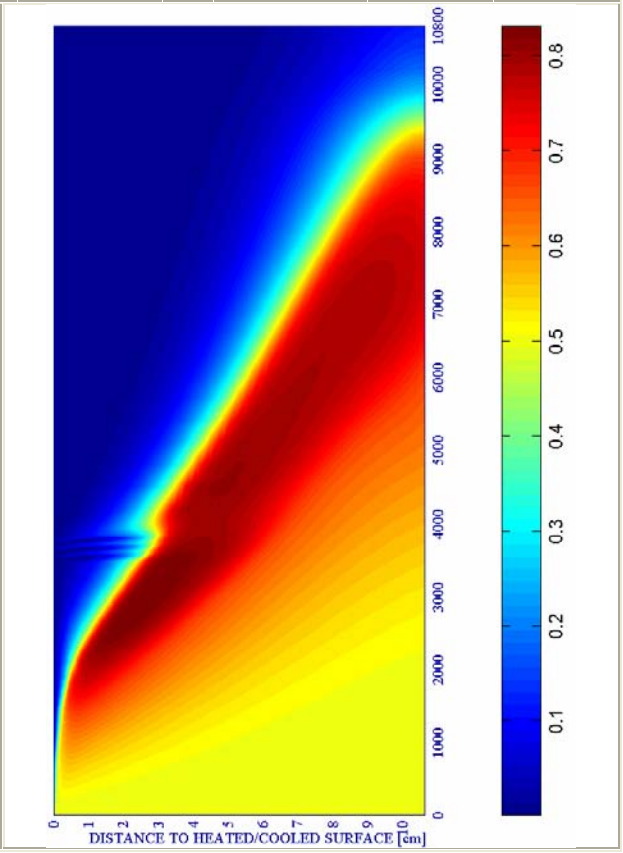

g) Saturation Degree S [-]

Figure 6-140. (continued)

h) Relative Humidity RH [-]

i) Temperature [K]

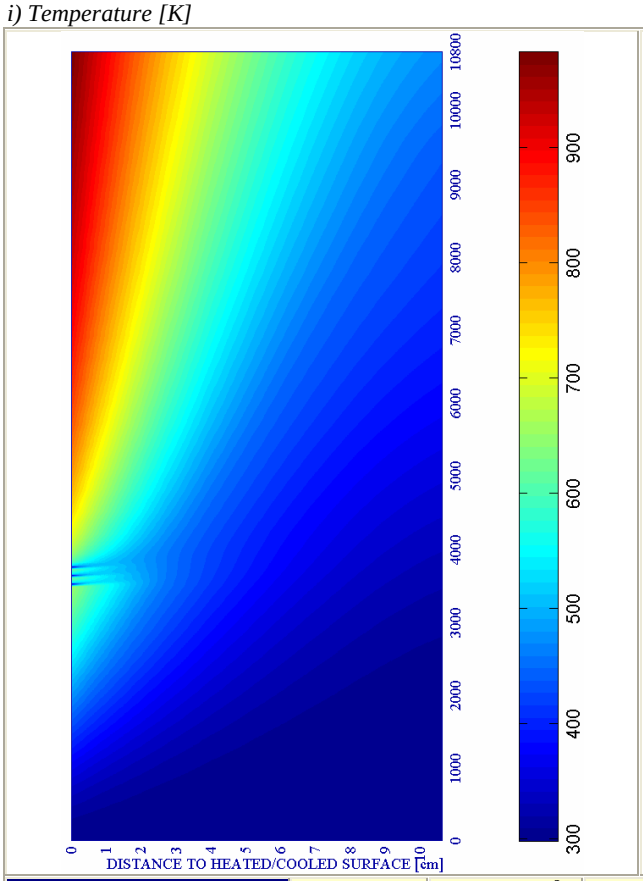

*j) Elastic Energy U · **10**$^{-4}$ [J/m^3]*

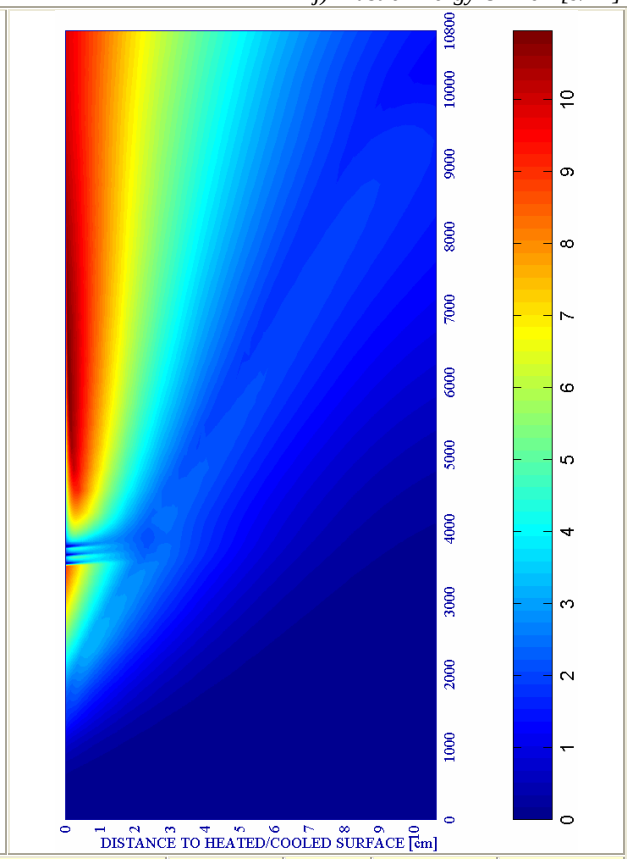

SURFACE COOL+REPEAT	PC1 - RH [%]			PC2 - K_0 [m^2]			PC4 - Heating curve			PC5 – Mat.		Cooling length[s]	Start of cooling [s]	End of cooling [s]
#	Combination	40	50	60	10^{-19}	10^{-18}	10^{-17}	PAR1	PAR2	PAR4	C60	C90			
14	TH12K018RH50PAR2C60		X			X			X		X		36 /33 / 33	3.480/3.600/3.717	3.516/3.633 /3.750

*k) Stress in longitudinal (xx) direction · **10**$^{-6}$ [Pa]*

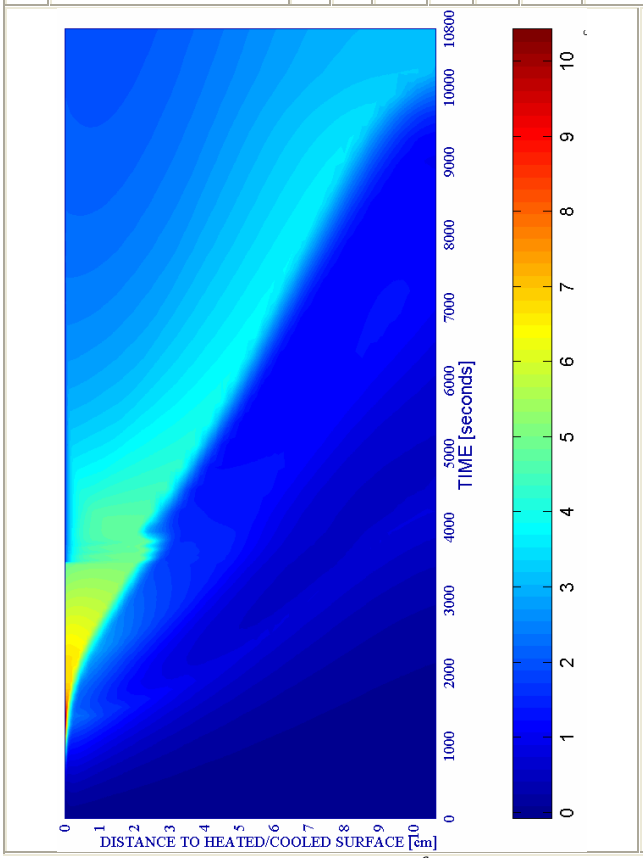

Figure 6-140. (continued)

*l) Stress in transversal (yy) direction · **10**$^{-7}$ [Pa]*

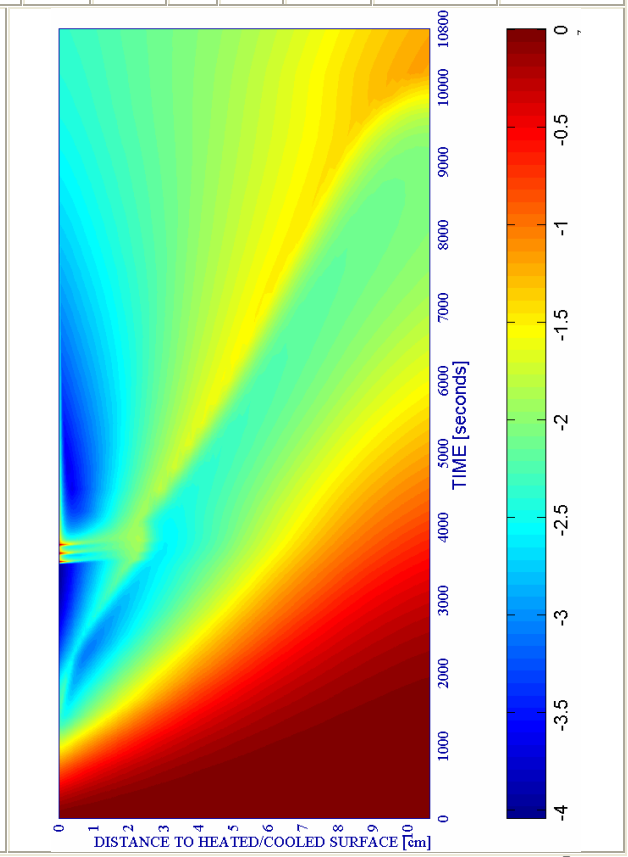

6.5.2.5.7 Environmental Heating up to Three hours Without any Cooling

Phenomenological and mechanistic analysis of this case is not qualitatively different from those corresponding to the heating stages analyzed within last paragraphs. However, the results exposed herein will be extremely useful for comparison purposes as it is detailed and dealt in depth on paragraph 6.5.3 of this chapter.

Next it is shown a collection of the main results cited in this subparagraph, as well as a description of each of the stages that compose the heating process analyzed herein.

Table 6-97. *Description of the Cooling Process Stages and Collection of the Main Results related to Spalling Index and velocity*

Stage description	Absolute Time Start [s]	Absolute Time End [s]	$IS4_{max}$ [-]	X_{IS4max} [cm]	t_{IS4max} [s]	v_{max} [m/s]	X_{vmax} [cm]	t_{vmax} [s]	v_{max}* [m/s]	X_{vmax*} [cm]	t_{vmax*} [s]
Heating up to 10.800s	0	10.800	0,1010	1,099	3.480	6,635	3,172	10.800	6,635	3,172	10.800

Remark †***:*** *These results are included for the Comparative Analysis developed on Paragraph 6.5.3*

Stage description	Absolute Time Start [s]	Absolute Time End [s]	d_{max} [-]	X_{dmax} [cm]	t_{dmax} [s]	T_{max} [K]	X_{Tmax} [cm]	t_{Tmax} [s]	p^g_{max} [MPa]	X_{pgmax} [cm]	t_{pgmax} [s]
Heating up to 10.800s	0	10.800	0,8115	0,000	10.800	982,90	0,000	10.800	0,8256	1,555	2.760

Table 6-98. *Description of the Cooling Process Stages and Collection of the Main Results related to mechanical damage, Temperature and Gas Pressure*

As it is shown on figure 6-141, beyond the Mechanical Damage maximum – values that appear on last table at depths close to the surface – Total Damage values are increased by Thermo-Chemical Damage (which reaches values of about 0,29) so Total Damage at the end of the three hours heating process has reached a quite high value – 0,87 – at the layers close to the surface. Nevertheless, the whole structural element presents at the end of the heating process a Total Damage level higher elsewhere than the 72 per cent, so it can be understood that the structural element will finally be almost completely destroyed.

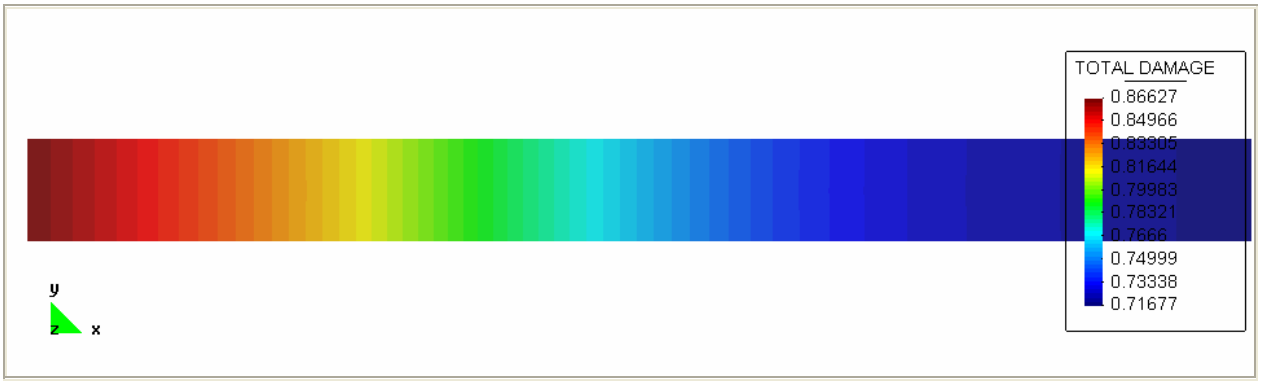

Figure 6-141. *Total Damage D [-] at the structural element at the end of the heating process without any cooling (time: 10.800 seconds)*

It is also remarkable that the maximum temperature achieved in this process (982,9 K) matches that corresponding to the process including one or three surface cooling intermediate stages (982,8 K and 982,5 K respectively). This fact initially suggests a rather local effect of the surface cooling processes considered in this chapter.

On figures 6-142 a) to l) it is shown a collection of twelve Time-Space graphics representing the evolution of all of the parameters cited in the last subparagraph and for all of the stages that compose the heating and cooling processes analyzed herein.

a) Spalling Index IS4 [-]

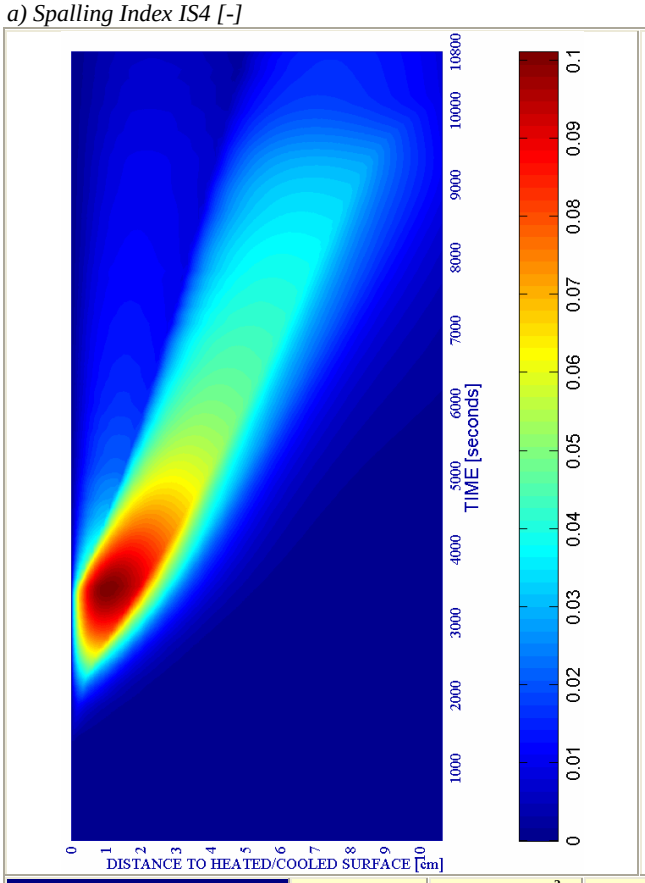

b) Mechanical damage d [-]

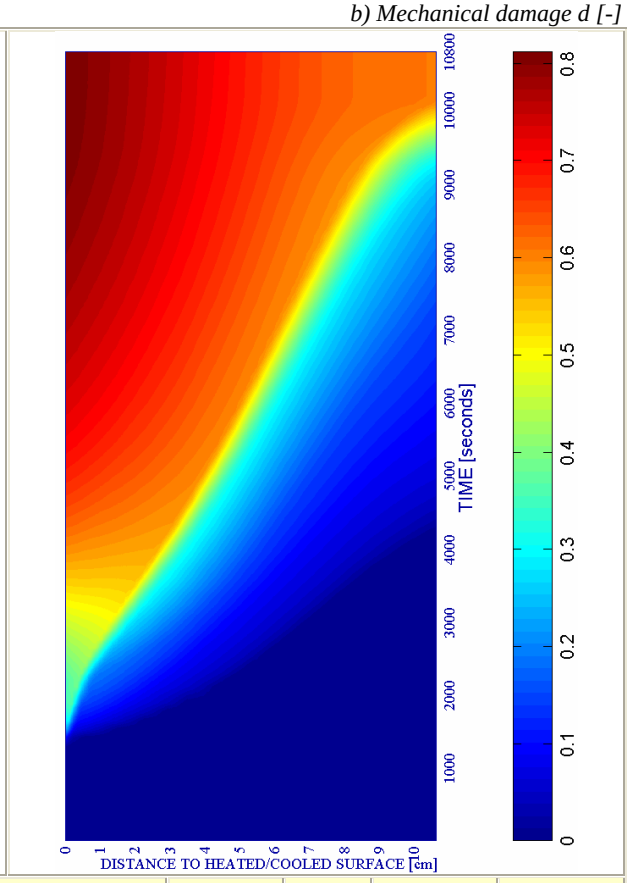

WITHOUT COOLING		PC1 - RH [%]			PC2 - K_0 [m^2]			PC4 - Heating curve			PC5 – Mat.		Cooling length[s]	Start of cooling [s]	End of cooling [s]
#	Combination	40	50	60	10^{-19}	10^{-18}	10^{-17}	PAR1	PAR2	PAR4	C60	C90			
14	TH12K018RH50PAR2C60		X			X			X		X		---	---	---

c) Velocity of spalled pieces v [m/s]

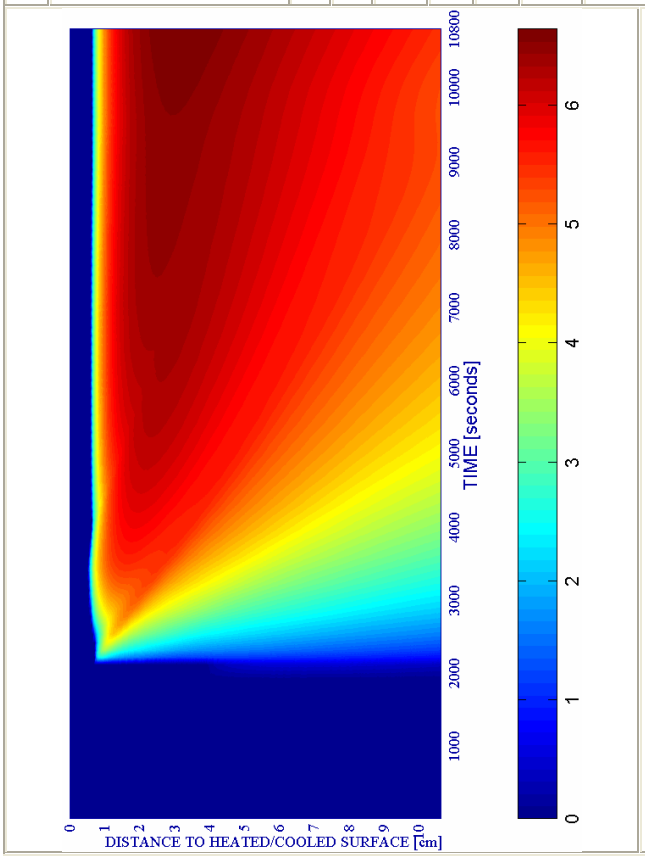

d) Velocity [m/s] where d ≥ 0,10

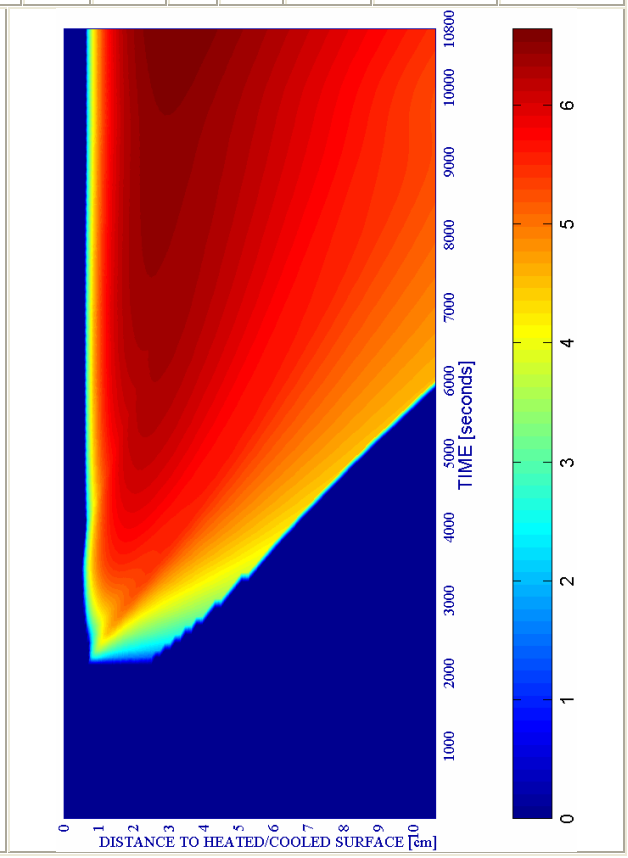

Figure 6-142.

e) Gas pressure $p^g \cdot 10^{-5}$ [Pa]

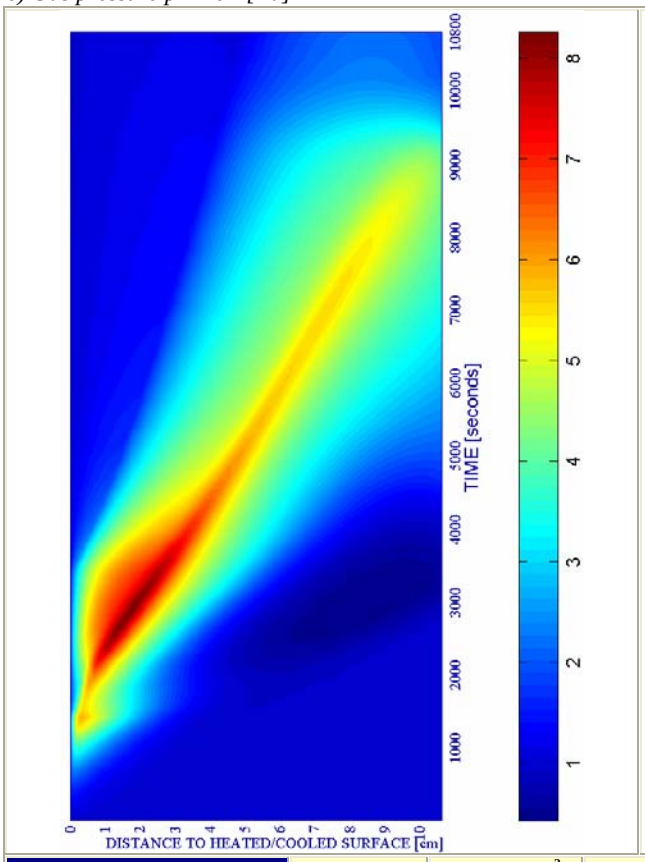

f) Vapour pressure $p^v \cdot 10^{-5}$ [Pa]

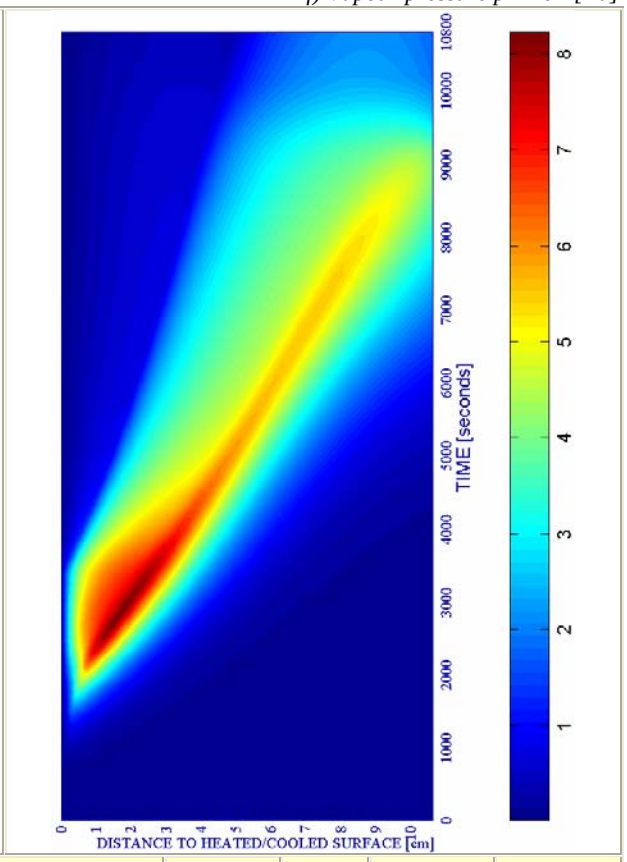

WITHOUT COOLING		PC1 - RH [%]			PC2 - K_0 [m^2]			PC4 - Heating curve			PC5 – Mat.		Cooling length[s]	Start of cooling [s]	End of cooling [s]
#	Combination	40	50	60	10^{-19}	10^{-18}	10^{-17}	PAR1	PAR2	PAR4	C60	C90			
14	TH12K018RH50PAR2C60		X			X			X		X		---	---	---

g) Saturation Degree S [-]

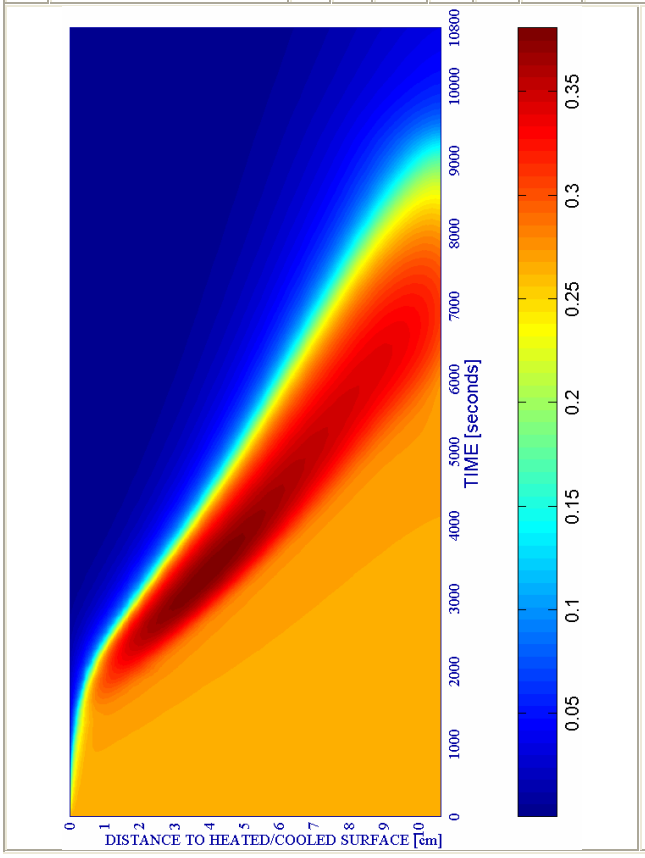

Figure 6-142. (continued)

h) Relative Humidity RH [-]

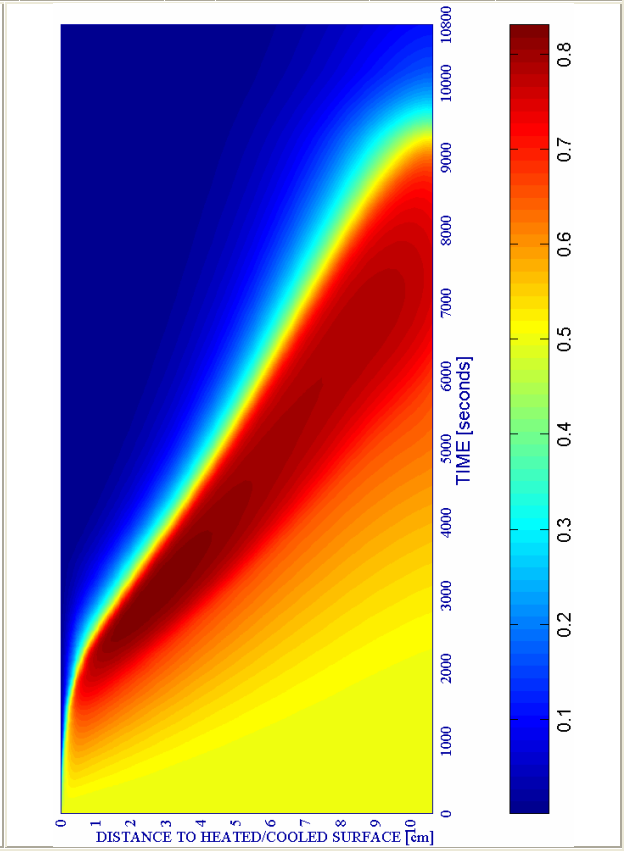

i) Temperature [K]

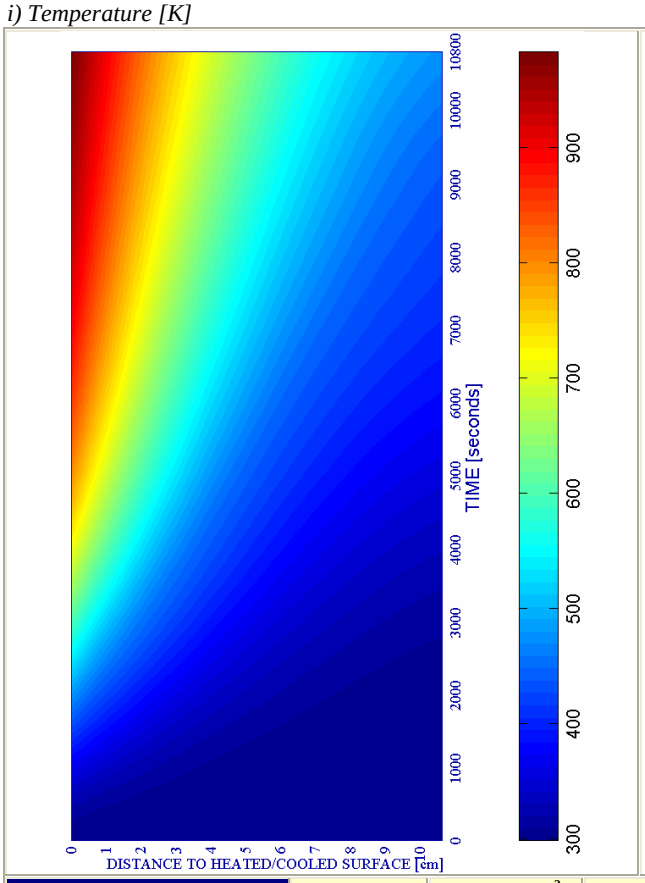

*j) Elastic Energy U · **10**$^{-4}$ [J/m^3]*

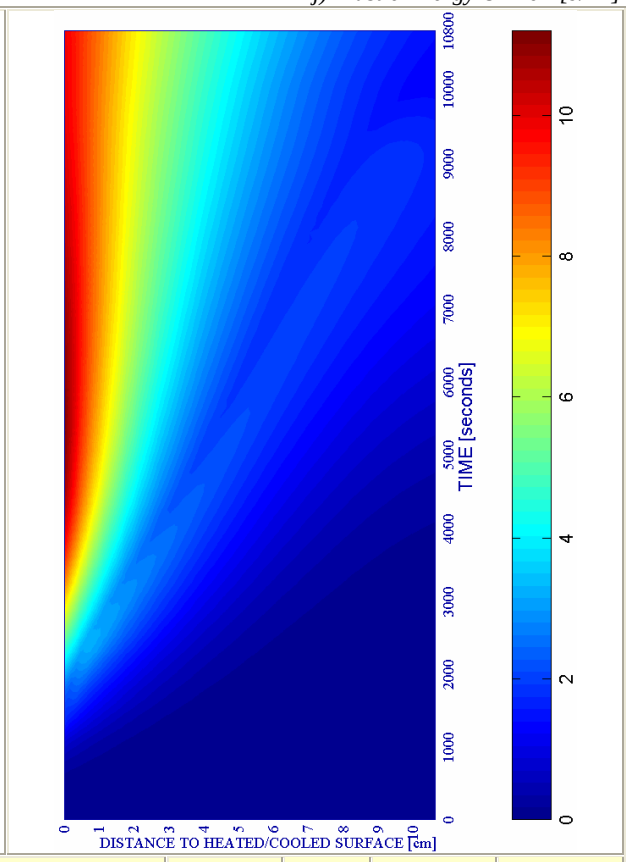

WITHOUT COOLING		PC1 - RH [%]			PC2 - K_0 [m^2]			PC4 - Heating curve			PC5 – Mat.		Cooling length[s]	Start of cooling [s]	End of cooling [s]
#	Combination	40	50	60	10^{-19}	10^{-18}	10^{-17}	PAR1	PAR2	PAR4	C60	C90			
14	TH12K018RH50PAR2C60		X			X			X		X		---	---	---

*k) Stress in longitudinal (xx) direction · **10**$^{-6}$ [Pa]*

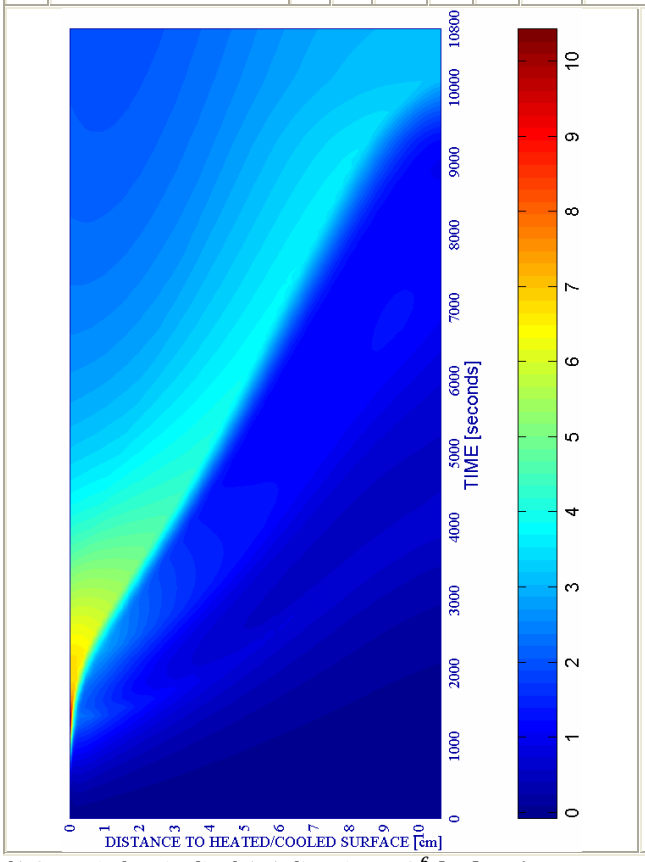

Figure 6-142. (continued)

*l) Stress in transversal (yy) direction · **10**$^{-7}$ [Pa]*

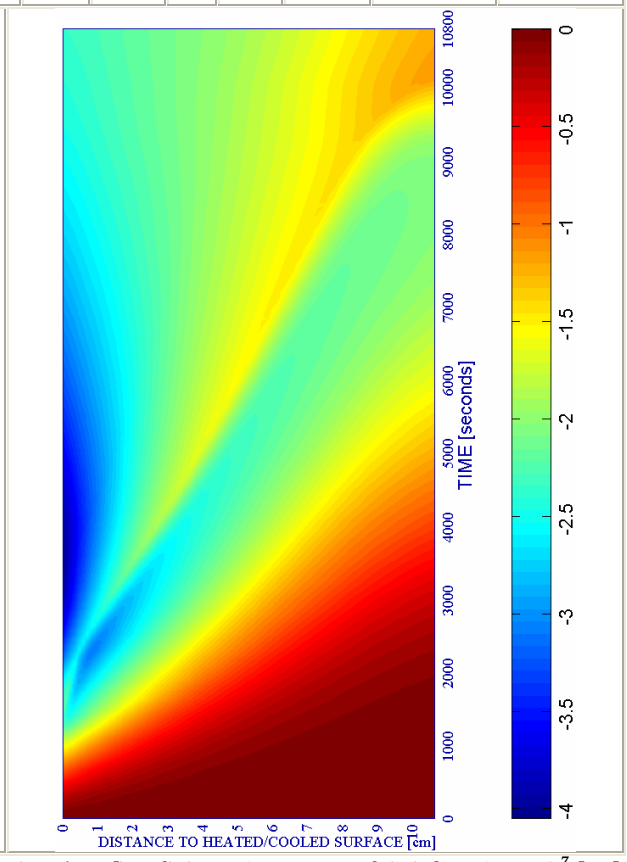

6.5.2.6 REFERENCE CASE # 14 – TH12K018RH50PAR2C60 – START OF COOLING: 3.360S WITH THE HIGH COOLING RATES CORRESPONDING TO HIGH-PRESSURE HOSE NOZZLES

Within this paragraph are analyzed the results corresponding to the cases where the most extreme cooling rates values obtained from the computational fluids dynamics simulations – i.e. those corresponding to High-Pressure Hose Nozzles – are applied to the surface of the structural element in order to discern if the conclusions arisen in this Chapter are valid for the complete range of expectable cooling rates during a fire fighting in a High-Rise Building.

The main features of this reference case are the following ones:

		PC1 (RH) [%]			PC2 (K) [m^2]			PC3 (TH) [cm]			PC4 (Heating curve)			PC5 (Mat)	
#	Combination	40	50	60	10^{-19}	10^{-18}	10^{-17}	12	24	50	PAR1	PAR2	PAR3	C60	C90
14	TH12K018RH50PAR2C60		X			X						X		X	

Table 6-99. *Main Features of the Reference Case #14 – TH12K018RH50PAR2C60.*

with an starting instant of the first cooling process at 3.360 seconds. The types and subtypes of cooling processes analyzed in this reference case are the following ones:

Type of Cooling	*Subtype of Cooling*	*Related Paragraph*	*Figures numbers*
Surface (-136,6 K/s)	Followed by an imposed constant Surface Temperature	6.5.2.6.1	6-143 to 6-153
Surface (-32,36 K/s)	Followed by an imposed constant Surface Temperature	6.5.2.6.2	6-154 a) to l)

Remark: *See each Paragraph for more details on the features of the Cooling Processes.*

Table 6-100. *Types and Subtypes of Cooling Processes Analyzed in the Reference Case #14 – TH12K018RH50PAR2C60 with the Start of Cooling Process at 3.360 seconds*

with two different cooling rates, namely, -136,6 K/second and -32,36 K/second respectively (values obtained from paragraph 6.4.3.2.4.3 in this Chapter).

6.5.2.6.1 Surface Cooling followed by an imposed Constant Surface Temperature: Cooling Rate -136,6 K/s

Herein is analyzed the most extreme value of the cooling rate applied to the surface of the structural element. Although in figure 6-151 is shown the complete time evolution of the parameters describing the hygro-thermo-chemo-mechanical behaviour of the structural element, a deeper emphasis is put on the cooling process, this is, from 3.480 to 3.482,7 seconds where the cooling rate is applied and, later, from 3.482,7 to 3.719,4 seconds where an ambient temperature is kept constant at the surface of the structural element.

Hence, figures 6-143 (and figure 6-151 a)) and 6-144 (figure 6-151 b)) show the evolution of the Spalling Index I_{s4} and the mechanical damage d respectively during these stages. It is clearly observed (figure 6-143) that despite mechanical damage increases significantly during cooling (more than a 30 per cent near the surface, figure 6-144) Spalling Index values decrease and, hence, the risk of experimenting thermal spalling also decreases.

This is mainly due, in part, to a sharp decrease of the gas pressure values (figure 6-145 and figure 6-151 e)) consequence, in the meantime, of a fast decrease of the vapour pressure ones during the cooling process (figure 6-146 and figure 6-151 f)). The fast decrease in temperature (figure 6-147 and figure 6-151 i)) – leading to higher values of the tensile strength of concrete –, the fast decrease in the constrained elastic energy (figure 6-148 and figure 6-151 j)) – except in the late stage of the constant ambient temperature situation, but arising to values of the elastic energy much lower than those corresponding to the start of the cooling – and the compressive longitudinal stresses arisen near the cooled surface during the process (figure 6-149 and figure 6-151 k)) impede the increase of the Spalling Index I_{s4} values.

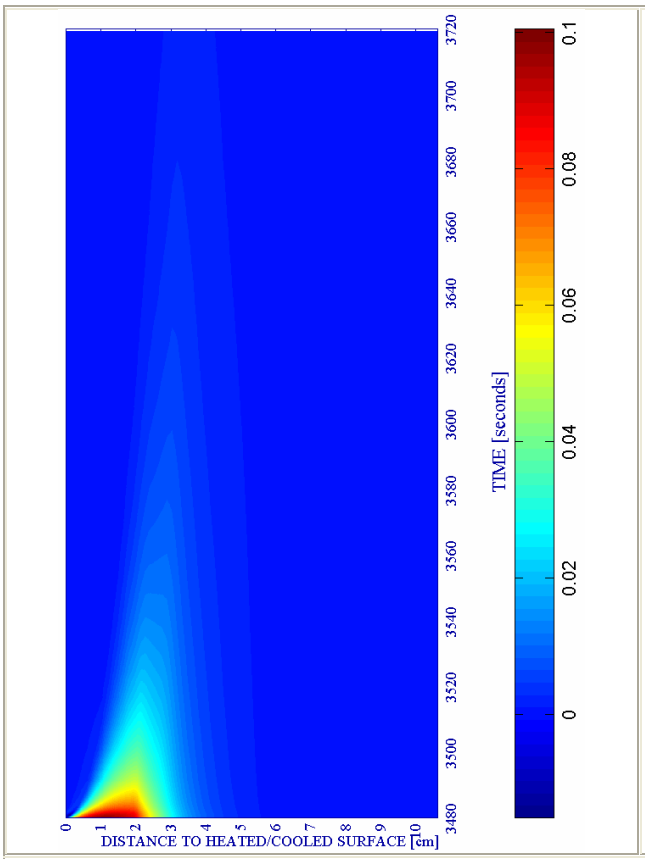

Figure 6-143. *Spalling Index IS4 [-]*

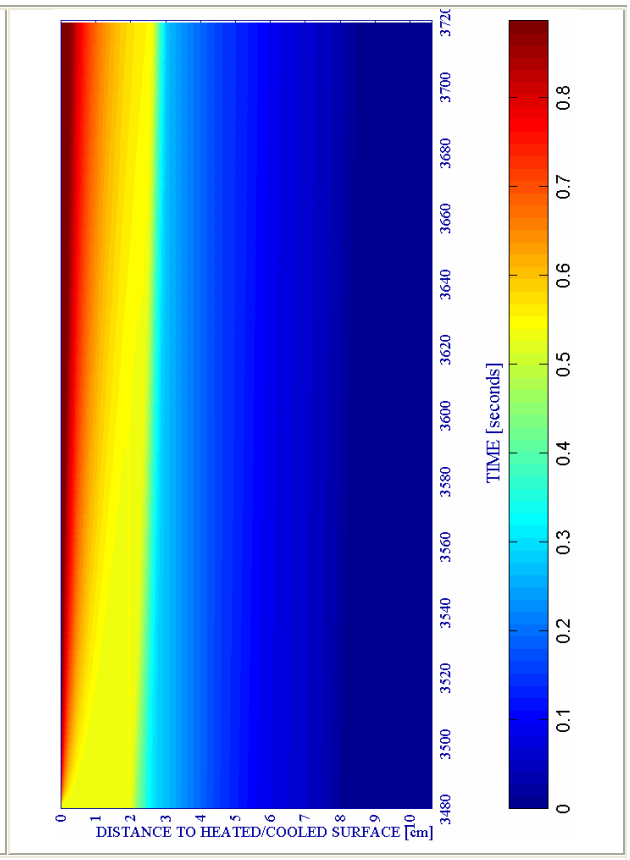

Figure 6-144. *Mechanical Damage d [-]*

at the structural element from the start of the cooling process until the end of the calculation.

Figure 6-145. *Gas pressure $p^g \cdot 10^{-5}$ [Pa]*

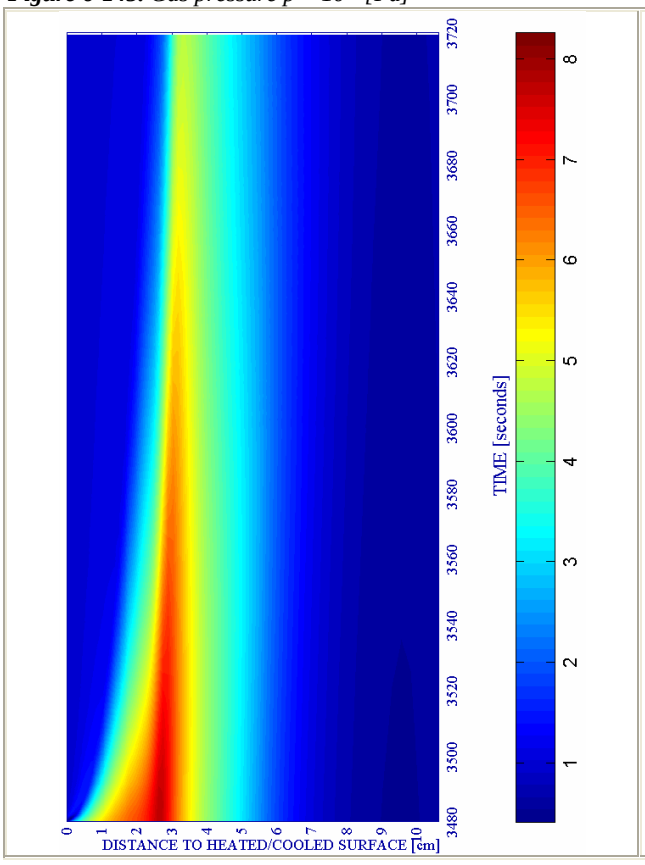

Figure 6-146. *Vapour pressure $p^v \cdot 10^{-5}$ [Pa]*

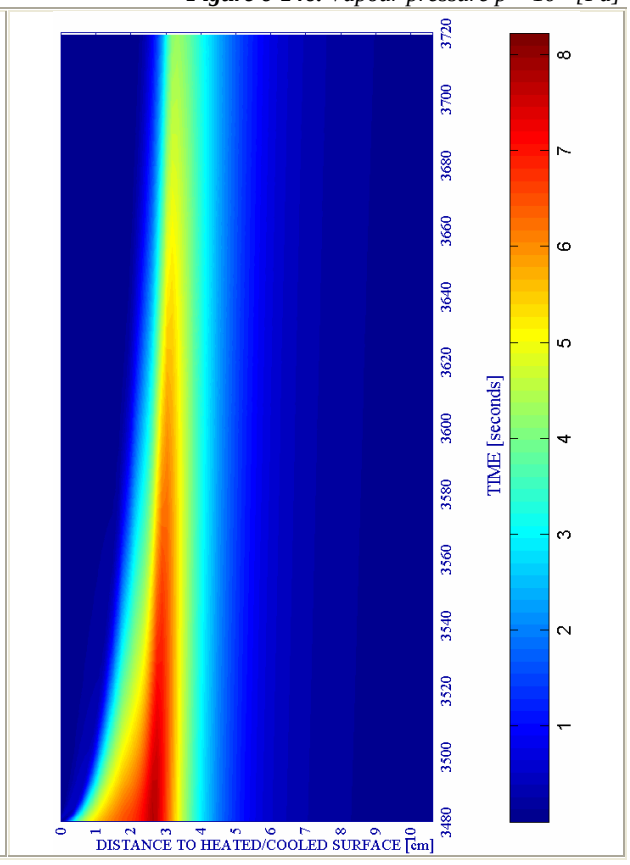

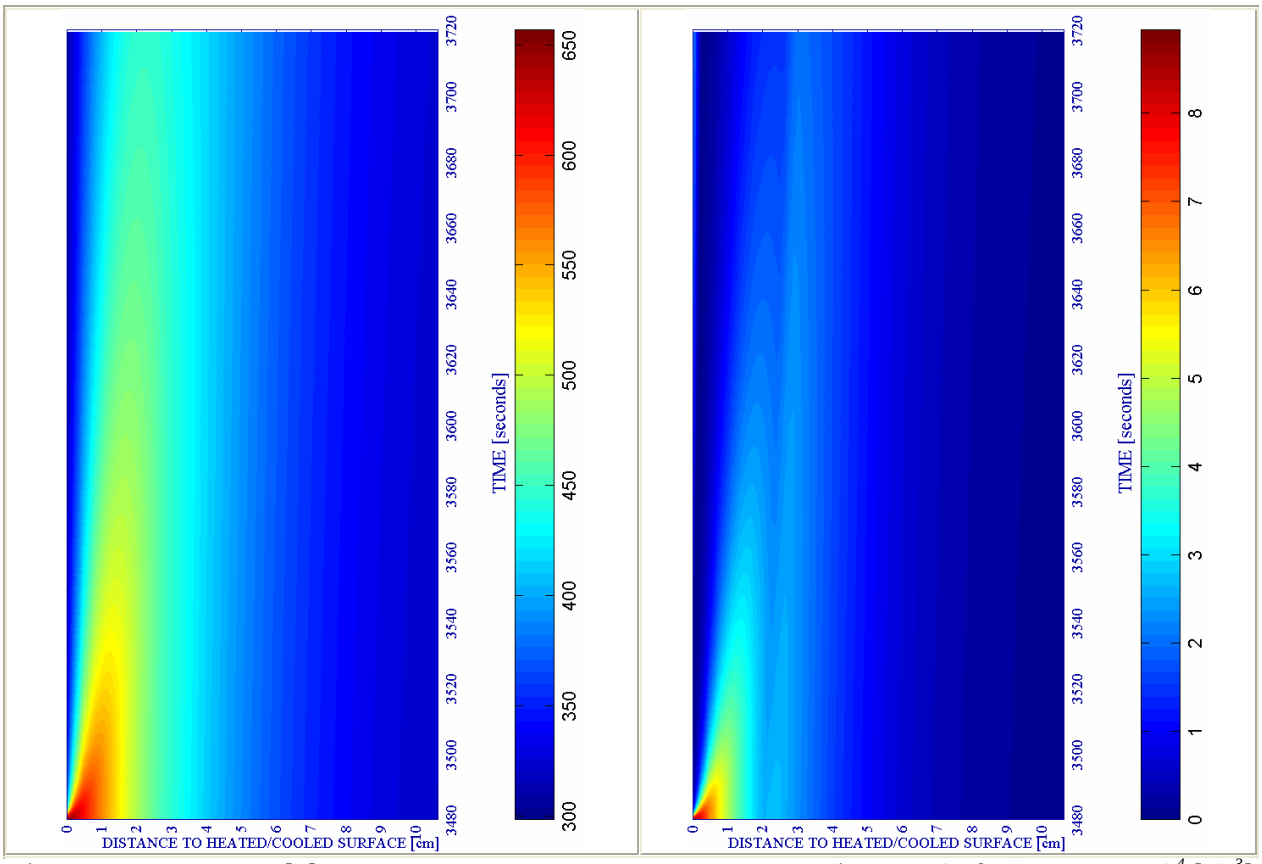

Figure 6-147. *Temperature [K]*

Figure 6-148. *Elastic energy U · 10^{-4} [J/m^3]*

at the structural element from the start of the cooling process until the end of the calculation.

Figure 6-149. *Stress in longitudinal (xx) direction · 10^{-7} [Pa]*

Figure 6-150. *Saturation Degree S [-]*

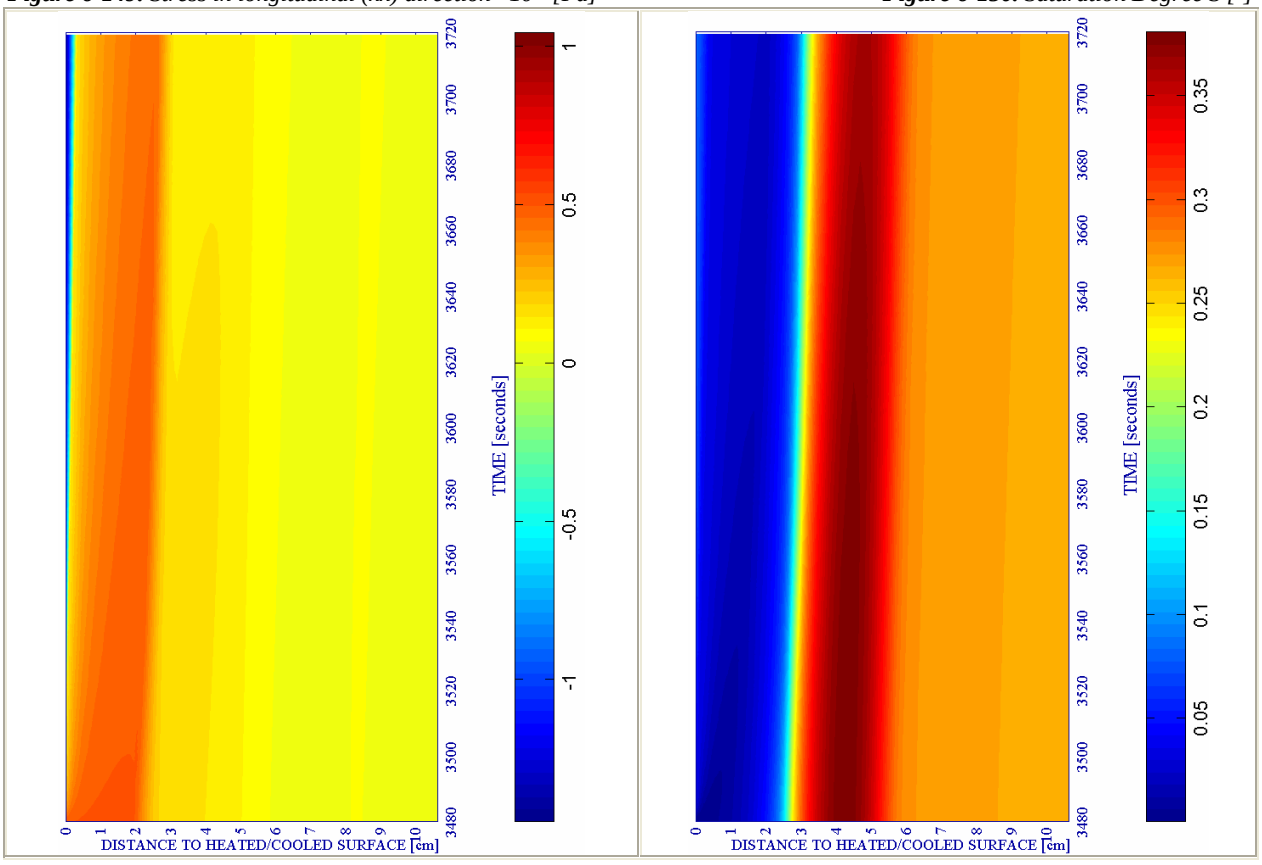

The complete evolution of these parameters is shown on figure 6-151.

a) Spalling Index IS4 [-] *b) Mechanical damage d [-]*

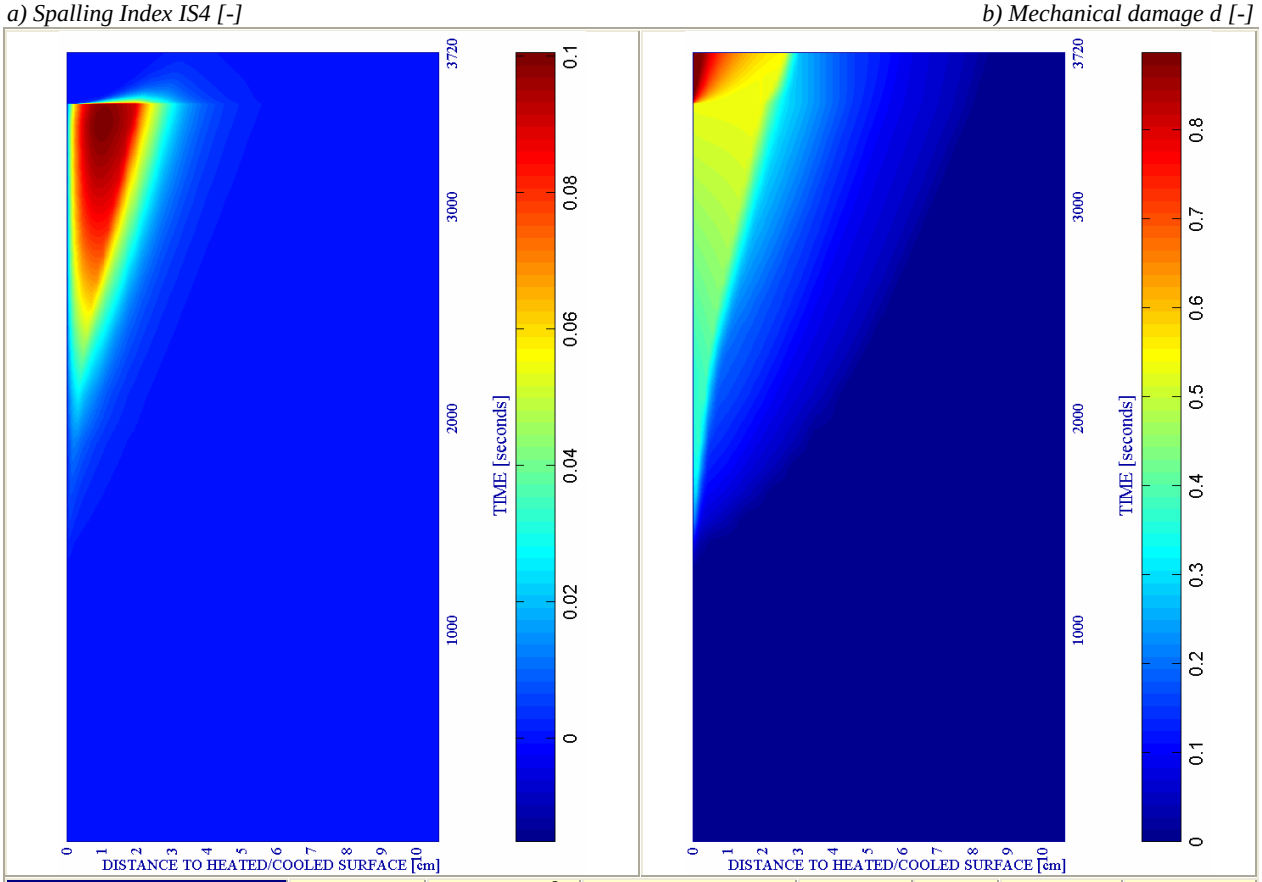

SURFACE COOL+KEEP		PC1 - RH [%]			PC2 - K_0 [m^2]			PC4 - Heating curve			PC5 – Mat.		Cooling length[s]	Start of cooling [s]	End of cooling [s]
#	Combination	40	50	60	10^{-19}	10^{-18}	10^{-17}	PAR1	PAR2	PAR4	C60	C90			
14	TH12K018RH50PAR2C60		X			X			X		X		2,7	3.360+120	3.482,70

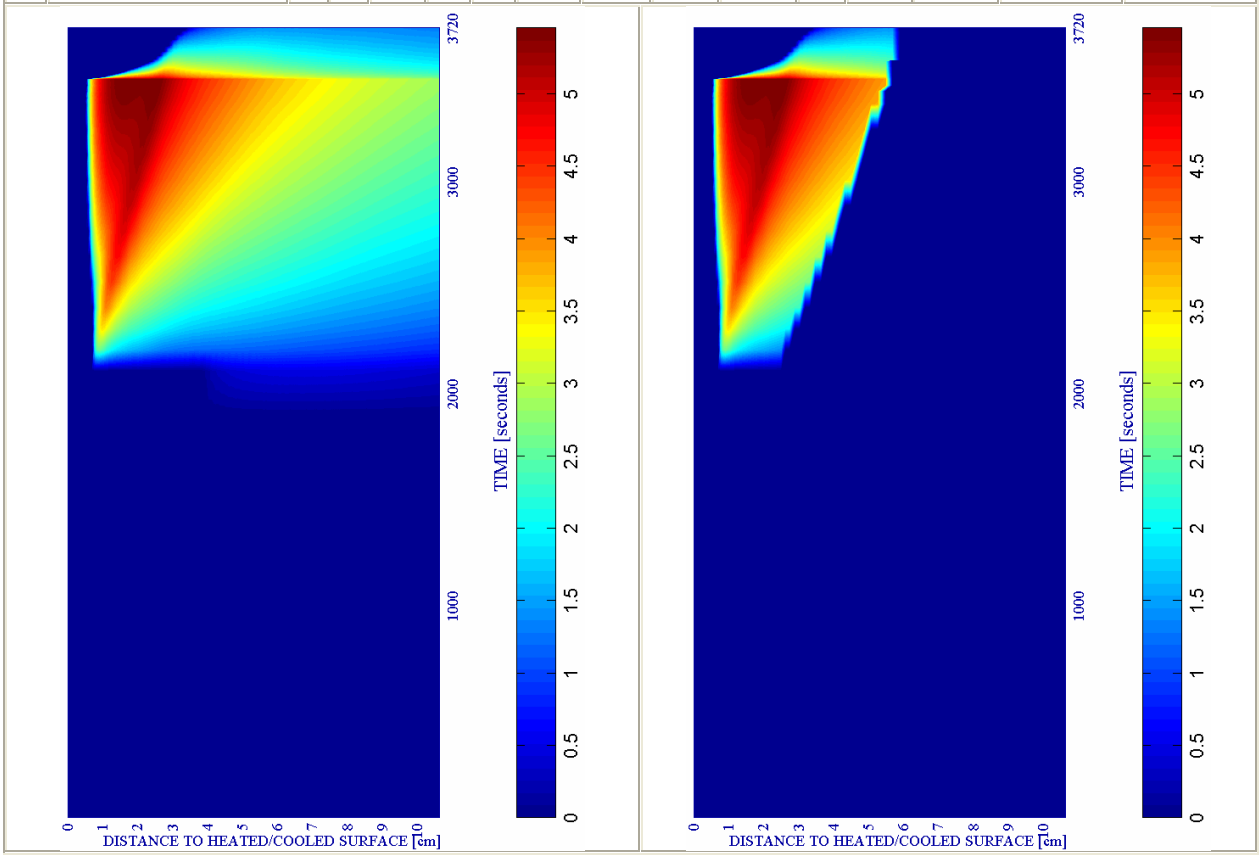

c) Velocity of spalled pieces v [m/s] ***Figure 6-151.*** ***(Cooling rate = -136,6 K/s)*** *d) Velocity [m/s] where d ≥ 0,10*

e) Gas pressure $p^g \cdot 10^{-5}$ [Pa]

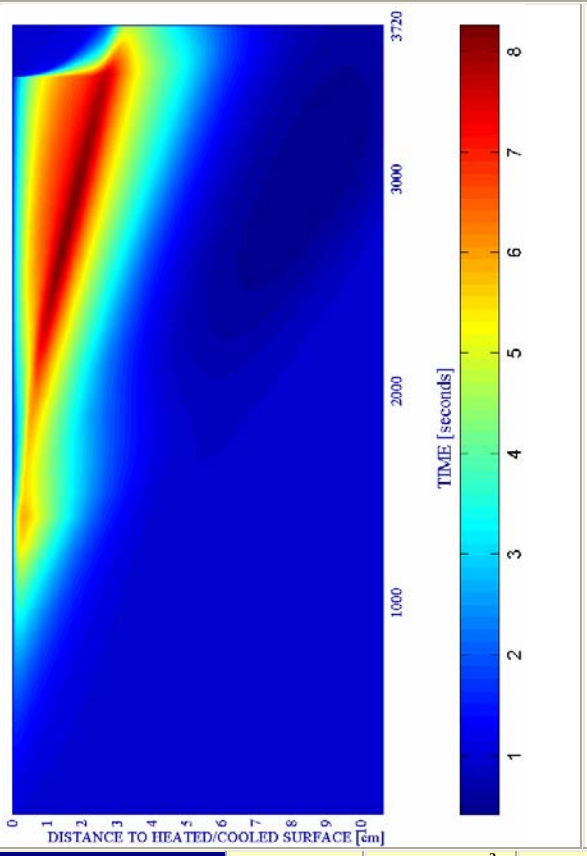

f) Vapour pressure $p^v \cdot 10^{-5}$ [Pa]

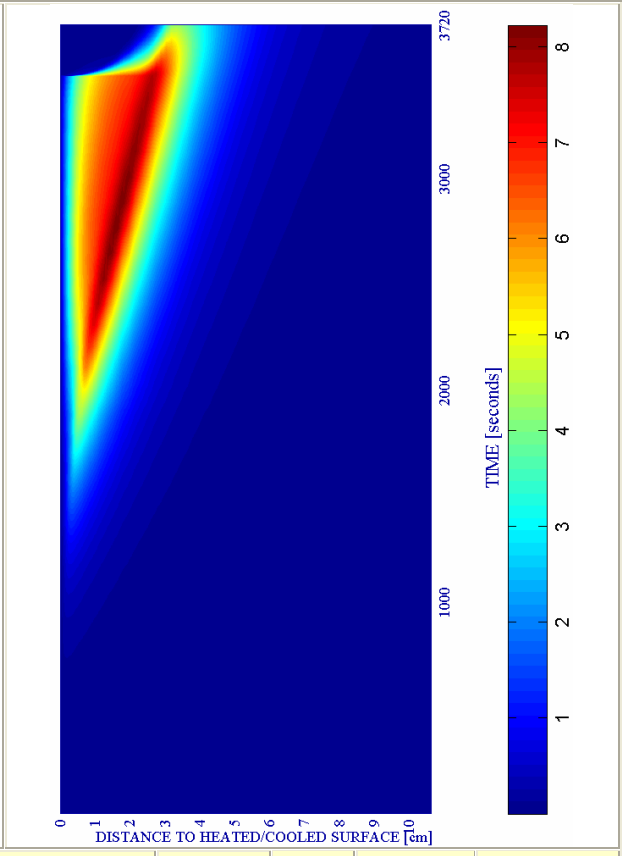

SURFACE COOL+KEEP		PC1 - RH [%]			PC2 - K_0 [m^2]			PC4 - Heating curve			PC5 – Mat.		Cooling length[s]	Start of cooling [s]	End of cooling [s]
#	Combination	40	50	60	10^{-19}	10^{-18}	10^{-17}	PAR1	PAR2	PAR4	C60	C90			
14	TH12K018RH50PAR2C60		X			X			X		X		2,7	3.360+120	3.482,70

g) Saturation Degree S [-]

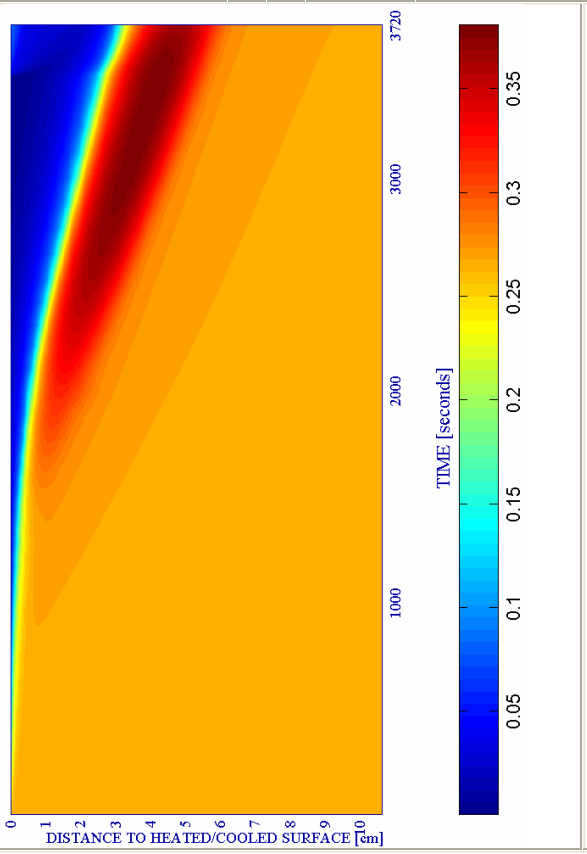

Figure 6-151. (continued) ***(Cooling rate = -136,6 K/s)***

h) Relative Humidity RH [-]

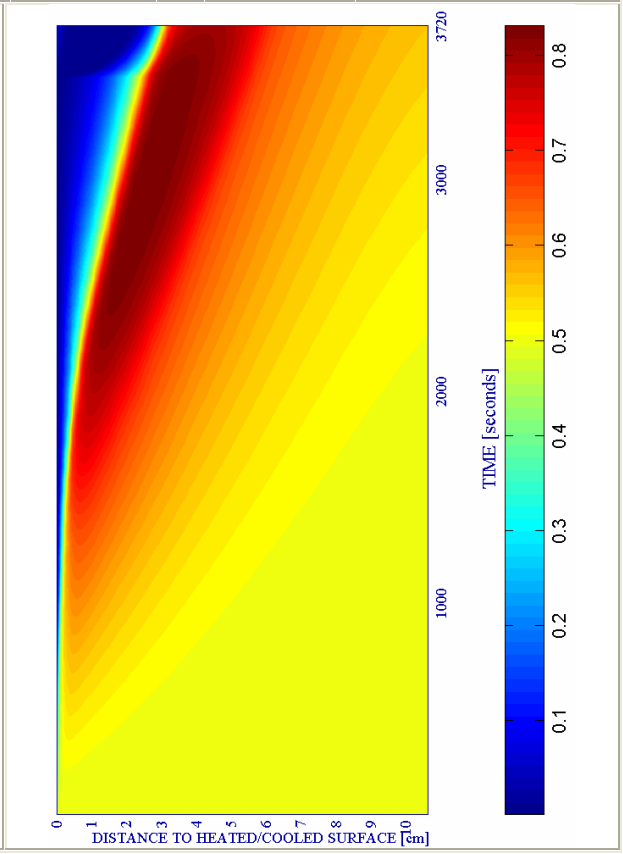

i) Temperature [K]

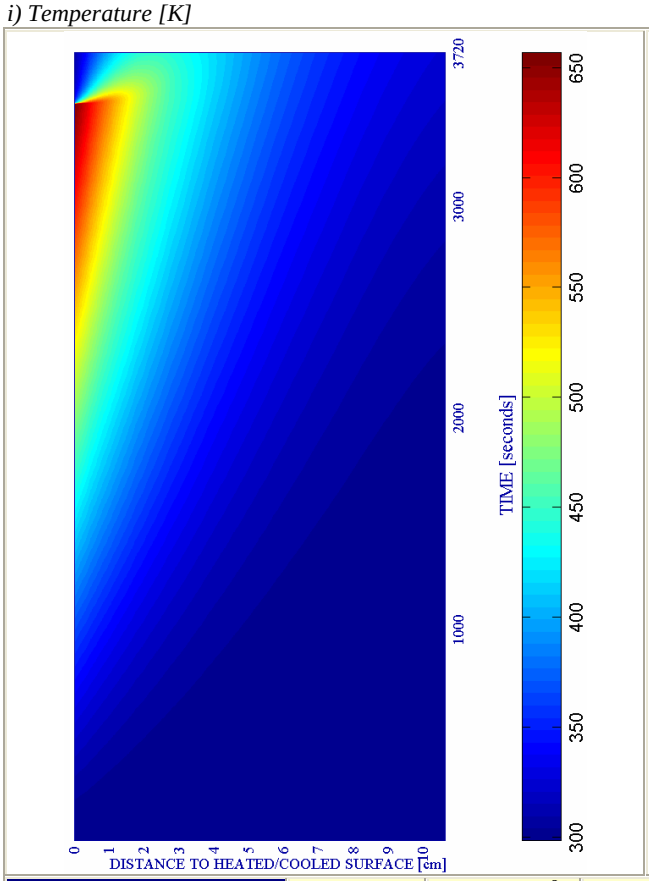

*j) Elastic Energy U · **10**$^{-4}$ [J/m^3]*

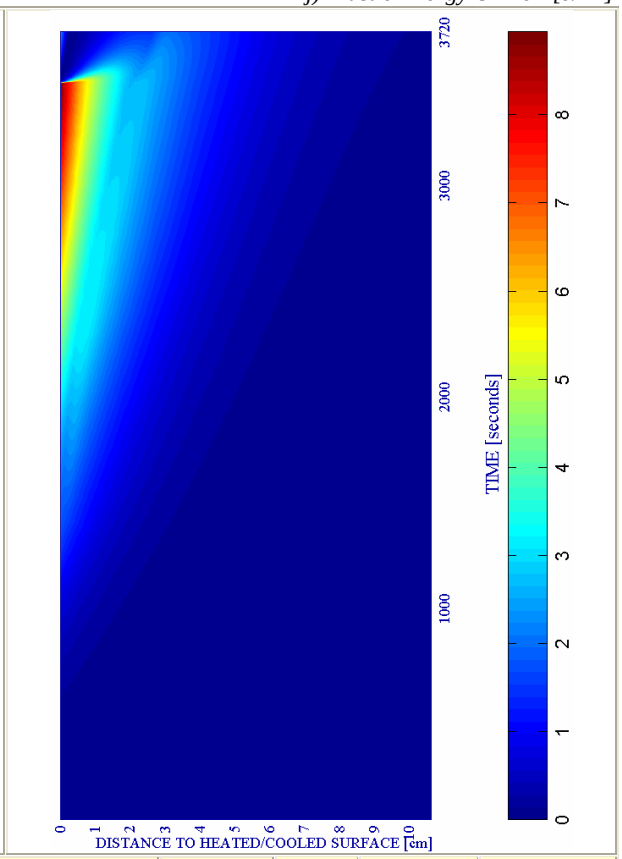

SURFACE COOL+KEEP		PC1 - RH [%]			PC2 - K_0 [m^2]			PC4 - Heating curve			PC5 – Mat.		Cooling length[s]	Start of cooling [s]	End of cooling [s]
#	Combination	40	50	60	10^{-19}	10^{-18}	10^{-17}	PAR1	PAR2	PAR4	C60	C90			
14	TH12K018RH50PAR2C60		X			X			X		X		2,7	3.360+120	3.482,70

*k) Stress in longitudinal (xx) direction · **10**$^{-6}$ [Pa]*

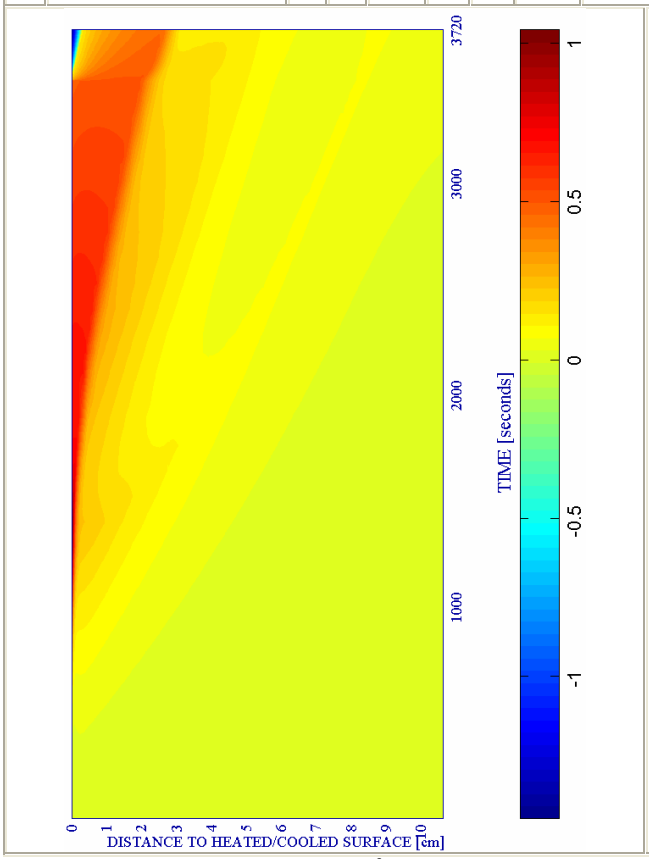

***Figure 6-151.** (Cooling rate = -136,6 K/s)*

*l) Stress in transversal (yy) direction · **10**$^{-7}$ [Pa]*

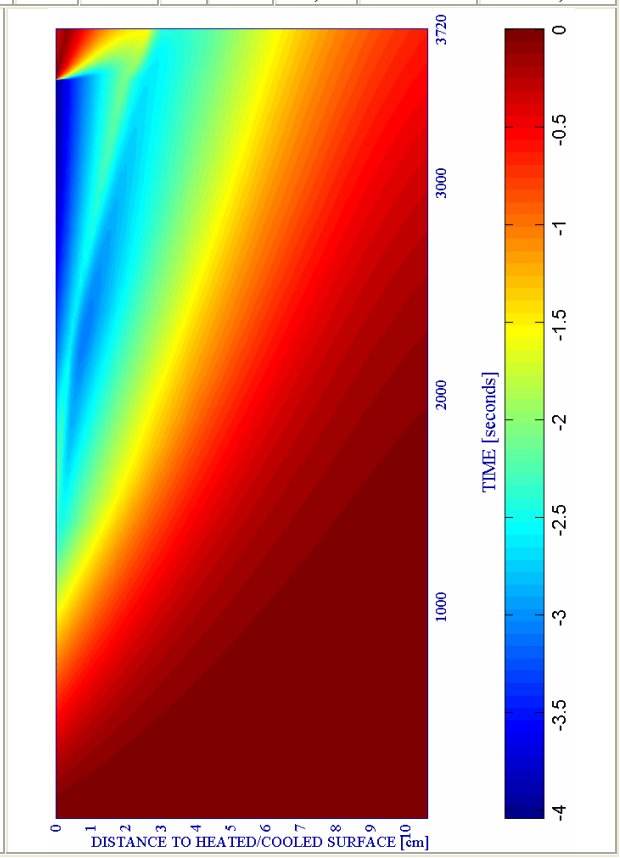

However, thermal spalling is energetically viable until the end of the time interval considered (despite compressive stresses appear close to the surface, tensile stresses keep present at the inner layers, where both the constrained energy and the gas pressure are still high enough to make thermal spalling viable) as it is shown on figures 152 (and figure 151 c)) and 153 (and figure 151 d)):

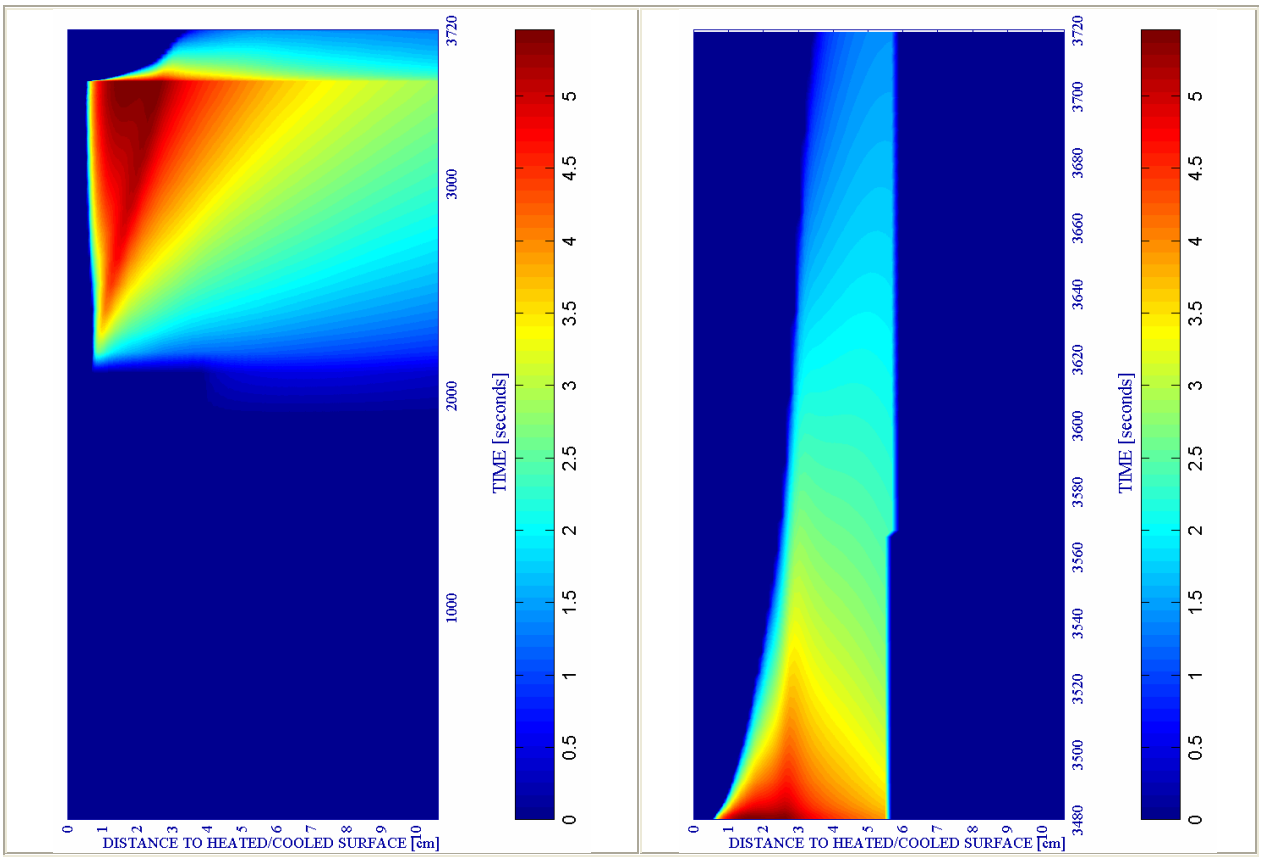

Figure 6-152. *Velocity of spalled pieces v [m/s]*

Figure 6-153. *Velocity [m/s] where d ≥ 0,10 at the structural element from the start of the cooling process until the end of the calculation.*

The set of results analyzed herein show that this extreme cooling rate is neither qualitatively different nor worse, from the Thermal Spalling risk point of view, than those corresponding to the case analyzed in paragraph 6.5.2.5.5 where a cooling rate of only the 7 per cent of that considered in this paragraph was applied.

Finally, it must also be observed that both undergoing atmospheric pressure in particular zones far from the cooled surface and the infiltration of humidity from the environment across the cooled surface phenomena are again appearing in this case.

6.5.2.6.2 Surface Cooling followed by an imposed Constant Surface Temperature: Cooling Rate -32,36K/s

The consideration of a cooling rate of -32,36 K/second instead of the extreme value considered in last paragraph leads to qualitatively identical results than those previously exposed, as it can be observed on figures 154 a) to l). However, this comparison will be analyzed in a deep detail within the comparative analysis developed on paragraph 6.5.3.

a) Spalling Index IS4 [-] *b) Mechanical damage d [-]*

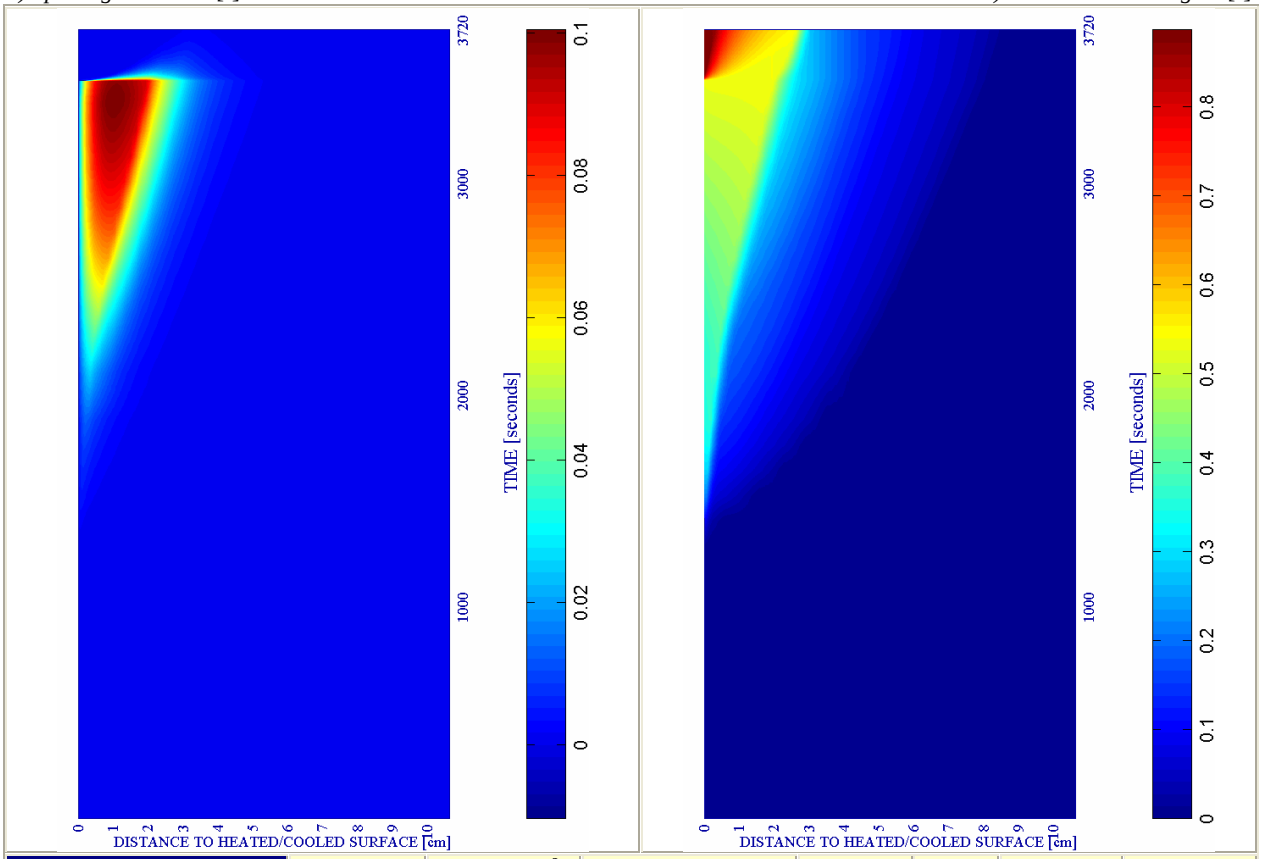

SURFACE COOL+KEEP		PC1 - RH [%]			PC2 - K_0 [m^2]			PC4 - Heating curve			PC5 – Mat.		Cooling length[s]	Start of cooling [s]	End of cooling [s]
#	Combination	40	50	60	10^{-19}	10^{-18}	10^{-17}	PAR1	PAR2	PAR4	C60	C90			
14	TH12K018RH50PAR2C60		X			X			X		X		10	3.360+120	3.490

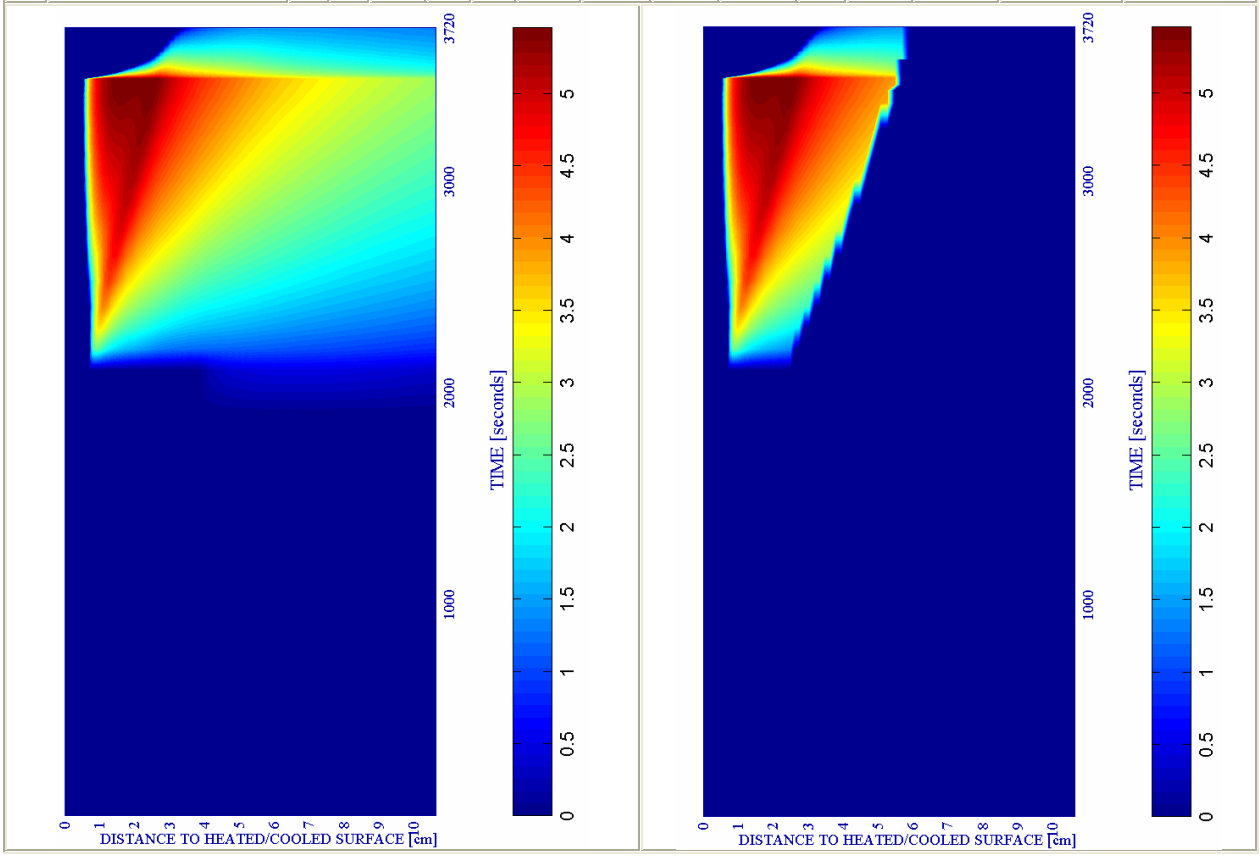

c) Velocity of spalled pieces v [m/s] ***Figure 6-154.*** ***(Cooling rate = -32,36 K/s)*** *d) Velocity [m/s] where d ≥ 0,10*

e) Gas pressure $p^g \cdot 10^{-5}$ [Pa]

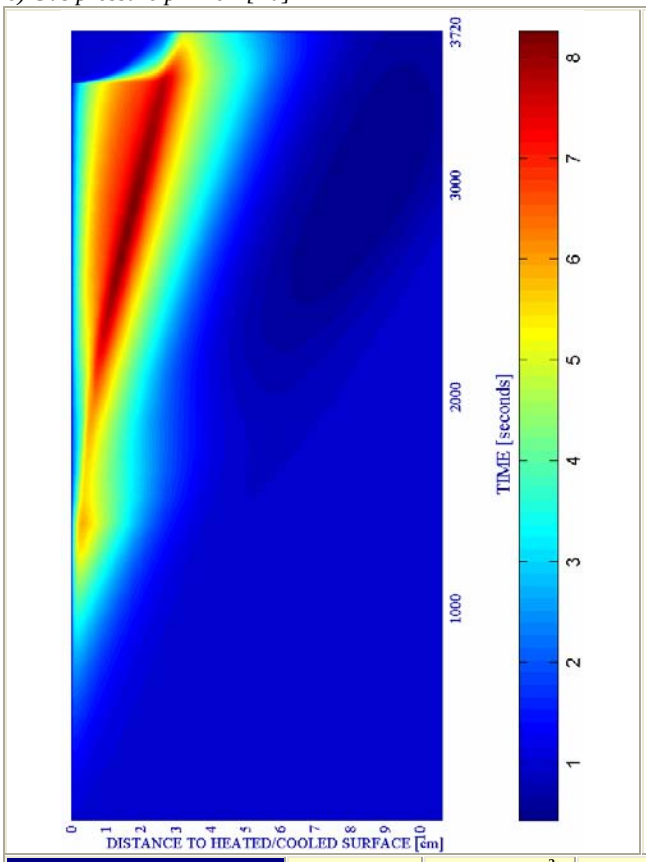

f) Vapour pressure $p^v \cdot 10^{-5}$ [Pa]

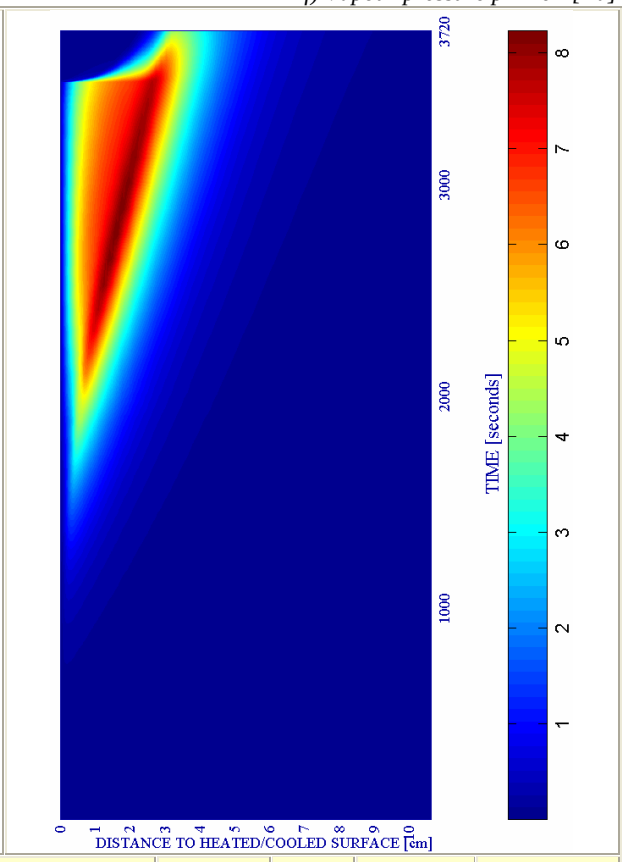

SURFACE COOL+KEEP		PC1 - RH [%]			PC2 - K_0 [m^2]			PC4 - Heating curve			PC5 – Mat.		Cooling length[s]	Start of cooling [s]	End of cooling [s]
#	Combination	40	50	60	10^{-19}	10^{-18}	10^{-17}	PAR1	PAR2	PAR4	C60	C90			
14	TH12K018RH50PAR2C60		X			X			X		X		10	3.360+120	3.490

g) Saturation Degree S [-]

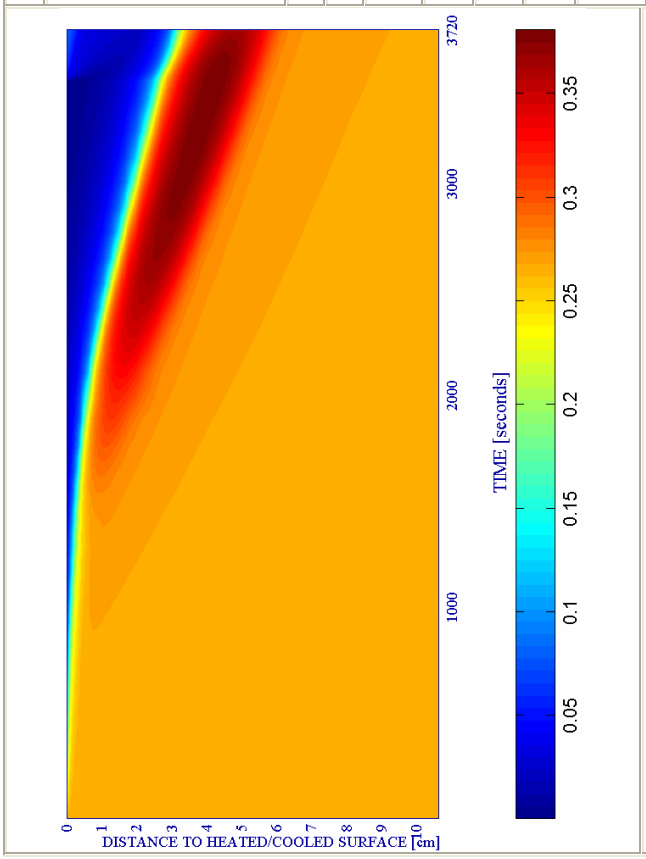

h) Relative Humidity RH [-]

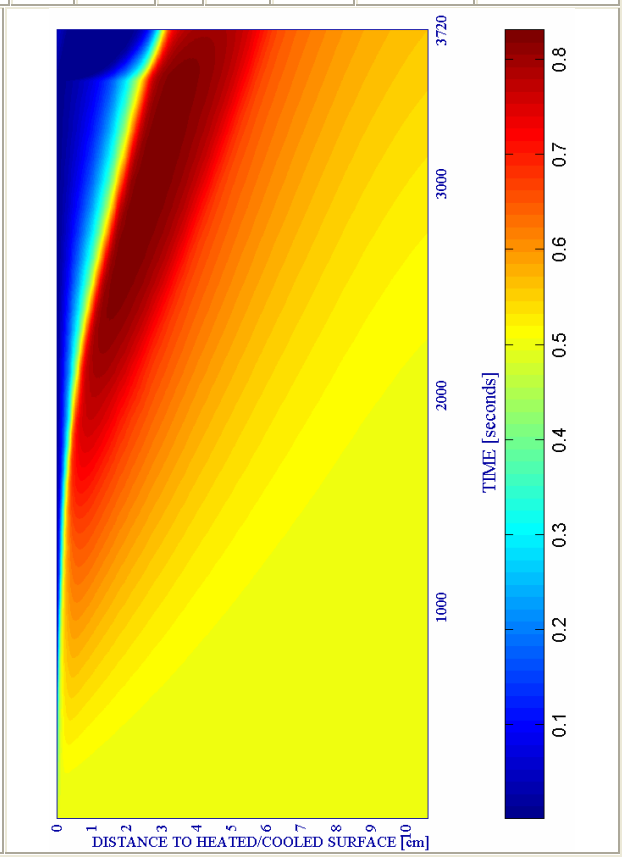

Figure 6-154. (continued) ***(Cooling rate = -32,36 K/s)***

i) Temperature [K] *j) Elastic Energy U · **10^{-4}** [J/m^3]*

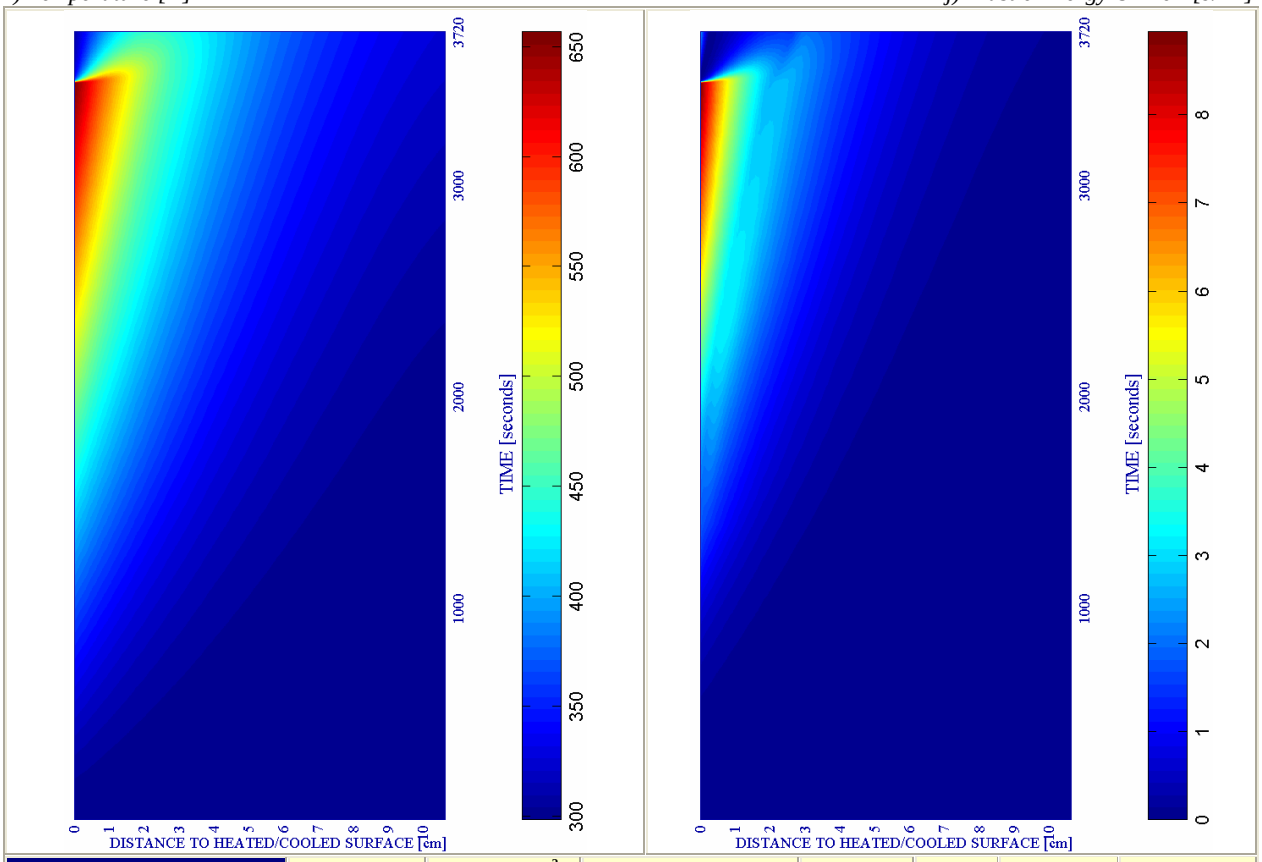

SURFACE COOL+KEEP		PC1 - RH [%]			PC2 - K_0 [m^2]			PC4 - Heating curve			PC5 – Mat.		Cooling length[s]	Start of cooling [s]	End of cooling [s]
#	Combination	40	50	60	10^{-19}	10^{-18}	10^{-17}	PAR1	PAR2	PAR4	C60	C90			
14	TH12K018RH50PAR2C60		X			X			X		X		10	3.360+120	3.490

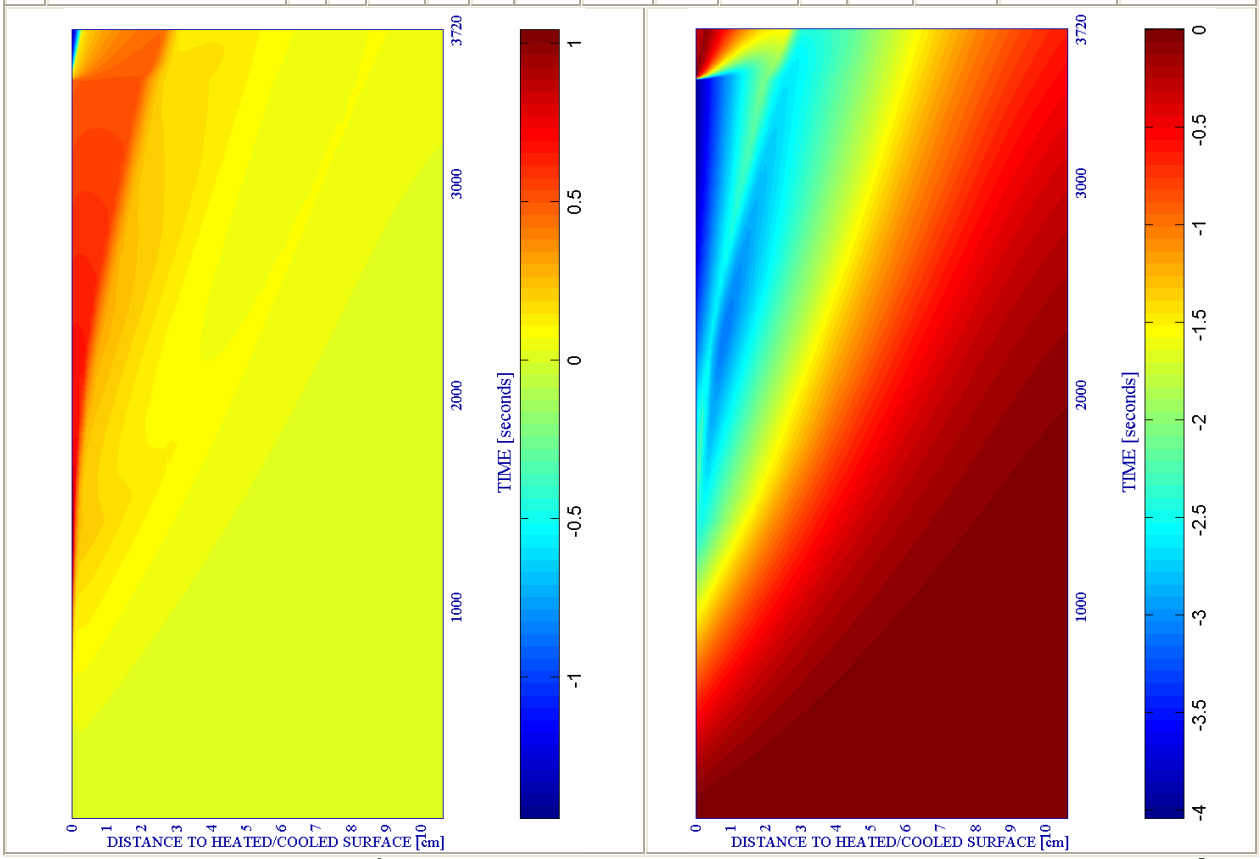

*k) Stress in longitudinal (xx) direction · **10^{-6}** [Pa]* ***Figure 6-154.** (Cooling rate = -32,36 K/s)* *l) Stress in transversal (yy) direction · **10^{-7}** [Pa]*

6.5.2.7 REFERENCE CASE # 100 – TH12K019RH50PAR4C90 – START OF COOLING: 4.800S

The main features of this reference case are the following ones:

		PC1 (RH) [%]			PC2 (K) [m^2]			PC3 (TH) [cm]			PC4 (Heating curve)			PC5 (Mat)	
#	**Combination**	**40**	**50**	**60**	10^{-19}	10^{-18}	10^{-17}	**12**	**24**	**50**	**PAR1**	**PAR2**	**PAR4**	**C60**	**C90**
100	TH12K019RH50PAR4C90		X		X			X					X		X

Table 6-101. *Main Features of the Reference Case #100 – TH12K019RH50PAR4C90.*

with an starting instant of the first cooling process at 4.800 seconds. The types and subtypes of cooling processes analyzed in this reference case are the following ones:

Type of Cooling	***Subtype of Cooling***	***Related Paragraph***	***Figures numbers***
Surface	Followed by Heating	6.5.2.7.1	6-155 to 6-156
Environment Heating up to three hours (10.800 seconds) without any cooling		6.5.2.7.2	6-157 a) to l)

Remark: *See each Paragraph for more details on the features of the Cooling Processes.*

Table 6-102. *Types and Subtypes of Cooling Processes Analyzed in the Reference Case #100 – TH12K019RH50PAR4C90 with the Start of Cooling Process at 4.800 seconds*

6.5.2.7.1 Surface First Cooling

Next it is shown a collection of the main results cited in this subparagraph, as well as a description of each of the stages that compose the heating process analyzed herein.

Table 6-103. *Description of the Cooling Process Stages and Collection of the Main Results related to Spalling Index and velocity*

Stage description	**Absolute Time Start [s]**	**Absolute Time End [s]**	$IS4_{max}$ [-]	X_{IS4max} [cm]	t_{IS4max} [s]	v_{max} [m/s]	X_{vmax} [cm]	t_{vmax} [s]	v_{max}* [m/s]	X_{vmax*} [cm]	t_{vmax*} [s]
First Heating	0	4.800	0,0690	0,710	4.800	6,096	0,175	2.925	4,021	1,238	4.800
Surface cooling	4.800	4.820	0,0690	0,710	4.800	4,021	1,238	4.800	4,021	1,238	4.800
Absolute Maximum	0	4.820	0,0690	0,710	4.800	6,096	0,175	2.925	4,021	1,238	4.800

Remark †***:*** *These results are included for the Comparative Analysis developed on Paragraph 6.5.3*

Stage description	**Absolute Time Start [s]**	**Absolute Time End [s]**	d_{max} [-]	X_{dmax} [cm]	t_{dmax} [s]	T_{max} [K]	X_{Tmax} [cm]	t_{Tmax} [s]	p^g_{max} [MPa]	X_{pgmax} [cm]	t_{pgmax} [s]
First Heating	0	4.800	0,6622	0,710	4.800	548,24	0,000	4.800	1,0564	0,194	2.925
Surface cooling	4.800	4.820	0,9246	0,001	4.820	548,24	0,000	4.800	0,9583	1,238	4.800
Absolute Maximum	0	4.820	0,9246	0,001	4.820	548,24	0,000	4.800	1,0564	0,194	2.925

Table 6-104. *Description of the Cooling Process Stages and Collection of the Main Results related to mechanical damage, Temperature and Gas Pressure*

On figure 6-155 it is shown the evolution, at the 2 first centimetres close to the heated/cooled surface, of several parameters favouring and impeding thermal spalling occurrence during the 20 seconds surface cooling considered. Hence, it is clearly observed how in a period as short as 20 seconds the values of mechanical damage (and therefore the level of cracking) close to the surface rise up in more than a 30 per cent while pressure in the first centimetre falls down to atmospheric values, elastic energy decreases significantly and the tensile longitudinal stresses level close to the surface descend to a 10 per cent of their value corresponding to the start of the cooling process.

This means that, once more, the values of the Spalling Index IS_4 (figure 6-156 a)) decrease during the surface cooling at all the depths of the structural element, as well as the available energy for the Thermal Spalling to occur (figures 6-156 c)) and 6-156 d)). Neither the considered values of the heating curve and the intrinsic permeability nor the material assumed, seem to affect these conclusions widely deducted from this Chapter, being the qualitative analysis of the involved phenomena analogous to those previously exposed.

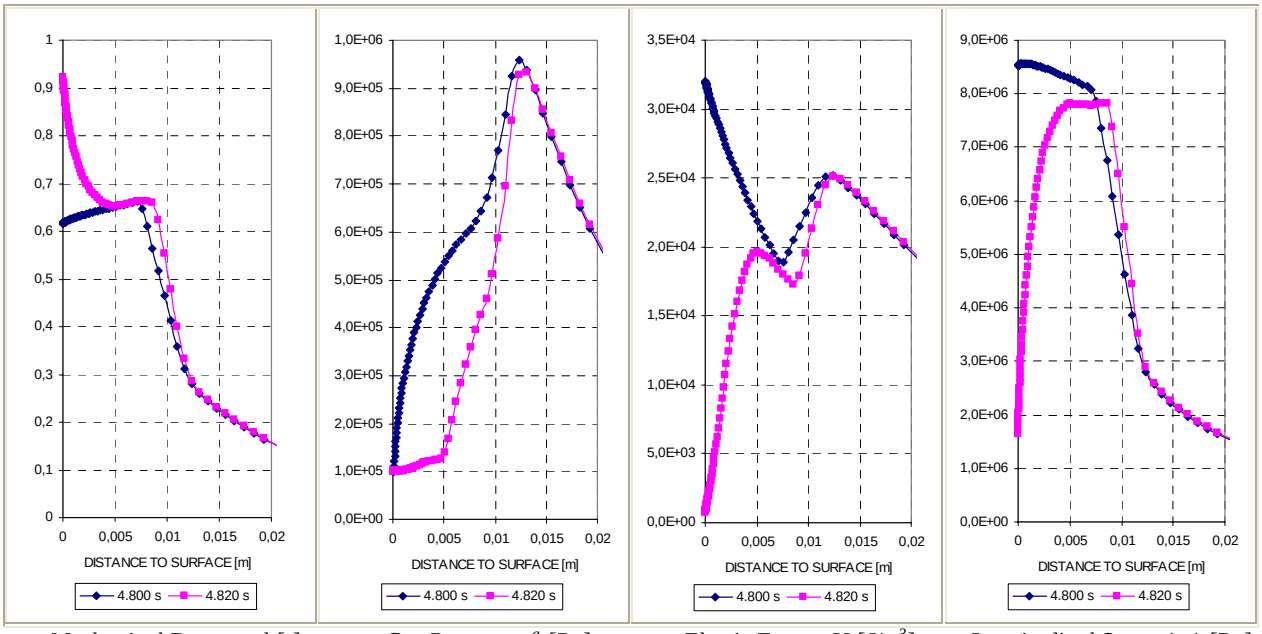

Mechanical Damage d [-] *Gas Pressure p^g [Pa]* *Elastic Energy U [J/m^3]* *Longitudinal Stress (xx) [Pa]*

Figure 6-155. *Evolution of several parameters during the surface cooling stage.*

6.5.2.7.2 Environmental Heating up to Three hours Without any Cooling

Next it is shown a collection of the main results cited in this subparagraph, as well as a description of each of the stages that compose the heating process analyzed herein.

Table 6-105. *Description of the Cooling Process Stages and Collection of the Main Results related to Spalling Index and velocity*

Stage description	Absolute Time Start [s]	Absolute Time End [s]	$IS4_{max}$ [-]	X_{IS4max} [cm]	t_{IS4max} [s]	v_{max} [m/s]	X_{vmax} [cm]	t_{vmax} [s]	v_{max}* [m/s]	X_{vmax*} [cm]	t_{vmax*} [s]
Heating up to 10.800s	0	10.800	0,0867	1,035	6.000	6,096	0,165	2.925	4,068	1,644	5.250

Remark †***:*** *These results are included for the Comparative Analysis developed on Paragraph 6.5.3*

Stage description	Absolute Time Start [s]	Absolute Time End [s]	d_{max} [-]	X_{dmax} [cm]	t_{dmax} [s]	T_{max} [K]	X_{Tmax} [cm]	t_{Tmax} [s]	p^g_{max} [MPa]	X_{pgmax} [cm]	t_{pgmax} [s]
Heating up to 10.800s	0	10.800	0,8517	0,000	10.800	800,71	0,000	10.800	1,0564	0,194	2.925

Table 6-106. *Description of the Cooling Process Stages and Collection of the Main Results related to mechanical damage, Temperature and Gas Pressure*

It is remarkable to observe from figure 6-157 e) that two peaks of gas pressure appear during the heating process: The first gas pressure peak, at approximately 2.925 seconds from the beginning of the heating, is mainly due to a sharp increase in the dry air pressure (vapour pressure is still low at all depths at this instant) and it leads to a 'spot' in the evolution map of the available energy (figure 6-157 c)) where Thermal Spalling would be possible if the cracking level were high enough.

After that the second gas pressure peak, appearing farther from the heated surface and at approximately 4.950 seconds from the beginning of the heating, is due to an increase in the vapour pressure (figure 6-157 f)) and leads to the maximum value of the Spalling Index IS_4, as it is seen in figure 6-157 a). This gas pressure peak translates into a double evolution of the constrained elastic energy (figure 6-157 j)) since it shows peak values not only next to the heated surface but also in a position progressively farther from this surface whose position matches the maximum of vapour pressure. The highest transversal (yy) stresses also appear in this second branch.

The comparison of this case against that including the surface cooling will be analyzed within the comparative analysis developed on paragraph 6.5.3.

a) Spalling Index IS4 [-]

b) Mechanical damage d [-]

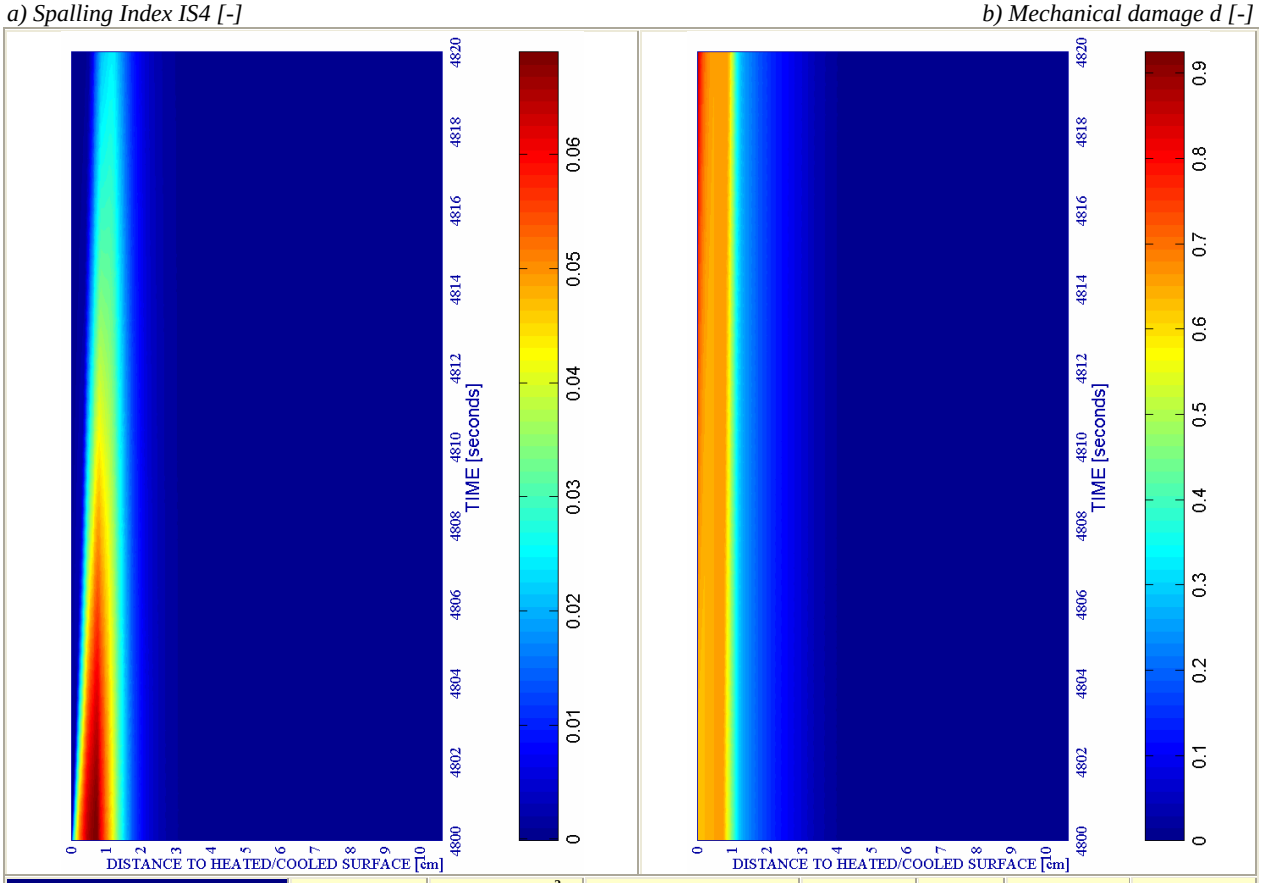

SURFACE FIRST COOLING		PC1 - RH [%]			PC2 - K_0 [m^2]			PC4 - Heating curve			PC5 – Mat.		Cooling length[s]	Start of cooling [s]	End of cooling [s]
#	Combination	40	50	60	10^{-19}	10^{-18}	10^{-17}	PAR1	PAR2	PAR4	C60	C90			
100	TH12K019RH50PAR4C90		X		X					X		X	20	4.800	4.820

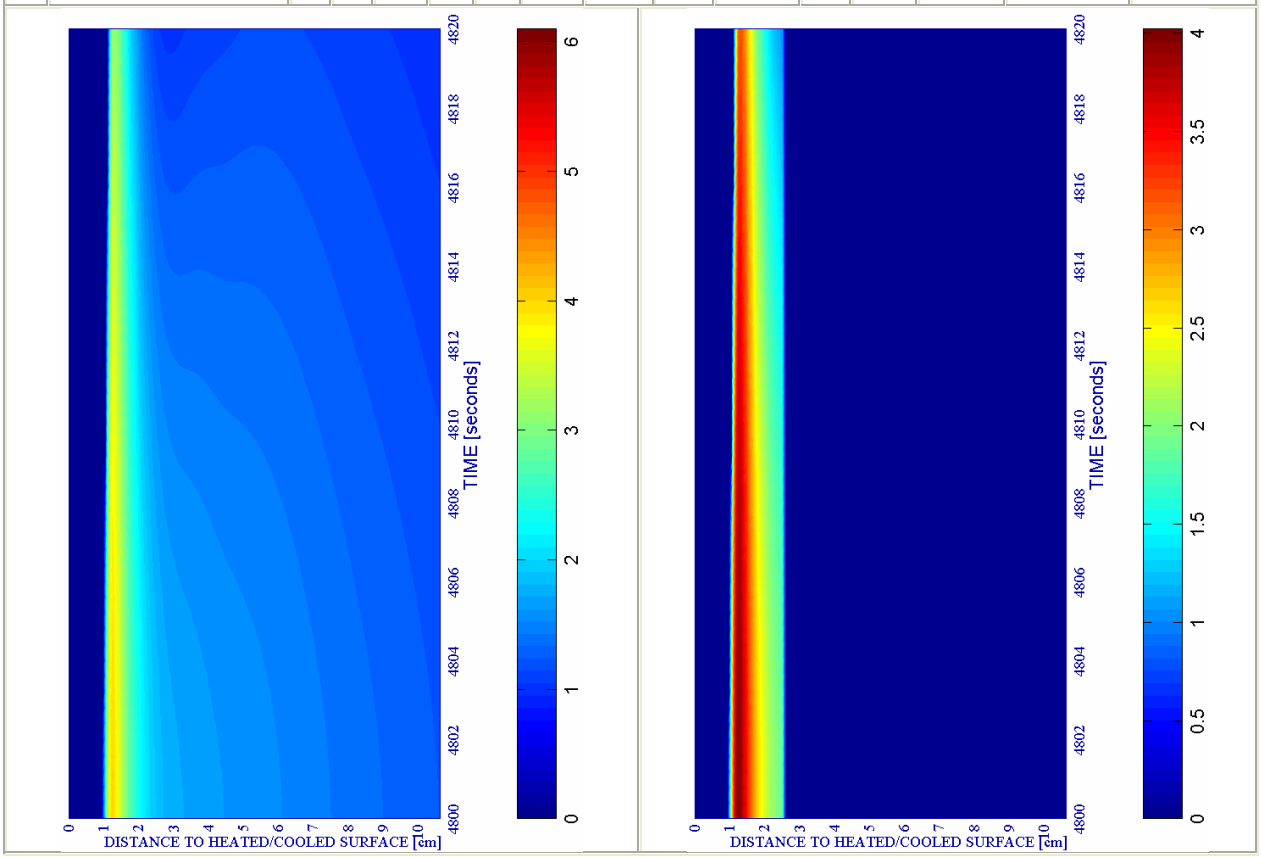

c) Velocity of spalled pieces v [m/s]

Figure 6-156.

d) Velocity [m/s] where d ≥ 0,10

e) Gas pressure $p^g \cdot 10^{-5}$ [Pa]

f) Vapour pressure $p^v \cdot 10^{-5}$ [Pa]

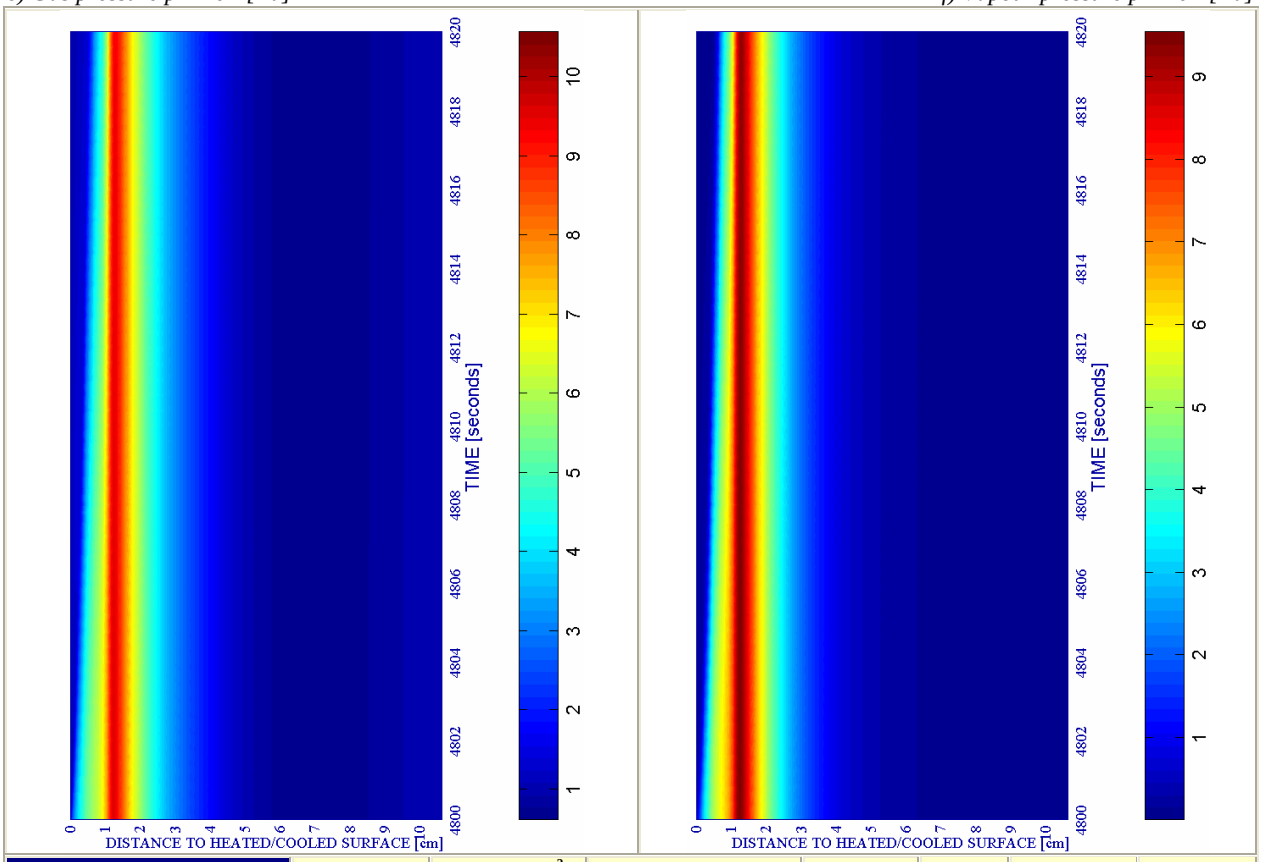

SURFACE FIRST COOLING		PC1 - RH [%]			PC2 - K_0 [m^2]			PC4 - Heating curve			PC5 – Mat.		Cooling length[s]	Start of cooling [s]	End of cooling [s]
#	Combination	40	50	60	10^{-19}	10^{-18}	10^{-17}	PAR1	PAR2	PAR4	C60	C90			
100	TH12K019RH50PAR4C90		X		X					X		X	20	4.800	4.820

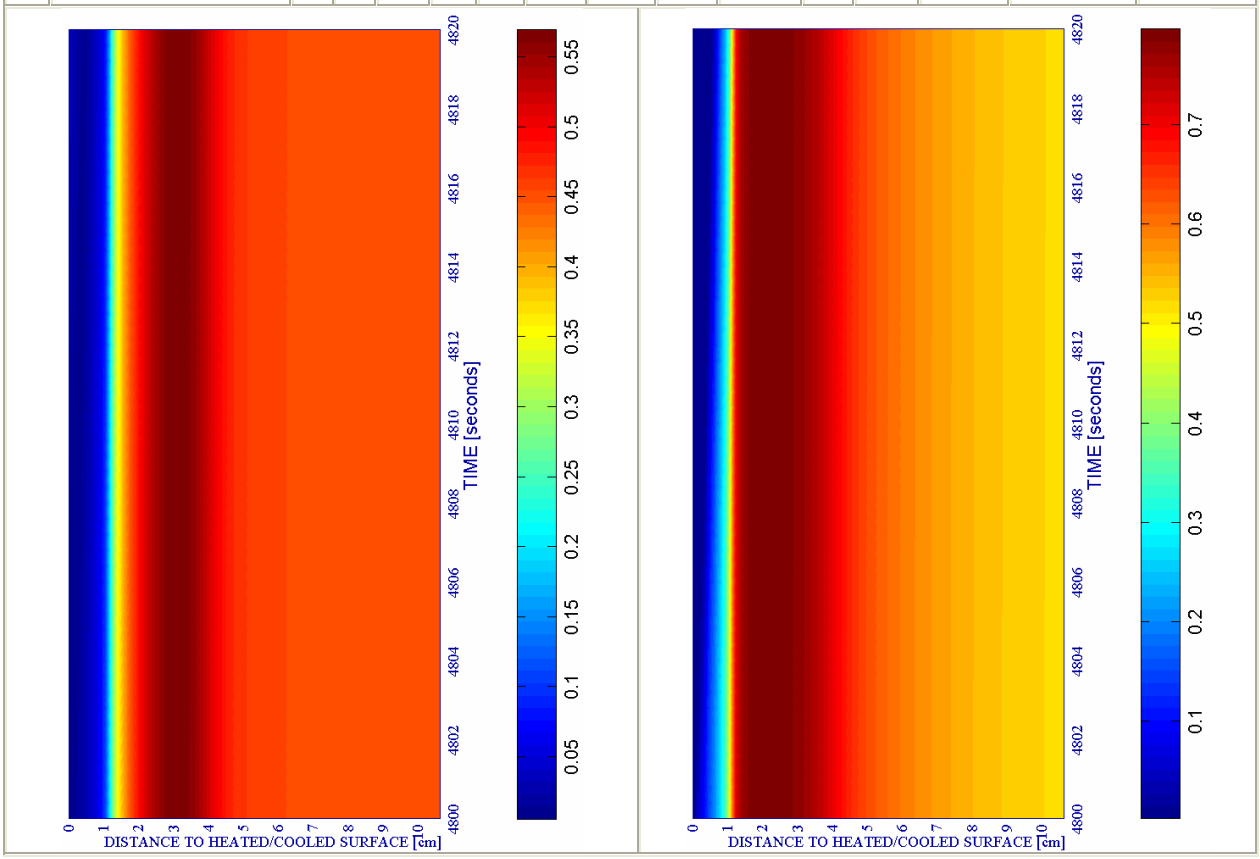

g) Saturation Degree S [-]

Figure 6-156. (continued)

h) Relative Humidity RH [-]

i) Temperature [K] *j) Elastic Energy U · 10^{-4} [J/m^3]*

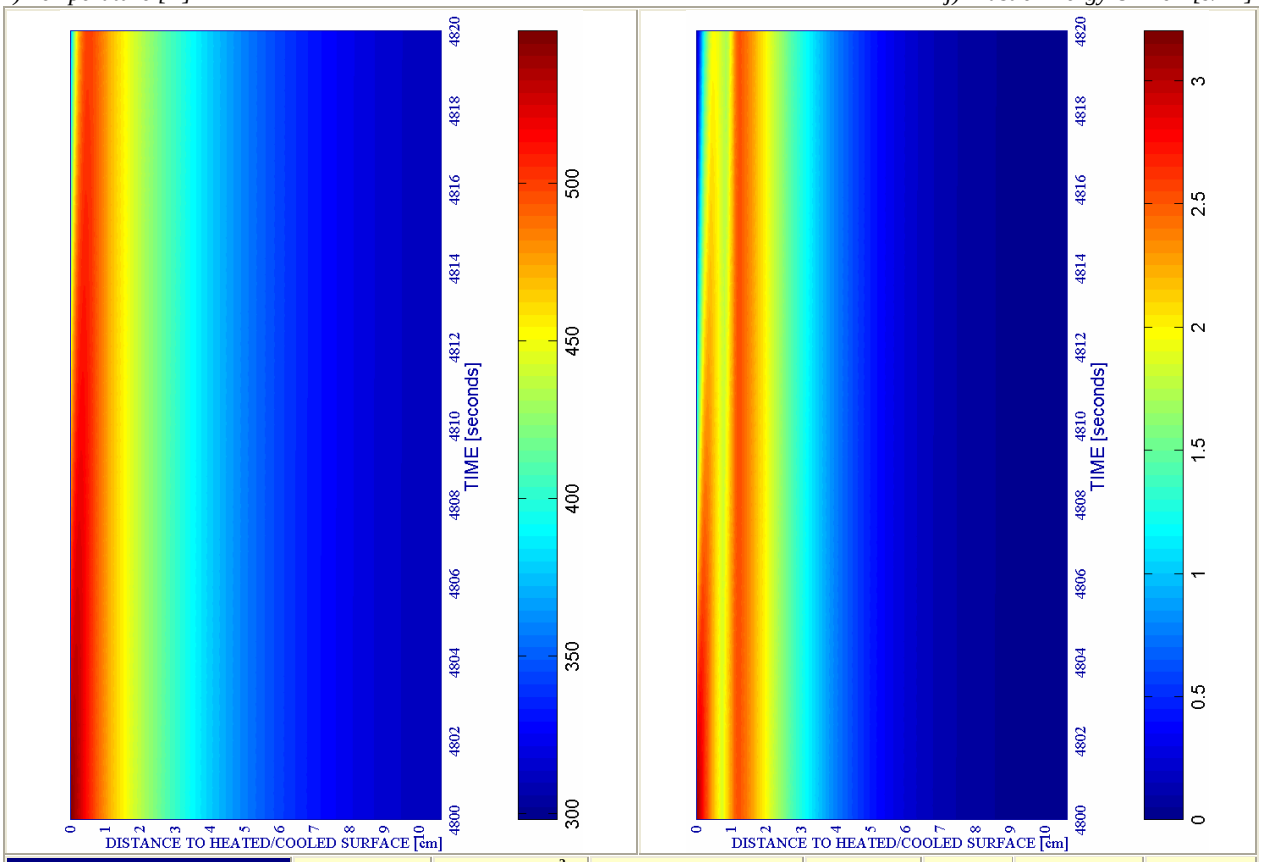

SURFACE FIRST COOLING	PC1 - RH [%]			PC2 - K_0 [m^2]			PC4 - Heating curve			PC5 – Mat.		Cooling length[s]	Start of cooling [s]	End of cooling [s]
#	Combination	40	50	60	10^{-19}	10^{-18}	10^{-17}	PAR1	PAR2	PAR4	C60	C90			
100	TH12K019RH50PAR4C90		X		X					X		X	20	4.800	4.820

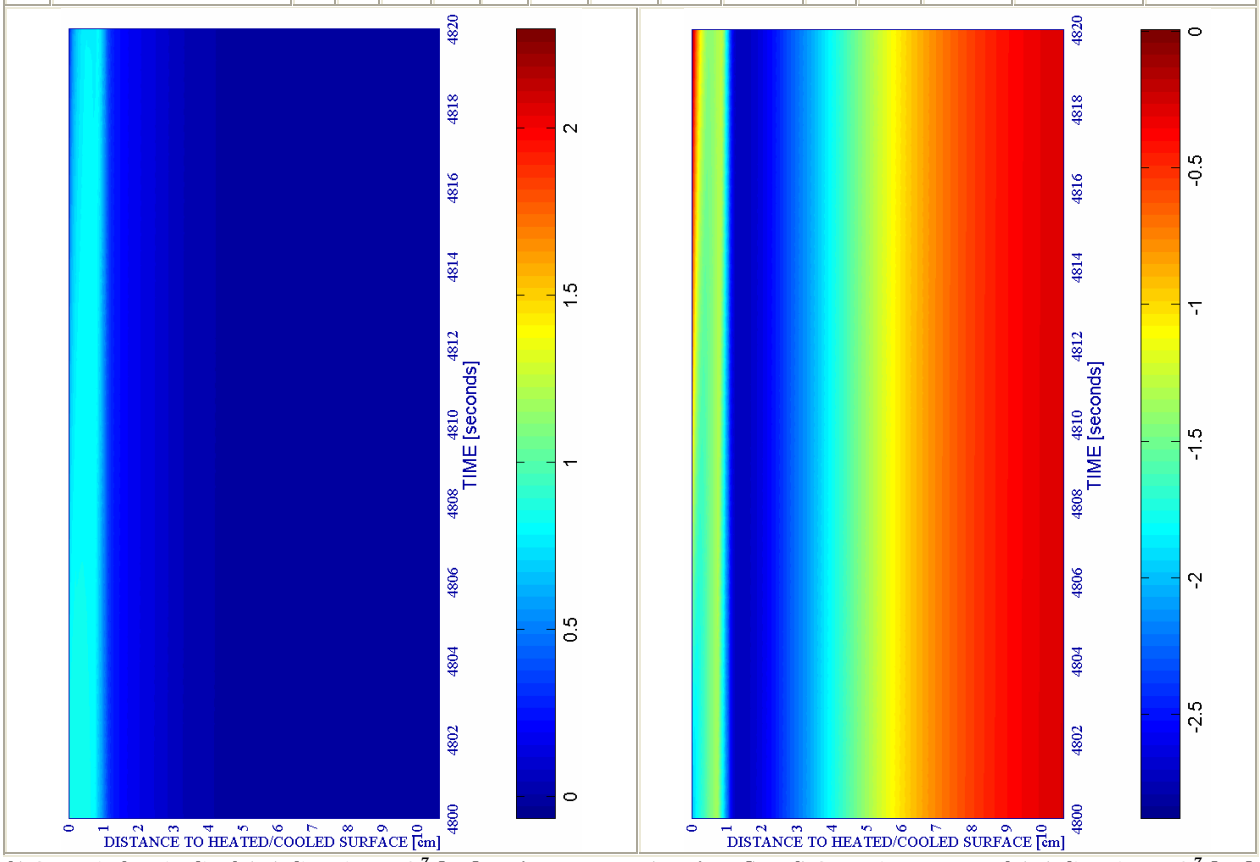

k) Stress in longitudinal (xx) direction · 10^{-7} [Pa] ***Figure 6-156. (continued)*** *l) Stress in transversal (yy) direction · 10^{-7} [Pa]*

a) Spalling Index IS4 [-]

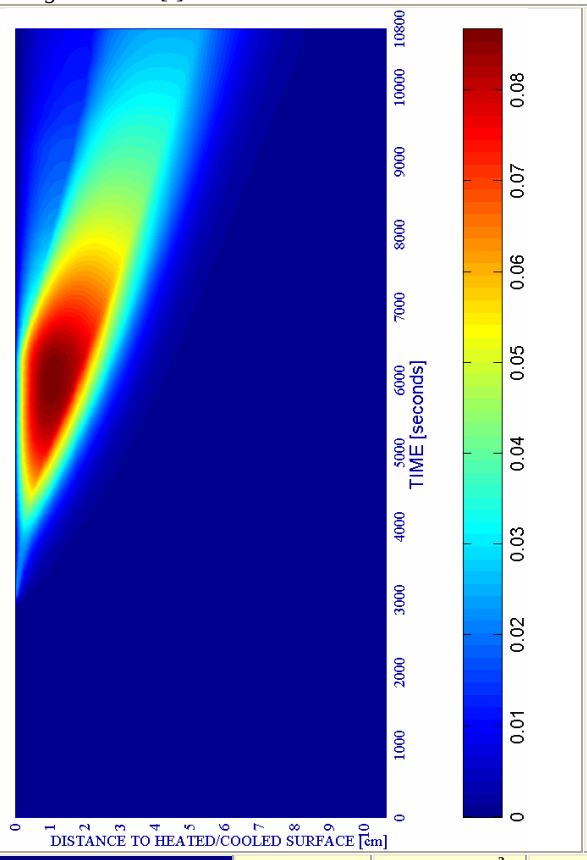

b) Mechanical damage d [-]

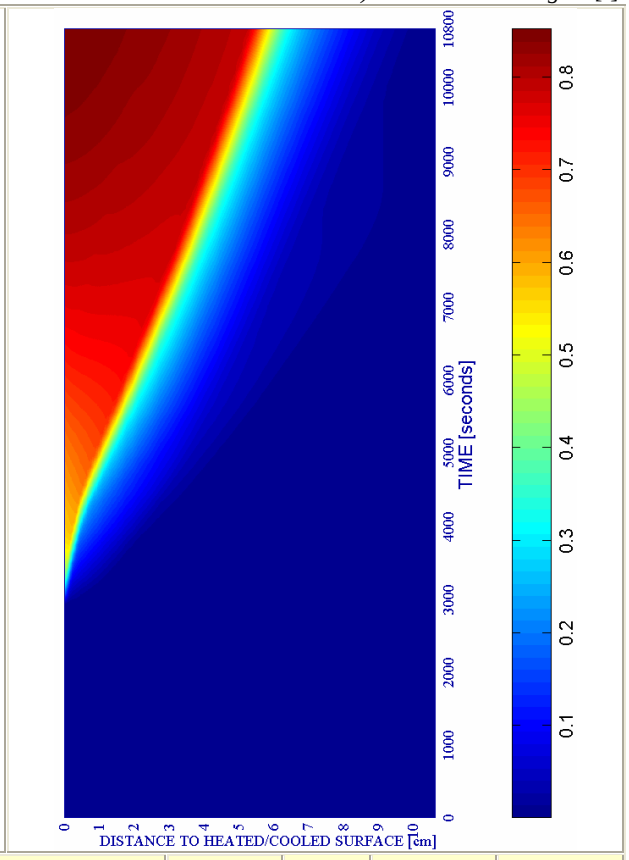

WITHOUT COOLING		PC1 - RH [%]			PC2 - K_0 [m^2]			PC4 - Heating curve			PC5 – Mat.		Cooling length[s]	Start of cooling [s]	End of cooling [s]
#	Combination	40	50	60	10^{-19}	10^{-18}	10^{-17}	PAR1	PAR2	PAR4	C60	C90			
100	TH12K019RH50PAR4C90		X		X					X		X	---	---	---

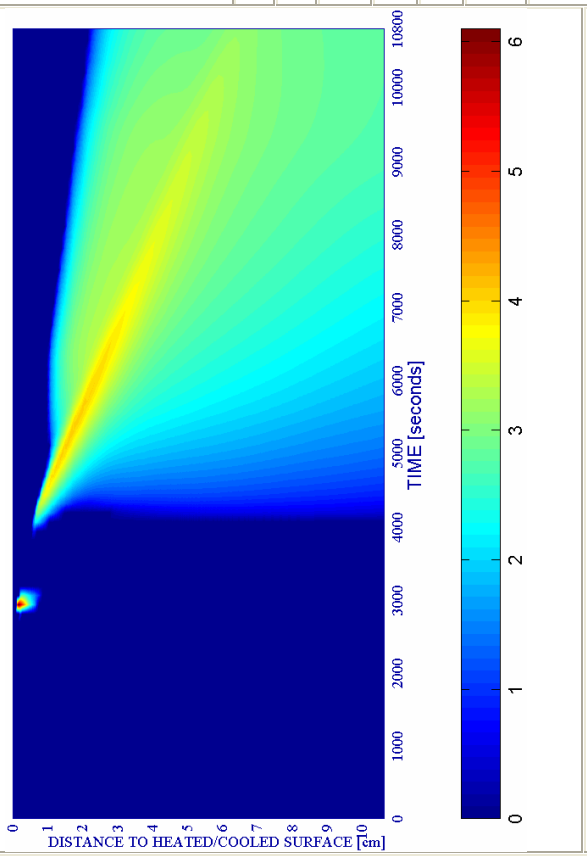

c) Velocity of spalled pieces v [m/s]

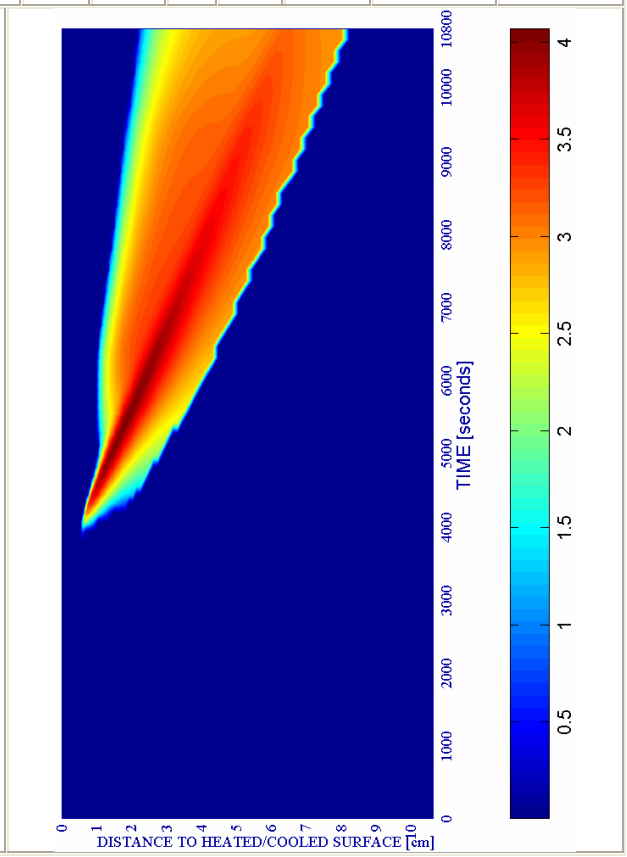

d) Velocity [m/s] where d ≥ 0,10

Figure 6-157.

e) Gas pressure $p^g \cdot 10^{-5}$ [Pa]

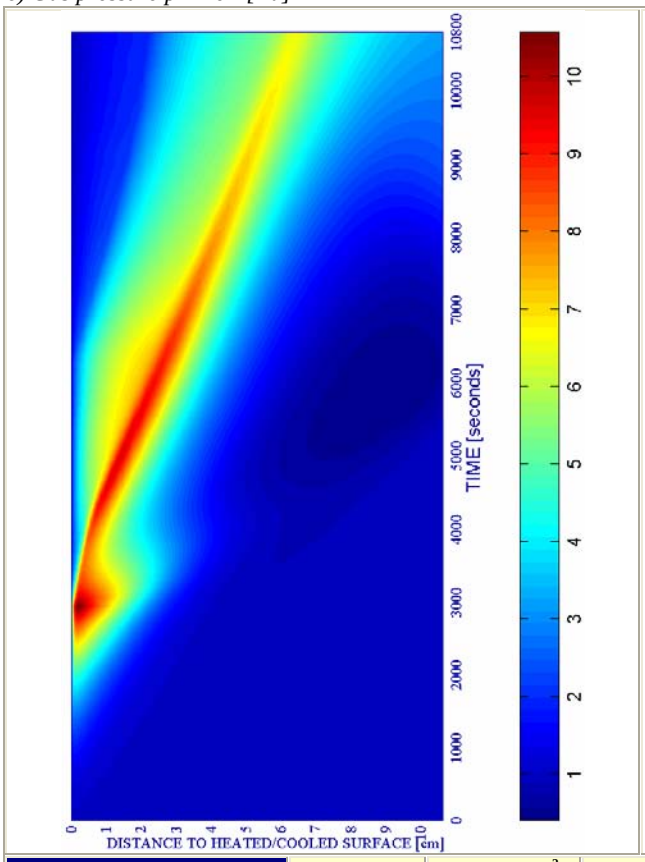

f) Vapour pressure $p^v \cdot 10^{-5}$ [Pa]

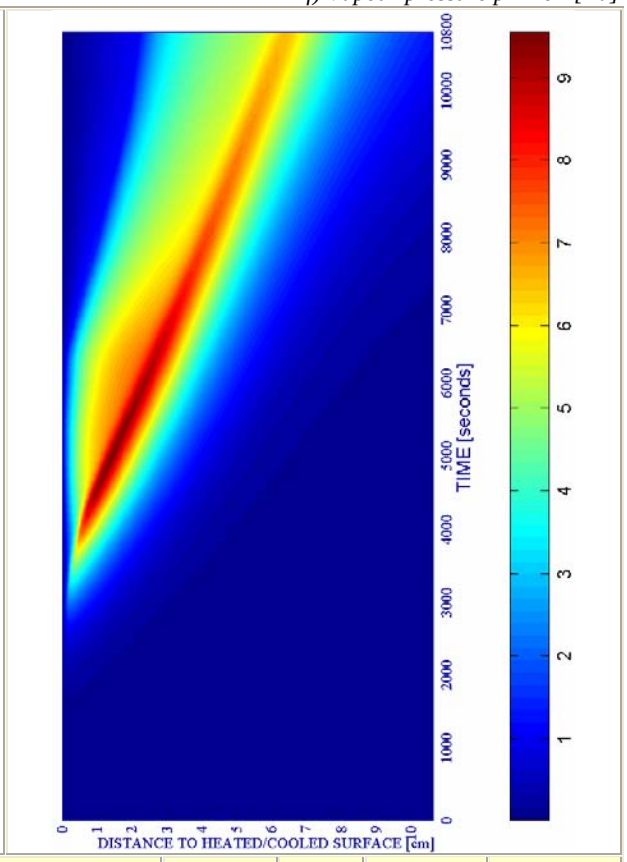

WITHOUT COOLING		PC1 - RH [%]			PC2 - K_0 [m^2]			PC4 - Heating curve			PC5 – Mat.		Cooling length[s]	Start of cooling [s]	End of cooling [s]
#	Combination	40	50	60	10^{-19}	10^{-18}	10^{-17}	PAR1	PAR2	PAR4	C60	C90			
100	TH12K019RH50PAR4C90		X		X					X		X	---	---	---

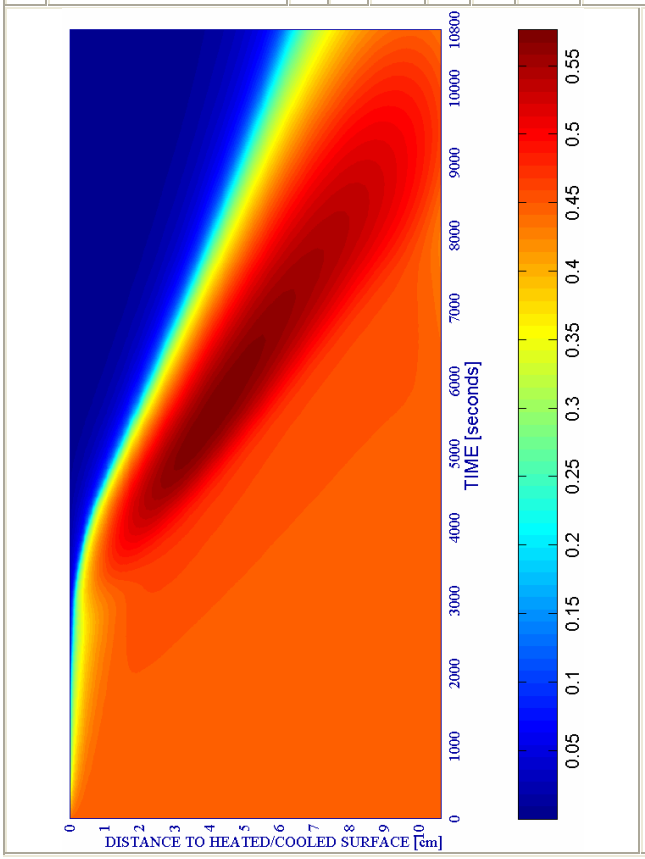

g) Saturation Degree S [-]

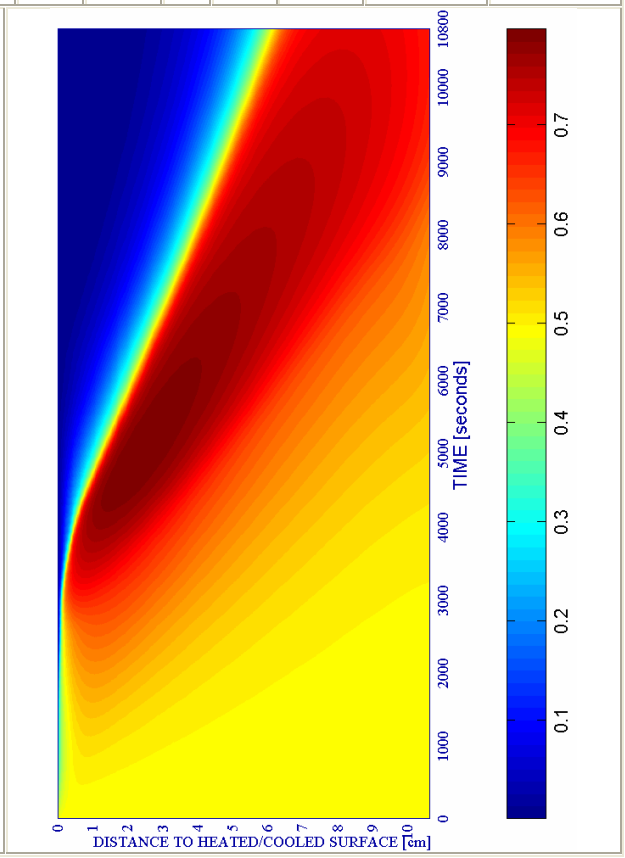

h) Relative Humidity RH [-]

Figure 6-157. (continued)

i) Temperature [K] *j) Elastic Energy U · **10^{-4}** [J/m^3]*

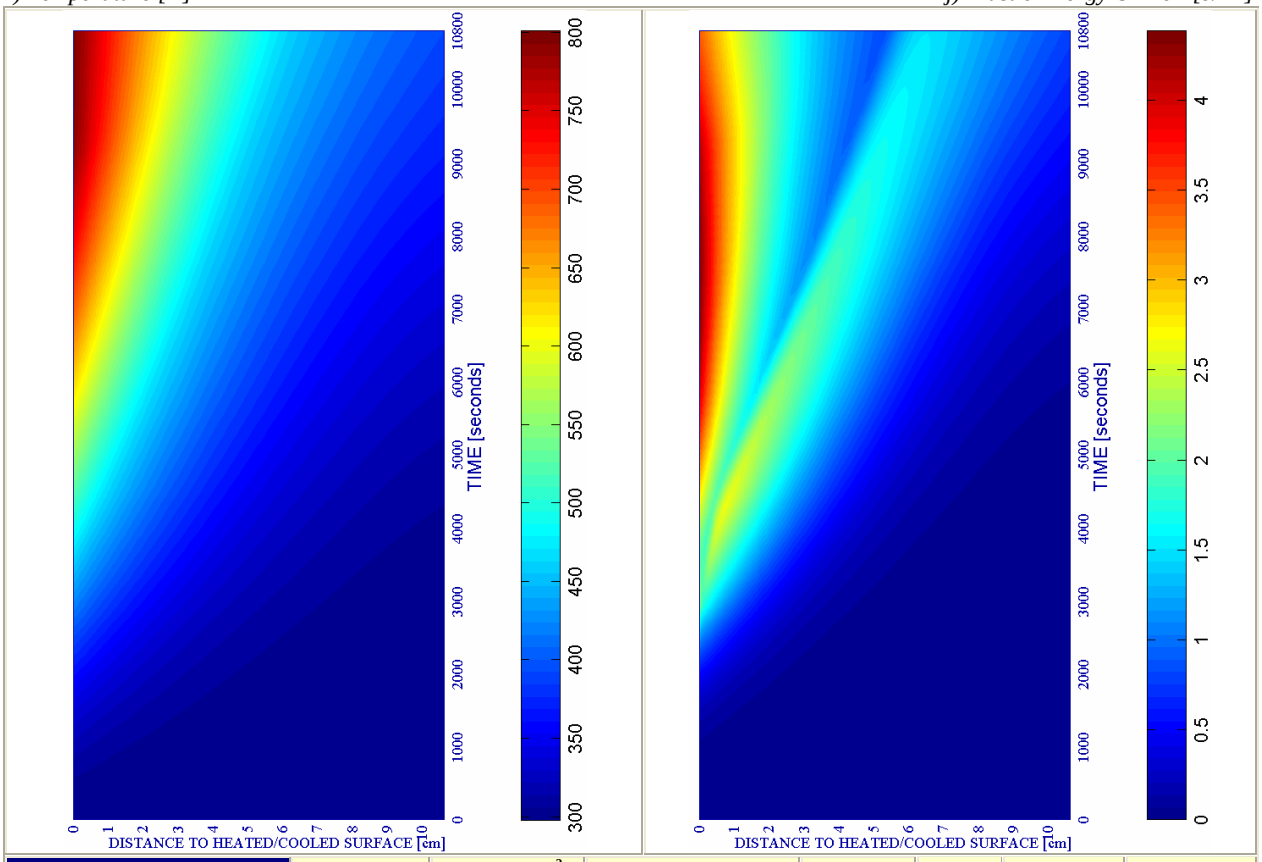

WITHOUT COOLING		PC1 - RH [%]			PC2 - K_0 [m^2]			PC4 - Heating curve			PC5 – Mat.		Cooling length[s]	Start of cooling [s]	End of cooling [s]
#	Combination	40	50	60	10^{-19}	10^{-18}	10^{-17}	PAR1	PAR2	PAR4	C60	C90			
100	TH12K019RH50PAR4C90		X		X					X		X	---	---	---

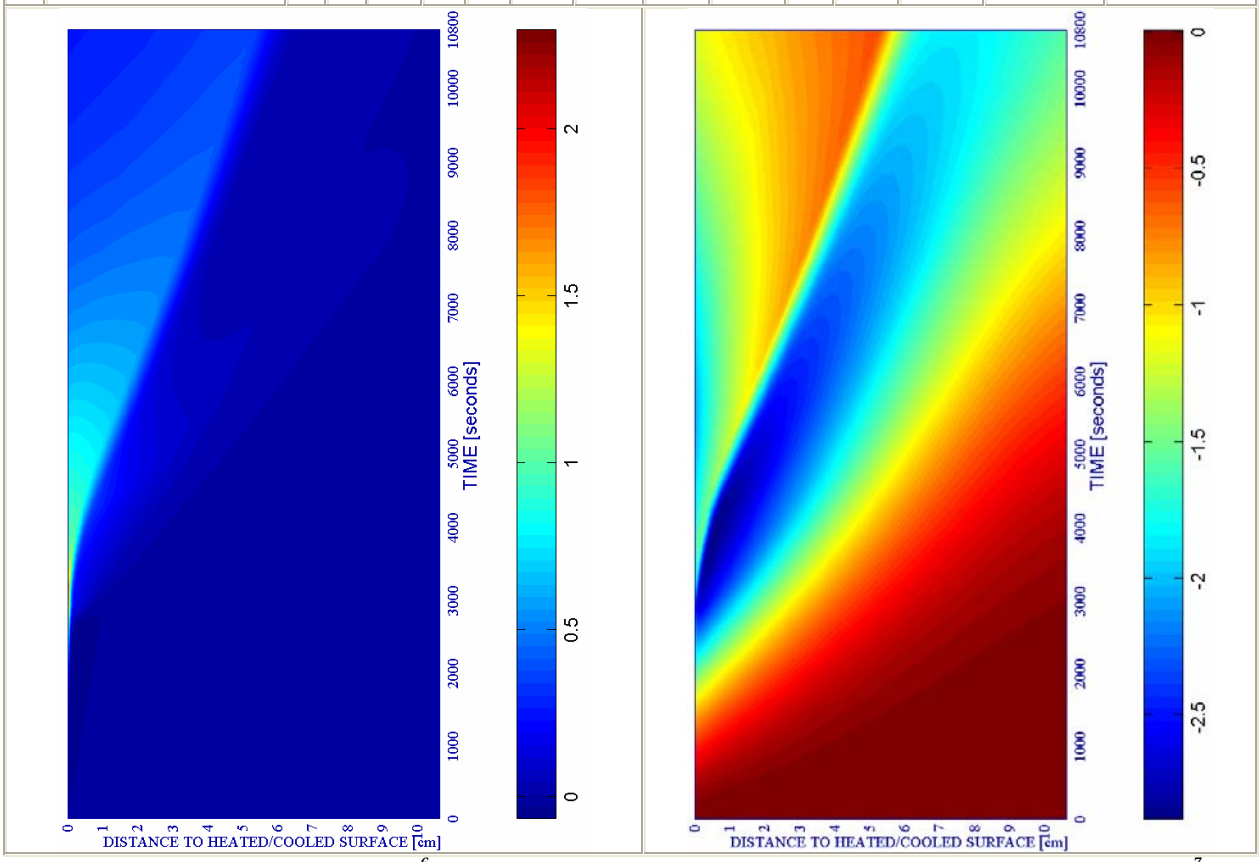

*k) Stress in longitudinal (xx) direction · **10^{-6}** [Pa]* ***Figure 6-157. (continued)*** *l) Stress in transversal (yy) direction · **10^{-7}** [Pa]*

6.5.2.8 PARTICULAR PHENOMENA AND ANALYSES OF INTEREST

Within this paragraph the description of some particular phenomena of interest and the development of certain analyses are included in order to enhance the usefulness of the results deducted in this Chapter as a necessary base to work out research tasks beyond the aims selected.

6.5.2.8.1 Compendium of Main Results

Particularly addressed to the comparative analyses developed in paragraph 6.5.3, a compendium of the main results obtained – and already described – on previous paragraphs of this Chapter is included on Table 6-108.

In order to identify correctly the case to which corresponds each set of results included this table, the equivalence described in table 6-107 must be studied first (see paragraph 6.3 for more details related to the nomenclature used herein):

CODE	COOLING START TIME (s)	COOLING TYPE	COOLING SUBTYPE	COMBINATION NAME	PC1 (RH) [%]			PC2 (K) [m²]			PC3 (TH) [cm]	PC4 (Heating curve)			PC5 (Mat)	
					40	50	60	10^{-19}	10^{-18}	10^{-17}	12	PAR1	PAR2	PAR4	C60	C90
1	600	ENV	SLOW	TH12K018RH50PAR1C60												
2			MEDIUM													
3			FAST													
4		SURF	HEAT			X			X		X	X			X	
5			KEEP													
6			REPEAT													
7	--/--	--/--	NO COOL													
8	1800	ENV	SLOW	TH12K018RH50PAR2C60												
9			MEDIUM													
10			FAST													
11		SURF	HEAT													
12			KEEP													
13			REPEAT													
14	2400	ENV	SLOW													
15			MEDIUM													
16			FAST													
17	3000	ENV	SLOW													
18			MEDIUM			X			X		X		X		X	
19			FAST													
20		SURF	KEEP													
21	3360	ENV	SLOW													
22			MEDIUM													
23			FAST													
24		SURF	HEAT													
25			KEEP													
26			REPEAT													
27	--/--	--/--	NO COOL													
28	4800	SURF	FIRST COOL	TH12K019RH50PAR3C90		X		X			X			X		X
29	--/--	--/--	NO COOL													

Table 6-107. *Equivalence table used to identify each case (highlighted in blue is the code assigned to each case that must be used to search the corresponding results on Table 6-108).*

In Table 6-108, the presented results for each case (results whose nomenclature is explained in detail in paragraph 6.5.2) are distributed in two rows: the row highlighted in blue corresponds to the maximum value of each parameter reached during the first three hours (10.800 seconds)

from the beginning of the fire. The second row of each case, always appearing in the environmental cooling cases but not in surface cooling ones, correspond to the maximum value of each parameter reached during the whole calculation (i.e. until the instant where the whole structural element temperature is lower than the ambient temperature plus 10 degrees).

CASE	$IS4_{max}$ [-]	X_{IS4max} [cm]	t_{IS4max} [s]	v_{max} [m/s]	X_{vmax} [cm]	t_{vmax} [s]	v_{max}* [m/s]	X_{vmax*} [cm]	t_{vmax*} [s]	d_{max} [-]	X_{dmax} [cm]	t_{dmax} [s]	T_{max} [K]	X_{Tmax} [cm]	t_{Tmax} [s]	p^g_{max} [MPa]	X_{pgmax} [cm]	t_{pgmax} [s]
1	0,3688	0,582	600	12,349	0,152	240	9,521	0,245	280	0,7304	0,000	10.800	754,18	0,000	720	1,3276	0,860	480
	0,3688	0,582	600	12,349	0,152	240	9,521	0,245	280	0,8773	3,028	42.420	754,18	0,000	720	1,3276	0,860	480
2	0,3688	0,582	600	12,349	0,152	240	9,521	0,245	280	0,7889	0,710	10.800	754,18	0,000	720	1,3276	0,860	480
	0,3688	0,582	600	12,349	0,152	240	9,521	0,245	280	0,8041	1,389	17.850	754,18	0,000	720	1,3276	0,860	480
3	0,3688	0,582	600	12,349	0,152	240	9,521	0,245	280	0,7925	0,758	10.800	754,18	0,000	720	1,3276	0,860	480
	0,3688	0,582	600	12,349	0,152	240	9,521	0,245	280	0,8021	1,167	15.153	754,18	0,000	720	1,3276	0,860	480
4	0,3688	0,582	600	12,349	0,152	240	9,521	0,245	280	0,9900	0-2,497	4.200	1.369,20	0,000	10.800	1,3276	0,860	480
	---	---	---	---	---	---	---	---	---	---	---	---	---	---	---	---	---	---
5	0,3688	0,582	600	12,349	0,152	240	9,521	0,245	280	0,8721	0,544	1.163	754,18	0,000	720	1,3276	0,860	480
	---	---	---	---	---	---	---	---	---	---	---	---	---	---	---	---	---	---
6	0,3688	0,582	600	12,349	0,152	240	9,521	0,245	280	0,9900	0 – 2,497	4.200	1.369,10	0,000	10.800	1,3276	0,860	480
	---	---	---	---	---	---	---	---	---	---	---	---	---	---	---	---	---	---
7	0,3688	0,582	600	12,349	0,152	240	9,521	0,245	280	0,9908	0 – 2,258	4.000	1.369,20	0,000	10.800	1,3276	0,860	480
	---	---	---	---	---	---	---	---	---	---	---	---	---	---	---	---	---	---
8	0,0129	0,227	1.920	0,000	---	---	0,000	---	---	0,6634	0,412	6.360	467,16	0,000	1.920	0,5967	0,582	1.920
	0,0129	0,227	1.920	0,000	---	---	0,000	---	---	0,6634	0,412	6.360	467,16	0,000	1.920	0,5967	0,582	1.920
9	0,0129	0,227	1.920	0,000	---	---	0,000	---	---	0,6641	0,412	6.360	467,16	0,000	1.920	0,5970	0,623	1.924
	0,0129	0,227	1.920	0,000	---	---	0,000	---	---	0,6641	0,412	6.360	467,16	0,000	1.920	0,5970	0,623	1.924
10	0,0129	0,227	1.920	0,000	---	---	0,000	---	---	0,6634	0,412	6.728	467,16	0,000	1.920	0,5967	0,582	1.920
	0,0129	0,227	1.920	0,000	---	---	0,000	---	---	0,6634	0,412	6.728	467,16	0,000	1.920	0,5967	0,582	1.920
11	0,0977	1,099	3.478	6,637	3,172	10.800	6,637	3,172	10.800	0,8115	0,000	10.800	982,85	0,000	10.800	0,8057	1,736	2.878
	---	---	---	---	---	---	---	---	---	---	---	---	---	---	---	---	---	---
12	0,0129	0,227	1.920	0,000	---	---	0,000	---	---	0,7863	0,265	2.129	467,16	0,000	1.920	0,5599	0,710	1.936
	---	---	---	---	---	---	---	---	---	---	---	---	---	---	---	---	---	---
13	0,0170	0,474	2.278	0,877	5,687	2.278	0,871	0,974	2.278,5	0,7445	0,000	2.298	506,97	0,000	2.278	0,6796	0,916	2.289,5
	---	---	---	---	---	---	---	---	---	---	---	---	---	---	---	---	---	---
14	0,0569	0,700	2.520	4,380	1,300	2.520	4,380	1,300	2.520	0,7158	0,200	10.800	542,44	0,000	2.520	0,8079	1,200	2.490
	0,0569	0,700	2.520	4,380	1,300	2.520	4,380	1,300	2.520	0,7901	1,300	23.760	542,44	0,000	2.520	0,8079	1,200	2.490
15	0,0569	0,700	2.520	4,380	1,300	2.520	4,380	1,300	2.520	0,7470	0,400	10.800	542,44	0,000	2.520	0,8079	1,200	2.490
	0,0569	0,700	2.520	4,380	1,300	2.520	4,380	1,300	2.520	0,7773	1,000	18.320	542,44	0,000	2.520	0,8079	1,200	2.490
16	0,0569	0,700	2.520	4,380	1,300	2.520	4,380	1,300	2.520	0,7481	0,400	10.800	542,44	0,000	2.520	0,8079	1,200	2.490
	0,0569	0,700	2.520	4,380	1,300	2.520	4,380	1,300	2.520	0,7754	0,900	16.436	542,44	0,000	2.520	0,8079	1,200	2.490
17	0,0894	0,974	3.090	5,228	2,037	3.090	5,228	2,037	3.090	0,7105	0,000	10.800	614,64	0,000	3.120	0,8256	1,555	2.760
	0,0894	0,974	3.090	5,228	2,037	3.090	5,228	2,037	3.090	0,8823	2,258	41.460	614,64	0,000	3.120	0,8256	1,555	2.760
18	0,0894	0,974	3.090	5,228	2,037	3.090	5,228	2,037	3.090	0,7376	0,000	10.800	614,64	0,000	3.120	0,8256	1,555	2.760
	0,0894	0,974	3.090	5,228	2,037	3.090	5,228	2,037	3.090	0,8543	2,258	36.960	614,64	0,000	3.120	0,8256	1,555	2.760
19	0,0894	0,974	3.090	5,228	2,037	3.090	5,228	2,037	3.090	0,7372	0,000	10.800	614,64	0,000	3.120	0,8256	1,555	2.760
	0,0894	0,974	3.090	5,228	2,037	3.090	5,228	2,037	3.090	0,8529	2,145	36.744	614,64	0,000	3.120	0,8256	1,555	2.760
20	0,0894	0,974	3.090	5,228	2,037	3.090	5,228	2,037	3.090	0,8911	0,033	3.182	614,64	0,000	3.120	0,8256	1,555	2.760
	---	---	---	---	---	---	---	---	---	---	---	---	---	---	---	---	---	---
21	0,1004	1,035	3.390	5,453	1,644	3.480	5,453	1,644	3.480	0,7149	0,000	10.800	656,65	0,000	3.480	0,8256	1,555	2.760
	0,1004	1,035	3.390	5,453	1,644	3.480	5,453	1,644	3.480	0,9204	3,964	102.000	656,65	0,000	3.480	0,8256	1,555	2.760
22	0,1004	1,035	3.390	5,453	1,644	3.480	5,453	1,644	3.480	0,7365	0,000	10.800	656,65	0,000	3.480	0,8256	1,555	2.760
	0,1004	1,035	3.390	5,453	1,644	3.480	5,453	1,644	3.480	0,8980	3,321	46.932	656,65	0,000	3.480	0,8256	1,555	2.760
23	0,1004	1,035	3.390	5,453	1,644	3.480	5,453	1,644	3.480	0,7411	0,000	10.800	656,65	0,000	3.480	0,8256	1,555	2.760
	0,1004	1,035	3.390	5,453	1,644	3.480	5,453	1,644	3.480	0,8995	2,753	44.304	656,65	0,000	3.480	0,8256	1,555	2.760
24	0,1004	1,035	3.390	6,631	3,172	10.800	6,631	3,172	10.800	0,8475	0,000	3.516	982,75	0,000	10.800	0,8256	1,555	2.760
	---	---	---	---	---	---	---	---	---	---	---	---	---	---	---	---	---	---
25	0,1004	1,035	3.390	5,453	1,644	3.480	5,453	1,644	3.480	0,8923	0,010	3.528	656,65	0,000	3.480	0,8256	1,555	2.760
	---	---	---	---	---	---	---	---	---	---	---	---	---	---	---	---	---	---
26	0,1004	1,035	3.390	6,622	3,172	10.800	6,622	3,172	10.800	0,8606	0,000	3.750	982,48	0,000	10.800	0,8256	1,555	2.760
	---	---	---	---	---	---	---	---	---	---	---	---	---	---	---	---	---	---
27	0,1010	1,099	3.480	6,635	3,172	10.800	6,635	3,172	10.800	0,8115	0,000	10.800	982,90	0,000	10.800	0,8256	1,555	2.760
	---	---	---	---	---	---	---	---	---	---	---	---	---	---	---	---	---	---
28	0,0690	0,710	4.800	6,096	0,175	2.925	4,021	1,238	4.800	0,9246	0,001	4.820	548,24	0,000	4.800	1,0564	0,194	2.925
	---	---	---	---	---	---	---	---	---	---	---	---	---	---	---	---	---	---
29	0,0867	1,035	6.000	6,096	0,165	2.925	4,068	1,644	5.250	0,8517	0,000	10.800	800,71	0,000	10.800	1,0564	0,194	2.925
	---	---	---	---	---	---	---	---	---	---	---	---	---	---	---	---	---	---

Table 6-108. *Compendium of the main results corresponding to each case described in Table 6-107.*

6.5.2.8.2 Environmental Humidity Infiltration

One secondary contribution of the analyses of this Chapter is the description of a particular phenomenon observed during the calculations: the infiltration of the environmental humidity inside the structural element during the cooling processes.

During the cooling processes analyzed it has been observed that there is an infiltration – across both surfaces – of the humidity of the environment towards the inner layers. This effect happens since a constant vapour pressure of the environment has been imposed at both sides of the structural element – see paragraph 6.4.1 explaining the boundary conditions used in the calculations – and, hence, as the temperature in the environment decreases its relative humidity increases (being approximately the 50% at the initial ambient temperature) and vice versa.

If, for instance, we analyze the case corresponding to the slow environmental cooling described in paragraph 6.5.2.1.1 (TH12K018RH50PAR1C60), the following evolution of relative humidity in the zones next to the heated/cooled surface are obtained:

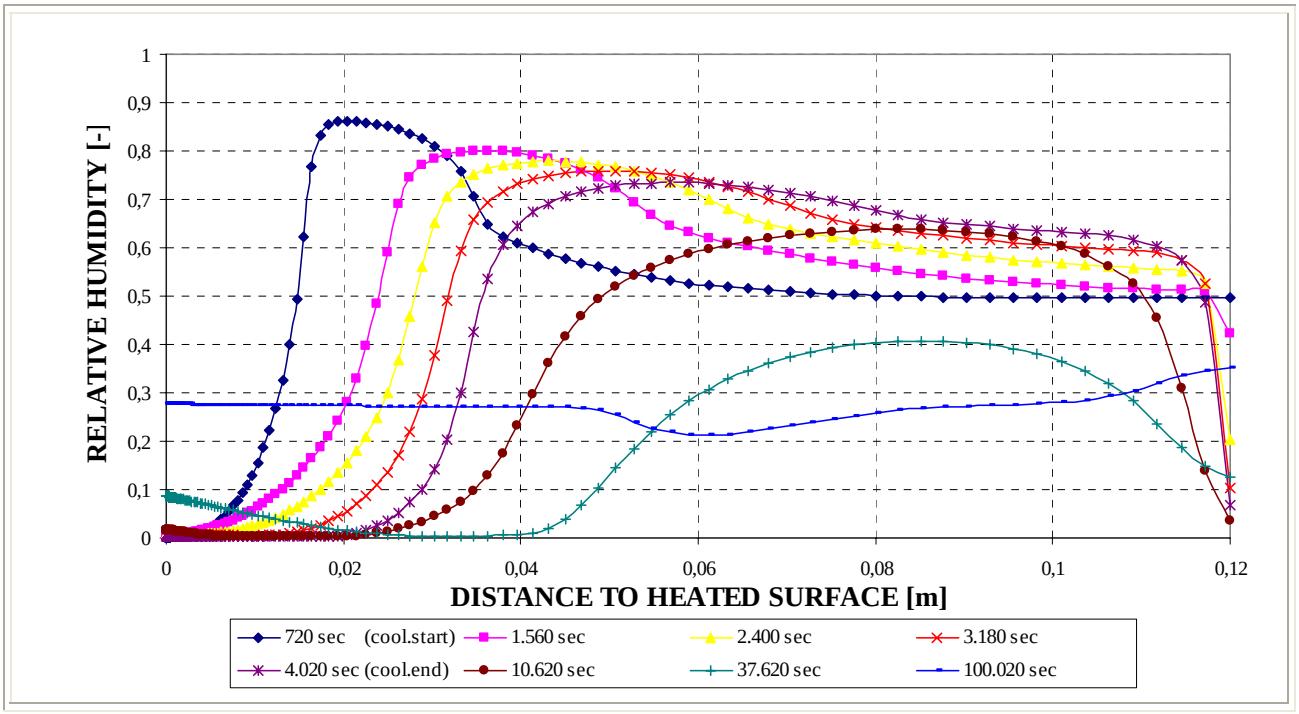

Figure 6-158. *Evolution of the relative humidity at all the depths during the prior heating and the environmental slow cooling.*

Figure 6-158 show that, at really late stages – from 3 hours after the beginning of the cooling process on – the relative humidity at both surfaces of the structural element begins to increase very slowly from an almost zero value up to levels around the 30 per cent (this increase starts at 9 hours after the beginning of the cooling process at the layers 3 centimetres far from the surface). The increase at the zones close to the surface can be more easily observed on figure 6-159.

Although a part of this increase is due to diffusion processes of the relative humidity present in the inner layers of the structural element, a part is unquestionably due to the infiltration of the environmental relative humidity since, as it will be observed on next figures, the relative humidity increase occurs first at the surface rather than at the inner layers close to the surface (in figure 6-159, for instance, it can be clearly observed that the surface is the position with higher relative humidity at every instant during the cooling process).

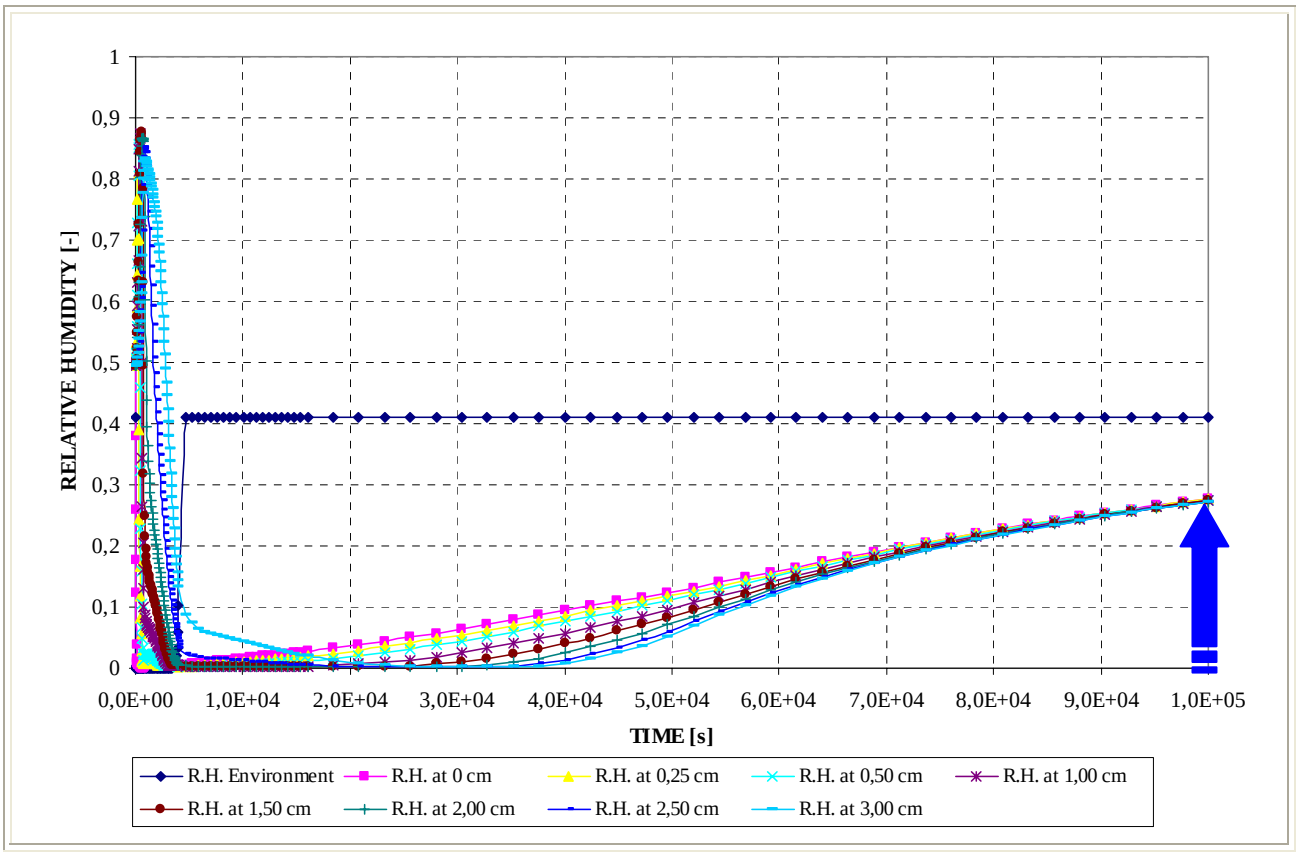

Figure 6-159. *Evolution of the relative humidity at the zones close to the heated/cooled surface during the prior heating and the environmental slow cooling (remember that the environmental cooling process starts at 720 seconds and finishes at 4.020 seconds).*

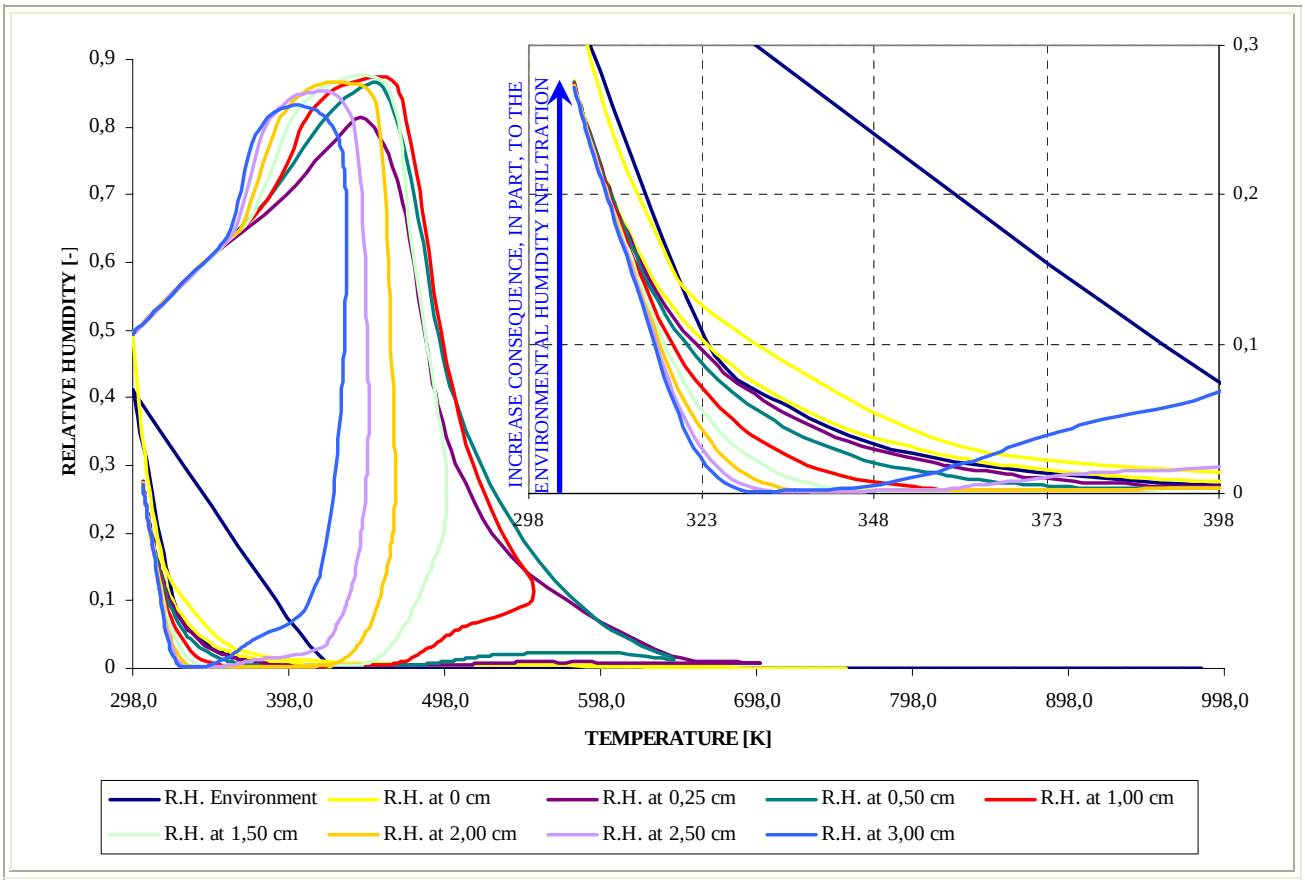

Figure 6-160. *Relation between the relative humidity at the zones close to the heated/cooled surface and their temperature.*

Figure 6-160 shows the relation between the relative humidity of several positions close to the heated/cooled surface and their temperature. Herein, the 30 per cent final level of the relative humidity of these zones is easily observed, whereas it is deducted that although the relative humidity at the surface is – at the beginning of the heating process – sharply reduced much faster than at any other layer, its increase during the cooling process is also the first (it must be remembered that the temperature at the surface is, during the cooling process, the lowest of all the layers).

Finally if, for instance, a comparison of the evolution of the relative humidity corresponding to the three subtypes of environmental cooling considered herein is developed, the following trends are observed:

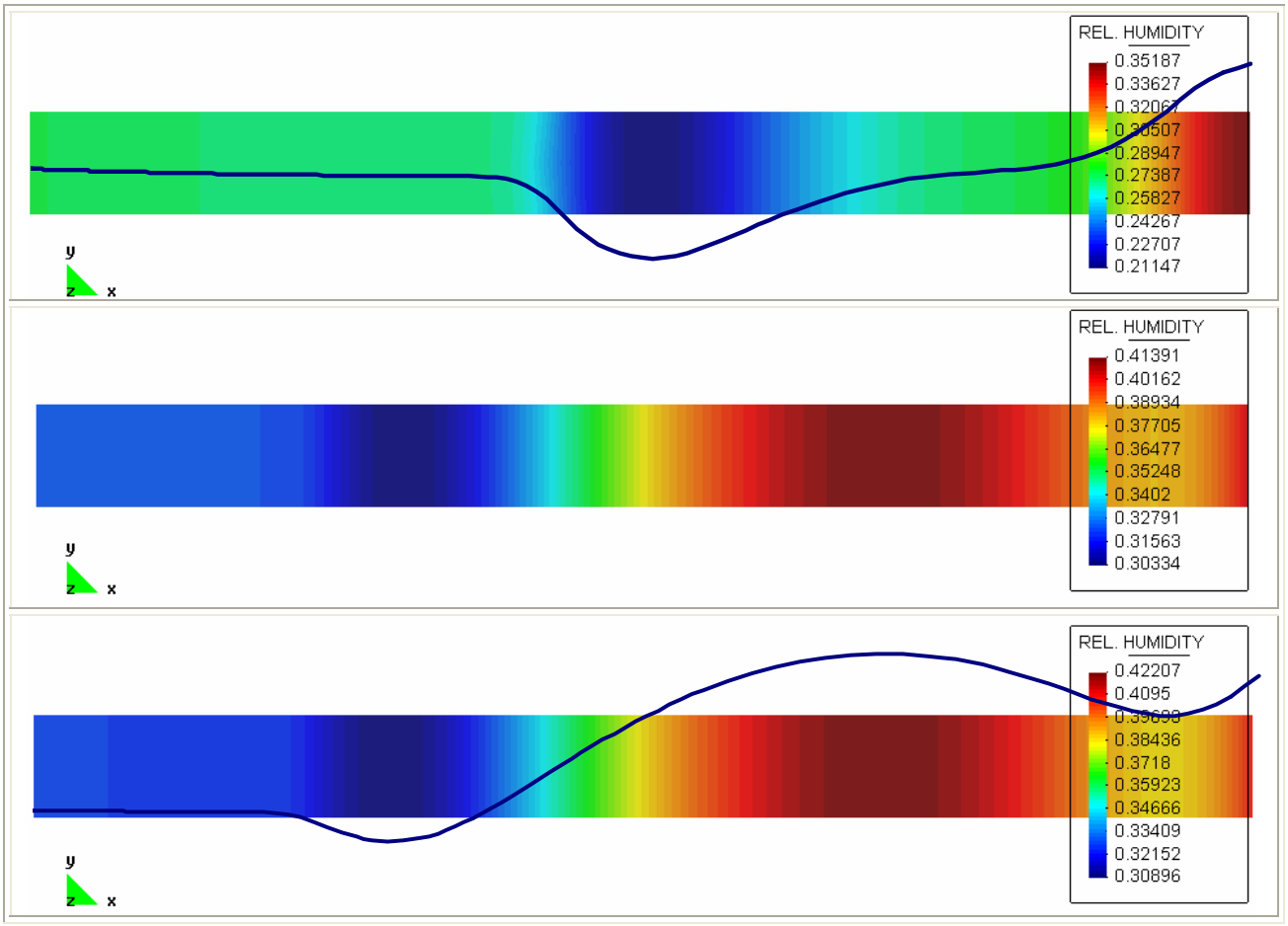

Figure 6-161. *Final distribution of the relative humidity (once the entire structural element has reached a temperature under ambient temperature plus 10 degrees K.*
Up: Environmental Slow Cooling; Middle: Environmental Medium Cooling; Down: Environmental Fast Cooling.

In figure 6-161 it is observed that in the environmental slow cooling case the maximum relative humidity at the end of the process is sited in a surface while, in the other cases, it is sited in an inner layer. In the meantime, in the environmental slow cooling the relative humidity is significantly higher than in inner zones while this is not so clear in faster environmental cooling processes.

This fact suggests that the slower the environmental cooling process is the greater the environmental relative humidity infiltration occurs (it must be remarked that the total simulation time corresponding to environmental slow and fast coolings are similar – 27,8 hours and 26,9 hours respectively – being even shorter in the slow cooling case).

6.5.2.8.3 Introduction to the Analysis of the Effect of the Maximum Temperature and Damage reached in Concrete

In paragraph 6.2.2.4 it has been justified the necessity of exploiting the maximum temperature reached at each position of the concrete matrix during the complete set of heating and cooling processes composing each case, in order to enable the evaluation the final value of several basic mechanical (and thermal) properties needed to calculate the load-carrying capacity of any structural element in a fire situation.

With this purpose, explained in detail in paragraph 6.2.4, figure 6-162 is included showing the maximum temperature reached at each position during several types and subtypes of cooling processes (not all of the considered cases are shown in next figure in order to ease its comprehension, only the reference ones):

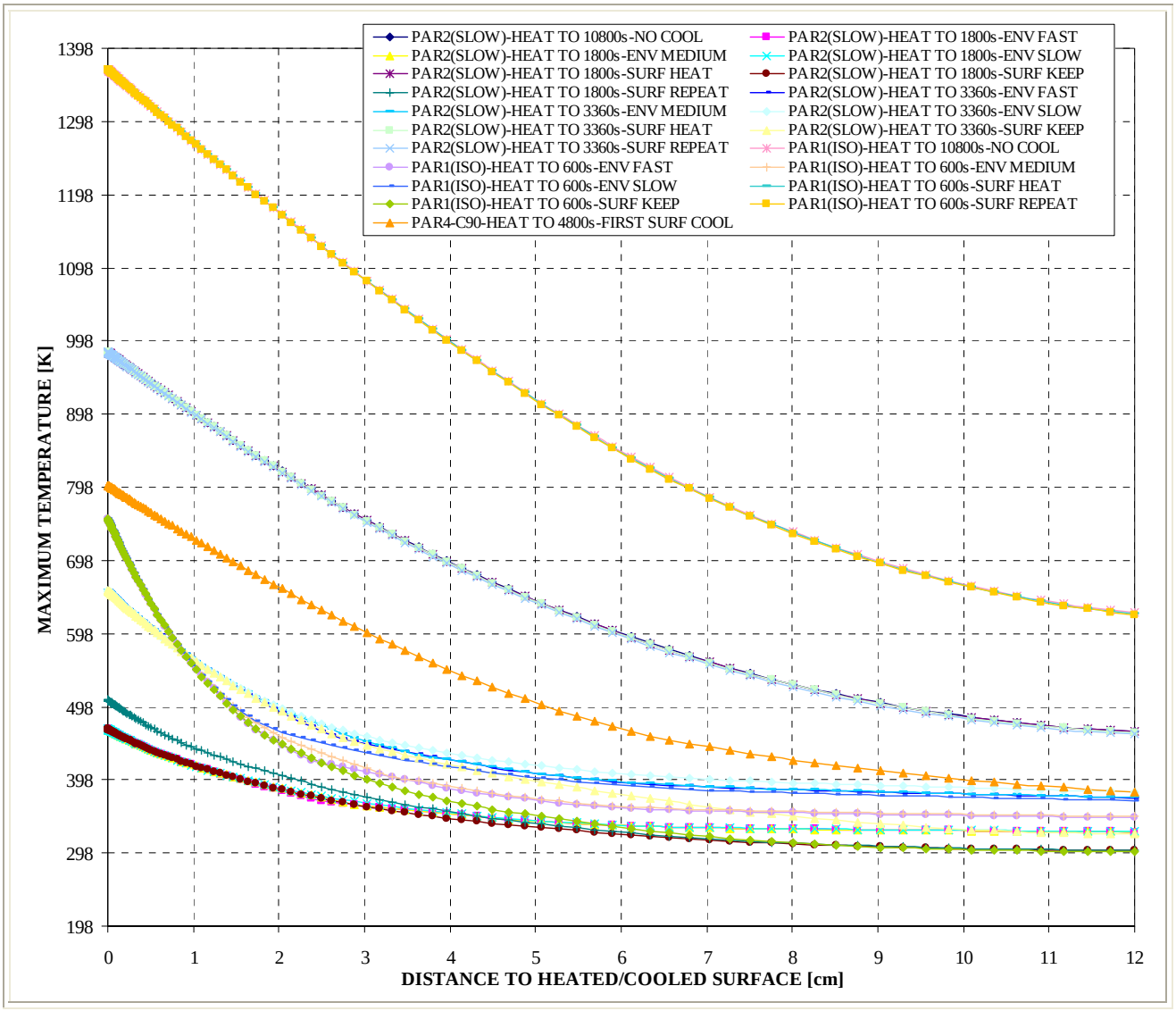

Figure 6-162. *Maximum temperature reached at each position during several types and subtypes of cooling processes.*

In case that, for instance, the minimum value of the compressive strength achieved during the heating/cooling process is needed to evaluate the structural state of a heated structural element, the reduction coefficients of the characteristic strength shown in Table 6-3 can be applied to the maximum temperatures distribution shown on last figure, obtaining the following values to be considered (see figures 6-163 and 6-164, where two types of heating curves are considered for a concrete with a characteristic compressive strength of 60 MPa):

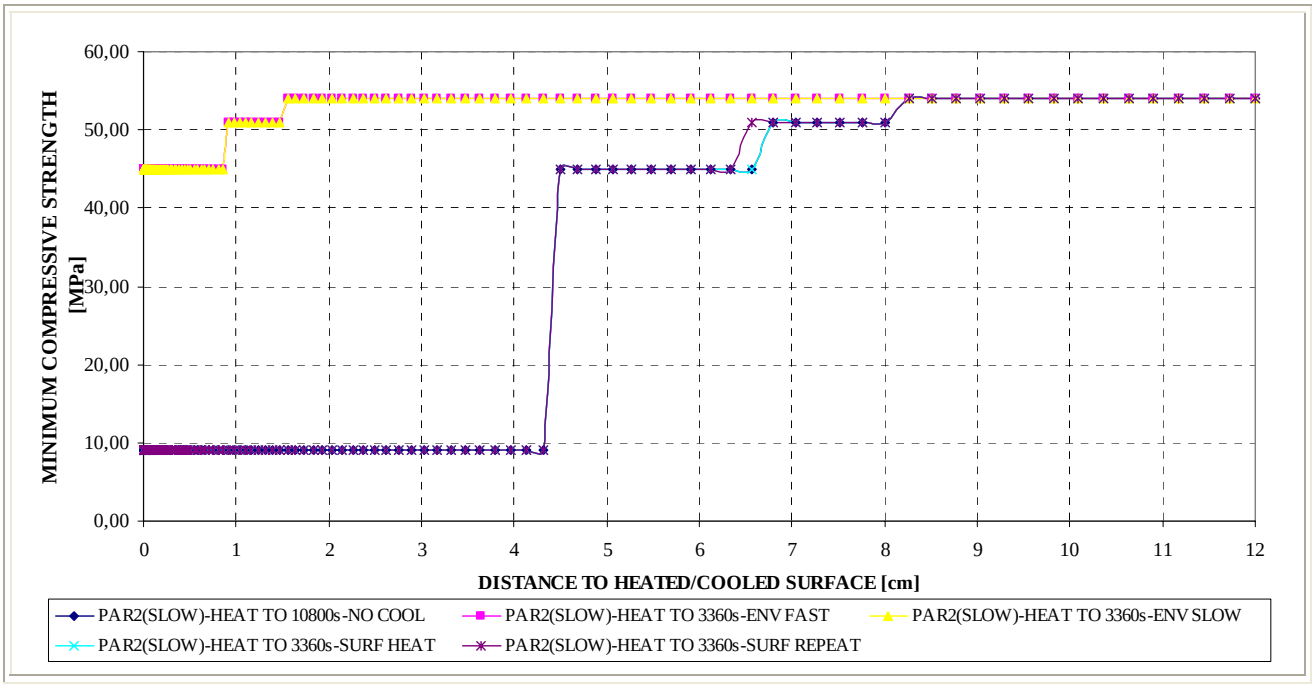

Figure 6-162. *Minimum values of the compressive strength reached at each position during several types of heating and cooling processes. PAR2 (slow) heating curve – cooling processes start at 3.360+120 seconds – (#14-3360-TH12K018RH50PAR2C60).*

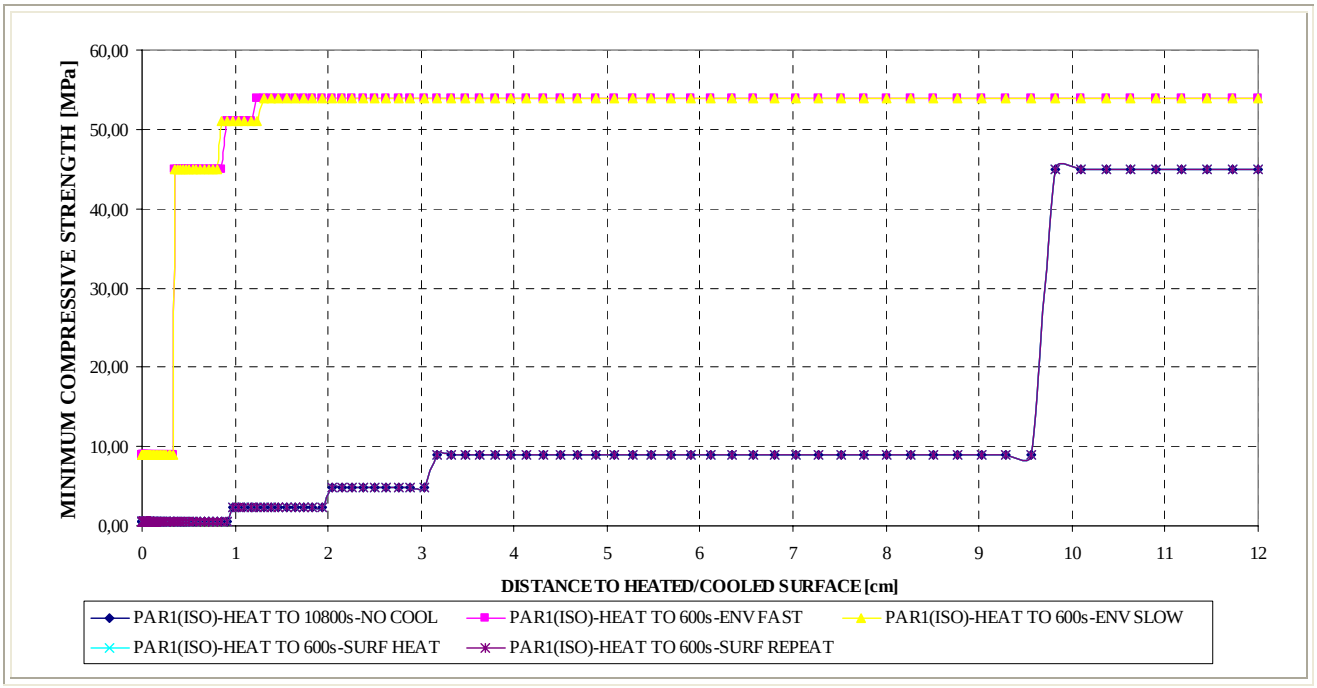

Figure 6-163. *Minimum values of the compressive strength reached at each position during several types of heating and cooling processes. PAR1 (ISO) heating curve – cooling processes start at 600+120 seconds – (#05-600-TH12K018RH50PAR1C60).*

Both figure 6-162 and 6-163 show the slight differences in the maximum temperature distributions corresponding to the environmental slow and fast cooling, leading to the lowest reductions in the characteristic compressive strength of concrete.

On the contrary, the highest reduction coefficient values are found within the surface cooling basically due to their short and quite local effect on temperature, leading to final (and maximum) temperature distributions non-significantly different from that corresponding to the case where no cooling is applied during the first three hours of fire progress.

As an additional use of the results obtained in this Chapter, the final distributions of the mechanical damage values may give a reasonable comprehension of the residual value of the Young's Modulus of concrete:

If, for instance, they are studied in the case corresponding to an ISO heating curve followed by an environmental slow cooling starting at 600+120 seconds (case #05-600-TH12K018RH50PAR1C60) figure 6-164 is obtained taking into account the relation between mechanical damage and Young's Modulus shown next: Mechanical damage of concrete is considered following the scalar isotropic model by Mazars [20,21]; in this model, the damaged material at given temperature, T, is supposed to behave elastically and to remain isotropic; its Young's modulus at this temperature, $E(T)$, can be obtained from the value of mechanically undamaged material at the same temperature, $E_o(T)$, and mechanical damage parameter, d, being a measure of cracks' volume density in the material,

$$E(T) = (1 - d)\,E_o(T) \tag{6.33}$$

Considering the final instant of the cooling process (once all the material presents a temperature lower than the ambient temperature plus 10 degrees) the following residual values of the Young's Modulus are obtained, observing that within the first four centimetres close to the heated/cooled surface the residual value of the Young's Modulus is lower than one sixth of its original value.

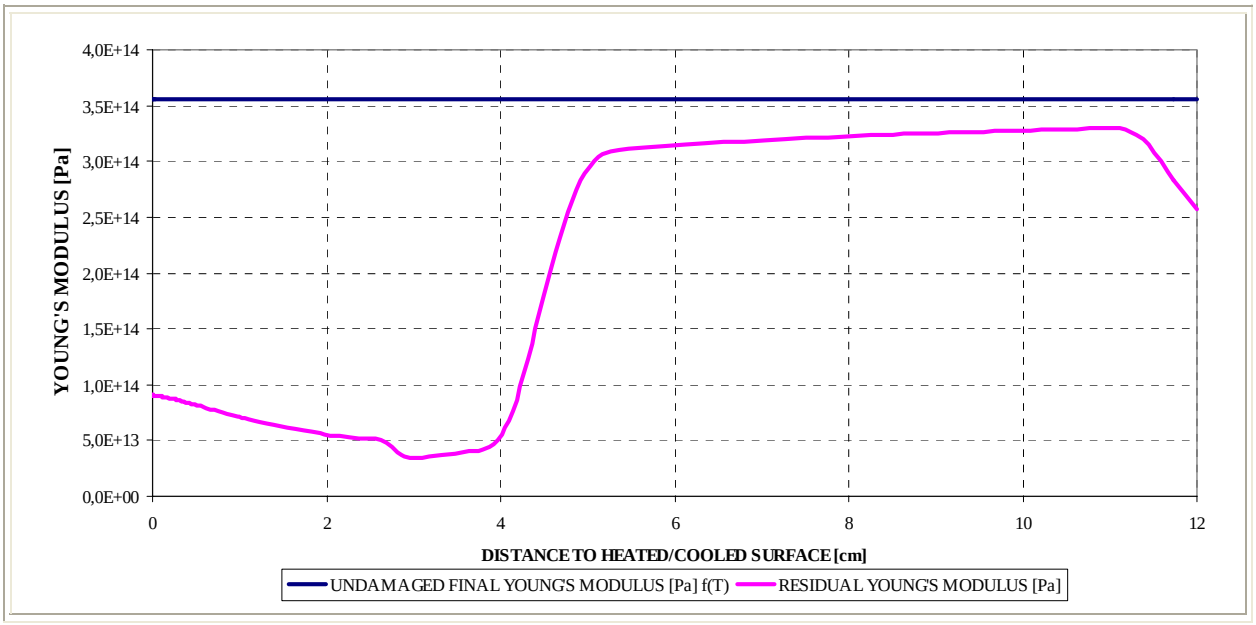

Figure 6-164. *Residual values of the Young's Modulus after the environmental slow cooling process has finished.*

The considerations exposed on this paragraph are just a sample of the possible post-uses of the results obtained in this Chapter, being these possible uses especially prone to serve to forensic engineering tasks, helping researchers to discern the extent of the overall structural pathologies arisen after a fire in a High-Rise Building. The same analyses exposed on this paragraph can be developed on any other set of results corresponding to any of the cases presented in this Chapter.

This constitutes another secondary original contribution of this Thesis since, up to this date, the only existing works addressed to evaluate, for instance, the residual Young's Modulus of a structural element after a fire are experimentally based.

6.5.2.8.4 Introduction to the Analysis of Temperature Effect on the Mechanical Properties of Steel Reinforcing Bars

Analogously to what has been done in the previous paragraph with concrete properties, knowing the maximum temperatures achieved at any position during the heating/cooling processes of each case the strength and deformation properties of steel reinforcing bars at elevated temperatures shall be obtained from the stress-strain relationships specified in figure 6-2 and tables 6-4 and 6-5. (*Eurocode 2: Design of concrete structures - Part 1.2* [23]) and used to assess the fire resistance of a concrete structural element.

If, for instance (see figure 6-3), a critical aspect in the case of structural elements under fire – the variation of the adherence between reinforcing bars and concrete – is evaluated taking into account the maximum temperatures reached at the reinforcing bars position, and taking into account that the perturbation of this feature is higher after the fire than when the maximum temperature is reached (and higher for higher temperatures reached), the following figure shows the residual relation between the adherence breakage stress ($\tau_{u,inc}$) after the fire and that previous to it (τ_u) (as it can be observed, the deterioration is very fast for temperatures higher than 300 ºC) – corresponding to an ISO heating curve followed by an environmental slow cooling starting at 600+120 seconds (case #05-600-ES-TH12K018RH50PAR1C60).

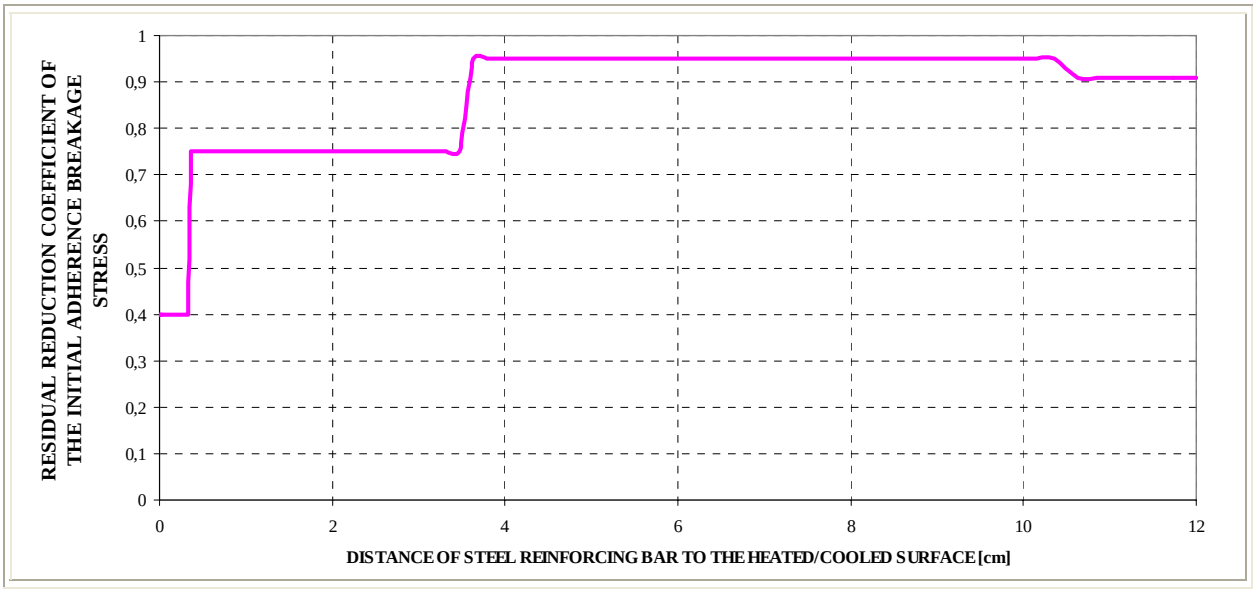

Figure 6-165. *Residual values of the reduction coefficient of the Initial adherence breakage stress after the environmental slow cooling process has finished.*

Through this methodology, the forensic engineer is capable to discern the residual value of the adherence breakage stress by entering in figure 6-165 (or in any other resulting from any of the cases analyzed in this Chapter) with the position of the steel reinforcing bars and deducting the residual value of its reduction coefficient.

Nevertheless, it must be taken into account that, as the relation between the adherence breakage stress and the temperature proposed in [25] depends on the temperature at the Interphase between concrete and steel, minor adjusts of the temperature arising from the calculations developed in this Chapter might be necessary in order to consider the local effect on the temperature distribution due to the presence of the steel reinforcing bars).

6.5.3 Comparative Analysis

Within this paragraph, a comparative analysis is developed from the results described previously in this Chapter in order to discern the effect of several factors on the hygro-thermo-chemo-mechanical state of a structural element. This comparison is developed on two of the selected reference cases: reference case #05 – TH12K018RH50PAR1C60 and reference case #14 – TH12K018RH50PAR2C60.

In the cases where an environmental cooling process has been considered, the analyzed state is that corresponding to the instant when the entire structural element has lowed down its temperature under the ambient temperature plus ten degrees (precisely, the ending instant of the calculations developed). In the meantime, in those cases where a surface cooling process has been applied, the structural element state after three hours from the beginning of the natural fire in a High-Rise Building is analyzed.

A qualitative comparison is also developed among the effect of the two types of cooling considered in this Chapter, i.e., the environmental cooling and the surface cooling.

Finally, the influence of other parameters such as the cooling process start instant are also analyzed for one of the selected reference cases (reference case #14 – TH12K018RH50PAR2C60).

6.5.3.1 ANALYSIS OF THE EFFECT OF THE TYPE AND SUBTYPE OF COOLING

As just stated, two types of cooling profiles are compared:

- Environmental Cooling Profiles, where cooling effect is applied to the air in contact with the surface of the structural element,
- Surface Cooling Profiles, where cooling effect is applied directly to the surface of the structural element.

Among them, several subtypes of cooling profiles are defined starting from different instants and depending on the actions following the cooling processes (see paragraph 6.4.3.2.5 for a deeper description):

- Environmental Cooling Profiles:
  - ‘*Slow cooling*’: It is characterized by a cooling rate of the air of only – 0,2 ºC/s.
  - ‘*Medium cooling*’: It is characterized by a cooling rate of the air of – 2,0 ºC/s.
  - ‘*Fast cooling*’: It is characterized by a cooling rate of the air of – 20,0 ºC/s.
- Surface Cooling Profiles: In general characterized by a cooling rate of the surface of the structural element of – 10,0 ºC/s
  - ‘*Followed by Heating*’: After the surface cooling stage, the environment heating profile keeps governing the evolution of the temperature in the structural element.
  - ‘*Followed by an imposed constant Surface Temperature*’: Herein, the surface temperature is also decreased at the cooling rate previously described until the ambient temperature is reached on the surface. At this instant the surface temperature is kept constant in order to simulate keeping the water jet applied on the surface for some time more.
  - ‘*Divided into Two/Three Periods*’: In this subtype of surface cooling is to simulate the action of the water jet applied on the surface of the structural element in several sweeps. Among the several cooling subprocesses, the temperature of the surface is assumed to evolution governed by the environment heating profile.

6.5.3.1.1 Comparison of the subtypes of Environmental Cooling

In order to compare the hygro-thermo-chemo-mechanical state of the structural element at the instant when the entire structural element has lowed down its temperature below the ambient temperature plus ten degrees (precisely, the ending instant of the calculations developed), the values and distributions of the parameters and criteria established in paragraph 6.2.2 are considered.

6.5.3.1.1.1 Reference case #05 – TH12K018RH50PAR1C60

First, an extract of the compendium of the main results already included in paragraph 6.5.2.8.1, particularized to the cases dealt herein, is included next. In order to identify correctly the case to which corresponds each set of results included this table, the equivalence described in next table must be studied first:

CODE	COOLING START TIME (s)	COOLING TYPE	COOLING SUBTYPE	COMBINATION NAME	PC1 (RH) [%]			PC2 (K) [m²]			PC3 (TH) [cm]	PC4 (Heating curve)			PC5 (Mat)	
					40	50	60	10^{-19}	10^{-18}	10^{-17}	12	PAR1	PAR2	PAR4	C60	C90
1	600	ENV	SLOW	TH12K018RH50PAR1C60		x			x		x	x			x	
2			MEDIUM													
3			FAST													

Table 6-109. *Equivalence table used to identify each case (highlighted in blue is the code assigned to each case that must be used to search the corresponding results on Table 6-110).*

CASE	$IS4_{max}$ [-]	X_{IS4max} [cm]	t_{IS4max} [s]	v_{max} [m/s]	X_{vmax} [cm]	t_{vmax} [s]	v_{max}* [m/s]	X_{vmax*} [cm]	t_{vmax*} [s]	d_{max} [-]	X_{dmax} [cm]	t_{dmax} [s]	T_{max} [K]	X_{Tmax} [cm]	t_{Tmax} [s]	p^g_{max} [MPa]	X_{pgmax} [cm]	t_{pgmax} [s]
1	0,3688	0,582	600	12,349	0,152	240	9,521	0,245	280	0,8773	3,028	42.420	754,18	0,000	720	1,3276	0,860	480
2	0,3688	0,582	600	12,349	0,152	240	9,521	0,245	280	0,8041	1,389	17.850	754,18	0,000	720	1,3276	0,860	480
3	0,3688	0,582	600	12,349	0,152	240	9,521	0,245	280	0,8021	1,167	15.153	754,18	0,000	720	1,3276	0,860	480

Table 6-110. *Extract of the Compendium of the maximum value of the main results corresponding to each case described in Table 6-109.*

Regarding the maximum value of the Spalling Index selected herein, I_{s4}, all of the cases dealt in this subparagraph (the three subtypes of environmental cooling) show an identical maximum value since this maximum appears at 600 seconds from the beginning of the fire and, hence, prior to the start of the cooling process. However, in both the Spalling Index value and the energy available for thermal spalling to occur at the end of the structural element environmental cooling the following differences are observed (see figure 6-166):

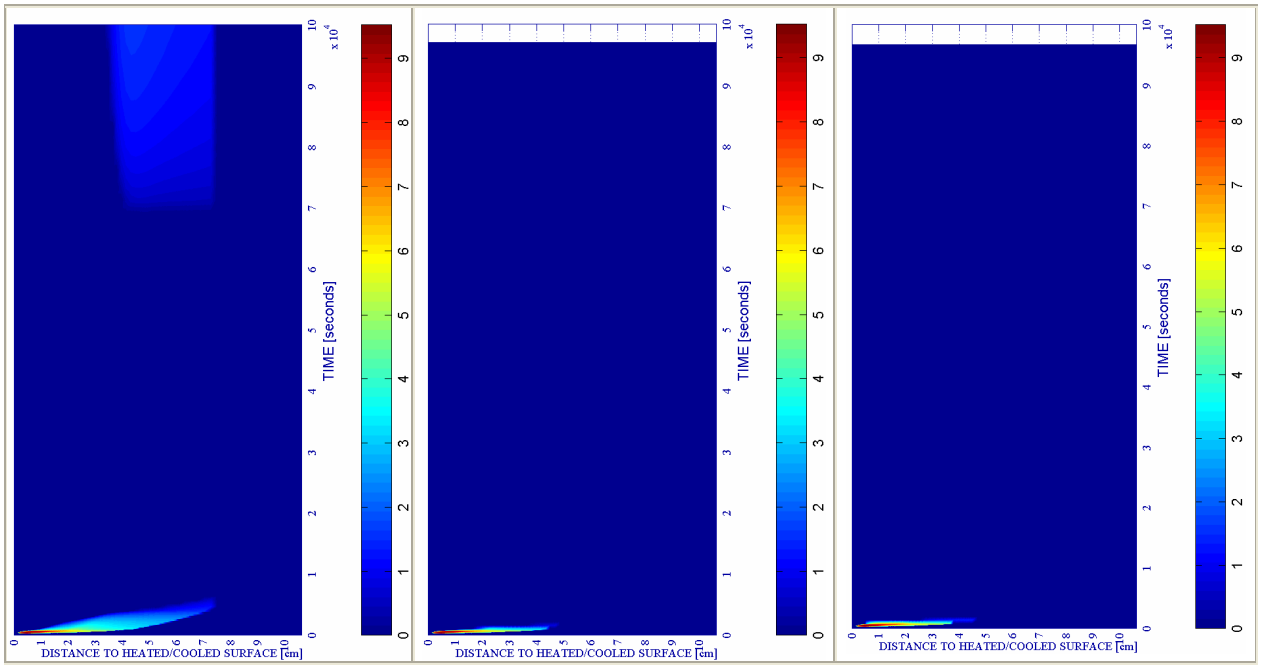

Slow environmental cooling *Medium environmental cooling* *Fast environmental cooling*

Figure 6-166. *Velocity of Spalled-off pieces [m/s] where mechanical damage $d \geq 0{,}10$*

In the case of the Slow environmental cooling, close to the end of the structural element cooling appears a second 'bag' of zones from 3 to 7 centimetres away from the surface where spalling would be again energetically viable at a stage as late as 27 hours after the start of the heating and more than 26 hours after the fire is supposed to be extinguished if longitudinal stresses at these instants were not of compressive nature.

Related to the final distribution of the mechanical damage values (and, hence, of the cracking level of the structural element) as it can be observed on figure 6-167 non-significant differences are found between those corresponding to Medium and Fast environmental cooling processes. However, the final state of the structural element after a Slow environmental cooling shows higher levels of cracking both in value (almost an 8 per cent higher) and, what it is equally unfavourable due to the loss of resistant surface, in its extent towards inner layers (in the Slow case, more than one third of the depth – the first 4,5 centimetres – of the structural element presents a mechanical damage value greater than 0,50, while this only happens in the first 2,5 centimetres in the Medium and Fast environmental cooling cases):

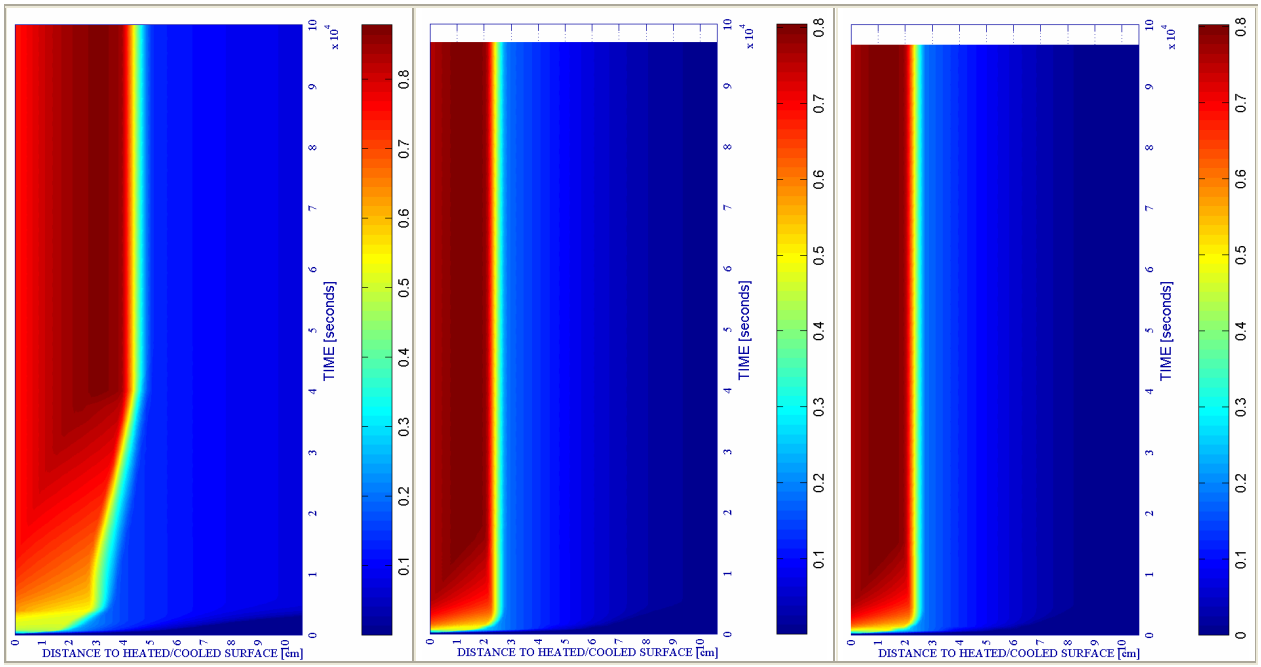

Slow environmental cooling *Medium environmental cooling* *Fast environmental cooling*

Figure 6-167. *Mechanical damage [-]*

However, in both the Medium and Fast environmental cooling cases the maximum values of the cracking level appear much sooner (approximately at 5 hours from the beginning of the fire in front of the 8 hours corresponding to the Slow case) which may lead to a longer and more severe exposition of the reinforcing bars to fire action during the period from 5 to 8 hours.

The relative humidity remaining in the structural element and its residual stress state at the end of its cooling process are also important to understand its future expectable hygro-thermo-chemo-mechanical behaviour.

As it is observed on figure 6-168, the final relative humidity corresponding to a Slow environmental cooling is lower at all the depths of the structural element than in the rest of cases, probably due both to a longer stay at high temperatures and to a higher level of cracking that enables water loss towards the environment.

Referred to the residual longitudinal stress (xx) although its distributions for all the cases are quite similar close to the heated/cooled surface (see figure 6-169) – where high compressive

stresses arise – in several inner layers the Slow environmental cooling case – from 2 to 5 centimetres from surface – is significantly more stressed.

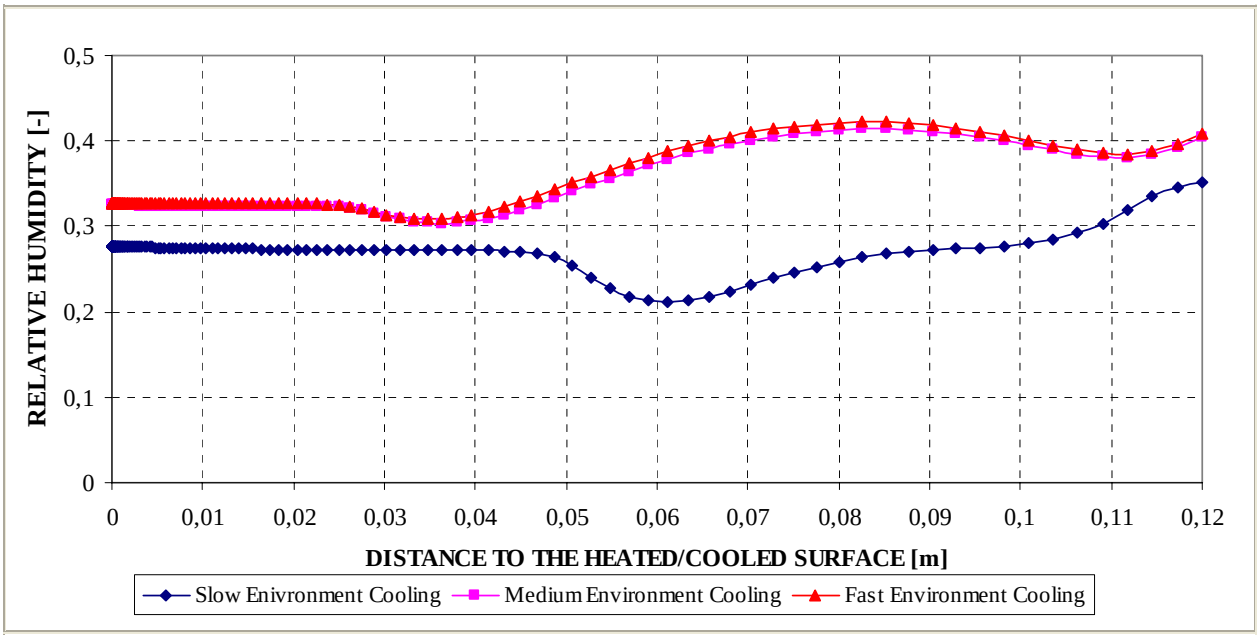

Figure 6-168. *Comparison of the final Relative Humidity [-] for each subtype of environmental cooling*

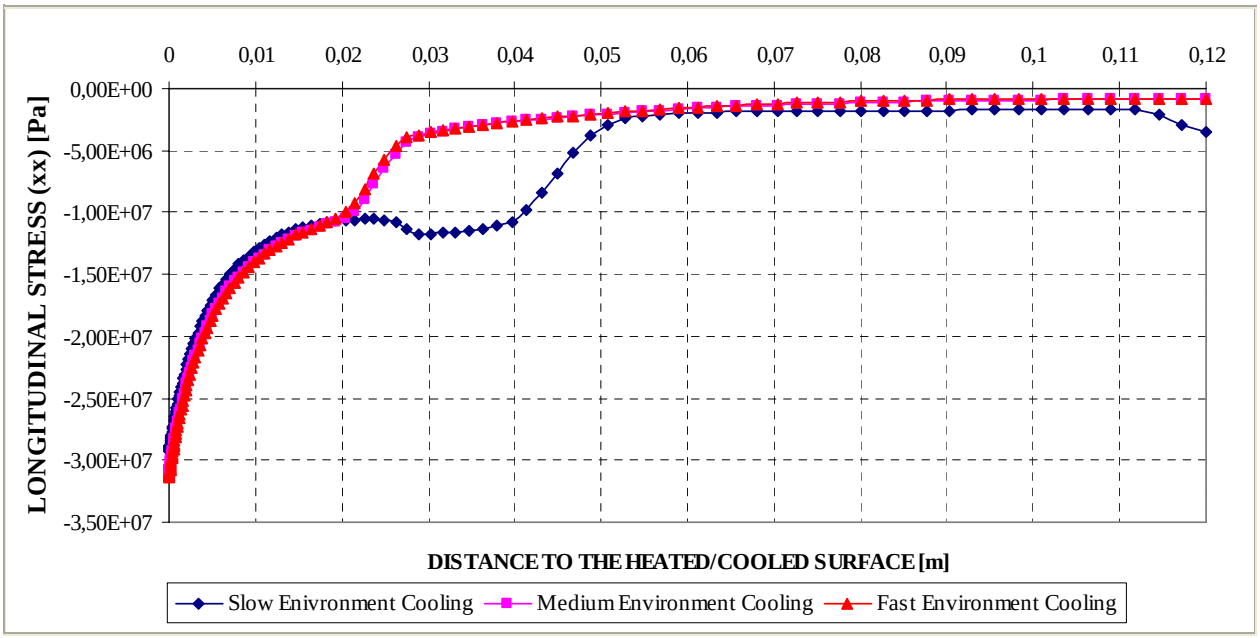

Figure 6-169. *Comparison of the final Longitudinal stress (xx) [Pa] for each subtype of environmental cooling*

In conclusion, from the comparison of these three subtypes of environmental cooling it is deducted that a low environmental cooling rate (i.e. Slow) leads – in the reference case analyzed in this subparagraph – to structural elements more widely damaged (cracked) and with higher residual stresses, being this an expected and quite intuitive conclusion.

6.5.3.1.1.2 Reference case #14 – TH12K018RH50PAR2C60

First, an extract of the compendium of the main results already included in paragraph 6.5.2.8.1, particularized to the cases dealt herein, is included next (it must be noted that 3.360 seconds is the reference cooling start instant considered in this subparagraph). In order to identify correctly the case to which corresponds each set of results included this table, the equivalence described in next table must be studied first:

CODE	COOLING START TIME (s)	COOLING TYPE	COOLING SUBTYPE	COMBINATION NAME	PC1 (RH) [%]			PC2 (K) [m²]			PC3 (TH) [cm]	PC4 (Heating curve)			PC5 (Mat)	
					40	50	60	10^{-19}	10^{-18}	10^{-17}	12	PAR1	PAR2	PAR4	C60	C90
21	3360	ENV	SLOW	TH12K018RH50PAR2C60		x			x		x		x		x	
22			MEDIUM													
23			FAST													

Table 6-111. *Equivalence table used to identify each case (highlighted in blue is the code assigned to each case that must be used to search the corresponding results on Table 6-112).*

CASE	$IS4_{max}$ [-]	X_{IS4max} [cm]	t_{IS4max} [s]	v_{max} [m/s]	X_{vmax} [cm]	t_{vmax} [s]	v_{max}* [m/s]	X_{vmax*} [cm]	t_{vmax*} [s]	d_{max} [-]	X_{dmax} [cm]	t_{dmax} [s]	T_{max} [K]	X_{Tmax} [cm]	t_{Tmax} [s]	p^g_{max} [MPa]	X_{pgmax} [cm]	t_{pgmax} [s]
21	0,1004	1,035	3.390	5,453	1,644	3.480	5,453	1,644	3.480	0,9204	3,964	102.000	656,65	0,000	3.480	0,8256	1,555	2.760
22	0,1004	1,035	3.390	5,453	1,644	3.480	5,453	1,644	3.480	0,8980	3,321	46.932	656,65	0,000	3.480	0,8256	1,555	2.760
23	0,1004	1,035	3.390	5,453	1,644	3.480	5,453	1,644	3.480	0,8995	2,753	44.304	656,65	0,000	3.480	0,8256	1,555	2.760

Table 6-112. *Extract of the Compendium of the maximum value of the main results corresponding to each case described in Table 6-111.*

Regarding the maximum value of the Spalling Index selected herein, I_{s4}, all of the cases dealt in this subparagraph (the three subtypes of environmental cooling) show an identical maximum value since this maximum appears at 3.390 seconds from the beginning of the fire and, hence, prior to the start of the cooling process.

However, in both the Spalling Index value and the energy available for thermal spalling to occur at the end of the structural element environmental cooling the following differences are observed (see figure 6-170):

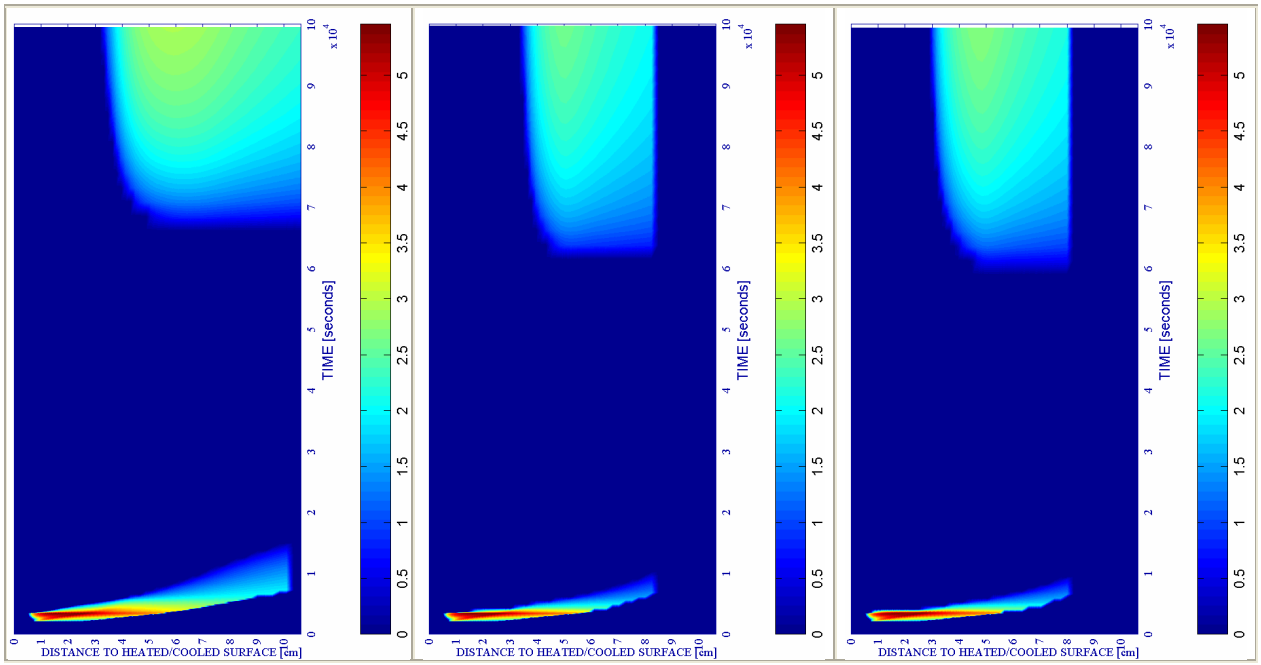

Slow environmental cooling *Medium environmental cooling* *Fast environmental cooling*

Figure 6-170. *Velocity of Spalled-off pieces [m/s] where mechanical damage $d \geq 0{,}10$*

In all of the cases, close to the end of the structural element cooling appears a second 'bag' of zones from 3 to 12 centimetres away from the surface (in Slow cooling, and from 3 to 8 centimetres in the rest of cases) where spalling would be again energetically viable at a stage as late as 20 hours after the start of the heating and more than 18 hours after the fire is supposed to be extinguished if longitudinal stresses at these instants were not of compressive nature (see figure 6-173).

Related to the final distribution of the mechanical damage values (and, hence, of the cracking level of the structural element) as it can be observed on figure 6-171 non-significant differences are found between those corresponding to Medium and Fast environmental cooling

processes. However, the final state of the structural element after a Slow environmental cooling shows high levels of cracking in wider and deeper extents towards inner layers (in the Slow case, almost two thirds of the depth – the first 8 of the total 12 centimetres – of the structural element present a mechanical damage value greater than 0,50, while this only happens in the first 5 centimetres in both the Medium and Fast environmental cooling cases). Despite this fact, the maximum value of the mechanical damage corresponding to the Slow case is only a 2 per cent higher than in the rest of the cases.

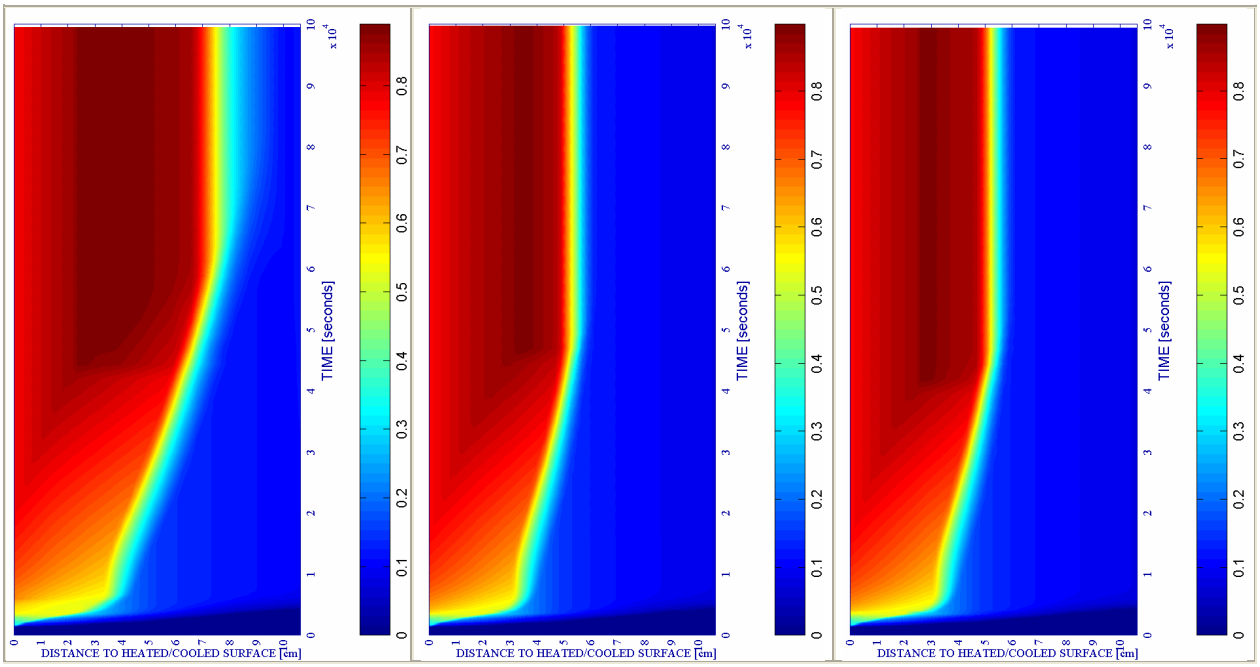

Slow environmental cooling *Medium environmental cooling* *Fast environmental cooling*

Figure 6-171. *Mechanical damage [-]*

Contrarily to what happened in the previous reference case (paragraph 6.5.3.1.1.1), all of the subtypes of environmental cooling lead to the appearance of the highest levels of cracking almost simultaneously, with the only difference that the values of the mechanical damage corresponding to the Slow case keep increasing slightly until the end of the process.

About the relative humidity remaining in the structural element and its residual stress state at the end of its cooling process, both also important to understand its future expectable hygro-thermo-chemo-mechanical behaviour, it is observed on figure 6-172 that the final relative humidity corresponding to a Slow environmental cooling is lower at most of the depths of the structural element than in the rest of cases, probably due both to a longer stay at high temperatures and to a higher level of cracking that enables water loss towards the environment.

Referred to the residual longitudinal stress (xx), its distributions for all the cases are quite similar close to the heated/cooled surface (see figure 6-173) – where high compressive stresses arise – but, as a difference with the previous reference case, in several inner layers (especially from 2 to 4 centimetres from surface) both Medium and Fast environmental cooling processes lead to higher residual stresses – while for deeper layers, again, the Slow case is residually more stressed).

In conclusion, from the comparison of these three subtypes of environmental cooling it is deducted that a low environmental cooling rate (i.e. Slow) leads – in the reference case analyzed in this subparagraph – to structural elements more widely (but not more severely) damaged (cracked) and with residual stresses not necessarily higher than those with faster cooling rates, being this a not so expected conclusion.

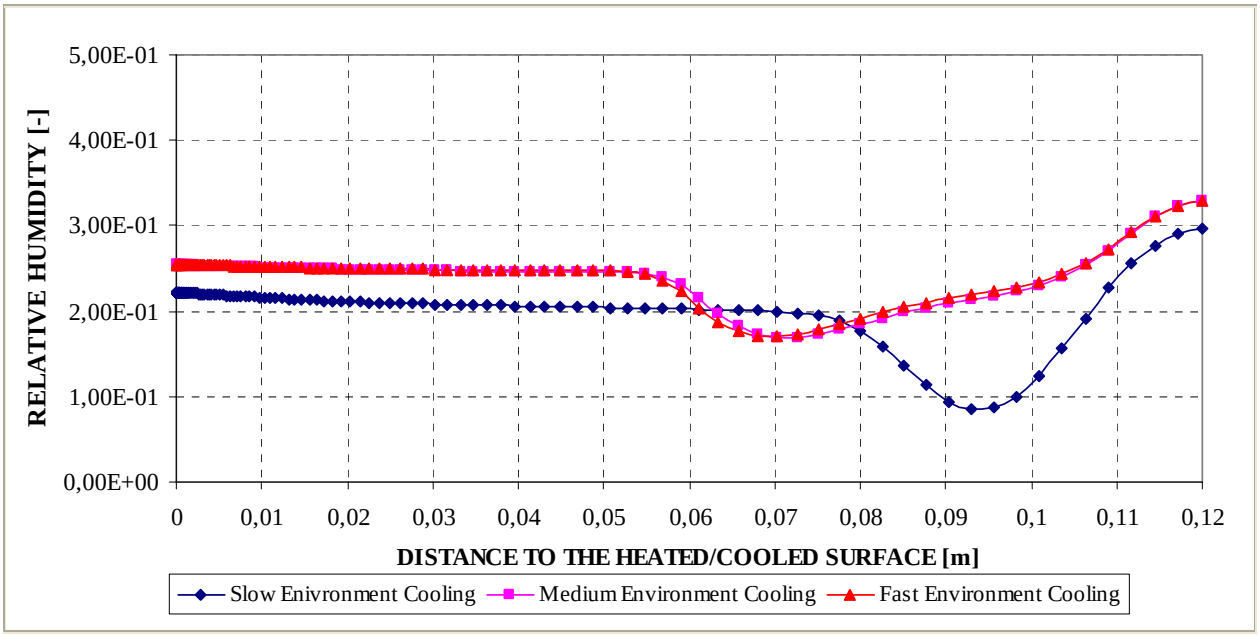

Figure 6-172. *Comparison of the final Relative Humidity [-] for each subtype of environmental cooling*

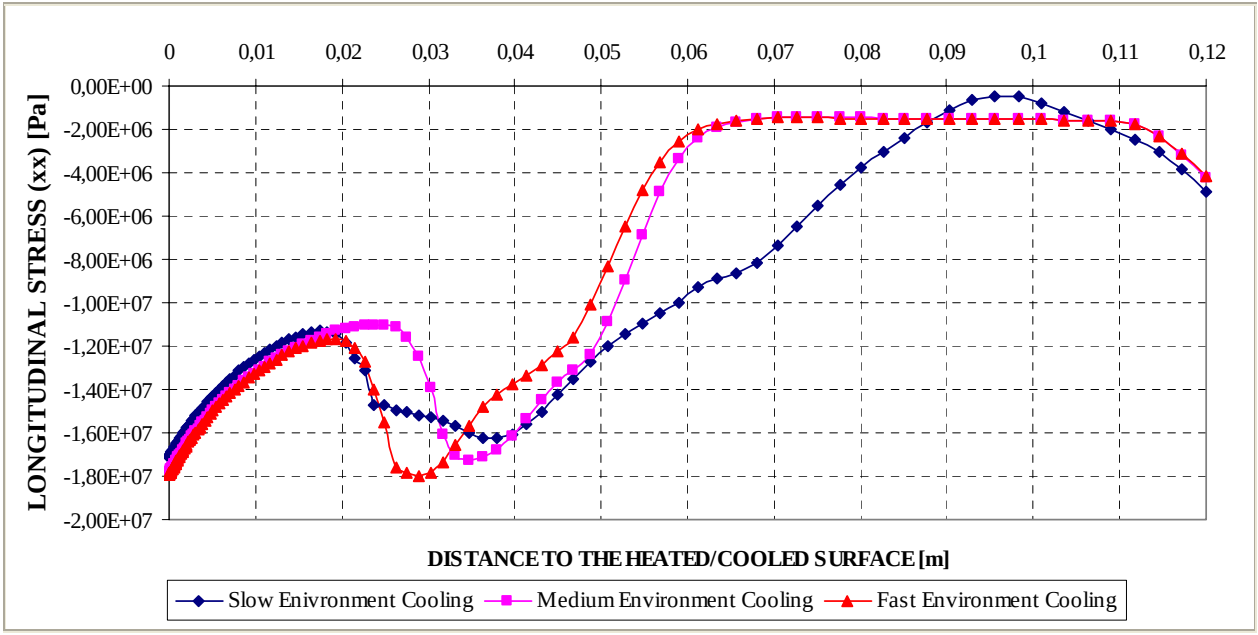

Figure 6-173. *Comparison of the final Longitudinal stress (xx) [Pa] for each subtype of environmental cooling*

6.5.3.1.2 Comparison of the subtypes of Surface Cooling

In order to compare the hygro-thermo-chemo-mechanical state of the structural element at the instant corresponding to three hours after the natural fire start (precisely, the ending instant of the calculations developed), the values and distributions of the parameters and criteria established in paragraph 6.2.2 are considered. Nevertheless, it is remarkable that the case named '*Followed by an imposed constant Surface Temperature*', where the surface temperature is kept constant in order to simulate keeping the water jet applied on the surface for some time more, the time extent of the calculations developed depends on the time when the superficial layers of the structural element become 'completely' damaged, since beyond this instant continuing the calculations is senseless. Therefore, the comparison of this case against the rest must be carefully analyzed since its calculation has not been extended up to three hours from the beginning of the fire but to shorter stages.

6.5.3.1.2.1. Reference case #05 – TH12K018RH50PAR1C60

First, an extract of the compendium of the main results already included in paragraph 6.5.2.8.1, particularized to the cases dealt herein, is included next. In order to identify correctly the case to which corresponds each set of results included this table, the equivalence described in next table must be studied first:

CODE	COOLING START TIME (s)	COOLING TYPE	COOLING SUBTYPE	COMBINATION NAME	PC1 (RH) [%]			PC2 (K) [m²]			PC3 (TH) [cm]	PC4 (Heating curve)			PC5 (Mat)	
					40	50	60	10^{-19}	10^{-18}	10^{-17}	12	PAR1	PAR2	PAR4	C60	C90
4	600	SURF	HEAT	TH12K018RH50PAR1C60												
5			KEEP			X			X		X	X			X	
6			REPEAT													

Table 6-113. *Equivalence table used to identify each case (highlighted in blue is the code assigned to each case that must be used to search the corresponding results on Table 6-114).*

CASE	$IS4_{max}$ [-]	X_{IS4max} [cm]	t_{IS4max} [s]	v_{max} [m/s]	X_{vmax} [cm]	t_{vmax} [s]	v_{max}* [m/s]	X_{vmax*} [cm]	t_{vmax*} [s]	d_{max} [-]	X_{dmax} [cm]	t_{dmax} [s]	T_{max} [K]	X_{Tmax} [cm]	t_{Tmax} [s]	p^g_{max} [MPa]	X_{pgmax} [cm]	t_{pgmax} [s]
4	0,3688	0,582	600	12,349	0,152	240	9,521	0,245	280	0,9900	0-2,497	4.200	1.369,20	0,000	10.800	1,3276	0,860	480
5	0,3688	0,582	600	12,349	0,152	240	9,521	0,245	280	0,8721	0,544	1.163	754,18	0,000	720	1,3276	0,860	480
6	0,3688	0,582	600	12,349	0,152	240	9,521	0,245	280	0,9900	0 – 2,497	4.200	1.369,10	0,000	10.800	1,3276	0,860	480

Table 6-114. *Extract of the Compendium of the maximum value of the main results corresponding to each case described in Table 6-113.*

Regarding the maximum value of the Spalling Index selected herein, I_{s4}, all of the cases dealt in this subparagraph (the three subtypes of surface cooling) show an identical maximum value since this maximum appears at 600 seconds from the beginning of the fire and, hence, prior to the start of the cooling process. However, in both the Spalling Index value and the energy available for thermal spalling to occur at the end of the three hours process the following differences are observed (see figure 6-174):

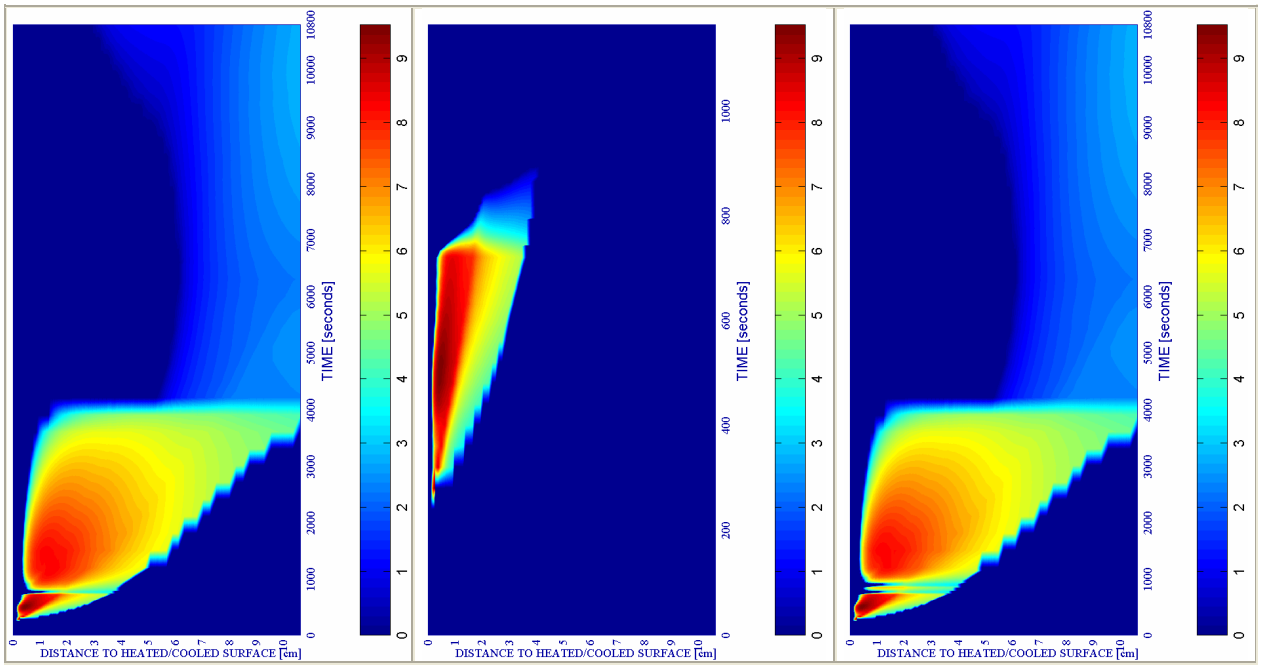

Surface cooling + heating *Surface cooling + imposed cnt. Temperature* *Surface cooling divided into 2 periods*

Figure 6-174. *Velocity of Spalled-off pieces [m/s] where mechanical damage d ≥ 0,10*

The cases '*Followed by heating*' and '*Divided into 2 periods*' lead to qualitative and quantitatively analogous results at the end of the 3 hours from the beginning of the fire, being thermal spalling energetically viable from really early stages up to the end (in this cases, tensile longitudinal stresses keep present until the end of the 3 hours process). On the contrary, the case '*Followed by an imposed constant temperature*' (see figure 6-174 in the centre) show that as

soon as 850 seconds from the beginning of the fire thermal spalling is not energetically viable any longer up to the end of the calculation (calculation that it must be reminded that it only continues until the superficial layers of the structural element become 'completely' damaged). This fact obviously occurs due to the contribution of the second (and third) heating processes that take place in the cases '*Followed by heating*' and '*Divided into 2 periods*' (otherwise, an unfavourable effect of the surface cooling on the thermal spalling risk would have to be understood, conclusion that has not derived from any of the cases analyzed in this Chapter).

Related to the final distribution of the mechanical damage values (and, hence, of the cracking level of the structural element) as it can be observed on figure 6-175 non-significant differences are found between those corresponding to '*Followed by heating*' and '*Divided into 2 periods*' processes, what suggests a quite local and limited effect of the second surface cooling process developed in the '*Divided into 2 periods*' case, as explained in previous paragraphs. In the meantime, in the '*Followed by an imposed constant temperature*' case it is remarkable the faster increase rate of mechanical damage close to the surface if compared to the others but only in a narrow layer close to the heated/cooled surface.

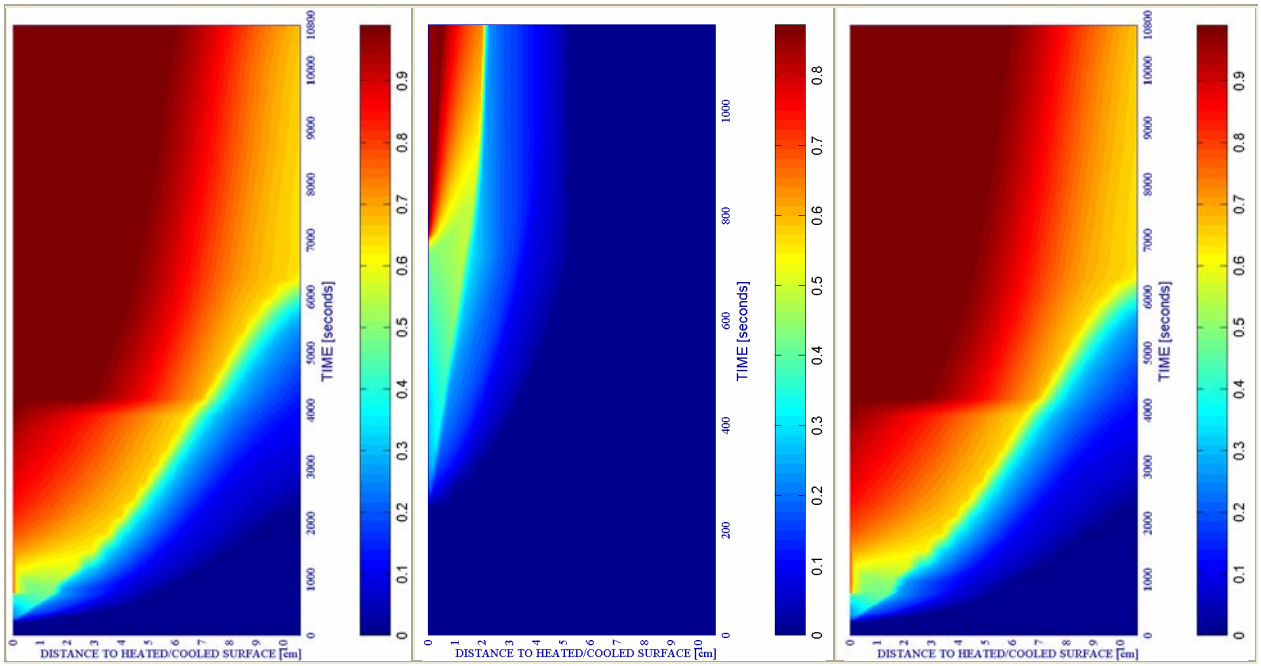

Surface cooling + heating *Surface cooling + imposed cnt. Temperature* *Surface cooling divided into 2 periods*

Figure 6-175. *Mechanical damage [-]*

In both '*Followed by heating*' and '*Divided into 2 periods*', the relative humidity remaining in the structural element after three hours from the beginning of the natural fire is not of interest since it is approximately zero at all the depths and with no significant differences (see figures 6-76 h) and 6-87 h)). Regarding the final distribution of temperature in the structural element, it is remarkable that no significant differences arise between the '*Followed by heating*' and '*Divided into 2 periods*' cases (see figures 6-76 i) and 6-87 i)) despite introducing in the latter an additional surface cooling process.

Referred to the residual longitudinal stress (xx), its distributions for both the '*Followed by heating*' and '*Divided into 2 periods*' cases are quite similar at all the depths (see figure 6-176) – arising elsewhere tensile stresses in the longitudinal directions and compressive in the transversal one – (remember that, in figure 6-179, the stress distribution corresponding to the '*Followed by an imposed constant temperature*' case is not represented at the same instant as the others but at a much earlier stage).

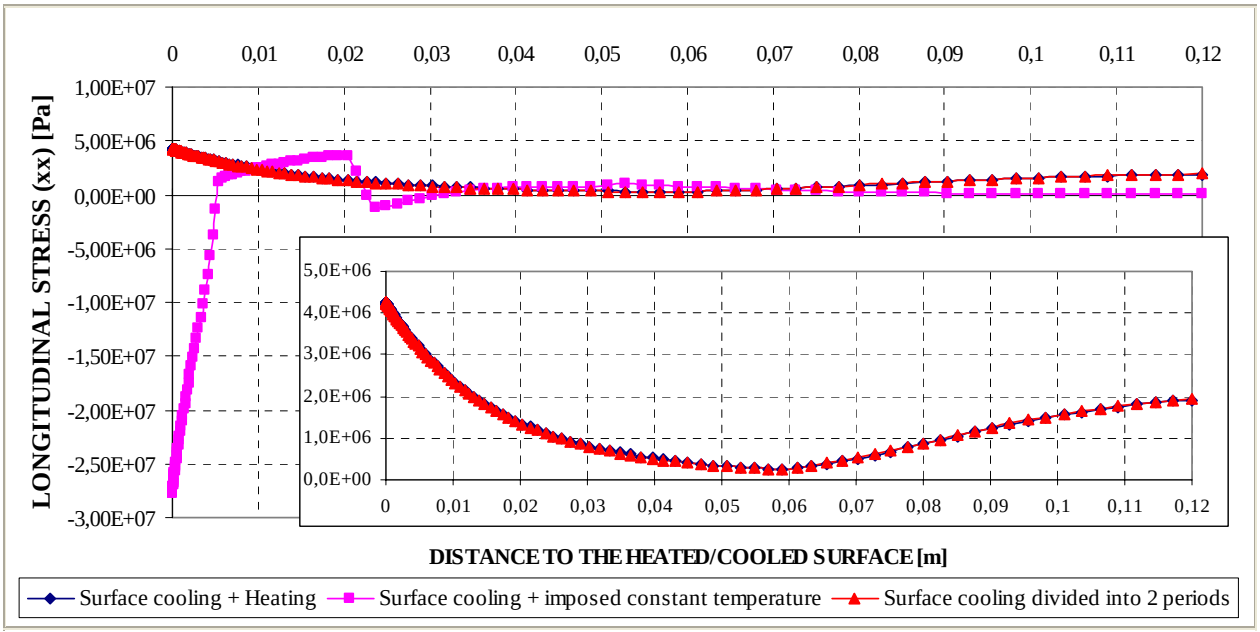

Figure 6-176. *Comparison of the Longitudinal stress (xx) [Pa] after 3 hours for each subtype of surface cooling*

In conclusion, from the comparison of these three subtypes of surface cooling it is deducted that the number of temperature cycles of similar amplitude – i.e. the number of sweeps done by the Fire-Fighter applying the water jet on the surface of the structural element (among one and two cycles/sweeps) – does not appear to lead to significant differences after 3 hours from the start of the natural fire. With respect to the case where the water jet is kept applied to the surface of the wall over a longer period, it is observed that higher cracking rates appear in a narrow layer close to the heated/cooled surface.

6.5.3.1.2.2. Reference case #14 – TH12K018RH50PAR2C60

First, an extract of the compendium of the main results already included in paragraph 6.5.2.8.1, particularized to the cases dealt herein, is included next. In order to identify correctly the case to which corresponds each set of results included this table, the equivalence described in next table must be studied first:

CODE	COOLING START TIME (s)	COOLING TYPE	COOLING SUBTYPE	COMBINATION NAME	PC1 (RH) [%]			PC2 (K) [m²]			PC3 (TH) [cm]	PC4 (Heating curve)			PC5 (Mat)	
					40	50	60	10^{-19}	10^{-18}	10^{-17}	12	PAR1	PAR2	PAR4	C60	C90
24	3360	SURF	HEAT	TH12K018RH50PAR2C60												
25			KEEP			X			X		X		X		X	
26			REPEAT													

Table 6-115. *Equivalence table used to identify each case (highlighted in blue is the code assigned to each case that must be used to search the corresponding results on Table 6-116).*

CASE	$IS4_{max}$ [-]	X_{IS4max} [cm]	t_{IS4max} [s]	v_{max} [m/s]	X_{vmax} [cm]	t_{vmax} [s]	v_{max}* [m/s]	X_{vmax*} [cm]	t_{vmax*} [s]	d_{max} [-]	X_{dmax} [cm]	t_{dmax} [s]	T_{max} [K]	X_{Tmax} [cm]	t_{Tmax} [s]	p^g_{max} [MPa]	X_{pgmax} [cm]	t_{pgmax} [s]
24	0,1004	1,035	3.390	6,631	3,172	10.800	6,631	3,172	10.800	0,8475	0,000	3.516	982,75	0,000	10.800	0,8256	1,555	2.760
25	0,1004	1,035	3.390	5,453	1,644	3.480	5,453	1,644	3.480	0,8923	0,010	3.528	656,65	0,000	3.480	0,8256	1,555	2.760
26	0,1004	1,035	3.390	6,622	3,172	10.800	6,622	3,172	10.800	0,8606	0,000	3.750	982,48	0,000	10.800	0,8256	1,555	2.760

Table 6-116. *Extract of the Compendium of the maximum value of the main results corresponding to each case described in Table 6-115.*

Regarding the maximum value of the Spalling Index selected herein, I_{s4}, all of the cases dealt in this subparagraph (the three subtypes of surface cooling) show an identical maximum value since this maximum appears at 3.390 seconds from the beginning of the fire and, hence, prior to the start of the cooling process. In both the Spalling Index value and the energy available for thermal spalling to occur at the end of the three hours process neither significant differences are observed after 3 hours from the start of the fire (see figure 6-177):

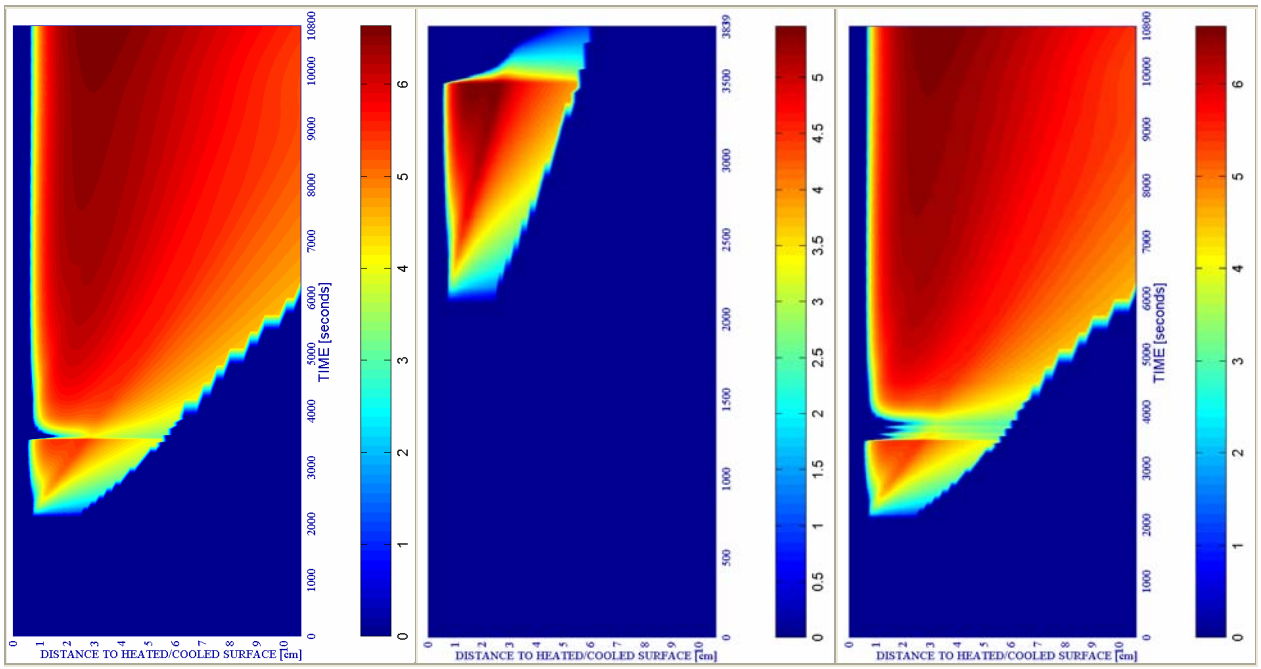

Surface cooling + heating *Surface cooling + imposed cnt. Temperature* *Surface cooling divided into 3 periods*

Figure 6-177. *Velocity of Spalled-off pieces [m/s] where mechanical damage d ≥ 0,10*

Hence, the cases '*Followed by heating*' and '*Divided into 3 periods*' lead to qualitative and quantitatively analogous results at the end of the 3 hours from the beginning of the fire, being thermal spalling energetically viable from really early stages up to the end (in this cases, tensile longitudinal stresses keep present until the end of the 3 hours process).

On the contrary, the case '*Followed by an imposed constant temperature*' (see figure 6-177 in the centre) show that as soon as 3.839 seconds from the beginning of the fire thermal spalling is not energetically viable any longer up to the end of the calculation (calculation that it must be reminded that it only continues until the superficial layers of the structural element become almost 'completely' damaged). This fact obviously occurs due to the contribution of the second (and third) heating processes that take place in the cases '*Followed by heating*' and '*Divided into 3 periods*' (otherwise, an unfavourable effect of the surface cooling on the thermal spalling risk would have to be understood, conclusion that has not derived from any of the cases analyzed in this Chapter).

Related to the final distribution of the mechanical damage values (and, hence, of the cracking level of the structural element) as it can be observed on figure 6-178 non-significant differences are found between those corresponding to '*Followed by heating*' and '*Divided into 3 periods*' processes, what suggests a quite local and limited effect of the second and third surface cooling processes developed in the '*Divided into 3 periods*' case, as explained in previous paragraphs.

What it is more relevant is that in the '*Followed by an imposed constant temperature*' case a considerably faster increase rate of mechanical damage close to the surface – if compared to the rest of the cases –, but only in a narrow layer close to the heated/cooled surface, arise. Hence, as soon as only 119 seconds (2 minutes) after the start of the cooling process, the mechanical damage level (0,8923 at the maximum) is already a five per cent higher than in the '*Followed by heating*' and '*Divided into 3 periods*' cases as late as 7.080 seconds (118 minutes) after the start of the cooling process. This trend denotes a quite unfavourable effect, from a mechanistic point of view, of a long application of a water jet on the heated surface of a structural element.

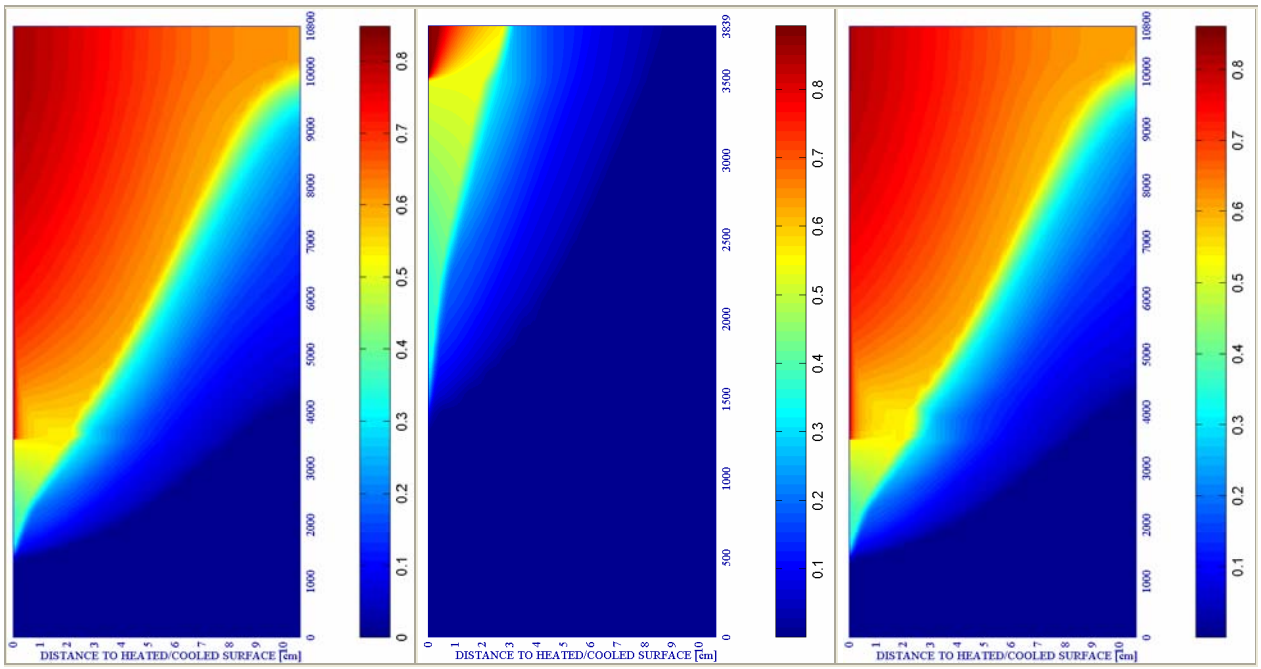

Surface cooling + heating | *Surface cooling + imposed cnt. Temperature* | *Surface cooling divided into 3 periods*

Figure 6-178. *Mechanical damage [-]*

In both '*Followed by heating*' and '*Divided into 2 periods*', the relative humidity remaining in the structural element after three hours from the beginning of the natural fire is not of interest since it is close to zero at all the depths and with no significant differences (see figures 6-129 h) and 6-140 h)). Regarding the final distribution of temperature in the structural element, it is remarkable that no significant differences arise between the '*Followed by heating*' and '*Divided into 2 periods*' cases (see figures 6-129 i) and 6-140 i)) despite introducing in the latter two additional surface cooling process. Referred to the residual longitudinal stress (xx), its distributions for both the '*Followed by heating*' and '*Divided into 3 periods*' cases are quite similar at all the depths (see figure 6-179) – arising elsewhere tensile stresses in the longitudinal directions and compressive in the transversal one – (remember that, in figure 6-179, the stress distribution corresponding to the '*Followed by an imposed constant temperature*' case is not represented at the same instant as the others but at a much earlier stage).

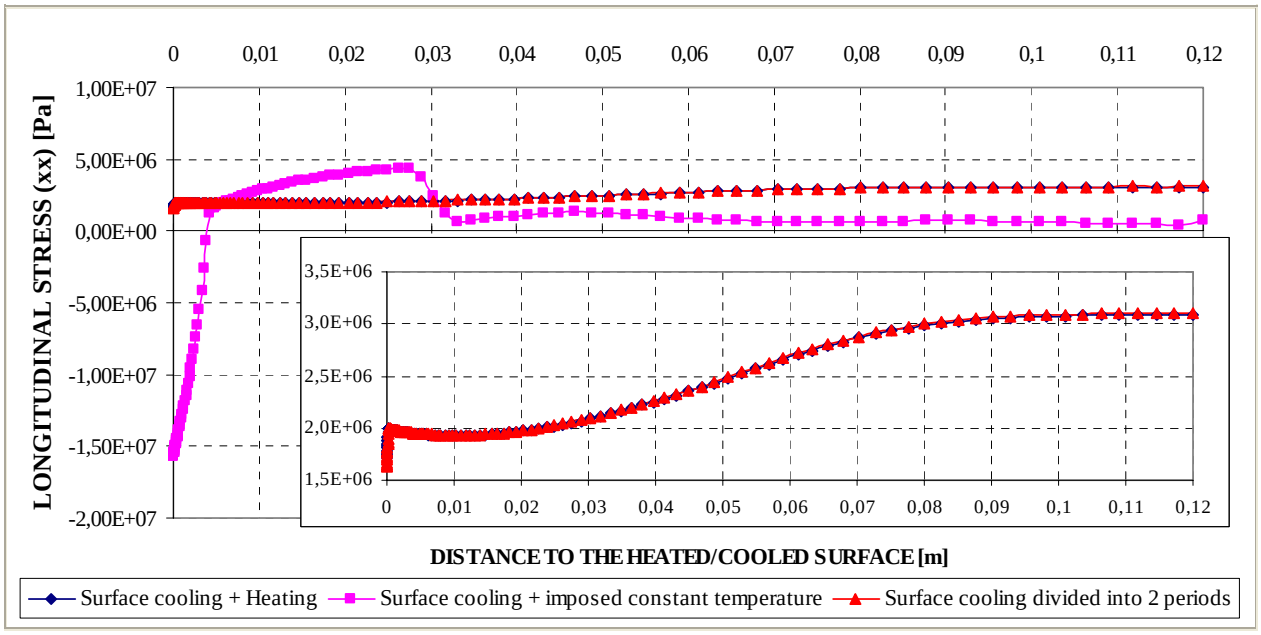

Figure 6-179. *Comparison of the Longitudinal stress (xx) [Pa] after 3 hours for each subtype of surface cooling*

In conclusion, from the comparison of these three subtypes of surface cooling it is deducted that the number of temperature cycles of similar amplitude (among one and three cycles) does not appear to lead to significant differences after 3 hours from the start of the natural fire. With respect to the case where the water jet is kept applied to the surface of the wall over a longer period, it is observed a considerably faster increase rate of mechanical damage close to the surface – if compared to the rest of the cases – arising hence the maximum of the mechanical damage value in this case, only in 2 minutes after the start of the cooling process, beyond the maximum cracking levels that are achieved in almost 2 hours in the '*Followed by heating*' and '*Divided into 3 periods*' cases. As already stated, this trend denotes a quite unfavourable effect, from a mechanistic point of view, of a long application of a water jet on the heated surface of a structural element.

6.5.3.1.3 Comparison of the Environmental Cooling versus the Surface Cooling and the No-Cooling case

Within this paragraph, a comparative analysis is developed from the results described previously in this Chapter in order to discern the effect of the type of cooling – environmental cooling, surface cooling or not cooling at all – on the hygro-thermo-chemo-mechanical state of a structural element (especially after the extinguishment of a fire in a High-Rise Building). This comparison is developed on one of the selected reference cases: reference case #14 – TH12K018RH50PAR2C60.

6.5.3.1.3.1. Comparison of the Slow Environmental Cooling versus the Natural Cooling cases

For this analysis, the calculation case where no cooling actions (neither environmental nor surface) are introduced during the three first hours from the beginning of the fire (case number 27 in Tables 6-107 and 6-117) has been extended by means of a subsequent 'natural' (parametric) cooling process of the structural element temperature down to ambient temperature. In this way it is provided enough information in order to compare the final hygro-thermo-chemo-mechanical states of a structural element existent in a room of a High-Rise Building where fire fighting actions (in the form of environmental slow cooling processes starting either at 1.800 or at 3.360 seconds) are / are not introduced during the natural fire evolution. Hence, the natural cooling curves adopted to accomplish this extension are the time-temperature parametric curves provided by Eurocode 1 Part 1-2 [28], as follows (for more details see paragraph 6.4.3.2.3.2):

$$
\begin{aligned}
&\Theta_g = \Theta_{\max} - 625 \cdot (t^* - t^*_{\max} \cdot x) \\
&\textit{where} \quad t^* = t \cdot \Gamma, \textit{with}\, \Gamma = 0{,}076\,(\textit{'slow curve' PAR2, opening coefficient}\, O = 0{,}02) \\
&\qquad t^*_{\max} = (0{,}2 \cdot 10^{-3} \cdot q_{t,d} / O) \cdot \Gamma = 0{,}228 \le 0{,}5 \\
&\qquad\quad (\textit{where}\, q_{t,d} = 286\, MJ/m^2, q_{f,d} = 1.145\, MJ/m^2) \\
&\qquad \Theta_{\max} = 1.021{,}3\, K\ (\textit{temperature at}\, t_{\max}) \\
&\qquad x = 1{,}0\,(t_{\max} > t_{\lim})\ (\textit{where}\, t_{\lim} = 20\,\min - \textit{medium fire} - \textit{and}\, t_{\max} = 180\,\min)
\end{aligned}
\tag{6.34}
$$

First, an extract of the compendium of the main results already included in paragraph 6.5.2.8.1, particularized to the cases dealt herein, is included next. In order to identify correctly the case to which corresponds each set of results included this table, the equivalence described in next table must be studied first:

CODE	COOLING START TIME (s)	COOLING TYPE	COOLING SUBTYPE	COMBINATION NAME	PC1 (RH) [%]			PC2 (K) [m²]			PC3 (TH) [cm]	PC4 (Heating curve)			PC5 (Mat)	
					40	50	60	10^{-19}	10^{-18}	10^{-17}	12	PAR1	PAR2	PAR4	C60	C90
8	1800	ENV	SLOW	TH12K018RH50PAR2C60		X			X		X		X		X	
21	3360	ENV	SLOW	TH12K018RH50PAR2C60		X			X		X		X		X	
27Ext.	10.800	NATURAL		TH12K018RH50PAR2C60		X			X		X		X		X	

Table 6-117. *Equivalence table used to identify each case (highlighted in blue is the code assigned to each case that must be used to search the corresponding results on Table 6-118).*

CASE	$IS4_{max}$ [-]	X_{IS4max} [cm]	t_{IS4max} [s]	v_{max} [m/s]	X_{vmax} [cm]	t_{vmax} [s]	v_{max}* [m/s]	X_{vmax*} [cm]	t_{vmax*} [s]	d_{max} [-]	X_{dmax} [cm]	t_{dmax} [s]	T_{max} [K]	X_{Tmax} [cm]	t_{Tmax} [s]	p^{g}_{max} [MPa]	X_{pgmax} [cm]	t_{pgmax} [s]
8	0,0129	0,227	1.920	0,000	---	---	0,000	---	---	0,6634	0,412	6.360	467,16	0,000	1.920	0,5967	0,582	1.920
21	0,1004	1,035	3.390	5,453	1,644	3.480	5,453	1,644	3.480	0,9204	3,964	102.000	656,65	0,000	3.480	0,8256	1,555	2.760
27Ext.	0,1010	1,099	3.480	6,635	3,172	10.800	6,635	3,172	10.800	0,9900	0,000	90.000	982,90	0,000	10.800	0,8256	1,555	2.760

Table 6-118. *Extract of the Compendium of the maximum value of the main results corresponding to each case described in Table 6-117.*

It is remarkable to explain that the calculation corresponding to the case named '27ext', where the natural (parametric) cooling is introduced at an absolute time of 10.800 seconds, has presented a lack of convergence at 90.000 seconds. At this instant, the temperature at the structural element surface is still of 367 K while the maximum temperature within the inner layers is still of 375 K. Since these values have not already achieved the ambient temperature (298,15K) the comparison against the other cases considered in this paragraph has to be developed carefully when related to the final state of the structural element.

Regarding the maximum value of the Spalling Index selected herein, I_{s4}, all of the cases dealt in this subparagraph show maximum values prior to the start of the corresponding cooling processes, being the highest that belonging to the case where no cooling actions are applied during the first three hours (case named '27ext').

However, related to the energy available for thermal spalling to occur at the end of the structural element environmental cooling the following differences are observed (see figure 6-180):

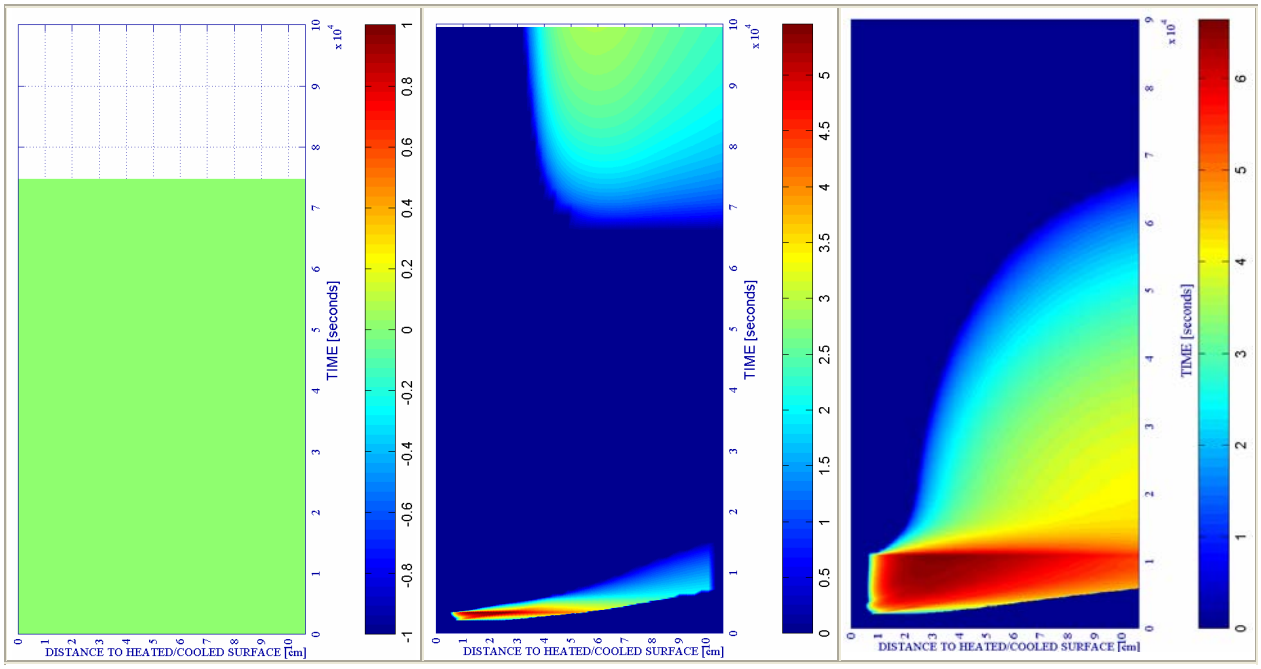

Slow environmental cooling (start 1.800s) *Slow environmental cooling (start 3.360s)* *Natural cooling (start 10.800s)*

Figure 6-180. *Velocity of Spalled-off pieces [m/s] where mechanical damage $d \geq 0{,}10$*

In the case where the slow environmental cooling process starts earlier (see figure 6-180 left) spalling is not energetically-mechanically viable at any instant during the whole process. With respect to the case where the slow environmental cooling process starts at 3.360 seconds (see figure 6-180 centre) close to the end of the structural element cooling appears a second 'bag' of zones from 3 to 12 centimetres away from the surface where spalling would be again energetically viable at a stage as late as 20 hours after the start of the heating and more than 18 hours after the fire is supposed to be extinguished if longitudinal stresses at these instants were not of compressive nature (see figure 6-184) so, in conclusion, for this case thermal spalling is not viable later than an absolute time of four hours. On the contrary, if it is analyzed the case

where no 'forced cooling' actions are introduced, i.e. the case with natural cooling (see figure 6-180 right), it is significant the very long period during the natural cooling process at which thermal spalling is energetically and mechanically viable, i.e. up to nineteen hours after the fire has begun.

Related to the final distribution of the mechanical damage values (and, hence, of the cracking level of the structural element), and keeping in mind that the case named '27ext', where the natural (parametric) cooling is introduced at an absolute time of 10.800 seconds, has not been developed until the ambient temperature is reached again in the whole structural element (so what it is exposed next will actually be more critical) as it can be observed on figure 6-181 extremely significant differences are found: the final state of the structural element after a Slow environmental cooling starting at 3.360 seconds (see figure 6-181 centre) shows high levels of cracking in much wider and deeper extents towards inner layers than when the cooling process is started earlier at 1.800 seconds (see figure 6-181 left) (almost two thirds of the depth of the structural element – the first 8 of the total 12 centimetres – present a mechanical damage value greater than 0,50, while this only happens in the first centimetre when the slow environmental cooling process starts earlier).

However, the more significant difference in the mechanical damage distribution and evolution appears at the case named '27ext', where the natural (parametric) cooling is introduced at an absolute time of 10.800 seconds (see figure 6-181 right): in this case, the mechanical damage values existent at 10.800 seconds, i.e. the start of the natural cooling process, are kept almost constant during a very long cooling period, i.e. from three to sixteen hours from the start of the fire, showing moderately high values (higher than the 60 per cent) at all the depths of the structural element. Then, at sixteen hours from the start of the fire, i.e. thirteen hours after the start of the natural cooling process, mechanical damage values begin to increase again at all the depths of the structural element without stopping this increase until the end of the calculation developed and reaching 'completely fractured' values at the layers close to the heated/cooled surface (being equal to 0,99 at this zone and probably being the reason for the lack of convergence of the calculation at this point).

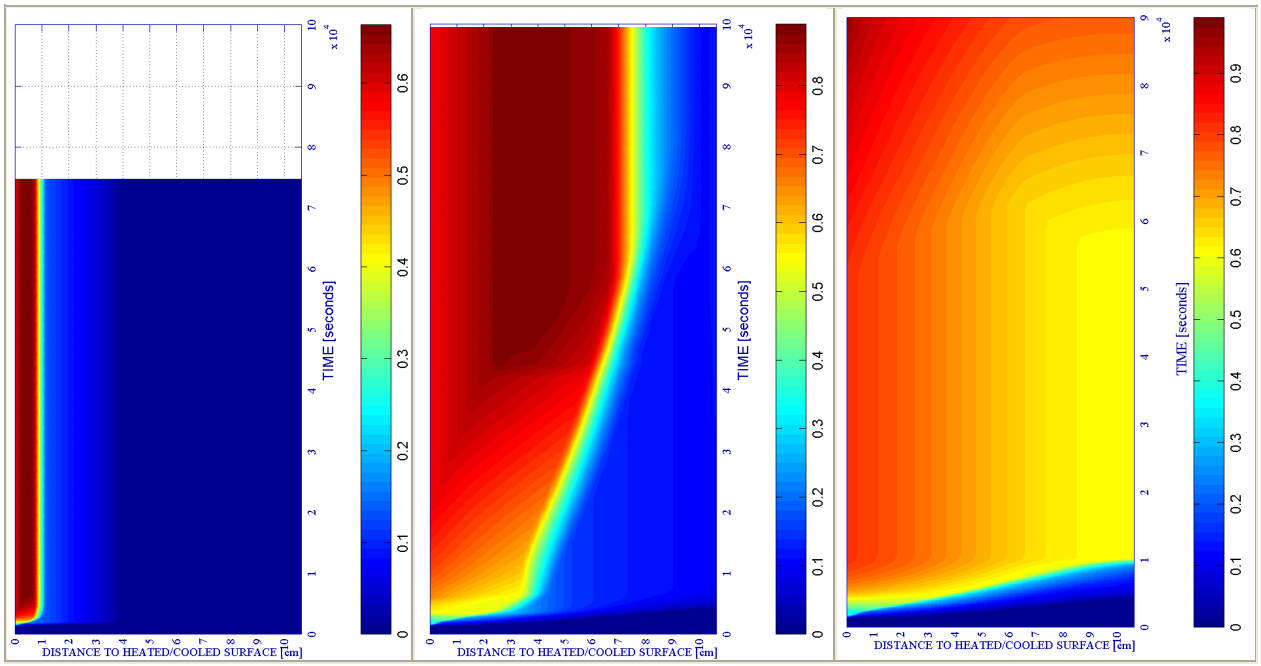

Slow environmental cooling (start 1.800s) *Slow environmental cooling (start 3.360s)* *Natural cooling (start 10.800s)*

Figure 6-181. *Mechanical damage [-]*

However, it is remarkable that the position of the most fractured layers is completely different in each case (at least, up to the extent of the available calculated instants in the case named '27ext'):

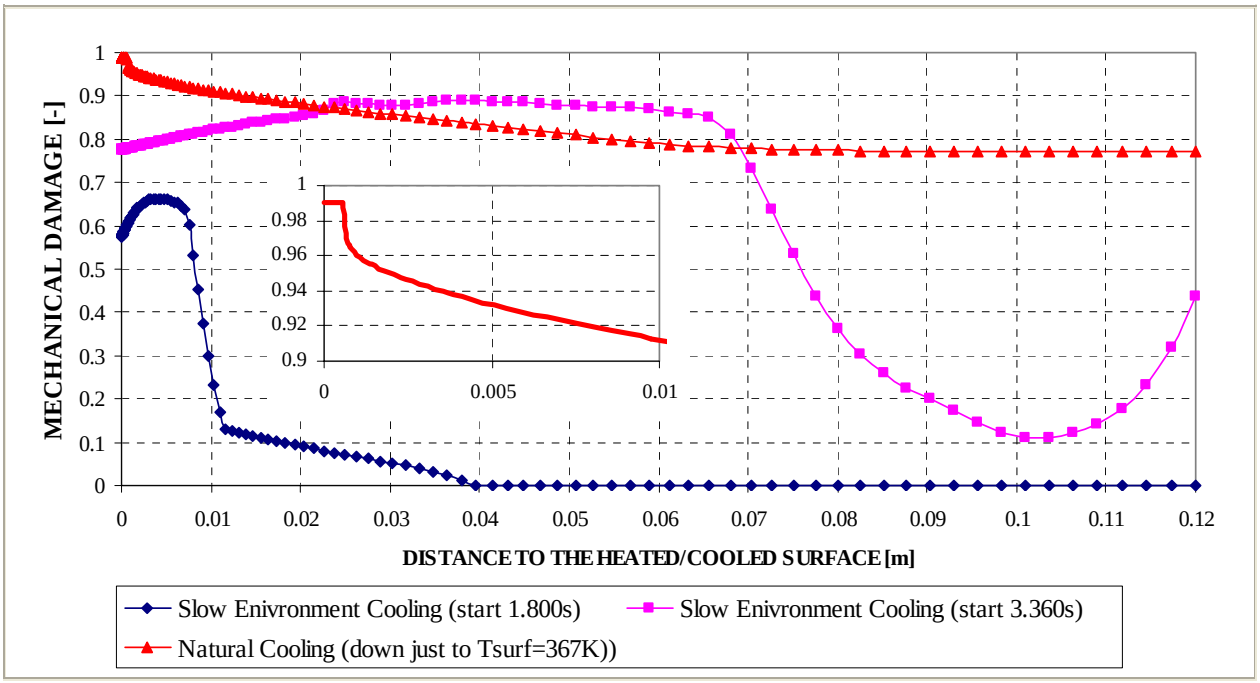

Figure 6-182. *Comparison of the final Mechanical Damage [-] for each type of cooling*

When the environmental slow cooling process starts earlier (at 1.800 seconds) the most fractured layers appear in the first centimetre close to the surface. If this process starts later, at 3.360 seconds, the maximum values of the mechanical damage appear farther from the surface, from two to four centimetres away from it. However, in the case where a natural cooling process is considered, the most fractured layers arise at the surface (and, more precisely, at the first five millimetres).

Nevertheless, it is very important to observe that at the positions where reinforcing bars are expected to be located (beyond three centimetres from surface) mechanical damage values arisen in the case with an environmental slow cooling starting at 3.360 seconds are higher (about a ten per cent) than those corresponding to the case including a natural cooling process (as previously said, at least up to the extent of the available calculated instants in the case named '27ext'). However, further developments of the numerical model used in the calculations would be needed to confirm this fact at the ultimate end of the cooling of case named '27ext', what obviously falls out of the scope of this Thesis, as it is explained in the paragraph corresponding to the extended tasks to go more deeply into Thermal Spalling study (see paragraph 6.6).

About the relative humidity remaining in the structural element and its residual stress state at the end of its cooling process, both also important to understand its future expectable hygro-thermo-chemo-mechanical behaviour, it is observed on figure 6-183 that the final relative humidity corresponding to a Slow environmental cooling (starting either at 1.800 or at 3.360 seconds) is higher at all of the depths of the structural element than in the case corresponding to the natural cooling process, probably due both to a longer stay at high temperatures and to a higher level of cracking that enables water loss towards the environment in the latter. However, this conclusion is not definitely confirmed since calculations corresponding to the natural cooling case stopped at a temperature about 75 degrees above the ambient temperature, so during the decrease of this temperature down to the ambient one the infiltration of environmental

humidity inside the structural element can be very pronounced as it is explained on paragraph 6.5.2.8.2.

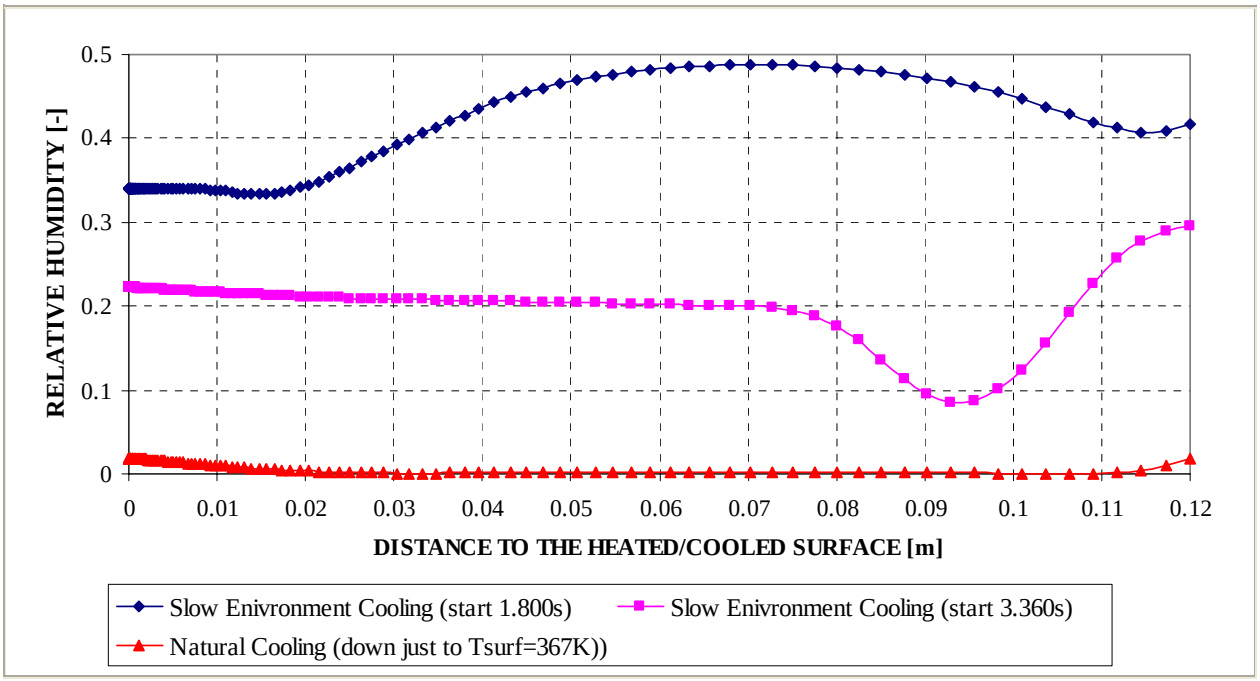

Figure 6-183. *Comparison of the final Relative Humidity [-] for each type of cooling*

Referred to the residual longitudinal stress (xx), although the final stresses distribution in the case of the natural cooling is of tensile nature and showing a really low-stressed state, as it has been repeatedly observed in this chapter late stages of environmental cooling processes may change this typology into compressive, so this conclusion is not definitely confirmed since calculations corresponding to the natural cooling case stopped at a temperature about 75 degrees above the ambient temperature.

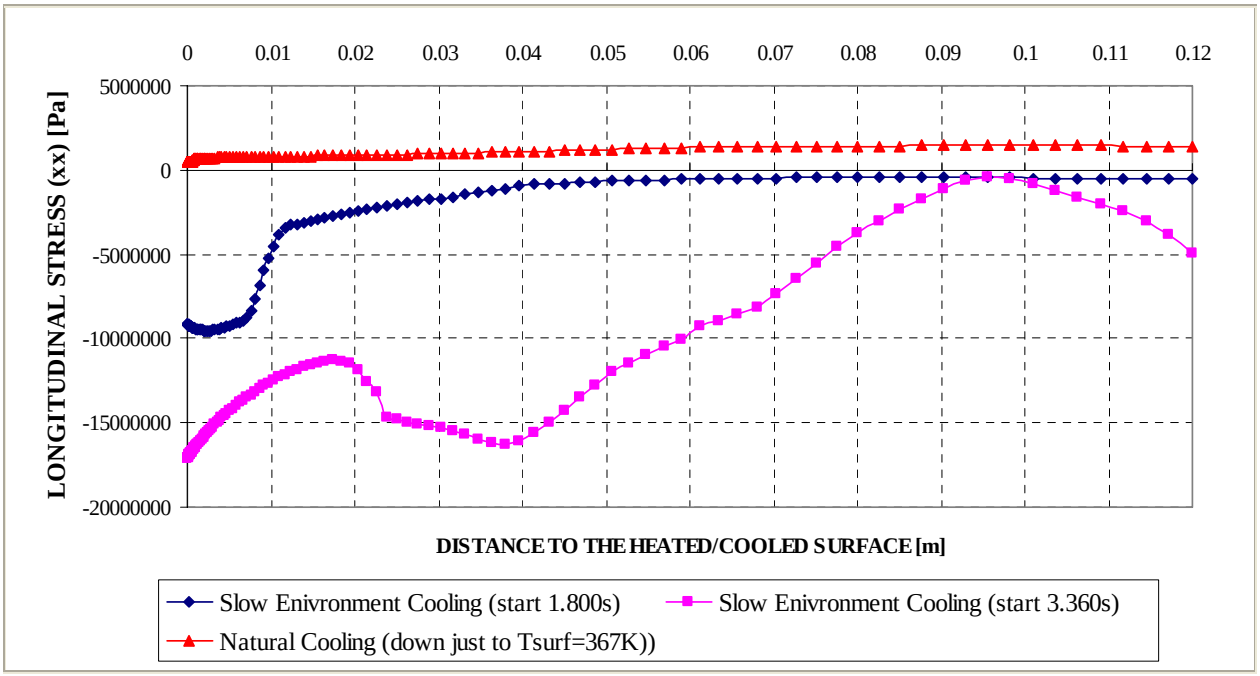

Figure 6-184. *Comparison of the final Longitudinal stress (xx) [Pa] for each type of cooling*

In conclusion, from the comparison of these three types of cooling it is deducted that a natural (parametric) cooling process leads – in the reference case analyzed in this subparagraph –

to structural elements more widely (and more severely) damaged (cracked) and with residual stresses not necessarily higher than those introducing environmental cooling actions, being this a not so expected conclusion. However, it is very important to observe that at the positions where reinforcing bars are expected to be located mechanical damage values (and, hence, the cracking level) arisen in the case with an environmental slow cooling starting at 3.360 seconds are higher (about a ten per cent) than those corresponding to the case including a natural cooling process (as previously said, at least up to the extent of the available calculated instants in the case named '27ext').

6.5.3.1.3.2. Comparison of the Surface Cooling + Heating/Repeating versus the No-Cooling cases

For this analysis, the calculation case where no cooling actions (neither environmental nor surface) are introduced during the three first hours from the beginning of the fire (case number 27 in Tables 6-107 and 6-119) is compared against the case where one/three surface cooling processes are introduced at 3.360 seconds from the beginning of the fire (case numbers 24 and 26 respectively in Tables 6-107 and 6-119):

CODE	COOLING START TIME (s)	COOLING TYPE	COOLING SUBTYPE	COMBINATION NAME	PC1 (RH) [%]			PC2 (K) [m²]			PC3 (TH) [cm]	PC4 (Heating curve)			PC5 (Mat)	
					40	50	60	10^{-19}	10^{-18}	10^{-17}	12	PAR1	PAR2	PAR4	C60	C90
24	3360	SURF	HEAT	TH12K018RH50PAR2C60		X			X		X		X		X	
26			REPEAT													
27	--/--	NO COOL		TH12K018RH50PAR2C60		X			X		X		X		X	

Table 6-119. *Equivalence table used to identify each case (highlighted in blue is the code assigned to each case that must be used to search the corresponding results on Table 6-120).*

CASE	$IS4_{max}$ [-]	X_{IS4max} [cm]	t_{IS4max} [s]	v_{max} [m/s]	X_{vmax} [cm]	t_{vmax} [s]	v_{max}* [m/s]	X_{vmax*} [cm]	t_{vmax*} [s]	d_{max} [-]	X_{dmax} [cm]	t_{dmax} [s]	T_{max} [K]	X_{Tmax} [cm]	t_{Tmax} [s]	p^g_{max} [MPa]	X_{pgmax} [cm]	t_{pgmax} [s]
24	0,1004	1,035	3.390	6,631	3,172	10.800	6,631	3,172	10.800	0,8475	0,000	3.516	982,75	0,000	10.800	0,8256	1,555	2.760
26	0,1004	1,035	3.390	6,622	3,172	10.800	6,622	3,172	10.800	0,8606	0,000	3.750	982,48	0,000	10.800	0,8256	1,555	2.760
27	0,1010	1,099	3.480	6,635	3,172	10.800	6,635	3,172	10.800	0,8115	0,000	10.800	982,90	0,000	10.800	0,8256	1,555	2.760

Table 6-120. *Extract of the Compendium of the maximum value of the main results corresponding to each case described in Table 6-119.*

The first unexpected result observed from the above cases analysis consist on the maximum values of the mechanical damage arisen after the three first hours from the start of the heating.

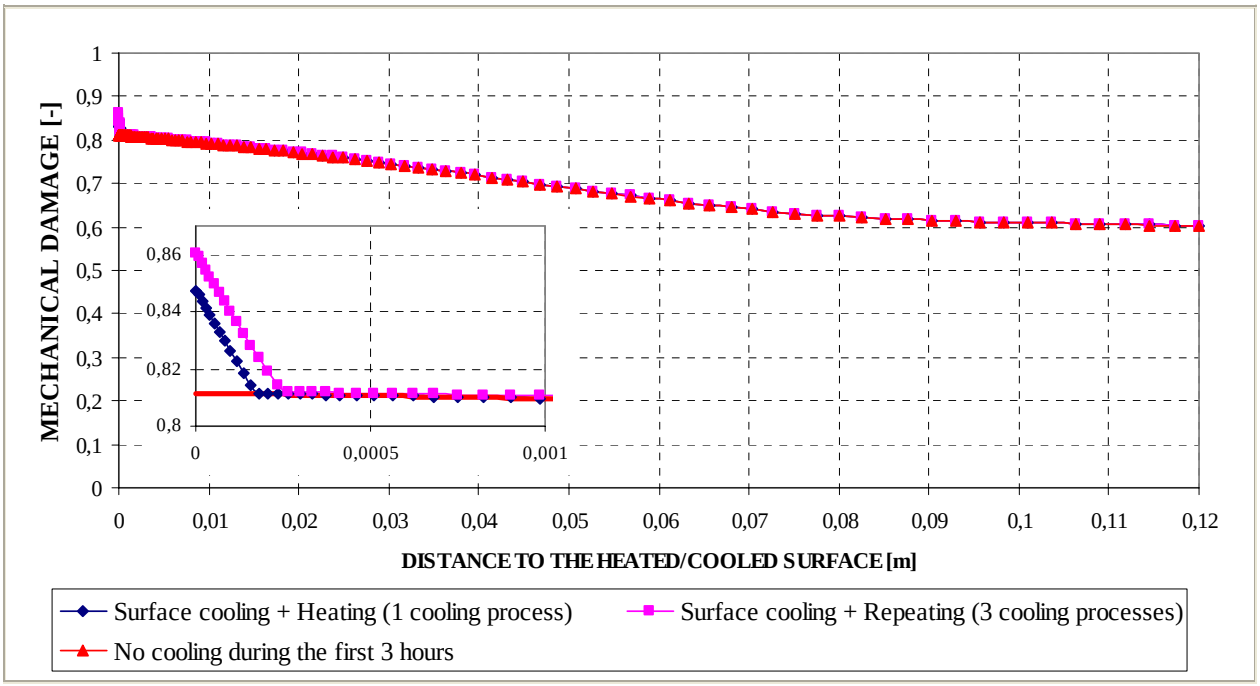

Figure 6-185. *Comparison of the final Mechanical Damage [-] for each type of cooling after three hours from the start of heating.*

As it is observed on figure 6-185, the mechanical damage values corresponding to each case are mainly identical but on the first millimetre close to the surface, where the cases introducing surface cooling processes show higher values. This fact initially suggests a rather local effect of the surface cooling processes considered in this chapter for the Surface + Heating and Surface + Repeating cases, what can also be observed on figure 6-186:

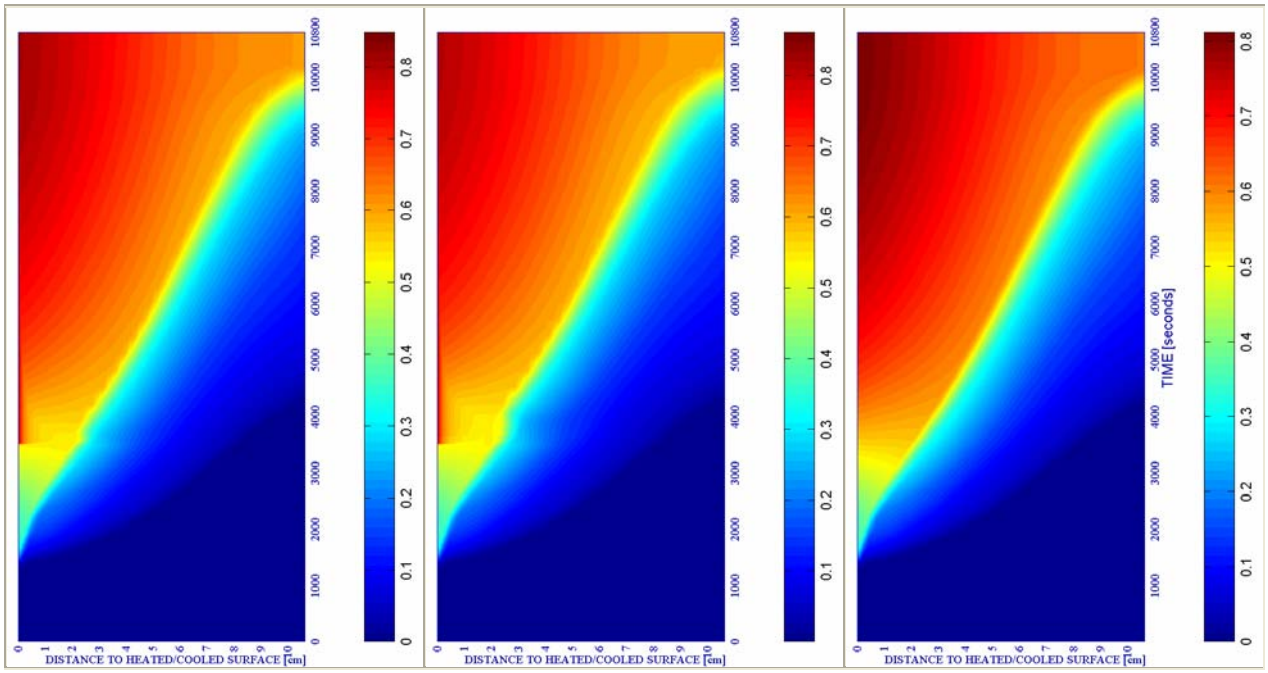

Surface cooling + Heating (1 cooling process) *Surface cooling + Repeating (3 cooling processes)* *No cooling processes*

Figure 6-186. *Mechanical damage [-]*

This local effect trend can also be observed in the final longitudinal stress state of the structural element after three hours of heating (figure 6-187):

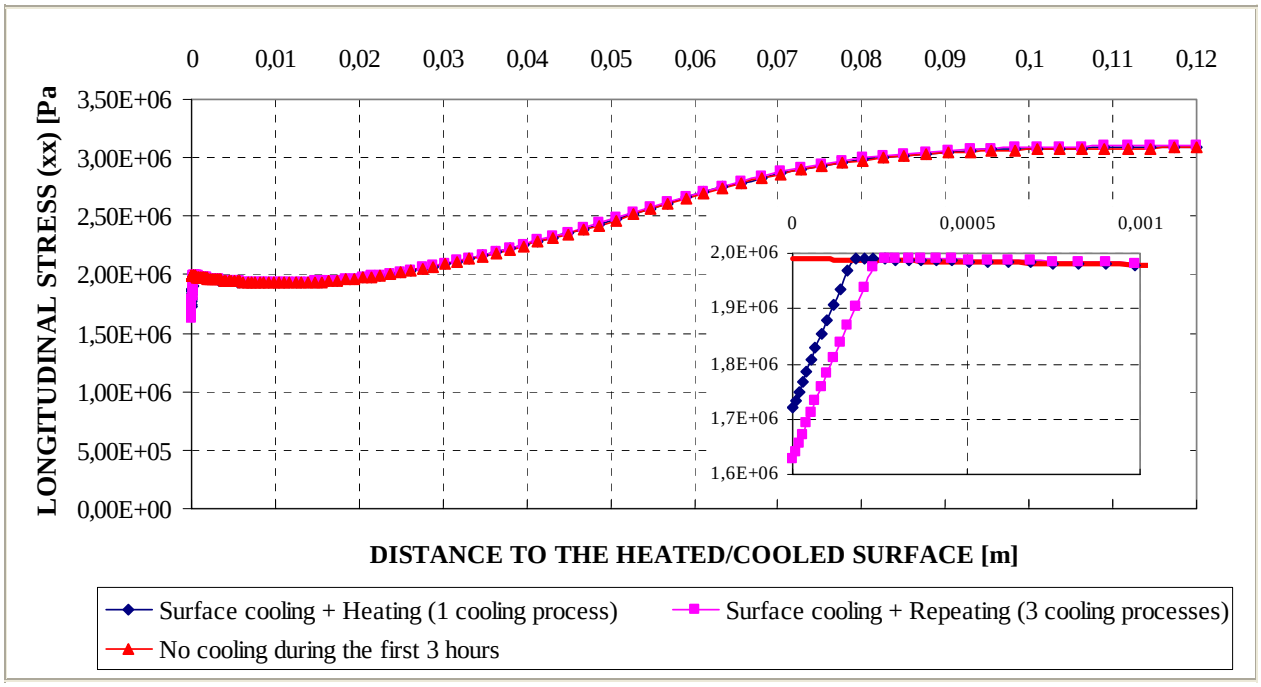

Figure 6-187. *Comparison of the longitudinal stress state [Pa] for each type of cooling after 3 hours from the start of heating.*

In conclusion, from the comparison of the cases analyzed herein it is deducted a rather local effect of the surface cooling processes considered in this chapter for the Surface + Heating and Surface + Repeating cases, with locally higher values of the cracking level when surface cooling

actions are introduced. It is remarkable, that this local effect trend is not extendable to the case Surface followed by an imposed constant ambient temperature where, as it is explained on paragraph 6.5.2.5.5, the cooling effect is not local. Regarding the maximum value of the Spalling Index selected herein, I_{s4}, and the energy available for Thermal Spalling, no significant differences are observed among the cases analyzed herein (see Table 6-120).

6.5.3.2 ANALYSIS OF THE EFFECT OF THE COOLING START INSTANT

6.5.3.2.1 Reference case #14-TH12K018RH50PAR2C60

6.5.3.2.1.1 Comparison of the effect of the cooling start instant on Environmental Slow Cooling cases

For this analysis, four start instants of the environmental slow cooling process are considered (1.800, 2.400, 3.000 and 3.360 seconds) in order to discern the effect of the cooling start instant on the final state of the structural element once it has cooled to ambient temperature (case numbers 8, 14, 17 and 21 respectively in Tables 6-107 and 6-121):

CODE	COOLING START TIME (s)	COOLING TYPE	COOLING SUBTYPE	COMBINATION NAME	PC1 (RH) [%]			PC2 (K) [m²]			PC3 (TH) [cm]	PC4 (Heating curve)			PC5 (Mat)	
					40	50	60	10^{-19}	10^{-18}	10^{-17}	12	PAR1	PAR2	PAR4	C60	C90
8	1800	ENV	SLOW	TH12K018RH50PAR2C60		x			x		x		x		x	
14	2400	ENV	SLOW													
17	3000	ENV	SLOW													
21	3360	ENV	SLOW													

Table 6-121. *Equivalence table used to identify each case (highlighted in blue is the code assigned to each case that must be used to search the corresponding results on Table 6-122).*

CASE	$IS4_{max}$ [-]	X_{IS4max} [cm]	t_{IS4max} [s]	v_{max} [m/s]	X_{vmax} [cm]	t_{vmax} [s]	v_{max}* [m/s]	X_{vmax*} [cm]	t_{vmax*} [s]	d_{max} [-]	X_{dmax} [cm]	t_{dmax} [s]	T_{max} [K]	X_{Tmax} [cm]	t_{Tmax} [s]	p^g_{max} [MPa]	X_{pgmax} [cm]	t_{pgmax} [s]
8	0,0129	0,227	1.920	0,000	---	---	0,000	---	---	0,6634	0,412	6.360	467,16	0,000	1.920	0,5967	0,582	1.920
14	0,0569	0,700	2.520	4,380	1,300	2.520	4,380	1,300	2.520	0,7901	1,300	23.760	542,44	0,000	2.520	0,8079	1,200	2.490
17	0,0894	0,974	3.090	5,228	2,037	3.090	5,228	2,037	3.090	0,8823	2,258	41.460	614,64	0,000	3.120	0,8256	1,555	2.760
21	0,1004	1,035	3.390	5,453	1,644	3.480	5,453	1,644	3.480	0,9204	3,964	102.000	656,65	0,000	3.480	0,8256	1,555	2.760

Table 6-122. *Extract of the Compendium of the maximum value of the main results corresponding to each case described in Table 6-121.*

Regarding the maximum value of the Spalling Index selected herein, I_{s4}, the cases dealt in this subparagraph (the four starting instants of the slow environmental cooling) show that the later the cooling starts the higher the Spalling Index maximum value becomes (and the deeper is located this maximum value), as it can be observed on Table 6-122.

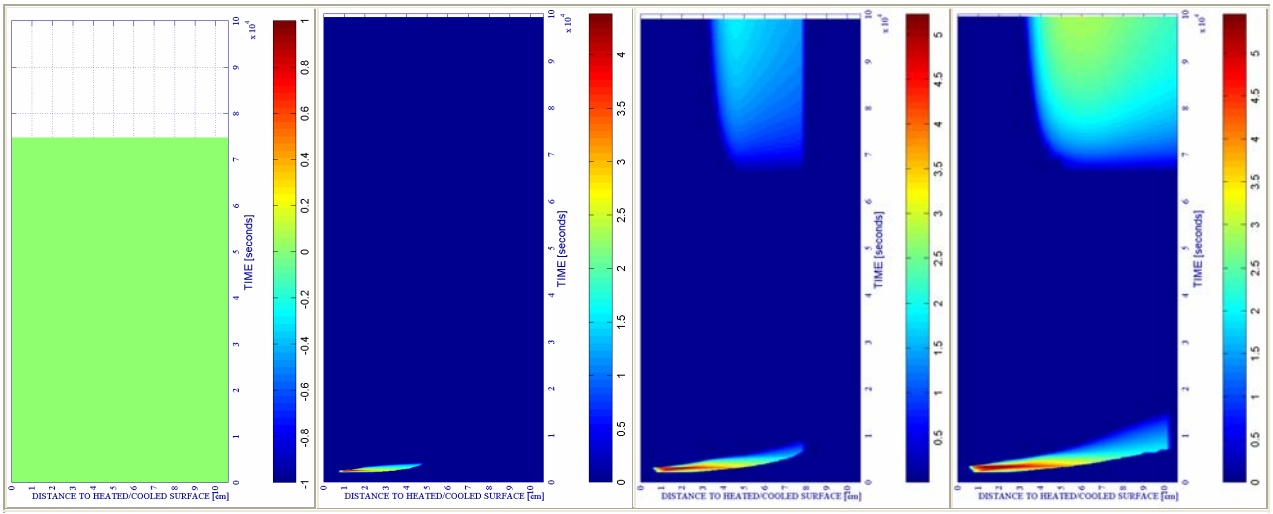

Start: 1.800 seconds *Start: 2.400 seconds* *Start: 3.000 seconds* *Start: 3.360 seconds*

Figure 6-188. *Velocity of Spalled-off pieces [m/s] where mechanical damage d ≥ 0,10*

With respect to the energetic-mechanic viability of Thermal Spalling, in figure 6-188 is observed that the later the cooling starts the higher amount of energy is available. However, taking into account that the type of residual longitudinal stresses is compressive (see figure 6-189), as it was explained on previous paragraphs the second 'bag' of available energy does not represent a state where Thermal Spalling might be mechanically viable. It is also remarkable that the later the cooling starts the higher residual longitudinal compressive stresses arise.

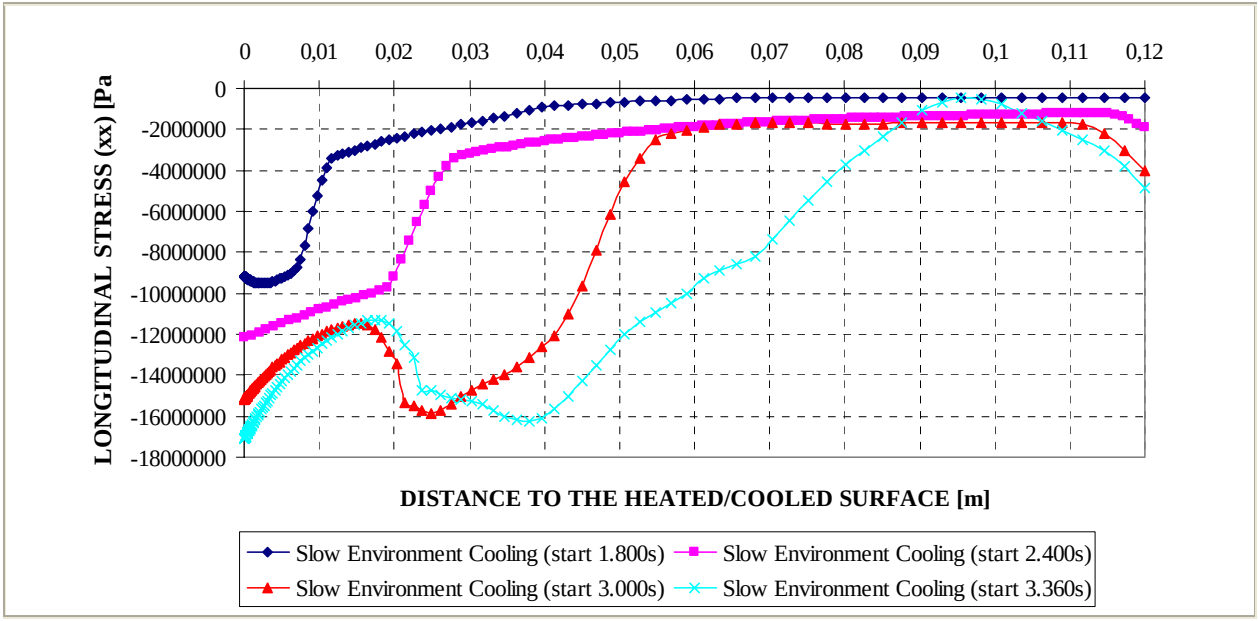

Figure 6-189. *Comparison of the final longitudinal stresses [Pa] for each type of cooling after the structural element cooling to ambient temperature.*

Related to the final distribution of the mechanical damage values (and, hence, of the cracking level of the structural element), in figures 6-190 and 6-191 it is observed that the later the cooling starts the higher the cracking level becomes at inner layers (while mechanical damage values close to the surface do not increase significantly for start instants higher than 2.400 seconds).

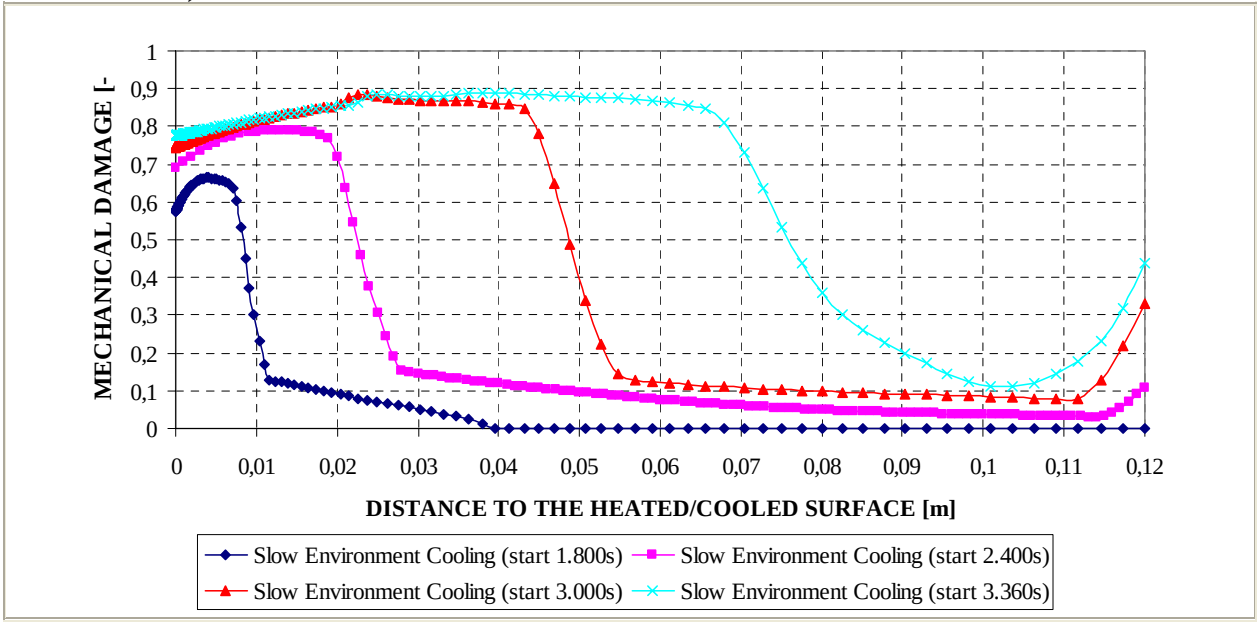

Figure 6-190. *Comparison of the final Mechanical Damage [-] for each type of cooling after the structural element cooling to ambient temperature.*

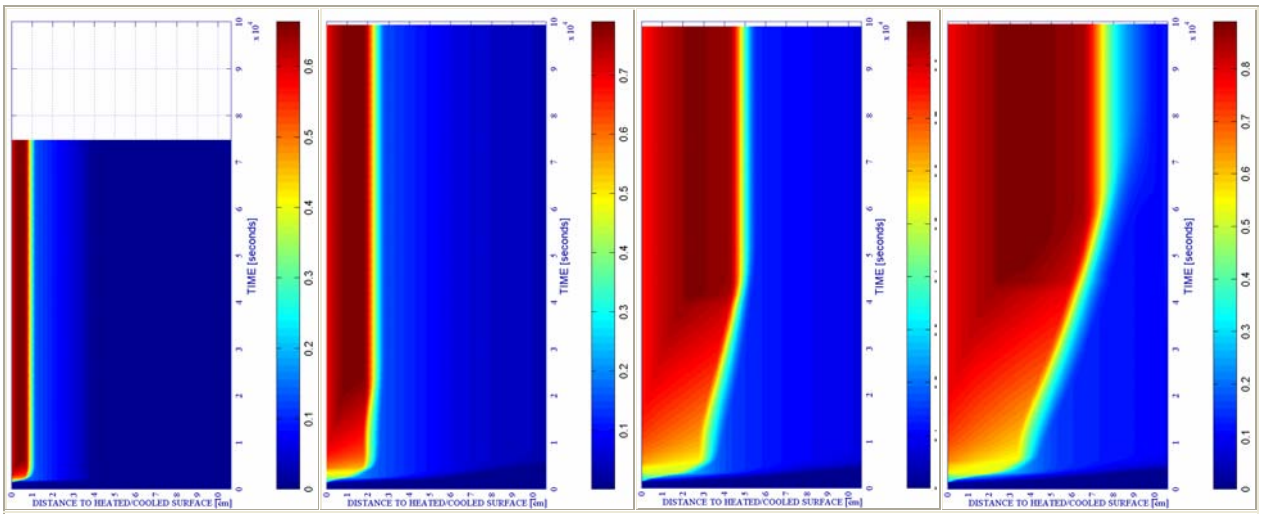

Start: 1.800 seconds *Start: 2.400 seconds* *Start: 3.000 seconds* *Start: 3.360 seconds*

Figure 6-191. *Mechanical Damage d [-]*

About the relative humidity remaining in the structural element at the end of its environmental cooling process, also important to understand its future expectable hygro-thermo-chemo-mechanical behaviour, it is observed in figures 6-192 and 6-193 that the later the cooling starts the lower the final relative humidity is in all the depths of the structural element.

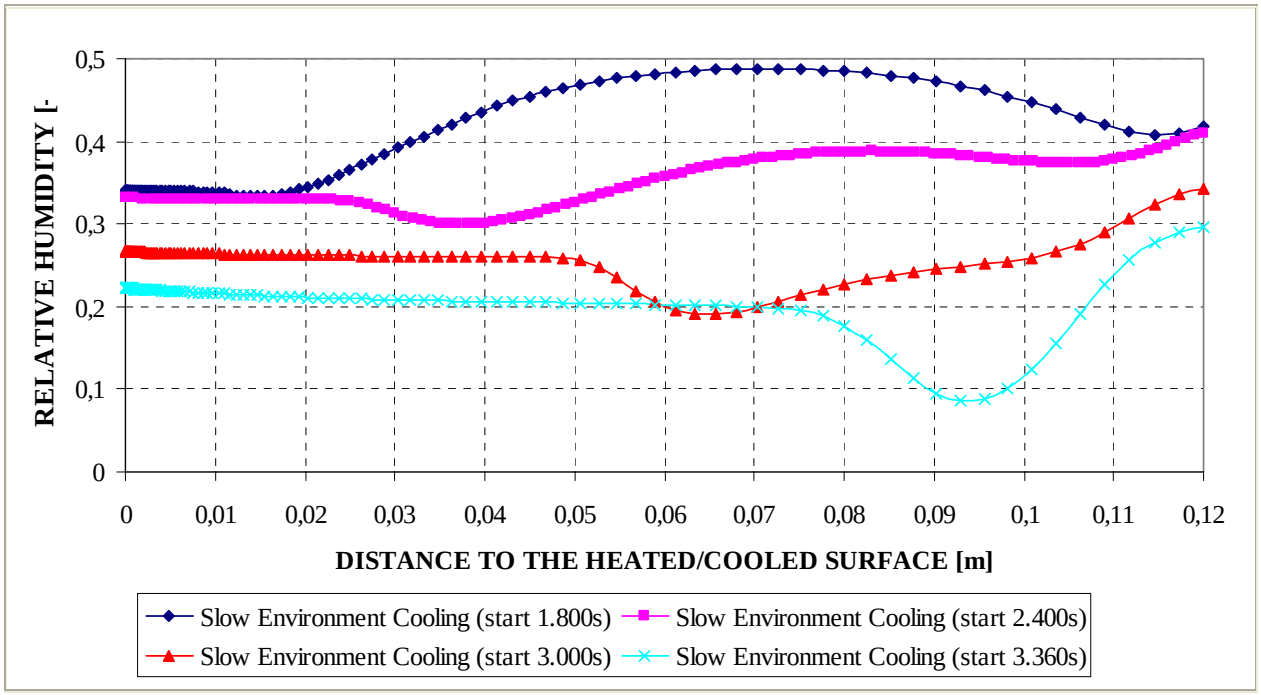

Figure 6-192. *Comparison of the final Relative Humidity [-] for each start instant of the cooling process.*

In conclusion, the later the slow environmental cooling starts:

- The higher the Spalling Index maximum value becomes,
- The higher amount of energy is available for Thermal Spalling (although it is not mechanically viable due to longitudinal compressive stresses),
- The higher residual longitudinal compressive stresses arise,
- The higher the cracking level becomes at inner layers, and
- The lower the remaining relative humidity results in all the depths of the structural element.

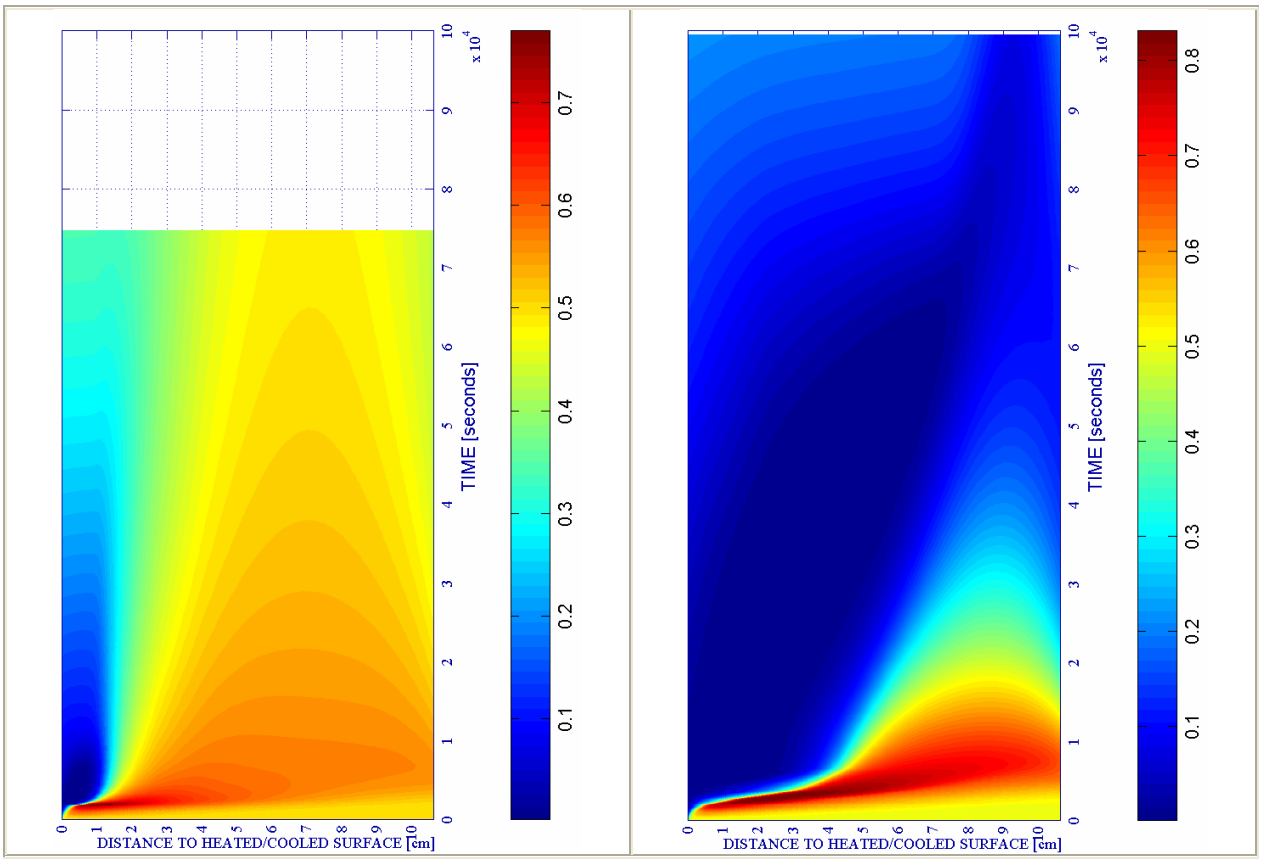

Start: 1.800 seconds *Start: 3.360 seconds*

Figure 6-193. *Relative Humidity RH [-] at the end of the slow environmental cooling of the structural element to ambient temperature.*

6.5.3.2.1.2 Comparison of the effect of the cooling start instant on Surface Cooling + Heating cases

For this analysis, two start instants of the surface cooling followed by a heating process up to 10.800 seconds are considered (1.800 and 3.360 seconds) in order to discern the effect of the cooling start instant on the final state of the structural element once it has been heated by a natural fire during three hours (case numbers 11 and 24 respectively in Tables 6-107 and 6-123):

CODE	COOLING START TIME (s)	COOLING TYPE	COOLING SUBTYPE	COMBINATION NAME	PC1 (RH) [%]			PC2 (K) [m²]			PC3 (TH) [cm]	PC4 (Heating curve)			PC5 (Mat)	
					40	50	60	10^{-19}	10^{-18}	10^{-17}	12	PAR1	PAR2	PAR4	C60	C90
11	1800	SURF	HEAT	TH12K018RH50PAR2C60		X			X		X		X		X	
24	3360	SURF	HEAT													

Table 6-123. *Equivalence table used to identify each case (highlighted in blue is the code assigned to each case that must be used to search the corresponding results on Table 6-124).*

CASE	$IS4_{max}$ [-]	X_{IS4max} [cm]	t_{IS4max} [s]	v_{max} [m/s]	X_{vmax} [cm]	t_{vmax} [s]	v_{max}* [m/s]	X_{vmax*} [cm]	t_{vmax*} [s]	d_{max} [-]	X_{dmax} [cm]	t_{dmax} [s]	T_{max} [K]	X_{Tmax} [cm]	t_{Tmax} [s]	p^g_{max} [MPa]	X_{pgmax} [cm]	t_{pgmax} [s]
11	0,0977	1,099	3.478	6,637	3,172	10.800	6,637	3,172	10.800	0,8115	0,000	10.800	982,85	0,000	10.800	0,8057	1,736	2.878
24	0,1004	1,035	3.390	6,631	3,172	10.800	6,631	3,172	10.800	0,8475	0,000	3.516	982,75	0,000	10.800	0,8256	1,555	2.760

Table 6-124. *Extract of the Compendium of the maximum value of the main results corresponding to each case described in Table 6-123.*

Regarding the maximum value of the Spalling Index selected herein, I_{s4}, the cases dealt in this subparagraph (the two starting instants of the surface cooling) show that the later the cooling starts the higher the Spalling Index maximum value becomes (but not the deeper is located this maximum value), as it can be observed on Table 6-124.

With respect to the viability of Thermal Spalling, in figure 6-195 is observed that the amount of available energy at the end of the first three hours of heating is not significantly affected by the start instant of the surface cooling process.

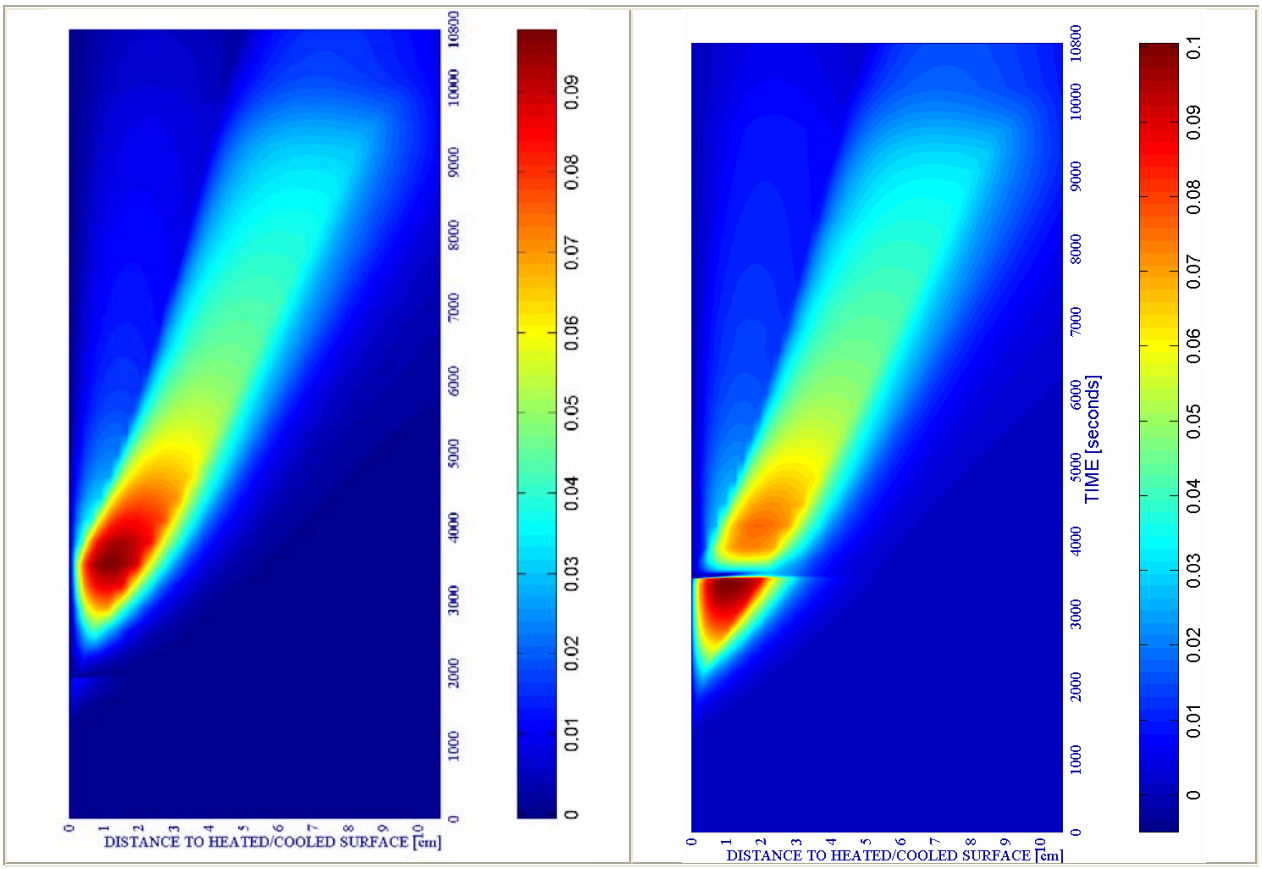

Start: 1.800 seconds *Start: 3.360 seconds*

Figure 6-194. *Spalling Index I_{s4} [-]*

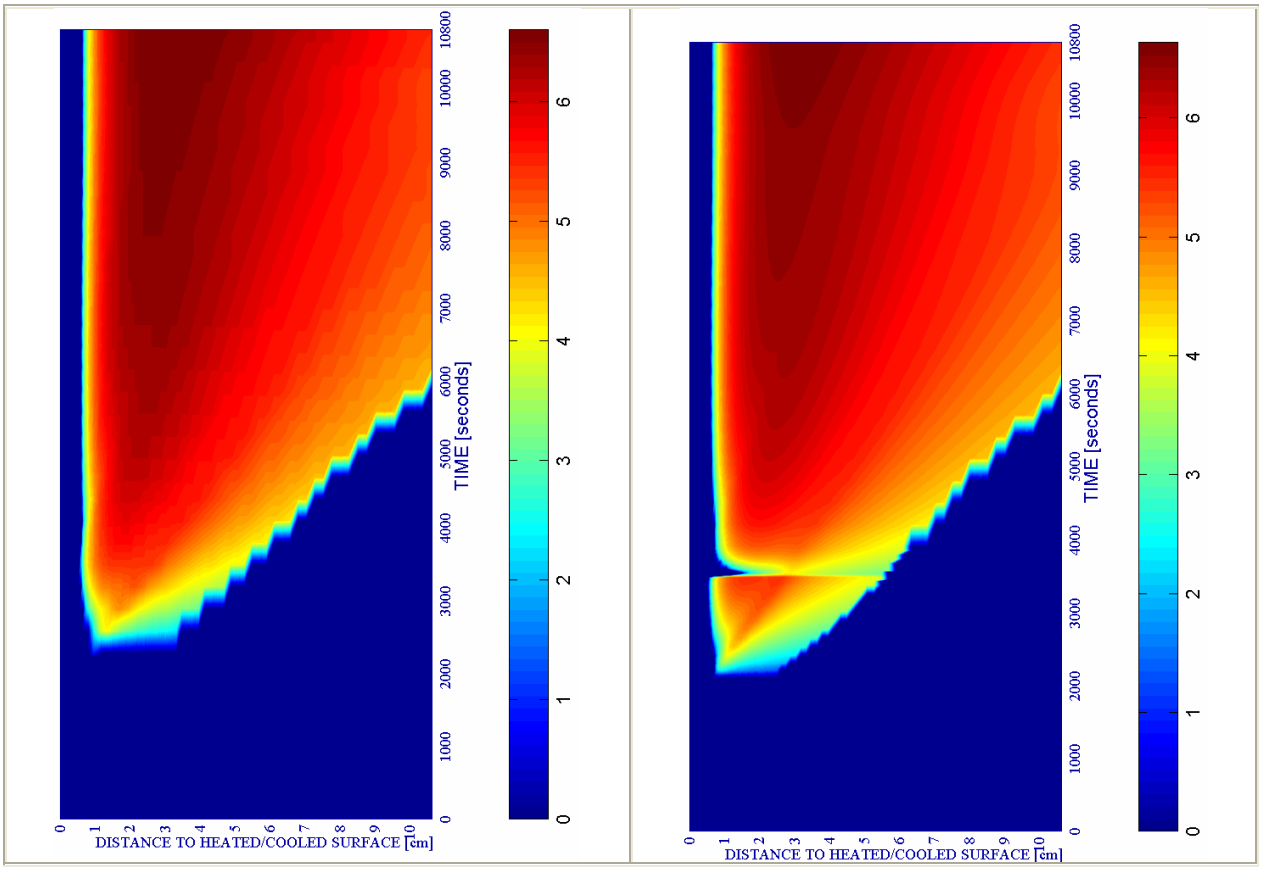

Start: 1.800 seconds *Start: 3.360 seconds*

Figure 6-195. *Velocity of Spalled-off pieces [m/s] where mechanical damage $d \geq 0{,}10$*

Related to the distribution of the mechanical damage values (and, hence, of the cracking level of the structural element) at the end of the first three hours of heating, in figures 6-196 and 6-197 it is observed that no significant differences arise (not greater than a 5 per cent), confirming once more the local effect of the surface cooling processes (followed by heating) already exposed on paragraph 6.5.3.1.3.2, independently on the cooling start instant.

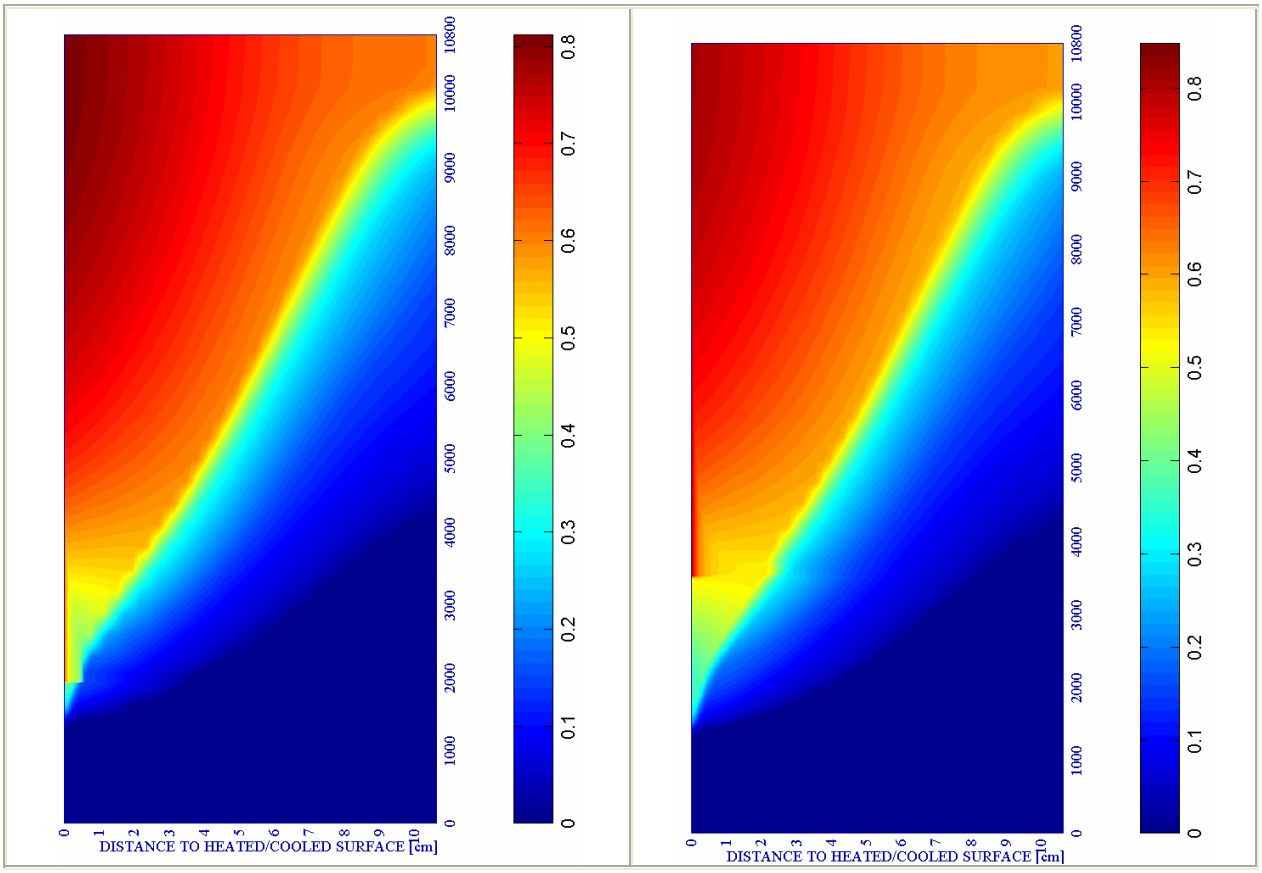

Start: 1.800 seconds *Start: 3.360 seconds*

Figure 6-196. *Mechanical Damage d [-]*

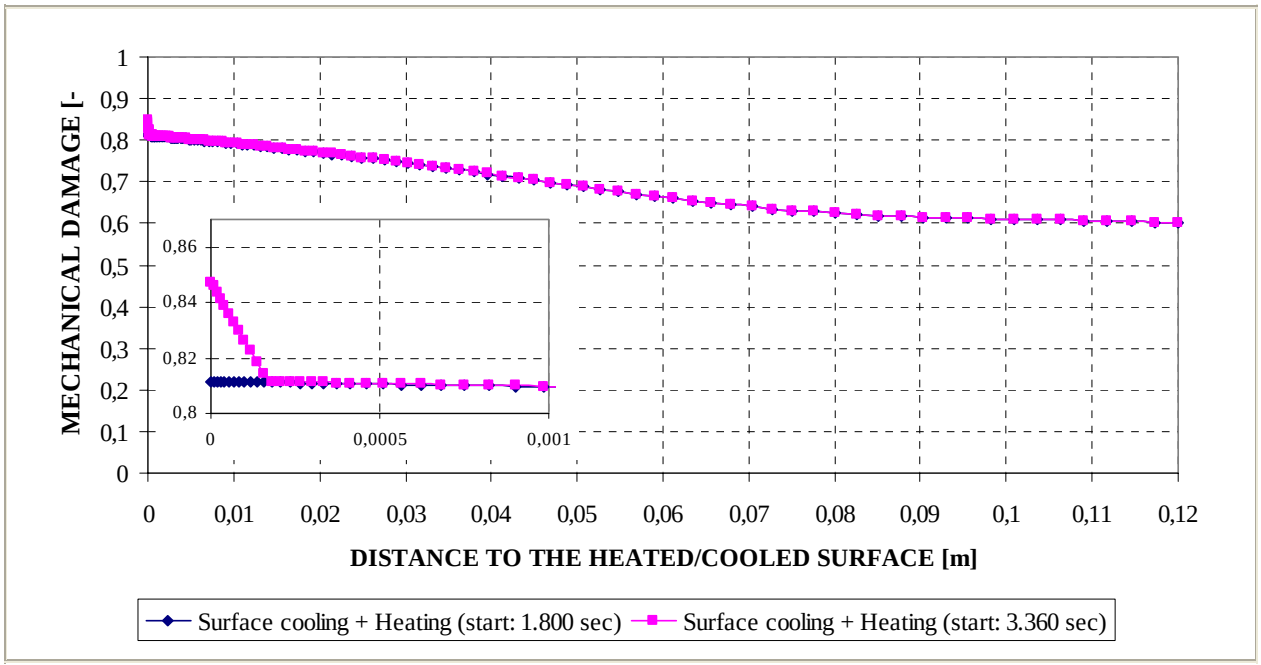

Figure 6-197. *Comparison of the final Mechanical Damage [-] for each start instant of the surface cooling, after 3 hours of heating.*

This clearly local influence of the start instant of the surface cooling processes (followed by heating) is also observed on the final distribution of longitudinal stresses at all the depths of the structural element after three hours of heating (see figure 6-198):

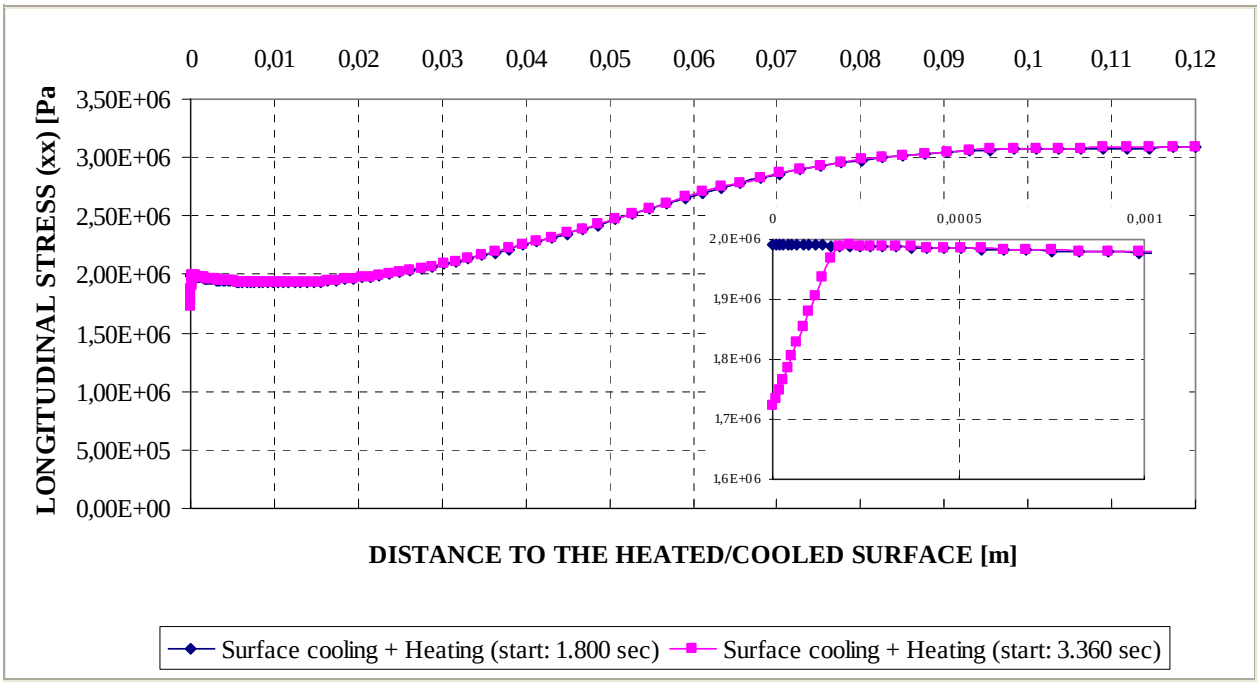

Figure 6-198. *Comparison of the final longitudinal stresses [Pa] for each start instant of the surface cooling, after 3 hours of heating.*

In conclusion, on the contrary of what has been observed on the previous paragraph related to the effect of the cooling start on the environmental cooling cases, herein this effect is only local and does not result significant at all after three hours of heating.

6.5.4 Atlas of Information for the Analysis of the Influence on Cooling of Parameters not related to Cooling Process

The works introduced in this paragraph are addressed, as it was explained on paragraph 6.3, to supply the information needed for the analysis of the influence on the hygro-thermo-chemo-mechanical behaviour of the structural element during the cooling processes of several parameters non-related to the own cooling processes – such as the initial moisture content of concrete, its intrinsic permeability, the rate of temperature increase (fire intensity), the porosity, compressive strength, type of aggregate and, in general, the whole set of hygro-thermo-chemical properties of concrete –.

The stated information is included in a separate Appendix – Appendix 6A – as an atlas of information that enables the generation of an extension of the Spalling Nomograms initially obtained just for heating processes and previously described on Chapter 4. In this way, the comprehension of the Chapter and its effectiveness towards the reader will be improved. A complete explanation of the methodology developed to supply this information is included in paragraph 6.3.

As it was explained in paragraph 6.1, although the generation of the stated Spalling Nomograms for the cooling stage is not an aim of this Thesis and it is proposed as an extended task for future research works, in Appendix 6A it is analyzed if the variation of any of these parameters leads to an increase of the maximum value of the adopted Spalling Index I_{s4} (i.e. the risk of Thermal Spalling) during the cooling stage of the cases dealt in this Chapter.

6.6 RESUME OF THE CONCLUSIONS OF THE CHAPTER

6.6.1 About the Cooling Phenomenological and Mechanistic Analysis

The phenomenological and mechanistic analysis of the effect of a spectrum of cooling processes – representative of the most expectable actions to be developed by the Fire Fighting Services during the progress of a natural fire in a High-Rise Building – on the hygro-thermo-chemo-mechanical state of a structural element manufactured with High-Strength concrete has been developed by means of the advanced Hitecosp Software [2] (see paragraph 6.5.2).

The structural element selected for the analyses developed in this chapter is analogous to that considered in *Chapter 4 – Spalling Nomograms*, since it was as more versatile as possible in order to achieve results applicable to most of the High Strength Concrete structural elements usually found in High-Rise Buildings. Its complete typological description is included in paragraph 4.3 of Chapter 4.

The adopted Heating profiles have been obtained, analogously to what is done in *Chapter 4*, from the time-temperature parametric curves defined in the Eurocode 1, Part 1-2 [28], since this is an European regulation widely spread and prestigious document where parametric curves have been defined on an experimental bases, definition that is described on paragraph 4.3.2.4.1 of Chapter 4. The complete description of the adopted Heating profiles is included in paragraph 6.4.3.1.

The definition of the Cooling profiles has been developed in sight of their Physical Background and of Fire Fighting Experiences described in the available bibliography (see paragraph 6.4.3.2.3) and from the development of several Computational Fluid Dynamics simulations of natural fires in an office (see paragraph 6.4.3.2.4), being the basic aim of these simulations to arrange more information about the temperature evolution of the surface of structural elements where a water jet/spray is directly applied, since this was a basic information needed to discern the cooling effect on the hygro-thermo-chemo-mechanical state of a structural element manufactured with High-Strength concrete. The selected office is where this Thesis is being written, owned by the PhD Student and writer, as it constitutes a typical-plan office common to many High-Rise Buildings sited in a building exclusively containing offices and consisted of an actual typical-plan office of A_f = 43,12 m^2, a total walls surface of A_t = 152,70 m^2 and 2,50 m in height:

A total amount of 16 Computational Fluid Dynamics simulations (requiring each a computational effort longer than four days) have been developed by means of *Fire Dynamics Simulator* software [48,49] on a 135.000 uniformly distributed cells model for several flow rates of a hose-nozzle ranging from 96 up to 220 litres per minute, different droplets mean diameters ranging from 250 to 1.000 μm, several cone angles ranging from 3º-6º to 3º-60º and different initial velocities of the droplets ranging from 10 to 15 m/s. The evolution of the temperature at the wall surface where the water jet has been applied has been deducted by means of a set of 36 thermocouples, resulting a general cooling rate of -10 ºC/s and two particular extremely high cooling rates of -136,6 ºC/s and -32,36 ºC/s respectively, all of them introduced in the subsequent hygro-thermo-chemo-mechanical calculations.

Two types of cooling profiles have been chosen in sight of what has been exposed on previous paragraphs (see paragraph 6.4.3.2.5): Environmental Cooling Profiles, where the cooling action is applied to the air in contact with the surface of the structural element, and Surface Cooling Profiles, where the cooling effect is applied directly to the surface of the structural element. Among them, several subtypes of cooling profiles are defined starting from different instants and depending on the actions following the cooling processes: within the Environmental Cooling Profiles, the environmental temperature has been progressively

decreased according to three cooling rates (–0,2 ºC/s, –2,0 ºC/s. and –20,0 ºC/s.) until it has reached ambient temperature, which is considered 25 ºC, following the calculations with a constant ambient temperature until the whole structural element show a temperature within the range *Ambient Temperature* ± 10ºC; on the other hand, within the Surface Cooling Profiles, as just explained all of them have been, in general, characterized by a cooling rate of the surface of the structural element of – 10,0 ºC/s (by apart of some particular analyses introducing the most extreme values of the cooling rates), followed by three different actions after the end of the surface cooling process to ambient temperature: '*Followed by Heating*', where after the surface cooling stage the environment heating profile keeps governing the evolution of the temperature in the structural element, '*Followed by an imposed constant Surface Temperature*', where the surface temperature is also decreased at the cooling rate previously described until the ambient temperature is reached on the surface and then it is kept constant in order to simulate keeping the water jet applied on the surface for some time more, and finally '*Divided into Two/Three Periods*', where the intention of this subtype of surface cooling has been to simulate the action of the water jet applied on the surface of the structural element in several sweeps, which might be a realistic situation when fire fighters move the nozzle around in cyclic sweeps.

Next, the cooling phenomenological and mechanistic analysis of a total amount of 29 reference cases have been developed by means of the advanced Hitecosp Software [2] (see Table 6-30 on paragraph 6.5.1 for an Atlas of the analyzed cases) (requiring each a computational effort longer than three days).

The phenomenological and mechanistic analysis of each reference case is deeply described in each corresponding subparagraph of paragraph 6.5.2, including the analysis of the evolution of several critical parameters such as the selected Spalling Index I_{s4}, the mechanical damage d, the velocity of spalled-off pieces v, the gas pressure p^g, the vapour pressure p^v, the saturation degree S, the relative humidity RH, the temperature T, the elastic energy U, the stress in the longitudinal direction σ_{xx} and the stress in the transversal direction σ_{yy}.

The only conclusion common to all of the reference cases consists on that from none of them have resulted increasing values of the selected Spalling Index I_{s4} during the cooling stages (neither during environmental cooling processes nor during surface cooling processes) not increasing, therefore, the Thermal Spalling risk during cooling stages. However, especially within the environmental cooling cases the mechanical damage – i.e. the cracking level – increases dramatically during the cooling stage both in value and in extent towards the inner layers increasing, hence, the depth of the structural element where Thermal Spalling is both energetically and mechanically viable and leading to more massive Thermal Spalling phenomena being expectable. On the other hand, surface cooling processes followed either by a heating stage or divided into two/three periods introduce a quite local effect on the overall hygro-thermo-chemo-mechanical behaviour of the structural element limited to the layers close to the heated/cooled surface. For a deeper and particularized description of the conclusions arisen from each analysis the reader is addressed to the corresponding paragraph of this Chapter.

Additionally, some particular phenomena of interest and the development of certain analyses have also been included in order to enhance the usefulness of the results deducted in this Chapter as a necessary base to work out research tasks beyond the aims selected.

Hence, as a secondary contribution of the analyses of this Chapter the description and analysis of the infiltration of the environmental humidity inside the structural element during the cooling processes has been developed (see paragraph 6.5.2.8.2): during the cooling processes analyzed it has been observed that there is an infiltration – across both surfaces of the structural element – of the humidity of the environment towards the inner layers. This effect happens since a constant vapour pressure of the environment has been imposed at both sides of the structural

element – see paragraph 6.4.1 explaining the boundary conditions used in the calculations – and, hence, as the temperature in the environment decreases its relative humidity increases (being approximately the 50% at the initial ambient temperature) and vice versa. These increases in the structural element relative humidity are significant since it rises from almost zero at the beginning of the cooling processes values up to a 30 per cent value at the end of the cooling. It has also been observed that the slower the environmental cooling process is the greater the environmental relative humidity infiltration occurs.

Introductory analyses of the effect of the maximum temperature and damage reached in the concrete of the structural element have also been included in paragraph 6.5.2.8.3 in order to enable the evaluation the final value of several basic mechanical (and thermal) properties needed to calculate the load-carrying capacity of any structural element during and after a fire situation, introducing several examples showing the usefulness of exploiting the results obtained in this Chapter to estimate, for instance, the minimum value of the compressive strength achieved during the heating/cooling process – d needed to evaluate the structural state of a heated structural element – or the residual value of the Young's Modulus of concrete (a reasonable comprehension of which is obtained from the final distributions of the mechanical damage). This constitutes another secondary original contribution of this Thesis since, up to this date, the only existing works addressed to evaluate, for instance, the residual Young's Modulus of a structural element after a fire are experimentally based.

Further introductory analyses have been also included in paragraph 6.5.2.8.4 in order to show, by means of an example, the usefulness of knowing the maximum temperatures achieved at any position during the heating/cooling processes of each case to estimate the strength and several deformation properties of steel reinforcing bars at elevated temperatures such as the residual relation between the adherence breakage stress ($\tau_{u,inc}$) after the fire and that previous to it (τ_u).

6.6.2 About the Comparative Analysis

The development of a comparative analysis to compare the final hygro-thermo-chemo-mechanical state of a structural element after the development of different types – and subtypes – of cooling processes, including comparisons about the Environment vs. Structural element's Surface cooling attacks, among different start instants and for several velocities of the cooling processes has been developed (see paragraph 6.5.3). This comparison has been developed on two of the selected reference cases: reference case #05 – TH12K018RH50PAR1C60 and reference case #14 – TH12K018RH50PAR2C60.

Within the comparison of the cases where an environmental cooling process has been considered (see paragraph 6.5.3.1.1), the analyzed state has been that corresponding to the instant when the entire structural element has lowed down its temperature under the ambient temperature plus ten degrees. The main conclusions of this comparative analysis have shown that, regarding the maximum value of the Spalling Index selected herein, I_{s4}, all of the cases dealt (the three subtypes of environmental cooling) lead to identical maximum values since these maxima jave appeared prior to the start of the cooling process. Related to the final distribution of the mechanical damage values (and, hence, of the cracking level of the structural element) non-significant differences have been found between those corresponding to Medium and Fast environmental cooling processes. However, the final state of the structural element after a Slow environmental cooling have shown higher levels of cracking both in value and, what it is equally unfavourable due to the loss of resistant surface, in its extent towards inner layers. While in the reference case #05 – TH12K018RH50PAR1C60, in both the Medium and Fast environmental cooling cases the maximum values of the cracking level have appeared much sooner – what may lead to a longer and more severe exposition of the reinforcing bars to fire action –, in the

reference case #14 – TH12K018RH50PAR2C60 all of the subtypes of environmental cooling have lead to the appearance of the highest levels of cracking almost simultaneously, with the only difference that the values of the mechanical damage corresponding to the Slow case have kept increasing slightly until the end of the process. Related to the final relative humidity corresponding to a Slow environmental cooling this has resulted lower at all the depths of the structural element than in the rest of cases, probably due both to a longer stay at high temperatures and to a higher level of cracking that has enabled water loss towards the environment. Finally, referred to the residual longitudinal stress (xx) although its distributions for all the cases are quite similar close to the heated/cooled surface – where high compressive stresses have arisen – in several inner layers the Slow environmental cooling case has resulted significantly more stressed in the reference case #05 – TH12K018RH50PAR1C60, while both Medium and Fast environmental cooling processes have lead to higher residual stresses in the reference case #14 – TH12K018RH50PAR2C60. In conclusion, from the comparison of these three subtypes of environmental cooling it has been deducted that a low environmental cooling rate (i.e. Slow) leads to structural elements more widely damaged (cracked) and with residual stresses higher in the reference case #05 – TH12K018RH50PAR1C60 but not in the reference case #14 – TH12K018RH50PAR2C60, being the latter a not so expected conclusion.

In the meantime, in those cases where a surface cooling process has been applied (see paragraph 6.5.3.1.2), the structural element state after three hours from the beginning of the natural fire in a High-Rise Building has been analyzed and compared. Again, regarding the maximum value of the Spalling Index selected herein, I_{s4}, all of the cases dealt (the three subtypes of surface cooling) have lead to identical maximum values since these maxima appear prior to the start of the cooling process. The cases '*Followed by heating*' and '*Divided into 2/3 periods*' have lead to qualitative and quantitatively analogous results at the end of the 3 hours from the beginning of the fire, being Thermal Spalling energetically viable from really early stages up to the end (in this cases, tensile longitudinal stresses keep present until the end of the 3 hours process). On the contrary, the case '*Followed by an imposed constant temperature*' has shown that at early stages Thermal Spalling is not energetically viable any longer up to the end of the calculation. This fact obviously occurs due to the contribution of the second (and third) heating processes that take place in the cases '*Followed by heating*' and '*Divided into 2/3 periods*' (otherwise, an unfavourable effect of the surface cooling on the thermal spalling risk would have to be understood, conclusion that has not derived at all from any of the cases analyzed in this Chapter). Related to the final distribution of the mechanical damage values (and, hence, of the cracking level of the structural element) non-significant differences have been found between those corresponding to '*Followed by heating*' and '*Divided into 2/3 periods*' processes, what suggests a quite local and limited effect of the second and third surface cooling process developed in the '*Divided into 2/3 periods*' case. In the meantime, in the '*Followed by an imposed constant temperature*' case it is remarkable the faster increase rate of mechanical damage close to the surface if compared to the others but only in a narrow layer close to the heated/cooled surface. Regarding the final distribution of temperature in the structural element, it is remarkable that no significant differences have arisen between the '*Followed by heating*' and '*Divided into 2/3 periods*' cases despite introducing in the latter additional surface cooling processes. Referred to the residual longitudinal stress (xx), its distributions for both the '*Followed by heating*' and '*Divided into 2/3 periods*' cases have resulted quite similar at all the depths– arising elsewhere tensile stresses in the longitudinal directions and compressive in the transversal one –. In conclusion, from the comparison of these three subtypes of surface cooling it is deducted that the number of temperature cycles of similar amplitude – i.e. the number of sweeps done by the Fire-Fighter applying the water jet on the surface of the structural element (among one and three cycles/sweeps) – does not appear to lead to significant differences after 3 hours from the start of the natural fire. With respect to the case where the water jet is kept

applied to the surface of the wall over a longer period: in the reference case #05 – TH12K018RH50PAR1C60 it has been observed that higher cracking rates appear in a narrow layer close to the heated/cooled surface; on the other hand, in the reference case #14 – TH12K018RH50PAR2C60 it has been observed a considerably faster increase rate of mechanical damage close to the surface – if compared to the rest of the cases – arising hence the maximum of the mechanical damage value in this case, only in 2 minutes after the start of the cooling process, beyond the maximum cracking levels that are achieved in almost 2 hours in the '*Followed by heating*' and '*Divided into 3 periods*' cases, denoting this trend a quite unfavourable effect, from a mechanistic point of view, of a long application of a water jet on the heated surface of a structural element.

A comparative analysis has also been developed in order to discern the effect of the type of cooling – environmental cooling, surface cooling or not cooling at all – on the hygro-thermo-chemo-mechanical state of a structural element (especially after the extinguishment of a fire in a High-Rise Building) in the reference case #14 – TH12K018RH50PAR2C60 (see paragraph 6.5.3.1.3):

First (see paragraph 6.5.3.1.3.1), a comparison of the final state of a structural element existent in a room of a High-Rise Building where fire fighting actions (in the form of environmental slow cooling processes starting either at 1.800 or at 3.360 seconds) are / are not introduced during the natural fire evolution – for this purpose, the parametric cooling curves provided by Eurocode 1 Part 1-2 [28] have been adopted to simulate the natural cooling of the enclosure –. Hence, it is remarkable that the case where no 'forced cooling' actions are introduced, i.e. the case with natural cooling, has resulted the only case (among those compared) showing a very long period during the natural cooling process at which Thermal Spalling has been energetically and mechanically viable, i.e. up to nineteen hours after the fire has begun. Related to the final distribution of the mechanical damage values (and, hence, of the cracking level of the structural element) extremely significant differences have been found: the final state of the structural element after a Slow environmental cooling starting at 3.360 seconds have shown high levels of cracking in much wider and deeper extents towards inner layers than when the cooling process has been started earlier at 1.800 seconds. However, the more significant difference in the mechanical damage distribution and evolution have appeared at the natural cooling case, in which the mechanical damage values existent at 10.800 seconds, i.e. the start of the natural cooling process, have resulted kept almost constant during a very long cooling period, i.e. from three to sixteen hours from the start of the fire, showing moderately high values (higher than the 60 per cent) at all the depths of the structural element whereas, at sixteen hours from the start of the fire – i.e. thirteen hours after the start of the natural cooling process – mechanical damage values have begun to increase again at all the depths of the structural element without stopping this increase until the end of the calculation developed and reaching 'completely fractured' values at the layers close to the heated/cooled surface. The main conclusion of the comparison of these three types of cooling is that a natural cooling process has lead – in the reference case analyzed – to structural elements more widely (and more severely) damaged (cracked) but with residual stresses not necessarily higher than those introducing environmental cooling actions, being this a not so expected conclusion. However, it is important to observe that at the positions where reinforcing bars are expected to be located mechanical damage values arisen in the case with an environmental slow cooling starting at 3.360 seconds have resulted higher (about a ten per cent) than those corresponding to the case including a natural cooling process (at least up to the extent of the available calculated instants in the natural cooling case named).

Second (see paragraph 6.5.3.1.3.2), the calculation case where no cooling actions (neither environmental nor surface) have been introduced during the three first hours from the beginning

of the fire has been compared against the case where one/three surface cooling processes have been introduced at 3.360 seconds from the beginning of the fire. The main conclusion arisen from this comparison has been to describe a rather local effect of the surface cooling processes considered in this chapter for the *Surface + Heating* and *Surface + Repeating* cases, with locally higher values of the cracking level when surface cooling actions have been introduced. It is remarkable, that this local effect trend has not been extendable to the case *Surface followed by an imposed constant ambient temperature* where the cooling effect is not local.

Finally, the influence of other parameters such as the cooling process start instant has also been analyzed for the reference case #14 – TH12K018RH50PAR2C60. Within the environmental cooling cases (see paragraph 6.5.3.2.1.1), the main conclusions arisen have shown that the later the slow environmental cooling starts the higher the Spalling Index maximum value becomes, the higher amount of energy is available for Thermal Spalling (although it is not mechanically viable due to longitudinal compressive stresses), the higher residual longitudinal compressive stresses arise, the higher the cracking level becomes at inner layers, and the lower the remaining relative humidity results in all the depths of the structural element. On the contrary, within the *Surface cooling + Heating* cases (see paragraph 6.5.3.2.1.2) has been observed that the effect of the cooling start on the surface cooling cases is only local and does not result significant at all after three hours of heating.

6.6.3 About the Atlas of Information for the Analysis of the Influence of Parameters not related to Cooling Processes

The information needed for the analysis of the influence on the hygro-thermo-chemo-mechanical behaviour of the structural element during the cooling processes of several parameters non-related to the own cooling processes – such as the initial moisture content of concrete, its intrinsic permeability, the rate of temperature increase (fire intensity), the porosity, compressive strength, type of aggregate and, in general, the whole set of hygro-thermo-chemical properties of concrete –, and for the generation of an extension of the Spalling Nomograms initially obtained just for heating processes and described previously on Chapter 4 has been provided (see paragraph 6.5.4 and Appendix 6A) as an atlas of information constituted by four Cartesian continuum representations of those parameters more representative of the Thermal Spalling risk for each of the forty five cases analyzed (what has represented a total amount of 180 figures).

Although the generation of the stated Spalling Nomograms for the cooling stage has not been an aim of this Thesis and it is proposed as an extended task for future research works, in Appendix 6A it has been analyzed if the variation of any of these parameters leads to an increase of the maximum value of the adopted Spalling Index Is4 (i.e. the risk of Thermal Spalling) during the cooling stage of the cases dealt in this Chapter.

From the analysis of the evolution of the Spalling Index I_{s4} resulting at each case it has been clearly observed that the values of the Spalling Index I_{s4} always decrease at all the depths as soon as the surface cooling process starts being reduced, hence, the risk of Thermal Spalling during this process (what does not mean that Thermal Spalling is no longer viable during the surface cooling process if, for instance, layers where Thermal Spalling would be energetically viable but mechanical damage showed too low values during heating increase their level of cracking during the cooling stage enabling mechanically the development of Thermal Spalling).

The latter situation has been clearly detected in several of the analyzed cases.

6.6.4 About the extended tasks to go more deeply into Thermal Spalling research during Cooling processes

1. In Chapter 5 it was already observed that thermal creep may have a significant effect on the results dealt in this Chapter. If the conclusions deducted herein are needed for structural elements where strong restraints are expected, there is a prior need to develop a software release capable to predict hygro-thermo-chemo-mechanical behaviour considering thermal creep during cooling processes.

2. The degree of saturation with liquid water S (considering together hygroscopic and capillary water, if the latter is contained in the pores) is an experimentally determined function of capillary pressure (matrix potential) p^c, and temperature T (since hysteresis phenomena are not considered here, it is assumed to be a unique function of capillary pressure). Usually presented graphically in the form of the sorption isotherms, this function is needed for realistic modelling of hygro-thermic behaviour of concrete and it must be determined during sorption tests at several temperatures. Within all of the calculations included in this Chapter the sorption isotherms corresponding to the heating stages have also been considered during the cooling ones, being therefore still a need to work out sorption isotherms specific for cooling stages.

3. Since the concrete cover of the steel reinforcing bars is reduced due to the spalled-off pieces, there is a need of studying what will happen after the first superficial pieces have spalled-off, being possible – but not corroborated – that Thermal Spalling phenomena accelerates as successive layers are progressively spalled-off until the reinforcement bars are reached and exposed directly to fire.

4. On the other hand, there is still a need for a mathematical model allowing analysing the hygro-thermal, chemical and deterioration processes in concrete structures at high temperature more precisely, and which will allow us to predict the Thermal Spalling phenomenon using purely 'mechanical' criteria, and not 'heuristic' ones, as the presented here. This should possibly take into account a stochastic nature of the phenomenon and its both local and global character. In some authors' opinion [1], the latter could be considered, for example, by using a multi-scale type model, involving a micro-level for predicting physical properties of the concrete components (i.e. cement paste, Inter-phase Transition Zone and aggregate), a meso-level for analysis of their interactions (e.g. by means of fracture mechanics), and finally, a macro-scale for evaluation of the whole structure performance at given ambient conditions. The model used in this chapter, after appropriate modifications, could be used for the macro-scale analysis.

5. As it was exposed on the State-Of-The-Art Chapter, there is an almost absolute lack of experimental phenomenological and mechanistic information about cooling processes in High Strength concretes. This is an unavoidable prior work to accomplish if the software release described on the first proposed extended task is to be developed.

6. The analysis of the influence on the hygro-thermo-chemo-mechanical behaviour of the structural element during the cooling processes of several parameters non-related to the own cooling processes – such as the initial moisture content of concrete, its intrinsic permeability, the rate of temperature increase (fire intensity), the porosity, compressive strength, type of aggregate and, in general, the whole set of hygro-thermo-chemical properties of concrete –, and the generation of an extension of the Spalling Nomograms initially obtained just for heating processes and described previously on Chapter 4 is still pending and may be fulfilled starting from the atlas of information provided in Appendix 6A.

7. Finally, an extension of all of these works – basically the development of Spalling Indexes correlated against experimental data – to cases with bidimensional fluxes of heat and mass are necessary to excerpt conclusions for cooling processes on certain structural elements

such as square columns, where Corner Thermal Spalling is often the most dangerous type. For this reason, the analyses of square columns included in Chapter 7 may only be developed from a 'heuristic' point of view.

6.7 BIBLIOGRAPHY OF THE CHAPTER

Bibliography of the chapter

[1] D. Gawin, F. Pesavento, B.A. Schrefler, *Towards prediction of the thermal spalling risk through a multi-phase porous media model of concrete*, Comput. Methods Appl. Mech. Engrg . 195 (2006) 5707-5729.

[2] Brite Euram III BRPR-CT95-0065 HITECO, *Understanding and industrial application of High Performance Concrete in High Temperature Environment – Final report*, 1999.

[3] R. Felicetti, P. Gambarova, M.P. Natali Sora, G. Rosati, *Caratterizzazione mecánica di calcestruzzi ad alta ed altissima resistenza esposti ad alta temperatura*, Brite Euram III report, 1999.

[4] D. Gawin, F. Pesavento, B.A. Schrefler, *Modelling of Hygro-Thermal behaviour of Concrete at High Temperature with Thermo-Chemical and Mechanical Material Degradation*, Comput. Methods Appl. Mech. Engrg . 192 (2003) 1731-1771.

[5] W.G. Gray, *Macroscale Equilibrium Conditions for Two-Phase Flow in Porous Media*, Int. J. Multiphase Flow, 26 (2000) 467-50.

[6] G.L. England, N. Khoylou, *Moisture Flow in Concrete Under Steady State Non-Uniform Temperature States: Experimental Observations and Theoretical Modelling*, Nucl. Eng. Des. 156 (1995) 83-107.

[7] R.H. Nochetto, M. Paolini, C. Verdi, *An Adaptive Finite Element Method for Two-Phase Stefan Problems in Two Space Variables*, Math. Comput. (1991) 78-108

[8] M. Picasso, *An Adaptive Finite Element Algorithm for a Two-Dimensional Stationary Stefan-Like Problem*, Comput. Methods Appl. Mech. Engng. 124 (1995) 213-230.

[9] D. Gawin, F. Pesavento, B.A. Schrefler, *Modelling of Hygro-Thermal Behaviour and Damage of Concrete at Temperature Above the Critical Point of Water*, Int. J. Numer. Anal. Meth. Geomech. 26 (2002) 537-562.

[10] Z.P. Bazant, W. Thonguthai, *Pore pressure and drying of concrete at high temperature*, J. Engrg. Mech. ASCE 104 (1978) 1059-1079.

[11] Z.P. Bazant, W. Thonguthai, *Pore Pressure in Heated Concrete Walls: Theoretical Prediction*, Mag. Concr. Res. 31 (1979) 67-76.

[12] D. Gawin, B.A. Schrefler, *Thermo- Hydro- Mechanical Analysis of Partially Saturated Porous Materials*, Eng. Comput. 13 (1996) 113-143.

[13] D. Gawin, P. Baggio, B.A. Schrefler, *Modelling heat and moisture transfer in deformable porous building materials*, Arch. of Civil Engng. 42 (1996) 325-349.

[14] D. Gawin, C.E. Majorana, B.A. Schrefler, *Numerical Analysis of Hygro-Thermic Behaviour and Damage of Concrete at High Temperature*, Mech. Cohes.-Frict. Mater. 4 (1999) 37-74.

[15] D. Gawin. F. Pesavento, B.A. Schrefler, *Simulation of Damage – Permeability Coupling in Hygro-Thermo-Mechanical Analysis of Concrete at High Temperature*, Commun. Numer. Meth. Engng. 18 (2002) 113-119.

[16] W.G. Gray, B.A. Schrefler, *Thermodynamic Approach to Effective Stress in Partially Saturated Porous Media*, Eur. J. Mech. A/Solids, 20 (2001) 521-538.

[17] B.A. Schrefler, D. Gawin, *The Effective Stress Principle: Incremental or Finite Form?*, Int. J. Numer. Anal. Meth. Geomech. 20 (1996) 785-815.

[18] G.A. Khoury, C.E. Majorana, F. Pesavento, B.A. Schrefler, *Modelling of Heated Concrete*, Mag. Concr. Res. 54 (2002) 1-25.

[19] D. Gawin, C. Alonso, C. Andrade, C.E. Majorana, F. Pesavento, *Effect of damage on permeability and hygro-thermal behaviour of high performance concretes at elevated temperatures*, (in preparation).

[20] J. Mazars, *Application de la mecanique de l' endommagement au comportament non lineaire et la rupture du beton de structure*, Thèse de Doctorat d' Etat, L.M.T., Universite de Paris, France, 1984.

[21] J. Mazars, *Description of the behaviour of composite concretes under complex loadings through continuum damage mechanics*, in: Proc. Tenth U.S. National Congress of Applied Mechanics, (ed. by J.P. Lamb, ASME, 1989).

[22] M.D. Kachanov, *Time of Rupture Process under Creep Conditions*, Izvestia akademii nauk, (in Russian) 8 (1958) 26-31.

[23] UNE-ENV 1992-1-2, *Eurocode 2: Design of concrete structures - Part 1.2: General rules – Structural fire design*, July 2002

[24] L.T. Phan, *High-Strength concrete at High Temperature – An overview*, Building Fire Research Laboratory Online Library, National Institute of Standards and Technology, Gaitherburg, 2002.

[25] J. Calavera, *Patología de Estructuras de Hormigón Armado y Pretensado – Tomo I*, Book, Instituto Técnico de Materiales y Construcciones, 3rd edition, 1996.

[26] Matlab, The Language of Technical Computing, Release 13, June 2002, The MathWorks, Inc.
[27] J.G. Quintiere, *Principles of Fire Behaviour*, Book, Delmar Publishers, 1st edition 1998.
[28] UNE-EN 1991-1-2, *Eurocódigo 1: Acciones en estructuras. Parte 1-2: Acciones generales. Acciones en estructuras expuestas al fuego*, Mayo 2004.
[29] P. Grimwood, E. Hartin, J. Mc Donough, S. Raffel, *3D FIRE Fighting, Training, Techcnics and Tactics*, Book, Fire Protection Publications, 1st edition, May 2005.
[30] J.R. Mawhinney, *Water Mist Extinguishing Properties*, 4th Symposium on Fire Safety Science 1994.
[31] K Giselsson, M Rosander, *Making the Best of Water for Extinguishing Purposes*, Fire Magazine (UK), October 1984.
[32] A. Jones, P.F. Nolan, *Discussions On The Use Of Fine Water Sprays or Mist for Fire Suppression*, Journal Loss Prev. Process Ind., Volume 8, Buterworth-Heinemann Ltd, pp 17-21, 1995.
[33] Alageel, Ewan and Swithenbank, *Mitigation of Compartment Jet Fires Using Water Sprays*, University of Sheffield UK, 1998.
[34] Svensson, Sardqvist, *Fire tests in a large Hall*, Report LUTVDG/TVBB-1025-SE, Lund University Sweden, 2002.
[35] Rasbash, *FRDG 1/97*, Fire Research & Development Group UK, 1997.
[36] P Grimwood, *Flashover & Nozzle Techniques*, 1999, Firetactics.com.
[37] Z. Liu; A. Kashef; G.D. Lougheed; N. Benichou, *RR124*, National Research Council, Canada, 2002.
[38] S. Sardqvist, *Report 7003*, Lund University Sweden, 1998.
[39] P. Beever, B. Davy, *A rational approach to firefighting water supplies*, AFAC Conference, Australia, 1999.
[40] S. Hunt, G. Roberts, *BDAG – ODPM*, Office of the Deputy Prime Minister, 2004.
[41] P Grimwood, *Fire Fighting Flow-Rate*, 2005, Firetactics.com.
[42] A. Hangell, *Utvärdering av dimstralrörs effektivitet vid brandgaskyling*, Lund University, Sweden, Report 5065, 2000.
[43] Quadrafog manufacturer, *Technical Sheets*, wfrfire.com, 2006.
[44] B.P. Husted, *The physics behind water mist system*, Proc. IWMA Conference, Rome, October 2004.
[45] B.P. Hume, *Water Mist Suppression in Conjunction with Displacement Ventilation*, Fire Engineering Research Report 03/4, University of Canterbury, New Zealand, February 2003.
[46] Arcelor, TNO, CTICM, Labein, University of Hannover, RuukkI OyJ, *Divulgación del conocimiento de Ingeniería de Seguridad Ante Incendio en Estructuras, DIFISEK Project*, 2005.
[47] J.R. Lawson, R.L. Vettoni, *NIST NCSTAR 1-8 (Draft) – Federal Building and Fire Safety Investigation of the World Trade Center Disaster. The Emergency Response Operations (Draft)*, Building and Fire Research Laboratory, NIST National Institute of Standards and Technology – Technology Administration, U.S. Department of Commerce, USA, September 2005.
[48] K. McGrattan, S. Hostikka, J. Floyd, H. Baum, R. Rehm, W. Mell, R. McDermott, *NIST Special Publication 1018-5 – Fire Dynamics Simulator (Version 5) Technical Reference Guide, Volume 1. Mathematical Model*, NIST National Institute of Standards and Technology (US Department of Commerce) in cooperation with VTT Technical Research Centre of Finland, October 2007.
[49] K. McGrattan, B. Klein, S. Hostikka, J. Floyd, *NIST Special Publication 1019-5 – Fire Dynamics Simulator (Version 5) User's Guide.*, NIST National Institute of Standards and Technology (US Department of Commerce) in cooperation with VTT Technical Research Centre of Finland, October 2007.
[50] V. Babrauskas, *Glass breakage in fires*, Fire Science and Technology Inc., March 2005, www.doctorfire.com/glass.html
[51] *Real Decreto 1942/1993, de 5 de noviembre, por el que se aprueba el Reglamento de Instalaciones de Protección Contra Incendios*, Boletín Oficial del Estado núm. 298 de 14 de diciembre de 1993, Spanish Government.
[52] *Real Decreto 2059/1981, de 10 de abril, por el que se aprueba la Norma Básica de la Edificación "Condiciones de protección contra incendio en los edificios"*, Boletín Oficial del Estado núm. 224 de 18 de septiembre de 1981, Spanish Government.
[53] N. Khoylou, *Modelling of moisture migration and spalling behaviour in non-uniformly heated concrete*, Ph.D. thesis, Imperial College, London, 1997, pp.1147.

Bibliography of the annexes

[B.1] K. McGrattan, S. Hostikka, J. Floyd, H. Baum, R. Rehm, W. Mell, R. McDermott, *NIST Special Publication 1018-5 – Fire Dynamics Simulator (Version 5) Technical Reference Guide, Volume 1. Mathematical Model*, NIST National Institute of Standards and Technology (US Department of Commerce) in cooperation with VTT Technical Research Centre of Finland, October 2007.

[B.2] K. McGrattan, B. Klein, S. Hostikka, J. Floyd, *NIST Special Publication 1019-5 – Fire Dynamics Simulator (Version 5) User's Guide*., NIST National Institute of Standards and Technology (US Department of Commerce) in cooperation with VTT Technical Research Centre of Finland, October 2007.

Appendix 6A. ATLAS OF INFORMATION FOR THE ANALYSIS OF THE INFLUENCE ON COOLING OF PARAMETERS NOT RELATED TO COOLING PROCESS

Appendix 6B. INPUT FILES FOR FIRE DYNAMICS SIMULATOR (FDS) CALCULATIONS

(See next pages)

THIS PAGE IS INTENTIONALLY
LEFT BLANK